Environmental modeling and remote sensing linked to lacustrine climate proxies: the rift basin Chew Bahir (Ethiopia) during the late Pleistocene

Dissertation

der Mathematisch-Naturwissenschaftlichen Fakultät

der Eberhard Karls Universität Tübingen

zur Erlangung des Grades eines

Doktors der Naturwissenschaften

(Dr. rer. nat.)

vorgelegt von

Markus Lothar Fischer

aus Jena

Tübingen

2022

Gedruckt mit Genehmigung der Mathematisch-Naturwissenschaftlichen Fakultät der Eberhard Karls Universität Tübingen.

DISSERTATION

Environmental modeling and remote sensing linked to lacustrine climate proxies: the rift basin Chew Bahir (Ethiopia) during the late Pleistocene

Markus Lothar Fischer

2022

Department of Geoscience, Eberhard-Karls University of Tuebingen

ACKNOWLEDGEMENTS

Table of Content

List of Abbreviations

AHP   African Humid Period

asl   above sea level

EARS   East African Rift System

ITCZ   Intertropical Convergence Zone

ka   Thousand Years Before Present

LBM   Lake Balance Model

LGM   Last Glacial Maximum

PVM   Predictive Vegetation Model

List of Figures

Summary

Eastern Africa, a hotspot of hominin evolution, is a diverse and fragile landscape, shaped by the ongoing rifting and the large orographic and climatic gradients between green and lush mountainous regions and dry and hot rift floors, which are partly deserted today, such as the Chew Bahir basin, in southern Ethiopia and north-east of Lake Turkana. Orbital-induced climate change caused the last African Humid Period (AHP) from 15–5 ka (thousand years before present), leading to large rift lakes, such as the paleo-lake Chew Bahir with up to 2500 km² in size. Drilled lacustrine sediment proxies from the Chew Bahir Basin revealed the climate dynamics for the last AHP and the past 620 ka. Because proxies provide qualitative spatially point-wise and temporally continuous data about the past climate and environment, this thesis aims to complement these results using catchment-scaled environmental models to gain quantitative and spatial data about the past hydroclimate and vegetation in the vicinity of Chew Bahir. Therefore, this cumulative thesis provides a collection of model applications in the Chew Bahir vicinity and discusses the consequences for early humans living in this region. First, a Lake Balance Model (LBM) extrapolated the necessary paleo-precipitation of +25–41% compared to today during the AHP and revealed the high importance of paleo-hydro-connectivity between different lake basins in the East African Rift System. Model results showed paleo-lake Chew Bahir may have desiccated within decades and flooded within the same time afterward as soon as humid conditions prevailed. Second, a Predictive Vegetation Model (PVM) linked with the LBM provided spatial estimates of the paleo-vegetation during the Last Glacial Maximum (LGM) time and the AHP. A comparison with the archeological record indicates a human preference for open landscapes in southern Ethiopia. The model yields a precipitation reduction of -17.5% during LGM times. Third, a comprehensive perspective on the lake level evolution within the Turkana Depression indicates that besides paleo-lake Chew Bahir, there was a paleo-lake Chalbi, similar in size and, presumably, even more climate-sensitive than paleo-lake Chew Bahir. Fourth, developing an isotope-enabled quantitative model using the geological gradient between the modern-day catchment and the extended paleo-catchment may be possible for the Chew Bahir lacustrine sediments, as this modern-analog study shows. Fifth, the interdisciplinary discussion about the risk assessment of humans living close-by Chew Bahir and Lake Turkana during the termination of the AHP is shown. Sixth and last, the application of a hydrological model is shown exemplary in a different landscape in Georgia, and the impact of human behavior on the hydrosphere during the Holocene is revealed.

Kurzfassung

Ostafrika, ein Hotspot der Hominidenevolution, ist eine vielfältige Landschaft, die durch den Grabenbruch und die großen orografischen und klimatischen Kontraste zwischen grünen üppigen Bergregionen und den trocken-heißen heißen Riftbecken geprägt ist, welche heute teilweise desertifiziert sind, wie das Chew Bahir Becken im Süden Äthiopiens. Orbital bedingte Klimaveränderungen haben die letzte Afrikanische Feuchtperiode (AHP) von 15–5 ka (vor tausend Jahren) verursacht, die zu der Entstehungen großer Riftseen führte, wie dem 2500 km² großen Paläosee Chew Bahir. Lakustrine Sedimente aus dem Chew Bahir Becken geben Aufschluss über die Klimadynamik während der letzten AHP und der letzten 620 ka. Da Proxies qualitative, räumlich punktuelle und zeitlich kontinuierliche Daten über das vergangene Klima und die Umwelt liefern, zielt diese Arbeit darauf ab, diese Ergebnisse mit Hilfe von Umweltmodellen auf Einzugsgebietsebene zu ergänzen, um wichtige quantitative und räumliche Daten über das vergangene Hydroklima und die Vegetation zu gewinnen. Daher zeigt diese kumulative Dissertation eine Sammlung von Modellanwendungen in der Umgebung von Chew Bahir, sowie Diskussionen über die potenziellen Folgen für die in der Region beheimateten frühen Menschen. Zunächst wird mit einem Wasserbilanzmodel (LBM) der notwendige Paläoniederschlag von +25-41% während der AHP extrapoliert und die große Bedeutung der Paläo-Hydro-Konnektivität zwischen verschiedenen Seebecken im Ostafrikanischen Grabensystem aufgezeigt. Die Modellergebnisse zeigten, dass der Paläosee Chew Bahir innerhalb weniger Jahrzehnte ausgetrocknet und anschließend innerhalb der gleichen Zeit überflutet worden sein könnte. Zweitens lieferte ein Vegetationsmodel (PVM) in Verbindung mit dem LBM räumliche Abschätzungen der Paläovegetation während des Letzten Glazialen Maximums (LGM) und der AHP. Ein Vergleich mit den archäologischen Daten zeigt, dass der Mensch im Süden Äthiopiens vermutlich offene Landschaften bevorzugte. Das Modell approximiert einen Niederschlagsrückgang von -17,5 % zur Zeit des LGM. Drittens zeigt ein umfassender Blick auf die Entwicklung des Seespiegels in der Turkana-Senke, dass es neben dem Paläosee Chew Bahir einen Paläosee Chalbi gab, welcher eine ähnliche Größe erreichte und möglicherweise eine noch drastischere Klimasensitivität aufwies. Viertens könnte die Entwicklung eines isotopengestützten quantitativen Modells unter Verwendung des geologischen Gradienten zwischen dem heutigen Einzugsgebiet und dem erweiterten Paläo-Einzugsgebiet für die lakustrinen Sedimente des Chew Bahir möglich sein. Fünftens wird die interdisziplinäre Diskussion über das Risikoadaptionsverhalten für Menschen, welche in der Nähe des Turkana-Sees lebten, dargestellt. Zuletzt wird die Anwendung eines hydrologischen Modells exemplarisch in einer anderen Landschaft in Georgien gezeigt und der Einfluss des menschlichen Verhaltens auf die Hydrosphäre während des Holozäns dargestellt.

1 Introduction

1.1 Background and Relevance

Eastern Africa is, due to the ongoing rifting and its position within the global atmospheric circulation system, a highly diverse and intricate geo-, climate- and ecosystem and a unique hotspot of hominin fossils and stone tool findings (Nicholson, 2019). It is called the cradle of humankind in popular science because of the proposed evolutionary emergence of our very own species, *Homo Sapiens* (Maslin, 2016). New findings challenge this simplistic narrative and suggest a multiregional pan-African origin (Bergström et al., 2021; Scerri et al., 2019). Nevertheless, a majority of crucial fossils documenting significant evolutionary steps have been found in eastern Africa. In the vicinity of Lake Turkana, for example, has been an almost wholly preserved *Homo Erectus* fossil with an age of around 1.5 million years (Brown et al., 1985), and one of the oldest *Homo Sapiens* fossils from Omo-Kibish with an age of about 233 ka (Thousand Years Ago) been excavated (Leakey, 1969; Vidal et al., 2022). The first documented stone tools with an age of 3.3 million years (Harmand et al., 2015), the oldest emergence of the Acheulean technology with an age of 1.7 million years (Diez-Martín et al., 2016), and the transition to the Middle Stone Age (MSA) at around 305 to 320 ka (Deino et al., 2018) are documented in eastern Africa and spread, presumably, from there throughout the world, contributing to our understanding of human evolution, cultural development, and expansion.

Multiple theories provide frameworks to explain the interaction of human evolution, landscape, and environmental change (Maslin et al., 2015). The Savanna Hypothesis (Dart, 1925; Darwin, 1871; de Lamarck, 1809), as a widely falsified theory (Trauth et al., 2010), explained the adaption to bipedalism with gradual aridification of the climate and a tendency to more open landscapes. In contrast, the Turnover Pulse Hypothesis (Vrba, 1980) explains evolution linked to northern hemisphere glaciation cycles and during relatively short periods when increased extinction and speciation occur. The Variability Selection Hypothesis (Potts, 1998) endorses environmental instability and unpredictability as a driver to adapt for behavioral or ecological flexibility (Maslin et al., 2015). Then, the Pulsed Climate Variability hypothesis (Maslin & Trauth, 2009) advocates the punctuation of the long-term aridification trend of Africa by orbital forced periods of extreme aridity and humidity, which gets even amplified by the exceptional topographic structure of the East African Rift System (EARS), which causes the rapid occurrence and disappearance of large and deep rift lakes, the so so-called Amplifier Lakes (Trauth et al., 2010).

The EARS topography formed intense gradients between the precipitation-rich highlands and the low elevated rift floors with enormous evaporation rates. This extreme gradient and the specific geometry make these endorheic rift basins extremely sensitive to climate change (Olaka et al., 2010; Street, 1980; Trauth et al., 2010). Small scale changes in the climate may force rapid lake expansion and vice versa, rapid lake desiccation.
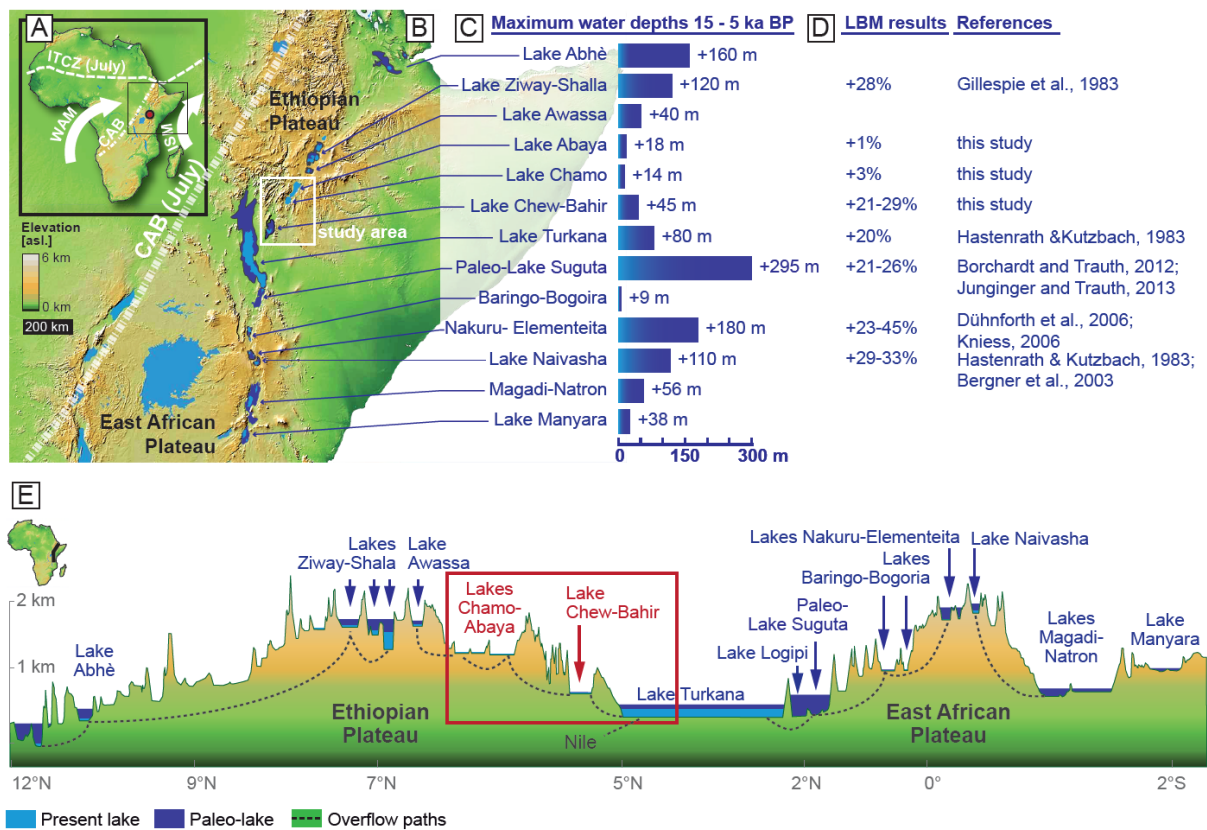
Figure 1: Overview of the study area (A & B) Elevation map of Africa and the positions of major air boundaries. (C & D) Known paleo-lake depths within the EARS during the African Humid Period (AHP) and published paleo-precipitation rates estimates using different lake-balance approaches and associated references. (E) Transect of the EARS from north-east to south, with modern and paleo level lake extents (light and dark blue, respectively), the study area (red box). Figure was modified after Junginger and Trauth (2013) and published in this version by Fischer et al. (2020).

Paleo-lake evidence, climate, and human evolution on time scales of 10^4 to 10^5 years correlate with orbital forcing, particularly with the eccentricity-modulated precession (Demenocal, 1995; Trauth et al., 2005; Trauth et al., 2007). Eccentricity, as a metric for the elliptical shape of the Earth's orbit, is the longest Milankovitch Cycle, with periods of 95, 125, and 412 ka (Berger & Loutre, 1991). The axial precession with a periodicity of 19 to 23.5 ka reflects the precession of the Earth's rotational axis (Maslin, 2020). This rotational shifting of the earth's axis superimposed by the Earth's orbit eccentricity intensifies, respectively weakens, the insolation seasonality. This has tremendous impacts on Africa's hydroclimate. In times of a precession

minimum and during northern hemisphere summer, the insolation in the northern tropics is increased, allowing the ITCZ (Intertropical Convergence Zone) to penetrate further north, which intensifies the North African summer monsoon (Berger et al., 2006; Kutzbach et al., 2020; Trauth et al., 2009). So then, today's arid northern Africa receives increased rainfall, which has led to the last African Humid Period (AHP, 15–5 ka), a greening of the Sahara, and the appearance of mega-lakes throughout northern and eastern Africa (Barker et al., 2004; Demenocal et al., 2000; Drake et al., 2022; Grant et al., 2017; Larrasoaña, 2021; Larrasoana et al., 2013).

The last AHP during the late Pleistocene to Middle Holocene is associated with the reoccupation of the Sahara ~10.5 ka (Drake et al., 2013; Kuper & Kropelin, 2006; Larrasoana et al., 2013; Manning & Timpson, 2014), cultural innovations (Lario et al., 1997) and accompanied with the transition to the Neolithic age (Honegger & Williams, 2015; Manning & Timpson, 2014). The aridification at the end of the AHP is related to the appearance of the first pastoralists in eastern Africa and the development of complex state-level societies (Brooks, 2006; Kuper & Kropelin, 2006). This environmental change may have forced human adaption and presumably provided constraints and opportunities as freshwater resources and food availability changed.

To better understand potential causal links between climate and environmental change on the one side and human evolution and cultural adaption on the other, paleoclimate archives and archaeological records can be used.

The Hominin Sites and Paleo Lake Drilling Project (HSPDP) aimed to provide a continuous paleoclimate archive based on lacustrine sediments from five sites throughout eastern Africa to cover critical phases of human evolution during the past four million years (Cohen et al., 2016). The Chew Bahir basin in southern Ethiopia, close to the Omo-Kibish formation, is one of the sites that have been drilled. The lacustrine archive covers the past 620 ka (Roberts et al., 2021). The hydroclimate is reconstructed using multiple proxies and foremost potassium XRF (Foerster et al., 2018; Schaebitz et al., 2021) and shows an aridification trend in eastern Africa lasting from approximately 200 to 60 ka superimposed by multiple orbital forced AHPs and a presumed influence of the paleo-ENSO dynamics (Kaboth-Bahr et al., 2021; Schaebitz et al., 2021; Trauth et al., 2021). This includes the last AHP during the late Pleistocene to Middle Holocene, where multiple short cores (Foerster et al., 2012; Foerster et al., 2015) from the Chew Bahir basin revealed, in a decadal resolution, a stable wet main phase in southern Ethiopia and intensive short (20–80 years) dry-spells punctuating the termination of the AHP (Trauth et al., 2018).

The late Pleistocene to Middle Holocene time allows the study of human-environmental interactions in great detail, as the archeological, geomorphological, and paleoclimate record is still dense compared to the sparse data points in the early- to mid-Pleistocene time. Nevertheless, proxies, such as the potassium record from the Chew Bahir basin (Foerster et al., 2018), provide qualitative spatially point-wise and temporally continuous data about the past climate and environment. In contrast, Proxy System Modelling (Dee et al., 2015; Dee et al., 2018; Evans et al., 2013) can be used to gain important quantitative data about the past hydroclimate. Spatialized results may help to correlate proxy results from the Chew Bahir drill cores with more distant (e.g., archeological) records. Therefore, improving the understanding of a local and regional environmental system with a holistic approach may help to decipher proxy data in greater detail, allowing to draw more precise or new conclusions.

1.2   Research Objectives

This dissertation aims to complement the paleoenvironmental understanding and the paleoenvironmental consequences for early humans during the late Pleistocene to Middle Holocene time in the Chew Bahir vicinity using catchment scaled models and to explore their capacity for interdisciplinary research. This comprises the quantification of the Hydro- and Biosphere processes and the alignment with the proxy results from the Chew Bahir basin. The exploration of alignment concepts accompanies this thesis. Furthermore, the consequences for human ancestors in these regions are discussed.

The Hydro- and Biosphere behavior in the Chew Bahir catchment is explored using Lake Balance Modelling (LBM) and Predictive Vegetation Modelling (PVM). This complements the conclusion drawn from the lacustrine proxies from the Chew Bahir basin. This emerges the following questions:

> **Q1**   What has been the magnitude of precipitation change in the Chew Bahir catchment since the late Pleistocene?
>
> **Q2**   What is the possible pace of Chew Bahir's paleo-lake level change given different climate transitions during the last AHP, and what are the implications for early humans?
>
> **Q3**   What was the paleo-vegetation in southern Ethiopia during the last AHP and the Last Glacial Maximum (LGM) time?
>
> **Q4**   How does a changing seasonality affect the paleo-water balance and the paleo-vegetation?

Q5 Has there been a preference of early humans for open or closed landscapes?

Q6 Do lake levels in the basins of Turkana, Chew Bahir, Suguta, and Chalbi in northern Kenya and southern Ethiopia follow the same climatic forcing and reaction?

Q7 Is a link between the Chew Bahir lacustrine sediments and the shoreline record from that region possible?

As a co-authored work, the potentials of an isotope-enabled hydro-balance model using the insights derived from the LBM (Fischer et al., 2020), comprehensive fieldwork, and laboratory data are studied. Therefore, the following questions arise:

Q8 Is it possible to use modern Oxygen, Hydrogen, and Strontium isotopes to reconstruct the paleohydrology of the Chew Bahir basin?

As human-environment interaction is a meaningful question in times of anthropogenic-induced climate change, the past may provide answers for the present. An interdisciplinary team reviewed the environmental and archeological records in the Lake Turkana realm, asking:

Q9 What are human strategies in the Turkana Basin to adapt to shrinking lake levels at the end of the last African Humid Period?

LBM is used to understand the amplitude and pace of change in space and time in the Chew Bahir proximity for the past 25 ka, and conclusions are drawn on the impact for human beings reacting to a changing environment. Such attempts may also be used in other landscapes, such as this interdisciplinary work from the Caucasus in Georgia. In this study, the impact of human behavior on the landscape is examined, trying to answer the following question:

Q10 Was human-induced landcover change a significant factor for lake formation during the Late Bronze to Early Iron Age in Shiraki Plateau, Georgia?

1.3   Thesis Structure

This is a cumulative dissertation, which provides a framework text and six publications in the Appendix. The published articles P1 and P2 are the core of this thesis, as they provide detailed modeling work of the Chew Bahir catchment system. P3 is in a very early preparation stage, completes the modeling work, and shows a failed attempt. P4 is a close collaboration paper, complementing the modeling work by developing a direct link between lake system, precipitation, and isotopes in the lacustrine sediments of the Chew Bahir basin. P5, as a co-authored work, is a review paper that shows the relevance of the conducted research for archeological and anthropological interpretations and hypothesis construction in the Turkana basin. P6, as a co-authored work, explores the capability of model applications in other biomes and reverse human-environment interactions.

P1   Fischer, M. L., Markowska, M., Bachofer, F., Foerster, V. E., Asrat, A., Zielhofer, C., Trauth, M. H., & Junginger, A. (2020). Determining the Pace and Magnitude of Lake Level Changes in Southern Ethiopia Over the Last 20,000 Years Using Lake Balance Modeling and SEBAL. Frontiers in Earth Science, 8. https://doi.org/10.3389/feart.2020.00197

Status: *Published*

Author contribution: Research design, model development, model interpretation and discussion, writing of the initial manuscript, and handling of the review process.

P2   Fischer, M. L., Bachofer, F., Yost, C. L., Bludau, I. J. E., Schepers, C., Foerster, V., Lamb, H., Schäbitz, F., Asrat, A., Trauth, M. H., & Junginger, A. (2021). A Phytolith Supported Biosphere-Hydrosphere Predictive Model for Southern Ethiopia: Insights into Paleoenvironmental Changes and Human Landscape Preferences since the Last Glacial Maximum. Geosciences, 11(10), 418. https://doi.org/10.3390/geosciences11100418

Status: *Published*

Author contribution: Funding acquisition, research design, model development, data acquisition, result interpretation, discussion, writing of the initial manuscript, and handling of the review process.

P3   Fischer, M.L.& Junginger A. (in prep.). The Turkana Lake System during the last African Humid Period: A Review

Status: *In preparation*

Author contribution: Funding acquisition, research design, data acquisition, interpretation and discussion, writing of the initial manuscript, and handling of the review process.

P4   Markowska, M., Martin, A. N., Vonhof, H. B., Guinoiseau, D., Fischer, M. L., Zinaye, B., Galer, S. J. G., Asrat, A., & Junginger, A. (2022). A multi-isotope and modelling approach for constraining hydro-connectivity in the East African Rift System, southern Ethiopia. Quaternary Science Reviews, 279. https://doi.org/10.1016/j.quascirev.2022.107387

Status: *Published*

Author contribution: Data acquisition, data analysis, contribution to writing and interpretation of results

P5   Hildebrand, E., Grillo, K., Kendra C., Fischer M.L., Goldstein S.T., Janzen A., Junginger, A., Kinyanjui R., Ndiema E., Sawchuk, E., Beyin, A., Pfeiffer, S.K. (2022). Buffering new risks? Environmental, social and economic changes in the Turkana Basin during and after the African Humid Period. The Holocene.

Status: *Published*

Author contribution: Contribution to writing and interpretation of results

P6   Suchodoletz, H., Kirkitadze, G., Koff, T., Fischer M. L., Poch R. M., Khosravichenar, A., Schneider B., Glaser B., Lindauer, S., Hoth, S., Skokan, A., Navrozashvili, L., Lobjanidze, M., Akhalaia, M., Losaberidze, L., Elashvili, M. (2022). Human-environmental interactions and seismic activity in a Late Bronze to Early Iron Age settlement center in the southeastern Caucasus. Frontiers in Earth Science.

Status: *Published*

Author contribution: Contribution to data analysis, discussion, writing, and interpretation of results

1.4   Regional Geography

The Omo-Turkana lows in eastern Africa contain the lake basins of Lake Turkana, paleo-lake Suguta, Chalbi, and Chew Bahir. These basins have an area of 259,000 km² ranging from 9.3°N to 0.8°S. They are located between the Ethiopian and the East African Plateau, part of

the 4000 km long EARS. Lake Turkana is the world's largest permanent desert lake (Ojwang et al., 2016), with a lake size of 6,400 km² and a catchment size of 75,000 km². It drains the western Ethiopian Plateau by the Omo River and the East African Plateau through the rivers Keiro and Turkwel. Lake Turkana (at 2.4°N-4.5°N and 35.8°E-36.8°E, 73 m deep, 360 m asl) is endorheic today and has its potential overflow sill at 35.15°E, 5.03°N to the White Nile and is hydrologically connected to the Mediterranean Sea. Paleo-lake Suguta (at ca. 2.2°N and 36.5°E) in the southern extension of Lake Turkana would potentially drain the modern-day endorheic Kenyan rift basins Baringo and Nakuru-Elmenteita and would potentially overspill with an increased lake level of + ~300 m to Lake Turkana. Paleo-lake Chalbi (at ca. 2.9°N and 37.6°E) is a vast desert today and apart from the paleo-hydrological network of Chew Bahir, Suguta, and Turkana. Paleo-lake Chalbi's potential overflow sill towards the Indian Ocean at 37.57°E and 2°N (Fischer et al., in prep.).

Chew Bahir (4.1–6.3°N, 36.5–38.1°E, ~498m asl) in southern Ethiopia is a 210 km² saline mudflat most of the year. Paleo-lake Chew Bahir would potentially drain the south of the Main Ethiopian Rift with today's endorheic rift lakes Abaya (6.4°N, 37.95°E, 7 m deep, and lake surface area of 1,081 km²) and Chamo (5.8°N, 37.6°E, ~1,109 m asl, 14 m deep, 310 km² lake surface area) through the river Segen and the northern Broadly Rifted Zone through the Weyto River. In case of overflowing, paleo-lake Chew Bahir would drain to Lake Turkana at 36.66°E and 4.22°N. The catchment is 20,650 km² in size and bound by the Main Ethiopian Rift shoulders with the Teltele Plateau (up to 1,600 m asl) in the east and the Hammar Range (up to 1,300 m asl) in the west (Fischer et al., 2020).

The geology of the study area is shaped by the rifting of the EARS, which leads to a complex relief ranging from vast highlands with elevations up to 4,000 m asl, steep rift shoulders to broad rift basins, such as the Chew Bahir or the Turkana basin. Elevations at the rift floor range from 300 to 500 m asl. The southwestern Ethiopian highlands are made up of up to 3000 m thick basalts and intercalated silicic volcanic of the Eocene to Late Oligocene age (Chorowicz, 2005; Corti, 2009; Mohr & Zanettin, 1988). Half-graben basins with a North to North-East orientation shape the Broadly Rifted Zone (Emishaw et al., 2017). Precambrian basement is exposed at the rift shoulders, such as at the western Hammar range (Davidson, 1983). To the south of Chew Bahir, the Cenozoic rift volcanic separate the Chew Bahir basin from the Turkana basin and the Turkana basin from the Chalbi and Suguta basin (Brown & Mcdougall, 2011; Levin et al., 2011). The rift basins are filled with Cenozoic sediments up to multiple km in depth (Corti, 2009).

The modern-day climate in the Omo-Turkana lows and the close vicinity of paleo-lake Chew Bahir is classified as hot semiarid (Koeppen climate classification), with precipitation being

lower than evapotranspiration. In contrast, the Ethiopian highlands in the north of Lake Turkana and Chew Bahir receive a higher precipitation amount and are classified as humid, with precipitation reaching partly 2,000 mm per year (Segele & Lamb, 2005).

The seasonality in Chew Bahir is linked to the annual migration of the ITCZ, which is primarily fueled by the Indian Ocean (Levin et al., 2009; Nicholson, 2017). The ITCZ migrates between 10° North and South of the equator, leading to a bimodal precipitation pattern close to the equator and unimodal close to the Tropic of Cancer and the Capricorn (Nicholson, 2019). So then, the southern lower elevated part of the Chew Bahir catchment receives a bimodal precipitation pattern with the long rains "Belg" from Match to May and the "short rains" in October and November. In contrast, the highlands in the north of Chew Bahir , the Omo River's upstream area, and the Lake Abaya catchment experience a unimodal rainfall pattern with a wet season lasting from March to November (Segele & Lamb, 2005; Williams & Funk, 2011). This long-lasting damp season has two sources- the "Belg" rains from March to May and the "Kiremt" from June to September. The "Kiremt" rains presumably are fueled by the West African Monson and reach their easternmost limit in southern Ethiopia, the so-called Congo Air Boundary (CAB) (Camberlin, 1997; Nicholson, 2019). It is hypothesized that during times of precession minima, as during the AHP, the CAB dragged east-wards leading to an additional rainy season in the Chew Bahir lowlands (Costa et al., 2014; Junginger & Trauth, 2013; Tierney et al., 2011).

The vegetation (see Figure 2) follows the topography and the precipitation gradients, forming a complex mosaic with desert shrubland along Lake Turkana's shore, woodlands and wooded grasslands in the Omo River lowlands and the paleo-lake Chew Bahir catchment, afro-montane forests of the Ethiopian highlands, and afro-alpine vegetation in most elevated parts (see Figure 2) (Asefa et al., 2020; Friis et al., 2011). While the eastern part of the study area is classified as *Acacia-Commiphora* woodland and bushland, the western part is dominated by *Combretum-Terminalia* woodland and wooded grassland (Friis et al., 2011).
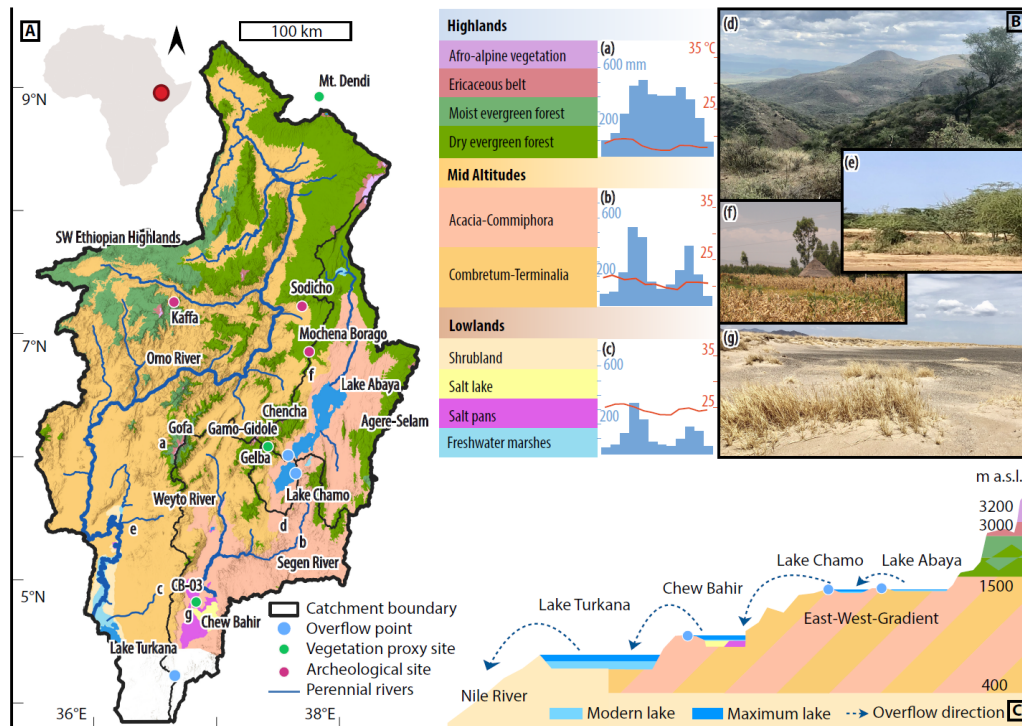
Figure 2: Overview of the study area with modern-day potential vegetation. (A) Potential vegetation is based on Friis, et al. (Friis et al., 2011). (B) monthly temperature means in °C and precipitation in mm per month (a–c, IRI, last accessed 12/2020). Representative vegetation regimes (d – g, photos from Annett Junginger) (C) Cross-section from Lake Abaya to Lake Turkana showing the overflow direction. Published in this version by Fischer et al. (2021).

2 Results and Discussion

2.1 Research Question Objectives

Six manuscripts address the given ten research questions, overarched by the main objective of the thesis – the exploration of the potentials of catchment scaled model applications focused on the Chew Bahir basin. The results are circumstantial in the publications (Appendix P1 to P6). Here, the results are briefly summarized.

Q1 What has been the magnitude of precipitation change in the Chew Bahir catchment since the late Pleistocene?

LBMs have been used to model multiple rift basins in the EARS during the AHP and to estimate necessary paleo precipitation rates to compensate for the increased open water evaporation, as explained in detail in publications P1 and P2 (Fischer et al., 2021; Fischer et al., 2020). Paleo-lake extents are given by digital elevation model analysis and are partly confirmed by shoreline observations. The magnitude of estimated precipitation rates in the EARS during the

AHP range from ca. 20 to 45%, as shown in Figure 1. This includes estimates from Ziway–Shala, +28%, (Gillespie et al., 1983), Lake Turkana, +20% (Hastenrath & Kutzbach, 1983), Suguta Valley, +26% (Junginger & Trauth, 2013), Lake Nakuru– Elmenteita, +23–45% (Dühnforth et al., 2006), and Lake Naivasha, +29–33% (Bergner et al., 2003; Hastenrath & Kutzbach, 1983). Besides the increased open water evaporation, other factors control the paleo water balance, such as biosphere feedback (Bergner et al., 2003), paleo-drainage networks, and a shift in the seasonality (Fischer et al., 2020).

We modeled the necessary precipitation increase to compensate for the increased open water evaporation. We developed a multi-basin LBM to understand the potential effect of overflooding lake systems on each other. We calculated a necessary paleo-precipitation of +6.5%. Using a monthly water balance, we analyzed the possible impact of a changing seasonality on the water balance of the lake system of Chew Bahir. A hypothetical east shift of the CAB would cause an additional rainy season (Junginger et al., 2014). As quantified within the EARS during the AHP, this effect would increase the paleo-precipitation necessity by +6.9%, summing up to +13.4%.

In the follow-up study (see Appendix P2), we focused on the biosphere feedback on the water balance and extended the studied time frame to the LGM period. We linked the developed multi-basin LBM with a newly engineered PVM to quantify the Biosphere-Hydrosphere feedback. Here, we identify an overall paleo-precipitation threshold of +25–40% to have been necessary during the AHP to lead to the observed lake level of paleo-lake Chew Bahir at the overflow sill to Lake Turkana.

We applied this Biosphere-Hydrosphere Predictive Model to the LGM time, assuming a desiccated paleo-lake Chew Bahir, as the lacustrine record suggests. The model suggests a decreased paleo-precipitation during LGM times of -15–25% compared to modern times due to the reduced evapotranspiration above land and the decreased temperature.

    Q2   What is the possible pace of Chew Bahir's paleo-lake level change given different climate transitions during the last AHP, and what are the implications for early humans?

The landscape architecture in the Chew Bahir and extended catchment is unique, as explained in detail in P1 (Fischer et al., 2020). The extended catchments of the lakes Abaya and Chamo are inherently necessary for the water balance of paleo-lake Chew Bahir. Given moderate increases of precipitation in the model, lakes Abaya and Chamo would overspill and drain

significant amounts of water through the river Segen to paleo-lake Chew Bahir. This implies a rapid lake flooding in the model as soon as Lake Chamo reaches its overflow sill, giving different scenarios (see Figure 3 for model results). This implies rapid desiccation if the water supply from the extended catchment is cut off. It can be summarized that paleo-lake Chew Bahir has a decadal reaction time to climate forcing and observed 20 to 80 years lasting dry spells at the end of the AHP (Trauth et al., 2018) had been long enough to lead to complete lake desiccation and a complete lake flooding. This is a rapid (decadal) lake response time to a climate signal and implies a reaction to changing environment and the disappearance of a potential primary food and water resource within a lifetime of a human being. As discussed in P1, Fischer et al. (2020) p.27: "… short-term episodes of pronounced aridity in the lower elevated lake basins, such as Chew Bahir could have been a push-factor for a refugium-directed vertical movement of groups with highly mobile hunter-gatherers […]. A now further specified variable is the climatic component in this comparison as shown in our study. The Southern Ethiopian Rift has responded sensitively to even shorter dry spells, so that living conditions would have deteriorated quickly when the rift floor became too dry. One of the reasons why hunter-gatherers might have returned to the South Ethiopian Rift region after such dry spells, could have been their dietary style at that time, that was mainly devoted to fishing (Hildebrand et al., 2018; Owen et al., 1982). The long-term transitions, on the other hand, driven by changes in orbital controlled insolation, could have fueled cultural adaptation and significant changes in the social organization within groups. Only after the gradual end of the AHP with the near-desiccation of almost all lakes in the Kenyan and Ethiopian rift over a longer period (>1,000 years), a cultural transition from hunter-gathering to pastoralism occurred (Garcin et al., 2012; Lesur et al., 2014; Marshall & Hildebrand, 2002). The change from fishing to herding seems to have been a dynamic process, since the introduction of cattle was catalyzed by the immigration of herders that were escaping the progressively drying Sahara region, where pastoralism had been introduced much earlier (Hildebrand & Grillo, 2012; Kuper & Kropelin, 2006). The dried up lake beds and former lake margins could have provided new land and grazing grounds for this new life style, which also made people independent from fishing (Garcin et al., 2012)."
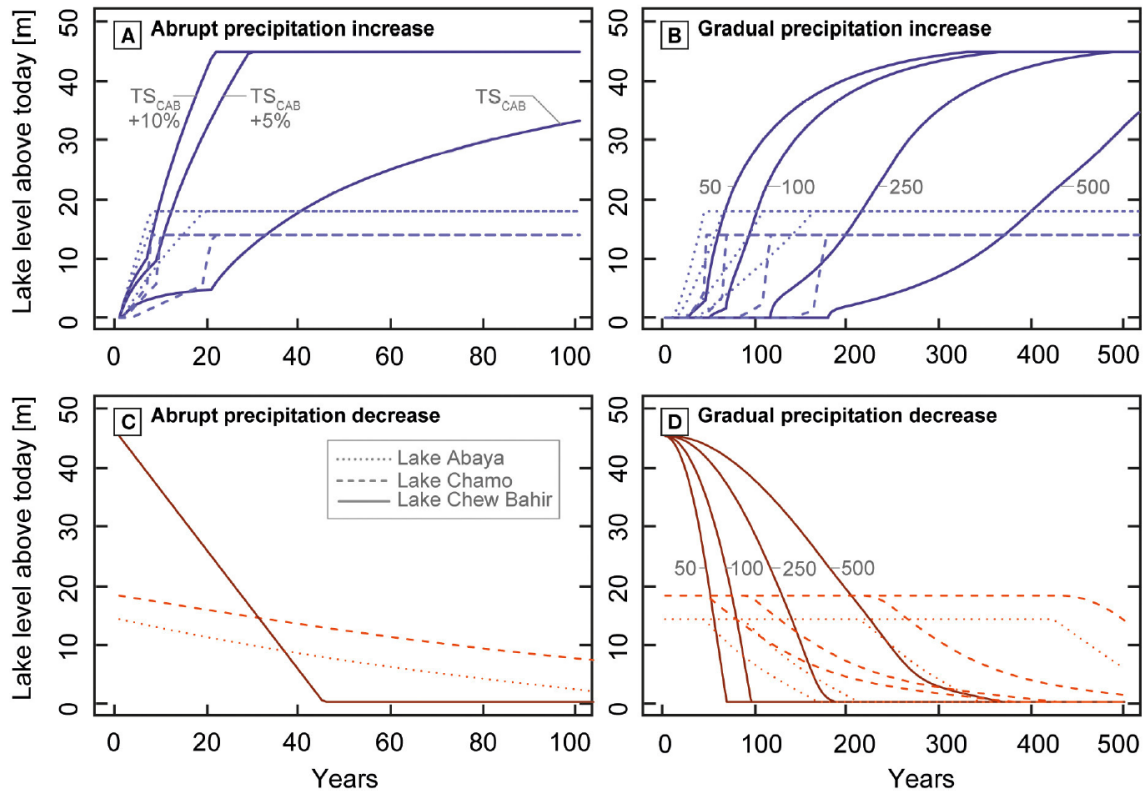
Figure 3: Modelled pace of lake transitions under abrupt and gradual precipitation changes: (A) Abrupt increase in precipitation from modern values to TS$_{CAB}$ values (13.4%) as a minimum possible amount of rainfall to fill up the investigated lake basins. TS$_{CAB}$ +5% and TS$_{CAB}$ +10% are provided as examples for even higher precipitation that was provided during the AHP, for example. (B) Lake fill scenario under gradual increase in precipitation from modern values to TS$_{CAB}$ values over 50, 100, 250, and 500 years. (C) Abrupt decrease in precipitation from TS$_{CAB}$ to modern values. (D) Lake regression scenario under gradual decrease in precipitation from TS$_{CAB}$ to modern values over 50, 100, 250, and 500 years.

Q3   What was the paleo-vegetation in southern Ethiopia during the last AHP and the during the Last Glacial Maximum (LGM) time?

Using predictive modeling linked to the LBM, the paleo vegetation during the AHP and LGM time has been mapped, as shown in Figure 4. Given the predictors monthly precipitation and elevation, the spatial prediction is unavoidably an estimation and modulated by local microclimate, hydrology, geology, and soils. Nevertheless, the model provides a reasonable estimate, as explained in detail in P2 (Fischer et al., 2021). During the AHP, forests prevailed in the mid-altitudes and formed a complex mosaic due to the diverse topography. There are two scenarios for the AHP time. Scenario 2a uses the same seasonality pattern today, whereas scenario 2b assumes an additional rainy season due to an east shift of the CAB. The LGM time landscape was presumably dominated by open vegetation, grasslands, and almost desert-like conditions in the rift floor surrounding of paleo-lake Chew Bahir and Lake Turkana. The sparse vegetation cover was accompanied by widespread afro-alpine vegetation above ca. 2000 m asl.
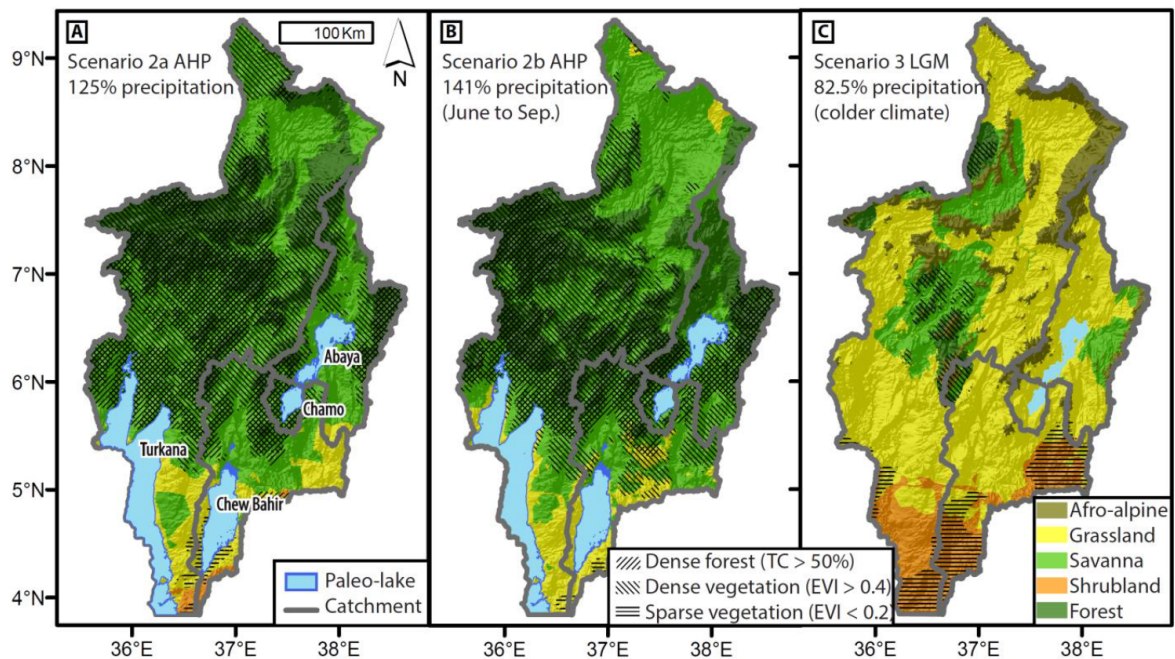
Figure 4: Paleo vegetation model result map for scenario 2a, 2b and 3: (A) Scenario 2a AHP. (B) Scenario 2b AHP (with CAB). (C) Scenario 3 LGM time. Figure published in P2, Fischer et al. (2021).

Q4   How does a changing seasonality affect the paleo-water balance and the paleo-vegetation?

An east shift of the CAB during times of low precession might be the reason for the increased moisture availability in the EARS, such as during the AHP, which implies an additional rainy season. Hence, modern-day dry months would receive additional rainfall, which would change the evaporative potential on land compared to today (see P1, Fischer et al., 2020, for further explanations). Without the biosphere feedback, this would imply around 7% additional precipitation required to flood paleo-lake Chew Bahir until its overflow sill. Incorporating the biosphere feedback, as explained in P2 (Fischer et al., 2021), the additional precipitation required compared to a scenario with the same seasonality yields +16%. The third rainy season would shorten the dry season, especially in the mid-altitudes in southern Ethiopia. In the CAB scenario 2b (see Figure 4), it would require at least 41% more precipitation than current levels to sustain the observed lake changes. It would produce less dense vegetation in the high altitudes and favor forest coverage at the mid-altitudes (between 1000 and 2000 m asl).

Q5   Has there been a preference of early humans for open or closed landscapes?

As discussed in P2, Fischer et al. (2021) p.25f: "Our model shows that the landscape in the study area during the LGM is dominated by a mixture of grasslands with a variety of vegetation types, resulting in a complex, mosaic landscape that would have offered a wide range of resources for hunter-gatherers. […] Trees are almost nonexistent at Mochena Borago according to our modelling results during the LGM, and the absence of evidence of human activity (Brandt et al., 2017; Brandt et al., 2012) may indicate that humans avoided the afro-alpine belt. Our modelling results support the refugium character of Ethiopian highlands during cold and dry conditions (Brandt et al., 2017; Brandt et al., 2012; Fischer et al., 2020; Foerster et al., 2015; Hensel et al., 2021; Vogelsang & Wendt, 2018). In summary, it seems that humans in southern Ethiopia lived in a rather open grassland with some trees during the LGM.
For the AHP, the modelling results indicate a vast expansion of forests and dense vegetation in southern Ethiopia. According to the results, forests and dense vegetation covered the known obsidian outcrops in the area that were intensively used by humans during the LGM. […] After the AHP, human activity is recorded again in the archaeological record of Mochena Borago and Sodicho Caves (Gutherz et al., 2002; Hensel et al., 2019; Hensel et al., 2021). The

modelling results show that Mochena Borago and Sodicho Cave may have been surrounded by grassland once again. Within the last 25 ka, hunter-gatherers used Mochena Borago and Sodicho Caves when the vicinity of the sites were characterized by grassland and solitary trees. With caution, we may propose that during the LGM and Middle Holocene, humans in southern Ethiopia occupied or even may have preferred open landscapes."

Q6   Do lake levels in the basins of Turkana, Chew Bahir, Suguta, and Chalbi in northern Kenya and southern Ethiopia follow the same climatic forcing and reaction?

The shoreline record from the lakes between the Ethiopian and Kenyan Plateau, including Lake Turkana, paleo-lake Chew Bahir, Suguta, and Chalbi, was analyzed as explained in detail in detail P3 (Fischer & Junginger, in prep.). On a millennial time scale, the shoreline record (see Figure 5) shows the climate evolution as suggested for the AHP with a wet phase, an unstable phase, and a dry state (Trauth et al., 2018). Nevertheless, there is no significant correlation between lakes in time on a decadal to centennial time scale. There may be multiple reasons beside the insufficiency of the record itself. Different response times may lead to delayed reaction to a potential supra-regional climate forcing. Furthermore, each basin differs in its topographical basin structure. For example, paleo-lake Chalbi was the only lake within the Turkana Basin that has not received additional moisture from an extended catchment and overflowing lakes from either the East African Plateau or the Ethiopian Plateau.

The record seems to have a high amount of noise, which may have multiple reasons, as written in Fischer & Junginger (in prep.): "Nevertheless, the shoreline record from the Turkana realm has high noise and uncertainty. Shoreline samples based on a few surface shells, either *M. tuberculata* or *Etheria elliptica*, are not certainly in situ depositions. Gravitational transport may dislocate them, especially in the studied millennial time scales. Outcrops, shell layer or subsurface samples avoid this problem but are relatively scarce in this record. Vertical uncertainty remains, as aquatic species live up to a couple of meters underwater and may be displaced due to water movement. So then, the shoreline is a lower boundary but may have been significantly higher. Archaeological sites, on the other hand, act as an upper limit of the lake level, as they have not necessarily been at the lake surface but have not been under water.

With 192 uneven distributed data points, of which 162 are shorelines, and 30 are archaeological sites for 15,000 years, the record is limited in its temporal resolution. The

vertical accuracy is dominated by high noise, which superimposes the climate signal. In contrast, the potassium record shows the rapid onset, the stable humidity, and the gradual fluctuating offset of the AHP in a decadal resolution (Fischer et al., 2020). As the potassium record is analyzed following one procedure, it may have the same proxy-system bias for each data point. This makes trend analysis more suitable in contrast to the multi-method, multi-procedure, and multi-laboratory shoreline record, where each datapoint has its own bias."
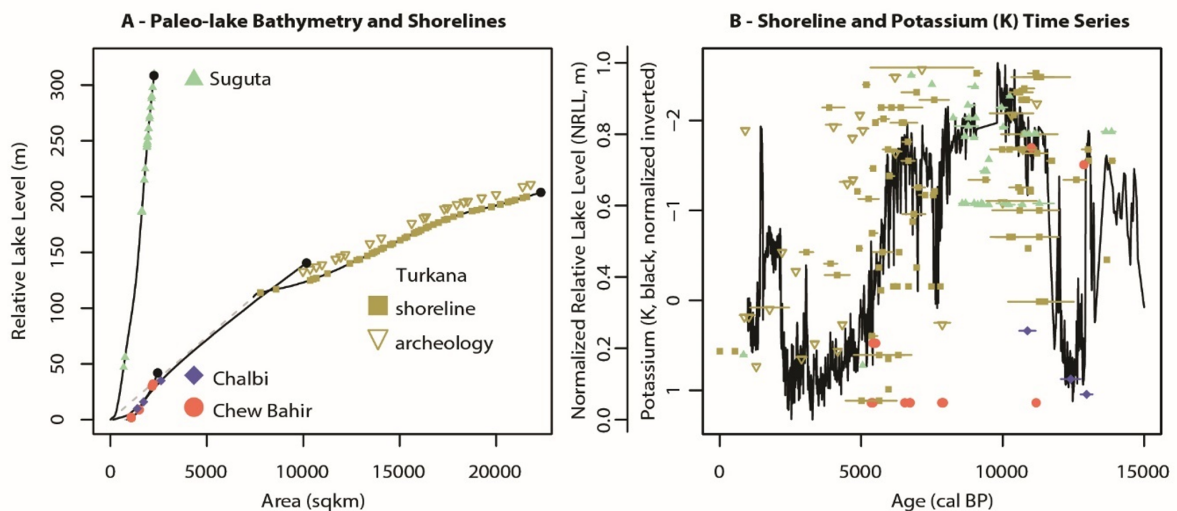
Figure 5: Analysis of the Shoreline. (A) Paleo-lake bathymetries and location of the shorelines and archeological sites. (B) time series of CB-01 and the normalized relative lake levels. Figure from P3, Fischer & Junginger (in prep.)

Q7   Is a link between the Chew Bahir lacustrine sediments and the shoreline record from that region possible?

Non-parametric statistics were used to evaluate the correlation between the potassium record from the Chew Bahir basin and the shoreline record. This has shown no significant correlation, as explained in P3, Fischer & Junginger (in prep.). Besides the quality of the shoreline record, further factors are impeding an empiric transfer function using shorelines and a continuous lacustrine proxy, as explained in Fischer & Junginger (in prep.): "The link between two paleo records inherits both age model-related uncertainties. In this case, the new dataset inherits the age model uncertainty of the lacustrine potassium record and the uncertainty of every single dated shoreline. We tested different methods to align them by taking the uncertainty of the shorelines into account but taking the age model of the potassium record as invariable. The single-age merge may catch specific maxima and minima of the potassium record, but, by

chance, it may match to a chronological close-by inverse peak, which adds random noise to the new aligned dataset. The two-sigma averaged alignment decreases the likelihood of random noise but decreases the signal. For example, a high-stand shoreline, which would correspond with a low peak in potassium, would not be recorded. Instead, a centennial averaged potassium signal is aligned to a decade-lasting shoreline. Aligning all potassium values within the given age range of the shoreline forces a higher signal but also a higher noise within the dataset. This makes this method a non-improvement, too. Nevertheless, none of these methods led to a dataset with a significant correlation, suitable for a potential transfer function between lacustrine μ-XRF and shoreline elevations. Age control remains one of the biggest challenges in paleoclimate research."

Q8   Is it possible to use modern Oxygen, Hydrogen, and Strontium isotopes to reconstruct the paleohydrology of the Chew Bahir basin?

The LBM of the southern Ethiopian Rift suggests the increasing importance of the extended catchment of lakes Abaya and Chamo for the water supply of paleo-lake Chew Bahir when precipitation increases (Fischer et al., 2020). Furthermore, the geological gradient between the catchment of paleo-lake Chew Bahir and the extended catchment of lakes Abaya and Chamo leads to different $^{87}Sr/^{86}Sr$. The catchment of paleo-lake Chew Bahir is partly dominated by Precambrian basement, which yields a higher ratio of $^{87}Sr/^{86}Sr$. In contrast, the catchments of lakes Abaya and Chamo are dominated by Cenozoic rift volcanic with a lower $^{87}Sr/^{86}Sr$ ratio. This could be used to develop a quantitative transfer function using the $^{87}Sr/^{86}Sr$ ratio to reconstruct absolute paleo-precipitation rates. The modern-analog study P4 (Markowska et al., 2022, p. 18) concluded: "Our study provides the first known major hydrochemical investigation of the Lake Chew Bahir catchment in southern Ethiopia. The major, trace, and Sr and O isotopic composition of surface and groundwaters reported in this study are within the range of previously published data in the EARS, suggesting the LCB catchment is a good analogue for other semi-arid catchments in the region. Groundwater-surface water interactions at terminal, semiarid LCB [Lake Chew Bahir] plays a significant role in water hydrochemistry. The Sr mass balance of LCB [Lake Chew Bahir] cannot be achieved by only including surface water inflows, or explain the modern lake water $^{87}Sr/^{86}Sr_L$ ratios. This demonstrates the important role of groundwater in dryland lake basins and supports the hypothesis that perennial springs likely play a central buffering role in sustaining water supplies in areas which typically experience climatically induced large-scale surface water fluctuations (Cuthbert et al., 2019).

Based on model simulations, LCB [Lake Chew Bahir] has short (1–55 years) Sr residence times, and $d^{18}O$ is sensitive to the evaporative conditions and lake water residence times. Higher $d^{18}O$ is likely indicative of a larger closed-lake system. Lake $d^{18}O_L$ values greater than +12.0‰ suggest a closed lake system, whereas a decreasing trend in $d^{18}O_L$ indicates a flow-through lake and subsequent connectivity to Lake Turkana. Coupled lower $^{87}Sr/^{86}Sr$ and higher $d^{18}O$ would suggest large-scale hydrological reorganisation, able to support a flowthrough lake system where the Sr budget was dominated by surface inflows. Isotopic data from microfossils could provide key insights on paleo-hydrological connectivity between LCB [Lake Chew Bahir] and Lake Turkana and allow time periods of cascading lake systems to be identified. Conversely, periods dominated and buffered by groundwater inflows indicated by lower $d^{18}O_L$ and higher $^{87}Sr/^{86}Sr_L$ may also be readily identified. This likely played an integral role in the availability of freshwater resources for our human ancestors in the region during documented climatic instability over the late Quaternary (Foerster et al., 2018; Viehberg et al., 2018). The combined use of $^{87}Sr/^{86}Sr_C$ and $d^{18}O_C$ can provide important insights to change in hydroclimate in southern Ethiopia, and other similar arid and semi-arid lowland sites."

Q9 What are human strategies in the Turkana Basin to adapt to shrinking lake levels at the end of the last African Humid Period?

It requires comprehensive interdisciplinary research to reconstruct the paleo-environment and it requires complex interdisciplinary research to reassemble the archeological records and the human cultural and evolutionary development. Studying human-environmental interactions and finding causal relationships requires expertise from both perspectives. Hence, interdisciplinary review publications provide the opportunity to discuss spatiotemporal processes all-encompassing. Here, the risk assessment faced by fishing and herding communities and the end of the AHP in the Turkana Basin were analyzed. Hildebrand et al. (P5, 2022) concluded: "Decades of fieldwork near Lake Turkana have generated extensive paleoenvironmental sequences and rich archaeological assemblages that do not yet support unequivocal answers but rather reveal the complexity of the task before us. Contrary to previous suggestions that AHP conditions offered stable resources, we find that fishing communities likely faced substantial risks throughout the AHP. As the AHP ended, lake levels dropped rapidly but terrestrial vegetation may have changed more gradually than previously thought. The mechanisms through which herding took hold around Lake Turkana are still murky. There is an extensive middle ground between diffusionist interpretations (e.g., that

fishers encountering catastrophic lake level changes adopted livestock obtained through exchange), and migrationist interpretations (e.g., that pastoralists moved into the area and took over, with little interest in lacustrine resources). For example, it may be that both fishers and herders were encountering new risks and new opportunities together and joined forces to invent a hybrid livelihood, retaining some economic and cultural features from both groups. Equally, incoming pastoralists may already have had their own traditions of fishing and aquatic resource use before reaching Turkana's shores. While these potential interpretations do not negate the general idea of risk as an influential mechanism, they demonstrate how difficult it is to pinpoint exactly how risks might have operated, and evaluate risk reduction against other possible motives for socioeconomic change. They also may serve as a caution in other parts of Africa where datasets are less secure, and will eventually contribute to productive comparisons of fishing-to-herding transitions between regions, between areas with different rainfall regimes, and between lacustrine vs. riverine vs. inland settings (e.g.,Garcea, 2006; Khalidi et al., 2020).

Methodological advances offer encouraging opportunities for paleoenvironmental analysis that can help evaluate risk on more local geographic scales in Turkana and other research areas. They also provide more direct ways to assess mobility of people, livestock, and objects that might - or might not - indicate human strategies to mitigate risk. While these research tools will generate exciting new datasets, the paramount challenge is to situate interpretations within a framework that incorporates momentary, seasonal, and long-term dilemmas faced by communities of fishers and pastoralists. This requires explicit efforts to understand mobility systems, attitudes toward risk and risk mitigation, and other factors that structure decision-making by communities actively practicing these economic strategies. Archaeologists should continue to incorporate existing ethnographic data into their models, and gain new perspectives via ethnoarchaeological research with fishing and pastoralist communities. Finally, as demonstrated elsewhere by Duwe and Preucel (2019), new collaborations with local research partners from these communities should yield insights that enhance interpretive frameworks."

Q10   Was human-induced landcover change a significant factor for lake formation during the Late Bronze to Early Iron Age in Shiraki Plateau, Georgia?

The quantification of hydrological processes such as evaporation as a function of climate and surface parameters was done in the African Tropics to understand paleoenvironmental

conditions due to climate forcing and the reaction of human ancestors have been discussed. A catchment scaled hydrological model may also be used to test hypotheses about the impact of human behavior on the water balance. In the Shiraki plateau, Georgia, an interdisciplinary research team revealed a lake formation in a semi-arid plain during the Late Bronze/ Iron Age. It was postulated that the clear-cutting of the basin may have changed the water balance, because it decreased the evapotranspiration in the basin and, hence, forced lake formation. Using the same evapotranspiration quantification method (see Figure 6) as applied in P1 and P2 (Fischer et al., 2021; Fischer et al., 2020) Suchodoletz et al. (P6, 2022) concluded: "Our study demonstrates that the Holocene hydrological balance of the Shiraki Plain was and is situated near a major hydrological threshold. Consequently, also relatively small-scale human or natural influences on this semi-arid landscape can cause significant geoecological changes that strongly affected the living conditions of local societies due to lake formation or desiccation in the central part of the plain. Hence, the results of our study underline the high fragility of drylands towards also small-scale external perturbations and demonstrate the high value of multi-disciplinary approaches to investigate their long-term evolution on millennial and centennial time scales."
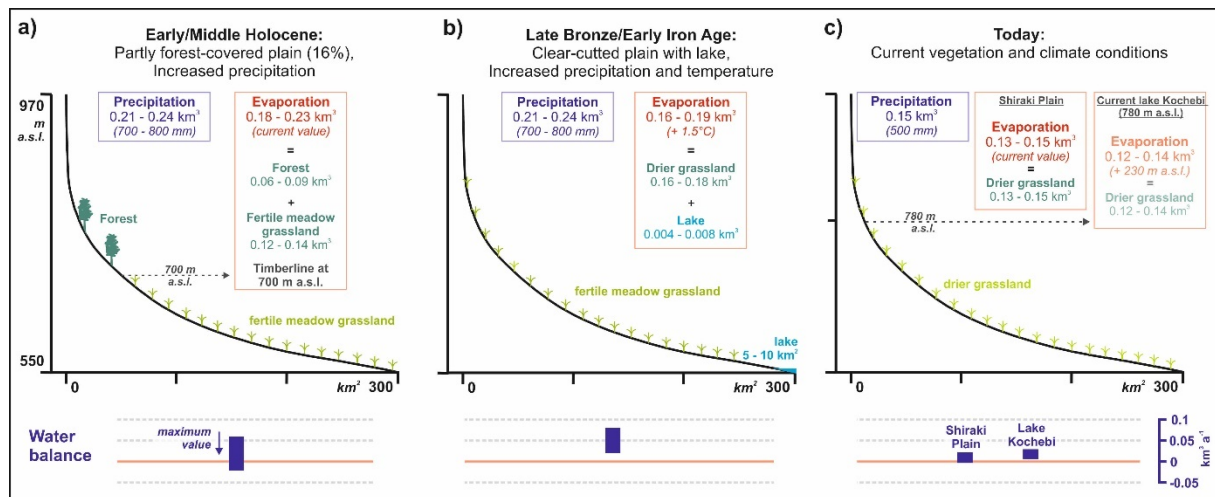
Figure 6: Water balance model of the Shiraki Plain for three different scenarios during the Holocene based on annual precipitation and evapotranspiration values. Figure from P6, Suchodoletz et al. (2022).

2.2   A Synthesis of the Paleoenvironment

Southern Ethiopia and Northern Kenya have undergone intense climate and environmental changes since the LGM time. Paleo-lake Chew Bahir was presumably dried out during LGM times (see P2), and model results suggest a decreased precipitation of around -17.5%. The

onset of humid conditions occurred with the beginning of the AHP around 15 ka. Shorelines indicate a maximum flooded paleo-lake Chew Bahir at the overflow sill elevation (see P3) due to a precipitation increase of around +25–41% compared to today (see P2). Freshwater conditions prevailed presumably until the termination of the AHP when massive lake level fluctuations occurred due to 20–80 years of lasting dry spells, which may have forced paleo-lake Chew Bahir to dry out completely multiple times (see P1). Since then, paleo-lake Chew Bahir was a shallow, seasonal, or completely dried-out mudflat.

Despite significant temperature decrease during LGM times, the dominant vegetation in the rift floor vicinity of paleo-lake Chew Bahir and Lake Turkana was rather desert-like, sparse, and governed by xerophytic vegetation. Widespread grasslands with refugial forests and savanna regions dominated the Ethiopian Plateau and the surrounding lakes Abaya and Chamo. Afro-alpine vegetation may have reached elevations of down to 2000 m asl (above sea level) giving the global average temperature decrease and the steepening of the lapse rate in the EARS. Then, during the AHP, vegetation density increased significantly. Dense forest cover prevailed in the mid to high altitudes, with a gradual transition to savanna and grassland cover towards the lower elevated south of Ethiopia and the vicinity of paleo-lake Chew Bahir (see P2).

Humans living close to the shore of paleo-lake Chew Bahir may have faced drastic changes in their freshwater and food resources. Model results suggest complete lake desiccation within decades (see P1). Therefore, model results support the hypothesis of vertical migration to the more humid mountainous regions during times of dry spells (Foerster et al., 2015). As the lowland region between the Ethiopian and East African Plateau was shaped by multiple mega-lakes, the asynchronous reaction of the lakes may have led to various reorganization pressure of food and water resources within the lowlands (see P3). The vegetation model and archeological records suggest a preference for open landscapes (see P2).

2.3   A Synthesis of the Modelling Approaches

During this thesis, multiple models and proxy-model links have been applied to reconstruct the hydroclimate and the paleo-vegetation. The LBM (P1) and the PVM (P2) are independent modern-analogue catchment-scaled models. While the LBM is a process-based model with a physical-based parametrized evapotranspiration model as a central sub-unit, the PVM has a machine learning-based predictive algorithm as a major component. Both use models use modern-day environmental conditions for calibration that are extrapolated to a defined paleo-environmental state. This state is determined using the paleo-lake observations based on shorelines. The link to the lacustrine potassium XRF scan data (P1) and phytoliths (P2) data is qualitative and utilized for a vice-versa interpretation. A direct quantitative relation between

the lacustrine proxy results and the shorelines was studied in P3 with insufficient results. In the Chew Bahir catchment and research project, these models provided an understanding of the paleo-environmental boundary conditions, the catchment system dynamics and allowed to extrapolate results spatially, making the comparison with the spacious distributed archeological record possible. The model results output was then used to understand potential implications for early humans living in this environment. This includes lake level (P1, P3, P5) and vegetation dynamics (P2). In comparison, as published by Suchodoletz et al. (2022, P6), the impact of human behavior on the hydro- and biosphere was studied in the Shiraki plain, Georgia. Here, the boundary conditions and the hypothesis were set using paleo proxy and archeological data. Catchment scaled modeling allowed then to test the plausibility of the hypothesis and to quantify if human-induced processes, such as the clear-cutting of the forests, are sufficient to explain environmental processes, such as the lake appearance.

The qualitative link between the LBM and the potassium record, as well as the vice-versa interpretation of the vegetation model output and the phytolith record, provided detailed knowledge about past ecosystem conditions and potential dynamics but lacked precise temporal continuous reconstructions. A possible empiric link between the shoreline record and the potassium record (P3) would have allowed using potassium to directly predict the hydroclimate. Another attempt to do so is the development of an isotope-enabled process-based model (P4), which has the potential to predict the hydroclimate continuously. Here, the modern analog provides a framework to do so.

Catchment scaled models may fulfill a bridge between global scale general circulation models or coupled east system models and proxy or sedimentary models. Independent meso-scaled models allow for an intercomparison with both, the point-wise proxy data and model, and the low resolved global simulations. So then, as done in Chew Bahir (see e.g., P2), catchment scaled environmental models provided the opportunity to relate the lacustrine proxy results with regional quantitative parameters (vegetation, precipitation) and then with global simulation metric for s specific time slice, such as the LGM time or the last AHP.

3   Conclusion and Prospect

During this thesis, many-sided aspects of the paleo-environment, the -climate, and -landscape in the Chew Bahir basin and the regional vicinity have been deciphered. Different modeling approaches were applied and compared with the lacustrine proxy data from the Chew Bahir basin. The application of the LBM provided evidence of multiple lake level fluctuations of paleo-lake Chew Bahir at the termination of the AHP. Precipitation thresholds for the LGM time and the AHP provide quantitative insights and may be used for further modeling applications. PVM allowed the creation of detailed paleo-vegetation maps and the comparison with archeological records throughout the region. Detailed digital elevation model analysis produced paleo-lake extents, bathymetries, remote-sensing-based shoreline surveys, and comparisons. The proposed interdisciplinary research was able to answer specific research questions, contributing to the understanding of our ancestors' potential habitats, climate dynamics and human-environment interactions in eastern Africa.

Future research may provide a comprehensive multi-basin LBM not only for the southern Ethiopian Rift but also for the paleo-lake Chalbi, Turkana, and Suguta. A link between the shoreline and the potassium record may be possible by incorporating the water balance implications and the lake dynamics. The shoreline localities in the paleo-lake Chalbi vicinity may be future locations for field campaigns as they may provide possible shoreline samples and presumably archeological sites. The developed approach to predict vegetation can be improved using an increase in learning data, predictors and could be enhanced with more profound vegetation classes to be expected. Those models can be applied to future climate change scenarios to develop maps of potential vegetation in eastern Africa. The development of direct quantitative links between proxies and precipitation using the unique landscape architecture in southern Ethiopia, as revealed during this thesis, may allow to time-progressively understand the paleo-environment, which provided constraints and opportunities for our ancestors in eastern Africa.

References

Asefa, M., Cao, M., He, Y., Mekonnen, E., Song, X., & Yang, J. (2020). Ethiopian vegetation types, climate and topography. *Plant Diversity*, *42*(4), 302-311. https://doi.org/10.1016/j.pld.2020.04.004

Barker, P. A., Talbot, M. R., Street-Perrott, F. A., Marret, F., Scourse, J., & Odada, E. O. (2004). Late Quaternary climatic variability in intertropical Africa. In *Past climate variability through Europe and Africa* (pp. 117-138). Springer.

Berger, A., & Loutre, M.-F. (1991). Insolation values for the climate of the last 10 million years. *Quaternary Science Reviews*, *10*(4), 297-317.

Berger, A., Loutre, M.-F., & Mélice, J. (2006). Equatorial insolation: from precession harmonics to eccentricity frequencies. *Climate of the Past*, *2*(2), 131-136.

Bergner, A. G. N., Trauth, M. H., & Bookhagen, B. (2003). Paleoprecipitation estimates for the Lake Naivasha basin (Kenya) during the last 175 k.y. using a lake-balance model. *Global and Planetary Change*, *36*(1-2), 117-136. https://doi.org/10.1016/s0921-8181(02)00178-9

Bergström, A., Stringer, C., Hajdinjak, M., Scerri, E. M. L., & Skoglund, P. (2021). Origins of modern human ancestry. *Nature*, *590*(7845), 229-237. https://doi.org/10.1038/s41586-021-03244-5

Brandt, S., Hildebrand, E., Vogelsang, R., Wolfhagen, J., & Wang, H. (2017). A new MIS 3 radiocarbon chronology for Mochena Borago Rockshelter, SW Ethiopia: Implications for the interpretation of Late Pleistocene chronostratigraphy and human behavior. *Journal of Archaeological Science: Reports*, *11*, 352-369. https://doi.org/10.1016/j.jasrep.2016.09.013

Brandt, S. A., Fisher, E. C., Hildebrand, E. A., Vogelsang, R., Ambrose, S. H., Lesur, J., & Wang, H. (2012). Early MIS 3 occupation of Mochena Borago Rockshelter, Southwest Ethiopian Highlands: Implications for Late Pleistocene archaeology, paleoenvironments and modern human dispersals. *Quaternary International*, *274*, 38-54. https://doi.org/10.1016/j.quaint.2012.03.047

Brooks, N. (2006). Cultural responses to aridity in the Middle Holocene and increased social complexity. *Quaternary International*, *151*(1), 29-49. https://doi.org/10.1016/j.quaint.2006.01.013

Brown, F., Harris, J., Leakey, R., & Walker, A. (1985). Early Homo erectus skeleton from west Lake Turkana, Kenya. *Nature*, *316*(6031), 788-792. https://doi.org/10.1038/316788a0

Brown, F. H., & Mcdougall, I. (2011). Geochronology of the Turkana Depression of Northern Kenya and Southern Ethiopia. *Evolutionary Anthropology: Issues, News, and Reviews*, *20*(6), 217-227. https://doi.org/10.1002/evan.20318

Camberlin, P. (1997). Rainfall Anomalies in the Source Region of the Nile and Their Connection with the Indian Summer Monsoon.

Chorowicz, J. (2005). The East African rift system. *Journal of African Earth Sciences*, *43*(1-3), 379-410. https://doi.org/10.1016/j.jafrearsci.2005.07.019

Cohen, A., Campisano, C., Arrowsmith, R., Asrat, A., Behrensmeyer, A. K., Deino, A., Feibel, C., Hill, A., Johnson, R., Kingston, J., Lamb, H., Lowenstein, T., Noren, A., Olago, D., Owen, R. B., Potts, R., Reed, K., Renaut, R., Schäbitz, F., . . . Zinaye, B. (2016). The Hominin Sites and Paleolakes Drilling Project: inferring the environmental context of human evolution from eastern African rift lake deposits. *Scientific Drilling*, *21*, 1-16. https://doi.org/10.5194/sd-21-1-2016

Corti, G. (2009). Continental rift evolution: From rift initiation to incipient break-up in the Main Ethiopian Rift, East Africa. *Earth-Science Reviews*, *96*(1-2), 1-53. https://doi.org/10.1016/j.earscirev.2009.06.005

Costa, K., Russell, J., Konecky, B., & Lamb, H. (2014). Isotopic reconstruction of the African Humid Period and Congo Air Boundary migration at Lake Tana, Ethiopia. *Quaternary Science Reviews*, *83*, 58-67. https://doi.org/10.1016/j.quascirev.2013.10.031

Cuthbert, M., Gleeson, T., Moosdorf, N., Befus, K. M., Schneider, A., Hartmann, J., & Lehner, B. (2019). Global patterns and dynamics of climate–groundwater interactions. *Nature Climate Change*, *9*(2), 137-141.

Dart, R. (1925). Australopithecus africanus the man-ape of South Africa. In (Vol. 115, pp. 195 - 199): Nature Publishing Group.

Darwin, C. (1871). The descent of man, and selection in relation to sex. *London: Murray*, *415*, 1871.

Davidson, A. (1983). The Omo river project, reconnaissance geology and geochemistry of parts of Ilubabor, Kefa, Gemu Gofa and Sidamo, Ethiopia. *Ethiop. Inst. Geol. Surv. Bull.*, *2*, 1-89.

de Lamarck, J.-B. d. M. (1809). *Philosophie zoologique, ou Exposition des considérations relatives à l'histoire naturelle des animaux* (Vol. 1). Dentu.

Dee, S., Emile-Geay, J., Evans, M. N., Allam, A., Steig, E. J., & Thompson, D. M. (2015). PRYSM: An open-source framework for PRoxY System Modeling, with applications to oxygen-isotope systems. *Journal of Advances in Modeling Earth Systems*, *7*(3), 1220-1247. https://doi.org/10.1002/2015ms000447

Dee, S. G., Russell, J. M., Morrill, C., Chen, Z., & Neary, A. (2018). PRYSM v2.0: A Proxy System Model for Lacustrine Archives. *Paleoceanography and Paleoclimatology*, *33*(11), 1250-1269. https://doi.org/10.1029/2018pa003413

Deino, A. L., Behrensmeyer, A. K., Brooks, A. S., Yellen, J. E., Sharp, W. D., & Potts, R. (2018). Chronology of the Acheulean to Middle Stone Age transition in eastern Africa. *Science*, *360*(6384), 95-98.

Demenocal, P., Ortiz, J., Guilderson, T., Adkins, J., Sarnthein, M., Baker, L., & Yarusinsky, M. (2000). Abrupt onset and termination of the African Humid Period: . *Quaternary Science Reviews*, *19*(1-5), 347-361. https://doi.org/10.1016/s0277-3791(99)00081-5

Demenocal, P. B. (1995). Plio-pleistocene African climate. *Science*, *270*(5233), 53-59.

Diez-Martín, F., Sánchez Yustos, P., Uribelarrea, D., Baquedano, E., Mark, D. F., Mabulla, A., Fraile, C., Duque, J., Díaz, I., Pérez-González, A., Yravedra, J., Egeland, C. P., Organista, E., & Domínguez-Rodrigo, M. (2016). The Origin of The Acheulean: The 1.7 Million-Year-Old Site of FLK West, Olduvai Gorge (Tanzania). *Scientific Reports*, *5*(1), 17839. https://doi.org/10.1038/srep17839

Drake, N. A., Breeze, P., & Parker, A. (2013). Palaeoclimate in the Saharan and Arabian Deserts during the Middle Palaeolithic and the potential for hominin dispersals. *Quaternary International*, *300*, 48-61. https://doi.org/10.1016/j.quaint.2012.12.018

Drake, N. A., Candy, I., Breeze, P., Armitage, S. J., Gasmi, N., Schwenninger, J. L., Peat, D., & Manning, K. (2022). Sedimentary and geomorphic evidence of Saharan megalakes: A synthesis. *Quaternary Science Reviews*, *276*. https://doi.org/10.1016/j.quascirev.2021.107318

Dühnforth, M., Bergner, A. G. N., & Trauth, M. H. (2006). Early Holocene water budget of the Nakuru-Elmenteita basin, Central Kenya Rift. *Journal of Paleolimnology*, *36*(3), 281-294. https://doi.org/10.1007/s10933-006-9003-z

Duwe, S., & Preucel, R. W. (2019). *The continuous path: Pueblo movement and the archaeology of becoming*. University of Arizona Press.

Emishaw, L., Laó-Dávila, D. A., Abdelsalam, M. G., Atekwana, E. A., & Gao, S. S. (2017). Evolution of the broadly rifted zone in southern Ethiopia through gravitational collapse and extension of dynamic topography. *Tectonophysics*, *699*, 213-226. https://doi.org/10.1016/j.tecto.2016.12.009

Evans, M. N., Tolwinski-Ward, S. E., Thompson, D. M., & Anchukaitis, K. J. (2013). Applications of proxy system modeling in high resolution paleoclimatology.

Quaternary Science Reviews, *76*, 16-28.
https://doi.org/10.1016/j.quascirev.2013.05.024

Fischer, M. L., Bachofer, F., Yost, C. L., Bludau, I. J. E., Schepers, C., Foerster, V., Lamb, H., Schäbitz, F., Asrat, A., Trauth, M. H., & Junginger, A. (2021). A Phytolith Supported Biosphere-Hydrosphere Predictive Model for Southern Ethiopia: Insights into Paleoenvironmental Changes and Human Landscape Preferences since the Last Glacial Maximum. *Geosciences*, *11*(10), 418. https://doi.org/10.3390/geosciences11100418

Fischer, M. L., Markowska, M., Bachofer, F., Foerster, V. E., Asrat, A., Zielhofer, C., Trauth, M. H., & Junginger, A. (2020). Determining the Pace and Magnitude of Lake Level Changes in Southern Ethiopia Over the Last 20,000 Years Using Lake Balance Modeling and SEBAL. *Frontiers in Earth Science*, *8*. https://doi.org/10.3389/feart.2020.00197

Foerster, V., Deocampo, D. M., Asrat, A., Günter, C., Junginger, A., Krämer, K. H., Stroncik, N. A., & Trauth, M. H. (2018). Towards an understanding of climate proxy formation in the Chew Bahir basin, southern Ethiopian Rift. *Palaeogeography, Palaeoclimatology, Palaeoecology*, *501*, 111-123. https://doi.org/10.1016/j.palaeo.2018.04.009

Foerster, V., Junginger, A., Landkamp, O., Gebru, T., Asrat, A., Umer, M., Lamb, H. F., Wennrich, V., Rethemeyer, J., N, N., Trauth, M. H., & Schaebitz, F. (2012). Climatic change recorded in the sediments of the Chew Bahir basin, southern Ethiopia, during the last 45,000 years. *Quaternary International*, *274*, 25. https://doi.org/10.1016/j.quaint.2012.06.028

Foerster, V., Vogelsang, R., Junginger, A., Asrat, A., Lamb, H. F., Schaebitz, F., & Trauth, M. H. (2015). Environmental change and human occupation of southern Ethiopia and northern Kenya during the last 20,000 years. *Quaternary Science Reviews*, *129*, 333-340. https://doi.org/10.1016/j.quascirev.2015.10.026

Friis, I., Demissew, S., & van Breugel, P. (2011). Atlas of the potential vegetation of ethiopia.

Garcea, E. A. (2006). Semi-permanent foragers in semi-arid environments of North Africa. *World Archaeology*, *38*(2), 197-219.

Garcin, Y., Melnick, D., Strecker, M. R., Olago, D., & Tiercelin, J.-J. (2012). East African mid-Holocene wet–dry transition recorded in palaeo-shorelines of Lake Turkana, northern Kenya Rift. *Earth and Planetary Science Letters*, *331-332*, 322-334. https://doi.org/10.1016/j.epsl.2012.03.016

Gillespie, R., Street-Perrott, F. A., & Switsur, R. (1983). Post-glacial arid episodes in Ethiopia have implications for climate prediction. *Nature*, *306*(5944), 680-683.

Grant, K. M., Rohling, E. J., Westerhold, T., Zabel, M., Heslop, D., Konijnendijk, T., & Lourens, L. (2017). A 3 million year index for North African humidity/aridity and the implication of potential pan-African Humid periods. *Quaternary Science Reviews*, *171*, 100-118. https://doi.org/10.1016/j.quascirev.2017.07.005

Gutherz, X., Jallot, L., Lesur, J., Pouzolles, G., & Sordoillet, D. (2002). Les fouilles de l'abri sous-roche de Moche Borago (Soddo, Wolyata). Premier bilan. Annales d'Ethiopie,

Harmand, S., Lewis, J. E., Feibel, C. S., Lepre, C. J., Prat, S., Lenoble, A., Boës, X., Quinn, R. L., Brenet, M., Arroyo, A., Taylor, N., Clément, S., Daver, G., Brugal, J.-P., Leakey, L., Mortlock, R. A., Wright, J. D., Lokorodi, S., Kirwa, C., . . . Roche, H. (2015). 3.3-million-year-old stone tools from Lomekwi 3, West Turkana, Kenya. *Nature*, *521*(7552), 310-315. https://doi.org/10.1038/nature14464

Hastenrath, S., & Kutzbach, J. E. (1983). Paleoclimatic estimates from water and energy budgets of East African lakes. *Quaternary Research*, *19*(2), 141-153.

Hensel, E. A., Bödeker, O., Bubenzer, O., & Vogelsang, R. (2019). Combining geomorphological–hydrological analyses and the location of settlement and raw material sites – a case study on understanding prehistoric human settlement activity in the southwestern Ethiopian Highlands. *E&G Quaternary Science Journal*, *68*(2), 201-213. https://doi.org/10.5194/egqsj-68-201-2019

Hensel, E. A., Vogelsang, R., Noack, T., & Bubenzer, O. (2021). Stratigraphy and Chronology of Sodicho Rockshelter – A New Sedimentological Record of Past Environmental Changes and Human Settlement Phases in Southwestern Ethiopia. *Frontiers in Earth Science, 8*. https://doi.org/10.3389/feart.2020.611700

Hildebrand, E. A., & Grillo, K. M. (2012). Early herders and monumental sites in eastern Africa: dating and interpretation. *Antiquity, 86*(332), 338-352.

Hildebrand, E. A., Grillo, K. M., Sawchuk, E. A., Pfeiffer, S. K., Conyers, L. B., Goldstein, S. T., Hill, A. C., Janzen, A., Klehm, C. E., Helper, M., Kiura, P., Ndiema, E., Ngugi, C., Shea, J. J., & Wang, H. (2018). A monumental cemetery built by eastern Africa's first herders near Lake Turkana, Kenya. *Proc Natl Acad Sci U S A, 115*(36), 8942-8947. https://doi.org/10.1073/pnas.1721975115

Honegger, M., & Williams, M. (2015). Human occupations and environmental changes in the Nile valley during the Holocene: The case of Kerma in Upper Nubia (northern Sudan). *Quaternary Science Reviews, 130*, 141-154. https://doi.org/10.1016/j.quascirev.2015.06.031

Junginger, A., Roller, S., Olaka, L. A., & Trauth, M. H. (2014). The effects of solar irradiation changes on the migration of the Congo Air Boundary and water levels of paleo-Lake Suguta, Northern Kenya Rift, during the African Humid Period (15–5ka BP). *Palaeogeography, Palaeoclimatology, Palaeoecology, 396*, 1-16. https://doi.org/10.1016/j.palaeo.2013.12.007

Junginger, A., & Trauth, M. H. (2013). Hydrological constraints of paleo-Lake Suguta in the Northern Kenya Rift during the African Humid Period (15–5kaBP). *Global and Planetary Change, 111*, 174-188. https://doi.org/10.1016/j.gloplacha.2013.09.005

Kaboth-Bahr, S., Gosling, W. D., Vogelsang, R., Bahr, A., Scerri, E. M. L., Asrat, A., Cohen, A. S., Düsing, W., Foerster, V., Lamb, H. F., Maslin, M. A., Roberts, H. M., Schäbitz, F., & Trauth, M. H. (2021). Paleo-ENSO influence on African environments and early modern humans. *Proceedings of the National Academy of Sciences, 118*(23), e2018277118. https://doi.org/10.1073/pnas.2018277118

Khalidi, L., Mologni, C., Ménard, C., Coudert, L., Gabriele, M., Davtian, G., Cauliez, J., Lesur, J., Bruxelles, L., & Chesnaux, L. (2020). 9000 years of human lakeside adaptation in the Ethiopian Afar: Fisher-foragers and the first pastoralists in the Lake Abhe basin during the African Humid Period. *Quaternary Science Reviews, 243*, 106459.

Kuper, R., & Kropelin, S. (2006). Climate-controlled Holocene occupation in the Sahara: motor of Africa's evolution. *Science, 313*(5788), 803-807.

Kutzbach, J. E., Guan, J., He, F., Cohen, A. S., Orland, I. J., & Chen, G. (2020). African climate response to orbital and glacial forcing in 140,000-y simulation with implications for early modern human environments. *Proc Natl Acad Sci U S A, 117*(5), 2255-2264. https://doi.org/10.1073/pnas.1917673117

Lario, J., Sanchez-Moral, S., Fernandez, V., Jimeno, A., & Menendez, M. (1997). Palaeoenvironmental evolution of the blue Nile (Central Sudan) during the early and mid-holocene (Mesolithic-Neolithic transition). *Quaternary Science Reviews, 16*(6), 583-588.

Larrasoaña, J. C. (2021). A review of West African monsoon penetration during Green Sahara periods; implications for human evolution and dispersals over the last three million years. *Oxford Open Climate Change, 1*(1). https://doi.org/10.1093/oxfclm/kgab011

Larrasoana, J. C., Roberts, A. P., & Rohling, E. J. (2013). Dynamics of green Sahara periods and their role in hominin evolution. *PLoS One, 8*(10), e76514. https://doi.org/10.1371/journal.pone.0076514

Leakey, R. E. F. (1969). Early Homo sapiens Remains from the Omo River Region of South-west Ethiopia: Faunal Remains from the Omo Valley. *Nature, 222*(5199), 1132-1133. https://doi.org/10.1038/2221132a0

Lesur, J., Hildebrand, E. A., Abawa, G., & Gutherz, X. (2014). The advent of herding in the Horn of Africa: New data from Ethiopia, Djibouti and Somaliland. *Quaternary International*, *343*, 148-158. https://doi.org/10.1016/j.quaint.2013.11.024

Levin, N. E., Brown, F. H., Behrensmeyer, A. K., Bobe, R., & Cerling, T. E. (2011). Paleosol carbonates from the Omo Group: Isotopic records of local and regional environmental change in East Africa. *Palaeogeography, Palaeoclimatology, Palaeoecology*, *307*(1-4), 75-89. https://doi.org/10.1016/j.palaeo.2011.04.026

Levin, N. E., Zipser, E. J., & Cerling, T. E. (2009). Isotopic composition of waters from Ethiopia and Kenya: Insights into moisture sources for eastern Africa. *Journal of Geophysical Research*, *114*(D23). https://doi.org/10.1029/2009jd012166

Manning, K., & Timpson, A. (2014). The demographic response to Holocene climate change in the Sahara. *Quaternary Science Reviews*, *101*, 28-35. https://doi.org/10.1016/j.quascirev.2014.07.003

Markowska, M., Martin, A. N., Vonhof, H. B., Guinoiseau, D., Fischer, M. L., Zinaye, B., Galer, S. J. G., Asrat, A., & Junginger, A. (2022). A multi-isotope and modelling approach for constraining hydro-connectivity in the East African Rift System, southern Ethiopia. *Quaternary Science Reviews*, *279*. https://doi.org/10.1016/j.quascirev.2022.107387

Marshall, F., & Hildebrand, E. (2002). Cattle before crops: the beginnings of food production in Africa. *Journal of World prehistory*, *16*(2), 99-143.

Maslin, M. (2016). *The Cradle of Humanity: How the changing landscape of Africa made us so smart*. Oxford University Press.

Maslin, M. (2020). Tying celestial mechanics to Earth's ice ages. *Physics Today*, *73*(5), 48-53. https://doi.org/10.1063/pt.3.4474

Maslin, M. A., Shultz, S., & Trauth, M. H. (2015). A synthesis of the theories and concepts of early human evolution. *Philos Trans R Soc Lond B Biol Sci*, *370*(1663), 20140064. https://doi.org/10.1098/rstb.2014.0064

Maslin, M. A., & Trauth, M. H. (2009). Plio-Pleistocene East African pulsed climate variability and its influence on early human evolution. In *The First Humans–Origin and Early Evolution of the Genus Homo* (pp. 151-158). Springer.

Mohr, P., & Zanettin, B. (1988). The Ethiopian flood basalt province. In *Continental flood basalts* (pp. 63-110). Springer.

Nicholson, S. E. (2017). Climate and climatic variability of rainfall over eastern Africa. *Reviews of Geophysics*, *55*(3), 590-635. https://doi.org/10.1002/2016rg000544

Nicholson, S. E. (2019). A review of climate dynamics and climate variability in Eastern Africa. *The limnology, climatology and paleoclimatology of the East African lakes*, 25-56.

Ojwang, W. O., Obiero, K. O., Donde, O. O., Gownaris, N., Pikitch, E. K., Omondi, R., Agembe, S., Malala, J., & Avery, S. T. (2016). Lake Turkana: World's Largest Permanent Desert Lake (Kenya). In *The Wetland Book* (pp. 1-20). Springer Netherlands. https://doi.org/10.1007/978-94-007-6173-5_254-1

Olaka, L. A., Odada, E. O., Trauth, M. H., & Olago, D. O. (2010). The sensitivity of East African rift lakes to climate fluctuations. *Journal of Paleolimnology*, *44*(2), 629-644. https://doi.org/10.1007/s10933-010-9442-4

Owen, R. B., Barthelme, J. W., Renaut, R., & Vincens, A. (1982). Palaeolimnology and archaeology of Holocene deposits north-east of Lake Turkana, Kenya. *Nature*, *298*(5874), 523-529.

Potts, R. (1998). Variability selection in hominid evolution. *Evolutionary Anthropology: Issues, News, and Reviews: Issues, News, and Reviews*, *7*(3), 81-96.

Roberts, H. M., Ramsey, C. B., Chapot, M. S., Deino, A. L., Lane, C. S., Vidal, C., Asrat, A., Cohen, A., Foerster, V., Lamb, H. F., Schäbitz, F., Trauth, M. H., & Viehberg, F. A. (2021). Using multiple chronometers to establish a long, directly-dated lacustrine record: Constraining >600,000 years of environmental change at Chew Bahir,

Ethiopia. *Quaternary Science Reviews*, *266*, 107025. https://doi.org/10.1016/j.quascirev.2021.107025

Scerri, E. M. L., Chikhi, L., & Thomas, M. G. (2019). Beyond multiregional and simple out-of-Africa models of human evolution. *Nature Ecology & Evolution*, *3*(10), 1370-1372. https://doi.org/10.1038/s41559-019-0992-1

Schaebitz, F., Asrat, A., Lamb, H. F., Cohen, A. S., Foerster, V., Duesing, W., Kaboth-Bahr, S., Opitz, S., Viehberg, F. A., Vogelsang, R., Dean, J., Leng, M. J., Junginger, A., Ramsey, C. B., Chapot, M. S., Deino, A., Lane, C. S., Roberts, H. M., Vidal, C., . . . Trauth, M. H. (2021). Hydroclimate changes in eastern Africa over the past 200,000 years may have influenced early human dispersal. *Communications Earth & Environment*, *2*(1). https://doi.org/10.1038/s43247-021-00195-7

Segele, Z. T., & Lamb, P. J. (2005). Characterization and variability of Kiremt rainy season over Ethiopia. *Meteorology and Atmospheric Physics*, *89*(1-4), 153-180. https://doi.org/10.1007/s00703-005-0127-x

Street, F. (1980). The relative importance of climate and local hydrogeological factors in influencing lake-level fluctuations.

Tierney, J. E., Russell, J. M., Sinninghe Damsté, J. S., Huang, Y., & Verschuren, D. (2011). Late Quaternary behavior of the East African monsoon and the importance of the Congo Air Boundary. *Quaternary Science Reviews*, *30*(7-8), 798-807. https://doi.org/10.1016/j.quascirev.2011.01.017

Trauth, M. H., Asrat, A., Cohen, A. S., Duesing, W., Foerster, V., Kaboth-Bahr, S., Kraemer, K. H., Lamb, H. F., Marwan, N., Maslin, M. A., & Schäbitz, F. (2021). Recurring types of variability and transitions in the ~620 kyr record of climate change from the Chew Bahir basin, southern Ethiopia. *Quaternary Science Reviews*, *266*. https://doi.org/10.1016/j.quascirev.2020.106777

Trauth, M. H., Foerster, V., Junginger, A., Asrat, A., Lamb, H. F., & Schaebitz, F. (2018). Abrupt or gradual? Change point analysis of the late Pleistocene–Holocene climate record from Chew Bahir, southern Ethiopia. *Quaternary Research*, *90*(2), 321-330. https://doi.org/10.1017/qua.2018.30

Trauth, M. H., Larrasoaña, J. C., & Mudelsee, M. (2009). Trends, rhythms and events in Plio-Pleistocene African climate. *Quaternary Science Reviews*, *28*(5-6), 399-411.

Trauth, M. H., Maslin, M. A., Deino, A., & Strecker, M. R. (2005). Late cenozoic moisture history of East Africa. *Science*, *309*(5743), 2051-2053.

Trauth, M. H., Maslin, M. A., Deino, A. L., Junginger, A., Lesoloyia, M., Odada, E. O., Olago, D. O., Olaka, L. A., Strecker, M. R., & Tiedemann, R. (2010). Human evolution in a variable environment: the amplifier lakes of Eastern Africa. *Quaternary Science Reviews*, *29*(23-24), 2981-2988. https://doi.org/10.1016/j.quascirev.2010.07.007

Trauth, M. H., Maslin, M. A., Deino, A. L., Strecker, M. R., Bergner, A. G., & Dühnforth, M. (2007). High-and low-latitude forcing of Plio-Pleistocene East African climate and human evolution. *Journal of Human Evolution*, *53*(5), 475-486.

Vidal, C. M., Lane, C. S., Asrat, A., Barfod, D. N., Mark, D. F., Tomlinson, E. L., Tadesse, A. Z., Yirgu, G., Deino, A., Hutchison, W., Mounier, A., & Oppenheimer, C. (2022). Age of the oldest known Homo sapiens from eastern Africa. *Nature*, *601*(7894), 579-583. https://doi.org/10.1038/s41586-021-04275-8

Viehberg, F. A., Just, J., Dean, J. R., Wagner, B., Franz, S. O., Klasen, N., Kleinen, T., Ludwig, P., Asrat, A., & Lamb, H. F. (2018). Environmental change during MIS4 and MIS 3 opened corridors in the Horn of Africa for Homo sapiens expansion. *Quaternary Science Reviews*, *202*, 139-153.

Vogelsang, R., & Wendt, K. P. (2018). Reconstructing prehistoric settlement models and land use patterns on Mt. Damota/SW Ethiopia. *Quaternary International*, *485*, 140-149.

Vrba, E. S. (1980). Evolution, species and fossils: how does life evolve. *South African Journal of Science*, *76*(2), 61-84.

Williams, A. P., & Funk, C. (2011). A westward extension of the warm pool leads to a westward extension of the Walker circulation, drying eastern Africa. *Climate Dynamics, 37*(11-12), 2417-2435. https://doi.org/10.1007/s00382-010-0984-y

Appendix P1 – Determining the Pace and Magnitude of Lake Level Changes in Southern Ethiopia Over the Last 20,000 Years Using Lake Balance Modeling and SEBAL

Determining the Pace and Magnitude of Lake Level Changes in Southern Ethiopia Over the Last 20,000 Years Using Lake Balance Modeling and SEBAL

Markus L. Fischer[1,2]*, Monika Markowska[1,3], Felix Bachofer[4], Verena E. Foerster[5], Asfawossen Asrat[6], Christoph Zielhofer[7], Martin H. Trauth[8] and Annett Junginger[1,2]

[1] Department of Geosciences, Eberhard Karls University Tübingen, Tübingen, Germany, [2] Senckenberg Centre for Human Evolution and Paleoenvironment (S-HEP), Tübingen, Germany, [3] Department of Climate Geochemistry, Max Planck Institute for Chemistry, Mainz, Germany, [4] Earth Observation Centre, German Aerospace Center (DLR), Wessling, Germany, [5] Institute of Geography Education, University of Cologne, Cologne, Germany, [6] School of Earth Sciences, Addis Ababa University, Addis Ababa, Ethiopia, [7] Institute of Geography, University of Leipzig, Leipzig, Germany, [8] Institute of Geosciences, University of Potsdam, Potsdam, Germany

The Ethiopian rift is known for its diverse landscape, ranging from arid and semi-arid savannahs to high and humid mountainous regions. Lacustrine sediments and paleo-shorelines indicate water availability fluctuated dramatically from deep fresh water lakes, to shallow highly alkaline lakes, to completely desiccated lakes. To investigate the role lakes have played through time as readily available water sources to humans, an enhanced knowledge of the pace, character and magnitude of these changes is essential. Hydro-balance models are used to calculate paleo-precipitation rates and the potential pace of lake level changes. However, previous models did not consider changes in hydrological connectivity during humid periods in the rift system, which may have led to an overestimation of paleo-precipitation rates. Here we present a comprehensive hydro-balance modeling approach that simulates multiple rift lakes from the southern Ethiopian Rift (lakes Abaya, Chamo, and paleo-lake Chew Bahir) simultaneously, considering their temporal hydrological connectivity during high stands of the African Humid Period (AHP, ~15–5 ka). We further used the Surface Energy Balance Algorithm for Land (SEBAL) to calculate the evaporation of paleo-lake Chew Bahir's catchment. We also considered the possibility of an additional rainy season during the AHP as previously suggested by numerous studies. The results suggest that an increase in precipitation of 20–30% throughout the southern Ethiopian Rift is necessary to fill paleo-lake Chew Bahir to its overflow level. Furthermore, it was demonstrated that paleo-lake Chew Bahir was highly dependent on the water supply from the upper lakes Abaya and Chamo and dries out within ~40 years if the hydrological connection is cut off and the precipitation amount decreases to present day conditions. Several of such rapid lake level fluctuations, from a freshwater to a saline lake, might have occurred during the termination of the AHP, when humid conditions were less stable. Fast changes in fresh water availability requires high adaptability for humans living in the area and might have exerted severe environmental stress on humans in a sub-generational timescale.

Keywords: African humid period, precipitation changes, abrupt and gradual changes, Chew Bahir, Lake Abaya, Lake Chamo, human-environment interaction

INTRODUCTION

Eastern African precipitation is characterized by large interannual to centennial variability (Lamb et al., 1998; Nicholson, 2000; Junginger et al., 2014; Liu et al., 2017), controlling water resource availability in the region. This is accentuated by the uneven spatial distribution of precipitation, from the lowlands (<500 m) to the high plateaus (>4,000 m), due to the extreme topography of the East African Rift System (EARS) (Nicholson, 2017). In recent decades a decline in precipitation has led to an increase in the intensity and frequency of drought periods (Funk et al., 2008; Viste, 2012; Rowell et al., 2015).

Water availability has always played a fundamental role in eastern Africa, and fluctuations in eastern Africa's hydroclimate in the past have had a dramatic impact on human societies. Changes in orbital insolation during the late Pleistocene to Middle Holocene caused an "African Humid Period" (AHP; ~15–5 ka BP; deMenocal et al., 2000; Barker et al., 2004), when increased precipitation triggered changes in vegetation (Lamb et al., 2004), dust dynamics (Zielhofer et al., 2017), lake expansion and increased river flow (Barker et al., 2004; Costa et al., 2014; Revel et al., 2014; Bloszies et al., 2015). In the wider region, these environmental changes during the AHP have been associated with multiple migration dynamics, such as the reoccupation of the Sahara ~10.5 ka BP (Kuper and Kröpelin, 2006; Drake et al., 2013; Larrasoaña et al., 2013; Manning and Timpson, 2014), cultural innovation (Lario et al., 1997) and overlapped with a demographic transition to the Neolithic age (Manning and Timpson, 2014; Honegger and Williams, 2015). An increase in arid conditions has been documented during the termination of the AHP ~5 ka BP in eastern Africa (e.g., deMenocal et al., 2000; Barker et al., 2004; Foerster et al., 2012; Junginger et al., 2014; Bloszies et al., 2015). This aridification trend coincides with societal adaptations, such as the introduction of pastoralism to eastern Africa, and the emergence of highly organized and complex state-level societies (demenocal, 1995; Brooks, 2006; Kuper and Kröpelin, 2006; Garcin et al., 2012; Foerster et al., 2015). Environmental changes likely provide both opportunities and constraints, due to variability in water resources and food availability, necessitating adaptation. To better understand potential links between cultural changes and climate variability, paleoclimate records can be used in conjunction with archaeological records to reconstruct major influences on modern civilizations.

In eastern Africa, however, there are still spatial and chronological gaps in paleoclimate records, which are largely non-quantitative and often regionally specific. Discrepancies particularly occur between records from marine archives, and lacustrine sites and also whether lacustrine sites are located within or outside the EARS. Existing records covering the AHP, report conflicting accounts of past climate variability in the region, with some studies suggesting a rapid onset and termination of the AHP (deMenocal et al., 2000; Tierney et al., 2013; Collins et al., 2017), while others indicate a rapid onset but more gradual termination and climate evolution in response to insolation forcing (Renssen et al., 2006; Asrat et al., 2007; Foerster

et al., 2012; Junginger et al., 2014; Trauth et al., 2018). While lakes with a constant groundwater/geothermal supply were mostly stable (e.g., Lake Tilo on the Ethiopian Plateau, Telford and Lamb, 1999), river-fed EARS lakes, such as Chew Bahir or Ziway-Shala in Ethiopia (Gillespie et al., 1983; Foerster et al., 2012) or Lakes Elementeita-Nakuru (Richardson and Dussinger, 1986), paleo-Lake Suguta in Kenya (Junginger et al., 2014) or Lake Manyara (Bachofer et al., 2015) demonstrated greater variability in lake levels in response to short-term precipitation-evaporation changes (**Figure 1**).

The first steps toward quantifying precipitation rates during the AHP and lake responses to a changing precipitation-evaporation budget were conducted for several basins in the EARS by applying Lake Balance Modeling (LBM) (**Figure 1**; Hastenrath and Kutzbach, 1983; Bergner et al., 2003; Dühnforth et al., 2006; Kniess, 2006; Borchardt and Trauth, 2012; Junginger and Trauth, 2013). LBM uses field observations, such as ^{14}C dated shorelines and overflow sills high above modern lakes (indicative of higher moisture availability), to calculate paleo-lake volumes, levels and paleo-precipitation rates. Such attempts of quantifying environmental parameters using field observations (e.g., shorelines) or proxy data (e.g., leaf waxes, stable isotopes, dust, pollen) through modeling approaches are defined as so-called Proxy System Modeling (PSM), as presented by Evans et al. (2013) or Dee et al. (2018).

For the AHP, the reconstruction of environmental parameters, such as paleo-temperatures, is based for example on GDGT and Tex$_{86}$ proxies from lake sediments (e.g., Verschuren, 2004; Berke et al., 2012a; Damsté et al., 2012; Loomis et al., 2012, 2014, 2015). Precipitation reconstructions are usually created using pollen (e.g., Lamb et al., 2004; Vincens et al., 2005; Umer et al., 2007; Rucina et al., 2009; Marchant et al., 2018), stalagmites (e.g., Baker et al., 2010), leaf waxes (e.g., Berke et al., 2012b; Costa et al., 2014), and the aforementioned LBMs. Due to the lack of the aforementioned proxy data in our study region, Chew Bahir in southern Ethiopia, an LBM is chosen to calculate paleo-precipitation rate changes.

Previously developed LBMs for the EARS, however, only looked at individual basins and therefore did not consider the hydrological connection via surface overflow of many rift basins (**Figure 1**). Consequently, the hydrological inflow budget of these interconnected lakes may have been underestimated, affecting the calculated paleo-precipitation estimates from the LBMs. Another aspect that was not considered in previous LBMs is change in seasonality. For the AHP it is hypothesized that an additional rainy season developed due to a shift of the Congo Air Boundary (CAB) during the northern hemisphere summer months, therefore tremendously impacting seasonality, environment and associated feedback mechanisms (e.g., Junginger and Trauth, 2013; Costa et al., 2014; Bloszies et al., 2015; Beck et al., 2019).

Here we present a comprehensive hydro-balance modeling approach that simulates firstly multiple rift lakes from the southern Ethiopian Rift (**Figure 1**; Abaya, Chamo, Chew Bahir). For this purpose, we developed a LBM for the region, which is a further development of the former models (e.g., Blodgett et al., 1997; Lenters and Cook, 1999). We have applied a combined
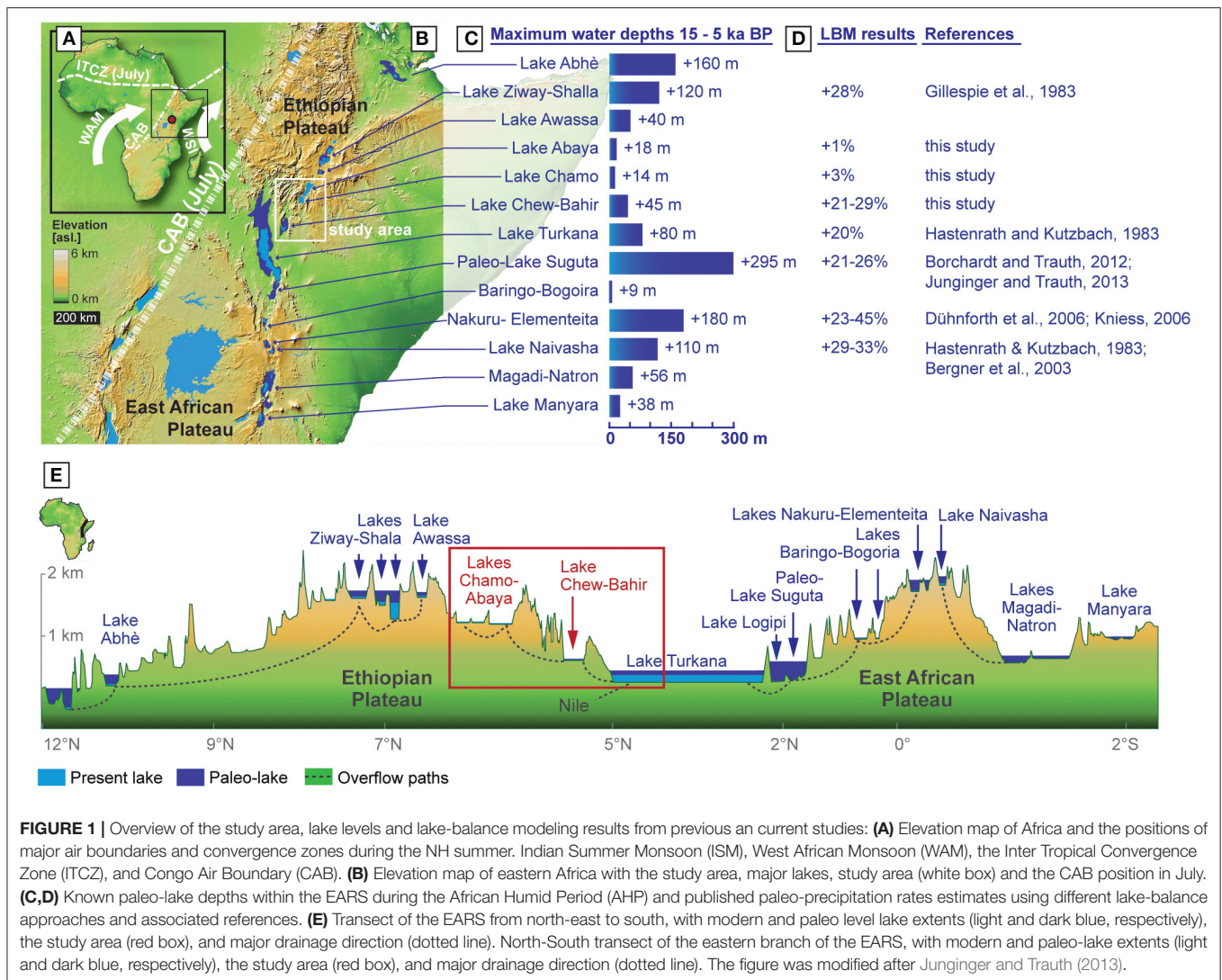
FIGURE 1 | Overview of the study area, lake levels and lake-balance modeling results from previous an current studies: **(A)** Elevation map of Africa and the positions of major air boundaries and convergence zones during the NH summer. Indian Summer Monsoon (ISM), West African Monsoon (WAM), the Inter Tropical Convergence Zone (ITCZ), and Congo Air Boundary (CAB). **(B)** Elevation map of eastern Africa with the study area, major lakes, study area (white box) and the CAB position in July. **(C,D)** Known paleo-lake depths within the EARS during the African Humid Period (AHP) and published paleo-precipitation rates estimates using different lake-balance approaches and associated references. **(E)** Transect of the EARS from north-east to south, with modern and paleo level lake extents (light and dark blue, respectively), the study area (red box), and major drainage direction (dotted line). North-South transect of the eastern branch of the EARS, with modern and paleo-lake extents (light and dark blue, respectively), the study area (red box), and major drainage direction (dotted line). The figure was modified after Junginger and Trauth (2013).

catchment approach including surface and subsurface flows. Two approaches were used to estimate the evapotranspiration; a bulk transfer equation and the Surface Energy Balance Algorithm for Land (SEBAL). The paleo-precipitation required during the AHP to fill lakes to their previous high-stands will be calculated under different scenarios including the incorporation of an additional rainy season as previously suggested by multiple studies (e.g., Junginger et al., 2014; Bloszies et al., 2015; Beck et al., 2019) and the theoretical feedback due to vegetation changes. We furthermore provide lake regression and transgression times under abrupt and gradual changes, in order to demonstrate the sensitivity of the investigated lake systems to changes in precipitation. Based on the outcome of the model, we compare lake response times to abrupt and gradual precipitation changes to aridity proxy data of an 11 m-long sediment core from the margin of paleo-lake Chew Bahir, which was published by Foerster et al. (2015) to reconstruct the paleo-lake level evolution of Chew Bahir during the past 20 ka.

REGIONAL SETTING

The Investigated Catchments

There are three adjoining North-South trending, endorheic basins at the southern end of the Main Ethiopian Rift (MER) which are part of the greater (4,000 km) EARS. These are the basins of Lake Abaya, Lake Chamo, and paleo-lake Chew Bahir, from north to south, respectively (**Figure 1**). Lake Abaya (6.4°N, 37.95°E, 7 m deep, and lake surface area of 1,081 km^2) is the northern-most and highest elevated (1,176 m a.s.l.) basin with a catchment size of 16,203 km^2 (**Figure 2**). The major rivers draining into Lake Abaya include the Gelana, Bilate, Gidabo, Hare, Baso, and Amesa Rivers (Tiruneh, 2005). Lake Chamo (5.8°N,37.6°E, ∼1,109 m a.s.l., 14 m deep, 310 km^2 lake surface area) to the south is separated from Lake Abaya by the Quaternary Tosa Sucha Volcano (Ebinger et al., 1993; **Figure 2J**). The Kulfo River to the west is the main tributary, while Sile and Wezeka rivers are smaller tributaries into Lake Chamo (Tiruneh, 2005). The Kulfo River is also connected to Lake
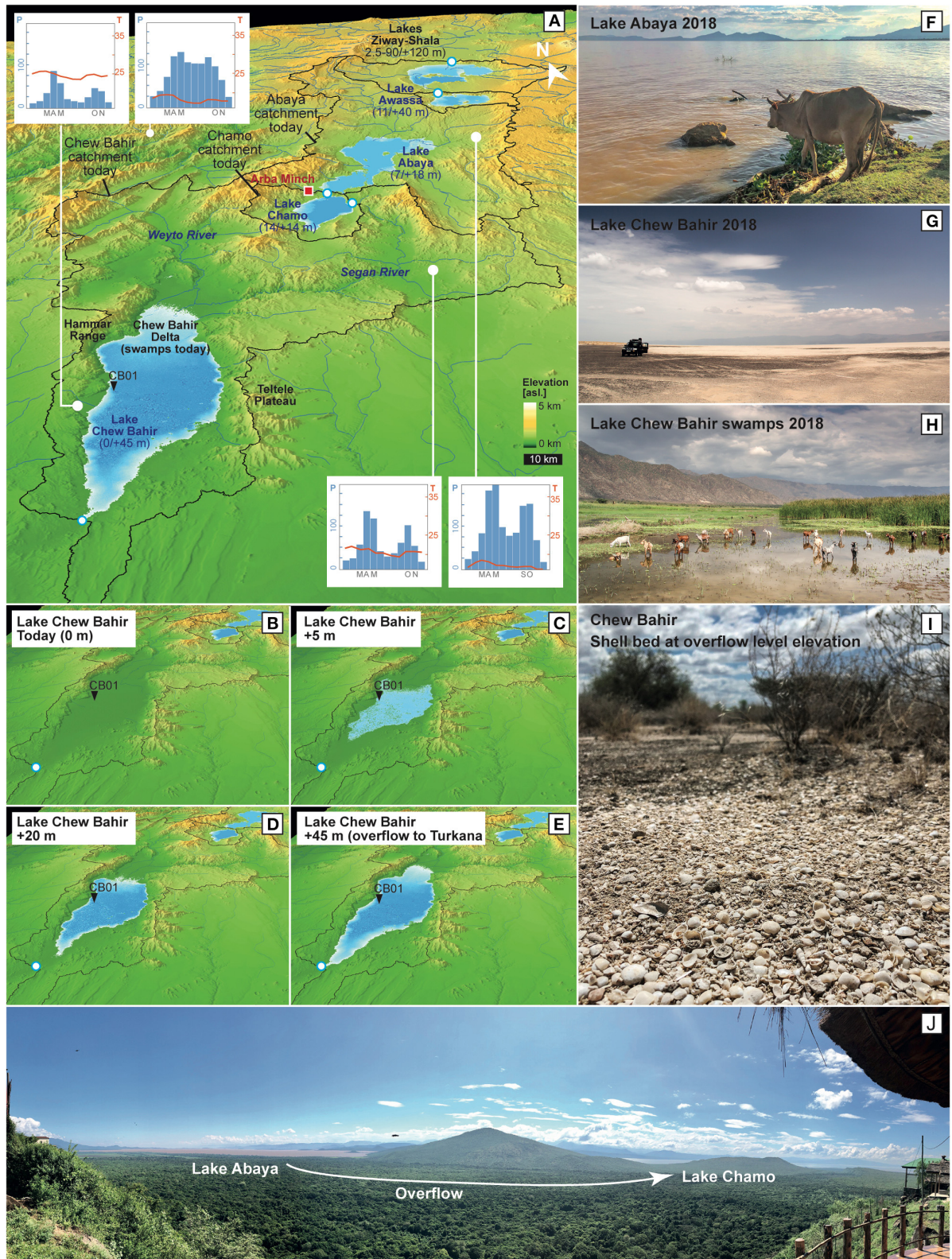
FIGURE 2 | Geographical features of the studied lake basins: **(A)** Modern catchment boundaries, monthly temperature means in °C and precipitation in mm/month (IRI, last accessed 11/2019), overflow sill locations (white-blue circles), and paleo-lake dimensions with modern/paleo-depths in numbers. **(B–E)** Modeling outputs of paleo-lake Chew Bahir's dimension during different lake filling steps from modern to +5, +20, and +45 m when reaching the overflow level. **(F–J)** Pictures from study sites by A. Junginger.

Abaya during wet periods when lake levels are higher (Tiruneh, 2005). The catchment area of Lake Chamo is ~1,793 km². Both lakes, Chamo and Abaya are bounded by the Gamo-Gidole horst to the west and the Amaro horst to the east reaching elevations over 3,000 m a.s.l. and consisting mainly of Cenozoic rift volcanics unconformably overlaying Precambrian basement rocks (Davidson, 1983; Ebinger et al., 1993). Paleo-lake Chew Bahir (4.1–6.3°N, 36.5–38.1°E, ~498 m a.s.l, **Figures 1**, **2**) to the south is most of the year a 210 km² saline mudflat and the lowest in elevation of the herein investigated basins. The Chew Bahir surface comprises deltaic ephemeral swamps at its northerly and north easterly reaches, where the perennial Weyto and Segan rivers drain the north-western and north-eastern sides of the catchment, respectively (**Figure 2**). The catchment (20,650 km²) is bound by the MER rift shoulders, in the east by the Teltele Plateau (up to 1,600 m a.s.l.) and in the west by the Hammar Range (up to 1,300 m a.s.l.). The elevation of the rift shoulders decreases in a southerly direction. The northern side of the catchment is bound by uplifted Proterozoic metamorphic rocks and Cenozoic rift volcanics (Davidson, 1983; **Figures 1**, **2**), hydrologically separating it from the Chamo and Abaya catchments. To the south, Cenozoic rift volcanics from the foothills of the Hammar Range prevent a direct hydrological link with the Turkana basin, today. The dry southern-most part of the catchment borders Kenya.

Overflow Regime

Several paleo-shorelines, wave cut notches and sediment characteristics in the Ethiopian Rift and plateau regions, such as Lake Abhé (Gasse and Street, 1978), Lake Ziway-Shala-Abiyata (Gillespie et al., 1983; Chalié and Gasse, 2002), Lake Dendi (Wagner et al., 2018), or Lake Ashenge (Marshall et al., 2009) show evidence of deep lakes during the AHP. During those high stands, these lakes were overflowing into rivers that connected to other lake basins. Awulachew (2006) reported that lakes Abaya and Chamo were previously connected via surface streams. Here, Lake Abaya connected via an old channel through the Kulfo river with Lake Chamo (**Figure 2**). Awulachew (2006) and Kassa (2015) report of evidence that during high stands, Lake Chamo overflowed into the river Metenafesha and into the Sermale stream, both being tributaries of the Segan river, which in turn feeds paleo-lake Chew Bahir. During a field campaign in November 2018, paleo-shoreline deposits (shell beds) at Chew Bahir could be identified at the same elevation as the overflow sill (**Figure 2**). As calculated in section Digital Elevation Model Analysis, Lake Abaya's overflow sill to the Chamo catchment is at 1,194 m a.s.l. (6°0′40.38″N, 37°34′50.45″E) 18 m above its present lake level. Lake Chamo reaches its overflow sill to the Chew Bahir catchment at 1,123 m a.s.l. (5°51′49.66″N, 37°38′31.78″E), which is 14 m above its modern lake surface. The Chew Bahir basin has an overflow sill at 543 m a.s.l. (4°13′30.58″N, 36°39′35.19″E) to Lake Turkana, 45 m above the basin floor.

Vegetation

Modern vegetation in the Chew Bahir catchment is typically sparse and follows an east-west gradient (Friis et al., 2010). The eastern part of the Chew Bahir basin is classified as Acacia-Commiphora woodland and bushland, whereas the western part is described as Combretum-Terminalia woodland and wooded grassland (Friis et al., 2010). The higher elevated parts of the study area, such as close to Arba Minch (**Figure 2**), comprise evergreen Afro-Montane forest and grassland complex, which transitions to moist evergreen Afro-Montane forest in the north. The vegetation in the even higher mountainous areas are dominated by Afro-alpine vegetation with an Ericaceous Belt (Friis et al., 2010).

Climate

Seasonal rainfall in Chew Bahir is associated with the annual passage of a tropical rain belt (often referred to as the Inter Tropical Convergence Zone, ITCZ), which is predominantly fueled by the Indian Ocean (**Figure 1**, Levin et al., 2009; Nicholson, 2017). Generally, the tropical rain belt migrates between 10° North and South of the equator, resulting in a bimodal precipitation pattern close to the equator and an unimodal pattern at its limits (Nicholson, 1996). Consequently, the lower elevations of the Chew Bahir catchment precipitation is bimodal, with the "Belg" rains from March to May (long rains) and the "short rains" in October–November (**Figure 2**). The highlands northwest of Chew Bahir, including the Abaya and Chamo catchments, experience an unimodal rainfall pattern with only one longer wet season from March to November (Segele and Lamb, 2005; Williams and Funk, 2011). This wet season is, fueled by two different sources, with the "Belg" rains lasting from March to May and the "Kiremt" rains from June to September. The Kiremt rains are hypothesized to originate from the Atlantic Ocean-derived southwestern humid Congo air stream (Nicholson, 1996; Camberlin, 1997; Lamb et al., 2000). The eastern limit of this air stream is marked by the Congo Air Boundary, which separates the humid air masses from the west from dry air masses in the east (Nicholson, 1996). Annual to decadal fluctuations in the intensity and strength of precipitation are possibly related to a direct response to sea-surface temperature variations in the Indian and Atlantic Oceans (Nicholson, 2017). Compared to other areas at similar latitudes in Africa, Ethiopia receives considerably more rainfall due to its position in the MER and the resulting orographic effects (Nicholson, 2017).

MATERIALS AND METHODS

We developed a LBM to quantify the present day and paleo-water balances of paleo-lake Chew Bahir, Lake Chamo and Lake Abaya. The model was coded in R and is available at GitHub (https://github.com/MLFischer/Lake-Balance-Model, 03/2019). In summary, a Digital Elevation Model (DEM) was used to delineate the catchment boundaries, lake bathometry, lake volumes and overflow sills (section Digital Elevation Model Analysis). The annual modern water balances were calculated for Lakes Abaya, Chamo and paleo-lake Chew Bahir (section Lake Balance of Lakes Abaya, Chamo, and Paleo-Lake Chew Bahir). Evaporation was estimated for the paleo-lake Chew Bahir catchment using SEBAL [section Surface Energy Balance

Algorithm for Land (SEBAL)]. After parametrizing the model based on present-day conditions, we modeled the most recent lake high-stands of Lake Chamo, Abaya and paleo-lake Chew Bahir during the AHP (section Paleo-Lake Modeling). In section Calculation of Amplifier Lake Characteristics, we calculated the Hypsometric Integral (HI) and Aridity Index (AI) for the paleo-lake Chew Bahir, Lake Abaya and Chamo catchments which are used to define the Amplifier Lake characteristic of lake basins in the EARS following Olaka et al. (2010). In section Lake Level Reconstruction of Paleo-Lake Chew Bahir, we apply the modeled lake responses of paleo-lake Chew Bahir to various changes is precipitation and thus lake-level scenarios to changes in a K-proxy record from a drill-core taken from the paleo-lake Chew Bahir basin (Foerster et al., 2012, 2015; Trauth et al., 2018) and reconstruct the paleo-lake level of the past 20 ka.

Digital Elevation Model Analysis

The catchment boundary delineation was based on the DEM resulting from the Shuttle Radar Topography Mission (SRTM C-band; http://www2.jpl.nasa.gov/srtm/). The flow directions, flow accumulations, catchment boundaries and hydro-junctions (maximum possible lake extent) were calculated with the workflow for deranged terrains from the ArcHydro toolbox of ArcGIS 10.3 (Merwade, 2012). The DEM of each catchment was processed using the *freq* function in the R raster-package to produce an elevation frequency table, which then is used to compute the basin hypsometry and paleo-lake bathymetry (R Core Team, 2019).

Lake Balance Model

Three processing steps were applied for calculating the modern day annual water balance as later summarized in Equation (3). The parameters used in this model are climate parameter based on interpolated global gridded climate data (New et al., 2002), remote sensing data (Friedl et al., 2010; Platnick et al., 2015) and evaporation parametrization approaches (Schmugge and André, 1991). The input parameters are annual averages and they are summarized in **Table 1**.

The first was to calculate surface temperatures by a radiation-based surface energy flux (Equation 1). The energy balance was calculated using Newton's method to determine the surface temperature. The energy fluxes were assumed to be in an equilibrium state and include: the incoming short-wave radiation (R_{sw}), the incoming long-wave radiation (R_{ld}) with the surface emissivity (ε), the long-wave radiation (R_{lu}) emitted by the Earth's surface, the sensible heat flux (H) and the latent heat flux ($L \cdot ET_a$), with L being the latent heat of vaporization, and ET_a the rate of actual evaporation (Blodgett et al., 1997; Lenters and Cook, 1999).

$$R_{sw} - R_{lu} + \epsilon\, R_{ld} - H - L \cdot ET_a = 0 \qquad (1)$$

In the second step (Equation 2), ET_a was calculated using the bulk transfer formula described by Brutsaert (1982), with the surface-drag coefficient (C_D), the wind speed (U), the soil moisture availability (f), the gas constant for dry air (R), the surface (T_s) and air (T_a) temperatures, the relative humidity (rh), and the saturation vapor pressure ($es(T_s)$) as a function of surface and air temperature.

$$ET_a = \frac{0.622 \cdot C_D \cdot U \cdot f}{RT_a}\left[es\left(T_s\right) - rh \cdot es\left(T_a\right)\right] \qquad (2)$$

The resulting ET_a on land and water was calculated with Equations (1) and (2) from the environmental parameters summarized in **Table 1**. A sensitivity analysis of ET_a for paleo-lake Chew Bahir to major environmental parameters, such as air temperature (T_a), cloud cover, relative humidity (rh), and wind speed (U) was performed.

The third step involved calculating the annual lake water balance of lakes Abaya, Chamo and paleo-lake Chew Bahir using ET_a on land (E_l) and water (E_w), the precipitation amount from the Tropical Rainfall Measuring Mission (TRMM, Bookhagen, in review) (P_{bas}) and the basin-wide subsurface outflow/inflow (S_{bas}) following Equation (3). A positive and negative water balance suggest an increase and decrease in lake water volume,

TABLE 1 | Summary of input parameters for the LBM of Chew Bahir, Chamo, and Abaya.

Parameter	Symbol (Unit)	Chew Bahir		Chamo		Abaya		Confidence	References
		Lake	Land	Lake	Land	Lake	Land		
Cloud free shortwave radiation	R_sw (W/m²)	415		415		415		±3	Berger and Loutre, 1991
Shortwave cloud parameters	a, b	0.39, 0.38		0.39, 0.38		0.39, 0.38		–	Bookhagen et al., 2001
Longwave cloud parameters	a_2, b_2	0.22, 2.0		0.22, 2.0		0.22, 2.0		–	Bookhagen et al., 2001
Air pressure	p (kPa)	95.67	88.5	88.7	85.13	87.9	81.7	–	Barometric elevation formula
Cloud coverage	cc	0.44	0.61	0.37	0.55	0.31	0.54	±0.05	Platnick et al., 2015
Relative humidity	rh	0.55	0.57	0.57	0.57	0.57	0.58	±0.05	New et al., 2002
Windspeed	ws (m s⁻¹)	2.56	2.13	1.71	1.72	1.46	1.42	±0.3	New et al., 2002
Air temperature	t_a (°C)	26.35	22.75	21.95	20.15	21.55	18.35	±0.5	New et al., 2002
Surface drag coefficient	cds	7.3×10^{-4}	5.9×10^{-3}	7.3×10^{-4}	6.6×10^{-3}	7.3×10^{-4}	7.6×10^{-3}	$±0.2 \times 10^{-3}$	Schmugge and André, 1991
Surface albedo	albedo	0.06	0.14	0.06	0.126	0.06	0.136	±0.02	Friedl et al., 2010
Surface emissivity	emis	0.98	0.96	0.98	0.96	0.98	0.96	±0.02	Friedl et al., 2010
Moisture availability	f	1.00	0.137	1.00	0.198	1.00	0.25	±0.05	Schmugge and André, 1991

respectively. The modern-day conditions of Lake Abaya, Lake Chamo and paleo-lake Chew Bahir were assumed to be in equilibrium, where $\Delta V = 0$ as suggested in previous studies, such as Bookhagen et al. (2001), Bergner et al. (2003), and Junginger and Trauth (2013). The water surplus was assumed to be groundwater recharge in contrast to previous LBM studies, which used a fixed precipitation to groundwater ratio (Blodgett et al., 1997), a fix value (Bergner et al., 2003) or that the groundwater recharge rate is zero (e.g., Bookhagen et al., 2001; Dühnforth et al., 2006; Junginger and Trauth, 2013).

$$\Delta V_{lake} = P_{bas} - \left[E_w \alpha_w + E_l (1 - \alpha_w)\right] - S_{bas} = 0 \quad (3)$$

The SEBAL Method

Southern Ethiopia is a data-sparse region, with few continuously monitored weather stations, making quantification of the evaporation difficult on a catchment scale. Hence, we used a second approach called Surface Energy Balance Algorithm for Land (SEBAL; Bastiaanssen et al., 1998a,b). SEBAL calculates the Earth's surface instantaneous energy flux (Equation 4) at the moment of satellite overpass, to determine the latent heat flux as the residual (Bastiaanssen et al., 1998a,b).

In order to populate the SEBAL input parameters, satellite remote sensing data products of the Moderate-Resolution Imaging Spectroradiometer (MODIS) were identified and resampled to an uniform spatial resolution of 500 m (**Table 2**). To quantify monthly evaporation (Zhang et al., 2011; Borchardt and Trauth, 2012), the available MODIS datasets for an average reference year (2010 CE, Kiptala et al., 2013) were processed. The selection criterion applied was a clear sky coverage of higher than 90 percent. The Land Cover MCD12Q1 was further utilized to estimate the surface roughness length and the surface drag coefficient, following Wieringa (1992).

To calculate ET_a based on the surface energy fluxes we employed the net radiation (R_n) equation (Equation 4). ET_a was

calculated using the soil heat flux G, which accounts for the amount of radiant energy released or absorbed at the soil surface per unit time, the sensible heat flux H and the latent heat flux λE, which resolves as residual of Equation (4):

$$R_n = G + H + \lambda E \quad (4)$$

R_n was estimated following the clear sky approach described in Allen et al. (2007) as a function of the day of the year, longitude, latitude, altitude, α, ε and atmospheric emissivity.

G was calculated with Equation (5) as a function of R_n, α and the Normalized Difference Vegetation Index (NDVI), which is a standardized proxy for vegetation density and greenness (Bastiaanssen, 2000).

$$\frac{G}{R_n} = \frac{T_s}{\alpha} \left(0.0038\alpha + 0.0074\alpha^2\right) \left(a - 0.98 \cdot NDVI^4\right) \quad (5)$$

H was determined using Equation (6), with the specific heat of air at a constant pressure (C_p), density of moist air (p), the vertical temperature gradient (dT), and the aerodynamic heat transfer resistance (r_{ah}) (Bastiaanssen et al., 1998a).

$$H = \frac{pC_p dT}{r_{ah}} \quad (6)$$

To solve Equation (6) we applied an approach by Zhang et al. (2011) that utilizes the wind field data by New et al. (2002). The frictional velocity and the aerodynamic resistance to heat transport were calculated for each pixel according to the wind-field and the logarithmic wind-profile. Both variables converge through an iterative atmospheric stability correction depending on the Monin-Obukov-Length (Bastiaanssen et al., 1998a,b). The resulting calculated dT leads to H (Bastiaanssen et al., 1998a,b). The evaporation fraction (Δ) was calculated to solve for daily evaporation (ET_{24}) from the instantaneous heat fluxes (Bastiaanssen, 2000; Bastiaanssen et al., 2005) with Equation (7).

$$\Delta = \frac{\lambda E}{R_n - G} = \frac{\lambda E}{\lambda E + H} \quad (7)$$

ET_{24} is a function of daily net radiation (R_{n24}) and Δ (Bastiaanssen, 2000). R_{n24} was calculated following De Bruin and Stricker (2000) through the integrated sinusoidal daily illumination and the extra-terrestrial solar radiation.

$$ET_{24} = \frac{86300 \cdot 10^3}{\lambda p_w} \Delta R_{n24} \quad (8)$$

The daily evaporation (ET_{24}) was averaged each month to calculate the monthly evaporation. Missing data for months with only cloudy days were interpolated from the adjacent months. To calculate ET_a, we applied a slight modification of the water balance by Thornthwaite and Mather (1955). We defined the modeled monthly evaporation as ET_p. Following that, we calculated the catchment average ET_p per month and compared them to the precipitation average from the TRMM dataset (Bookhagen, in review). Two assumptions have been

TABLE 2 | Moderate-Resolution Imaging Spectroradiometer (MODIS) products and bands used for SEBAL calculation.

Product	Band	Temporal granularity	Pixel size (m)	Data references
MOD11A1	Land Surface Temperature Daily	Daily	1,000	Wan et al., 2015
	Emissivity Band 31			
	Emissivity Band 32			
	Day View Time			
	Clear Day Coverage			
MOD09GA	Surface Reflectance Band 1–7	Daily	500	Vermote and Wolfe, 2015
	Solar Azimuth			
	Solar Zenith			
MOD13Q1	NDVI	16 day	250	Didan, 2015
MCD12Q1	Land Cover Type 2 (UMD)	Yearly	500	Friedl et al., 2010

considered when calculating the monthly water balance: (1) The total monthly ET_a is smaller than the total monthly precipitation (P) and the available soil water (SW) in the catchment. (2) 50% of the monthly water surplus, if occurring, is stored in the soil for the next month (SW) and 50% of the water surplus results in groundwater recharge (GW). In months where $ET_p < P$, we set $ET_a = ET_p$. However, in months where $ET_p > P$ the monthly ET_a was calculated by multiplying ET_p by the ratio of available water and ET_p (Thornthwaite and Mather, 1955; Borchardt and Trauth, 2012). The ET_a spatial distribution of humid months does not need to be corrected, as it remains the ET_p distribution. During dry months ET_a was further modified using the normalized Topographic Wetness Index (TWI; Kirkby and Beven, 1979) as shown in Equation (9). This spatial correction factor using the TWI reflects the orographic influence on the soil water distribution.

$$ET_a(x,y) = ET_p(x,y) \cdot [TWI_{norm}(x,y)$$
$$+ (\frac{\sum availableWater}{\sum potentialEvaporation} - TWI\_norm)] \quad (9)$$

In a last step, we compared the SEBAL and the bulk transfer LBM derived ET_a estimates on land, as well as the subsurface recharge rates for the Chew Bahir catchment to assess the two different approaches. Lake evaporation estimates for Chamo and Abaya were compared to measured pan evaporation data over the years 1985–2005 from the Arba Minch weather station ($6°2'$N, $37°33'$E), which is located between lakes Abaya and Chamo (Belete, 2009).

Paleo-Lake Modeling Method
Model Calculation
In order to assess the sensitivity of lake levels to changes in precipitation and the impact of hydrological connectivity between basins, we combined the LBM's of Lake Abaya, Lake Chamo and paleo-lake Chew Bahir. The annual water balance of each catchment (Equation 3) and the consequent lake volumes were calculated to derive the potential change of lake surface areas. Annual changes in the total lake surface area were considered at the end of each annually modeled time-step and the ratio of land and water were adjusted to reflect the new surface evaporation fluxes for each modeled year. Furthermore, at each annual time step the overflow threshold was considered and an additional drainage function was activated if the lake water level exceeded the height of the overflow sill that was calculated in the DEM analysis (section Digital Elevation Model Analysis). For example, if the surface water level for Lake Abaya equals the overflow threshold, the water surplus is accounted for as inflow into the Chamo catchment and added to the water balance. The TRMM derived precipitation rates were multiplied by the total area of each catchment to calculate the volume of the total water influx. The computed ET_a over water was multiplied by the lake area to derive the evaporated water volume above each lake and the ET_a over land was multiplied by the remaining catchment areas to calculate the total ET_a.

Modeling Increased Precipitation Scenarios
We modeled various changes in precipitation over the Abaya, Chamo, and Chew Bahir catchments to estimate the increase in precipitation that was required for paleo-lake Chew Bahir to reach its overflow sill, the point where paleo-lake Chew Bahir drained into Lake Turkana during lake high-stands in the AHP (Foerster et al., 2012). Covering both decadal and centennial transitions of paleo-lake Chew Bahir (Trauth et al., 2018), we ran 500-years simulations of the LBM. The precipitation is increasing by 0.1% in each simulation, providing a total of 300 simulations with modeled precipitation increases from 0 to 30% of present day. This allowed us to calculate both the transition times for paleo-lake Chew Bahir; to go from "no lake" conditions to a "flooded basin" and the amount of increased precipitation that would be required. In the simulations, the exchange rates between the basins were calculated and the amount of the water volume influx from Lake Abaya to Lake Chamo and Lake Chamo to paleo-lake Chew Bahir were quantified as a proportion of its total water budget. Due to a lack of paleo-vegetation information and its impact on the actual evaporation and resulting precipitation in the study region for the AHP, we used the estimates of a 7–15% increased precipitation during the AHP in the Kenyan Rift published by Bergner et al. (2003). Those estimates are presented as vegetation threshold within our results and are based on the same parametrization approach as our LBM and are coming from a comparable landscape composition.

Modeling Seasonality Changes in Precipitation
Previous studies have suggested a change in the seasonality of precipitation during the AHP, due to a shift in the Congo Air Boundary, resulting in additional precipitation during July to September in equatorial regions in eastern Africa (e.g., Junginger, 2011; Junginger and Trauth, 2013; Costa et al., 2014; Junginger et al., 2014; Bloszies et al., 2015; Beck et al., 2019). This would have resulted in a change of the evaporative potential on land, compared to present day, due to an increased potential moisture source over what were previously dry months ($ET_p > P$). We calculate the difference between ETa and ET_p using SEBAL from July to September and add this evaporation amount to Chew Bahir's catchment actual evaporation rate on land. We omit the catchment of the lakes Abaya and Chamo from this procedure as they don't have this modern day lack ($ET_p < P$) of evaporable water for these months.

Transition Times for Onset and Termination of AHP
The timing of precipitation change was also modeled using different scenarios to estimate the temporal reaction of paleo-lake Chew Bahir's volume to abrupt and gradual precipitation changes during the onset and termination of the AHP. The first scenario (S1) was an abrupt transition, simulated by an instantaneous increase in precipitation to the threshold (TS) amount required to force paleo-lake Chew Bahir to the overflow sill. However, this only represents the minimum precipitation required to fill Paleo-lake Chew Bahir to the overflow level, therefore we additionally considered two scenarios, in which the threshold could have been exceeded (S2: TS+5%, S3:

TS+10%). We simulated a gradual increase in precipitation from modern day conditions to TS over 50, 100, 250, and 500 years. The termination of the AHP was also simulated, where the abrupt scenario saw an immediate transition from increased precipitation rates (TS) to modern day precipitation. The gradual offset was simulated by decreasing the precipitation amount linearly from TS to the modern day amount within 50, 100, 250, and 500 years.

Amplifier Lake Characteristics

In order to compare the basins of Lake Abaya, Lake Chamo and paleo-lake Chew Bahir with other lakes within the EARS, we calculated the hypsometric integral (*HI*; Pike and Wilson, 1971) following Equation (10).

$$ HI = \frac{mean\ elevation - minimum\ elevation}{maximum\ elevation - minimum\ elevation} \quad (10) $$

We calculated the *AI* of each, individual catchment as the quotient precipitation (mm a^{-1}) and potential evaporation (mm a^{-1}, Thornthwaite, 1948) within each catchment. The term amplifier lake characterizes lakes in the EARS that react very sensitively to even moderate climate changes (Street-Perrott, 1985; Olaka et al., 2010; Trauth et al., 2010). We compared the HI and AI of paleo-lake Chew Bahir, lakes Abaya, and Chamo with other lake basins and classified amplifier lakes in the EARS based on Olaka et al. (2010).

Chew Bahir Lake Level Reconstruction

To translate changes indicated by climate proxies in the Chew Bahir drill core sediments into actual lake level changes, we used the established aridity proxy potassium (K) (Foerster et al., 2012, 2015, 2018; Trauth et al., 2018). High K concentrations in the sedimentary record have been documented to be strongly controlled by the hydrochemistry of the paleo-lake and porewaters. Such changes in salinity and alkalinity are typically caused by a drier climate and associated lake water evaporation (Foerster et al., 2018). For our study, we are using the most complete and high resolution record from Chew Bahir for the last 20 ka BP, a composite of pilot core CB-01 and CB-03, as discussed in Foerster et al. (2015). In our study, we compare the timing of K-changes with modeled response times of paleo-lake Chew Bahir's lake level, and interpret whether long-term and short-term fluctuations can be explained by abrupt or gradual changes in precipitation based on their duration and also K content.

RESULTS

DEM Analysis Overflow Regime

As summarized in **Table 3**, an additional 25.2 km^3 of water would be required to initiate drainage at the overflow sill from Lake Abaya toward Lake Chamo, resulting in an increased lake surface area of 3.6%. To initiate overflow from Lake Chamo toward Chew Bahir, only an additional 5.2 km^3 is required, which would increase the lake area by 5%. Paleo-lake Chew Bahir would require 83.2 km^3 for the lake level to reach the overflow sill and initiate drainage into Lake Turkana. In this

TABLE 3 | Summary of major output parameters.

Parameter	Unit	Chew Bahir	Chamo	Abaya
DIGITAL ELEVATION MODEL ANALYSIS				
Catchment size	km²	20,650	1,793	16,203
Modern day lake level	m a.s.l.	498	1,109	1,176
Maximum lake level	m a.s.l.	543	1,123	1,194
Modern day lake area	km²	0	310	1,081
Maximum lake area	km²	2,486	394	1,557
Additional lake volume	km³	83	5	25
Modern day lake area ratio, α$_w$	%	0	17	6
Maximum lake area ratio, α$_w$	%	12	22	9.6
Hypsometric Integral		0.23	0.15	0.25
Aridity Index		0.83	1.33	1.72
LAKE BALANCE MODEL				
Precipitation modern, P$_{bas}$ (rate, volume)	(mm a^{-1}, km³)	917, 18.9	1,211, 2.2	1,407, 22.8
Precipitation paleo 20–30% increased, P$_{bas}$ (rate)	(mm a^{-1})	1,100–1,192	1,453–1,574	1,688–1,829
Groundwater, S$_{bas}$ (rate, volume)	(mm a^{-1}, km³)	24, 0.5	80, 0.1	260, 4.2
Evaporation on land, E$_l$ (rate, volume)	(mm a^{-1}, km³)	892, 18.4	1,060, 1.6	1,123, 17
Evaporation on water, E$_w$ (rate, volume)	(mm a^{-1}, km³)	1,908, 0	1,550, 0.5	1,513, 1.6

scenario, paleo-lake Chew Bahir would cover 12% of the total catchment area.

Lake Balance Model Results

Sensitivity tests of the major environmental parameters in the LBM including temperature, cloud cover, humidity and wind speed were calculated for the paleo-lake Chew Bahir catchment (**Figure 3**). For example, a modeled mean temperature rise of 1°C with an error below 1°C (New et al., 2002) would result in an increase of 4.7% (42 mm a^{-1}) in ET$_a$ for the average land evaporation in the paleo-lake Chew Bahir catchment (**Figure 3A**). Cloud cover measurements from MODIS typically have an error below 5% (Platnick et al., 2015). An increase in average cloud cover by 5% would decrease ET$_a$ by ∼4% (367 mm a^{-1}, **Figure 3B**). The dataset of the relative humidity shows errors up to ±15% (New et al., 2002). Hence, an increase in the average relative humidity of 15% would decrease ET$_a$ on land by 8.7% (78 mm a^{-1}, **Figure 3C**). The windspeed dataset has the highest errors and according to New et al. (2002) the maximum deviation for specific measures sites in eastern Africa ranges between 40 and 60%. For example, an increase in wind speed of 1 m s^{-1} (corresponding to a 45% deviation) would enhance ET$_a$ by 19.5% (174 mm a^{-1}, **Figure 3C**).

SEBAL Results

Using 43 days with a clear sky of the reference year, the calculated mean R_n was 459 W m^{-2} (σ = 54 W m^{-2}), the average G was 75 W m^{-2} (σ = 8.6 W m^{-2}), and H was 130 W m^{-2} (σ
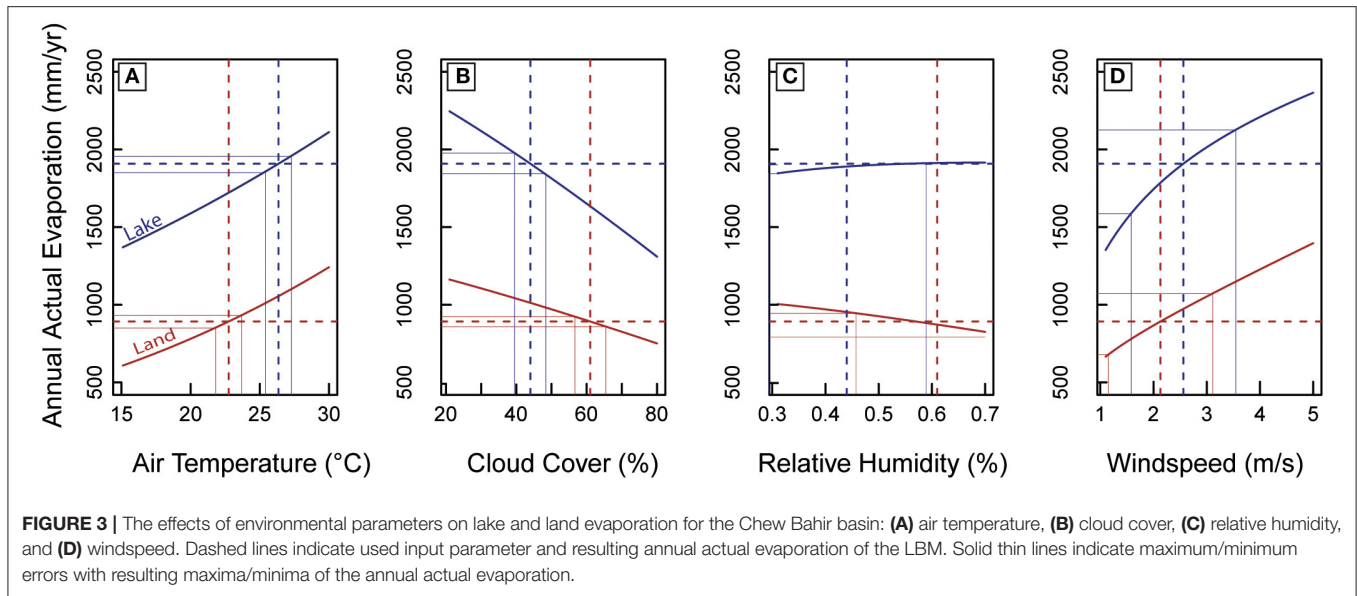
FIGURE 3 | The effects of environmental parameters on lake and land evaporation for the Chew Bahir basin: **(A)** air temperature, **(B)** cloud cover, **(C)** relative humidity, and **(D)** windspeed. Dashed lines indicate used input parameter and resulting annual actual evaporation of the LBM. Solid thin lines indicate maximum/minimum errors with resulting maxima/minima of the annual actual evaporation.

= 27.3 W m^{-2}). Those fluxes result in Δ of 0.64 (σ = 0.074) and λE of 0.38 mm h^{-1} (σ = 0.07). RN_{24} was 137 W m^{-2} (σ = 7.07 W m^{-2}), resulting in ET_{24} of 3.18 mm d^{-1} (σ = 0.33 mm d^{-1}).

The annual water balance shows a bimodal precipitation (916 mm a^{-1}) and ET_a (847 mm a^{-1}) and an unimodal ET_p (see **Figure 4B**). The spatial distribution (see **Figure 4A**) of ET_a ranges from 52 to 1,360 mm a^{-1}. The southern part of the catchment has the lowest values, whereas the northern and elevated rift shoulders, with streams and adjacent wetlands, has the highest ET_a due to greater water availability.

Evaporation Estimate Comparison

Using the SEBAL approach, ET_a was 847 mm a^{-1} for the paleo-lake Chew Bahir catchment, compared to 892 mm a^{-1} using the bulk transfer method, which is a relative difference of 5% (45 mm a^{-1}). This leads to a shift in the closed water balance of the paleo-lake Chew Bahir catchment and a difference in the estimated catchment-wide groundwater recharge rates between 69 mm a^{-1} (SEBAL) and 24 mm a^{-1} (LBM). We calculated annual lake evaporation for Lake Abaya of 1,513 mm and for Lake Chamo of 1,550 mm a^{-1} using the bulk transfer Lake Balance Model. At the Arba Minch metrological station (6°2'N, 37°33'E), class A pan evaporation was measured from 1985 to 2005 AD, with an average of 2,191 mm a^{-1}. This results, with a correction factor of 0.85, in a 20-years average annual lake evaporation of 1,862 mm a^{-1} as calculated by Belete (2009). These values differ from our model results by 16.7 to 18.7%, which could be related to a high uncertainty of the individually determined correction factor for pan evaporation data.

Combined Lake Balance Model and Paleo-Water Balances Results
Modeling Increased Precipitation Scenarios

The transition of paleo-lake Chew Bahir from "no lake" to "overflow conditions" at a lake surface level of 543 m a.s.l., 45 m

above basin floor, was simulated over a period of 500 years. The transition occurs at a minimum precipitation increase at a TS of 6.5% compared to modern day 12-years TRMM average and occurs within 302 years (**Figure 5A**). The transition time required to go from "no lake" to "overflow conditions" decreases with increasing precipitation to, for example, 39 years (TS+5% = 11.5%) and 21 years (TS+10% = 16.5%), as indicated by stars in **Figure 5A**.

The water flux from one basin to the next basin increases linearly as soon as the overflow threshold of each basin is reached (**Figure 5B**). For example, the water flux from Lake Chamo to paleo-lake Chew Bahir increases starting from zero when precipitation is enhanced by 1.1%, and rises up to 3.9 km^3 a^{-1} when precipitation is 16.5% higher than today.

The calculated inflow ratio for paleo-lake Chew Bahir describes the ratio between the annual water derived by precipitation within the catchment and the inflow from Lake Chamo (**Figure 5C**). The inflow ratio quantifies the high importance of the extended catchment of Lake Abaya and Lake Chamo for the water balance of paleo-lake Chew Bahir. The inflow ratio of Chew Bahir increases starting from 0 to 1.1% enhanced precipitation and reaches 6.3% when precipitation enhances to the threshold precipitation (TS = 6.5%) for overflow conditions.

Seasonality Changes Results

The difference in annual evaporation on land of 167.6 mm for the paleo-lake Chew Bahir catchment that we assessed needs to be considered to compensate for the additional rainy months from June to September according to the SEBAL processing. This difference in annual evaporation on land results in an increased threshold to achieve the transition from "no lake" to "overflow conditions." When considering a third rainy season to have been active during the AHP, the threshold precipitation to fill paleo-lake Chew Bahir up to its overflow level would have increased

FIGURE 4 | SEBAL results for paleo-lake Chew Bahir catchment: **(A)** Map of actual evaporation distribution throughout the catchment. **(B)** Monthly precipitation and monthly water balance of the Chew Bahir catchment.

FIGURE 5 | The effects of precipitation increase on the investigated lake basins: **(A)** Transition times of paleo-lake Chew Bahir from "no lake" to "overflowing lake" into Lake Turkana under minimum threshold (TS) conditions where seasonality has not changed; under the consideration of an additional rainy season caused by a shift of the location of the Congo Air Boundary (TS$_{CAB}$); and the incorporation of theoretically vegetation feedback (TS$_{VEG}$) with values taken from Bergner et al. (2003), since no local paleo-data are available. The graph shows the increasing pace of lake level rise with increasing precipitation. **(B)** Water mass exchange between the three investigated basins for the scenarios, TS and TS$_{CAB}$. **(C)** Precipitation and overflowing Lake Chamo-Abaya as relative water sources of paleo-lake Chew Bahir showing the importance of an enlarged catchment of Chew Bahir during overflow times of all lakes. Whereas, under TS conditions Chew Bahir inflow ratio is at 6.3%, the inflow doubles up to 12.7% when considering an additional rainy season.

by 6.9% (TS$_{CAB}$ = TS+6.9% = 13.4%) compared to the modern day precipitation amount (**Figures 5A,C**). The consideration of a changing vegetation on the evaporation and the resulting necessity of an increased precipitation is 7–15%, as suggested

by Bergner et al. (2003). This leads to a combined threshold TS$_{VEG}$ of 20.6 to 28.6% (TS$_{VEG}$ = TS+TS$_{CAB}$+ 7–15% = 20.6–28.6%; 20–30% rounded) compared to the modern day annual precipitation (**Figures 5A,C**).

AHP Transition Times Results

For abrupt "lake fill" scenarios (**Figure 6A**), the lake filling curve using the minimum precipitation amount of 13.4% (TS_{CAB}) required to fill paleo-lake Chew Bahir up its overflow sill, leads to a slow, around 300 years, asymptotic reaction of the lake surface level over time as soon as paleo-lake Chew Bahir derives a constant water flux from Lake Chamo. Whereas, an increase of the precipitation amount for example by 5% (TS_{CAB}+5%) or 10% (TS_{CAB}+10%) above the threshold (TS_{CAB}) leads to a fast transition of paleo-lake Chew Bahir from "no lake" to "overflow conditions" within 30 and 22 years, respectively. Lake Abaya and Lake Chamo, however, are showing for all simulated precipitation signals decadal to sub-decadal transition times.

For gradual "lake fill" scenarios (**Figure 6B**) within 50, 100, 250, and 500 years from the modern day precipitation amount to the threshold, the same asymptotic lake surface level reaction pattern in time is identified, but it is delayed through the gradual precipitation signal. This gradual delay factor leads to corresponding centennial transition (>350 years) times. Lake Abaya and Lake Chamo show for all simulated gradual

"lake fill" scenarios filling times between 40–160 and 50–180 years, respectively.

We simulated abrupt "lake drain" scenarios (**Figure 6C**) starting with lakes at their specific overflow sill: Lake Abaya at +18 m, Lake Chamo at +14 m, and paleo-lake Chew Bahir at +45 m above the modern day lake surface levels. For this scenario paleo-lake Chew Bahir would have been dried out within 45 years, whereas Lake Chamo and Lake Abaya would need more than 100 years to reach their new equilibrium state.

The simulation of gradual "lake drain" scenarios within 50, 100, 250, or 500 years to modern day conditions leads to delayed transition times of paleo-lake Chew Bahir from 70 up to 370 years before drying up (**Figure 6D**). Under gradual precipitation decrease Lake Abaya dries up between 170 and >500 years, and Lake Chamo takes the longest with 370 to >500 years.

Amplifier Lake Characteristic Results

Following the main principles for amplifier lake characterization (HI 0.23–0.3; Olaka et al., 2010; **Figure 7**), Chew Bahir (HI: 0.23, AI: 0.83) and Abaya (HI: 0.25, AI: 1.72) can be characterized as amplifier lakes. Chew Bahir is with an AI < 1 characterized as a

FIGURE 6 | Modeled pace of lake transitions under abrupt and gradual precipitation changes: **(A)** Abrupt increase in precipitation from modern values to TS_{CAB} values (13.4%) as a minimum possible amount of rainfall to fill up the investigated lake basins. TS_{CAB} +5% and TS_{CAB} +10% are provided as examples for even higher precipitation that was provided during the AHP, for example. **(B)** Lake fill scenario under gradual increase in precipitation from modern values to TS_{CAB} values over 50, 100, 250, and 500 years. **(C)** Abrupt decrease in precipitation from TS_{CAB} to modern values. **(D)** Lake regression scenario under gradual decrease in precipitation from TS_{CAB} to modern values over 50, 100, 250, and 500 years.

FIGURE 7 | The characterization of amplifier lakes: Hypsometric integral (HI) and Aridity Index (AI) of major lake basins within the EARS as published by Olaka et al. (2010) including new calculated values of paleo-lake Chew Bahir, Lake Abaya, and Lake Chamo (in yellow) from this study. Amplification of precipitation changes occurs in lakes with HI of 0.23–0.3 according to Olaka et al. (2010). We postulate that AI has changed in the course of climatic changes and thus amplification influences, such as groundwater and precipitation.

lake with slightly higher potential evaporation than precipitation, whereas Abaya is the wettest of all investigated basins with AI>1 (**Figure 7**). Lake Chamo (HI: 0.15, AI: 1.33) cannot be considered as an amplifier lake.

DISCUSSION

Advantages and Limitation of the LBM
Paleo-Precipitation Estimates
The results from the hydro-balance modeling show that a surplus in precipitation of 20–30% compared to present day values is required to fill the presently dry paleo-lake Chew Bahir to its overflow sill at 545 m a.s.l. and a depth of ~45 m, resulting in a ~2,500 km^2 large freshwater lake. These final estimates are the result of three different assumptions: (1) TS of +6.5% accounts for the minimum precipitation required to fill paleo-lake Chew Bahir to its overflow level (classical hydro-balance approach), (2) TS_{CAB} equals the sum of TS+6.9% to include extra precipitation outside the current rainy season from the theoretical shift of the CAB over the rift region during the AHP as suggested by previous studies (e.g., Junginger, 2011; Costa et al., 2014; Junginger et al., 2014; Bloszies et al., 2015; Beck et al., 2019), and (3) TS_{VEG} equals the sum TS+TS_{CAB} +7–15% precipitation to include the impact of vegetation feedback (**Figure 5**). Vegetation feedback, which increases transpiration and thus precipitation was approximated in our model, based on biosphere-feedback modeling results (7–15%; Bergner et al., 2003) from the nearby Lake Naivasha basin

in the central Kenya rift, due to a lack of direct paleo-vegetation data. Numerous studies from eastern Africa strongly suggest a pronounced vegetation change between the AHP and today (e.g., Lamb et al., 2004; Vincens et al., 2005; Umer et al., 2007; Rucina et al., 2009; Marchant et al., 2018) and that vegetation feedback played an important role in precipitation (e.g., Claussen et al., 2017). However, local and regional information during the AHP (e.g., pollen, non-pollen palynomorphs, charcoal or phytoliths from sediments) are currently lacking and would help refine estimates of paleo-precipitation changes due to vegetation feedback, allowing for improved estimations of past hydrological budgets in southern Ethiopia.

Our modeling results of precipitation increase (20–30%) for paleo-lake Chew Bahir are of the same order of magnitude as results for similar studies within the EARS during the AHP (**Figure 1**), such as Ziway–Shala (+28%, Gillespie et al., 1983), Lake Turkana (+20%, Hastenrath and Kutzbach, 1983), Suguta Valley (+26%, Junginger and Trauth, 2013), Lake Nakuru–Elmenteita (+23–45%%, Dühnforth et al., 2006; Kniess, 2006), and Lake Naivasha (+29–33%, Hastenrath and Kutzbach, 1983; Bergner et al., 2003). However, almost all results stem from different modeling approaches. None of the previous models have considered hydrological connectivity or the impact on evaporation (ET_a) due to a third rainy season. The latter would have had especially affected the catchments of Lake Turkana, Lake Nakuru-Elmenteita, Lake Naivasha and paleo-Lake Suguta, as they most likely experienced a precipitation increase due to the

change in the position of the CAB during the AHP (Junginger et al., 2014). We therefore propose that lake catchments and LBM results in the EARS under the potential influence of the CAB during the AHP would require additional increased precipitation.

Another important aspect in hydrological modeling of eastern African rift lakes is the inclusion of basin surface connectivity in major humid periods (**Figure 1**). Paleo-lake Chew Bahir received 15–25% of its additional water during the AHP from overflowing lakes Abaya and Chamo via the Segan River. Such hydrological connectivity during the AHP almost doubled the catchment size of Chew Bahir from 20,650 to 38,647 km^2 (**Figure 2**). However, hydrological basin connectivity was likely intermittent, only occurring during strong humid phases (**Figure 8**). Intermittent connectivity during high-stands could have been caused by short-term abrupt changes in the position of the CAB and associated temporal cut offs from the surplus of water. Such intermittent surficial hydrological connectivity is likely relevant for all EARS lakes in the mid and lower altitudes, such as lakes Abhé, Turkana, Suguta, Baringo-Bogoria, Magadi, and Manyara (**Figure 1E**).

The water balance has varied due to increased precipitation and changes in other environmental parameters (e.g., as mentioned in **Table 1**) which influence the inflows and outflows into the basin. It is difficult to quantify these parameters (e.g., cloud cover, wind speed, and relative humidity) during the AHP. Proxy record reconstructions over the AHP however, can provide some insights. The GDGT based temperature reconstruction for eastern Africa by Loomis et al. (2012) reveals a colder climate at the beginning of the AHP at around 15 ka BP and a climate which was up to 3°C between 12 and 5 ka BP. Based on our sensitivity analysis for environmental parameters (section Lake Balance Model), an increase of around three Kelvin could increase the actual evaporation by up to 14%. A decrease in temperature of three Kelvin could lower the evaporation by the same amount. In terms of the resulting precipitation estimates, the early AHP with a slightly colder climate would need a slightly lower precipitation amount to reach a positive water budget, whereas the late phase of the AHP would need a slight higher precipitation amount to reach a positive water budget.

In summary, our study reveals the same magnitude of precipitation increase (+20–30% of modern day) in eastern Africa for the AHP as most other studies, but separates this threshold into parts. Those parts would need to be added (precipitation during modern day dry months) or subtracted (paleo hydrological connectivity) for other lake basins within the EARS, but can only be quantified in a site specific manner.

### Evaporation Estimates Discussion
We compensated the lack of ground measured climate data by using remote sensing MODIS products, modeled climate data and calculated the actual evaporation additionally through SEBAL. This algorithm as proposed by Bastiaanssen et al. (1998a,b) has been applied in numerous variations depending on the data, landscapes and research designs. Studies showed inaccuracy of SEBAL at a field-scale and suggested to use METRIC or SEBS instead (e.g., Losgedaragh and Rahimzadegan,

2018). Mkhwanazi et al. (2015) implemented advective conditions within the SEBAL for crop evaporation studies on a field-scale, because the algorithm underestimate actual evaporation with a mean bias Error of 17.1%. SEBAL for catchment-scale studies instead showed an accuracy above 95% (Bastiaanssen et al., 2005). A 3 years SEBAL application in Tanzania and Kenya with a comparable research design as our application achieved a difference between the SEBAL results and the water balance of the catchment of 12%. For a SEBAL application in the Suguta Valley the SEBAL ET_a is 5% lower than the bulk transfer calculated ET_a of the LBM (Borchardt and Trauth, 2012; Junginger and Trauth, 2013).

The evaporation estimates of the SEBAL, the bulk-transfer formula and the pan-evaporation measurement have been compared and vary between 5 and 18.7%. This means the input water fluxes for the LBM could vary at the same magnitude. But those fluxes are not independent, instead the modern day water budget for each year is in balance. An increase in ET_a on land would necessarily imply, ET_a on water or the groundwater recharge rate is overestimated. The same yields for the sensitivity analysis of the bulk-transfer derived ET_a. The variation of the evaporation rate depending on the environmental parameters shows possible inter-annual variability and possible micro-climate caused differences within the catchment. This spatial variety is mapped by SEBAL. However, besides the sensitivity, spatial variety and inter-annual variability, the accuracy of each multi-annual average water flux rate is due to the multi-method verification and the closed water balance of each catchment with an definite error below 20%. The different subdivisions of precipitation within each catchment between ET_a on water and land affects the paleo-precipitation threshold in approximately one-tenth of the maximum deviation between ET_a on water and land. This leads to a robust error of the threshold of 2% and an overall paleo-precipitation threshold for paleo-lake Chew Bahir of plus 20–30% precipitation in a multi-annual average compared to the modern day conditions.

Subsurface Flows Discussion
Endorheic basins, and their subsequent lakes, can be classified into three groups; (1) flow-through lakes, (2) discharge lakes, and (3) recharge lakes (e.g., Olaka, 2011 and references therein). Flow-through lakes are balanced ($S_{bas} = 0$). Discharge lakes are positively affected by groundwater flowing into the lake ($S_{bas} > 0$) and recharge lakes lake water seeps into the groundwater ($S_{bas} < 0$). During the AHP, when the overall moisture availability in the atmosphere was much higher and lake levels rose, changes in the groundwater levels may have changed the classification and status of the basin. Changes in groundwater inflows and outflows, would have subsequent impacts on the overall lake water balance. For example, groundwater discharge into lake basins could reduce their sensitivity to reduced precipitation input in short-term dry periods and potentially delay lake desiccation in protracted dry phases. This is a possible mechanism to explain why extremely arid catchments, such as paleo-Lake Suguta or Lake Nakuru-Elementeita, developed and maintained paleo-lakes which were 10–300 m deeper than today (Olaka et al.,
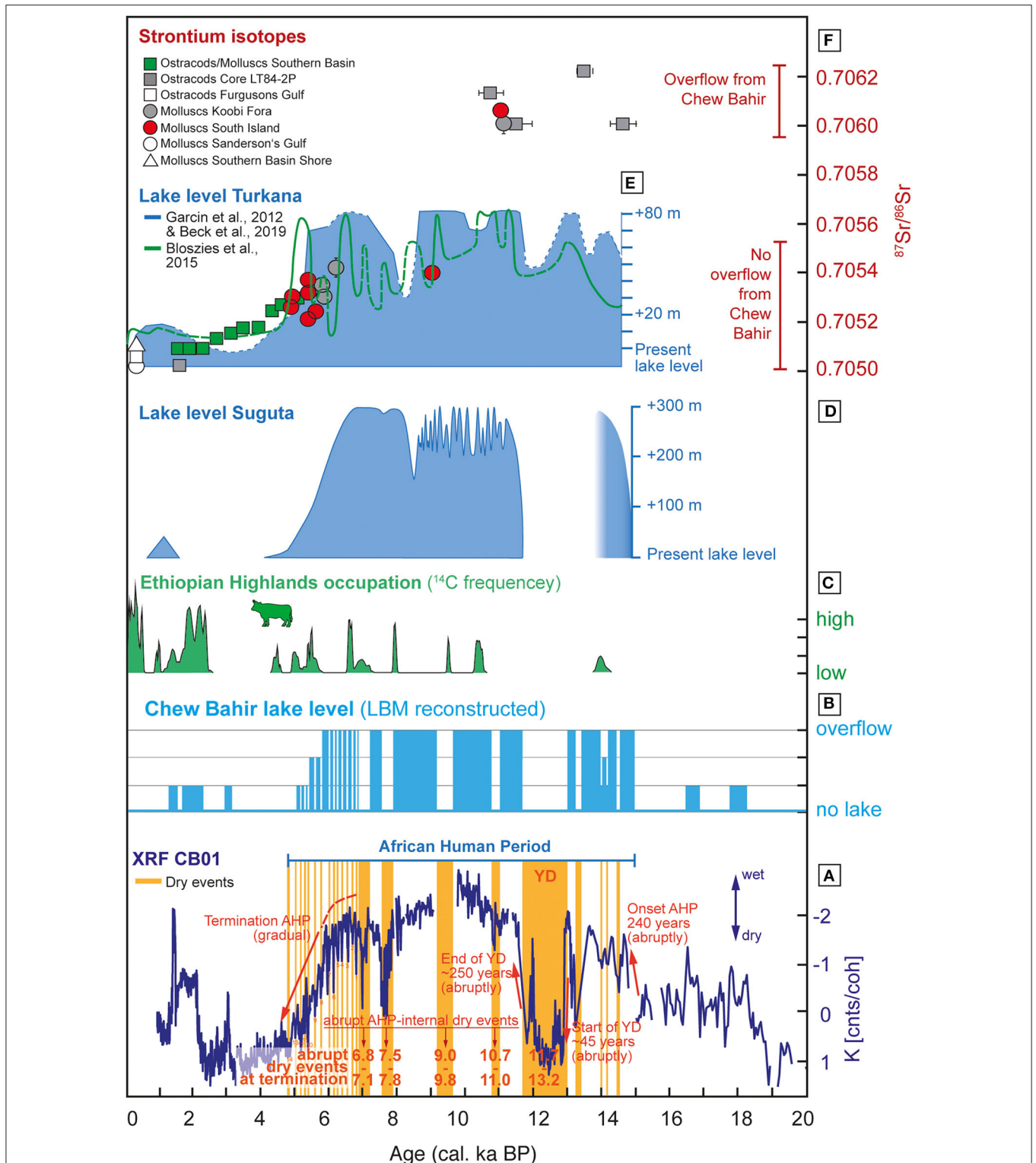
FIGURE 8 | Chew Bahir LBM-based paleo-lake level reconstruction and comparison to adjacent lakes: **(A)** CB01 K proxy-record by Foerster et al. (2015) with dry events discussed in the text and transition modes. **(B)** Reconstructed lake level curve of Chew Bahir based on the lake-balance model (LBM) applied to changes in the K concentration of CB01. **(C)** Human occupation history of the Ethiopian highlands implies enhanced activities when lakes in the lower elevated rift basins, such as paleo-lake Chew Bahir became to saline or even dried up. The Ethiopian highlands may thus have been a refuge area during unfavorable times as Foerster et al. (2015) suggested. Cow indicates cultural transition from fishing/hunting/gathering to herding in the Ethiopian Highlands. **(D)** Lake level reconstruction of Suguta Valley (Junginger et al., 2014) as the mirror basin of Chew Bahir. **(E)** Lake level reconstruction of Lake Turkana by Garcin et al. (2012) and Beck et al. (2019) (blue, shaded curve), and by Bloszies et al. (2015) (green). **(F)** Strontium isotopes measured on aquatic fossils from lake Turkana sediments (van der Lubbe et al., 2017).

2010). For example, Olaka (2011) estimated response times of 2–2.7 ka for groundwater to drain a 41 km³ large aquifer underneath the Eburro volcano complex located between Lake Naivasha and Lake Nakuru in the central Kenya Rift (**Figure 1**). Unfortunately, the southern MER lack this kind of information, despite preliminary evidence of significant groundwater aquifers in the central part of the Ethiopian rift (Kebede and Travi, 2012).

In terms of the groundwater recharge rate and the subsequent effect on the paleo-precipitation threshold for the African Humid Period, we parameterised the groundwater recharge rate as the surplus of the water balance budget, which is in contrast to previous LBM studies (see section Lake Balance of Lakes Abaya, Chamo, and Paleo-Lake Chew Bahir). Based on Chernet (1993) recharge rates between 50 and 150 mm a^{-1} are typical, which would be ~5–15% of the annual precipitation within the Chew Bahir catchment. We calculated a groundwater recharge rate of 24 mm a^{-1} using the LBM and 69 mm a^{-1} using SEBAL. These comparisons show the possible errors of our modeling results due to this uncertainty, which are a quantity smaller than the annual fluxes in precipitation and evaporation (Dühnforth et al., 2006).

Lake Response Times Discussion
Amplifier Lake Characteristics
Olaka et al. (2010) postulated that amplifier lakes, where AI < 1 (ET$_p$ > P), likely received greater groundwater or surface inputs during the AHP, in order to maintain expansive lake systems in semiarid to arid regions in the EARS. In contrast, lakes with AI > 1 (ET$_p$ < P), which are prevalent on the high plateaus of the rift margins and Ethiopian Domes (**Figure 1**), are and were during the AHP amplified through precipitation. However, these calculations are based on present day conditions and may be irrelevant in a paleo context where P and ET$_p$ would have been vastly different, and consequently the AI. We expect in a paleo context, that the position of the AI for the respective paleo lakes would likely shift vertically along the y-axes of **Figure 7** over time periods of 10–10,000 years. Based on our LBM, for example, the rate of groundwater feeding paleo-lake Chew Bahir today remains smaller than the rate of groundwater discharge within the catchment and is furthermore a magnitude smaller than the water mass exchange rates due to precipitation, evaporation and surface basin connectivity. However, the groundwater system could act as a millennial-scale buffer, which is recharged during major humid periods may slow the transition to lake desiccation in drier periods (e.g., Garcin et al., 2009; Olaka, 2011).

Although Lake Chamo is not characterized as an amplifier lake, it can receive additional surface inflows from Lake Abaya, due to the very shallow overflow between the two lakes (**Figures 1**, **2**). Due to the extremely shallow overflow sill of Lake Abaya toward Lake Chamo and toward paleo-lake Chew Bahir, we hypothesize that even sub-decadal precipitation shifts may have triggered overflow to the paleo-lake Chew Bahir basin, and thus would have caused abrupt changes in the water budget of paleo-lake Chew Bahir. It is therefore highly likely that paleo-lake Chew Bahir was able to change during the AHP from a fresh-water lake to a desert within only a couple of decades. Such sensitivity to even moderate climate changes makes the paleo-lake Chew Bahir basin responsive to even sub-decadal

climate fluctuations in contrast to, for example the Suguta Valley, which has a greater buffering capacity to short-term variability in precipitation, due to its larger size and depth of the paleo-lake (paleo-lake depth of 295 m), and higher overflow sill (**Figures 1**, **8**).

We understand paleo-lake Chew Bahir as a double amplifier lake, pronouncing the unique and high sensitivity of the landscape and lakes water-level reaction to precipitation signals. This is due to (1) the classification of its catchment as an amplifier lake (**Figure 1**) and (2) the importance of the catchment of lakes Chamo and Abaya for the paleo water balance of paleo-lake Chew Bahir. This expansion of paleo-lake Chew Bahirs catchment in case of over-spilling lakes Abaya and Chamo into the Chew Bahir basin amplifies the lakes reaction to precipitation changes and causes rapid filling if there is a significant water drain, or rapid draining if this hydrological connectivity gets cut off.

Pace and Magnitude of Lake Level Changes
In a previous study by Trauth et al. (2018) a change point analysis was applied to the aridity proxy K-record by Foerster et al. (2012, 2015) to investigate the timing and duration of climatic changes. Our study now is able to add the character and magnitude of lake level changes and thus allows to infer direct implications to biosphere impacts.

Trauth et al. (2018) stated that the most dramatic changes occurred during the onset of the AHP and the interruption by the Younger Dryas (YD), a global cold event, known as a pronounced dry episode in eastern Africa (e.g., Barker et al., 2004). The onset of the AHP in the Chew Bahir basin, so Trauth et al. (2018), occurred within ~240 years (15.7–15.46 ka BP). Within such period of time, paleo-lake Chew Bahir would have been able to reach the overflow sill toward Lake Turkana (**Figures 1**, **8**). The extreme arid interval in Chew Bahir between 13.2 and 11.73 ka BP, largely coinciding with the YD chronozone, shows abrupt changes in the K- record. Those were presumably expressed in an abrupt lake level drop (within 45 years) and lake level rise (within 250 years) in Chew Bahir. After the return to full humid conditions, the AHP main phase was interrupted by four dry spells at 11–10.7, 9.8–9.0, 7.8–7.5 and 7.1–6.8 ka BP. Those dry events are also reflected in records from lakes Turkana and paleo-lake Suguta (**Figure 8**), Mount Kilimanjaro (Thompson et al., 2002), Arabia (Fleitmann et al., 2003), as well as marine records off the NE coast of Africa (e.g., Gupta et al., 2003). Most of these dry episodes have lasted around 300 years. We expect, from a modeling perspective, these dry spells to have been long enough to desiccate paleo-lake Chew Bahir completely.

Trauth et al. (2018) highlights fourteen 20–80 years lasting dry events within the K-proxy record during the overall gradual termination of the AHP. According to our LBM, decadal dry events of 40 years or longer were able to dry up the Chew Bahir basin completely. Dry periods of 40 years or shorter still caused a considerable reduction in lake level though not a complete desiccation (**Figure 8**). Over the entire length of the AHP termination, Chew Bahir appears to have been under severe desiccation pressure. Such rainfall variability was also recorded in stalagmites in the near-by south-eastern rift shoulders of

Ethiopia during times of a progressively drier climate (Baker et al., 2010). However, short-term precipitation changes may have filled lakes Abaya and Chamo up to their shallow overflow sills and provided Chew Bahir every now and then with enough water to delay the drying up process. The short-term flickers at the end of the AHP suggest, that paleo-lake Chew Bahir had not enough time between those flickers to have reached the overflow sill again. This assumption is supported by the finding of van der Lubbe et al. (2017), who used strontium isotopes as a water provenance proxy over the AHP and found no indication of a contribution of Chew Bahir water after 6 ka into Lake Turkana (**Figure 8F**).

The recent dry period after the termination of the AHP, which has left the Chew Bahir basin dry for most of the time, is interrupted by brief excursions to wetter conditions at 3, 2.2, and 1.3 ka BP (**Figure 8A**). Such a lowering of K concentration in the sediments of paleo-lake Chew Bahir points toward a lake transgression and thus a positive water budget during this time. Based on the results of our LBM, we conclude that even though the duration of these events would have allowed a rise of Chew Bahir's paleolake level, it is unlikely that the lake has reached maximum lake depths during these short-term humid episodes. This conclusion is supported by two arguments: (1) We expect a different climatic forcing mechanism than during the AHP, where a precession minimum caused enhanced humidity and the shift of rain belts over the study region (e.g., Costa et al., 2014; Junginger et al., 2014; Bloszies et al., 2015; Beck et al., 2019). For the past ∼5 ka, for example, short-term changes in sea surface temperatures and associated circulation systems could account for these short-term increases in precipitation (e.g., Nicholson, 2017; Bayon et al., 2019). (2) The second argument against maximum water levels in Chew Bahir is that K concentrations do not reach AHP minima. A clear signal whether our assumption, that lake Chew Bahir has not reached its overflow level, is true may only be proved by poxies that could reflect paelo-water provenance, such as strontium isotopes in aquatic fossils, as van der Lubbe et al. (2017) have shown. In summary, paleo-lake Chew Bahir was a large paleo-lake during the AHP that dried up abruptly at least 19 times within decades resulting in a desert-like rift floor similar to today. Such rapid environmental changes must have had a tremendous impact on the biosphere including humans.

Implications for Human Adaptations

A first attempt of comparing an available archaeological record from hypothesized refuge areas in the region with inferred phases of climatic stress from the Chew Bahir K-proxy record was made by Foerster et al. (2015, 2016) for the last 20 ka. The study used scarce but available radiocarbon frequencies of documented archaeological sites in the lush mountainous regions of SW Ethiopia as a possible indicator for changes in settlement activities in the highlands during dry periods in the lowlands, which are indicated by high K content in the drill core sediments of Chew Bahir (note inverse scale, **Figure 8**). Even though age model uncertainties, the indefinite incompleteness and natural biases in the archaeological record naturally constrain the possibility to directly correlate climatic

and archaeological data sets (see Foerster et al., 2015, 2016) and references therein), the patterns found in the comparative study are a valuable starting point to indirectly infer shifts in human settlement activity, bearing the role of external factors in mind. The results tentatively suggest that both, long and short-term climatic change could have affected settlement patterns and cultural innovation differently, though the factor of human decision-making within environmental boundaries played an important but further incalculable role (Foerster et al., 2015).

On the one hand, short-term episodes of pronounced aridity in the lower elevated lake basins, such as Chew Bahir could have been a push-factor for a refugium-directed vertical movement of groups with highly mobile hunter-gatherers (**Figure 8C**). A now further specified variable is the climatic component in this comparison as shown in our study. The Southern Ethiopian Rift has responded sensitively to even shorter dry spells, so that living conditions would have deteriorated quickly when the rift floor became too dry. One of the reasons why hunter-gatherers might have returned to the South Ethiopian Rift region after such dry spells, could have been their dietary style at that time, that was mainly devoted to fishing (e.g., Owen et al., 1982; Hildebrand et al., 2018). The long-term transitions, on the other hand, driven by changes in orbital controlled insolation, could have fueled cultural adaptation and significant changes in the social organization within groups. Only after the gradual end of the AHP with the near-desiccation of almost all lakes in the Kenyan and Ethiopian rift over a longer period (>1,000 years), a cultural transition from hunter-gathering to pastoralism occurred (e.g., Marshall and Hildebrand, 2002; Garcin et al., 2012; Lesur et al., 2014). The change from fishing to herding seems to have been a dynamic process, since the introduction of cattle was catalyzed by the immigration of herders that were escaping the progressively drying Sahara region, where pastoralism had been introduced much earlier (e.g., Kuper and Kröpelin, 2006; Hildebrand and Grillo, 2012). The dried up lake beds and former lake margins could have provided new land and grazing grounds for this new life style, which also made people independent from fishing (e.g., Garcin et al., 2012).

Trauth et al. (2010) introduced the theoretical concept of allopatric speciation through precession forced long-term (>10,000 years) population separation and remixing within the EARS due to appearing and disappearing rift lakes. Based on our study results, the Chew Bahir, Abaya, and Chamo basins can be excluded from this concept, due to their extreme sensitive amplifier lake characteristics. We expect, from a modeling perspective, that these lakes reacted on much shorter time scales (<100 a), suggesting that intensive adaption was required from humans living at the lakes margins (cultural buffering; Galway-Witham et al., 2019). One of those adaptive strategies could have been short-term migration, either vertically to the nearby more humid higher elevated grounds (Foerster et al., 2015; Ossendorf et al., 2019) or longitudinally and latitudinally to lake or river refugia that were not affected by the dry spells. Both would have contributed to a periodic cultural and genetic exchange, which is thought to be one of the key drivers in cultural innovation and, on longer time scales, evolution (Lahr and Foley, 1998;

Scerri et al., 2018; Galway-Witham et al., 2019), with innovations being generally favored by the exchange of cultural information (Ackermann et al., 2016).

CONCLUSION

We developed a comprehensive Lake Balance Model (LBM) for the southern Ethiopian rift with focus on paleo-lake Chew Bahir and its catchment as a first contribution to better understand the potential response of paleo-lake Chew Bahir to precipitation changes. We conclude that the following paleo-precipitation estimates would have been necessary to fill paleo-lake Chew Bahir until its overflow level: (1) the classic LBM approach resulted in a 6.5% (TS) precipitation increase, (2) the addition of a third rainy season in the region from July to September would cause a 6.9% (TS$_{CAB}$) increase, leading to a total of TS+TS$_{CAB}$ = 13.4%. (3) The inclusion of vegetation feedback of +7–15%, resulted in an additional precipitation, which sums up to a robust estimate of ~20–30% increased precipitation compared to the modern day amount for the paleo-lake Chew Bahir during the African Humid Period. We furthermore determined the amplifier lake characteristics of Lakes Abaya (HI = 0.25, AI = 1.72), Chamo (HI = 0.15, AI = 1.33) and Chew Bahir (HI = 0.23, AI = 0.83). We found that the sensitivity of lake levels is greatly increased during periods of high humidity due to overflowing lakes along the EARS axis and enhanced surface flow. Such additional water resources should be taken into account in the analysis of the paleo-hydrology of other lakes in the EARS when abrupt or gradual changes in the proxies are observed. Accordingly, we implemented all additional factors in our new LBM and were able to calculate lake level response times to abrupt and gradual precipitation changes and characterize lake level changes from K-proxy changes in a drill core from Chew Bahir. Based on our LBM results, we can now support the proposed abruptness of the onset of the AHP in southern Ethiopia by Trauth et al. (2018), similar to the beginning and end of the millennial-scale dry episode during the Younger Dryas. The results of our LBM furthermore support the gradual termination of the AHP, with the model indicating that the reported 20–80 years lasting dry events that are punctuating the termination could have been able to dry up the paleo-lake completely, when caused by abrupt precipitation changes.

DATA AVAILABILITY STATEMENT

The hydro-balance model coded in R is available at GitHub (https://github.com/MLFischer/Lake-Balance-Model, 03/2019).

AUTHOR CONTRIBUTIONS

This study was designed and financed by AJ and MF. MF developed and performed the final LBM. MM, FB, VF, MT, and AJ contributed the data and analysis tools. All authors contributed to the article and approved the submitted version.

REFERENCES

Ackermann, R. R., Mackay, A., and Arnold, M. L. (2016). The hybrid origin of "modern" humans. *Evol. Biol.* 43, 1–11. doi: 10.1007/s11692-015-9348-1

Allen, R. G., Tasumi, M., Morse, A., Trezza, R., Wright, J. L., Bastiaanssen, W., et al. (2007). Satellite-based energy balance for mapping evapotranspiration with internalized calibration (METRIC)—applications. *J. Irrig. Drainage Eng.* 133, 395–406. doi: 10.1061/(ASCE)0733-9437(2007)133:4(395)

Asrat, A., Baker, A., Mohammed, M. U., Leng, M. J., Calsteren, P. V., and Smith, C. (2007). A high-resolution multi-proxy stalagmite record from Mechara, Southeastern Ethiopia: palaeohydrological implications for speleothem palaeoclimate reconstruction. *J. Quat. Sci.* 22, 53–63. doi: 10.1002/jqs.1013

Awulachew, S. B. (2006). Investigation of physical and bathymetric characteristics of Lakes Abaya and chamo, Ethiopia, and their management implications. *Lakes Reserv. Res. Manag.* 11, 133–140. doi: 10.1111/j.1440-1770.2006.00300.x

Bachofer, F., Quénéhervé, G., Maerker, M., and Hochschild, V. (2015). Comparison of SVM and boosted regression trees for the delineation of lacustrine sediments using multispectral ASTER data and topographic indices in the Lake

Manyara basin. *Photogrammetrie-Fernerkundung-Geoinformation* 2015, 81–94. doi: 10.1127/pfg/2015/0251

Baker, A., Asrat, A., Fairchild, I. J., Leng, M. J., Thomas, L., Widmann, M., et al. (2010). Decadal-scale rainfall variability in Ethiopia recorded in an annually laminated, holocene-age, stalagmite. *Holocene* 20, 827–836. doi: 10.1177/0959683610365934

Barker, P. A., Talbot, M. R., Street-Perrott, F. A., Marret, F., Scourse, J., Odada, E. O. (2004). "Late Quaternary climatic variability in intertropical Africa," in *Past Climate Variability through Europe and Africa, Developments in Paleoenvironmental Research*, vol. 6. eds R. W. Battarbee, F. Gasse, C. E. Stickley (Dordrecht: Springer), 117–138. doi: 10.1007/978-1-4020-2121-3_7

Bastiaanssen, W. G. (2000). SEBAL-based sensible and latent heat fluxes in the irrigated Gediz Basin, Turkey. *J. Hydrol.* 229, 87–100. doi: 10.1016/S0022-1694(99)00202-4

Bastiaanssen, W. G., Menenti, M., Feddes, R. A., and Holtslag, A. A. M. (1998a). A remote sensing surface energy balance algorithm for land (SEBAL). 1. Formulation. *J. Hydrol.* 212, 198–212. doi: 10.1016/S0022-1694(98)00253-4

Bastiaanssen, W. G., Pelgrum, H., Wang, J., Ma, Y., Moreno, J. F., Roerink, G. J., et al. (1998b). A remote sensing surface energy balance algorithm for land (SEBAL).: Part 2: validation. *J. Hydrol.* 212, 213–229. doi: 10.1016/S0022-1694(98)00254-6

Bastiaanssen, W. G. M., Noordman, E. J. M., Pelgrum, H., Davids, G., Thoreson, B. P., and Allen, R. G. (2005). SEBAL model with remotely sensed data to improve water-resources management under actual field conditions. *J. Irrig. Drainage Eng.* 131, 85–93. doi: 10.1061/(ASCE)0733-9437(2005)131:1(85)

Bayon, G., Schefuß, E., Dupont, L., Borges, A. V., Dennielou, B., Lambert, T., et al. (2019). The roles of climate and human land-use in the late Holocene rainforest crisis of Central Africa. *Earth Planet. Sci. Lett.* 505, 30–41. doi: 10.1016/j.epsl.2018.10.016

Beck, C. C., Feibel, C. S., Wright, J. D., and Mortlock, R. A. (2019). Onset of the African humid period by 13.9 kyr BP at kabua gorge, turkana Basin, Kenya. *Holocene* 29, 1011–1019. doi: 10.1177/0959683619831415

Belete, A. (2009). *Climate change impact on lake abaya water level* (M.Sc. thesis), Addis Ababa University, Ethiopia. Available online at: http://etd.aau.edu.~et/dspace/bitstream/123456789/2635/1/17730248189668230838464212617211563806

Berger, A., and Loutre, M. F. (1991). Insolation values for the climate of the last 10 million years. *Quat. Sci. Rev.* 10, 297–317. doi: 10.1016/0277-3791(91)90033-Q

Bergner, A. G., Trauth, M. H., and Bookhagen, B. (2003). Paleoprecipitation estimates for the Lake Naivasha basin (Kenya) during the last 175 ky using a lake-balance model. *Global Planet Change.* 36, 117–136. doi: 10.1016/S0921-8181(02)00178-9

Berke, M. A., Johnson, T. C., Werne, J. P., Grice, K., Schouten, S., and Damsté, J. S. S. (2012b). Molecular records of climate variability and vegetation response since the late pleistocene in the lake victoria basin, East Africa. *Quat. Sci. Rev.* 55, 59–74. doi: 10.1016/j.quascirev.2012.08.014

Berke, M. A., Johnson, T. C., Werne, J. P., Schouten, S., and Damsté, J. S. S. (2012a). A mid-Holocene thermal maximum at the end of the African Humid Period. *Earth Planet. Sci. Lett.* 351–352, 95–104. doi: 10.1016/j.epsl.2012.07.008

Blodgett, T. A., Isacks, B. L., and Lenters, J. D. (1997). Constraints on the origin of paleolake expansions in the central andes. *Earth Interact.* 1, 1–28.doi: 10.1175/1087-3562(1997)001<0001:COTOOP>2.3.CO;2

Bloszies, C., Forman, S. L., and Wright, D. K. (2015). Water level history for lake turkana, Kenya in the past 15,000 years and a variable transition from the African humid period to holocene aridity. *Glob. Planet. Change.* 132, 64–76. doi: 10.1016/j.gloplacha.2015.06.006

Bookhagen, B. (in review). *High resolution spatiotemporal distribution of rainfall seasonality and extreme events based on a 12-year TRMM time series, in review. [Data set]* Available online at: http://www.geog.ucsb.edu/~bodo/TRMM/ (accessed Agust 1, 2018).

Bookhagen, B., Haselton, K., and Trauth, M. H. (2001). Hydrological modelling of a pleistocene landslide-dammed lake in the santa maria basin, NW Argentina. *Palaeogeogr. Palaeoclimatol. Palaeoecol.* 169, 113–127. doi: 10.1016/S0031-0182(01)00221-8

Borchardt, S., and Trauth, M. H. (2012). Remotely-sensed evapotranspiration estimates for an improved hydrological modeling of the early holocene mega-lake suguta, northern Kenya Rift. *Palaeogeogr. Palaeoclimatol. Palaeoecol.* 361, 14–20. doi: 10.1016/j.palaeo.2012.07.009

Brooks, N. (2006). Cultural responses to aridity in the middle holocene and increased social complexity. *Quat. Int.* 151, 29–49. doi: 10.1016/j.quaint.2006.01.013

Brutsaert, W. (1982). *Evaporation Into the Atmosphere: Theory, History, and Applications.* Dordrecht: Reidel.

Camberlin, P. (1997). Rainfall anomalies in the source region of the Nile and their connection with the Indian summer monsoon. *J. Clim.* 10, 1380–1392. doi: 10.1175/1520-0442(1997)010<1380:RAITSR>2.0.CO;2

Chalié, F., and Gasse, F. (2002). Late glacial–holocene diatom record of water chemistry and lake level change from the tropical east african rift lake abiyata (Ethiopia). *Palaeogeogr. Palaeoclimatol. Palaeoecol.* 187, 259–283. doi: 10.1016/S0031-0182(02)00480-7

Chernet, T. (1993). *Hydrogeology of Ethiopia and Water Resources Development.* Addis Ababa: EIGS.

Claussen, M., Dallmeyer, A., and Bader, J. (2017). "Theory and modeling of the African humid period and the green Sahara," in *Oxford Research Encyclopedia of Climate Science*. doi: 10.1093/acrefore/9780190228620.013.532

Collins, J. A., Prange, M., Caley, T., Gimeno, L., Beckmann, B., Mulitza, S., et al. (2017). Rapid termination of the african humid period triggered by northern high-latitude cooling. *Nat. Commun.* 8:1372. doi: 10.1038/s41467-017-01454-y

Costa, K., Russell, J., Konecky, B., and Lamb, H. (2014). Isotopic reconstruction of the african humid period and congo air boundary migration at lake tana, Ethiopia. *Quat. Sci. Rev.* 83, 58–67. doi: 10.1016/j.quascirev.2013.10.031

Damsté, J. S. S., Ossebaar, J., Schouten, S., and Verschuren, D. (2012). Distribution of tetraether lipids in the 25-ka sedimentary record of Lake Challa: extracting reliable TEX86 and MBT/CBT palaeotemperatures from an equatorial African lake. *Quat. Sci. Rev.* 50, 43–54. doi: 10.1016/j.quascirev.2012.07.001

Davidson, A. (1983). The Omo river project, reconnaissance geology and geochemistry of parts of Ilubabor, kefa, gemu gofa and sidamo, Ethiopia. *Ethiop. Inst. Geol. Surv. Bull.* 2, 1–89.

De Bruin, H. A. R., and Stricker, J. N. M. (2000). Evaporation of grass under non-restricted soil moisture conditions. *Hydrol. Sci. J.* 45, 391–406. doi: 10.1080/02626660009492337

Dee, S. G., Russell, J. M., Morrill, C., Chen, Z., and Neary, A. (2018). PRYSM v2.0: a proxy system model for lacustrine archives. *Paleoceanogr. Paleoclimatol.* 33, 1250–1269. doi: 10.1029/2018PA003413

deMenocal, P., Ortiz, J., Guilderson, T., Adkins, J., Sarnthein, M., Baker, L., et al. (2000). Abrupt onset and termination of the African Humid Period: rapid climate responses to gradual insolation forcing. *Quat. Sci. Rev.* 19, 347–361. doi: 10.1016/S0277-3791(99)00081-5

demenocal, P. B. (1995). Plio-pleistocene African climate. *Science* 270, 53–59. doi: 10.1126/science.270.5233.53

Didan, K. (2015). *MOD13Q1 MODIS/Terra Vegetation Indices 16-Day L3 Global 250m SIN Grid V006 [Data set]*. NASA EOSDIS Land Processes DAAC. Available online at: https://doi.org/10.5067/MODIS/MOD13Q1.006 (accessed August 1, 2018).

Drake, N. A., Breeze, P., and Parker, A. (2013). Palaeoclimate in the saharan and arabian deserts during the middle palaeolithic and the potential for hominin dispersals. *Quat. Int.* 300, 48–61. doi: 10.1016/j.quaint.2012.12.018

Dühnforth, M., Bergner, A. G., and Trauth, M. H. (2006). Early holocene water budget of the nakuru-elmenteita basin, central Kenya Rift. *J. Paleolimnol.* 36, 281–294. doi: 10.1007/s10933-006-9003-z

Ebinger, C. J., Yemane, T., Woldegabriel, G., Aronson, J. L., and Walter, R. C. (1993). Late eocene–recent volcanism and faulting in the southern main Ethiopian rift. *J. Geol. Soc.* 150, 99–108. doi: 10.1144/gsjgs.150.1.0099

Evans, M. N., Tolwinski-Ward, S. E., Thompson, D. M., and Anchukaitis, K. J. (2013). Applications of proxy system modeling in high resolution paleoclimatology. *Quat. Sci. Rev.* 76, 16–28. doi: 10.1016/j.quascirev.2013.05.024

Fleitmann, D., Burns, S. J., Mudelsee, M., Neff, U., Kramers, J., Mangini, A., et al. (2003). Holocene forcing of the Indian monsoon recorded in a stalagmite from southern Oman. *science* 300, 1737–1739. doi: 10.1126/science.1083130

Foerster, V., Deocampo, D. M., Asrat, A., Günter, C., Junginger, A., Krämer, K. H., et al. (2018). Towards an understanding of climate proxy formation in the chew bahir basin, southern Ethiopian Rift. *Palaeogeogr. Palaeoclimatol. Palaeoecol.* 501, 111–123. doi: 10.1016/j.palaeo.2018.04.009

Foerster, V., Junginger, A., Langkamp, O., Gebru, T., Asrat, A., Umer, M., et al. (2012). Climatic change recorded in the sediments of the chew bahir basin, southern Ethiopia, during the last 45,000 years. *Quat. Int.* 274, 25–37. doi: 10.1016/j.quaint.2012.06.028

Foerster, V., Vogelsang, R., Junginger, A., Asrat, A., Lamb, H. F., Schaebitz, F., et al. (2015). Environmental change and human occupation of southern Ethiopia and northern Kenya during the last 20,000 years. *Quat. Sci. Rev.* 129, 333–340. doi: 10.1016/j.quascirev.2015.10.026

Foerster, V., Vogelsang, R., Junginger, A., Asrat, A., Lamb, H. F., Schaebitz, F., et al. (2016). Reply to the comment on "Environmental change and human occupation of southern Ethiopia and northern Kenya during the last 20,000 years. Quaternary Science Reviews 129: 333-340". *Quat. Sci. Revi.* 141, 130–133. doi: 10.1016/j.quascirev.2016.04.003

Friedl, M. A., Sulla-Menashe, D., Tan, B., Schneider, A., Ramankutty, N., Sibley, A., et al. (2010). MODIS Collection 5 global land cover: algorithm refinements and characterization of new datasets. *Remote Sens. Environ.* 114, 168–182. doi: 10.1016/j.rse.2009.08.016

Friis, I., Demissew, S., and Breugel, P. V. (2010). Atlas of the potential vegetation of Ethiopia. *Biol. Skrif.* 58, 1–307. doi: 10.1093/aob/mcq242

Funk, C., Dettinger, M. D., Michaelsen, J. C., Verdin, J. P., Brown, M. E., Barlow, M., et al. (2008). Warming of the Indian ocean threatens eastern and southern african food security but could be mitigated by agricultural development. *Proc. Natl. Acad. Sci. U.S.A.* 105, 11081–11086. doi: 10.1073/pnas.0708196105

Galway-Witham, J., Cole, J., and Stringer, C. (2019). Aspects of human physical and behavioural evolution during the last 1 million years. *J. Quat. Sci.* 34, 355–378. doi: 10.1002/jqs.3137

Garcin, Y., Junginger, A., Melnick, D., Olago, D. O., Strecker, M. R., and Trauth, M. H. (2009). Late pleistocene–holocene rise and collapse of lake suguta, northern Kenya Rift. *Quat. Sci. Rev.* 28, 911–925. doi: 10.1016/j.quascirev.2008.12.006

Garcin, Y., Melnick, D., Strecker, M. R., Olago, D., and Tiercelin, J. J. (2012). East African mid-holocene wet–dry transition recorded in palaeo-shorelines of lake turkana, northern Kenya Rift. *Earth Planet. Sci. Lett.* 331, 322–334. doi: 10.1016/j.epsl.2012.03.016

Gasse, E., and Street, F. A. (1978). Late Quaternary lake-level fluctuations and environments of the northern Rift Valley and Afar region (Ethiopia and Djibouti). *Palaeogeogr. Palaeoclimatol. Palaeoecol.* 24, 279–325. doi: 10.1016/0031-0182(78)90011-1

Gillespie, R., Street-Perrott, F. A., and Switsur, R. (1983). Post-glacial arid episodes in Ethiopia have implications for climate prediction. *Nature* 306:680. doi: 10.1038/306680a0

Gupta, A. K., Anderson, D. M., and Overpeck, J. T. (2003). Abrupt changes in the Asian southwest monsoon during the Holocene and their links to the North Atlantic Ocean. *Nature* 421:354. doi: 10.1038/nature01340

Hastenrath, S., and Kutzbach, J. E. (1983). Paleoclimatic estimates from water and energy budgets of East African lakes. *Quat. Res.* 19, 141–153. doi: 10.1016/0033-5894(83)90001-7

Hildebrand, E. A., and Grillo, K. M. (2012). Early herders and monumental sites in eastern Africa: dating and interpretation. *Antiquity* 86, 338–352. doi: 10.1017/S0003598X00062803

Hildebrand, E. A., Grillo, K. M., Sawchuk, E. A., Pfeiffer, S. K., Conyers, L. B., Goldstein, S. T., et al. (2018). A monumental cemetery built by eastern Africa's first herders near Lake Turkana, Kenya. *Proc. Natl. Acad. Sci. U.S.A.* 115, 8942–8947. doi: 10.1073/pnas.1721975115

Honegger, M., and Williams, M. (2015). Human occupations and environmental changes in the Nile valley during the holocene: the case of kerma in upper nubia (northern Sudan). *Quat. Sci. Rev.* 130, 141–154. doi: 10.1016/j.quascirev.2015.06.031

Junginger, A. (2011). *East African climate variability on different time scales: the Suguta Valley in the African-Asian Monsoon Domain* (Doctoral dissertation), University of Potsdam, Germany.

Junginger, A., Roller, S., Olaka, L. A., and Trauth, M. H. (2014). The effects of solar irradiation changes on the migration of the congo air boundary and water levels of paleo-lake suguta, northern Kenya Rift, during the African humid period (15–5 ka BP). *Palaeogeogr. Palaeoclimatol. Palaeoecol.* 396, 1–16. doi: 10.1016/j.palaeo.2013.12.007

Junginger, A., and Trauth, M. H. (2013). Hydrological constraints of paleo-lake suguta in the northern kenya rift during the African humid period (15–5 ka BP). *Glob. Planet. Change* 111, 174–188. doi: 10.1016/j.gloplacha.2013.09.005

Kassa, T. G. (2015). *Holocene Environmental History of Lake Chamo, South Ethiopia* (Doctoral dissertation), University of Cologne, Germany.

Kebede, S., and Travi, Y. (2012). Origin of the δ18O and δ2H composition of meteoric waters in Ethiopia. *Quat. Int.* 257, 4–12. doi: 10.1016/j.quaint.2011.09.032

Kiptala, J. K., Mohamed, Y., Mul, M. L., and Van der Zaag, P. (2013). Mapping evapotranspiration trends using MODIS and SEBAL model in a data scarce and heterogeneous landscape in Eastern Africa. *Water Resour. Res.* 49, 8495–8510. doi: 10.1002/2013WR014240

Kirkby, M. J., and Beven, K. J. (1979). A physically based, variable contributing area model of basin hydrology. *Hydrol. Sci. J.* 24, 43–69. doi: 10.1080/02626667909491834

Kniess, U. (2006). *Hydrologische Modellierung im Zentralen Kenya-Rift* (Unpublished Diploma thesis), University of Potsdam, Germany.

Kuper, R., and Kröpelin, S. (2006). Climate-controlled Holocene occupation in the Sahara: motor of Africa's evolution. *Science* 313, 803–807. doi: 10.1126/science.1130989

Lahr, M., and Foley, R. A. (1998). Towards a theory of modern human origins: geography, demography, and diversity in recent human evolution. *Am. J. Phys. Anthropol.* 107, 137–176. doi: 10.1002/(SICI)1096-8644(1998)107:27+<137::AID-AJPA6>3.0.CO;2-Q

Lamb, A. L., Leng, M. J., Lamb, H. F., and Mohammed, M. U. (2000). A 9000-year oxygen and carbon isotope record of hydrological change in a small Ethiopian crater lake. *Holocene* 10, 167–177. doi: 10.1191/095968300677444611

Lamb, A. L., Leng, M. J., Mohammed, M. U., and Lamb, H. F. (2004). Holocene climate and vegetation change in the main ethiopian rift valley, inferred from the composition (C/N and δ13C) of lacustrine organic matter. *Quat. Sci. Rev.* 23, 881–891. doi: 10.1016/j.quascirev.2003.06.010

Lamb, P. J., Bell, M. A., and Finch, J. D. (1998). "Varibility of Sahelian disturbance lines and rainfall during 1951-87," in *Water Resources Variability in Africa during XXth Century*, eds E. Servat et al. (IAHS), 19–26.

Lario, J., Sanchez-Moral, S., Fernandez, V., Jimeno, A., and Menendez, M. (1997). Palaeoenvironmental evolution of the blue Nile (Central Sudan) during the early and mid-holocene (Mesolithic-Neolithic transition). *Quat. Sci. Rev.* 16, 583–588. doi: 10.1016/S0277-3791(96)00053-4

Larrasoaña, J. C., Roberts, A. P., and Rohling, E. J. (2013). Dynamics of green Sahara periods and their role in hominin evolution. *PLoS ONE* 8:e76514. doi: 10.1371/journal.pone.0076514

Lenters, J. D., and Cook, K. H. (1999). Summertime precipitation variability over South America: Role of the large-scale circulation. *Monthly Weather Rev.* 127, 409–431. doi: 10.1175/1520-0493(1999)127<0409:SPVOSA>2.0.CO;2

Lesur, J., Hildebrand, E. A., Abawa, G., and Gutherz, X. (2014). The advent of herding in the horn of africa: new data from Ethiopia, Djibouti and Somaliland. *Quat. Int.* 343, 148–158. doi: 10.1016/j.quaint.2013.11.024

Levin, N. E., Zipser, E. J., and Cerling, T. E. (2009). Isotopic composition of waters from Ethiopia and Kenya: insights into moisture sources for eastern Africa. *J. Geophys. Res. Atmospheres.* 114:D23. doi: 10.1029/2009JD012166

Liu, C., Ikeda, K., Rasmussen, R., Barlage, M., Newman, A. J., Prein, A. F., et al. (2017). Continental-scale convection-permitting modeling of the current and future climate of North America. *Clim. Dynam.* 49, 71–95. doi: 10.1007/s00382-016-3327-9

Loomis, S. E., Russell, J. M., Eggermont, H., Verschuren, D., and Damsté, J. S. S. (2014). Effects of temperature, pH and nutrient concentration on branched GDGT distributions in East African lakes: Implications for paleoenvironmental reconstruction. *Org. Geochem.* 66, 25–37. doi: 10.1016/j.orggeochem.2013.10.012

Loomis, S. E., Russell, J. M., Ladd, B., Street-Perrott, F. A., and Damsté, J. S. S. (2012). Calibration and application of the branched GDGT temperature proxy on East African lake sediments. *Earth Planet. Sci. Lett.* 357, 277–288. doi: 10.1016/j.epsl.2012.09.031

Loomis, S. E., Russell, J. M., and Lamb, H. F. (2015). Northeast African temperature variability since the Late Pleistocene. *Palaeogeogr. Palaeoclimatol. Palaeoecol.* 423, 80–90. doi: 10.1016/j.palaeo.2015.02.005

Losgedaragh, S. Z., and Rahimzadegan, M. (2018). Evaluation of SEBS, SEBAL, and METRIC models in estimation of the evaporation from the freshwater lakes (Case study: Amirkabir dam, Iran). *J. Hydrol.* 561, 523–531. doi: 10.1016/j.jhydrol.2018.04.025

Manning, K., and Timpson, A. (2014). The demographic response to Holocene climate change in the Sahara. *Quat. Sci. Rev.* 101, 28–35. doi: 10.1016/j.quascirev.2014.07.003

Marchant, R., Richer, S., Boles, O., Capitani, C., Courtney-Mustaphi, C. J., Lane, P., et al. (2018). Drivers and trajectories of land cover change in East Africa: Human and environmental interactions from 6000 years ago to present. *Earth Sci. Rev.* 178, 322–378. doi: 10.1016/j.earscirev.2017.12.010

Marshall, F., and Hildebrand, E. (2002). Cattle before crops: the beginnings of food production in Africa. *J. World Prehistory* 16, 99–143. doi: 10.1023/A:1019954903395

Marshall, M. H., Lamb, H. F., Davies, S. J., Leng, M. J., Kubsa, Z., Umer, M., et al. (2009). Climatic change in northern Ethiopia during the past 17,000 years: a diatom and stable isotope record from Lake Ashenge. *Palaeogeogr. Palaeoclimatol. Palaeoecol.* 279, 114–127. doi: 10.1016/j.palaeo.2009.05.003

Merwade, V. (2012). *Watershed and Stream Network DelineationUsing Arc Hydro Tools*. Available online at: https://web.ics.purdue.edu/~vmerwade/education/terrain_processing.pdf (accessed August 2018).

Mkhwanazi, M., Chavez, J. L., and Andales, A. A. (2015). SEBAL-A: A remote sensing ET algorithm that accounts for advection with limited data. Part I: Development and validation. *Remote Sens.* 7, 15046–15067. doi: 10.3390/rs71115046

New, M., Lister, D., Hulme, M., and Makin, I. (2002). A high-resolution data set of surface climate over global land areas. *Clim. Res.* 21, 1–25. doi: 10.3354/cr021001

Nicholson, S. E. (1996). A review of climate dynamics and climate variability in Eastern Africa. *Limnol. Climatol. Paleoclimatol.* 25–56. doi: 10.1201/9780203748978-2

Nicholson, S. E. (2000). The nature of rainfall variability over Africa on time scales of decades to millenia. *Glob. Planet. Change* 26, 137–158. doi: 10.1016/S0921-8181(00)00040-0

Nicholson, S. E. (2017). Climate and climatic variability of rainfall over eastern Africa. *Rev. Geophys.* 55, 590–635. doi: 10.1002/2016RG000544

Olaka, L. A. (2011). *Hydrology across scales: sensitivity of East African lakes to climate changes* (Doctoral dissertation), Universität Potsdam, Germany.

Olaka, L. A., Odada, E. O., Trauth, M. H., and Olago, D. O. (2010). The sensitivity of East African rift lakes to climate fluctuations. *J. Paleolimnol.* 44, 629–644. doi: 10.1007/s10933-010-9442-4

Ossendorf, G., Groos, A. R., Bromm, T., Tekelemariam, M. G., Glaser, B., Lesur, J., et al. (2019). Middle stone age foragers resided in high elevations of the glaciated bale mountains, Ethiopia. *Science* 365, 583–587. doi: 10.1126/science.aaw8942

Owen, R. B., Barthelme, J. W., Renaut, R. W., and Vincens, A. (1982). Palaeolimnology and archaeology of holocene deposits north-east of lake turkana, Kenya. *Nature* 298:523. doi: 10.1038/298523a0

Pike, R. J., and Wilson, S. E. (1971). Elevation-relief ratio, hypsometric integral, and geomorphic area-altitude analysis. *Geol. Soc. Am. Bull.* 82, 1079–1084. doi: 10.1130/0016-7606(1971)821079:ERHIAG2.0.CO;2

Platnick, S., Ackerman, S. A., King, M. D., Meyer, K., Menzel, W. P., Holz, R. E., et al. (2015). *MODIS atmosphere L2 cloud product (06_L2), NASA MODIS Adaptive Processing System.* Goddard Space Flight Center. doi: 10.5067/MODIS/MYD06_L2.006

R Core Team (2019). *R: A Language and Environment for Statistical Computing.* Vienna: R Foundation for Statistical Computing. Available online at: http://www.R-project.org/

Renssen, H., Brovkin, V., Fichefet, T., and Goosse, H. (2006). Simulation of the holocene climate evolution in northern Africa: the termination of the African humid period. *Quat. Int.* 150, 95–102. doi: 10.1016/j.quaint.2005.01.001

Revel, M., Colin, C., Bernasconi, S., Combourieu-Nebout, N., Ducassou, E., Grousset, F. E., et al. (2014). 21,000 Years of Ethiopian African monsoon variability recorded in sediments of the western nile deep-sea fan. *Reg. Environ. Change* 14, 1685–1696. doi: 10.1007/s10113-014-0588-x

Richardson, J. L., and Dussinger, R. A. (1986). Paleolimnology of mid-elevation lakes in the Kenya Rift Valley. *Hydrobiologia* 143, 167–174. doi: 10.1007/BF00026659

Rowell, D. P., Booth, B. B., Nicholson, S. E., and Good, P. (2015). Reconciling past and future rainfall trends over East Africa. *J. Clim.* 28, 9768–9788. doi: 10.1175/JCLI-D-15-0140.1

Rucina, S. M., Muiruri, V. M., Kinyanjui, R. N., McGuiness, K., and Marchant, R. (2009). Late quaternary vegetation and fire dynamics on mount Kenya. *Palaeogeogr. Palaeoclimatol. Palaeoecol.* 283, 1–14. doi: 10.1016/j.palaeo.2009.08.008

Scerri, E. M., Thomas, M. G., Manica, A., Gunz, P., Stock, J. T., Stringer, C., et al. (2018). Did our species evolve in subdivided populations across Africa, and why does it matter? *Trends Ecol. Evol.* 33, 582–594. doi: 10.1016/j.tree.2018.05.005

Segele, Z. T., and Lamb, P. J. (2005). Characterization and variability of Kiremt rainy season over Ethiopia. *Meteorol. Atmospher. Phys.* 89, 153–180. doi: 10.1007/s00703-005-0127-x

Street-Perrott, F. A., and Harrison, S. P. (1985). "Lake levels and climate reconstruction," in *Paleoclimate Analysis and Modeling,* ed A. D. Hecht (New York, NY: John Wiley), 291–340.

Telford, R. J., and Lamb, H. F. (1999). Groundwater-mediated response to Holocene climatic change recorded by the diatom stratigraphy of an Ethiopian crater lake. *Quat. Res.* 52, 63–75. doi: 10.1006/qres.1999.2034

Thompson, L. G., Mosley-Thompson, E., Davis, M. E., Henderson, K. A., Brecher, H. H., Zagorodnov, V. S., et al. (2002). Kilimanjaro ice core records: evidence of holocene climate change in tropical Africa. *Science* 298, 589–593. doi: 10.1126/science.1073198

Thornthwaite, C. W. (1948). An approach toward a rational classification of climate. *Geogr. Rev.* 38, 55–94. doi: 10.2307/210739

Thornthwaite, C. W., and Mather, J. R. (1955). *The Water Balance.* Centerton: Drexel Institute of Technology, Laboratory of Climatology.

Tierney, J. E., Smerdon, J. E., Anchukaitis, K. J., and Seager, R. (2013). Multidecadal variability in East African hydroclimate controlled by the Indian Ocean. *Nature* 493:389. doi: 10.1038/nature11785

Tiruneh, A. T. (2005). *Water quality monitoring in lake abaya and lake chamo region* (Doctoral dissertation), University of Siegen, Germany.

Trauth, M. H., Foerster, V., Junginger, A., Asrat, A., Lamb, H. F., and Schaebitz, F. (2018). Abrupt or gradual? Change point analysis of the late pleistocene–holocene climate record from chew bahir, southern Ethiopia. *Quat. Res.* 90, 321–330. doi: 10.1017/qua.2018.30

Trauth, M. H., Maslin, M. A., Deino, A. L., Junginger, A., Lesoloyia, M., Odada, E. O., et al. (2010). Human evolution in a variable environment: the amplifier lakes of Eastern Africa. *Quat. Sci. Rev.* 29, 2981–2988. doi: 10.1016/j.quascirev.2010.07.007

Umer, M., Lamb, H. F., Bonnefille, R., Lézine, A. M., Tiercelin, J. J., Gibert, E., et al. (2007). Late pleistocene and holocene vegetation history of the Bale mountains, Ethiopia. *Quat. Sci. Rev.* 26, 2229–2246. doi: 10.1016/j.quascirev.2007.05.004

van der Lubbe, H. J. L., Krause-Nehring, J., Junginger, A., Garcin, Y., Joordens, J. C. A., Davies, G. R., et al. (2017). Gradual or abrupt? Changes in water source of Lake Turkana (Kenya) during the African Humid Period inferred from Sr isotope ratios. *Quat. Sci. Rev.* 174, 1–12. doi: 10.1016/j.quascirev.2017.08.010

Vermote, E., and Wolfe, R. (2015). "MOD09GA MODIS/terra surface reflectance daily L2G global 1kmand 500m SIN grid V006 [Data set]," in *NASA EOSDIS Land Processes DAAC.* Available online at: https://doi.org/10.5067/MODIS/MOD09GA.006 (accessed January 8, 2020).

Verschuren, D. (2004). "Decadal and century-scale climate variability in tropical Africa during the past 2000 years," in *Past Climate Variability through Europe and Africa. Developments in Paleoenvironmental Research,* vol 6, eds R. W. Battarbee, F. Gasse, C. E. Stickley (Dordrecht: Springer), 139–158. doi: 10.1007/978-1-4020-2121-3_8

Vincens, A., Buchet, G., Williamson, D., and Taieb, M. (2005). A 23,000 yr pollen record from Lake Rukwa (8 S, SW Tanzania): new data on vegetation dynamics and climate in Central Eastern Africa. *Rev. Palaeobot. Palynol.* 137, 147–162. doi: 10.1016/j.revpalbo.2005.06.001

Viste, E. M. (2012). *Moisture transport and precipitation in Ethiopia* (Doctoral dissertation), University of Bergen, Norway.

Wagner, B., Wennrich, V., Viehberg, F., Junginger, A., Kolvenbach, A., Rethemeyer, J., et al. (2018). Holocene rainfall runoff in the central Ethiopian highlands and evolution of the River Nile drainage system as revealed from a sediment record from Lake Dendi. *Glob. Planet. Change* 163, 29–43. doi: 10.1016/j.gloplacha.2018.02.003

Wan, Z., Hook, S., and Hulley, G. (2015). "MOD11A1 MODIS/Terra land surface temperature/emissivity daily L3 global 1km SIN grid V006 [Data set]," in *NASA EOSDIS Land Processes DAAC.* Available online at: https://doi.org/10.5067/MODIS/MOD11A1.006 (accessed January 8, 2020).

Wieringa, J. (1992). Updating the Davenport roughness classification. *J. Wind Eng. Indus. Aerodyn.* 41, 357–368. doi: 10.1016/0167-6105(92)90434-C

Williams, A. P., and Funk, C. (2011). A westward extension of the warm pool leads to a westward extension of the walker circulation, drying eastern Africa. *Clim. Dyn.* 37, 2417–2435. doi: 10.1007/s00382-010-0984-y

Zhang, X. C., Wu, J. W., Wu, H. Y., and Li, Y. (2011). Simplified SEBAL method for estimating vast areal evapotranspiration with MODIS data. *Water Sci. Eng.* 4, 24–35. doi: 10.3882/j.issn.1674-2370.2011.01.003

Zielhofer, C., von Suchodoletz, H., Fletcher, W. J., Schneider, B., Dietze, E., Schlegel, M., et al. (2017). Millennial-scale fluctuations in Saharan dust supply across the decline of the African humid period. *Quat. Sci. Rev.* 171, 119–135. doi: 10.1016/j.quascirev.2017.07.010

Appendix P2 – A Phytolith Supported Biosphere-Hydrosphere Predictive Model for Southern Ethiopia: Insights into Paleoenvironmental Changes and Human Landscape Preferences since the Last Glacial Maximum

A Phytolith Supported Biosphere-Hydrosphere Predictive Model for Southern Ethiopia: Insights into Paleoenvironmental Changes and Human Landscape Preferences since the Last Glacial Maximum

Markus L. Fischer [1,2,*], Felix Bachofer [3], Chad L. Yost [4], Ines J. E. Bludau [1,2], Christian Schepers [5], Verena Foerster [6], Henry Lamb [7,8], Frank Schäbitz [6], Asfawossen Asrat [9,10], Martin H. Trauth [11] and Annett Junginger [1,2,*]

1   Department of Geosciences, Eberhard Karls University Tuebingen, Hoelderlinstr. 12, 72074 Tuebingen, Germany; ines.thate@ifg.uni-tuebingen.de
2   Senckenberg Centre for Human Evolution and Paleoenvironment (S-HEP), Sigwartstr. 10, 72076 Tuebingen, Germany
3   Observation Centre, German Aerospace Center (DLR), Muenchener Str. 29, 82234 Wessling, Germany; felix.bachofer@dlr.de
4   Department of Earth and Environmental Systems, Indiana State University, Terre Haute, IN 47809, USA; Chad.Yost@indstate.edu
5   Institute of Prehistoric Archaeology, University of Cologne, 50931 Cologne, Germany; christian.schepers@uni-koeln.de
6   Institute of Geography Education, University of Cologne, 50931 Cologne, Germany; V.Foerster@uni-koeln.de (V.F.); frank.schaebitz@uni-koeln.de (F.S.)
7   Department of Geography and Earth Sciences, Aberystwyth University, Aberystwyth SY23 3FL, UK; hfl@aber.ac.uk
8   Botany Department, School of Natural Sciences, Trinity College, D02 DP21 Dublin, Ireland
9   Department of Mining and Geological Engineering, Botswana International University of Science and Technology, Private Bag 16, Palapye, Botswana; asfawossen.asrat@aau.edu.et
10 School of Earth Sciences, Addis Ababa University, P.O. Box 1176, Addis Ababa, Ethiopia
11 Institute of Geosciences, University of Potsdam, 14476 Potsdam, Germany; Martin.Trauth@geo.uni-potsdam.de
*   Correspondence: markus_fischer@posteo.de (M.L.F.); annett.junginger@uni-tuebingen.de (A.J.)

Abstract: During the past 25 ka, southern Ethiopia has undergone tremendous climatic changes, from dry and relatively cold during the Last Glacial Maximum (LGM, 25–18 ka) to the African Humid Period (AHP, 15–5 ka), and back to present-day dry conditions. As a contribution to better understand the effects of climate change on vegetation and lakes, we here present a new Predictive Vegetation Model that is linked with a Lake Balance Model and available vegetation-proxy records from southern Ethiopia including a new phytolith record from the Chew Bahir basin. We constructed a detailed paleo-landcover map of southern Ethiopia during the LGM, AHP (with and without influence of the Congo Air Boundary) and the modern-day potential natural landcover. Compared to today, we observe a 15–20% reduction in moisture availability during the LGM with widespread open landscapes and only few remaining forest refugia. We identify 25–40% increased moisture availability during the AHP with prevailing forests in the mid-altitudes and indications that modern anthropogenic landcover change has affected the water balance. In comparison with existing archaeological records, we find that human occupations tend to correspond with open landscapes during the late Pleistocene and Holocene in southern Ethiopia.

1. Introduction

The formation of the East African Rift System (EARS) led to large topographical contrasts in southern Ethiopia [1] and is thus responsible for an extreme precipitation gradient between the dry lowlands of the Omo-Turkana and Chew Bahir basins and the moist Southwestern Ethiopian Highlands [2] (Figure 1). Due to this topography and its position within the global atmospheric circulation system, the prevailing vegetation is partitioned into a complex mosaic of forests, bushlands and grasslands [3]. In the past several centuries, intensified agriculture, de- and reforestation pronouncedly reorganised the biosphere in Ethiopia [3]. Such human induced landcover change may have affected ecosystem climatic boundary conditions with subsequent effects on the hydrosphere and potential consequences for the local economy and food security.
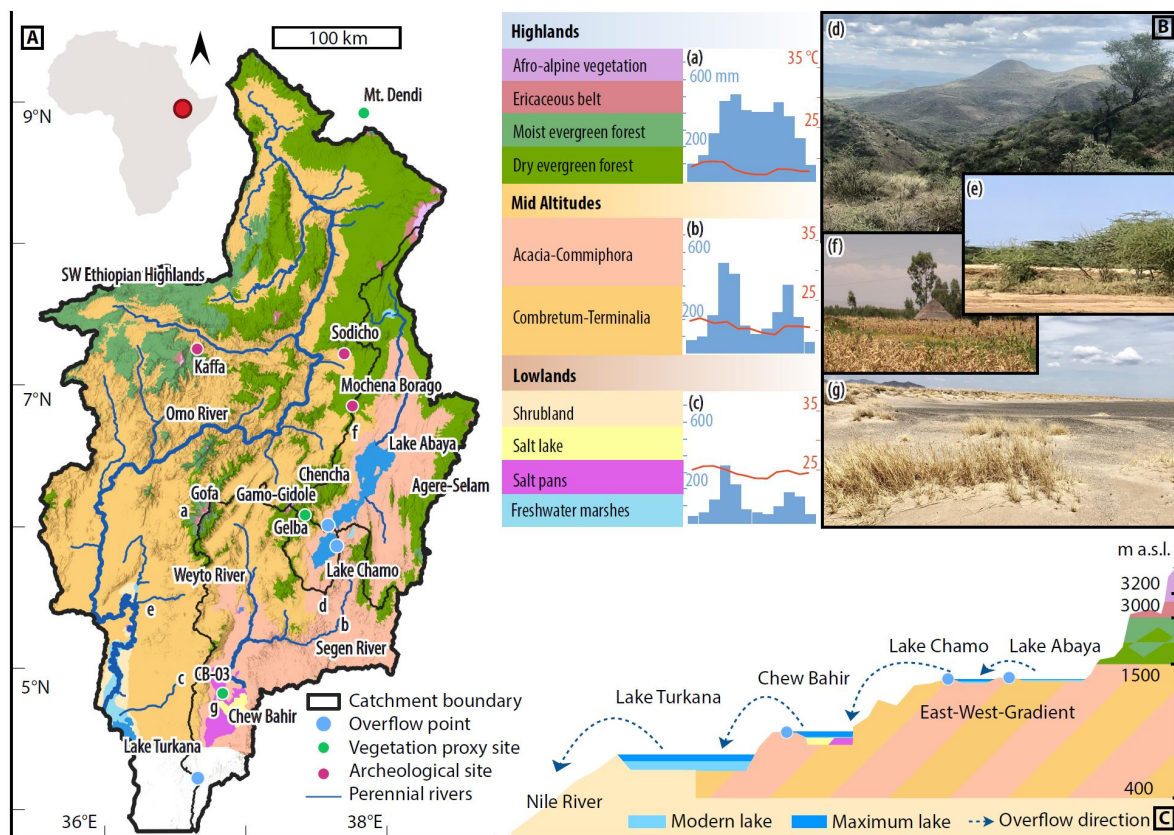
Figure 1. Overview of the study area with sites mentioned in the text, investigated lakes, overflow dynamics and modern-day potential vegetation. (**A**) Catchment of the Omo River, lakes Abaya and Chamo and paleo-lake Chew Bahir with lake's overflow locations. Hill-shaded potential vegetation is based on Friis, et al. [3]. (**B**) Legend of potential vegetation arranged by altitude with (a to c) monthly temperature means in °C and precipitation in mm per month (IRI, last accessed 12/2020). The locations of the photographs of representative vegetation regimes (d to g, photos from Annett Junginger) are marked on the catchment map. (**C**) Cross-section from Lake Abaya to Lake Turkana showing the overflow direction and lake ladder with their prevailing potential vegetation (numbers correspond to the potential vegetation types marked on **A** and **B**).

Highly variable water availability in the EARS during the Pleistocene and Holocene must have caused a significant reorganization-pressure on plant habitats and subsequent adaptation of habitat preferences of early humans [4,5]. During the past 25,000 calibrated years before present (herein ka), the region has been characterized by high amplitude climatic change, including the drier and colder episode during the Last Glacial Maximum (LGM, 25–18 ka) [6,7], the African Humid Period (AHP, 15–5 ka) [8,9] and present-day dry conditions. These climatic fluctuations caused tremendous changes in lake water levels in eastern Africa [10–13], river flow [8,14] and vegetation composition and patterns [15–18].

The human preference for certain landscape types remains a recurring question. According to the savanna hypothesis [19,20], humans originated within a savanna landscape, and the perception of the savanna as an ideal habitat was evolutionarily imprinted onto humans [21]. Another hypothesis by Tveit, et al. [22] resulted in a more variable notion about human landscape preferences. The archaeological record shows that over time, humans lived in a wide range of landscapes.

Forested and humid landscapes were supposedly preferred habitats in Tiemassas in western Africa 44 ka [23]. In eastern Africa at Panga ya Saidi, humans lived in a forest-grassland landscape at the coast during the transition from the Middle to the Later Stone Age around 67 ka [24–26]. Other studies indicate that humans survived in a grassland environment along the shores of Lake Victoria during the Late Pleistocene Middle Stone Age 40–60 ka [27] and, at 105 ka, they lived in a relatively humid Kalahari far away from the coast [28]. It has been shown that humans were able to adapt to alpine conditions with gallery forests in small valleys and collected raw materials along mountain glaciers above 4000 m a.s.l. at Fincha Habera, Ethiopia from 47 to 31 ka [29]. On top of the Dendi caldera, Ethiopia (3000 m a.s.l) humans created handaxes [30]. Thus, based on the Upper Pleistocene and Holocene archaeological record, humans seem not to have shown a preference for a specific single landscape type, but rather occupied complex landscapes and developed flexible strategies to respond to a transforming environment [4,5,31,32]. For southern Ethiopia, a comparison of occupation frequencies between the lowlands and hypothesised refuge areas in, e.g., the SW Ethiopian Highlands suggested that during short-term dry spells puncturing the AHP the humid highlands could have been the sink area for vertical migration of highly mobile hunter-gatherer groups [33]. However, paleo-vegetation and paleoclimatic data covering the entire southern Ethiopian region, particularly during the LGM, the AHP and the late Holocene are scarce, yet they play a key part in understanding the potential constraints of natural resources for humans.

In an effort to address this lack of environmental context Fischer, et al. [10] have recently developed a Lake Balance Model (LBM) to reconstruct paleo-lake Chew Bahir's response to moisture changes during the AHP. The LBM identified the importance of temporarily interconnected lake catchments during major humid periods. The LBM suggested a precipitation increase of +6.5% to compensate for increased open water evaporation. Furthermore, an additional +7% increase was calculated to account for the increased ET on land due to a change in rainfall seasonality. Some studies suggest that increased precipitation during the AHP in the EARS was due to an eastward-shift of the Congo Air Boundary (CAB) [34,35]. However, the magnitude of vegetation changes was not a well-constrained parameter in our LBM, due to the lack of reliable information on regional vegetation. Instead, Fischer, et al. [10] used estimations from a Kenyan LBM study, that suggested an +7–15% precipitation increase to compensate for the biosphere-hydrosphere feedback during the AHP [36]. Hence, the LBM reconstructs a total precipitation increase of +20 to 30% during the AHP to explain maximum observed lake levels for paleo-lake Chew Bahir.

Since specific information about the paleo-vegetation and its effect on the hydrosphere is missing for southern Ethiopia, we present here the results of a Predictive Habitat or Predictive Vegetation Modelling (PVM). PVM is a common approach used to understand habitat suitability and possible habitat shifts due to changes in the environmental conditions (predictors) such as elevation and precipitation [37–39]. PVMs are widely used to model the impact of modern-day climate change on landcover and vegetation. If there is a strong relationship between the environmental predictors and the vegetation, the models can be used to forecast future scenarios using projected data. For this purpose, numerous techniques have been proposed in the past such as Generalized Linear Models [37,40], Generalized Additive Models [40,41], Bioclimatic Envelopes [42] and Bayesian statistics [43]. Recently, machine learning approaches have been used more frequently in this research field, such as Support Vector Machines [44,45], Neural Networks [46], Random Forest [45] and Boosted Regression Trees (BRT), also called Stochastic Gradient Boosting [37,45,47,48].

In order to understand the effect of the precipitation and the temperature on the paleo vegetation and subsequently the paleo-hydrosphere during the climatic extremes of the past 25 ka and to provide a profound discussion about human landscape preferences in southern Ethiopia, we link a PVM (based on BRTs) with the previously established LBM by Fischer, et al. [10]. BRTs combine the strength of regression or classification trees with the boosting algorithm to combine multiple weak models for improved predictive performance. BRTs work for different predictor variables with different scales and are robust against outliers [47]. The resulting model is subsequently tested using a new phytolith proxy record from the Chew Bahir basin. The combination provides independent catchment-scale estimates of paleo-precipitation during the LGM and the AHP, as well as detailed maps of the prevailing vegetation mosaic covering the orographic gradient of the EARS in southern Ethiopia.

2. Regional Setting

2.1. Geology, Hydrology and Climate

The 115,613 km^2 study area covers the southwestern Ethiopian highlands, which is the source region of the Omo River and the catchment of lakes Abaya, Chamo and paleo-lake Chew Bahir (Figure 1). The Omo River is the main tributary of Lake Turkana with a catchment of 75,000 km^2. Lake Turkana and paleo-lake Chew Bahir (20,650 km^2) are both part of the Broadly Rifted Zone (BRZ) with rift floor elevations of ~500 m a.s.l. The Lake Abaya catchment (16,200 km^2) and the Lake Chamo catchment (1800 km^2) are part of the Southern Main Ethiopian Rift. Lake Abaya and Lake Chamo are located at around 1000 m a.s.l. [10]. The southwestern Ethiopian highlands consists of 500 to 1500 m thick (up to 3000 m thick in places) basalts and intercalated silicic volcanics of Eocene to Late Oligocene age [1,49]. The rift floor between the Ethiopian and Somalian Plateaus is filled with Late Miocene to Quaternary sediments. In the Broadly Rifted Zone, Precambrian basement is exposed at the rift shoulders, particularly at the Hammar range.

During major humid periods, such as the AHP, a cascading lake system developed, with Lake Abaya (+18 m) and Lake Chamo (+14 m), overspilling into paleo-lake Chew Bahir (+45 m; 2500 km^2), which in turn was overspilling into Lake Turkana [10]. Despite increased moisture availability during the AHP, intense lake level fluctuations have been recorded. Since the recent past, paleo-lake Chew Bahir is a desiccated playa with a seasonally flooded wetland [11]. Lake Turkana is the world's largest permanent desert lake with a modern-day extent of 7000 km^2 and a catchment area of 148,000 km^2 [12,50]. During the AHP, the Lake Turkana water table was +100 m higher due to increased precipitation and inflow from paleo-lake Chew Bahir (and lakes Abaya and Chamo) as well as lakes Nakuru-Elementeita, Baringo-Bogoria and Suguta from the Kenyan plateau [13].

Today's climate in the BRZ lowlands of paleo-lake Chew Bahir and Lake Turkana can be classified as hot semiarid (Koeppen climate classification), with precipitation (P) below evapotranspiration (ET). In contrast, the majority of the southwestern Ethiopian highlands and the catchments of lakes Abaya and Chamo receive higher P with a bi-modal precipitation pattern, despite intervening intense dry seasons. The most elevated parts are humid with P > ET and a unimodal P pattern of up to 2000 mm per year [51].

2.2. Vegetation

The prevailing vegetation is a complex mosaic with desert shrubland along Lake Turkana's shore, woodlands and wooded grasslands in the Omo River lowlands and the paleo-lake Chew Bahir catchment, afro-montane forests of the Ethiopian highlands, and afro-alpine vegetation in most elevated parts (Figure 1) [3,52]. Friis, et al. [3] summarized and mapped distinguishable vegetation classes based on characteristic species in the "Atlas of the potential vegetation in Ethiopia" as follows:

The desert and semi-desert shrubland in Ethiopia, according to Friis, et al. [3], is located below 400 m a.s.l. and characterized as scarcely vegetated with highly drought tolerant species such as *Poaceae* (grasses) with mainly *Dactyloctenium aegyptium*, and rela-

tively fewer perennials, such as *Panicum turgidum*. The *Acacia-Commiphora* woodland and bushland covers vast parts of the dry lowlands in eastern and southern Ethiopia and is located between 400 to 900 and 1600 to 1900 m a.s.l. with a high physiognomical diversity. It overlaps with the desert and semi-desert shrubland, as well as the *Combretum-Terminalia* woodland and wooded grassland. Species within the *Acacia-Commiphora* unit are typically drought resistant trees and shrubs with, either deciduous or small, evergreen leaves. The western boundary of the *Combretum-Terminalia* unit is not sharply defined, due to the shift from a bimodal to primarily unimodal precipitation pattern. Partly, on steep slopes and areas with tall grasses on deep, loamy soils, fire regimes lead to the dominance of *Combretum-Terminalia*, whereas flat and sandy soils are dominated by *Acacia-Commiphora*. Typical for the *Combretum-Terminalia* strata are small to moderate trees with rather large deciduous leaves of the name inherent genera *Combretum* and *Terminalia*. The ground layer is comprised of dense grass vegetation, primarily from the genera *Hyparrhenia*, *Panicum* and *Pennisetum*, and productivity (biomass) is strongly correlated with the seasonality of precipitation [3]. This *Combretum-Terminalia* vegetation unit is dominant in the lowlands of western Ethiopia and penetrates into the Ethiopian highlands through the river valleys. The elevational range of this unit is 400 to 1800 m a.s.l. [3].

Currently, the dry evergreen afro-montane forest and grassland between 1800 and up to 3000 m a.s.l. is a complex mosaic due to agricultural intensification since the late Holocene that led to soil erosion and various succession stages from grasslands to forests. *Juniperus procera* and *Podocarpus falcatus* are characteristic, while *Podocarpus falcatus* is also present in the drier parts of the moist evergreen afro-montane forest. *Pouteria adolfi-friederici* is typical of the moist forests, which are closed forests with tree heights up to 30–40 m, separated from dry forests by a mean annual precipitation >700 mm per year. This unit ranges from 1500 to 3000 m a.s.l. The *Ericaceous* belt is a common high-elevation vegetation type throughout eastern Africa and ranges from 3000 to 3200 m a.s.l., with local variations. The afro-alpine vegetation unit, characterised by the giant herb *Lobelia rhynchopetalum*, covers the highest elevations of Ethiopia [3,53].

The aquatic vegetation unit is separated into freshwater and salt-water species. Below 1000 ppm dissolved salt, open freshwater *Lemnaceae* are typical. Floodplain and lake shore vegetation is characteristically dominated by sedges of the genus *Cyperus* (primarily C_3 [54]), and the characteristic grass species *Leersia hexandra* (C_3) and *Panicum hygrocharis* ($C_3 C_3/C_4$ [55]). The salt-lake vegetation unit is highly dependent on salinity and mostly characterized by salt tolerant taxa *Suaeda monoica*, *Atriplex* spp. and *Salicornia* spp. [3].

2.3. Overview of Archaeological Records of the Last 25 ka in Ethiopia

At several archaeological sites in Ethiopia, cultural sequences end just before the Last Glacial Maximum and continue after a distinct hiatus starting around 14 ka or even later in the Holocene. No human activity is visible in the cultural stratigraphy of Goda Buticha from ~25–8 ka [56–58]. In the stratigraphy of Mochena Borago, a gap in human activity is reported from ~36–10 ka [33,59,60]. Combining the different sites in the Ziway-Shala Basin, it appears that humans were not active in the area from ~22–14 ka [33,61]. The youngest date at Fincha Habera is ~31 ka [29]. The youngest radiocarbon dates from Porc Epic are ~35 ka [62,63]. All these archaeological records point towards the absence of human activities at the investigated sites during the LGM [57,64].

In addition to the absence of humans, other scenarios might have caused this gap, such as erosion of sediments with artefacts and research bias [56,65]. Indications for such bias come from Sodicho Cave 40 km away from Mochena Borago [64]. Here, the lowermost cultural layers are dated to ~27–15 ka before a gap occurs that corresponds to the AHP [64]. After the AHP, indications for human activity starts again at ~4.8 ka [64]. So far, only Sodicho Cave indicates human activity in southern Ethiopia during the LGM [64].

Signs of human activity during the AHP remain, however, scarce in southern Ethiopia. The age-depth model from Sodicho Cave and manganese concentrations indicate a decline of human activities at ~15 ka [64]. Younger radiocarbon dates at 13.5 ka stem from sieve

finds and were therefore not included in the age-depth model [64]. The only other site with a similar age in the study area so far is the Harurona Cave record, dated to 14 ka [66]. Outside of the study area, human activity at Aladi Springs is dated to around 13 ka [67,68], at Laga Oda to ~12 ka [69] and at the Ziway-Shala sites to ~14 ka, ~13 ka and ~11 ka [61]. Another possible gap at Ziway-Shala corresponds to the Younger Dryas that also marks the end of the Pleistocene and the beginning of the Holocene [11,33,61]. Other Ethiopian sites with archaeological records originating from the beginning of the Holocene are Baahti Nebait [70] and Dibé Rockshelter, both dated to 11 ka [71]. During the later stages of the AHP, human activity is dated to ~10 ka at Mochena Borago [60]. Examples are three caves in the Gamo highlands [72] and six caves or rockshelters in the Kaffa region [73] (Figure 1). The Dendi Lake Rockshelter is one example of humans using high-altitude landscapes during the Middle and Late Holocene [74].

3. Materials and Methods

To understand the interrelation of precipitation and vegetation we developed a new PVM in R (available at Github: https://github.com/MLFischer/Paleo-Vegetation-Model (accessed 1 October 2021) and linked it to the previously published LBM of the southern Main Ethiopian Rift [10]. The four major steps of this study are summarized in Figure 2.
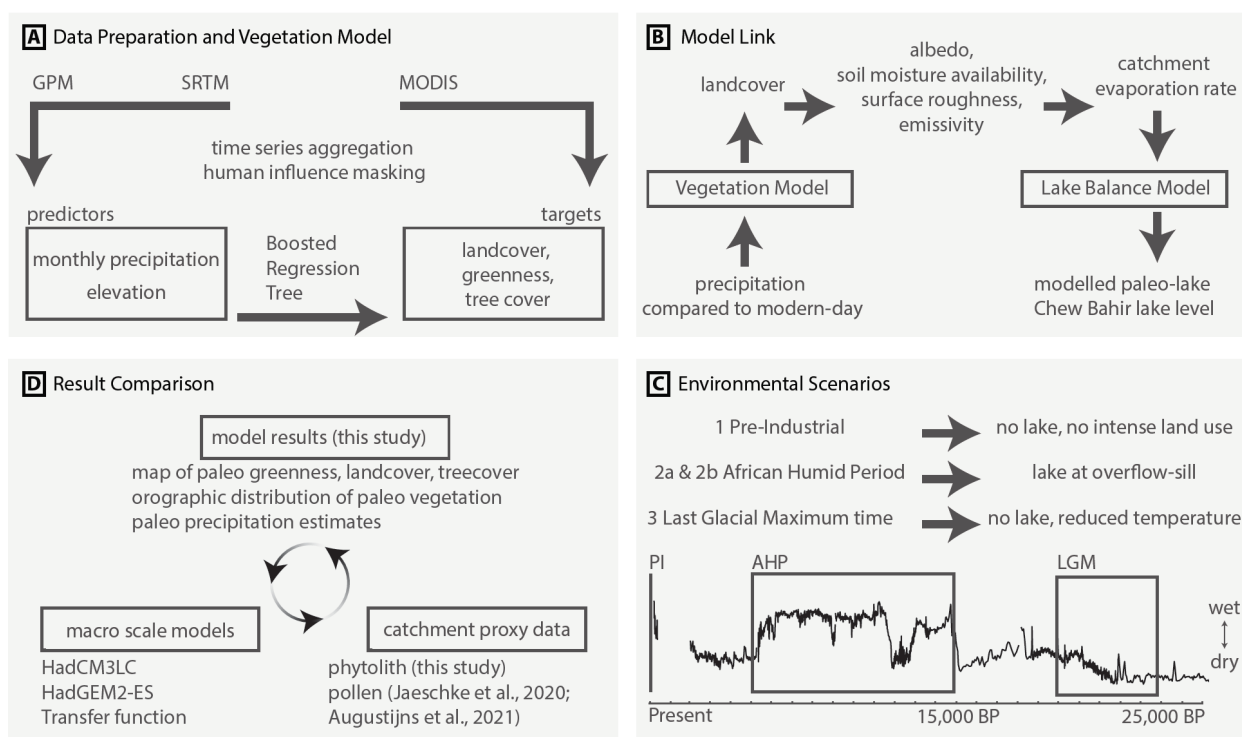
Figure 2. Summary of methods in this study. (**A**) Dataset collection: Modern Global Precipitation Measurement (GPM), Shuttle Radar Topography Mission (SRTM) elevation data, Moderate Resolution Imaging Spectroradiometer (MODIS) vegetation and landcover data. Dataset preparation included time series aggregation from 2001 to 2018 with human influence masked using Open Street Maps, and Boosted Regression Tree model training. (**B**) Vegetation and LBM link using precipitation as input to predict landcover, resulting surface parameters and ET based on [75], the resulting lake balance of lakes Abaya, Chamo and paleo-lake Chew Bahir and, hence, the lake surface elevation of paleo-lake Chew Bahir. (**C**) Three different environmental scenarios are applied in this study: Pre-Industrial time with modern-day climate, reduced or eliminated human influence and to be modelled potential landcover, and AHP and LGM time based with major assumption for this model. All three scenarios are visible in the Potassium record in the lacustrine sediments of paleo-lake Chew Bahir [33]. (**D**) Comparison with global paleo reconstructions (macro scale) and catchment (small scale) proxy-based reconstructions including the phytoliths from the current study.

3.1. Training and Prediction Data

A multi-source and multi-annual (2001 to 2018) dataset of the Omo River and lakes Abaya, Chamo and paleo-lake Chew Bahir catchments was created, containing modern-day elevation of the Shuttle Radar Topography Mission (SRTM) [76], monthly precipitation derived from Global Precipitation Measurement (GPM) [77], landcover (LC) [78] and Vegetation Continuous Fields (VCF) [79], as well as the monthly Enhanced Vegetation Index (EVI) [80] (Table 1). The input datasets were processed in R [81] with the packages raster [82] and rgdal [83]. The boundary of the study area was determined by catchment delineation in ArcGIS 10.4.1 using the SRTM elevation. To minimize the direct human impact on the modern environmental parameters, Open Street Map [84] based streets, buildings and industrial areas were delineated with a 500 m buffer to mask these areas from further analysis. In addition, all areas represented by a LC property [85] that is neither evergreen broadleaf forest (>60% woody cover, >2 m height), open shrubland (shrub cover 10–60%, <2 m height), savanna (forest cover 10–30%, >2 m height) nor grassland (tree cover < 10%) in at least one of the years from 2001 to 2018 were excluded. To produce a consistent LC dataset, the remaining multi-annual layers have been temporally aggregated by applying a majority decision. The aggregation of the monthly EVI (vegetation greenness) and the annual VCF (tree, non-tree and barren soil distribution) was achieved with an arithmetic mean function. Out of the monthly EVI, the annual average EVI was calculated. The average monthly precipitation from the years 2001 to 2018 was accessed and calculated using the Giovanni online data system [86]. To link the spatial domain of these datasets, all layers (bilinear resampling for continuous and natural neighbour for discrete data) have been resampled to a spatial resolution of 926 m, which is the native resolution of the EVI dataset. One raster-stack was created for training (data_tr) composed of elevation, precipitation, LC and vegetation data, that was excluded using the Open Street Map and LC mask. Another raster-stack of the entire study area for prediction (data_pr) was created, containing the elevation and monthly precipitation only.

Table 1. Summary of input dataset.

Data	Specification	Temporal Resolution	Spatial Resolution
Elevation	Shuttle Radar Topography Mission	-	~90 m
Precipitation	Global Precipitation Measurement	Monthly	0.1°
Landcover	MODIS, MCD12Q1, UMD	Annual	~500 m
Greenness	MODIS, MOD13A3, EVI	Monthly	~1000 m
Vegetation Cover	MODIS, MOD44B, VCF	Annual	~250 m

3.2. Model Training and Validation

For the prediction of LC, VCF and annual EVI based on the elevation and monthly precipitation, Boosted Regression Trees were used [37,47], which combine classification and regression trees with the gradient boosting algorithm [87] using the R package gbm [88]. Individual models for each target were trained (LC-BRT, EVI-BRT and VCF-BRT) based on the data_tr dataset. To predict LC, a multinomial loss function, a training fraction of 75%, a five-fold cross validation and a maximum of 1000 trees was chosen. Subsequently, the bag fraction, the learning rate and the interaction depth were hyper-tuned and a weighting coefficient were set to achieve the best multiclass ROC (Receiver Operating Characteristic, R package pROC, [89]) and an optimized confusion matrix based on the R package caret [90]. To avoid overfitting, we used the number of trees with the minimized loss in the 25% validation fraction. To validate the model performance, we separately calculated the confusion matrix and the resulting accuracy, Cohen's Kappa and ROC for wildlife reserves, national parks and controlled hunting areas within the study area and further tested the model on protected areas outside of the study area (test dataset) using the balanced accuracy for each class. To predict annual EVI, a Gaussian loss function and a training fraction of 75% has been used. The model has been hyper-tuned in the same

manner, but without the weighting coefficient, to optimize the resulting determination coefficient between predicted and observed annual EVI. To predict VCF, separate models were built for the tree cover (TC), non-tree cover (NTC) and non-vegetation cover (NVC) and optimized the same way. For both EVI and VCF, the determination coefficient and the average residuum of observation and prediction were calculated separately for each protected area type.

3.3. Model Link and Scenarios

To reconstruct the biosphere-hydrosphere interaction from the LGM onwards, three scenarios are defined to be modelled: (1) the hypothetical pre-industrial scenario (PI), with the potential LC (reduced human influence) based on the same precipitation amount and temperature as modern-day, (2a) the AHP with an increased precipitation amount that is distributed equally as modern day, (2b) the AHP with an CAB-based precipitation increase, assuming that the precipitation increase is happening between the months of June and September, as the increased precipitation was due to an eastward-shift of the Congo Air Boundary (CAB) [13,35] and (3) the LGM with a decreased temperature and a presumably decreased precipitation amount.

To assess the effect of paleo-precipitation changes on paleo-vegetation for each scenario, the central concept is to link this new PVM to the existing LBM from our precursor study [10]. This model link is divided into three stages: The first one is to calculate the effect of an expected range of precipitation change on the vegetation as compared to modern-day precipitation and to compute the resulting vegetation distribution in the catchments of lakes Abaya, Chamo and paleo-lake Chew Bahir. The second stage is the application of an established parametrization approach [36,75,91] to calculate the resulting ET on land as a function of the precipitation-vegetation distribution for each lake's catchment, separately. In the final, third stage, this precipitation-vegetation derived ET is used as input for the existing LBM of lakes Abaya, Chamo and paleo-lake Chew Bahir to model the new threshold of appearance (AHP and AHP-CAB) and disappearance (LGM) of paleo-lake Chew Bahir.

3.3.1. Stage 1—Precipitation to Vegetation

For each scenario, the data_pr dataset and the LC-BRT were used to predict the LC. For the PI scenario, the original data_pr dataset was utilised. The output of the multinomial LC-BRT is applied to classify each datapoint according to its most likely class. For the AHP scenario, the precipitation amount of each month and data point was changed by multiplying it with the percentage of the precipitation change (e.g., 1.3 for 130% precipitation amount as compared to modern-day conditions) starting from 100 to 150% with increments of 1%. For each precipitation amount within each scenario, the LC distribution in the catchments (Abaya, Chamo and Chew Bahir) is retained in a scenario specific spreadsheet for the next analysis step. For the AHP-CAB scenario, the absolute annual difference for each percentage change is calculated as an absolute value for each datapoint and converted to a percentage change in the months from June to September, covering the same precipitation range. For the LGM scenario, the significant temperature difference from modern-day conditions is considered by using the GDGT based temperature reconstructions [7,92]. For this purpose, the modern-day elevation (E) was converted into an elevation equivalent (EE) using the modern-day lapse rate (MDLR) over eastern Africa of $-5.8\,°C\,km^{-1}$, the LGM calculated lapse rate of $-6.7\,°C\,km^{-1}$ [7], their difference of $0.9\,°C\,km^{-1}$ (LRD) and a base cooling (BC) between 3 and 4 °C [92]. Afterwards, EE is calculated according to equation 1. With this EE, the paleo-vegetation is predicted, covering the precipitation range from 50 to 100% with increments of 1% compared to the modern-day amount. For the LGM LC-BRT model, a condition was added to classify each datapoint as afro-alpine vegetation if the EE exceeds 3000 m a.s.l. [3]. For the modern-day elevation and temperature gradient, the ratio of areas within the modelled area that have elevations higher than this threshold is negligible. Based on Fischer, et al. [10],

we here use the assumption of similar temperatures during the AHP as today to simplify the approach.

$$EE = E + (LRD * E + BC)/(MDLR) \tag{1}$$

3.3.2. Stage 2—Vegetation to ET

A parametrization approach was applied to calculate ET by a vegetation-precipitation dependent albedo, emissivity, soil moisture availability and surface drag coefficient [36,75,91]. The parameters have been calibrated meticulously (Table 2) to acquire the same results as calculated by Fischer, et al. [10] and to account for the closed basin balanced water budget for the modern-day vegetation coverage, maintaining the parameter gradients in between the classes. ET calculation is based on the surface-drag coefficient, the wind speed, the soil moisture availability, the gas constant for dry air, the surface and air temperatures, the relative humidity and the saturation vapor pressure as a function of surface and air temperature [10]. The resulting ET for the scenario specific precipitation-vegetation distribution (AHP, AHP-CAB, LGM) has been calculated separately. Furthermore, the average temperature decrease for each catchment and lake in the LGM scenario was calculated based on the GDGT temperature reconstructions [7,92], which also resulted in an updated lake evaporation for lakes Abaya, Chamo and paleo-lake Chew Bahir.

Table 2. Summary of input parameters used for each LC with UMD, name, albedo, emissivity, Soil Moisture Availability (SMA) and roughness length (cm).

UMD	Name	Albedo	Emissivity	SMA	Roughness Length (cm)
0	Water Bodies	0.06	0.99	1	0.01
2	Evergreen Broadleaf Forest	0.07	0.96	0.5	50
6	Closed Shrubland	0.085	0.96	0.5	50
7	Open Shrubland	0.2	0.8	0.075	15
8	Woody Savanna	0.095	0.96	0.5	40
9	Savanna	0.13	0.96	0.18	25
10	Grassland	0.14	0.98	0.14	20
11	Permanent Wetland	0.055	1	0.8	0.01
12,14	Cropland	0.1	0.95	0.5	50
13	Urban or Built-Up	0.275	0.75	0.02	1
15	Non vegetated	0.25	0.75	0.02	1
16	Afro-alpine	0.125	0.97	0.5	27.5

3.3.3. Stage 3—ET to Lake Levels and Paleo-Precipitation

In the third stage, precipitation and the precipitation-dependent ET of each scenario was used as input for the LBM. The model used a change in precipitation of 100 to 150% for the AHP and AHP-CAB scenario and of 50 to 100% for the LGM (the upper and lower limit are set generously to cover definitely the expected precipitation amount for each scenario). For any amount of precipitation, the lake's reaction was simulated over 500 years, which is sufficient time for the system to reach its ET-precipitation equilibrium [10]. For simulation of each scenario, we analysed the resulting equilibrium lake level of paleo-lake Chew Bahir, the water fluxes between the catchments (Lake Abaya—Lake Chamo—paleo-lake Chew Bahir—Lake Turkana) and the relative importance of the extended catchment (lakes Abaya and Chamo) for the water balance of paleo-lake Chew Bahir. The precipitation threshold of the transition of lake appearance (to go from "no lake" conditions to a "flooded basin") in the AHP and AHP-CAB scenario is used as a precipitation estimate for the final LC prediction. The precipitation interval (comparison of 3 to 4 °C base cooling during LGM) of lake disappearance (to go from "flooded basin" conditions to a "no lake") is used as precipitation estimate in the LGM scenario.

3.3.4. Paleo-Vegetation Maps

Using the precipitation estimate from the prior step as input for the BRT model for LC, VCF and EVI, the vegetation distribution (LC, VCF and EVI) for each scenario from the LGM onwards until the modern-day conditions was modelled, presenting the most likely spatial distribution of vegetation type and density.

3.4. Phytolith Proxy

To infer and test the modelling results with proxies of past vegetation, lacustrine sediment samples covering the past 25 ka from the paleo-lake Chew Bahir basin CB-03 short-core were used [11,33,93,94]. Pollen is a well-known proxy for paleo-vegetation reconstruction but are not preserved in the Chew Bahir lacustrine sediments. Instead, phytoliths were used to gain information about paleo-vegetation, as phytoliths are particularly valuable for the identification of grass type composition [95]. Phytoliths are microscopic opal silica infillings of plant cells [95,96]. With sheet-wash, fluvial or aeolian transport distances typically up to 10 km from the sample (core) location, phytoliths reflect a mixed signal of the landscape mosaic [95,97].

We analysed 27 samples using a wet-oxidation and heavy-liquid density separation method described in Yost, et al. [95]. Phytoliths were identified using a modern comparative collection from C. Yost and the descriptive phytolith references listed in Yost, et al. [95]. Phytoliths were classified according to the International Code for Phytolith Nomenclature (ICPN 1.0; [98]) and only grass short-cell phytolith morphotypes were assigned to C_4 mesophytic, C_4 xerophytic and C_3 grass functional type (GFT) categories for percentage calculations following Table 1 from Yost, et al. [95] and the results of a modern *phytoscape* approach from the adjacent Turkana Basin [99]. The Iph aridity index, also used to discriminate short-grass xerophytic (Sahelian) savanna from tall-grass mesophytic (Sudanian) savanna [100], was calculated as described in Bremond, et al. [101]. The 95% confidence intervals in GFT percentages and Iph index values were calculated using the nonparametric bootstrap resampling method described in Yost, et al. [95]. Phytolith preservation was assessed using the criteria discussed in Yost, et al. [95] and was ranked on a numerical scale from good to poor to none. Phytolith concentrations were calculated by counting a *Lycopodium* spike added to each sample at the end of the phytolith extraction steps. Phytolith relative abundance was calculated based on the total grass short-cell phytolith count for each sample. These efforts led to a time series of phytolith preservation and C_4 mesic, C_4 xeric and C_3 grass phytolith relative abundance. Additionally, diatoms, sponge spicules, burned phytoliths and microcharcoal were counted but are not discussed in this study.

4. Results

4.1. Dataset Exploration and Description

The data_tr dataset contains 65,052 datapoints, the data_pr dataset 135,368 datapoints. The elevation ranges from 360 to 3593 m a.s.l. with a mean of 1450 m a.s.l. as shown in Figure 3A. The precipitation ranges from 410 mm a^{-1} to 1740 mm a^{-1} with a mean of 1120 mm a^{-1}. The highest precipitation is recorded in the Southwestern Highlands (located in the north-western part of the study area, Figure 1), while the lowest annual amount is close to the shores of Lake Turkana and the southern Chew Bahir basin. The seasonality is unimodal with a strong peak during northern hemisphere summer in the forest classified areas and less intense in the savanna classified areas (Figure 3B,C). The precipitation seasonality for grassland and open shrubland classified areas is bimodal with peaks during northern hemisphere spring and autumn, with the latter's rainy season being less intense. Roughly 45% of the study area is classified as grassland, 47% as savanna, 3% as open shrubland and around 5% as forest. EVI varies from 0.06 to 0.55 with a mean of 0.29. TC ranges from 0 to 82% with a median of 17%. Forest has the highest TC with a median of 71%, followed by savanna (18%) and grassland with a median of 8%, as shown in Figure 3B. The area with NTC comprises 0 to 87% with a median of 16%. Grasslands and savanna have a similar NTC median of 70%, in contrast to forests (27.5%) and open

shrubland (22.5%). The NVC spans from 0 to 100% and has a median of 18%. The highest NVC median of 77% is encountered within the open shrubland areas. Grasslands have a higher median NVC (19%) than savanna classified areas (10%) and forest areas (2%).
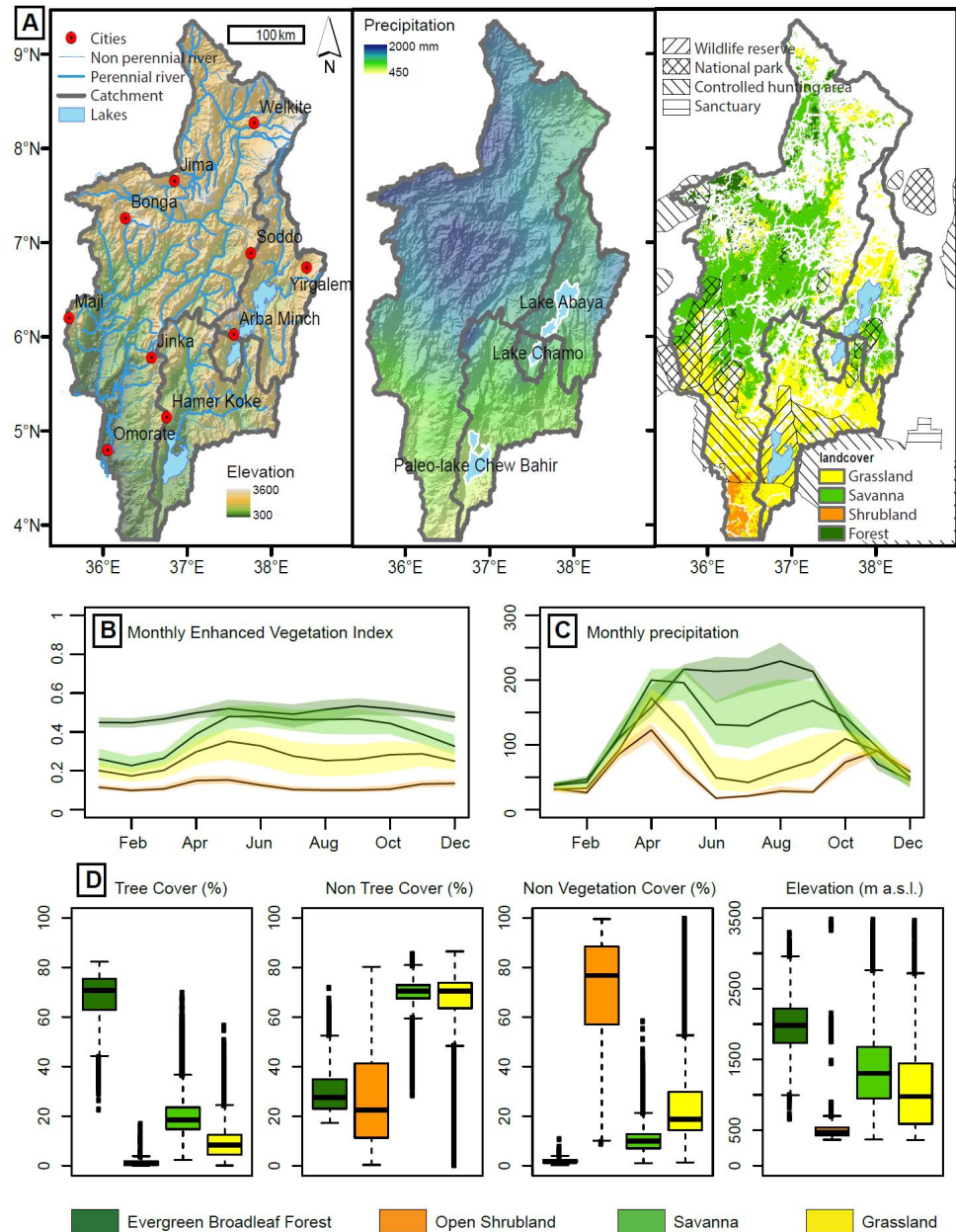
Figure 3. Dataset exploration used for training and prediction: (**A**) Maps of the datasets used in this study with SRTM based elevation, annual precipitation and LC with protected areas. Plots of the datasets used in this study with (**B**) monthly EVI interquartile range for each landcover class, (**C**) monthly GPM precipitation (mm) interquartile range for each class and (**D**) boxplots of the TC, NTC, NVC and elevation for each class.

4.2. Model Training and Validation

For the LC-BRT, the best fit to the data was achieved with a ROC of 0.79, 298 trees, a bag fraction of 0.5, an interaction depth of 1 and a learning rate of 0.05 (Table 3). The most important predictors are the September rains (24%), the elevation (20%), the precipitation in June (13%) and the precipitation in May (11%). The overall accuracy based on the confusion matrix (Table 4) for the multiclass prediction is 0.73 and the overall Cohen's Kappa is 0.57.

For wildlife reserves (Figure 3A), the accuracy is 0.81, kappa is 0.61 and the ROC is 0.76. In national parks, the accuracy is 0.86, kappa is 0.73 and the ROC is 0.87. In controlled hunting areas, the accuracy is 0.87, kappa is 0.5 and the ROC is 0.78. In the test dataset, containing protected areas outside the study area, we achieved a balanced accuracy for evergreen broadleaf forests (0.9), open shrublands (0.51), savanna (0.76) and grasslands (0.58). The ROC for the test dataset is 0.72. The spatial distribution of the model prediction agrees well with the training data in most of the study area (Figure 4), but disagrees in the transition areas, especially in the surroundings of forests and open shrubland areas.

Table 3. Summary of BRT hyper parameters and performance.

BRT	Distribution	Interaction Depth	Shrinkage	Bag Fraction	Trees	ROC/R^2
LC	multinomial	1	0.05	0.5	298	0.79
EVI	gaussian	1	0.05	0.75	3096	0.8
TC	gaussian	3	0.05	0.5	1771	0.8
NTC	gaussian	5	0.05	0.5	3408	0.49
NVC	gaussian	3	0.05	0.5	2671	0.55

Table 4. Confusion matrix for landcover classification.

	Forest	Open Shrubland	Savanna	Grassland
Forest	2784	0	4313	1024
Open Shrubland	0	1198	4	4260
Savanna	237	1	23,289	4015
Grassland	14	839	2757	20,317

The determination coefficient (R^2) for EVI prediction is 0.8. The most important predictors are the precipitation in February (26%), May (21%), September (13%) and the elevation (11%). The R^2 for wildlife reserves within the study area is 0.58 and the EVI is overestimated by 5.6%. The determination coefficient for national parks is 0.64 and the EVI is underestimated by 1.4%. In controlled hunting areas, the R^2 is 0.59 and EVI is overestimated by 2.9%. In the test dataset outside the study area, the determination coefficient is 0.68 and EVI is overestimated by 14% on average.

For TC prediction, R^2 is 0.8. The most important predictors are the September rains (17%), the elevation (14%), December rains (10%) and precipitation in August (10%). The R^2 in wildlife reserves is 0.53 and TC is underestimated by around 1% in average. For national parks, the R^2 is 0.51 and the residuum is -0.28% on average. In controlled hunting areas, R^2 is 0.78 and the average residuum is -1.4%. In the test areas, the determination coefficient is 0.76 and the average residuum is -2.5%.

Even after fine-tuning the hyperparameters for the NTC, the coefficient of determination is only 0.49, indicating an insufficient correlation between the observed and predicted NTC. In the test area, R^2 is even lower with only 0.34, which makes a further use of the NTC-BRT unfeasible. For the NVC, the determination coefficient is 0.55 within the study area and only 0.4 in the test areas, making an application of the NVC-BRT also impracticable.
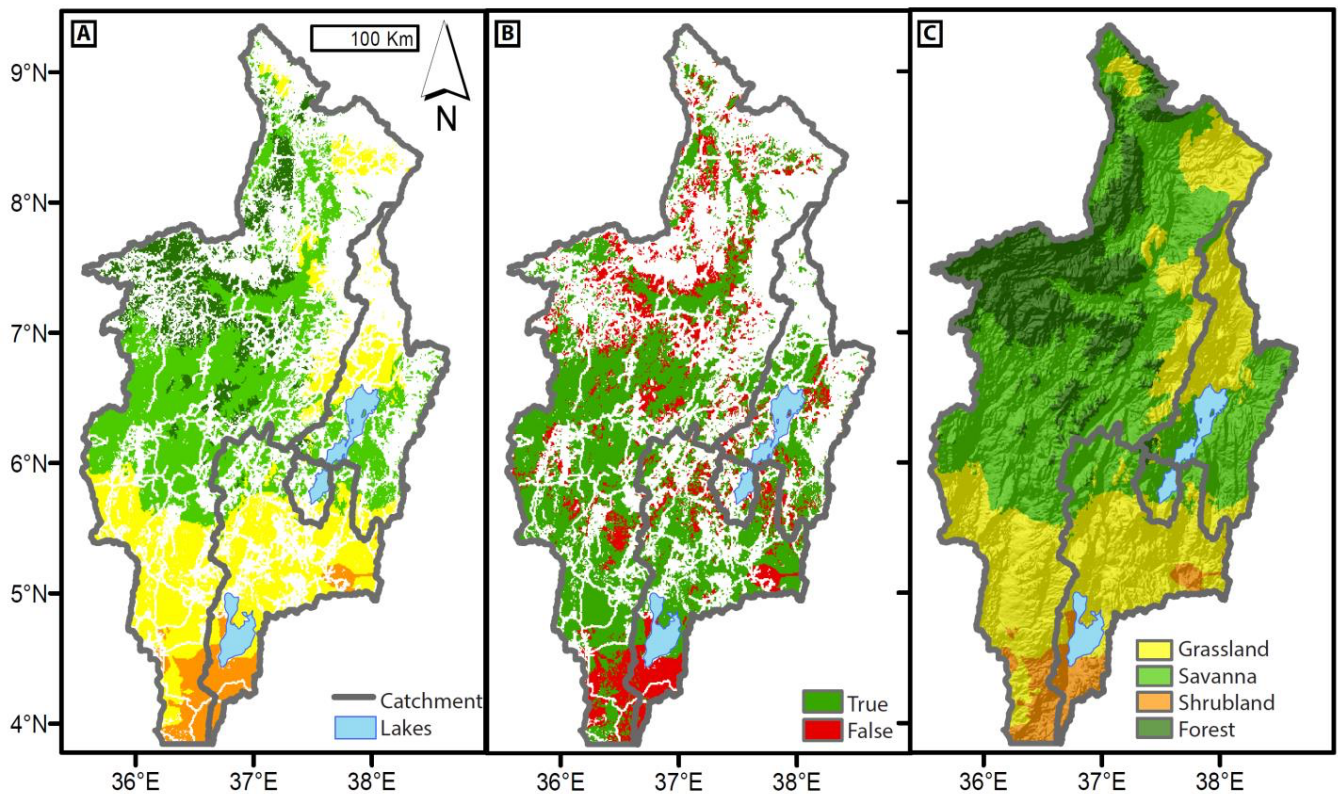
Figure 4. Spatial model performance, extrapolation and PI LC: (**A**) Result of the LC-BRT using the original data_tr dataset. (**B**) Model performance with correct (green) and incorrect (red) classified data points, based on comparison of panel 3 of Figures 3A and 4A. (**C**) Resulting extrapolated LC representing the PI scenario using the original data_pr dataset and LC-BRT.

4.3. Model Link and Scenarios

4.3.1. Modern-Day and Pre-Industrial LC and ET

The modern-day and supposed PI LC distribution of lakes Abaya, Chamo and paleo-lake Chew Bahir is summarized in Table 5. The most significant changes in the catchments of lakes Abaya and Chamo are the decrease of agricultural areas from 19% (Abaya) and 10.8% (Chamo) to 0% and the increase of savanna covered areas by 14% (Abaya) and 24% (Chamo). In the catchment of paleo-lake Chew Bahir, the model suggests a precipitation-elevation based difference of open shrubland covered areas by around 14%. The forest covered areas are increasing moderately (0.4 to 4.1%) throughout all the catchments.

Based on the parametrizations of the LCs, we calculated a modern-day ET of 1072 mm a^{-1} for the catchment of Lake Abaya, which differs by −51 mm a^{-1} from the previously calculated value of Fischer, et al. [10]. In the Lake Chamo catchment, ET is 28 mm a^{-1} higher relative to the previous study, resulting in an annual ET of 1088 mm a^{-1}. In the paleo-lake Chew Bahir catchment, the MD ET is 939 mm a^{-1} compared to 892 mm a^{-1} of Fischer, et al. [10].

The PI (scenario 1) leads to a decreased estimated ET (PI ET of 845 mm a^{-1}) in the Lake Abaya catchment, due to a decrease of agricultural area. This decrease results in a positive water budget within the catchment of Lake Abaya, which would then overflow to Lake Chamo and, hence, to the Chew Bahir basin. The estimated PI ET for the Lake Chamo catchment is 1026 mm a^{-1}, while it is 872 mm a^{-1} for the paleo-lake Chew Bahir catchment.

Table 5. Modern-day (MD) and pre-industrial (PI) landcover distribution (%) in the catchments of lakes Abaya, Chamo and paleo-lake Chew Bahir.

	Lake Abaya Catchment		Lake Chamo Catchment		Chew Bahir Catchment	
	MD	**PI**	**MD**	**PI**	**MD**	**PI**
Water	6.1	6.1	15	15	0	0
Forest	1.2	1.8	0.1	4.5	0.2	0.6
Open Shrubland	0.1	0	0	0	0.6	14.5
Savanna	34	48	26.8	50.1	16.8	18.8
Grassland	37.3	44	44.9	30	75.2	62.2
Cropland	19	0	10.8	0	3.3	0
Sparsely Vegetated	0.5	0.5	0.4	0.4	3.9	3.9

4.3.2. Scenario 2a—AHP, no CAB

The simulation of the precipitation dependent vegetation-ET for the 2a scenario (AHP, no CAB) is shown in Figure 5A. The forest coverage in the Lake Abaya catchment is increasing almost linearly to the 120% precipitation threshold and is then stabilizing, whereas the grassland coverage is decreasing, starting from around 45% and reaching 5% at around 125% precipitation. This forces a positive water budget at the modern-day precipitation amount and a decrease of the water surplus until the forest saturation point at around 120%. The grassland coverage of the Lake Chamo catchment is decreasing rapidly, being replaced by savanna, whereas the forest coverage is increasing slowly until ~120% precipitation, after which it begins to decrease. The water budget is slightly positive within the simulated precipitation increase and ET is following the precipitation amount, starting to increase after the forest saturation point at ~120%. In the paleo-lake Chew Bahir catchment, the model shows a positive water budget for the modern-day precipitation amount. The open shrubland coverage is decreasing to almost zero, whereas the forest coverage is increasing slightly with increasing precipitation. The main process in the paleo-lake Chew Bahir catchment is the replacement of grassland by savanna.

4.3.3. Scenario 2b—AHP, with CAB

In the CAB scenario 2b, the precipitation dependent vegetation-ET interrelation for each catchment is summarized in Figure 5B. The potential increase of forest coverage with increasing precipitation is higher compared to the 2a scenario and remains linear in the Lake Abaya catchment until a threshold at ~140% precipitation. In the Lake Chamo catchment, forest coverage reacts at a greater precipitation increase and reaches 20% at ~120% precipitation. In both mid-altitude catchments (Abaya and Chamo), grassland is replaced quickly by savanna due to increased precipitation. In the catchment of paleo-lake Chew Bahir, the 2b scenario leads to the same vegetation reaction to precipitation increase as in the 2a scenario, with a more pronounced increase of the forest coverage and a less pronounced decrease in grasslands.

4.3.4. Scenario 3—LGM

The simulation of scenario 3 (LGM) shows a ~20% temperature-driven coverage of the Lake Abaya catchment with afro-alpine vegetation, which is independent from the precipitation amount (Figure 5C). Within all catchments, the forest coverage is zero and the savanna is replaced by grassland, due to the decreased precipitation amount. In the paleo-lake Chew Bahir catchment, the savanna coverage is reaching almost zero at ~80% precipitation. The grassland coverage decreased and is replaced by open shrubland with a stable plateau at ~80% precipitation. In all catchments, ET is decreasing with a decline in precipitation. Water balance is positive for precipitation levels above ~80% (paleo-lake Chew Bahir) and 70% (Lake Abaya) of modern levels.
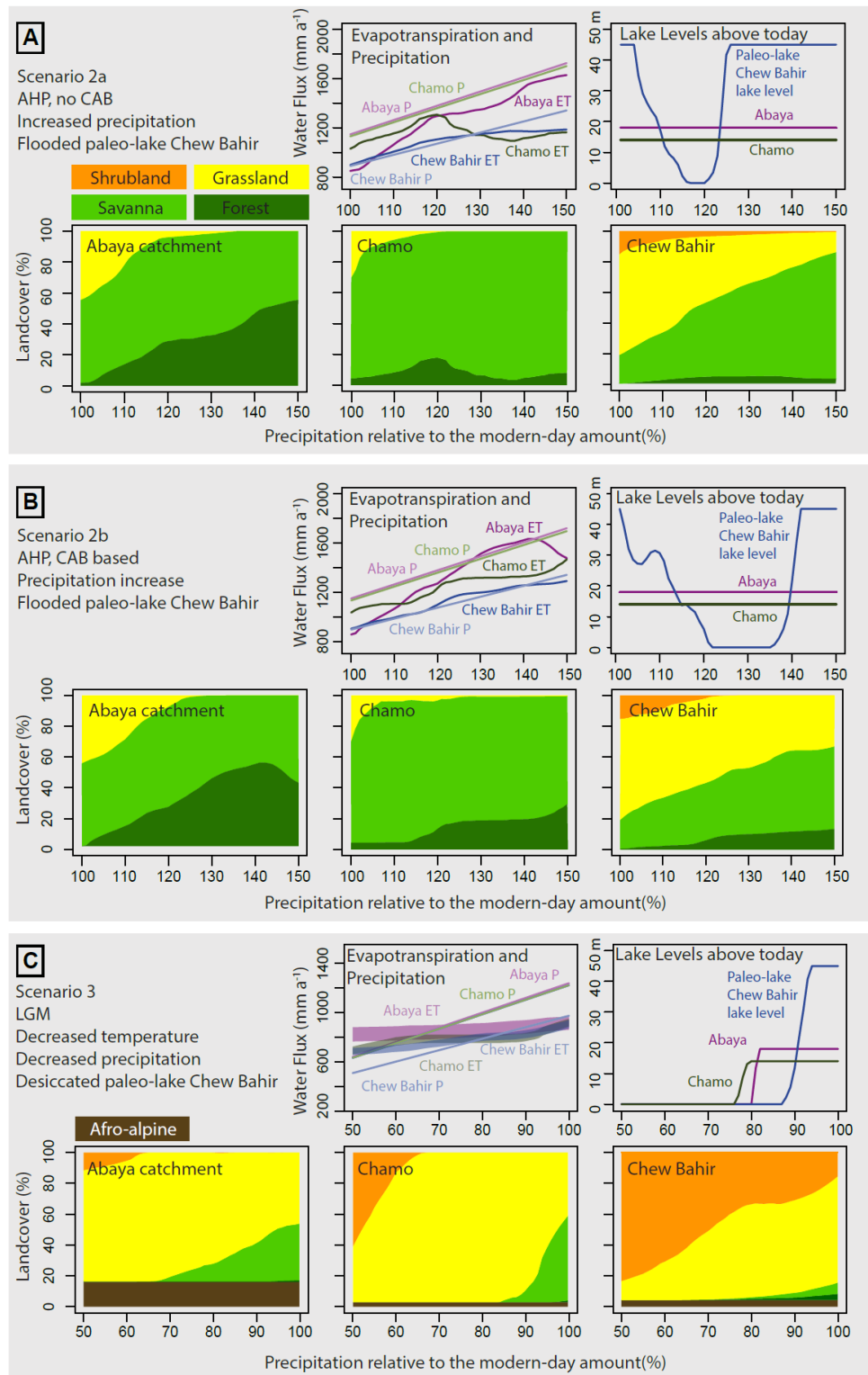
Figure 5. Model Results for Scenario 2a AHP (**A**), 2b AHP with CAB (**B**) and 3 LGM (**C**): modelled annual ET on land for each catchment (lakes Abaya, Chamo and paleo-lake Chew Bahir) for the given precipitation from 100 to 150%, respectively, 50 to 100%; LBM resulting lake levels of lakes Abaya, Chamo and paleo-lake Chew Bahir and vegetation model result with changing LC for each catchment. Scenario 3 ET has an upper and lower boundary due to the modelled temperature decrease range (3–4 °C).

4.3.5. PVM and LBM Model Link

The combined LBM for the 2a AHP scenario with no change in the seasonality of the precipitation shows a lake occurrence of paleo-lake Chew Bahir under modern-day precipitation conditions. With increasing precipitation from 15 to 20%, the model shows initially no lake, which changes as soon as the threshold of 25% precipitation is reached and a lake is (re)established. In the 2b scenario, as a theoretical contrast scenario with additional precipitation in June to September, the threshold for lake appearance is at ~41% more precipitation compared to today. For scenario 3, the modelled LGM environmental conditions, caused the lakes to disappear below 80–85% of the modern-day precipitation. We used these thresholds (2a—125%, 2b—141%, 3—82.5%) as minimum (AHP) and maximum (LGM) precipitation thresholds and as input parameters for the spatial reconstruction of the vegetation mosaic during these time periods by combining the LC-BRT, the EVI-BRT and the TC-BRT (Figure 6). We added the maximum lake extents of lakes Abaya, Chamo and paleo-lake Chew Bahir [10], as well as Lake Turkana [12] for the AHP scenarios. During the LGM, the model suggests that a desiccation of lakes Abaya and Chamo would have required 10% further reduction in precipitation than required for the desiccation of paleo-lake Chew Bahir (Figure 5C).
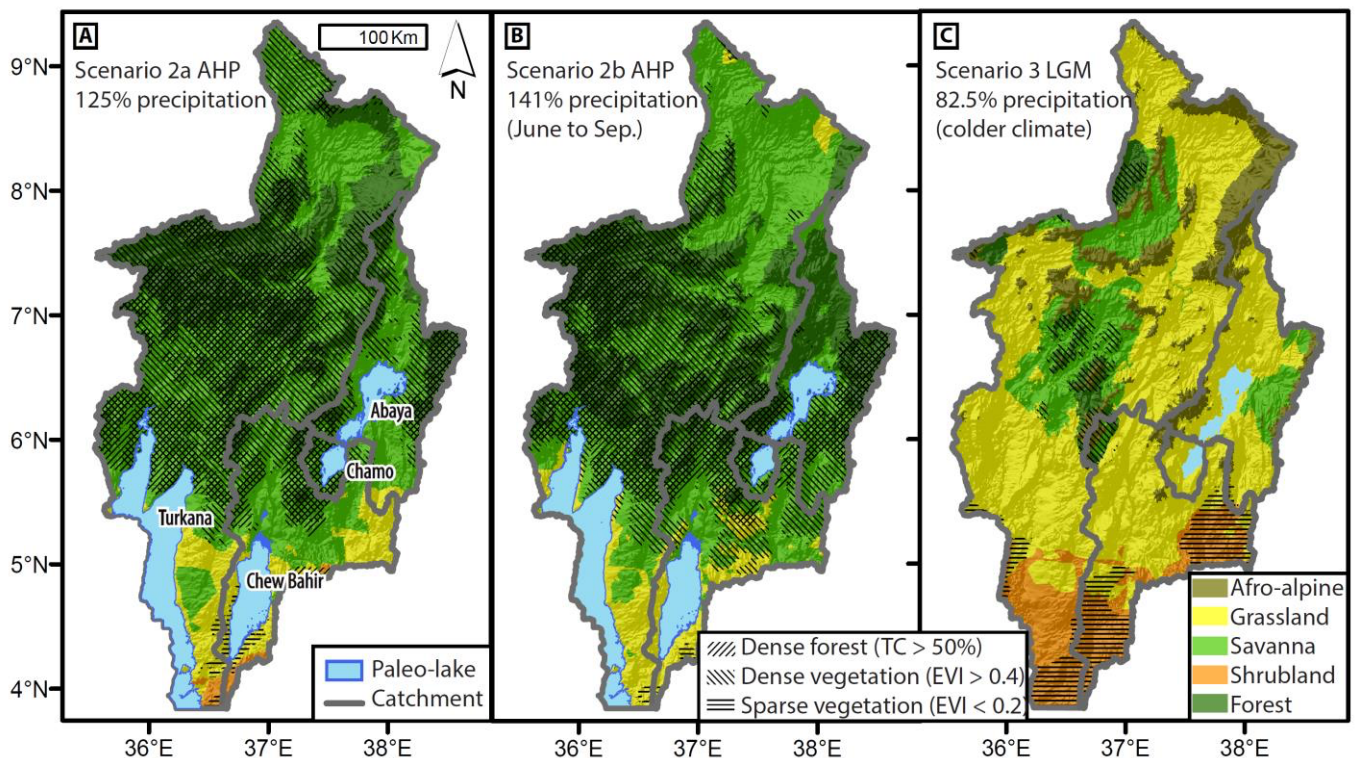
Figure 6. Model result map for scenario 2a, 2b and 3: (**A**) Scenario 2a AHP with spatial application of the LC-BRT, EVI-BRT and TC-BRT using modern-day elevation and 125% precipitation (threshold for lake appearance for scenario 2a). (**B**) Scenario 2b AHP (with CAB) with spatial application of the LC-BRT, EVI-BRT and TC-BRT using modern-day elevation and 141% increased precipitation (threshold for lake appearance for scenario 2b). (**C**) Scenario 3 LGM with spatial application of the LC-BRT, EVI-BRT and TC-BRT using elevation equivalent due to cooler temperatures and 82.5% precipitation (threshold for lake disappearance for scenario 3).

4.4. Phytolith Proxy

Phytolith counts ranged from 0 to 252 per sample, with 16 (59%) yielding no phytoliths (Table 6). Almost no phytoliths were preserved before ~12 ka in the studied Chew Bahir Lake sediment record, except for a few that date to ~24 ka (Figure 7). During the AHP, preservation of phytoliths peaked at ~8 ka and decreased to almost zero at around

5 ka. Phytolith preservation remained low after the AHP. Hence, classification of the surrounding vegetation in the area is limited in this study to the AHP. With the exception of sample 524, uncertainties in the GFT percentages were on average ±9% (C$_3$ grasses), ±10% (C$_4$ mesic grasses) and ±7% (C$_4$ xeric grasses). Even though the sample 524 GFT percentage was plotted in Figure 7, it should be noted that only three phytoliths were used in the GFT calculation. Likewise, the youngest sample from a depth of 4 m yielded only 20 short-cell phytoliths and exhibited evidence of poor preservation, so the calculated GFT percentages have a high level of uncertainty (±20% for C$_3$ and C$_4$ mesic grasses) and are not used directly in our interpretations. The GFT distribution is showing the highest relative abundance of C$_4$ mesophytic grasses with a linear positive trend until the end of the AHP. C$_4$ xerophytic grasses are highest around 12 ka and are decreasing to zero at the end of the AHP. C$_3$ grasses have a comparatively low abundance but reach their highest values at 11 ka and 8 ka. With the exception of sample 464, Iph aridity index values during the AHP were all well below the 27.8 threshold at the 95% confidence level, indicating the presence of mesophytic tall-grass Sudanian savanna or mesic edaphic grasslands associated with paleo-lake Chew Bahir (Table 5). Even though no globular granulate phytolith morphotypes diagnostic of woody plants (trees and shrubs) were observed, during the AHP, ~8% of the total phytolith count at this time was comprised of morphotypes typically derived from woody plants.

Table 6. Phytolith counts and calculated results. 1 depth (m), 2 *Lycopodium* counts, 3 *Lycopodium* spike, 4 dry weight (1g +/−), 5 Trapeziform sinuate: Pooideae, 6 Rondel-keeled, 7 Rondel-angular keel: *Phalaris*, 8 Rondel > 15 microns, 9 Rondel: Bambosoideae, 10 Saddle-long: Bambusoideae, 11 Bilobate-scooped: Ehrhartoideae, 12 total C$_3$, 13 Saddle: Chloridoideae, 14 Saddle-tall: Chloridoideae, 15 total Saddles: C$_4$ Xeric, 16 Saddle-plateau: *Sporobolus*-type, 17 Cross-3-lobed, 18 Cross, 19 Polylobate: Panicoideae, 20 Bilobate: Panicoideae, 21 total Bilobates, 22 total Crosses, 23 total C$_4$ Mesic, 24 Rondel < 15 microns, 25 Grass epidermis, 26 Bulliform, 27 Stomatal cell, 28 Dendriform, 29 total various grasses, 30 Trichome, 31 Elongate-psilate, 32 Elongate-echinate, 33 Blocky-grass/sedge type, 34 total grass/sedge types, 35 thin w/ridges: Cyperaceae (stem), 36 Irreg w/tubular proj: Cyperaceae (root), 37 Cone cell: *Cyperus*-type, 38 Cone cell: *Carex*-type, 39 total Cyperaceae, 40 total Graminoid, 41 Sclereid-branched, 42 Sclereid-elongate, 43 Sclereid-pitted, 44 Elongate-facetate, 45 Blocky-facetate, 46 Blocky-irregular, 47 Globular-decorated, 48 Globular granulate, 49 Globular-facetate, 50 Globular-psilate, 51 Annonaceae-type, 52 Anticlinal-deciduous leaves, 53 Ellipsoid-echinate, 54 Nodular, 55 Granular, 56 Blocky clavate: *Celtis*-type, 57 total semi-deciduous, 58 Globular-echinate, 59 Conical echinate: *Borassus*-type, 60 total Arecaceae, 61 Podostemaceae, 62 *Commelina*-type, 63 *Tradescantia* sp., 64 *Murdannia simplex*, 65 *Cyanotis* sp., 66 Opaque perf plate: Asteraceae, 67 total Herbaceaous, 68 unknown, 69 total phytoliths counted, 70 Sponge spicules, 71 Sponge spherasters, 72 Diatoms, 73 Charcoal < 50 microns, 74 Charcoal > 50 microns, 75 Burned phytoliths, 76 % C$_3$, 77 % C$_3$ confidence interval (+/−) in percent, 78 % C$_4$ Mesic, 79 % C$_4$ Mesic confidence interval (+/−) in percent, 80 % C$_4$ Xeric, 81% C$_4$ Xeric confidence interval (+/−) in percent, 82 Iph Index, 83 Iph confidence interval (−), 84 Iph confidence interval (+).

| 1	4	24	64	104	124	164	196	224	264	304	344	386	464	524	564	624	684	704	744	784	864	944	998	1004	1024	1064	1098
2	98	242	200	336	329	141	155	51	7	19	17	34	18	227	150	346	355	43	298	295	267	203	272	294	289	273	286
3	9666	9666	9666	9666	9666	9666	9666	9666	9666	9666	9666	9666	9666	9666	9666	9666	9666	9666	9666	9666	9666	9666	9666	9666	9666	9666	9666
4	0.011	0.01	0.027	0.005	0.035	0.010	0.008	0.005	0.009	0.011	0.006	0.003	0.007	0.026	0.012	0.011	0.011	−0.04	0.004	0.001	0	0.001	0.005	0.006	0.042	0.004	0.003
5	0	0	0	0	0	0	0	0	0	4	0	0	0	0	0	0	0	0	0	0	0	0	0	0	0	0	0
6	0	0	0	0	0	0	0	0	0	0	0	0	0	0	0	0	0	0	0	0	0	0	0	0	0	0	0
7	0	0	0	0	0	0	0	0	0	0	0	0	0	0	0	0	0	0	0	0	0	0	0	0	0	0	0
8	10	0	0	0	0	0	0	0	0	0	10	1	9	0	0	0	0	0	0	0	0	0	0	0	0	0	0
9	0	0	0	0	0	0	0	0	0	0	0	0	0	0	0	0	0	0	0	0	0	0	0	0	0	0	0
10	0	0	0	0	0	0	0	0	0	0	0	0		0	0	0	0	0	0	0	0	0	0	0	0	0	0
11	0	0	0	0	0	0	0	0	0	0	0	0	0	0	0	0	0	0	0	0	0	0	0	0	0	0	0
12	10	0	0	0	0	0	0	0	0	4	10	1	9	0	0	0	0	0	0	0	0	0	0	0	0	0	0
13	2	0	0	0	0	0	0	0	2	4	9	7	9	1	0	0	0	0	0	0	0	0	0	0	0	0	0
14	0	0	0	0	0	0	0	0	0	0	0	0	0	0	0	0	0	0	0	0	0	0	0	0	0	0	0
15	2	0	0	0	0	0	0	0	2	4	9	7	9	1	0	0	0	0	0	0	0	0	0	0	0	0	0
16	0	0	0	0	0	0	0	0	0	0	0	0	0	0	0	0	0	0	0	0	0	0	0	0	0	0	0
17	0	0	0	0	0	0	0	17	0	33	10	9	8	0	0	0	0	0	0	0	0	0	0	0	0	0	0
18	6	0	0	0	0	0	0	0	7	0	0	0	0	0	0	0	0	0	0	0	1	0	0	0	0	0	0
19	0	0	0	0	0	0	0	0	0	4	0	1	0	0	0	0	0	0	0	0	0	0	0	0	0	0	0
20	2	0	0	0	0	1	0	30	19	54	58	51	5	2	0	0	0	0	0	0	0	1	0	0	0	0	0
21	2	0	0	0	0	1	0	30	19	58	58	52	5	2	0	0	0	0	0	0	0	1	0	0	0	0	0
22	6	0	0	0	0	0	0	17	7	33	10	9	8	0	0	0	0	0	0	0	0	1	0	0	0	0	0
23	8	0	0	0	0	1	0	47	26	91	68	61	13	2	0	0	0	0	0	0	0	2	0	0	0	0	0
24	0	0	0	0	0	0	0	17	0	0	0	1	0	0	0	0	0	0	0	0	0	0	0	0	0	0	0
25	0	0	0	0	0	0	0	0	0	0	0	0	0	0	0	0	0	0	0	0	0	0	0	0	0	0	0

Table 6. *Cont.*

1	4	24	64	104	124	164	196	224	264	304	344	386	464	524	564	624	684	704	744	784	864	944	998	1004	1024	1064	1098
26	0	0	0	0	0	0	0	26	1	0	5	0	4	0	0	0	0	1	0	0	0	2	0	0	0	0	0
27	0	0	0	0	0	0	0	0	0	0	0	0	0	0	0	0	0	0	0	0	0	0	0	0	0	0	0
28	0	0	0	0	0	0	0	0	0	0	0	0	0	0	0	0	0	0	0	0	0	0	0	0	0	0	0
29	0	0	0	0	0	0	0	43	1	0	5	1	4	0	0	0	0	1	0	0	0	2	0	0	0	0	0
30	0	0	0	0	0	1	0	60	8	42	38	95	36	3	0	0	0	0	0	0	0	2	0	0	0	0	0
31	0	0	0	0	0	0	0	13	6	30	58	39	58	3	0	0	0	4	0	0	0	1	0	0	0	0	0
32	0	0	0	0	0	0	0	9	2	13	34	15	34	1	0	0	0	0	0	0	0	0	0	0	0	0	0
33	0	0	0	0	0	0	0	0	0	0	0	6	0	0	0	0	0	0	0	0	0	0	0	0	0	0	0
34	0	0	0	0	0	1	0	82	16	85	130	155	128	7	0	0	0	4	0	0	0	3	0	0	0	0	0
35	0	0	0	0	0	0	0	0	0	0	0	0	0	0	0	0	0	0	0	0	0	0	0	0	0	0	0
36	0	0	0	0	0	0	0	0	0	0	0	0	0	0	0	0	0	0	0	0	0	0	0	0	0	0	0
37	0	0	0	0	0	0	0	0	0	0	0	0	0	0	0	0	0	0	0	0	0	0	0	0	0	0	0
38	0	0	0	0	0	0	0	0	0	0	0	0	0	0	0	0	0	0	0	0	0	0	0	0	0	0	0
39	0	0	0	0	0	0	0	0	0	0	0	0	0	0	0	0	0	0	0	0	0	0	0	0	0	0	0
40	20	0	0	0	0	2	0	172	45	184	222	225	163	10	0	0	0	5	0	0	0	7	0	0	0	0	0
41	0	0	0	0	0	0	0	0	0	0	0	0	0	0	0	0	0	0	0	0	0	0	0	0	0	0	0
42	0	0	0	0	0	0	0	0	0	0	15	12	14	0	0	0	0	0	0	0	0	0	0	0	0	0	0
43	0	0	0	0	0	0	0	0	0	0	0	0	0	0	0	0	0	0	0	0	0	0	0	0	0	0	0
44	0	0	0	0	0	0	0	0	0	0	0	0	0	0	0	0	0	0	0	0	0	0	0	0	0	0	0
45	0	0	0	0	0	0	0	0	0	0	0	0	0	0	0	0	0	0	0	0	0	0	0	0	0	0	0
46	0	0	0	0	0	0	0	0	0	0	0	0	0	0	0	0	0	0	0	0	0	0	0	0	0	0	0
47	0	0	0	0	0	0	0	0	0	0	0	0	0	0	0	0	0	0	0	0	0	0	0	0	0	0	0
48	0	0	0	0	0	0	0	0	1	0	0	0	0	0	0	0	0	0	0	0	0	0	0	0	0	0	0
49	0	0	0	0	0	0	0	0	0	0	0	0	0	0	0	0	0	0	0	0	0	0	0	0	0	0	0
50	0	0	0	0	0	0	0	0	0	8	10	0	10	0	0	0	0	0	0	0	0	0	0	0	0	0	0
51	0	0	0	0	0	0	0	0	0	0	0	0	0	0	0	0	0	0	0	0	0	0	0	0	0	0	0
52	0	0	0	0	0	0	0	0	0	0	0	0	0	0	0	0	0	0	0	0	0	0	0	0	0	0	0
53	0	0	0	0	0	0	0	0	0	0	0	0	0	0	0	0	0	0	0	0	0	0	0	0	0	0	0
54	0	0	0	0	0	0	0	0	0	0	0	0	0	0	0	0	0	0	0	0	0	0	0	0	0	0	0
55	0	0	0	0	0	0	0	0	3	0	0	0	0	0	0	0	0	0	0	0	0	2	0	0	0	0	0
56	0	0	0	0	0	0	0	0	0	0	0	0	0	0	0	0	0	0	0	0	0	0	0	0	0	0	0
57	0	0	0	0	0	0	0	0	4	8	25	12	24	0	0	0	0	0	0	0	0	2	0	0	0	0	0
58	0	0	0	0	0	0	0	0	0	17	5	2	5	1	0	0	0	0	0	0	0	0	0	0	0	0	0
59	0	0	0	0	0	0	0	0	0	0	0	0	0	0	0	0	0	0	0	0	0	0	0	0	0	0	0
60	0	0	0	0	0	0	0	0	0	17	5	2	5	1	0	0	0	0	0	0	0	0	0	0	0	0	0
61	0	0	0	0	0	0	0	0	0	0	0	0	0	0	0	0	0	0	0	0	0	0	0	0	0	0	0
62	0	0	0	0	0	0	0	0	0	0	0	0	0	0	0	0	0	0	0	0	0	0	0	0	0	0	0
63	0	0	0	0	0	0	0	0	0	0	0	0	0	0	0	0	0	0	0	0	0	0	0	0	0	0	0
64	0	0	0	0	0	0	0	0	0	0	0	0	0	0	0	0	0	0	0	0	0	0	0	0	0	0	0
65	0	0	0	0	0	0	0	0	0	0	0	0	0	0	0	0	0	0	0	0	0	0	0	0	0	0	0
66	0	0	0	0	0	0	0	0	0	0	0	0	0	0	0	0	0	0	0	0	0	0	0	0	0	0	0
67	0	0	0	0	0	0	0	0	0	0	0	0	0	0	0	0	0	0	0	0	0	0	0	0	0	0	0
68	0	0	0	0	0	0	0	34.3	2	46.5	29	8.5	29	5	0	0	0	1	0	0	0	0	0	0	0	0	0
69	20	0	0	0	0	2	0	172	49	209	252	239	192	11	0	0	0	5	0	0	0	9	0	0	0	0	0
70	0	0	0	0	0	0	0	4	6	0	0	0	0	17	0	0	0	6	0	0	0	15	6	0	0	5	0
71	0	0	0	0	0	0	2	0	0	0	0	0	0	0	0	0	0	0	0	0	0	0	0	0	0	0	0
72	0	0	0	0	0	0	3	632	0	796	9019	852	9019	112	0	0	0	19	0	0	0	62	0	0	0	0	0
73	0	0	0	0	0	0	0	34.3	6	9	0	41	0	21	0	0	0	7	0	0	0	1	4	0	0	3	0
74	0	0	0	0	0	0	0	0	0	0	0	0	0	0	0	0	0	0	0	0	0	0	0	0	0	0	0
75	0	0	0	0	0	0	0	0	4	0	0	1.2	0	0	0	0	0	0	0	0	0	0	0	0	0	0	0
76	50					0		0	0	4.0	11.5	1.4	29.0	0								0					
77	20					0		0	0	3	7	0	16	0								0					
78	40					100		100	92.9	91.9	78.2	88.4	41.9	66.7								100					
79	20					0		0	11.0	6.0	9.0	9.0	16.0	67.0								0					
80	10					0		0	7.1	4.0	10.3	10.1	29.0	33.3								0					
81	5					0		0	4	4	7	7	16	33								0					
82	20					0		0.0	7.1	4.2	11.7	10.3	40.9	33.3								0					
83	20					0		0.0	7.1	4.2	7.8	7.4	22.7	19.9								0					
84	20					0		4.2	7.1	3.2	6.5	5.9	18.2	14.5								0					
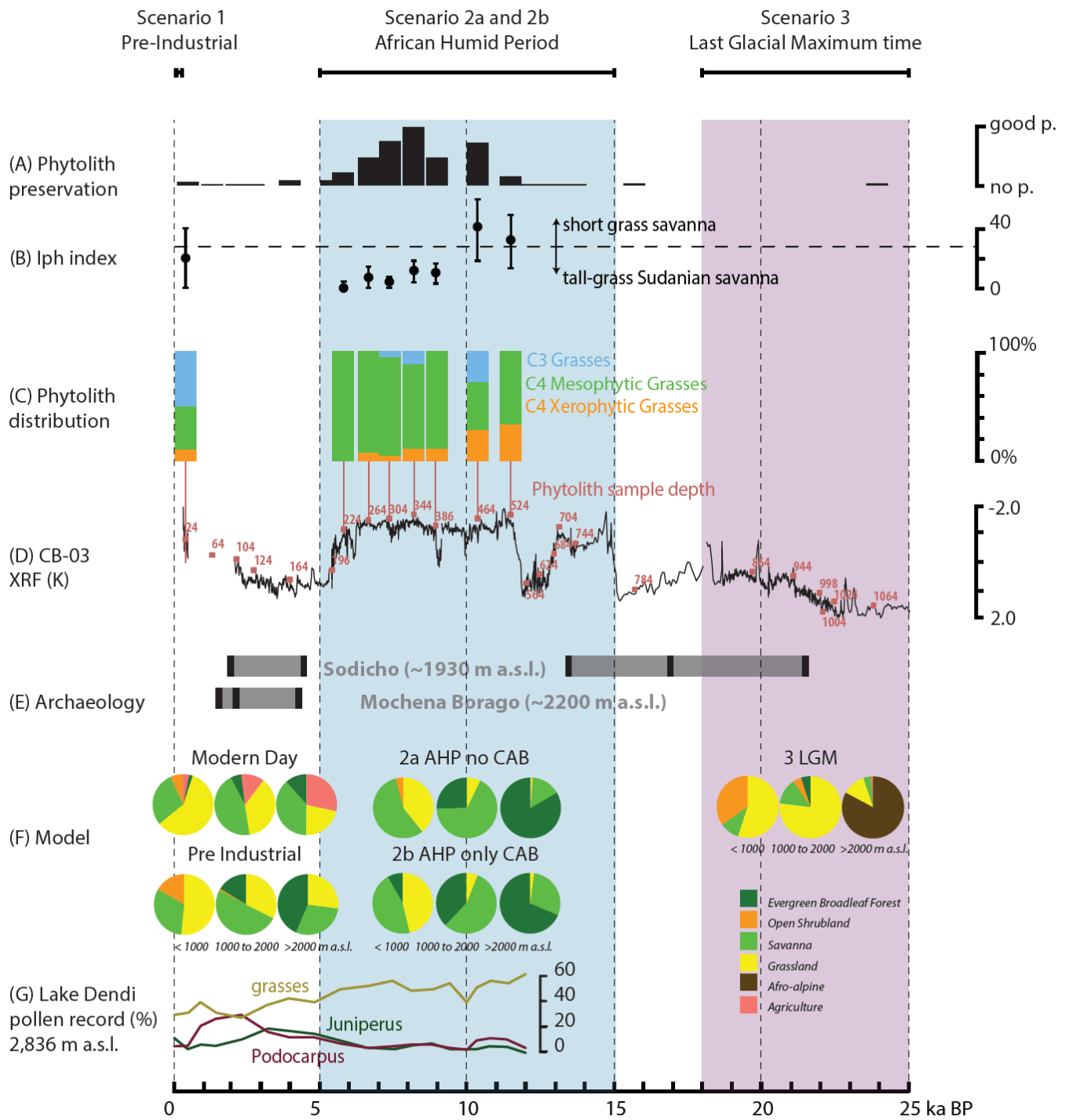
Figure 7. Proxy time series and model results: (**A**) Phytolith preservation. (**B**) Iph index. (**C**) Phytolith type distribution. (**D**) Potassium proxy record of CB-03 [33]. (**E**) Archaeological record with dated (confirmed) occupation (black) [59,60,64] and presumed occupation (grey). (**F**) Orographic strata model results with LC. (**G**) Lake Dendi pollen record summary [16].

5. Discussion

5.1. Results Synthesis

Our biosphere-hydrosphere modelling approach for southern Ethiopia from the LGM times to the present shows: (a) during the LGM, an annual precipitation decrease of at least 15 to 20%, along with decreased temperatures. This would explain the lake regression and would have resulted in extensive grassland cover and sparse vegetation in the lower

elevations and widespread afro-alpine vegetation above approximately 2000 m a.s.l. (b) A precipitation increase of at least 25% during the AHP, which would explain the observed high lake level of paleo-lake Chew Bahir reaching the overflow sill. This precipitation increase would produce dense forest cover in the high altitudes (above 2000 m a.s.l.) and dense vegetation cover in the vicinity of northern Lake Turkana, as well as along the shores of paleo-lake Chew Bahir. (c) In the CAB scenario, it would require at least 41% more precipitation than modern levels to sustain the observed lake changes and would produce less dense vegetation in the high altitudes and favour forest coverage at the mid-altitudes (between 1000 and 2000 m a.s.l.). (d) The modern-day land-use has about a fourth of the forest coverage (10%) at high-altitudes compared to the pre-industrial potential LC (44%) and reduced forest coverage at mid altitudes from 16 to 4%.

5.1.1. Scenario 3—LGM

Previous studies based on reconstructed vegetation and their potential hydro-climatic habitat on a pan-African scale revealed a reduction of around 25 to 27% annual precipitation during LGM times in eastern Africa, compared to the amount of modern-day precipitation [102]. The orographic temperature driven displacement of the vegetation belts was estimated to be around −700 m in the dry, high mountains and around −1000 m in the humid mountainous regions [15], which is also supported by our modelling results that suggest an orographic lowering of the afro-alpine vegetation to around −1000 m. The pan-African vegetation reconstruction (based on sea surface temperature derived paleo-precipitation estimates and resulting vegetation transfer functions) by Anhuf, et al. [15] suggests grass savanna cover in the surrounding of Lake Turkana, dry forest or savanna vegetation in the majority of the area and forests in the highland areas. The coupled earth system model HadCM3LC yields a forest cover of less than 40% in Ethiopia during LGM times, in contrast to partly 60 to 80% forest cover during pre-industrial time [103]. Our model results for the LGM times are in overall agreement with the earth system model [103] and transfer function results [102], but paleo-lake Chew Bahir would already dry out at a precipitation decrease of 15 to 20%. In contrast to Hopcroft and Valdes [104], who used HadGEM2-ES to infer global vegetation patterns, our modelling results do not show vast spatial distribution of forests in Ethiopia, neither in the western nor in the central highlands. There is no general decrease in the EVI (vegetation greenness or proxy for productivity), but instead a large decrease in EVI in the high altitudes of the western highlands and the southeastern escarpments. In contrast, an EVI increase is observed in the rift lakes region surrounding lakes Abaya and Chamo and the lowlands of the BRZ. For all altitudes, the tree cover decreased from 17 to 14%. Tree refugia during the LGM are mainly the Gofa range, the northwestern escarpments, as well as parts of the Agere-Selam escarpment (Figure 1). In contrast to the Agere-Selam escarpment, our model did not suggest a tree refuge in the Gamo-Gidole Horst, which suggests the possibility of a complex reorganisation of the vegetation mosaic in the EARS during the LGM.

The model result is tested with a new pollen record from the Gelba wetlands at 2300 m a.s.l. (Figure 1) [105], which are located in the Gamo-Gidole Horst at the catchment boundary of lakes Abaya and Chamo. Results from the Gelba wetland record show a high abundance of afro-alpine vegetation during late LGM times (*Ericaceous*, afro-montane forest), in addition to more dry conditions until about 13.5 ka BP, with increasing afro-alpine vegetation and wetlands/open water after 13 ka BP. Pollen from *Podocarpus*, *Juniperus*, *Artemisia*, *Rumex* and *Poaceae* are abundant in that region during the LGM [105], which indicates the presence of dry afro-montane forest species.

5.1.2. Scenario 2—AHP

In our preceding LBM study [10], it was estimated that a precipitation threshold of 120 to 130% during the AHP was required to allow paleo-lake Chew Bahir to reach the overflow sill at 543 m a.s.l., whereby +7–15% of the increase is due to vegetation feedback. However, the quantification of the vegetation feedback was previously used from a study

at Lake Naivasha in Kenya by Bergner, et al. [36], where paleo-vegetation was extrapolated based on pollen proxy information and subsequently parametrised to calculate ET in the same manner as explained in Section 3.3.2. Since pollen data as well as precise paleo-vegetation estimates are scarce in southern Ethiopia, a continuous PVM was used for all precipitation amounts and a new threshold was determined. This threshold shows an addition of +18–34% is needed to compensate for the biosphere feedback.

Other studies concerning the overall precipitation estimate for the EARS during the AHP based on LBMs yield: +20–30% (Ziway–Shala +28% [106]; Lake Turkana +20% [107]; Suguta Valley +26% [13]; Lake Nakuru–Elmenteita +23–45% [108] and Lake Naivasha +29–33% [36,107]). Apart from the estimate from Lake Naivasha, none of these model approaches considered the biosphere feedback, making those estimates presumably too small. A site specific or a pan-eastern African vegetation model, similar to the one presented here for paleo-lake Chew Bahir, could resolve these uncertainties.

The impact of changing seasonality on ET, due to a shift in the CAB (Scenario 2b), with the additional precipitation required to compensate for the increased ET during present-day dry months, was estimated at +7% based on SEBAL results for each month [10]. Our current hydrosphere-biosphere approach suggests an even larger effect of +16%, including the biosphere feedback. The 2b scenario (CAB caused seasonality changes) promotes the growth of forests in the mid-altitudes (between 1000 and 2000 m a.s.l.) which comprise most of the catchment areas for lakes Abaya and Chamo, both of which were significant water sources for paleo-lake Chew Bahir. Forest growth in these catchments would decrease the surface runoff to the lakes while significantly increasing ET on land. However, our modelling results provide possible realizations of a hydrosphere-biosphere interaction within the EARS as a minimum precipitation amount with two contrasting AHP scenarios, whereas a mixture of both (2a and 2b) seem most likely.

Scenario 2a (equally enhanced rainfall) suggests an approximately 40% increase in EVI and a 150% increase in tree cover throughout the study area compared to modern-day conditions. For scenario 2b, the tree cover increase is lower at 115%. The EVI increase is almost the same at 38%. In comparison, the CAB 2b scenario would increase EVI in the lowlands (below 1000 m a.s.l.) and the lake shores of Abaya and Chamo, as well as for the eastern escarpments, which are regions where the dry season is well pronounced. In contrast, the 2a scenario would increase EVI on the highlands in the northwestern part of the Omo River catchment, but the increase is not significant compared to the overall increase throughout the study area. The diverging model results between 2a and 2b for the southeastern escarpments also apply to the TC prediction. The 2b scenario produces forest growth, whereas the 2a scenario does not produce forests in that region. Furthermore, the 2b CAB scenario would result in an increase in forest coverage in the vicinity of Lake Abaya relative to modern-day conditions, which would not be the case in scenario 2a.

We conclude that the potential forest coverage during the AHP in southern Ethiopia is restructured and the overall trend observed in the modelling results is in agreement with the pollen record from Augustijns, et al. [105]. The pollen record shows wet to open water conditions and afro-montane forest pollen peaks at 13 ka and 7 ka. A pollen record from the central Ethiopian highlands from Lake Dendi (3270 m a.s.l.) revealed a low abundance of *Podocarpus* and *Juniperus* pollen during the AHP and instead yielded high *Poaceae* abundances [16], which would be in accordance with the modelling results of scenario 2b. This could be interpreted as supporting evidence for the concept of an eastward shift and intensification of the CAB.

5.1.3. Scenario 1—Pre-Industrial

How agriculture and grazing altered the landscape and affected the potential vegetation cover during the PI remains an open question. For instance, the Northwestern Ethiopian Highlands have been deforested since at least 3 ka, when agriculture and grazing progressively replaced hunting and gathering [109,110]. Soil erosion altered the landscape and may have degraded the ecosystem irreversibly [3]. This also affected the water run-off

coefficient and the water budget of the lake basins [110]. Such a complete deforestation is not visible in the pollen record from the Chencha bog (3000 m a.s.l.) on the Chencha Horst (Figure 1), where the afro-montane forest cover seems to decrease at 1.7 ka but recovers after 0.8 ka [105]. In contrast, around Lake Turkana, Gil-Romera, et al. [111] did not see indications for a human-induced ecosystem shift in the past 2 ka. Instead, they concluded that bush encroachment and retraction are predominately controlled by rainfall and fire on multi-decadal to centennial cycles.

Overall, the model suggests that 11.5% of afro-montane forests have been replaced by agricultural areas. The forest coverage decreased (pre-industrial to modern-day) from 44% to 10% in high altitudes and from 16 to 4% in mid to low altitudes, showing the immense impact of agriculture on the landscape in the highlands. The model results agree with the atlas of the potential vegetation of Ethiopia [3] for the moist evergreen afro-montane forest but classifies vast parts of the dry evergreen afro-montane forest as grassland. Either the lack of sufficient training data for the dry central Ethiopian highlands could bias the result as the model is based on a learning algorithm, or grassland may already be a proper classification for the degraded potential landscape. The grassland and savanna classified areas of the PI scenario are different to the results of the potential vegetation based on Friis, et al. [3]. The species perspective from Friis, et al. [3] does not match either the observed or the predicted landscape phenology and density of the MODIS LC, which follows a north-south gradient (Figure 3).

The shrinking of agricultural areas and the increase of savanna and grassland areas in the catchment of Lake Abaya reduces the ET rate on land for the PI scenario, which then leads to a modelled positive water budget within the lake system of lakes Abaya, Chamo and paleo-lake Chew Bahir. This could imply that agricultural activities in the Main Ethiopian Rift degraded the landscape and replaced high forest ET (low run-off) with high agricultural ET, conserving the water balance. However, if the actual soil-determined potential vegetation is a grassland complex (low ET, higher run-off), a hypothetical spontaneous end of agriculture would lead to a less negative water budget and increased lake levels. In contrast, a potential and realistic further increase in agriculture and extensive water use could result in a more negative water budget and decrease the lake levels of lakes Abaya and Chamo.

The LC in the Lake Abaya basin has been changing for decades [112], which may lead to an increase of areas with extensive water use and agriculture (coffee, banana) on the one hand, and gully eroded areas with a high run-off for the lake's water supply on the other. This explains the high sediment load of Lake Abaya, visible even in satellite imagery. For the PI, this could further imply that extensive agriculture has already affected the water budget of Lake Abaya and subsequently Lake Chamo and paleo-lake Chew Bahir. This extrapolation is supported by a report by von Höhnel [113], who observed in 1888 at the end of the dry season that the southern shore of paleo-lake Chew Bahir was occupied by a shallow lake, which is desiccated today. High lake levels after the termination of the Little Ice Age at the end of the 19th century have also been reported (e.g., Nicholson [114]) for lakes in the vicinity and under a similar climate regime. Based on the model results, we conclude that the persistent aridification of southern Ethiopia since the beginning of the 20th century, could be at least partly caused by LC changes.

5.2. Proxy Model Interference

While the atlas of the potential vegetation of Ethiopia [3] uses dominant and characteristic plant species to classify the broad variety of vegetation types, the MODIS LC uses remote sensing derived phenology and spectral properties to classify the vegetation and the landcover. Phytoliths as an environmental proxy from the Chew Bahir sediment cores [33], allow us to distinguish mesic and xeric as well as C_4 and C_3 grasses [95]. The best preservation of phytoliths is recorded during the AHP (Figure 7). The abundance of C_3 grass phytoliths is interpreted as the existence of aquatic vegetation of a wetland (dominated by C_3) near the sediment core site, similar to today. Due to changes in the water level

of paleo-lake Chew Bahir over the past 20 ka, the wetland vegetation may have migrated up to 100 km northwards. If the wetlands are close to the drill location, the C_3 signals prevails. The wetland, with its dense aquatic vegetation seen today, may act as a phytolith filter that filters out long-distance phytolith transport. We thus assume that the origin of C_4 phytoliths in the Chew Bahir sediments are sourced in the catchment of the Hamar Range and in particular the catchment that is related to the alluvial fan 6 km west of the drill site. C_4 xeric phytolith types may indicate the existence of open shrubland to grassland on these alluvial fans, which would be the desert and semi-desert shrubland unit based on Friis, et al. [3]. C_4 mesic phytolith types indicate a grassland to savanna landscape, which would belong to the *Acacia-Commiphora*, respectively, the *Combretum-Terminalia* woodland and wooded grassland [3], especially *Combretum-Terminalia* woodland, as it is typically covered by dense (mesic) grass vegetation.

During the LGM, the absence of phytoliths (most likely caused by dissolution) supports the scenario of a highly alkaline paleo-Lake Chew Bahir. Our model uses this condition as a lake disappearance precipitation threshold (see Figure 5C). During the AHP, the rapid onset of phytolith preservation starting around 11 ka agrees with the rapid onset of humid conditions as recorded in the Chew Bahir K record and other records from paleo-lakes in the vicinity [13,34,35,93]. Phytolith preservation decreased continuously over a period of 3000 years (8 to 5 ka), again providing proxy evidence for a gradual decline of the AHP in the region, as previously also suggested by Foerster, et al. [33] and Fischer, et al. [10] and statistically analysed by Trauth, et al. [94]. During the main phase of the AHP (11 to 6 ka), the record shows the dominance of C_4 mesic phytoliths, and hence a savanna landscape with underlying dense productive grass, even close to the lake shore, which is a modern-day sparse grass and/or open shrubland area. The slow replacement of C_4 xeric grasses (suggesting open or semi-desert shrubland) could indicate either a slow climatic signal towards more and continuous precipitation in the lowlands, or a signal of the slow replacement process towards a more closed savanna landscape in the area. This trend could also be interpreted as a slow reaction of the landscape due to a groundwater-table-dependent vegetation structure, since groundwater may react over millennial time scales [115]. On the other hand, this trend could be an artefact in the phytolith record due to morphotype specific dissolution [116] during the AHP, showing the limitation of this phytolith record. The continuous upward trend is punctuated by two C_3 grass phytolith peaks at 10.5 ka and 9 ka, that is in agreement with the Chew Bahir K proxy record [11]. This could mark a brief period of dry conditions leading to rapid lake desiccation and a formation of a dense and productive wetland in the basin until it becomes flooded again. Fischer, et al. [10] concluded, based on the lake dynamics modelling and K-proxy results, that many of these lake level fluctuations interrupted the paleo-lake highstand during the AHP. A higher resolution phytolith analysis extending further back in time may detect additional lake desiccation phases.

5.3. Limitations and Advantages of the Method

We used elevation and monthly precipitation as the only predictors in our model, being aware that LC is also determined by other environmental factors, such as lithology, soil type or depth, geomorphological position (such as aspect, slope and terrain position) or windspeed and dry season length [117]. Precipitation and elevation, however, are the major determinants of the vegetation in tropical Africa [3,117]. Incorrect LC classifications, especially in the transition areas (forest to savanna and grassland to open shrubland), are below a significant error for our application on the hydrological cycle but may remain a consequence of the simple model structure. A better spatial precision for LC prediction could be achieved with the incorporation of more predictors, but testing, for example, the topographic position index on different spatial scales has not shown a significant effect. In addition to derivates of precipitation and elevation, reliable high-resolution data are especially scarce for soils and the lithology in southern Ethiopia. Additionally, a model with a higher complexity may lack traceability. Hence, we used these simple predictors for

our LC prediction, being aware that the interpretation of results for areas of smaller scales, such as archaeological sites, incorporate uncertainties.

With a ROC of 0.79, the model fits the LC prediction well. It was necessary, however, to include an additional weighting factor, making each class equally important, as the imbalance between them made a successful model training for all classes impossible. This has led to a higher classification importance for the open shrubland and forest classes, which increases their suitable habitat in the PI prediction tremendously. This effect is acceptable since the dry parts of the grassland classified areas of the MODIS product for example, may be classified as open shrubland as well. The parameter variability (greenness, phenology, precipitation and elevation) in the LC groups overlap with the neighbouring groups. Another effect is the higher importance of the forest class in the model training and hence the broad increase of forest coverage in the high altitudes for the PI scenario. Forests are mainly limited to refugia and inaccessible areas. Hence, the environmental boundaries of the predictors (precipitation, elevation) can only be partly learned by the algorithm. The algorithm cannot learn a potential habitat of forests, if there are no remaining broadleaf forests left today, which may be true especially for the drier parts of the Ethiopian highlands [3]. Moreover, the coarse data resolution of the precipitation, compared to the landcover, leads inherently to the overlapping predictor variable space in between the LC's.

While LC, EVI and TC prediction works well, NVC and NTC prediction was not possible. The model is not able to predict low NTC correctly, as low NTC could imply high TC or high NVC, either on densely green or sparsely vegetated areas (see Figure 8A). The prediction of NVC works well for low NVC but fails to predict high NVC (Figure 8B). The predicted NVC stabilizes at around 20-40%, while the observed NVC reaches almost 100%. Again, we encounter problems due to the coarse resolution of the GPM precipitation data and overlapping predictor variable space on a variety of plant phenology. This inappropriate model behaviour might also be caused by non-involved forcing factors such as the underlying soil. For instance, the white clayish lacustrine sediments of Chew Bahir, covering about 755 km^2, prevents plant growth, while the predictions based on the precipitation-elevation would predict sparse vegetation.
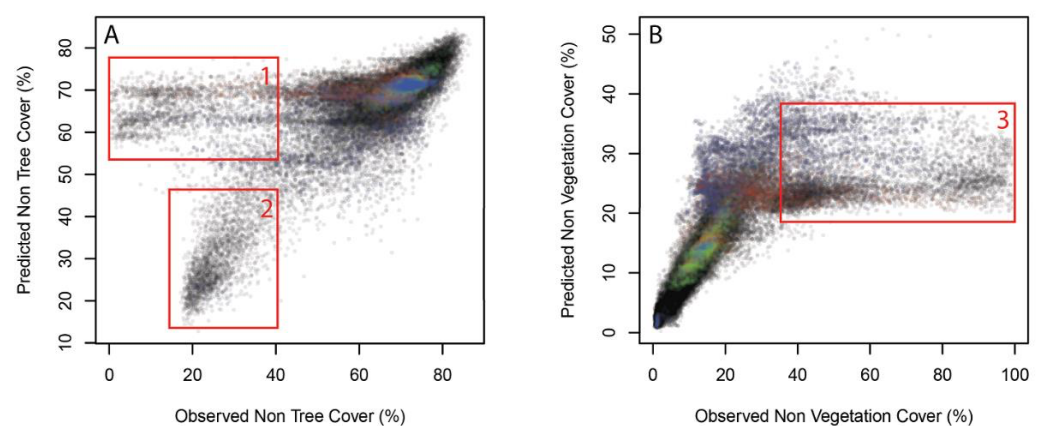
Figure 8. Observed vs. predicted NTC (**A**) and NVC (**B**): (**1**) low observed NTC with high predicted NTC; (**2**) good fit to the data; (**3**) predicted NVC saturation at around 20–40%; red = wildlife reserve; green = national parc; blue = controlled hunting area.

The model link is the central step in aligning the thresholds of the lake's system with the response of the surrounding vegetation. The parameter-based approach in estimating the annual ET [36,75,91] is widely used and tested for its sensitivity for the input parameter [10,36]. For the application, the LBM is dependent on precise input parameters, that are determined, tested and calibrated in our precursor study [10]. The calibrated surface parameters (albedo, emissivity, soil moisture availability and roughness length) were tested

carefully on the closed basins internal logic of the resulting ET in balance with P. This resulted in a difference of the LC surface parameters, compared to Bergner, et al. [36] and Lyons, et al. [91], but the in-between class differences remained. Land surface parameterization remains an approximation with classified LC's. The transitions between open shrublands, grasslands, savannas and forests are gradual. Continuous predictor models combined with ET land surface parameterization could improve the performance of the hydrosphere-biosphere prediction.

5.4. Human Landscape Preferences

Our model shows that the landscape in the study area during the LGM is dominated by a mixture of grasslands with a variety of vegetation types, resulting in a complex, mosaic landscape that would have offered a wide range of resources for hunter-gatherers. Hunter-gatherers at Sodicho Cave used exclusively obsidian raw material to produce their stone tools [118]. The use of the Humbo Baantu outcrop as obsidian source is attested for Sodicho Cave [64] and Mochena Borago [59,60]. The Humbo Baantu outcrop is around 20 km southeast from Mochena Borago [60] and around 60 km from Sodicho Cave (Figure 1). The use of these outcrops [64,118] shows the wide range of hunter-gatherers in the open landscape during the LGM. Movements through such landscapes to reach for example the Humbo Baantu obsidian outcrop, would have required at least a short-term camp and open water stop, that might have been available as residual water in the highlands [64,119] or even in the colder areas of afro-alpine vegetation or at small, temporal streams in the Lake Abaya catchment. The potential of alpine environments for human life/occupation is shown at Fincha Habera, although Ossendorf, et al. [29] suggest the existence of gallery forests within the Bale Mountain valleys. Trees are almost nonexistent at Mochena Borago according to our modelling results during the LGM, and the absence of evidence of human activity [59,60] may indicate that humans avoided the afro-alpine belt. Our modelling results support the refugium character of Ethiopian highlands during cold and dry conditions [10,33,59,60,64,120]. In summary, it seems that humans in southern Ethiopia lived in a rather open grassland with some trees during the LGM.

For the African Humid Period, the modelling results indicate a vast expansion of forests and dense vegetation in southern Ethiopia. According to the results, forests and dense vegetation covered the known obsidian outcrops in the area that were intensively used by humans during the LGM. So far, the archaeological record and our modeling results suggest that human activities ceased during very wet periods when dense vegetation and forests predominated. The exact reasons for this remain unknown, but it can be speculated that also pronounced wet phases were not necessarily favorable for humans, possibly because of dense vegetation constraining mobility or promoting the spread of diseases.

With obsidian becoming inaccessible due to the forest cover, the Main Ethiopian Rift lakes, such as Ziway-Shala presumably offered easier access to food, water and raw material [33,61,64]. The highly variable lithic technology along the lakes through time indicates a complex and changing settlement pattern coherent to changing lake levels [10,33,61]. Due to a gap in the archaeological record, rapidly changing lake levels seem to be unfavorable conditions for humans, however, it is also possible that signs of former human activities were simply washed away [33]. The shores of lakes Abaya and Chamo became densely vegetated and forested during the AHP, according to the model scenario 2b (CAB caused change in seasonality). If humans preferred more open landscapes in southern Ethiopia at this time, the closed landscape at the shores of lakes Abaya and Chamo would explain the absence of archaeological records. There are also no published archaeological records from the shores of paleo-lake Chew-Bahir, except for a brief report on rock engravings (5.66 ka $\pm$ 0.11; 4781–4274 cal BP) from an island in the southern part of the lake after the termination of the AHP [121]. The persistence of an open landscape, however, indicates a potential for archaeological sites during the AHP, similar to Lake Turkana [33]. After the AHP, human activity is recorded again in the archaeological record

of Mochena Borago and Sodicho Caves [64,118,122]. The modelling results show that Mochena Borago and Sodicho Cave may have been surrounded by grassland once again.

Within the last 25 ka, hunter-gatherers used Mochena Borago and Sodicho Caves when the vicinity of the sites were characterized by grassland and solitary trees. With caution, we may propose that during the LGM and Middle Holocene, humans in southern Ethiopia occupied or even may have preferred open landscapes.

6. Conclusions

We developed a new Predictive Vegetation Model (PVM) based on open-source methods and multi-source data, which we linked to a Lake Balance Model (LBM) of the southern Main Ethiopian Rift [10] to independently reconstruct and disentangle the environmental processes, changes and amplitudes for the Last Glacial Maximum (LGM), the African Humid Period (AHP) and the pre-industrial (PI) time. The model output was compared to a new phytolith proxy record from Chew Bahir basin and pollen records from southern Ethiopia. The model shows a 15–20% decrease of annual precipitation during the LGM, which was dominated by open landscapes in the low and high altitudes with only a few forest refuges remaining, leading to the desiccation of paleo-lake Chew Bahir. During the AHP, a 25–40% increase in the annual precipitation amount resulted in a doubling of forest-covered areas and would explain the maximum possible lake level of paleo-lake Chew Bahir. Additional rainfall during northern hemisphere summer due to an eastward shift of the CAB would lead to a dense forest coverage in the mid-altitudes and open landscape in the highlands, which is supported by pollen records. The phytolith record indicates a rapid onset of humid conditions at ~12 ka and a slow transition throughout the AHP to mesic conditions. Our comparison of model results and archeological records in that region suggests that humans may have largely occupied open landscapes. For the modern time, we conclude that the agriculturally altered landscape may endanger the water supply of the lakes Abaya and Chamo and may have contributed to the aridification of the Chew Bahir basin during the 20th century. This is of interest and concern for land and water management in Ethiopia in the near future, due to the increasing agricultural use of the Lake Abaya basin.

Author Contributions: This study was designed by M.L.F. and A.J.; M.L.F. developed and performed the vegetation model; Phytolith analysis was accomplished by C.L.Y. and A.J.; C.S. discussed archaeological implications. All authors contributed data and analysis tools. All authors contributed to the article and approved the submitted version. All authors have read and agreed to the published version of the manuscript.

Institutional Review Board Statement: Not applicable.

Informed Consent Statement: Not applicable.

Data Availability Statement: All scripts are available at Github: https://github.com/MLFischer/Paleo-Vegetation-Model (accessed 1 October 2021).

Conflicts of Interest: The authors declare no conflict of interest.

References

1. Corti, G. Continental rift evolution: From rift initiation to incipient break-up in the Main Ethiopian Rift, East Africa. *Earth Sci. Rev.* **2009**, *96*, 1–53. [CrossRef]
2. Nicholson, S.E. Climate and climatic variability of rainfall over eastern Africa. *Rev. Geophys.* **2017**, *55*, 590–635. [CrossRef]
3. Friis, I.; Demissew, S.; van Breugel, P. *Atlas of the Potential Vegetation of Ethiopia*; Det Kongelige Danske Videnskabernes Selskab: Copenhagen, Denmark, 2011.
4. Schaebitz, F.; Asrat, A.; Lamb, H.F.; Cohen, A.S.; Foerster, V.; Duesing, W.; Kaboth-Bahr, S.; Opitz, S.; Viehberg, F.A.; Vogelsang, R.; et al. Hydroclimate changes in eastern Africa over the past 200,000 years may have influenced early human dispersal. *Commun. Earth Environ.* **2021**, *2*, 123. [CrossRef]
5. Kaboth-Bahr, S.; Gosling, W.D.; Vogelsang, R.; Bahr, A.; Scerri, E.M.L.; Asrat, A.; Cohen, A.S.; Düsing, W.; Foerster, V.; Lamb, H.F.; et al. Paleo-ENSO influence on African environments and early modern humans. *Proc. Nat. Acad. Sci. USA* **2021**, *118*, e2018277118. [CrossRef]
6. Gasse, F. Hydrological changes in the african tropics since the last glacial maximum. *Quat. Sci. Rev.* **2000**, *19*, 189–211. [CrossRef]
7. Loomis, S.E.; Russell, J.M.; Verschuren, D.; Morrill, C.; De Cort, G.; Sinninghe Damsté, J.S.; Olago, D.; Eggermont, H.; Street-Perrott, F.A.; Kelly, M.A. The tropical lapse rate steepened during the Last Glacial Maximum. *Sci. Adv.* **2017**, *3*, e1600815. [CrossRef]
8. Barker, P.A.; Talbot, M.R.; Street-Perrott, F.A.; Marret, F.; Scourse, J.; Odada, E.O. Late quaternary climatic variability in intertropical Africa. In *Past Climate Variability through Europe and Africa*; Springer: Berlin, Germany, 2004; pp. 117–138.
9. Demenocal, P.; Ortiz, J.; Guilderson, T.; Adkins, J.; Sarnthein, M.; Baker, L.; Yarusinsky, M. Abrupt onset and termination of the African humid period. *Quat. Sci. Rev.* **2000**, *19*, 347–361. [CrossRef]
10. Fischer, M.L.; Markowska, M.; Bachofer, F.; Foerster, V.E.; Asrat, A.; Zielhofer, C.; Trauth, M.H.; Junginger, A. Determining the pace and magnitude of lake level changes in Southern Ethiopia over the last 20,000 years using lake balance modeling and SEBAL. *Front. Earth Sci.* **2020**, *8*, 197. [CrossRef]
11. Foerster, V.; Junginger, A.; Langkamp, O.; Gebru, T.; Asrat, A.; Umer, M.; Lamb, H.F.; Wennrich, V.; Rethemeyer, J.; Nowaczyk, N.; et al. Climatic change recorded in the sediments of the Chew Bahir basin, southern Ethiopia, during the last 45,000 years. *Quat. Int.* **2012**, *274*, 25. [CrossRef]
12. Garcin, Y.; Melnick, D.; Strecker, M.R.; Olago, D.; Tiercelin, J.-J. East African mid-Holocene wet–dry transition recorded in palaeo-shorelines of Lake Turkana, northern Kenya Rift. *Earth Planet. Sci. Lett.* **2012**, *331*, 322–334. [CrossRef]
13. Junginger, A.; Trauth, M.H. Hydrological constraints of paleo-Lake Suguta in the Northern Kenya Rift during the African Humid Period (15–5kaBP). *Glob. Planet. Change* **2013**, *111*, 174–188. [CrossRef]
14. Costa, K.; Russell, J.; Konecky, B.; Lamb, H. Isotopic reconstruction of the African Humid Period and Congo Air Boundary migration at Lake Tana, Ethiopia. *Quat. Sci. Rev.* **2014**, *83*, 58–67. [CrossRef]
15. Anhuf, D.; Ledru, M.P.; Behling, H.; Da Cruz, F.W.; Cordeiro, R.C.; Van der Hammen, T.; Karmann, I.; Marengo, J.A.; De Oliveira, P.E.; Pessenda, L.; et al. Paleo-environmental change in Amazonian and African rainforest during the LGM. *Palaeogeogr. Palaeoclimatol. Palaeoecol.* **2006**, *239*, 510–527. [CrossRef]
16. Jaeschke, A.; Thienemann, M.; Schefuß, E.; Urban, J.; Schäbitz, F.; Wagner, B.; Rethemeyer, J. Holocene hydroclimate variability and vegetation response in the Ethiopian highlands (Lake Dendi). *Front. Earth Sci.* **2020**, *8*, 585770. [CrossRef]
17. Lamb, A.L.; Leng, M.J.; Umer Mohammed, M.; Lamb, H.F. Holocene climate and vegetation change in the Main Ethiopian Rift Valley, inferred from the composition (C/N and δ13C) of lacustrine organic matter. *Quat. Sci. Rev.* **2004**, *23*, 881–891. [CrossRef]
18. Umer, M.; Lamb, H.F.; Bonnefille, R.; Lézine, A.M.; Tiercelin, J.J.; Gibert, E.; Cazet, J.P.; Watrin, J. Late pleistocene and holocene vegetation history of the Bale Mountains, Ethiopia. *Quat. Sci. Rev.* **2007**, *26*, 2229–2246. [CrossRef]
19. Darwin, C. The descent of man, and selection in relation to sex. *Lond. Murray* **1871**, *415*, 1871.
20. Dart, R. Australopithecus africanus the man-ape of South Africa. *S. Afr. J. Sci.* **1925**, *115*, 195–199. [CrossRef]
21. Falk, J.H.; Balling, J.D. Evolutionary influence on human landscape preference. *Environ. Behav.* **2010**, *42*, 479–493. [CrossRef]
22. Tveit, M.S.; Ode Sang, Å.; Hagerhall, C.M. Scenic beauty: Visual landscape assessment and human landscape perception. *Environ. Psychol. Introd.* **2018**, 45–54. [CrossRef]
23. Niang, K.; Blinkhorn, J.; Ndiaye, M. The oldest Stone Age occupation of coastal West Africa and its implications for modern human dispersals: New insight from Tiémassas. *Quat. Sci. Rev.* **2018**, *188*, 167–173. [CrossRef]
24. Shipton, C.; Blinkhorn, J.; Archer, W.; Kourampas, N.; Roberts, P.; Prendergast, M.E.; Curtis, R.; Herries, A.I.R.; Ndiema, E.; Boivin, N.; et al. The Middle to Later Stone Age transition at Panga ya Saidi, in the tropical coastal forest of eastern Africa. *J. Hum. Evolut.* **2021**, *153*, 102954. [CrossRef]
25. Shipton, C.; Roberts, P.; Archer, W.; Armitage, S.J.; Bita, C.; Blinkhorn, J.; Courtney-Mustaphi, C.; Crowther, A.; Curtis, R.; Errico, F.D.; et al. 78,000-year-old record of Middle and Later Stone Age innovation in an East African tropical forest. *Nat. Commun.* **2018**, *9*, 1832.
26. Roberts, P.; Prendergast, M.E.; Janzen, A.; Shipton, C.; Blinkhorn, J.; Zech, J.; Crowther, A.; Sawchuk, E.A.; Stewart, M.; Ndiema, E. Late Pleistocene to Holocene human palaeoecology in the tropical environments of coastal eastern Africa. *Palaeogeogr. Palaeoclimatol. Palaeoecol.* **2020**, *537*, 109438. [CrossRef]

27. Faith, J.T.; Tryon, C.A.; Peppe, D.J.; Beverly, E.J.; Blegen, N.; Blumenthal, S.; Chritz, K.L.; Driese, S.G.; Patterson, D. Paleoenvironmental context of the Middle Stone Age record from Karungu, Lake Victoria Basin, Kenya, and its implications for human and faunal dispersals in East Africa. *J. Hum. Evolut.* **2015**, *83*, 28–45. [CrossRef]

28. Wilkins, J.; Schoville, B.J.; Pickering, R.; Gliganic, L.; Collins, B.; Brown, K.S.; von der Meden, J.; Khumalo, W.; Meyer, M.C.; Maape, S. Innovative Homo sapiens behaviours 105,000 years ago in a wetter Kalahari. *Nature* **2021**, *592*, 248–252. [CrossRef] [PubMed]

29. Ossendorf, G.; Groos, A.R.; Bromm, T.; Tekelemariam, M.G.; Glaser, B.; Lesur, J.; Schmidt, J.; Akçar, N.; Bekele, T.; Beldados, A.; et al. Middle Stone Age foragers resided in high elevations of the glaciated Bale Mountains, Ethiopia. *Science* **2019**, *365*, 583–587. [CrossRef]

30. Vogelsang, R.; Bubenzer, O.; Kehl, M.; Meyer, S.; Richter, J.; Zinaye, B. When hominins conquered highlands—An acheulean site at 3000 m asl on mount dendi/Ethiopia. *J. Paleolit. Archaeol.* **2018**, *1*, 302–313. [CrossRef]

31. Bergström, A.; Stringer, C.; Hajdinjak, M.; Scerri, E.M.L.; Skoglund, P. Origins of modern human ancestry. *Nature* **2021**, *590*, 229–237. [CrossRef]

32. Nicholson, S.L.; Hosfield, R.; Groucutt, H.S.; Pike, A.W.G.; Fleitmann, D. Beyond arrows on a map: The dynamics of Homo sapiens dispersal and occupation of Arabia during Marine Isotope Stage 5. *J. Anthropol. Archaeol.* **2021**, *62*, 101269. [CrossRef]

33. Foerster, V.; Vogelsang, R.; Junginger, A.; Asrat, A.; Lamb, H.F.; Schaebitz, F.; Trauth, M.H. Environmental change and human occupation of southern Ethiopia and northern Kenya during the last 20,000 years. *Quat. Sci. Rev.* **2015**, *129*, 333–340. [CrossRef]

34. Junginger, A.; Roller, S.; Olaka, L.A.; Trauth, M.H. The effects of solar irradiation changes on the migration of the Congo Air Boundary and water levels of paleo-Lake Suguta, Northern Kenya Rift, during the African Humid Period (15–5ka BP). *Palaeogeogr. Palaeoclimatol. Palaeoecol.* **2014**, *396*, 1–16. [CrossRef]

35. Beck, C.C.; Feibel, C.S.; Wright, J.D.; Mortlock, R.A. Onset of the African Humid Period by 13.9 kyr BP at Kabua Gorge, Turkana Basin, Kenya. *Holocene* **2019**, *29*, 1011–1019. [CrossRef]

36. Bergner, A.G.N.; Trauth, M.H.; Bookhagen, B. Paleoprecipitation estimates for the Lake Naivasha basin (Kenya) during the last 175 k.y. using a lake-balance model. *Glob. Planet. Change* **2003**, *36*, 117–136. [CrossRef]

37. Elith, J.; Graham, C.H.; Anderson, R.P.; Dudík, M.; Ferrier, S.; Guisan, A.; Hijmans, R.J.; Huettmann, F.; Leathwick, J.R.; Lehmann, A.; et al. Novel methods improve prediction of species′ distributions from occurrence data. *Ecography* **2006**, *29*, 129–151. [CrossRef]

38. Guisan, A.; Zimmermann, N.E. Predictive habitat distribution models in ecology. *Ecol. Model.* **2000**, *135*, 147–186. [CrossRef]

39. Van Breugel, P.; Friis, I.; Demissew, S.; Wesche, K. The transitional semi-evergreen bushland in Ethiopia: Characterization and mapping of its distribution using predictive modelling. *Appl. Veg. Sci.* **2016**, *19*, 355–367. [CrossRef]

40. Guisan, A.; Edwards, T.C.; Hastie, T. Generalized linear and generalized additive models in studies of species distributions: Setting the scene. *Ecol. Model.* **2002**, *157*, 89–100. [CrossRef]

41. Duque-Lazo, J.; Van Gils, H.; Groen, T.A.; Navarro-Cerrillo, R.M. Transferability of species distribution models: The case of Phytophthora cinnamomi in Southwest Spain and Southwest Australia. *Ecol. Model.* **2016**, *320*, 62–70. [CrossRef]

42. Pearson, R.G.; Dawson, T.P. Predicting the impacts of climate change on the distribution of species: Are bioclimate envelope models useful? *Glob. Ecol. Biogeogr.* **2003**, *12*, 361–371. [CrossRef]

43. Termansen, M.; Mcclean, C.J.; Preston, C.D. The use of genetic algorithms and Bayesian classification to model species distributions. *Ecol. Model.* **2006**, *192*, 410–424. [CrossRef]

44. Drake, J.M.; Lodge, D.M. Allee effects, propagule pressure and the probability of establishment: Risk analysis for biological invasions. *Biol. Invasions* **2006**, *8*, 365–375. [CrossRef]

45. Fukuda, S.; De Baets, B.; Waegeman, W.; Verwaeren, J.; Mouton, A.M. Habitat prediction and knowledge extraction for spawning European grayling (*Thymallus thymallus* L.) using a broad range of species distribution models. *Environ. Model. Softw.* **2013**, *47*, 84. [CrossRef]

46. Rammer, W.; Seidl, R. A scalable model of vegetation transitions using deep neural networks. *Methods Ecol. Evol.* **2019**, *10*, 879–890. [CrossRef]

47. Elith, J.; Leathwick, J.R.; Hastie, T. A working guide to boosted regression trees. *J. Anim. Ecol.* **2008**, *77*, 802–813. [CrossRef]

48. Kleinbauer, I.; Dullinger, S.; Peterseil, J.; Essl, F. Climate change might drive the invasive tree *Robinia pseudacacia* into nature reserves and endangered habitats. *Biol. Conserv.* **2010**, *143*, 382–390. [CrossRef]

49. Mohr, P.; Zanettin, B. The Ethiopian flood basalt province. In *Continental Flood Basalts*; Springer: Berlin, Germany, 1988; pp. 63–110.

50. Johnson, T.C.; Malala, J.O. Lake Turkana and its link to the Nile. In *The Nile*; Springer: Berlin, Germany, 2009; pp. 287–304.

51. Segele, Z.T.; Lamb, P.J. Characterization and variability of Kiremt rainy season over Ethiopia. *Meteorol. Atmos. Phys.* **2005**, *89*, 153–180. [CrossRef]

52. Asefa, M.; Cao, M.; He, Y.; Mekonnen, E.; Song, X.; Yang, J. Ethiopian vegetation types, climate and topography. *Plant Divers.* **2020**, *42*, 302–311. [CrossRef]

53. Hedberg, O. *Features of Afroalpine Plant Ecology*; Sv. växtgeografiska sällsk: Upsala, Sweden, 1964.

54. Bruhl, J.; Wilson, K. Towards a comprehensive survey of C3 and C4 photosynthetic pathways in *Cyperaceae*. *Aliso* **2007**, *23*, 99–148. [CrossRef]

55. Brown, R.H.; Bouton, J.H.; Evans, P.T.; Malter, H.E.; Rigsby, L.L. Photosynthesis, morphology, leaf anatomy, and cytogenetics of hybrids between C3 and C3/C4Panicum species. *Plant Physiol.* **1985**, *77*, 653–658. [CrossRef] [PubMed]

56. Leplongeon, A.; Pleurdeau, D.; Hovers, E. Late Pleistocene and Holocene Lithic variability at Goda Buticha (Southeastern Ethiopia): Implications for the understanding of the Middle and Late Stone Age of the Horn of Africa. *J. Afr. Archaeol.* **2017**, *15*, 202–233. [CrossRef]

57. Tribolo, C.; Asrat, A.; Bahain, J.-J.; Chapon, C.; Douville, E.; Fragnol, C.; Hernandez, M.; Hovers, E.; Leplongeon, A.; Martin, L.; et al. Across the gap: Geochronological and sedimentological analyses from the late Pleistocene-Holocene sequence of Goda Buticha, Southeastern Ethiopia. *PLoS ONE* **2017**, *12*, e0169418. [CrossRef] [PubMed]

58. Pleurdeau, D.; Hovers, E.; Assefa, Z.; Asrat, A.; Pearson, O.; Bahain, J.-J.; Lam, Y.M. Cultural change or continuity in the late MSA/Early LSA of southeastern Ethiopia? The site of Goda Buticha, Dire Dawa area. *Quat. Int.* **2014**, *343*, 117–135. [CrossRef]

59. Brandt, S.A.; Fisher, E.C.; Hildebrand, E.A.; Vogelsang, R.; Ambrose, S.H.; Lesur, J.; Wang, H. Early MIS 3 occupation of Mochena Borago Rockshelter, Southwest Ethiopian Highlands: Implications for Late Pleistocene archaeology, paleoenvironments and modern human dispersals. *Quat. Int.* **2012**, *274*, 38–54. [CrossRef]

60. Brandt, S.; Hildebrand, E.; Vogelsang, R.; Wolfhagen, J.; Wang, H. A new MIS 3 radiocarbon chronology for Mochena Borago Rockshelter, SW Ethiopia: Implications for the interpretation of Late Pleistocene chronostratigraphy and human behavior. *J. Archaeol. Sci. Rep.* **2017**, *11*, 352–369. [CrossRef]

61. Ménard, C.; Bon, F.; Dessie, A.; Bruxelles, L.; Douze, K.; Fauvelle, F.-X.; Khalidi, L.; Lesur, J.; Mensan, R. Late Stone Age variability in the Main Ethiopian Rift: New data from the Bulbula River, Ziway–Shala basin. *Quat. Int.* **2014**, *343*, 53–68. [CrossRef]

62. Leplongeon, A. Microliths in the Middle and Later Stone Age of eastern Africa: New data from Porc-Epic and Goda Buticha cave sites, Ethiopia. *Quat. Int.* **2014**, *343*, 100–116. [CrossRef]

63. Assefa, Z. Faunal remains from Porc-Epic: Paleoecological and zooarchaeological investigations from a Middle Stone Age site in southeastern Ethiopia. *J. Hum. Evol.* **2006**, *51*, 50–75. [CrossRef]

64. Hensel, E.A.; Vogelsang, R.; Noack, T.; Bubenzer, O. Stratigraphy and chronology of Sodicho Rockshelter—A new sedimentological record of past environmental changes and human settlement phases in Southwestern Ethiopia. *Front. Earth Sci.* **2021**, *8*, 640. [CrossRef]

65. Khalidi, L.; Mologni, C.; Ménard, C.; Coudert, L.; Gabriele, M.; Davtian, G.; Cauliez, J.; Lesur, J.; Bruxelles, L.; Chesnaux, L.; et al. 9000 years of human lakeside adaptation in the Ethiopian Afar: Fisher-foragers and the first pastoralists in the Lake Abhe basin during the African Humid Period. *Quat. Sci. Rev.* **2020**, *243*, 106459. [CrossRef]

66. Bachechi, L. Notizie preliminari sulla campagna di scavo 2002 svolta nel deposito del riparo di Harurona. *CAVANNA C. A Cura di, Wolayta, una Regione d'Etiopia. Studi e Ricerche* **1995**, *2004*, 67–78.

67. Gossa, T.; Sahle, Y.; Negash, A. A reassessment of the Middle and Later Stone Age lithic assemblages from Aladi Springs, Southern Afar Rift, Ethiopia. *Azania Archaeol. Res. Afr.* **2012**, *47*, 210–222. [CrossRef]

68. Williams, M.A.J.; Bishop, P.M.; Dakin, F.M.; Gillespie, R. Late quaternary lake levels in southern Afar and the adjacent Ethopian Rift. *Nature* **1977**, *267*, 690–693. [CrossRef]

69. Kurashina, H. *An Examination of Prehistoric Lithic Technology in East-Central Ethiopia*; University of California, Berkeley: Berkeley, CA, USA, 1978.

70. Finneran, N.; Boardman, S.; Cain, C. Excavations at the Late Stone Age Site of Baahti Nebait, Aksum, Northern Ethiopia, 1997. *AZANIA J. Br. Inst. East. Afr.* **2000**, *35*, 53–73. [CrossRef]

71. Ashkenazy, H.; Sahle, Y. An early Holocene Lithic assemblage from Dibé Rockshelter, South-Central Ethiopia. *J. Afr. Archaeol.* **2021**, *1*, 1–15. [CrossRef]

72. Arthur, J.W.; Curtis, M.C.; Arthur, K.J.W.; Coltorti, M.; Pieruccini, P.; Lesur, J.; Fuller, D.; Lucas, L.; Conyers, L.; Stock, J.; et al. The transition from hunting–gathering to food production in the Gamo Highlands of Southern Ethiopia. *Afr. Archaeol. Rev.* **2019**, *36*, 5–65. [CrossRef]

73. Hildebrand, E.A.; Brandt, S.A.; Lesur-Gebremariam, J. The holocene archaeology of Southwest Ethiopia: New insights from the Kafa Archaeological project. *Afr. Archaeol. Rev.* **2010**, *27*, 255–289. [CrossRef]

74. Schepers, C.; Lesur, J.; Vogelsang, R. Hunter-gatherers of the high-altitude Afromontane forest—The Holocene occupation of Mount Dendi, Ethiopia. *Azania Archaeol. Res. Afr.* **2020**, *55*, 329–359. [CrossRef]

75. Rowntree, P. Atmospheric parameterization schemes for evaporation over land: Basic concepts and climate modeling aspects. In *Land Surface Evaporation*; Springer: Berlin, Germany, 1991; pp. 5–29.

76. Farr, T.G.; Rosen, P.A.; Caro, E.; Crippen, R.; Duren, R.; Hensley, S.; Kobrick, M.; Paller, M.; Rodriguez, E.; Roth, L.; et al. The shuttle radar topography mission. *Rev. Geophys.* **2007**, *45*, 1–33. [CrossRef]

77. Huffman, G.J.; Stocker, E.F.; Bolvin, D.T.; Nelkin, E.J.; Tan, J. *GPM IMERG Final Precipitation L3 1 Month 0.1 Degree x 0.1 Degree V06*; Goddard Earth Sciences Data and Information Services Center (GES DISC): Greenbelt, MD, USA, 2019.

78. Friedl, M.; Sulla-Menashe, D. *MCD12Q1 MODIS/Terra+Aqua Land Cover Type Yearly L3 Global 500m SIN Grid V006 (Data Set)*; NASA EOSDIS Land Processes DAAC: Sioux Falls, SD, USA, 2019. [CrossRef]

79. DiMiceli, C.; Carroll, M.; Sohlberg, R.; Kim, D.; Kelly, M.; Townshend, J. *MOD44B MODIS/Terra Vegetation Continuous Fields Yearly L3 Global 250m SIN Grid V006 (Data Set)*; NASA EOSDIS Land Processes DAAC: Sioux Falls, SD, USA, 2015. [CrossRef]

80. Didan, K. *MOD13A3 MODIS/Terra Vegetation Indices Monthly L3 Global 1km SIN Grid V006 (Data Set)*; NASA EOSDIS Land Processes DAAC: Sioux Falls, SD, USA, 2015. [CrossRef]

81. R Core Team, R. *A Language and Environment for Statistical Computing*; R Foundation for Statistical Computing: Vienna, Austria, 2021.

82. Hijmans, R.J. *raster: Geographic Data Analysis and Modeling*, R package version 3.1-5; 2020.

83. Bivand, R.; Keitt, T.; Rowlingson, B. *rgdal: Bindings for the 'Geospatial' Data Abstraction Library*, R package version 1.5-10; 2020.

84. OpenStreetMap, C. Planet Dump. 2017. Available online: https://planet.osm.org (accessed on 1 March 2020).

85. Friedl, M.A.; Sulla-Menashe, D.; Tan, B.; Schneider, A.; Ramankutty, N.; Sibley, A.; Huang, X. MODIS Collection 5 global land cover: Algorithm refinements and characterization of new datasets. *Remote Sens. Environ.* **2010**, *114*, 168–182. [CrossRef]

86. Acker, J.G.; Leptoukh, G. Online analysis enhances use of NASA earth science data. *Eos Trans. Am. Geophys. Union* **2007**, *88*, 14–17. [CrossRef]

87. Friedman, J.H. Greedy function approximation: A gradient boosting machine. *Ann. Stat.* **2001**, *29*, 1189–1232. [CrossRef]

88. Greenwell, B.; Boehmke, B.; Cunningham, J.; Developers, G. *gbm: Generalized Boosted Regression Models*, R package version 2.1.5; 2019.

89. Robin, X.; Turck, N.; Hainard, A.; Tiberti, N.; Lisacek, F.; Jean-Charles, S.; Müller, M. pROC: An open-source package for R and S+ to analyze and compare ROC curves. *BMC Bioinform.* **2011**, *12*, 77. [CrossRef]

90. Kuhn, M. *caret: Classification and Regression Training*, R package version 6.0-86; 2020.

91. Lyons, R.P.; Kroll, C.N.; Scholz, C.A. An energy-balance hydrologic model for the Lake Malawi Rift Basin, East Africa. *Glob. Planet. Change* **2011**, *75*, 83–97. [CrossRef]

92. Loomis, S.E.; Russell, J.M.; Ladd, B.; Street-Perrott, F.A.; Sinninghe Damsté, J.S. Calibration and application of the branched GDGT temperature proxy on East African lake sediments. *Earth Planet. Sci. Lett.* **2012**, *357*, 277–288. [CrossRef]

93. Foerster, V.; Deocampo, D.M.; Asrat, A.; Günter, C.; Junginger, A.; Krämer, K.H.; Stroncik, N.A.; Trauth, M.H. Towards an understanding of climate proxy formation in the Chew Bahir basin, southern Ethiopian Rift. *Palaeogeogr. Palaeoclimatol. Palaeoecol.* **2018**, *501*, 111–123. [CrossRef]

94. Trauth, M.H.; Foerster, V.; Junginger, A.; Asrat, A.; Lamb, H.F.; Schaebitz, F. Abrupt or gradual? Change point analysis of the late Pleistocene–Holocene climate record from Chew Bahir, southern Ethiopia. *Quat. Res.* **2018**, *90*, 321–330. [CrossRef]

95. Yost, C.L.; Ivory, S.J.; Deino, A.L.; Rabideaux, N.M.; Kingston, J.D.; Cohen, A.S. Phytoliths, pollen, and microcharcoal from the Baringo Basin, Kenya reveal savanna dynamics during the Plio-Pleistocene transition. *Palaeogeogr. Palaeoclimatol. Palaeoecol.* **2021**, *570*, 109779. [CrossRef]

96. Piperno, D.R. *Phytoliths: A Comprehensive Guide for Archaeologists and Paleoecologists*; Rowman Altamira: Lanham, MD, USA, 2006.

97. Li, R.; Fan, J.; Vachula, R.S.; Tan, S.; Qing, X. Spatial distribution characteristics and environmental significance of phytoliths in surface sediments of Qingshitan Lake in Southwest China. *J. Paleolimnol.* **2019**, *61*, 201–215. [CrossRef]

98. Madella, M.; Alexandre, A.; Ball, T. International code for phytolith nomenclature 1.0. *Ann. Bot.* **2005**, *96*, 253–260. [CrossRef]

99. Yost, C.L.; Lupien, R.L.; Beck, C.; Feibel, C.S.; Archer, S.R.; Cohen, A.S. Orbital influence on precipitation, fire, and grass community composition from 1.87 to 1.38 Ma in the Turkana Basin, Kenya. *Front. Earth Sci.* **2021**, *9*, 646. [CrossRef]

100. Novello, A.; Barboni, D.; Sylvestre, F.; Lebatard, A.-E.; Paillès, C.; Bourlès, D.L.; Likius, A.; Mackaye, H.T.; Vignaud, P.; Brunet, M. Phytoliths indicate significant arboreal cover at Sahelanthropus type locality TM266 in northern Chad and a decrease in later sites. *J. Hum. Evol.* **2017**, *106*, 66–83. [CrossRef] [PubMed]

101. Bremond, L.; Alexandre, A.; Peyron, O.; Guiot, J. Definition of grassland biomes from phytoliths in West Africa. *J. Biogeogr.* **2008**, *35*, 2039–2048. [CrossRef]

102. Anhuf, D. Vegetation history and climate changes in Africa north and south of the equator (10 S to 10 N) during the last glacial maximum. In *Southern Hemisphere Paleo-and Neoclimates*; Springer: Berlin, Germany, 2000; pp. 225–248.

103. Cowling, S.A.; Cox, P.M.; Jones, C.D.; Maslin, M.A.; Peros, M.; Spall, S.A. Simulated glacial and interglacial vegetation across Africa: Implications for species phylogenies and trans-African migration of plants and animals. *Glob. Change Biol.* **2008**, *14*, 827–840. [CrossRef]

104. Hopcroft, P.O.; Valdes, P.J. Last glacial maximum constraints on the Earth system model HadGEM2-ES. *Clim. Dyn.* **2015**, *45*, 1657–1672. [CrossRef]

105. Augustijns, F.; Broothaerts, N.; Verstraeten, G. Reconstructing vegetation changes in the Ethiopian Highlands: 18,000 years of Afromontane vegetation dynamics recorded in high altitude wetlands. In Proceedings of the EGU General Assembly Conference Abstracts, Vienna, Austria, 25–30 April 2021; p. EGU21-1340.

106. Gillespie, R.; Street-Perrott, F.A.; Switsur, R. Post-glacial arid episodes in Ethiopia have implications for climate prediction. *Nature* **1983**, *306*, 680–683. [CrossRef]

107. Hastenrath, S.; Kutzbach, J.E. Paleoclimatic estimates from water and energy budgets of East African lakes. *Quat. Res.* **1983**, *19*, 141–153. [CrossRef]

108. Dühnforth, M.; Bergner, A.G.N.; Trauth, M.H. Early holocene water budget of the Nakuru-Elmenteita basin, Central Kenya Rift. *J. Paleolimnol.* **2006**, *36*, 281–294. [CrossRef]

109. Darbyshire, I.; Lamb, H.; Umer, M. Forest clearance and regrowth in northern Ethiopia during the last 3000 years. *Holocene* **2003**, *13*, 537–546. [CrossRef]

110. Nyssen, J.; Poesen, J.; Moeyersons, J.; Deckers, J.; Haile, M.; Lang, A. Human impact on the environment in the Ethiopian and Eritrean highlands—A state of the art. *Earth Sci. Rev.* **2004**, *64*, 273–320. [CrossRef]

111. Gil-Romera, G.; Lamb, H.F.; Turton, D.; Sevilla-Callejo, M.; Umer, M. Long-term resilience, bush encroachment patterns and local knowledge in a Northeast African savanna. *Glob. Environ. Change* **2010**, *20*, 612–626. [CrossRef]

112. Woldeyohannes, A.; Cotter, M.; Kelboro, G.; Dessalegn, W. Land use and land cover changes and their effects on the landscape of Abaya-Chamo Basin, Southern Ethiopia. *Land* **2018**, *7*, 2. [CrossRef]

113. Von Höhnel, L. The Lake Rudolf region: Its discovery and subsequent exploration, 1888–1909. Part II. *J. R. Afr. Soc.* **1938**, *37*, 206–226.

114. Nicholson, S.E. Climatic and environmental change in Africa during the last two centuries. *Clim. Res.* **2001**, *17*, 123–144. [CrossRef]

115. Olaka, L.A. *Hydrology Across Scales: Sensitivity of East African Lakes to Climate Changes*; Universität Potsdam: Potsdam, Germany, 2011.

116. Cabanes, D.; Weiner, S.; Shahack-Gross, R. Stability of phytoliths in the archaeological record: A dissolution study of modern and fossil phytoliths. *J. Archaeol. Sci.* **2011**, *38*, 2480–2490. [CrossRef]

117. Greve, M.; Lykke, A.M.; Blach-Overgaard, A.; Svenning, J.-C. Environmental and anthropogenic determinants of vegetation distribution across Africa. *Glob. Ecol. Biogeogr.* **2011**, *20*, 661–674. [CrossRef]

118. Hensel, E.A.; Bödeker, O.; Bubenzer, O.; Vogelsang, R. Combining geomorphological–hydrological analyses and the location of settlement and raw material sites—A case study on understanding prehistoric human settlement activity in the southwestern Ethiopian Highlands. *E G Quat. Sci. J.* **2019**, *68*, 201–213. [CrossRef]

119. Basell, L. Middle Stone Age (MSA) site distributions in eastern Africa and their relationship to quaternary environmental change, refugia and the evolution of Homo sapiens. *Quat. Sci. Rev.* **2008**, *27*, 2484–2498. [CrossRef]

120. Vogelsang, R.; Wendt, K.P. Reconstructing prehistoric settlement models and land use patterns on Mt. Damota/SW Ethiopia. *Quat. Int.* **2018**, *485*, 140–149. [CrossRef]

121. Dekker, G.; Gebre Selassie, T. Rock engravings at Ch'ew Bahir. *Ann. Ethiop.* **1972**, *9*, 19. [CrossRef]

122. Gutherz, X.; Jallot, L.; Lesur, J.; Pouzolles, G.; Sordoillet, D. Les fouilles de l'abri sous-roche de Moche Borago (Soddo, Wolyata). Premier bilan. *Ann. Ethiop.* **2002**, *18*, 181–190. [CrossRef]

Appendix P3 – An Examination of the Great Lakes of Turkana in Eastern Africa during the last African Humid Period using Literature Review and Visual Remote Sensing

1   **The Turkana Lake System during the last African Humid Period: A Review**

2   Markus L. Fischer[1,*], Annett Junginger[1,2]

3   [1] Department of Geosciences, Eberhard Karls University Tuebingen, Hoelderlinstr. 12, 72074
4   Tuebingen, Germany

5   [2] Senckenberg Centre of Human Evolution and Paleoenvironment (S-HEP), Hoelderlinstr. 12,
6   72074 Tuebingen, Germany

7   * Correspondence: markus_fischer@posteo.de

8

9   **Abstract**

10   Lake Turkana in northern Kenya and southern Ethiopia is the last of numerous paleo-lakes
11   that has persisted in drying up entirely at the end of the last African Humid Period (AHP, 15 –
12   5 ka, thousand years before present). The adjacent paleo-lakes Suguta (2,000 km²) and Chew
13   Bahir (2,500 km²), which are desiccated today, have formed together with paleo-lake Turkana
14   (20,000 km²) a, N-S oriented lake system during the AHP that has been separated only by
15   small morphological barriers. While Turkana, Suguta, and Chew Bahir have been part of
16   intensive research during the past decades, paleo-lake Chalbi, located east of Turkana, was
17   out of sight for most archaeologists and geoscientists. Paleo-lake Chalbi was, with 2,500 km²
18   in size, the eastern extension of the Turkana Lake System. For now, each lake and its related
19   paleo-environment were discussed soloistic, and their interference in space and time was not
20   highlighted. The Turkana Depression, including the paleo-lake Chalbi basin, was a vast and,
21   presumably, resource-rich habitat during the AHP and a potential corridor of human migration
22   between the Ethiopian and Kenyan highlands. To fill this gap and to provide a paleo-
23   environmental framework for discussing possible human-environment interactions in this
24   region, we use literature and data review and -collection, visual remote sensing, data merging,
25   and -analysis. To summarize, paleo-lake Chalbi was the only lake in the Turkana Lake System
26   that did not reach its overflow sill. In contrast, paleo-lake Turkana, Suguta, and Chew Bahir
27   formed a hydro-network that connected the Ethiopian and the Kenyan highlands with the
28   Mediterranean Sea. The reviewed paleo-lake level record based on shorelines provides a
29   database for paleo-lake level evolution analysis. A potential quantitative correlation between
30   existing records in the region does not show a supra-regional climate forcing of the lake levels,
31   but we conclude that this may be due to the data quality of the shoreline record itself. Based
32   on our review and collection, we see a high relevance of the eastern shore of Lake Turkana
33   as potential refugia, as both, paleo-lake Chew Bahir and Chalbi, presumably have been the
34   most unstable lake environments throughout that region on a decadal to centennial time scale.

35   **Introduction**

36   Lake Turkana is the world's largest permanent desert lake and a unique ecosystem that
37   provides essential ecosystem services in the border region of Kenya and Ethiopia in Eastern
38   Africa (Ojwang et al., 2016). The stability of this ecoregion may be challenged due to
39   anthropogenic climate change, hydropower dams, irrigation schemes, and demographic-
40   economic growth (Ojwang et al., 2016). To better constrain potential future eco-climatic
41   changes and threats and to understand the environmental dynamic, a paleoenvironmental
42   perspective may help.

43   The most contrasting environmental conditions, compared to today, occurred during the last
44   African Humid Period (AHP, ~15 to 5 ka, thousand years before present), when orbital changes
45   caused insolation changes that had a significant impact on eastern Africa's hydroclimate
46   (Barker et al., 2004; Demenocal et al., 2000). Associated increased precipitation forced
47   vegetation change (Fischer et al., 2021; Jaeschke et al., 2020; Lamb et al., 2004; Umer et al.,
48   2007), river flow increase (Revel et al., 2014), new lakes formation, expansion, or deepening
49   with up to 300 m in water level (Fischer et al., 2020; Garcin et al., 2012; Junginger & Trauth,
50   2013; Nyamweru & D., 1989). The complex morphology of the East African Rift System (EARS)
51   and thus catchments, in which these lakes are located, with precipitation-rich highlands (>4000
52   m) and lowlands with exceeding high evaporation rates (<500 m), causes these lakes to be
53   highly climate-sensitive (Olaka et al., 2010; Trauth et al., 2010). This climate sensitivity is
54   recorded in fast-changing lake levels, preserved in paleo-shorelines, such as wave-cut
55   notches, sand shells, or ostracod layers (Garcin et al., 2012; Junginger & Trauth, 2013).

56   The Turkana Depression and its related climate sensitive lake systems connect the northern
57   Kenyan Plateau with the southern East African Plateau. This region is a major hotspot of
58   hominin fossils (Brown et al., 1985; Leakey, 1969), stone tool findings (Harmand et al., 2015),
59   and Holocene archeology (Hildebrand et al., 2010). The decline of the last AHP was
60   accompanied by the transition of hunting gatherer fishing communities to livestock farmers
61   (Hildebrand & Grillo, 2012) and the occurrence of first cemeteries in the Lake Turkana vicinity
62   (E. A. Hildebrand et al., 2018).

63   While the Lake Turkana surrounding provides one of the most impressive archeological
64   records, there are only a few published sites in the eastern part of the Turkana Depression,
65   the so-called Chalbi basin, respectively -desert, which seems to have a comparable
66   geographical setting. Still, until now, there are only a few mentions of this region in the
67   literature, which raises the question of whether there is a sampling bias or if the Chalbi basin
68   geography differs significantly. Furthermore, Lake Turkana was surrounded in the northeast
69   by the modern-day dried-out paleo-lake Chew Bahir (Fischer et al., 2020) and in the south by
70   paleo-lake Suguta (Junginger & Trauth, 2013). These lake basins overspilled into each other,
71   but if they followed the same lake level evolution in time is under debate and may impact the
72   landscape evolution perspective and the paleo-environmental consequences for humans living
73   close-by the lakes.

74   A precursor study in the Chew Bahir basin used a physical process Lake Balance Model that
75   was tied to a high-resolution μ-XRF (in particular potassium; Foerster et al., 2015) record of a
76   drill core to determine the paleo-lake behavior and paleo-precipitation threshold (Fischer et al.,
77   2020). For now, these models are tested and anchored using one shoreline at the overflow sill
78   elevation of paleo-lake Chew Bahir. A link between two independent datasets, such as
79   shorelines and lacustrine sediments, may help to enhance the paleo-environmental
80   understanding of the entire Lake Turkana region. This could be done if there is a correlation
81   between the temporal high-resolved lacustrine proxy and quantitative anchored shorelines.

82   Here, we aim to analyze the Turkana Lake System as a complex interacting environment in
83   terms of lake extents and lake level evolution over time. Furthermore, we aim to complement
84   potential gaps by first-step surveying remotely the geomorphological evidence of the extent of
85   paleo-lake Chalbi. We review significant publications of the paleo-lakes and the existing
86   records, such as shorelines, to create a shoreline dataset, to test the possibility of an
87   overarching lake level history. Furthermore, we complement the existing shoreline records with
88   new dates from the Chew Bahir basin. Last, we test the capability of a link between the
89   shoreline record and the potassium record from the Chew Bahir basin shore core CB-01

90 (Foerster et al., 2015) to potentially construct a transfer function between lake levels and
91 potassium, which may be used to back-propagate lake levels in the entire region on currently
92 new drill cores reaching further back in time until the mid-Pleistocene (e.g., Cohen et al., 2016;
93 Roberts et al., 2021; Schaebitz et al., 2021).

94
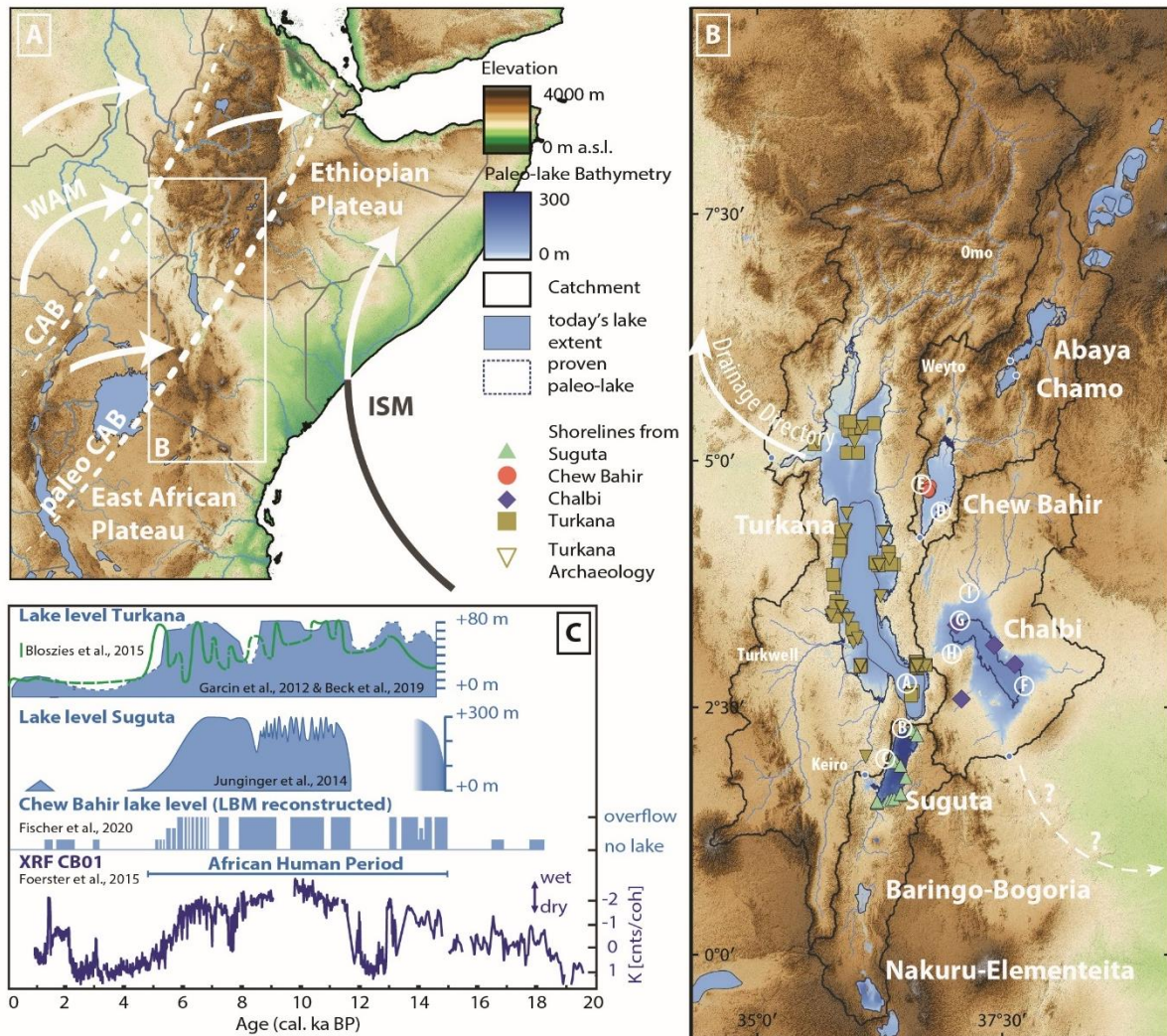
Figure 1 I Topography, major wind trajectories, modern-day lakes, paleo-lakes, and lake level evolution during the
past 20 ka. (A) Topography of Eastern Africa with modern-day Congo Air Boundary (CAB) and presumed paleo-
CAB as the eastern boundary of the West African Monsoon (WAM), Indian Summer Monsoon (ISM) trajectory. (B)
Topography of Lake Turkana's extended catchment during paleo-lake high stand with SRTM-based possible paleo-
lake bathymetry. Shoreline and archeological site locations and satellite images according to figure 2. (C) Time
series of the past 20 ka, including Chew Bahir short core CB01 potassium record, Chew Bahir, Suguta, and Turkana
published lake level curves.

Regional Setting

103 The Turkana lowland region consists of four major basins (Fig. 1): Lake Turkana, paleo-lake
104 Suguta, paleo-lake Chew Bahir, and the paleo-lake Chalbi basin or Chalbi desert today. The
105 catchments cover a total area of ca. 259,000 km² from 9.3°N to 0.8°S, whereby the Lake
106 Turkana catchment is the largest with 149,000 km². Lake Turkana also has the largest
107 catchment draining the western Ethiopian Plateau through the Omo river and the northern part
108 of the East African Plateau by the rivers Kerio and Turkwel. Chew Bahir drains the southern
109 Main Ethiopian Rift by the rivers Weyto and Segen. During the African Humid Period, the lakes
110 Abaya and Chamo overspilled and drained their surplus water by the river Segen to paleo-lake

111   Chew Bahir (Fischer et al., 2020). Suguta drains the northern Kenyan Rift and received the
112   overspilling water from the lakes Nakuru-Elementeita and Baringo-Bogoria. Paleo-lake Chalbi
113   has no persistent river today.

114   During the AHP, paleo-Lake Chew Bahir (+45 m; Fischer et al., 2020) in the Southern Ethiopian
115   basin and paleo-lake Suguta (+295 m, Garcin et al., 2009) enlarged so much, that both basins
116   reached their overflow sills (36.658°E, 4.220°N, and 36.104°E, 1.816°N) towards lake Turkana
117   which itself overflowed (+94 m; Garcin et al., 2012) into the White Nile and finally the
118   Mediterranean Sea (at 35.145°E, 5.030°N) (Garcin et al., 2012). In contrast, paleo-lake Chalbi
119   most likely did not overflow to Turkana, instead would potentially have drained towards the
120   Indian Ocean at 37.5729°E, 2.0057°N as digital elevation model analysis indicates.

121   The Turkana Depression is located between the East African Plateau to its South and the
122   Ethiopian Plateau to its North. Paleo-lake Chew Bahir is part of the Main Ethiopian rift, whereas
123   paleo-Lake Suguta belongs to the volcanically more active Northern Kenyan Rift. Both basins
124   are bound by steep North to North-East striking graben shoulders (Chorowicz, 2005). The
125   Turkana basin, also part of the Northern Kenya rift, is only bounded by steep graben shoulders
126   in the south and opens up further north when it converges with the ancient underlying E-W
127   Anza rift structure (Bruhn et al., 2011). The paleo-lake Chalbi basin is located east of Lake
128   Turkana in an appended basin (Chorowicz, 2005) which is not part of the EARS. It is
129   surrounded by the two volcanoes Mt. Kulal and Marsabit.

130   Volcano-sedimentary and Proterozoic metamorphic are abundant in the transition areas
131   towards the lowlands and Lake Turkana's surrounding. Cenozoic volcanism dominate the
132   mountainous regions of all catchments. All basins are filled with Pleistocene to Holocene
133   Sediments (Boone et al., 2018). The vegetation ranges from Afromontane forests in the
134   highlands to Combretum or Acacia-Commiphora woodland to bushland and semi-desert to
135   deserts in the lowlands and paleo-lake rift floors (van Breugel et al., 2015).

Methods

Literature Review and Shoreline Dataset

138   We reviewed the major recent publications that published dated shorelines or summarized
139   previously published shorelines in one of the basins (Beck et al., 2019; Bloszies et al., 2015;
140   Forman et al., 2014; Garcin et al., 2012; Junginger et al., 2014; Nyamweru, 1986; Nyamweru
141   & D., 1989; Wright et al., 2015). Next, we created a combined dataset of all shorelines,
142   including the original sample name, the sample type (e.g., *Melanoides tuberculata*, *Etheria
143   elliptica*, Ostracods, charcoal, humid acids, Bivalve, Stromatolites), sample elevation, latitude,
144   longitude, ^{14}C age (calibrated) and the two sigma minima and maximum age as well as optically
145   stimulated luminescence-based ages (Supplementary Tab. 1). Based on the SRTM elevation
146   data, we extracted the elevation for each site and calculated the relative lake level (sample
147   elevation – modern-day lake elevation or rift floor) and the normalized relative lake level for
148   each shoreline using z-transformation.

Chew Bahir Shoreline Dating

150   During a field campaign in 2018, an East-West transect along the western alluvial fan (Fig. 2-
151   E) of the Chew Bahir basin was surveyed for potential shoreline features, and four stromatolites
152   and two shell beds were collected. Samples were dated using the Accelerator Mass
153   Spectrometer (AMS) laboratory at ETH in Zurich. All ^{14}C ages have been calibrated using

154 OxCal version 4.3.2 and IntCal 13 (Ramsey, 2017). The original ^{14}C data set is evaluated and
155 discussed given in a parallel study by Junginger et al. in prep.

Remotely Sensed Shoreline Exploration

157 Google Earth images were used to locate published (and dated) shorelines of paleo-lakes
158 Suguta, Chew Bahir, and Turkana (see references above). Based on the remotely observed
159 features on these satellite images, potential shorelines of the nearly unexplored paleo-lake
160 Chalbi were identified. We carefully distinguished potential geological (e.g., faults) and
161 geomorphological features (e.g., wind ripples, dunes) to provide cautiously possible shoreline
162 localities. The potential paleo-lake Chalbi outlet and overflow sill were calculated using ArcGIS
163 10.3 and the toolbox ArcHydro (Merwade, 2012).

Shoreline Proxy Transfer Function

165 Previous drilling and drill core analyses in the Chew Bahir have provided a well-testified hydro-
166 climate proxy, namely potassium (K) from μ-XRF scanning in a high-resolution (tens of years)
167 (Foerster et al., 2012; 2018). We tested the capability to use the high-resolution K proxy record
168 to predict lake levels based on the collected shoreline record, a so-called transfer function.
169 Therefore, we merged both using three different methods to test if one of the methods provides
170 a robust correlation between the z-transformed μ-XRF potassium and the relative normalized
171 shoreline elevation. First, by merging the shoreline elevation, their exact age (or *single age*),
172 and the exact z-transformed μ-XRF potassium. Second, by merging the shoreline data with
173 the mean of z-transformed μ-XRF potassium given the *two-sigma* age range of the specific
174 shoreline. Third, by merging each shoreline data with *all values* of the z-transformed μ-XRF
175 potassium in the two-sigma age range of each particular shoreline. Next, we created a subset
176 of the shoreline dataset by using no archeological sites, no sites from the Suguta valley, and
177 by using only sites with an age precision below 200 years. To test the robustness of the
178 correlation, we used a non-parametric spearman rank correlation. All analysis steps are
179 conducted in R and available on Github (Github.com/MLFischer/Turkana-Lake-System,
180 08/22).

Results

Paleo-Shoreline Dataset

183 In eastern Africa, in the surrounding of Lake Turkana, intensive studies during the past
184 decades revealed a complex history and sensitivity of the surrounding paleo-lakes, primarily
185 based on numerous shoreline records. This includes Lake Turkana (Beck et al., 2019; Bloszies
186 et al., 2015; Forman et al., 2014; Garcin et al., 2012), paleo-lake Suguta (Garcin et al., 2009;
187 Junginger & Trauth, 2013), Chew Bahir (Fischer et al., 2020; Foerster et al., 2012; Foerster et
188 al., 2015; M. H. Trauth et al., 2018), and paleo-lake Chalbi (Nyamweru, 1986; Nyamweru & D.,
189 1989). The compiled dataset contains 192 dated sites, which includes 26 dated archeological
190 sites and 89 shorelines at Lake Turkana, 44 shoreline ages from the Suguta Valley, four
191 published ages from paleo-lake Chalbi, and eight new ages from paleo-lake Chew Bahir. A
192 review of the existing data on paleo-lake levels of the lowland lakes, including Lake Turkana,
193 is summarized below.

Lake Turkana

195 The dry climate encircling Lake Turkana preserved shorelines and archaeological sites from
196 the last AHP in good quality, which provides evidence of the lake's extent at a specific time.
197 Lake Turkana's shorelines cover the whole range in space (from the modern-day lake surface

198   until the overflow sill) and time, whereby a higher record density occurs during the termination
199   of the AHP from ca. 7 to 5 ka. Bloszies et al. (2015) and Forman et al. (2014) have summarized
200   the lake level history of Lake Turkana based on their own data complemented by intensive
201   research that has been done over the past decades (Butzer, 1980; Butzer et al., 1972; Butzer
202   & Thurber, 1969; Owen et al., 1982; Phillipson, 1977; Webster Barthelme, 1985) (Fig. 1). This
203   lake level curve, however, contradicts a reconstruction by Garcin et al. (2012), which got
204   updated using new dates from Beck et al. (2019). The primary contradictory focuses on the
205   termination of the AHP. For how long Turkana was an exoreic lake during the AHP and if the
206   ending of the AHP between 7 and 5 ka was either abrupt or gradual remains an open debate.

207   **Paleo-lake Suguta**

208   The first evidence for tremendously deep paleo-lake Suguta during the late Pleistocene using
209   shorelines was carried out by Baker and Lovenbury (1971) and Truckle (1976). A lake level
210   curve of the AHP was reconstructed using lake sediments, shoreline deposits, and a Lake
211   Balance Model by Junginger and Trauth (2013), including shorelines presented by Garcin et
212   al. (2009) that have been reservoir corrected (see Figure 1). The pure shoreline data based
213   on snail shells (mainly *M. tuberculata*) of paleo-lake Suguta covers only the upper third of the
214   nearly 300 m deep lake, primarily samples from the main phase of the AHP (ca. 11 to 8 ka).
215   The reconstructed paleo-lake level of Suguta shows a rapid onset and a gradual lake decline
216   at the end of the AHP, which contrasts with Lake Turkana's lake level data (Junginger & Trauth,
217   2013).

218   **Paleo-lake Chew Bahir**

219   The most detailed continuous regional und supra-regional paleoclimate record comes from the
220   Chew Bahir basin, as multiple drill cores covering the AHP have been intensely analyzed in
221   the last decade (Foerster et al., 2018; Foerster et al., 2012; Schaebitz et al., 2021; Trauth et
222   al., 2021). Despite the high-resolution μ-XRF data (particularly potassium as a hydro-climate
223   proxy), these records lack paleo-shoreline data. The potential paleo-lake level evolution during
224   the AHP of Chew Bahir thus has been reconstructed by Fischer et al. (2020) by linking a Lake
225   Balance Model of the southern Main Ethiopian Rift with the potassium record (Foerster et al.,
226   2018; Foerster et al., 2015) (Fig. 1). Model results showed that paleo-lake Chew Bahir
227   depended highly on water flux from the Main Ethiopian Rift and the overflowing lakes Abaya
228   and Chamo. The model provided evidence that fluctuations in the potassium record at the
229   termination of the AHP would have been sufficient to desiccate paleo-lake Chew Bahir multiple
230   times. New shoreline data from shell beds, presented in our study, show a lake 35 m deep at
231   9.7, 9.6, and 10.9 ka (Tab. 1). Stromatolites are mainly in the vicinity of the modern basin floor
232   and date to 7.1, 4.6 and 5.7 ka. As the analysis of stromatolites is still in progress by a parallel
233   study by Junginger et al. (in prep), where growth form and isotopes are applied for evaluation
234   of lake depth and lake status, the presented stromatolite data must be taken with caution.

235   **Paleo-lake Chalbi**

236   While Turkana, Suguta, and Chew Bahir have been examined intensively during the past
237   decades, the Chalbi desert got little attention. Fieldwork in the 80s revealed four sites with
238   dated *M. tuberculata* (Nyamweru, 1986; Nyamweru & D., 1989). Three indicate a permanent
239   water body using stable isotopes (Abell & Nyamweru, 1988). Based on a modern-day digital
240   elevation model, the shorelines' altitude was 35 m above the modern basin floor. Above the
241   40 m level, Nyamweru and D. (1989) do not see evidence of a more enormous lake. Instead,
242   a small sink in the southwest, called Olturo, suggests a wet and swampy environment

throughout the large flat plane. The existing data prove that a paleo-lake has covered approximately 20% of the total possible lake basin during the early and main phase of the AHP.

Results on Remotely Sensed Shoreline Exploration

We surveyed the potential outlets of the paleo-lakes. Based on known paleo-shoreline localities (Figure 2-A, B, C, E), we searched for potential shoreline sites at paleo-lake Chalbi and Chew Bahir. Explicit wave-cut notches, as visible around Lake Turkana based on Garcin et al. (2012) (see Figure 2-A, B), are not visible in the Chew Bahir paleo-lake outlet. The maximum extent of paleo-lake Chew Bahir was revealed using Google Earth Pro surveying, which got confirmed during our field campaign in 2018. Shell beds in Figure 2-E were dated at 9.6 ka. We did not find other explicit locations of a maximum extent shoreline of paleo-lake Chew Bahir. Instead, multiple shallow distinct features have been documented comparable with beach ridges from the Suguta Valley and Lake Turkana (see Figure 2-A, C, D, and E).

In the Chalbi desert, multiple weak noticeable (presumed) wave-cut notches are visible at the eastern flood basalt, indicating up to 45 m paleo-lake water level. At North Horr (Figure 2-G), white sediments are visible at the surface, which may be diatomite layers, as they are common in other East African Rift System paleo-lake basins. Those sediments have been dated by Nyamweru (1986) to 10.87 ka. White sediment layers are visible at multiple locations (e.g., Figure 2-H) and match the overflow sill elevations with a water column of ca. + 100 m. Indistinct features, such as possible beach ridges, wave ripples, or wind dunes at other localities, may provide further evidence of the paleo-lake extent and offer possible locations for sediment sampling and hypothesis testing.

Table 1 | 14C Ages from paleo-lake Chew Bahir (*preliminary stromatolite ages and currently still under investigation). A detailed discussion and evaluation on all 14C data is given in a parallel study by Junginger et al. (in prep.)

Location	Sample	Description	14C age	age [cal BP]	δ13C [‰]	14C conc.
M1*	M1Cii_14C_01	M1 top	7074 ± 31	7904 ± 58	-4.8 ± 1	0.4145
M2*	M2B_14C_02	M2 inner	4607 ± 30	5415 ± 39	- 1.2 ± 1	0.5635
M7*	M7C_14C_01	M7 top	5735 ± 30	6541 ± 92	- 6.1 ± 1	0.4897
M8*	M8B_14C_01	M8 top	4605 ± 30	5415 ± 40	2.5 ± 1	0.5637
B21	CB18-B21	corticula	10938 ±34	12871 ± 85	-3.7 ± 1	0.2562
B2	CB18-B2	inlet	9727 ± 33	11183 ± 24	-7.2 ± 1	0.2979
B18	CB18-B18	shell layer	9758 ± 33	11017 ± 125	-5.8 ± 1	0.2968
B18	CB18-B18	white hill	9643 ± 33	11017 ± 58	-8.2 ± 1	0.3010

Transfer Function

We tested three methods to merge the shoreline dataset with the potassium record from the CB-01 short core. The best spearman's rho is accessed for *single-age extraction* with 0.34, whereas the *two-sigma mean extraction* rho is 0.33, and the *all-value* extraction (Fig. 3-C) has a rho of 0.29. The further data cleaning led to a Spearman correlation rho of 0.34 (excluding archaeological sites, 145 sites left), 0.31 (no archaeological sites and no sites from paleo-lake Suguta, 103 sites left), and 0.33 (only sites with a dating two sigma range below 200 years, 63 sites left). These metrics do not show a significant correlation between the normalized relative lake levels of the shorelines and the related z-transformed μ-XRF potassium.
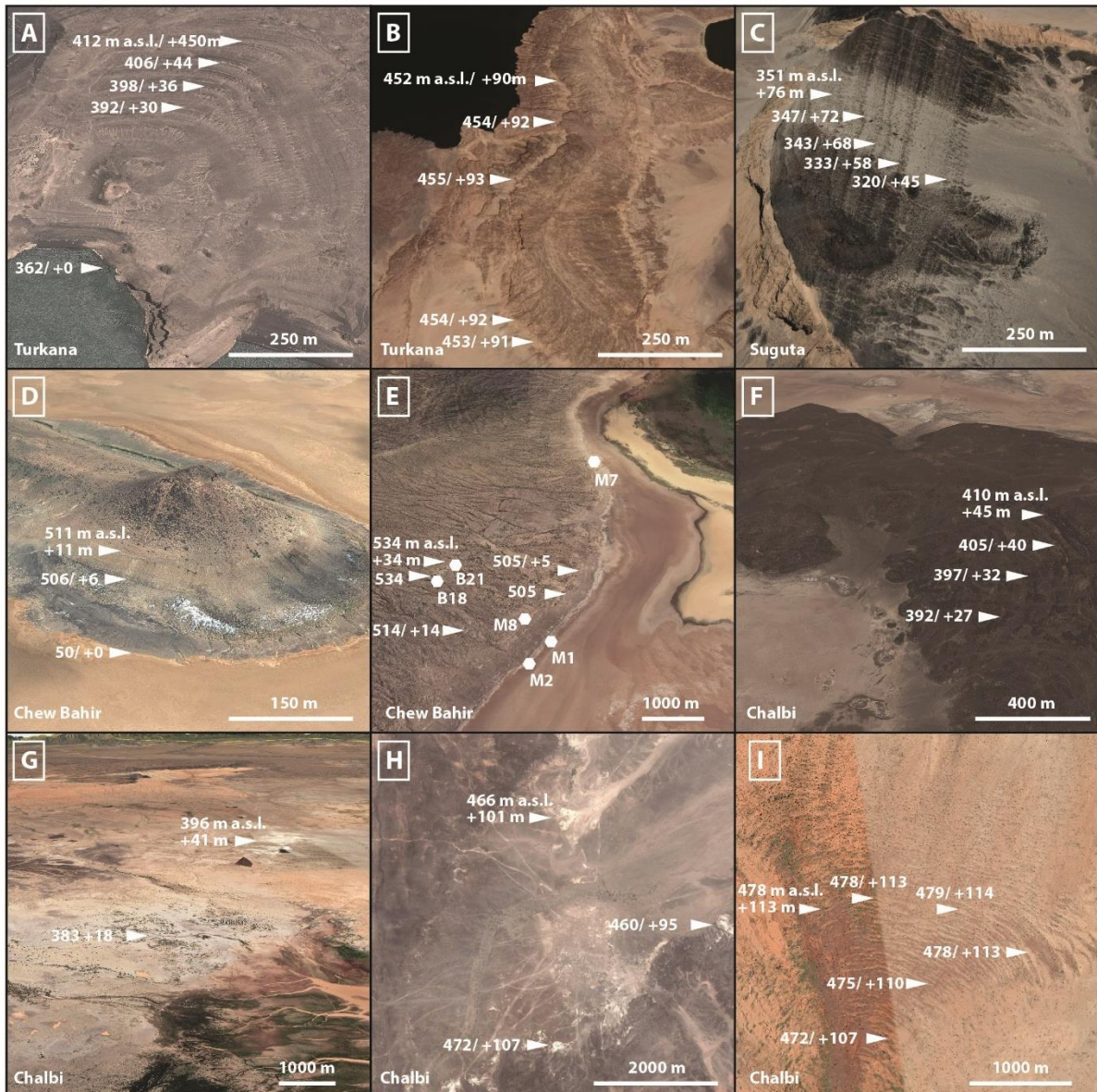
Figure 2 | Representative Google Earth snapshots of shorelines with ground truth (A, C, C, D, G), presumed shorelines (D, F) and ambiguous shoreline observations (H, I), and locations of the new Chew Bahir shoreline ages (E)

Discussion

We reviewed the literature about Lake Turkana and the adjacent paleo-lakes Suguta, Chew Bahir, and Chalbi, surveyed visual satellite imagery and provided new shorelines dates from paleo-lake Chew Bahir to determine their paleo-lake extents, their lake-level evolution, and to analyze the correlation of the lake-levels and the potassium μ-XRF scanning data from the CB-01 short core (Foerster et al., 2015). In summary, during the last AHP, the lakes had a size of 22,904 km² (Lake Turkana), 1,713 km² (paleo-lake Suguta), and 2,477 km² (paleo-lake Chew Bahir), and 2,460 km² (paleo-lake Chalbi). Today, Lake Turkana is the only lake with an outlet area of approximately 6,400 km². Shoreline ages indicate paleo-lake Chew Bahir and Chalbi may have reached their maximum extent only during the early phase of AHP at around 10 and 11 ka.
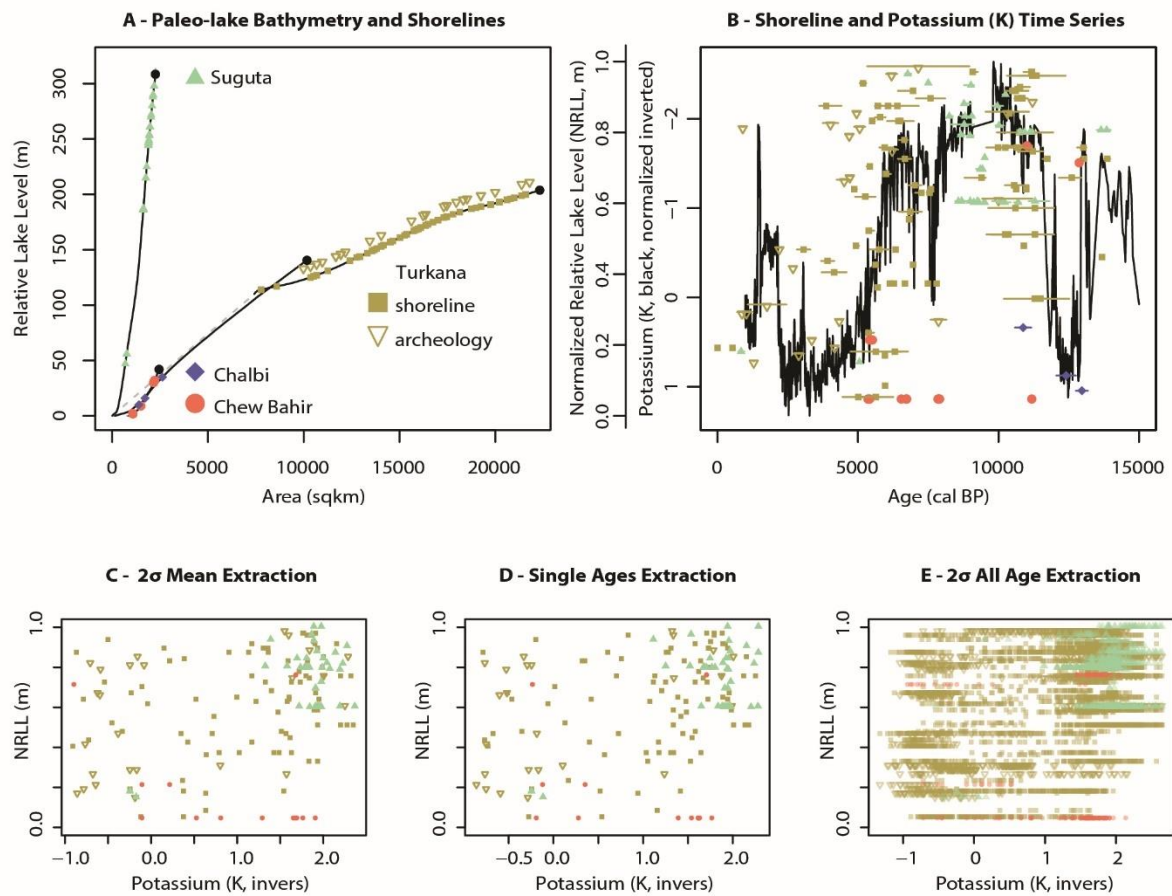
Figure 3. Analysis of the Shoreline. (A) Paleo-lake bathymetries and location of the shorelines and archeological sites. (B) time series of CB-01 and the normalized relative lake levels. (C) data space of the merged datasets using the three presented methods.

Lake Turkana interconnects the Hydrosphere of the rift lakes Abaya, Chamo, Chew Bahir, Suguta, Baringo, Nakuru-Elmenteita with the Mediterranean Sea (Dommain et al., 2022) and, regionally, the Ethiopian with the Kenyan rift lakes. Lake Abaya, Chamo, and paleo-lake Chew Bahir formed a cascading lake system, which drained into Lake Turkana (Fischer et al., 2020). Analogous, Nakuru-Elementeita, Baringo-Bogoria developed a lake system, which overspilled to paleo-lake Suguta and then towards Lake Turkana (Junginger et al., 2014). Paleo-lake Chalbi was not part of this paleo-drainage system and was the only lake that presumably did not reached its overflow sill. Lake Balance Modelling suggested the high importance of the surface water inflow from the extended catchment (Fischer et al., 2020). The missing overspilling influx of paleo-lake Chalbi may have led to insufficient water to compensate for the high evaporation. This hypothesis could be tested using water balance modelling, as applied for the Chew Bahir basin. The elevation of the proven water level of paleo-lake Chalbi (400 m asl) is below the absolute water level of Lake Turkana (455 m asl).

White sediments surrounding paleo-lake Chalbi (see Figure 2-H) are located at the overflow sill elevation and are presumably lacustrine deposits. Nevertheless, their age is yet unknown and may coincide with older lake phases during the Pleistocene. For example, during the Pliocene, the Chalbi and the Turkana basin were connected, forming a mega-lake, which

312 drained into the Indian Ocean (Bruhn et al., 2011). Basalt flows may have covered the
313 lacustrine sediments, which could provide a detailed archive of earlier lake phases.

314 The lake level evolution and the climate processes during the AHP remain debated. Paleo-
315 lake Chew Bahir and Chalbi have their highest localized and dated shorelines from the early
316 AHP. An incomplete record may lead to false conclusions but may be interpreted as a climate
317 signal: The shoreline record implies a rapid onset of humid conditions after the Younger Dryas
318 at around 10.9 ka and a gradual decline of precipitation (Junginger et al., 2014), which leads
319 to the desiccation of paleo-lake Chalbi. As the potassium record indicates, paleo-lake Chew
320 Bahir may have remained a freshwater throughout flow lake with stable climatic conditions
321 (Fischer et al., 2020; M. Trauth et al., 2018).

322 **Shoreline Record Dataset Discussion**

323 Shorelines as a paleoenvironmental proxy are valuable as they provide an archive that can be
324 used to gain spatial and quantitative information about the paleoenvironment and have been
325 used widely all over the globe in, for example, Africa (Drake et al., 2022; Quade et al., 2018),
326 Asia (Jarahi, 2021; Yang et al., 2008; Zhang, Zhao, Sheng, Chen, et al., 2022; Zhang, Zhao,
327 Sheng, Zhang, et al., 2022), America (Baedke et al., 2004; Lewis et al., 2012), and even on
328 the Mars (Irwin III et al., 2002). Shorelines are analyzed remotely based on digital elevation
329 models (Drake & Bristow, 2006; Irwin III et al., 2002), visual aerial or satellite image
330 interpretation (Jarahi, 2021), multi-spectral remote sensing (Bachofer et al., 2014), ground
331 surveys using outcrop or surface samples (Garcin et al., 2009; Huth et al., 2015; Mologni et
332 al., 2021), and even sub-merged paleo-shorelines using acoustic profiles (Lewis et al., 2012).
333 As a geomorphological or sedimentary feature, they are used to reconstruct paleo-lake extents
334 (Junginger & Trauth, 2013), paleo-drainage networks (Dommain et al., 2022), tectonics
335 (Melnick et al., 2012), limnological sedimentary processes (Schuster & Nutz, 2018), paleo-
336 water balance (Junginger & Trauth, 2013) and paleoclimate (Bouchette et al., 2010; Huth et
337 al., 2015; Irwin III et al., 2002).

338 Nevertheless, the shoreline record from the Turkana realm has high noise and uncertainty.
339 Shoreline samples based on a few surface shells, either *M. tuberculata* or *Etheria elliptica*, are
340 not certainly in situ depositions. Gravitational transport may dislocate them, especially in the
341 studied millennial time scales. Outcrops, shell layer or subsurface samples avoid this problem
342 but are relatively scarce in this record. Vertical uncertainty remains, as aquatic species live up
343 to a couple of meters underwater and may be displaced due to water movement. So then, the
344 shoreline is a lower boundary but may have been significantly higher. Archaeological sites, on
345 the other hand, act as an upper limit of the lake level, as they have not necessarily been at the
346 lake surface but have not been under water.

347 With 192 uneven distributed data points, of which 162 are shorelines, and 30 are
348 archaeological sites for 15,000 years, the record is limited in its temporal resolution. The
349 vertical accuracy is dominated by high noise, which superimposes the climate signal. In
350 contrast, the potassium record shows the rapid onset, the stable humidity, and the gradual
351 fluctuating offset of the AHP in a decadal resolution (Fischer et al., 2020). As the potassium
352 record is analyzed following one procedure, it may have the same proxy-system bias for each
353 data point. This makes trend analysis more suitable in contrast to the multi-method, multi-
354 procedure, and multi-laboratory shoreline record, where each datapoint has its own bias.

355 The normalized relative lake level allows for inter-lake comparison. But it is not entirely suitable
356 to generalize the lake processes in terms of climate forcing. Each basin has its specific Aridity

Index and Hypsometric Integral (Olaka et al., 2010) that modifies the pace and magnitude of lake level change to increased precipitation (Fischer et al., 2020). The ratio between the lake and land surface within the catchments is a function of the hypsometry of the basin and differs significantly. Paleo-lake Suguta, for example, has very steep graben shoulders. So then, increasing lake levels do not substantially increase the lake surface area and, hence, the evaporation volume. In contrast, paleo-lake Chew Bahir increases its surface area tremendously by slightly increasing the lake level. Paleo-lake Chalbi and Lake Turkana have comparable paleo-lake bathymetry. Little precipitation or temperature changes may lead to intense fluctuations in the lake level of paleo-lake Suguta. In contrast, those small changes would lead to drastic changes in the water budget of the other lakes and may therefore be recorded in their shoreline record.

Empiric Transfer Function Potentials

The link between two paleo records inherits both age model-related uncertainties. In this case, the new dataset inherits the age model uncertainty of the lacustrine potassium record and the uncertainty of every single dated shoreline. We tested different methods to align them by taking the uncertainty of the shorelines into account but taking the age model of the potassium record as invariable. The *single-age* merge may catch specific maxima and minima of the potassium record, but, by chance, it may match to a chronological close-by inverse peak, which adds random noise to the new aligned dataset. The *two-sigma* averaged alignment decreases the likelihood of random noise but decreases the signal. For example, a high-stand shoreline, which would correspond with a low peak in potassium, would not be recorded. Instead, a centennial averaged potassium signal is aligned to a decade-lasting shoreline. Aligning all potassium values within the given age range of the shoreline forces a higher signal but also a higher noise within the dataset. This makes this method a non-improvement, too. Nevertheless, none of these methods led to a dataset with a significant correlation, suitable for a potential transfer function between lacustrine μ-XRF and shoreline elevations. Age control remains one of the biggest challenges in paleoclimate research.

Lake Level and Landscape Implication

The Turkana lows interconnect the highland regions of the Ethiopian and Kenyan uplift dome and have been an important fossil-bearing site (Brown et al., 1985; Leakey, 1969; Walker et al., 1986) and network node (Bergström et al., 2021) on human evolutionary time scales. During the most intense pluvial period, e.g., at around 11 ka, four mega paleo-lakes and dense savanna vegetation led to a resource-rich environment, as shorelines and modeling work indicate (Fischer et al., 2021; Fischer et al., 2020; Garcin et al., 2012; Junginger & Trauth, 2013; Nyamweru & D., 1989). High climate sensitivity forced the eastern lakes (paleo-lakes Chew Bahir and Chalbi) even during the African Humid Period to dry out. Presumably, humid decadal intervals reactivated this region as a resource-rich environment. Still, every dry spell must have forced climate adaptability from humans living close to paleo-lake Chalbi or Chew Bahir, which may have led to population pressure at the eastern shore of Lake Turkana. In contrast, paleo-lake Suguta remained a large lake throughout the African Humid Period and provided a more stable environment. We see high importance, especially in the region between the (paleo-)lakes Turkana, Chew Bahir, and Chalbi. Whenever a turnover to dry conditions occurs, the eastern shore of Lake Turkana could have been a significant refugium beside distant vertical migration to the green and lush mountainous regions (Foerster et al., 2015). This condensation of resources in space at the Lake Turkana shore may have played a role in human behavior exchange and adaptability when the transition from fishing and hunter-gathering to animal husbandry and the occurrence of the first cemetery (Elisabeth A.

404 Hildebrand et al., 2018) at the end of the African Humid Period has taken place in the
405 surrounding of Lake Turkana.

406 **Conclusion**

407 We examined the lakes between the Ethiopian and Kenyan Plateau, which includes Lake
408 Turkana, paleo-lake Chew Bahir, Suguta, and Chalbi, using literature and data review and -
409 collection, visual remote sensing, data merging, and analysis to (a) reconstruct the paleo-lake
410 extents and depths (b) identify potential gaps in knowledge and (c) to combine multiple paleo
411 datasets. Based on the literature and remote sensing, we conclude that paleo-lake Chalbi was
412 the only lake in the Turkana Depression that did not reach its overflow sill, as it was the only
413 lake which did not received additional water influx from an extended catchment. We see high
414 importance as reliable resource region for humans during the AHP and termination of the
415 eastern shore of Lake Turkana, because the eastern paleo-lakes, Chew Bahir and Chalbi,
416 reacted hypersensitive to short dry spells. Developing a transfer function between lake levels
417 represented by shorelines and the lacustrine potassium proxy failed. We conclude that the
418 combined age model uncertainties and the data quality of shorelines are insufficient for this
419 approach.

420 **References**

421 Abell, P. I., & Nyamweru, C. K. (1988). Paleoenvironments in the Chalbi Basin of Kenya. *Chemical*
422 *Geology (Isotope Geoscience Section)*, *72*, 283-291.
423 Bachofer, F., Quénéhervé, G., & Märker, M. (2014). The delineation of paleo-shorelines in the Lake
424 Manyara basin using TerraSAR-X data. *Remote Sensing*, *6*(3), 2195-2212.
425 Baedke, S. J., Thompson, T. A., Johnston, J. W., & Wilcox, D. A. (2004). Reconstructing paleo lake levels
426 from relict shorelines along the Upper Great Lakes. *Aquatic Ecosystem Health & Management*,
427 *7*(4), 435-449.
428 Baker, M., & Lovenbury, H. (1971). The South Turkana Expedition Scientific Papers VII The 1969 Season
429 Survey. *Geographical Journal*, 349-360.
430 Barker, P. A., Talbot, M. R., Street-Perrott, F. A., Marret, F., Scourse, J., & Odada, E. O. (2004). Late
431 Quaternary climatic variability in intertropical Africa. In *Past climate variability through Europe*
432 *and Africa* (pp. 117-138). Springer.
433 Beck, C. C., Feibel, C. S., Wright, J. D., & Mortlock, R. A. (2019). Onset of the African Humid Period by
434 13.9 kyr BP at Kabua Gorge, Turkana Basin, Kenya. *The Holocene*, *29*(6), 1011-1019.
435 https://doi.org/10.1177/0959683619831415
436 Bergström, A., Stringer, C., Hajdinjak, M., Scerri, E. M. L., & Skoglund, P. (2021). Origins of modern
437 human ancestry. *Nature*, *590*(7845), 229-237. https://doi.org/10.1038/s41586-021-03244-5
438 Bloszies, C., Forman, S. L., & Wright, D. K. (2015). Water level history for Lake Turkana, Kenya in the
439 past 15,000years and a variable transition from the African Humid Period to Holocene aridity.
440 *Global and Planetary Change*, *132*, 64-76. https://doi.org/10.1016/j.gloplacha.2015.06.006
441 Boone, S. C., Kohn, B. P., Gleadow, A. J., Morley, C. K., Seiler, C., Foster, D. A., & Chung, L. (2018).
442 Tectono-thermal evolution of a long-lived segment of the East African Rift System:
443 Thermochronological insights from the North Lokichar Basin, Turkana, Kenya. *Tectonophysics*,
444 *744*, 23-46.
445 Bouchette, F., Schuster, M., Ghienne, J.-F., Denamiel, C., Roquin, C., Moussa, A., Marsaleix, P., &
446 Duringer, P. (2010). Hydrodynamics in Holocene Lake Mega-Chad. *Quaternary Research*, *73*(2),
447 226-236. https://doi.org/10.1016/j.yqres.2009.10.010
448 Brown, F., Harris, J., Leakey, R., & Walker, A. (1985). Early Homo erectus skeleton from west Lake
449 Turkana, Kenya. *Nature*, *316*(6031), 788-792. https://doi.org/10.1038/316788a0
450 Bruhn, R. L., Brown, F. H., Gathogo, P. N., & Haileab, B. (2011). Pliocene volcano-tectonics and
451 paleogeography of the Turkana Basin, Kenya and Ethiopia. *Journal of African Earth Sciences*,
452 *59*(2-3), 295-312. https://doi.org/10.1016/j.jafrearsci.2010.12.002

Butzer, K. W. (1980). The Holocene lake plain of North Rudolph, East Africa. *Physical Geography*, *1*(1), 42-58.

Butzer, K. W., Isaac, G. L., Richardson, J. L., & Washbourn-Kamau, C. (1972). Radiocarbon Dating of East African Lake Levels: New observations provide fresh insights into late Quaternary paleoclimates. *Science*, *175*(4026), 1069-1076.

Butzer, K. W., & Thurber, D. (1969). *Some late Cenozoic sedimentary formations of the Lower Omo Basin*. Fisher, Knight & Company.

Chorowicz, J. (2005). The East African rift system. *Journal of African Earth Sciences*, *43*(1-3), 379-410. https://doi.org/10.1016/j.jafrearsci.2005.07.019

Cohen, A., Campisano, C., Arrowsmith, R., Asrat, A., Behrensmeyer, A. K., Deino, A., Feibel, C., Hill, A., Johnson, R., Kingston, J., Lamb, H., Lowenstein, T., Noren, A., Olago, D., Owen, R. B., Potts, R., Reed, K., Renaut, R., Schäbitz, F., . . . Zinaye, B. (2016). The Hominin Sites and Paleolakes Drilling Project: inferring the environmental context of human evolution from eastern African rift lake deposits. *Scientific Drilling*, *21*, 1-16. https://doi.org/10.5194/sd-21-1-2016

Demenocal, P., Ortiz, J., Guilderson, T., Adkins, J., Sarnthein, M., Baker, L., & Yarusinsky, M. (2000). Abrupt onset and termination of the African Humid Period: . *Quaternary Science Reviews*, *19*(1-5), 347-361. https://doi.org/10.1016/s0277-3791(99)00081-5

Dommain, R., Riedl, S., Olaka, L. A., Demenocal, P., Deino, A. L., Owen, R. B., Muiruri, V., Müller, J., Potts, R., & Strecker, M. R. (2022). Holocene bidirectional river system along the Kenya Rift and its influence on East African faunal exchange and diversity gradients. *Proceedings of the National Academy of Sciences*, *119*(28). https://doi.org/10.1073/pnas.2121388119

Drake, N., & Bristow, C. (2006). Shorelines in the Sahara: geomorphological evidence for an enhanced monsoon from palaeolake Megachad. *The Holocene*, *16*(6), 901-911. https://doi.org/10.1191/0959683606hol981rr

Drake, N. A., Candy, I., Breeze, P., Armitage, S. J., Gasmi, N., Schwenninger, J. L., Peat, D., & Manning, K. (2022). Sedimentary and geomorphic evidence of Saharan megalakes: A synthesis. *Quaternary Science Reviews*, *276*. https://doi.org/10.1016/j.quascirev.2021.107318

Fischer, M. L., Bachofer, F., Yost, C. L., Bludau, I. J. E., Schepers, C., Foerster, V., Lamb, H., Schäbitz, F., Asrat, A., Trauth, M. H., & Junginger, A. (2021). A Phytolith Supported Biosphere-Hydrosphere Predictive Model for Southern Ethiopia: Insights into Paleoenvironmental Changes and Human Landscape Preferences since the Last Glacial Maximum. *Geosciences*, *11*(10), 418. https://doi.org/10.3390/geosciences11100418

Fischer, M. L., Markowska, M., Bachofer, F., Foerster, V. E., Asrat, A., Zielhofer, C., Trauth, M. H., & Junginger, A. (2020). Determining the Pace and Magnitude of Lake Level Changes in Southern Ethiopia Over the Last 20,000 Years Using Lake Balance Modeling and SEBAL. *Frontiers in Earth Science*, *8*. https://doi.org/10.3389/feart.2020.00197

Foerster, V., Deocampo, D. M., Asrat, A., Günter, C., Junginger, A., Krämer, K. H., Stroncik, N. A., & Trauth, M. H. (2018). Towards an understanding of climate proxy formation in the Chew Bahir basin, southern Ethiopian Rift. *Palaeogeography, Palaeoclimatology, Palaeoecology*, *501*, 111-123. https://doi.org/10.1016/j.palaeo.2018.04.009

Foerster, V., Junginger, A., O., L., T., G., Asrat, A., M., U., F, L. H., Wennrich, V., Rethemeyer, J., N, N., Trauth, M. H., & Schaebitz, F. (2012). Climatic change recorded in the sediments of the Chew Bahir basin, southern Ethiopia, during the last 45,000 years. *Quaternary International*, *274*, 25. https://doi.org/10.1016/j.quaint.2012.06.028

Foerster, V., Vogelsang, R., Junginger, A., Asrat, A., Lamb, H. F., Schaebitz, F., & Trauth, M. H. (2015). Environmental change and human occupation of southern Ethiopia and northern Kenya during the last 20,000 years. *Quaternary Science Reviews*, *129*, 333-340. https://doi.org/10.1016/j.quascirev.2015.10.026

Forman, S. L., Wright, D. K., & Bloszies, C. (2014). Variations in water level for Lake Turkana in the past 8500 years near Mt. Porr, Kenya and the transition from the African Humid Period to Holocene aridity. *Quaternary Science Reviews*, *97*, 84-101. https://doi.org/10.1016/j.quascirev.2014.05.005

505 Garcin, Y., Junginger, A., Melnick, D., Olago, D. O., Strecker, M. R., & Trauth, M. H. (2009). Late
506   Pleistocene–Holocene rise and collapse of Lake Suguta, northern Kenya Rift. *Quaternary*
507   *Science Reviews*, *28*(9-10), 911-925. https://doi.org/10.1016/j.quascirev.2008.12.006

508 Garcin, Y., Melnick, D., Strecker, M. R., Olago, D., & Tiercelin, J.-J. (2012). East African mid-Holocene
509   wet–dry transition recorded in palaeo-shorelines of Lake Turkana, northern Kenya Rift. *Earth*
510   *and Planetary Science Letters*, *331-332*, 322-334. https://doi.org/10.1016/j.epsl.2012.03.016

511 Harmand, S., Lewis, J. E., Feibel, C. S., Lepre, C. J., Prat, S., Lenoble, A., Boës, X., Quinn, R. L., Brenet,
512   M., Arroyo, A., Taylor, N., Clément, S., Daver, G., Brugal, J.-P., Leakey, L., Mortlock, R. A.,
513   Wright, J. D., Lokorodi, S., Kirwa, C., . . . Roche, H. (2015). 3.3-million-year-old stone tools from
514   Lomekwi 3, West Turkana, Kenya. *Nature*, *521*(7552), 310-315.
515   https://doi.org/10.1038/nature14464

516 Hildebrand, E. A., Brandt, S. A., & Lesur-Gebremariam, J. (2010). The Holocene Archaeology of
517   Southwest Ethiopia: New Insights from the Kafa Archaeological Project. *African Archaeological*
518   *Review*, *27*(4), 255-289. https://doi.org/10.1007/s10437-010-9079-8

519 Hildebrand, E. A., & Grillo, K. M. (2012). Early herders and monumental sites in eastern Africa: dating
520   and interpretation. *Antiquity*, *86*(332), 338-352.

521 Hildebrand, E. A., Grillo, K. M., Sawchuk, E. A., Pfeiffer, S. K., Conyers, L. B., Goldstein, S. T., Hill, A. C.,
522   Janzen, A., Klehm, C. E., Helper, M., Kiura, P., Ndiema, E., Ngugi, C., Shea, J. J., & Wang, H.
523   (2018). A monumental cemetery built by eastern Africa's first herders near Lake Turkana,
524   Kenya. *Proc Natl Acad Sci U S A*, *115*(36), 8942-8947.
525   https://doi.org/10.1073/pnas.1721975115

526 Hildebrand, E. A., Grillo, K. M., Sawchuk, E. A., Pfeiffer, S. K., Conyers, L. B., Goldstein, S. T., Hill, A. C.,
527   Janzen, A., Klehm, C. E., Helper, M., Kiura, P., Ndiema, E., Ngugi, C., Shea, J. J., & Wang, H.
528   (2018). A monumental cemetery built by eastern Africa's first herders near Lake Turkana,
529   Kenya. *Proceedings of the National Academy of Sciences*, *115*(36), 8942-8947.
530   https://doi.org/10.1073/pnas.1721975115

531 Huth, T., Hudson, A. M., Quade, J., Guoliang, L., & Hucai, Z. (2015). Constraints on Paleoclimate from
532   11.5 to 5.0 ka from Shoreline dating and Hydrologic Budget Modeling of Baqan Tso,
533   Southwestern Tibetan Plateau. *Quaternary Research*, *83*(1), 80-93.
534   https://doi.org/10.1016/j.yqres.2014.07.011

535 Irwin III, R. P., Maxwell, T. A., Howard, A. D., Craddock, R. A., & Leverington, D. W. (2002). A large
536   paleolake basin at the head of Ma'adim Vallis, Mars. *Science*, *296*(5576), 2209-2212.

537 Jaeschke, A., Thienemann, M., Schefuß, E., Urban, J., Schäbitz, F., Wagner, B., & Rethemeyer, J. (2020).
538   Holocene Hydroclimate Variability and Vegetation Response in the Ethiopian Highlands (Lake
539   Dendi). *Frontiers in Earth Science*, *8*. https://doi.org/10.3389/feart.2020.585770

540 Jarahi, H. (2021). Paleo Mega Lake of Rey Identification and Reconstruction of Quaternary Lake in
541   Central Iran. *Open Quaternary*, *7*. https://doi.org/10.5334/oq.94

542 Junginger, A., Roller, S., Olaka, L. A., & Trauth, M. H. (2014). The effects of solar irradiation changes on
543   the migration of the Congo Air Boundary and water levels of paleo-Lake Suguta, Northern
544   Kenya Rift, during the African Humid Period (15–5ka BP). *Palaeogeography,*
545   *Palaeoclimatology, Palaeoecology*, *396*, 1-16. https://doi.org/10.1016/j.palaeo.2013.12.007

546 Junginger, A., & Trauth, M. H. (2013). Hydrological constraints of paleo-Lake Suguta in the Northern
547   Kenya Rift during the African Humid Period (15–5kaBP). *Global and Planetary Change*, *111*,
548   174-188. https://doi.org/10.1016/j.gloplacha.2013.09.005

549 Lamb, A. L., Leng, M. J., Umer Mohammed, M., & Lamb, H. F. (2004). Holocene climate and vegetation
550   change in the Main Ethiopian Rift Valley, inferred from the composition (C/N and δ13C) of
551   lacustrine organic matter. *Quaternary Science Reviews*, *23*(7-8), 881-891.
552   https://doi.org/10.1016/j.quascirev.2003.06.010

553 Leakey, R. E. F. (1969). Early Homo sapiens Remains from the Omo River Region of South-west Ethiopia:
554   Faunal Remains from the Omo Valley. *Nature*, *222*(5199), 1132-1133.
555   https://doi.org/10.1038/2221132a0

Lewis, C. F. M., Cameron, G. D. M., Anderson, T. W., Heil, C. W., & Gareau, P. L. (2012). Lake levels in the Erie Basin of the Laurentian Great Lakes. *Journal of Paleolimnology*, *47*(3), 493-511. https://doi.org/10.1007/s10933-012-9578-5

Melnick, D., Garcin, Y., Quinteros, J., Strecker, M. R., Olago, D., & Tiercelin, J.-J. (2012). Steady rifting in northern Kenya inferred from deformed Holocene lake shorelines of the Suguta and Turkana basins. *Earth and Planetary Science Letters*, *331-332*, 335-346. https://doi.org/10.1016/j.epsl.2012.03.007

Merwade, V. (2012). Watershed and stream network delineation using ArcHydro tools. *School of Civil Engineering, Purdue University*, 1-7.

Mologni, C., Bruxelles, L., Schuster, M., Davtian, G., Ménard, C., Orange, F., Doubre, C., Cauliez, J., Taezaz, H. B., & Revel, M. (2021). Holocene East African monsoonal variations recorded in wave-dominated clastic paleo-shorelines of Lake Abhe, Central Afar region (Ethiopia & Djibouti). *Geomorphology*, *391*, 107896.

Nyamweru, C. K. (1986). Quaternary environments of the Chalbi basin, Kenya: sedimentary and geomorphological evidence. *Geological Society Special Publication*, *25*(Sedimentation in the African Rifts), 297-310.

Nyamweru, C. K., & D., B. (1989). Climatic changes in the Chalbi Desert, North Kenya.

Ojwang, W. O., Obiero, K. O., Donde, O. O., Gownaris, N., Pikitch, E. K., Omondi, R., Agembe, S., Malala, J., & Avery, S. T. (2016). Lake Turkana: World's Largest Permanent Desert Lake (Kenya). In *The Wetland Book* (pp. 1-20). Springer Netherlands. https://doi.org/10.1007/978-94-007-6173-5_254-1

Olaka, L. A., Odada, E. O., Trauth, M. H., & Olago, D. O. (2010). The sensitivity of East African rift lakes to climate fluctuations. *Journal of Paleolimnology*, *44*(2), 629-644. https://doi.org/10.1007/s10933-010-9442-4

Owen, R. B., Barthelme, J. W., Renaut, R., & Vincens, A. (1982). Palaeolimnology and archaeology of Holocene deposits north-east of Lake Turkana, Kenya. *Nature*, *298*(5874), 523-529.

Phillipson, D. W. (1977). Lowasera. *AZANIA: Journal of the British Institute in Eastern Africa*, *12*(1), 1-32.

Quade, J., Dente, E., Armon, M., Ben Dor, Y., Morin, E., Adam, O., & Enzel, Y. (2018). Megalakes in the Sahara? A Review. *Quaternary Research*, *90*(2), 253-275. https://doi.org/10.1017/qua.2018.46

Ramsey, C. B. (2017). Methods for summarizing radiocarbon datasets. *Radiocarbon*, *59*(6), 1809-1833.

Revel, M., Colin, C., Bernasconi, S., Combourieu-Nebout, N., Ducassou, E., Grousset, F. E., Rolland, Y., Migeon, S., Bosch, D., Brunet, P., Zhao, Y., & Mascle, J. (2014). 21,000 Years of Ethiopian African monsoon variability recorded in sediments of the western Nile deep-sea fan. *Regional Environmental Change*, *14*(5), 1685-1696. https://doi.org/10.1007/s10113-014-0588-x

Roberts, H. M., Ramsey, C. B., Chapot, M. S., Deino, A. L., Lane, C. S., Vidal, C., Asrat, A., Cohen, A., Foerster, V., Lamb, H. F., Schäbitz, F., Trauth, M. H., & Viehberg, F. A. (2021). Using multiple chronometers to establish a long, directly-dated lacustrine record: Constraining >600,000 years of environmental change at Chew Bahir, Ethiopia. *Quaternary Science Reviews*, *266*, 107025. https://doi.org/10.1016/j.quascirev.2021.107025

Schaebitz, F., Asrat, A., Lamb, H. F., Cohen, A. S., Foerster, V., Duesing, W., Kaboth-Bahr, S., Opitz, S., Viehberg, F. A., Vogelsang, R., Dean, J., Leng, M. J., Junginger, A., Ramsey, C. B., Chapot, M. S., Deino, A., Lane, C. S., Roberts, H. M., Vidal, C., . . . Trauth, M. H. (2021). Hydroclimate changes in eastern Africa over the past 200,000 years may have influenced early human dispersal. *Communications Earth & Environment*, *2*(1). https://doi.org/10.1038/s43247-021-00195-7

Schuster, M., & Nutz, A. (2018). Lacustrine wave-dominated clastic shorelines: modern to ancient littoral landforms and deposits from the Lake Turkana Basin (East African Rift System, Kenya). *Journal of Paleolimnology*, *59*(2), 221-243. https://doi.org/10.1007/s10933-017-9960-4

Trauth, M., Foerster, V., Junginger, A., Asrat, A., Lamb, H., & Schaebitz, F. (2018). Abrupt or Gradual? Change Point Analysis of the Late Pleistocene-Holocene Chew Bahir Record from Southern Ethiopia. *Quaternary Research*, *90*(2), 321-330.

Trauth, M. H., Asrat, A., Cohen, A. S., Duesing, W., Foerster, V., Kaboth-Bahr, S., Kraemer, K. H., Lamb, H. F., Marwan, N., Maslin, M. A., & Schäbitz, F. (2021). Recurring types of variability and

609   transitions in the ~620 kyr record of climate change from the Chew Bahir basin, southern
610   Ethiopia. *Quaternary Science Reviews*, *266*. https://doi.org/10.1016/j.quascirev.2020.106777
611 Trauth, M. H., Foerster, V., Junginger, A., Asrat, A., Lamb, H. F., & Schaebitz, F. (2018). Abrupt or
612   gradual? Change point analysis of the late Pleistocene–Holocene climate record from Chew
613   Bahir, southern Ethiopia. *Quaternary Research*, *90*(2), 321-330.
614   https://doi.org/10.1017/qua.2018.30
615 Trauth, M. H., Maslin, M. A., Deino, A. L., Junginger, A., Lesoloyia, M., Odada, E. O., Olago, D. O., Olaka,
616   L. A., Strecker, M. R., & Tiedemann, R. (2010). Human evolution in a variable environment: the
617   amplifier lakes of Eastern Africa. *Quaternary Science Reviews*, *29*(23-24), 2981-2988.
618   https://doi.org/10.1016/j.quascirev.2010.07.007
619 Truckle, P. (1976). Geology and late Cainozoic lake sediments of the Suguta Trough, Kenya. *Nature*,
620   *263*(5576), 380-383.
621 Umer, M., Lamb, H. F., Bonnefille, R., Lézine, A. M., Tiercelin, J. J., Gibert, E., Cazet, J. P., & Watrin, J.
622   (2007). Late Pleistocene and Holocene vegetation history of the Bale Mountains, Ethiopia.
623   *Quaternary Science Reviews*, *26*(17-18), 2229-2246.
624   https://doi.org/10.1016/j.quascirev.2007.05.004
625 van Breugel, P., Kindt, R., Lillesø, J., Bingham, M., Demissew, S., Dudley, C., Friis, I., Gachathi, F., Kalema,
626   J., Mbago, F., Moshi, H., Mulumba, J., Namaganda, M., Ndangalasi, H., Ruffo, C., Védaste, M.,
627   Jamnadass, R., & Graudal, L. (2015). *Potential Natural Vegetation Map of Eastern Africa
628   (Burundi, Ethiopia, Kenya, Malawi, Rwanda, Tanzania, Uganda and Zambia). Version 2.0*.
629   Forest and Landscape (Denmark) and World Agroforestry Centre (ICRAF).
630   //vegetationmap4africa.org
631 Walker, A., Leakey, R. E., Harris, J. M., & Brown, F. H. (1986). 2.5-Myr Australopithecus boisei from west
632   of Lake Turkana, Kenya. *Nature*, *322*(6079), 517-522. https://doi.org/10.1038/322517a0
633 Webster Barthelme, J. (1985). *Fisher-hunters and neolithic pastoralists in East Turkana, Kenya*. BAR
634   Publishing.
635 Wright, D. K., Forman, S. L., Kiura, P., Bloszies, C., & Beyin, A. (2015). Lakeside View: Sociocultural
636   Responses to Changing Water Levels of Lake Turkana, Kenya. *African Archaeological Review*,
637   *32*(2), 335-367. https://doi.org/10.1007/s10437-015-9185-8
638 Yang, L., Chen, F., Chun, X., Fan, Y., Sun, Y., Madsen, D. B., & Zhang, X. (2008). The Jilantai Salt Lake
639   shorelines in Northwestern arid China revealed by remote sensing images. *Journal of Arid
640   Environments*, *72*(5), 861-866.
641 Zhang, S., Zhao, H., Sheng, Y., Chen, S., Li, G., & Chen, F. (2022). Late Quaternary lake level record of
642   Orog Nuur, southern Mongolia, revealed by optical dating of paleo-shorelines. *Quaternary
643   Geochronology*, 101370.
644 Zhang, S., Zhao, H., Sheng, Y., Zhang, J., Zhang, J., Sun, A., Wang, L., Huang, L., Hou, J., & Chen, F. (2022).
645   Mega-lakes in the northwestern Tibetan Plateau formed by melting glaciers during the last
646   deglacial. *Quaternary Science Reviews*, *285*, 107528.

647

648

Supplementary

Table S1 I Shoreline record and archeological sites, archeological sites coordinates published with significant reduced precision (*B = Chew Bahir S = Suguta, C = Chalbi, T = Turkana, TA = Turkana archaeology; **M = Melanoides tuberculata, E = Etheria elliptica, O = Ostracods, C= charcoal, H = humid acids, B = Bivalve, O = oyster , Sn= snail, St= Stromatolites; *** cal BP).

ID	Site*	ID orig	Type**	Elev	Lat	Long	14C mean***	14C 2σ min***	14C 2σ max***	Reference
1	S	KIA35809	O	322	1,913	36,465	5050	5022	5114	Junginger et al., 2014
2	S	KIA36873	M	573	1,561	36,334	6770	6664	6901	Junginger et al., 2014
3	S	KIA36866	M	565	1,619	36,461	7500	7426	7581	Junginger et al., 2014
4	S	KIA33903	M	536	2,273	36,578	8250	8187	8376	Junginger et al., 2014
5	S	KIA33909	M	520	1,576	36,373	8660	8554	8791	Junginger et al., 2014
6	S	KIA33902	M	490	2,270	36,574	9350	9195	9440	Junginger et al., 2014
7	S	KIA33916	M	519	1,950	36,381	8990	8855	9124	Junginger et al., 2014
8	S	KIA36872	M	563	1,790	36,515	9020	8767	9137	Junginger et al., 2014
9	S	KIA33917	M	585	1,955	36,416	9030	8992	9143	Junginger et al., 2014
10	S	KIA33908	M	536	1,578	36,400	9050	8974	9139	Junginger et al., 2014
11	S	KIA33918	M	585	1,955	36,416	9790	9736	10168	Junginger et al., 2014
12	S	KIA33911	M	528	2,246	36,614	10020	9885	10194	Junginger et al., 2014
13	S	KIA33913	M	545	2,248	36,614	9960	9760	10172	Junginger et al., 2014
14	S	KIA33912	M	555	2,248	36,613	10250	10133	10267	Junginger et al., 2014
15	S	KIA37059	C	522	1,538	36,225	10750	10720	10870	Junginger et al., 2014
16	S	KIA37060	E	522	1,538	36,225	10790	10742	11166	Junginger et al., 2014
17	S	KIA37057	M,R	522	1,538	36,225	10930	10702	11109	Junginger et al., 2014
18	S	KIA37058	C,R	522	1,538	36,225	10930	10702	11109	Junginger et al., 2014
19	S	KIA37056	C	522	1,538	36,225	11120	10920	11110	Junginger et al., 2014
20	S	KIA37055	C	522	1,538	36,225	11200	11091	11243	Junginger et al., 2014
21	S	KIA37054	C	522	1,538	36,225	11210	11162	11252	Junginger et al., 2014
22	S	KIA33910	M	524	1,537	36,226	13650	13493	13813	Junginger et al., 2014
23	S	KIA33907	E	524	1,537	36,226	13850	13739	14000	Junginger et al., 2014
24	S	KIA33904	M	461	2,219	36,631	10700	10552	10793	Junginger et al., 2014
25	S	KIA33905	M	461	2,219	36,631	10220	10223	10432	Junginger et al., 2014
26	S	KIA33906	M	461	2,219	36,631	9510	9465	9546	Junginger et al., 2014
27	S	KIA37071	M	461	2,219	36,631	9495	9420	9537	Junginger et al., 2014
28	S	KIA33901	M	536	2,272	36,578	8810	8637	8984	Junginger et al., 2014
29	S	KIA37069	M,R	461	2,219	36,631	9300	9081	9329	Junginger et al., 2014
30	S	KIA37070	C,HA,R	461	2,219	36,631	9300	9081	9329	Junginger et al., 2014
31	S	KIA37068	Cb	461	2,219	36,631	9120	9010	9304	Junginger et al., 2014
32	S	KIA37067	C	462	1,630	36,465	8570	8453	8629	Junginger et al., 2014
33	S	KIA37065	M,R	462	1,630	36,465	8690	8593	8811	Junginger et al., 2014
34	S	KIA37066	C,R	462	1,630	36,465	8690	8593	8811	Junginger et al., 2014
35	S	KIA37064	C	462	1,630	36,465	8990	8767	9031	Junginger et al., 2014
36	S	KIA37063	C	462	1,630	36,465	9250	9021	9302	Junginger et al., 2014
37	S	KIA37062	M	462	1,630	36,465	10060	9767	10188	Junginger et al., 2014
38	S	KIA37061	C	462	1,630	36,465	11300	11073	11824	Junginger et al., 2014
39	S	KIA33919	M	547	1,550	36,222	8770	8720	9035	Junginger et al., 2014
40	S	KIA 33914	M	490	1,947	36,380	9430	9272	9482	Junginger et al., 2014
41	S	KIA33915	M	500	1,950	36,381	9510	9465	9564	Junginger et al., 2014
42	S	KIA43294	C	529	1,551	36,226	8780	8278	9139	Junginger et al., 2014
43	S	KIA43247	C,R	331	1,910	36,464	840	737	962	Junginger et al., 2014
44	S	KIA43248	M,R	331	1,910	36,464	840	795	886	Junginger et al., 2014
45	B	CB18-B21 C	B	530	4,707	36,733	12871	12786	12956	this study
46	B	CB18-B2 I	M	502	4,691	36,751	11183	11159	11206	this study
47	B	CB18-B18 SH	B	532	4,705	36,731	11017	10892	11141	this study
48	B	CB18-B18 WH	B	532	4,705	36,731	11017	10892	11141	this study
49	B	M1Cii_14C_01	St	502	4,695	36,753	7904	7846	7962	this study
52	B	M2B_14C_02	St	502	4,691	36,751	5415	5376	5454	this study
54	B	M7C_14C_01	St	502	4,742	36,761	6541	6449	6633	this study
57	B	M8B_14C_01	St	509	4,697	36,743	5415	5375	5455	this study
72	T	KIA 36856	M	453	2,661	36,588	9085	9015	9270	Garcin et al., 2012
73	T	KIA 36857	E	453	2,661	36,588	11190	10884	11247	Garcin et al., 2012

74	T	KIA 36858	M	428	2,627	36,572	5420	5306	5469	Garcin et al., 2012
75	T	KIA 36859	M	422	2,626	36,571	4865	4843	4969	Garcin et al., 2012
76	T	KIA 36860	M	411	2,626	36,572	5385	5316	5576	Garcin et al., 2012
77	T	KIA 36861	M	407	2,625	36,572	4925	4855	5040	Garcin et al., 2012
78	T	KIA 36862	B	402	2,624	36,571	5625	5590	5715	Garcin et al., 2012
79	T	KIA 36864	M	393	2,622	36,571	11500	11275	11764	Garcin et al., 2012
80	T	KIA 36865	M	384	2,619	36,571	5375	5319	5579	Garcin et al., 2012
81	T	Pa 2226	M	432	2,932	36,063	11215	10788	11606	Garcin et al., 2012
82	T	Pa 2227	B	421	3,219	36,003	7255	7024	7318	Garcin et al., 2012
83	T	Pa 2224	S	421	3,219	36,003	7550	7438	7576	Garcin et al., 2012
84	T	Pa 2223	B	449	3,748	35,785	10765	10585	11125	Garcin et al., 2012
85	T	TOP 02/11	O	435	3,845	35,772	6650	6446	6780	Garcin et al., 2012
86	T	LAPS 02/14	O	433	4,284	35,863	5950	5754	6263	Garcin et al., 2012
87	T	Pa 2230	O	440	4,118	35,851	5500	5474	5601	Garcin et al., 2012
88	T	Pa 2231	St	440	4,118	35,851	5500	5470	5594	Garcin et al., 2012
89	T	Pa 2225	O	444	4,151	35,852	6070	5992	6208	Garcin et al., 2012
90	T	Pa 2228	M	444	4,151	35,852	5710	5601	5875	Garcin et al., 2012
91	T	Pa 2229	O	426	4,086	35,838	6000	5927	6180	Garcin et al., 2012
92	T	Pa 2232	O	426	4,086	35,838	5995	5929	6178	Garcin et al., 2012
93	T	402648	C	422	3,458	35,782	10630	10560	10695	Beck et al., 2019
94	T	402649	S	422	3,458	35,782	10990	10913	10993	Beck et al., 2019
95	T	3775179	C	407	3,458	35,785	10900	10812	10987	Beck et al., 2019
96	T	396299	S	430	3,446	35,788	11740	11560	11745	Beck et al., 2019
97	T	396300	S	430	3,446	35,788	13040	12990	13090	Beck et al., 2019
98	T	396301	S	430	3,446	35,788	13870	13755	13980	Beck et al., 2019
99	T	ISGS A-1133	M	422	2,940	36,630	7600	7580	7620	Forman et al., 2014
100	T	ISGS A-1259	B	378	2,902	36,634	5960	5945	5975	Forman et al., 2014
101	T	ISGS A-1260	B	397	2,920	36,632	6275	6260	6290	Forman et al., 2014
102	T	ISGS A-1261	M	414	2,932	36,630	6820	6785	6855	Forman et al., 2014
104	T	ISGS A-1342	E	440	2,963	36,619	6440	6415	6465	Forman et al., 2014
105	T	SNU11-A023	M	370	2,895	36,634	5965	5905	6025	Forman et al., 2014
106	T	SNU11-A024	M	406	2,926	36,630	6340	6290	6390	Forman et al., 2014
107	T	SNU11-A027	M	397	2,920	36,632	7490	7445	7535	Forman et al., 2014
108	T	SNU11-A028	B	397	2,920	36,632	6135	6055	6215	Forman et al., 2014
109	T	SNU11-A029	B	397	2,921	36,633	6670	6600	6740	Forman et al., 2014
110	T	UIC2321	OSL	416	2,936	36,630	6860	6440	7280	Forman et al., 2014
111	T	UIC2497	OSL	440	2,963	36,619	6510	6030	6990	Forman et al., 2014
112	T	UIC2513	OSL	379	2,904	36,632	6315	5845	6785	Forman et al., 2014
113	T	UIC2513a	OSL	379	2,904	36,632	5635	4725	6545	Forman et al., 2014
114	T	UIC2514	OSL	380	2,902	36,633	0	0	45	Forman et al., 2014
115	T	UIC2719	OSL	446	2,961	36,622	7580	7055	8105	Forman et al., 2014
116	T	UIC2720	OSL	420	2,940	36,633	5260	4890	5630	Forman et al., 2014
117	T	UIC2721	OSL	380	2,902	36,633	540	490	590	Forman et al., 2014
118	T	UIC2958	OSL	403	2,924	36,632	3920	3680	4160	Forman et al., 2014
119	T	UIC2959	OSL	400	2,920	36,623	4150	3700	4600	Forman et al., 2014
120	T	UIC2960	OSL	406	2,926	36,630	5760	5400	6120	Forman et al., 2014
121	T	UIC2961	OSL	406	2,926	36,630	3065	2820	3310	Forman et al., 2014
122	T	SNU12-589	M	450	3,424	35,805	5180	5060	5300	Bloszies et al., 2015
123	T	SNU12-590	M	402	3,577	35,812	6960	6890	7030	Bloszies et al., 2015
126	T	SNU12-591	M	396	3,301	35,971	5700	5635	5765	Bloszies et al., 2015
128	T	SNU12-592	M	397	3,526	35,811	7800	7720	7880	Bloszies et al., 2015
129	T	SNU12-593	M	404	3,525	35,805	13680	13610	13750	Bloszies et al., 2015
130	T	SNU12-594	M	453	2,916	36,058	11175	11100	11250	Bloszies et al., 2015
131	T	SNU12-595	M	448	2,917	36,060	10610	10515	10705	Bloszies et al., 2015
132	T	SNU12-596	E	446	2,917	36,059	10830	10690	10970	Bloszies et al., 2015
133	T	SNU12-597	M	446	2,917	36,055	10670	10560	10780	Bloszies et al., 2015
134	T	SNU12-598	B	446	2,917	36,055	10850	10660	11040	Bloszies et al., 2015
135	T	SNU12-599	M	442	2,918	36,055	10395	10295	10495	Bloszies et al., 2015
136	T	ULN#	B	433	5,375	35,912	13020	12791	13132	Brown and Fuller, 2008
137	T	L-1203-I	B	441	5,303	35,984	5785	5600	5990	Butzer, 1980, Butzer and Thurber, 1972
138	T	L-1203-B	B	410	5,392	35,907	10240	9701	10576	Butzer and Thurber, 1969, Butzeret al., 1972
139	T	L-1203-C	B	410	5,392	35,907	11300	10804	11990	Butzer and Thurber, 1969, Butzeret al., 1972

140	T	L-1203-D	B	410	5,392	35,907	10250	9563	10776	Butzer and Thurber, 1969, Butzeret al., 1972
141	T	L-1203-E	B	410	5,392	35,907	10350	9785	11089	Butzer and Thurber, 1969, Butzeret al., 1972
142	T	L-1203-G	B	448	5,300	35,950	6960	6413	6900	Butzer and Thurber, 1969, Butzeret al., 1972
143	T	L-1203-H	B	444	5,315	35,929	3870	3615	4418	Butzer and Thurber, 1969, Butzeret al., 1972
144	T	L-1203-I	B	430	5,327	35,998	6670	6413	6900	Butzer and Thurber, 1969, Butzeret al., 1972
145	T	L-1203-J	B	417	5,377	36,193	11300	10804	11990	Butzer and Thurber, 1969, Butzeret al., 1972
146	T	L-1203-K	B	423	5,335	36,064	7020	6788	7267	Butzer and Thurber, 1969, Butzeret al., 1972
147	T	L-1203-L	E	425	5,083	35,917	9400	8785	9551	Butzer and Thurber, 1969, Butzeret al., 1972
148	T	L-1203-M	B	437	5,400	35,950	10750	9934	11953	Butzer and Thurber, 1969, Butzeret al., 1972
149	T	L-1303-A	B	444	5,167	35,586	6400	5609	7170	Butzeret al., 1972
150	T	L-1303-C	B	393	5,084	36,032	11290	10182	12525	Butzeret al., 1972
151	T	L-1303-H	B	417	5,396	35,946	10600	9627	11326	Butzeret al., 1972
152	T	R1-954	B	452	4,072	36,343	11350	10716	12394	Owen et al., 1982
153	T	SUA-635	B	448	3,948	36,397	10490	10221	11073	Owen et al., 1982
154	T	SUA-638	B	425	3,941	36,247	12610	12143	12958	Owen et al., 1982
155	T	Gx-5479	B	452	4,072	36,343	11200	10298	11813	Owen et al., 1982, Barthelme, 1985
156	T	Hel-1276	B	433	3,952	36,369	9980	9560	10273	Owen et al., 1982, Barthelme, 1985
157	T	Hel-1277	E	433	3,952	36,369	10240	9901	10655	Owen et al., 1982, Barthelme, 1985
158	T	SUA-635	B	423	3,943	36,238	10560	10223	11075	Owen et al., 1982, Barthelme, 1985
159	T	HEL-867	B	433	2,932	36,720	10650	10236	11206	Phillipson, 1977
160	T	Birm-540	E	367	3,968	36,213	5630	5053	6265	Williams and Johnson, 1976
161	T	Birm-540	E	367	3,968	36,213	5010	4441	5577	Williams and Johnson, 1976
162	TA	FwJh14	A	376	4,29	35,90	1290	1260	1320	Wright et al., 2015
163	TA	FwJh16	A	382	4,30	35,90	3355	3250	3460	Wright et al., 2015
164	TA	GaJi2	A	424	3,94	36,23	4509	4237	4781	Wright et al., 2015
165	TA	GaJi4	A	425	3,94	36,24	4710	4581	4839	Wright et al., 2015
166	TA	FwJj5	A	438	4,27	36,29	900	840	960	Wright et al., 2015
167	TA	FwJj25	A	439	4,27	36,28	4020	3740	4300	Wright et al., 2015
168	TA	GeJk4	A	433	2,91	36,71	10718	10235	11202	Wright et al., 2015
169	TA	GcJh1	A	391	3,40	35,92	1761	1068	2455	Wright et al., 2015
170	TA	GcJh2	A	406	3,39	35,92	2203	2061	2345	Wright et al., 2015
171	TA		A	389	3,19	36,02	1027	799	1255	Wright et al., 2015
172	TA	GdJi2	A	452	3,16	35,98	6195	5995	6394	Wright et al., 2015
173	TA	FvJh2	A	387	4,46	35,91	7866	7577	8156	Wright et al., 2015
174	TA		A	389	3,19	36,02	871	693	1049	Wright et al., 2015
175	TA		A	442	5,19	35,61	10316	9537	11096	Wright et al., 2015
176	TA		A	432	5,19	35,99	6214	5991	6437	Wright et al., 2015
177	TA	GaJi23	A	436	4,00	36,35	4690	4533	4847	Wright et al., 2015
178	TA	GbJj1	A	438	3,62	36,26	5061	4858	5265	Wright et al., 2015
179	TA	GcJh11	A	445	3,43	35,75	11211	11177	11246	Wright et al., 2015
180	TA	GeJi10	A	467	2,92	36,04	4851	4836	4866	Wright et al., 2015
181	TA	GeJh3	A	387	3,49	35,86	4331	4250	4413	Wright et al., 2015
182	TA	GeJh5	A	380	3,51	35,86	4171	4102	4240	Wright et al., 2015
183	TA		A	566	2,00	36,11	1114	937	1291	Wright et al., 2015
184	TA	GeJk10	A	378	2,90	36,63	2890	2695	3085	Wright et al., 2015
185	TA	GeJk13	A	401	2,92	36,63	2686	2622	2751	Wright et al., 2015
186	TA	GeJi11	A	454	2,91	36,05	7145	5320	8971	Wright et al., 2015
187	TA	GeJi9	A	442	2,92	36,05	4951	4870	5033	Wright et al., 2015
188	TA		A	419	5,34	36,07	10000	9415	11211	Wright et al., 2015
189	C	Maikona	M	375	2,93	37,630	12969	12752	13185	Nyamweru and Bowman, 1989
190	C	Kalacha	M	381	3,131	37,421	12406	12053	12758	Nyamweru and Bowman, 1989
191	C	Laga llama	M	400	3,336	37,037	10877	10581	11172	Nyamweru and Bowman, 1989
192	C	Olturot	M	541	2,585	37,087	12309	11940	12678	Nyamweru and Bowman, 1989

650

Appendix P4 – A multi-isotope and modelling approach for constraining hydroconnectivity in the East African Rift System, southern Ethiopia

A multi-isotope and modelling approach for constraining hydro-connectivity in the East African Rift System, southern Ethiopia

M. Markowska [a, b, *], A.N. Martin [c], H.B. Vonhof [b], D. Guinoiseau [b, d], M.L. Fischer [a, e], B. Zinaye [f, h], S.J.G. Galer [b], A. Asrat [g, h], A. Junginger [a, e]

[a] University of Tübingen, Department of Geosciences, Tübingen, Germany
[b] Max Planck Institute for Chemistry, Climate Geochemistry Department, Mainz, Germany
[c] Leibniz University Hannover, Institute of Mineralogy, Hannover, 30167, Germany
[d] UMR 8148 GEOPS, Université Paris-Saclay − CNRS, 91405, Cedex, France
[e] Senckenberg Centre for Human Evolution and Paleoenvironment (S-HEP), Tübingen, Germany
[f] University of Cologne, Department of Geosciences, Cologne, Germany
[g] Department of Mining and Geological Engineering, Botswana International University of Science and Technology, Palapye, Botswana
[h] Addis Ababa University, School of Earth Sciences, Addis Ababa, Ethiopia

ARTICLE INFO

ABSTRACT

During the last African Humid Period (AHP; 15−5 ka), many lakes in the East African Rift System (EARS) experienced pronounced lake-level variations that dramatically transformed the hydrological landscape. Currently dry, saline or marshy-wetland terminal lakes became vast waterbodies, interconnected via overflow sills resulting in the formation of a several thousand-kilometre-long chain of lakes in the EARS. A quantitative, process-based understanding of these hydrological systems can advance our interpretation of past hydroclimate variability from proxy records. Here, we provide a critical modern hydrological dataset for the data-sparse Lake Chew Bahir basin in southern Ethiopia. Driven by modern data, an isotope-enabled hydro-balance model was developed to assess how increases in rainfall modulate $\delta^{18}O$ and $^{87}Sr/^{86}Sr$ variability. Considering a terminal Lake Chew Bahir scenario, humid conditions resulted in higher lake $\delta^{18}O$ (~+14‰) due to increased evaporation and longer water residence times. At the same time $^{87}Sr/^{86}Sr$ decreased from 0.7064 to 0.7061 due to an increased riverine Sr flux characterised by lower, unradiogenic $^{87}Sr/^{86}Sr$ ratios. In a modelling scenario where Lake Chew Bahir became a flow-through system with interconnectivity between lakes Abaya, Chamo, Chew Bahir and Turkana, higher lake $\delta^{18}O$ (~+12‰) relative to present was found, but $\delta^{18}O$ was lower than in the terminal lake scenario. The lake water $^{87}Sr/^{86}Sr$ ratios (<0.7061) were also slightly lower. A moderate concomitant change in rainfall input $\delta^{18}O$ of −1‰ in step with hydrological reorganisation resulted in the lowest lake $\delta^{18}O$ (~+5‰). Modelled $\delta^{18}O$ values were similar to the $\delta^{18}O$ range of endogenic carbonates from sedimentary cores from Lake Chew Bahir at the onset of the AHP, supporting the validity of our model, and suggesting that evaporation and the lake water residence time strongly influence lake water $\delta^{18}O$. However, the reported $^{87}Sr/^{86}Sr$ of fossil carbonates from Lake Chew Bahir during the AHP (0.7065 −0.7060) could not be reproduced by our modelled scenarios without adjusting the surface-water-to-groundwater ratio, highlighting the potential role of groundwater as a water source in semi-arid regions. These results demonstrate the insights that can be gained from applying a process-based approach using O and Sr isotope hydro-balance modelling to aid interpretation of past hydro-balance and lake interconnectivity from lacustrine sedimentary records.

© 2022 Elsevier Ltd. All rights reserved.

1. Introduction

The East African Rift System (EARS) contains 80+ lake systems (Schagerl and Renaut, 2016), many of which fill, overflow and become hydrologically connected during wet periods, for instance,

* Corresponding author. Max Planck Institute for Chemistry, Climate Geochemistry Department, Mainz, Germany.
  E-mail address: monika.markowska@mpic.de (M. Markowska).

during the most recent pluvial episode, the African Humid Period (AHP) (Beck et al., 2019; Forman et al., 2014; Junginger and Trauth, 2013; Talbot et al., 2000). Since the AHP, some of these lakes, such as Lake Chew Bahir (LCB) in southern Ethiopia, receded into small endorheic marshes and wetlands (Foerster et al., 2012). A particular feature of the EARS lakes is their sensitivity to climatic variability due to higher precipitation rates on the high-elevation rift margins, coupled with high evaporation rates in the lower-elevation rift floors and have subsequently been termed 'amplifier lakes'(Street-Perrott and Harrison, 1985; Trauth et al., 2010).

Recurring extreme drought and flood conditions are common in the EARS, even on annual timescales. Extreme hydroclimate variability at LCB in southern Ethiopia, however, is not a uniquely recent phenomenon. For instance, rapid shifts from wet to dry conditions were reported in carbonate lake core records from 116 to 66 ka BP, transitioning to a more stable, drier period between 58 and 32 ka BP (Viehberg et al., 2018), which is supported by elemental variations in lacustrine sediments during 45−35 ka BP (Foerster et al., 2012). Variations in potassium (K) abundances in lacustrine sediments from 23 to 5 ka BP, in contrast, broadly followed a precession-forced increase in insolation. The AHP (15-5 ka) was interpreted as much wetter than present day, and punctuated by large changes in K abundances interpreted as rapid oscillations from wet to dry conditions (Foerster et al., 2012). However, it is difficult to use elemental abundances to quantify past changes in lake level, or identify the dominant moisture sources driving hydrological reorganisation.

Strontium (Sr) isotope ratios ($^{87}Sr/^{86}Sr$) of lacustrine carbonates and bioapatite preserved in paleo-shoreline deposits or recovered from sedimentary cores in the EARS may be used to reconstruct provenance of hydrological inputs and assess past changes in regional water balance (Baddouh et al., 2016; Doebbert et al., 2014; Hart et al., 2004; Joordens et al., 2011; Talbot et al., 2000; van der Lubbe et al., 2017). Appreciable amounts of calcium carbonate were precipitated in LCB over the AHP in the form of stromatolites, molluscan shells, and ostracods, as well as bioapatite such as fish bones and teeth. Strontium is present in these carbonates in trace amounts (10−1000 s ppm) and the $^{87}Sr/^{86}Sr$ of lake biota directly record the Sr isotope composition of lake waters (Hart et al., 2004). This is because any mass-dependent Sr isotope fractionation (natural or analytical) is corrected for during radiogenic Sr isotope analyses, physical or chemical isotope fractionation processes in the lake do not influence the $^{87}Sr/^{86}Sr$ ratio measured in lacustrine fossil carbonates. This is particularly useful in EARS catchments which have widely varying $^{87}Sr/^{86}Sr$, ranging from Precambrian metamorphic-granitic and gneissic rocks with more radiogenic $^{87}Sr/^{86}Sr$ to Cenozoic flood basalts with less radiogenic $^{87}Sr/^{86}Sr$ (Table 1).

Quaternary climate reconstructions using $^{87}Sr/^{86}Sr$ in lacustrine carbonate fossils from the adjacent Lake Turkana basin found that lake water $^{87}Sr/^{86}Sr$ during the AHP reflected inflow variability from the Omo River to the north and the Turkwel and Kerio Rivers

to the south (van der Lubbe et al., 2017). On longer timescales (~2.0−1.7 Ma), lake water $^{87}Sr/^{86}Sr$ was suggested to be governed exclusively by changes in surface inflows of the Omo River (Joordens et al., 2011). Both studies emphasised that $^{87}Sr/^{86}Sr$ in Lake Turkana is insensitive to interannual fluctuations and only responds to long-term orbitally-induced forcing. In other regions, $^{87}Sr/^{86}Sr$ has been shown to change with hydrological inflows and used to infer paleo-lake levels. For example, variations of paleo $^{87}Sr/^{86}Sr$ in the Bonneville paleolake system, U.S.A., was directly attributed to changes in lake level and the contribution of the Bear River to the dissolved Sr flux (Hart et al., 2004).

Although carbonate $^{87}Sr/^{86}Sr$ ($^{87}Sr/^{86}Sr_C$) and the oxygen isotope composition ($\delta^{18}O = [^{18}O/^{16}O_{sample}/^{18}O/^{16}O_{VPDB} − 1]$ x 1000)) of carbonate ($\delta^{18}O_C$) from EARS lakes have been successfully used to interpret past changes in climate (e.g. Viehberg et al., 2018; van der Lubbe et al., 2017), robust interpretations are limited by the paucity of the modern data available. This has necessitated key assumptions, including: 1) riverine $^{87}Sr/^{86}Sr$ ($^{87}Sr/^{86}Sr_R$) reflects that of the average lithology of the catchment area, i.e., congruent weathering conditions, 2) lake $^{87}Sr/^{86}Sr$ ($^{87}Sr/^{86}Sr_L$) and $\delta^{18}O$ ($\delta^{18}O_L$) are controlled by temporal changes in surface hydrological inflows, 3) minimal temporal changes in groundwater/surface water interactions with limited subsequent influence on $^{87}Sr/^{86}Sr_L$ and $\delta^{18}O_L$, and 4) no significant variations in lake water residence times. Addressing these uncertainties is critical for accurately interpreting lacustrine $^{87}Sr/^{86}Sr_C$ and $\delta^{18}O_C$ records and may have significant implications for our understanding of past hydrological changes in the EARS.

In this study, we aim to better constrain the controls on $^{87}Sr/^{86}Sr_L$ and $\delta^{18}O_L$ at LCB. Lake Chew Bahir is located some 100 km upstream of Lake Turkana, the world's largest permanent desert lake (Johnson and Malala, 2009). It is analogous to Lake Turkana as it has a similar range of lithological endmembers, and was a large expansive lake during the AHP (Bloszies et al., 2015). In contrast to Lake Turkana, modern LCB is a shallow wetland area with a much smaller maximum extent, and represents a simpler hydrological system with unidirectional overflow in a north-south direction from hydrological connectivity with upper catchments (Lake Chamo and Lake Abaya) during major humid periods. We determine whether the Sr isotope composition of catchment waters reflect the $^{87}Sr/^{86}Sr$ of local lithologies and assess the dominant inflows/outflows in terms of hydrological and Sr budgets. Following this, we combine isotope-enabled mass balance modelling of both $^{87}Sr/^{86}Sr_L$ and $\delta^{18}O_L$ as the two isotope systems together provide independent constraints on the driving mechanisms of hydrological change in lacustrine systems. Unlike Sr, $\delta^{18}O_L$ is controlled by the combination of source water inflows (e.g., rainfall, groundwater and surface water) and catchment-integrated evaporation (Cohen et al., 1997; Dettman et al., 2005; Leng and Marshall, 2004; Vonhof et al., 2013); thus lake $\delta^{18}O_C$ records are often interpreted in terms of water balance (Chamberlain et al., 2013; Doebbert et al., 2014; Leng et al., 1999a, b). We develop an isotope-enabled

Table 1
Mean Sr concentration and$^{87}Sr/^{86}Sr$ of rocks sampled in southern Ethiopia and northern Kenya. Precambrian metamorphic average$^{87}Sr/^{86}Sr$ values here are consistent with the measured bioavailable$^{87}Sr/^{86}Sr$ from catchments dominated by Precambrian lithology (0.72796; Janzen et al., 2020).

Southern Ethiopia				
Period/Eon	**$^{87}Sr/^{86}Sr$**	**Sr**	**n**	**Reference**
Precambrian	0.7271 ± 0.0286	323 ± 275	19	Kebede and Koeberl (2003); Kebede et al. (1999); Asrat and Barbey (2003); Teklay et al. (1998)
Neogene/Paleogene	0.7038 ± 0.0004	565 ± 268	43	Shinjo et al. (2011); Stewart and Rogers (1996); George and Rogers (2002)
Quaternary	0.7028 ± 0.0007	343 ± 378	12	Meshesha et al. (2011); Stewart and Rogers (1996)
Northern Kenya				
Neogene/Paleogene	0.7034 ± 0.0005	547 ± 251	10	Furman et al. (2006)
Quaternary	0.7043 ± 0.0012	352 ± 301	17	Furman et al. (2006); Clement et al. (2003)

hydro-balance model to mechanistically understand $\delta^{18}O_L$ and $^{87}Sr/^{86}Sr_L$ variations in LCB and the resulting lacustrine carbonates. By extending this to the Late Quaternary, we model hydroclimate variability at the onset of the AHP and assess whether catchment hydrological reorganisation can explain the measured range of $^{87}Sr/^{86}Sr$ (0.7065−0.7060; van der Lubbe et al., 2017; Junginger et al., unpublished data) and $\delta^{18}O$ (0.5−11.0‰ VPDB; Viehberg et al., 2018) at LCB during the AHP.

2. Regional setting

2.1. Geology

The LCB catchment is located within the southern Main Ethiopian Rift (MER) northeast of the Turkana Depression, and between the Ethiopian and the East African Plateaus (Fig. 1c,d). The metamorphic Precambrian basement is dominated by gneisses and granitic intrusions of the Mozambique Belt and the meta-volcano-sedimentary complexes of the Arabian-Nubian Shield (Davidson, 1983; Teklay et al., 1998; Asrat et al., 2001; Asrat and Barbey, 2003). Flood basalt volcanism and subordinate trachytic and rhyolitic rocks formed the Ethiopian highlands during the Oligocene, while over the Mid-Miocene to present volcano-tectonic

processes involving bi-modal (basaltic and rhyolitic) volcanism characterize the MER (Bonini et al., 2005). The deeper MER basins are covered by Quaternary sediments.

The average $^{87}Sr/^{86}Sr$ of each surface lithology found in our study catchments (LCB, Lake Chamo, Lake Abaya and Lake Turkana) are summarised in Table 1 and were grouped according to average $^{87}Sr/^{86}Sr$ (Table 2). In LCB, the dominant surface lithologies are Precambrian basement rocks (40%) and Quaternary sediment cover (40%), with lesser proportions of Neogene/Paleogene volcanics (17%) and Quaternary volcanics (2%), with the remaining 1% representing the lake surface. The greatest proportion of exposed Precambrian basement rocks within LCB sub-catchments are in the Segen River and unnamed dry valleys to the west of LCB (hereafter 'dry western valley'), whereas Neogene/Paleogene volcanics dominate the dry eastern valley (55%), as well as the Abaya and Chamo catchments with 43% and 49% coverage, respectively. The Lake Chamo and Lake Abaya catchments have minor contributions from Precambrian metamorphic units in the southeast (6% and 3%, respectively). In comparison, the Lake Turkana catchment is comprised of predominately Paleogene/Neogene volcanic units (52%) with less Precambrian surface cover (20%), which is mainly localised to the Turkwel sub-catchment (68%).
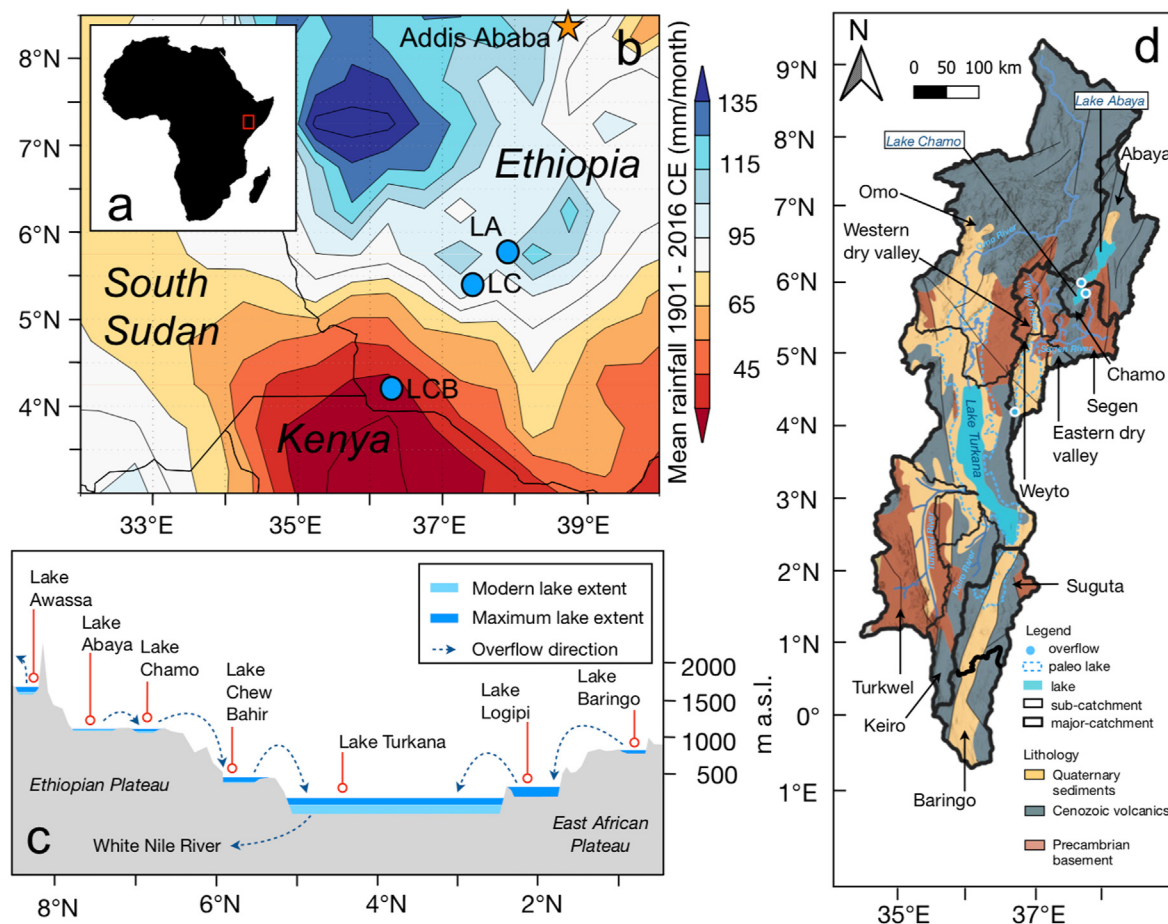
Fig. 1. Panel a: Map of continental Africa where the red box denotes the study region. Panel b: Mean monthly rainfall over the period 1901−2016 CE using the CRU TS 4.01 (land) 0.5° high-resolution grids of monthly climate precipitation observations dataset and compiled in KNMI Climate Explorer (https://climexp.knmi.nl/start.cgi), where the blue circles show the locations of LCB, Lake Abaya (LA) and Lake Chamo (LC), and the yellow star denotes the Ethiopian capital city Addis Ababa. Panel c: Cross section along the East African Rift System from NE to SW, indicating lake level changes in the African Humid Period relative to today following Junginger and Trauth (2013). Panel d: Simplified geological map of southern Ethiopian and northern Kenyan catchments. Catchment shapefiles were used to extract the percentage of rock types in the northern Kenyan catchments from the 1:10M-scale geological map of Africa (Thieblemont, 2016) and for southern Ethiopia using the SEAMIC GSE EN Geology 1:2 million scale Geology Map of Ethiopia. (For interpretation of the references to colour in this figure legend, the reader is referred to the Web version of this article.)

Table 2
Surface lithology of the Lake Chew Bahir (LCB), Lake Chamo (LC), Lake Abaya (LA), and Lake Turkana (LT) catchments (also see Fig. 5a). The percentage of exposed rock types in a given catchment was calculated using the SEAMIC GSE EN Geology 1:2 million scale Geology Map of Ethiopia for the catchments located in Ethiopia and the 1:10M-scale geological map of Africa for the northern Kenyan catchments (Thieblemont, 2016). The catchment lithology for the 'within catchment' samples was calculated by using the surface cover for the area upstream of the riverine sample points measured excluding CB18W08, which is not connected to a major tributary. The geological fractional mixing model shows the estimated lake and river water ^{87}Sr/^{86}Sr, and also incorporates the k flux (individual k fluxes for each catchment and given lithology). Lake areas were assumed to be Quaternary sediments. The lithological end-members Sr concentration and ^{87}Sr/^{86}Sr values used are given in in Table 1.

Major catchment	LCB											LC	LA	LT			
Sub-catchment	Weyto River			Segen River					Eastern dry valley	Western dry valley	Entire catchment	Entire catchment	Entire catchment	Keiro River	Turkwel River	Omo River	Entire catchment
within-catchment		CB18W4	CB18W11		CB18W1	CB18W12	CB18W3	CB18W16									
Precambrian Gneissic-granitic	39%	40%	40%	53%	51%	53%	100%	38%	7%	64%	40%	6%	3%	21%	68%	13%	20%
Paleogene/Neogene volcanics	17%	18%	18%	27%	27%	27%	0%	26%	55%	0%	17%	49%	43%	68%	4%	71%	52%
Paleogene/Neogene sedimentary	0%	0%	0%	0%	0%	0%	0%	0%	0%	0%	0%	0%	0%	0%	0%	1%	1%
Quaternary volcanics	0%	0%	0%	6%	7%	15%	0%	17%	0%	0%	2%	0%	32%	0%	0%	0%	1%
Quaternary sediments	44%	42%	42%	15%	15%	6%	0%	19%	39%	36%	40%	27%	15%	12%	28%	16%	21%
Lake	0%	0%	0%	0%	0%	0%	0%	0%	0%	0%	1%	18%	7%	0%	0%	0%	5%
Geological mixing model																	
Measured ^{87}Sr/^{86}Sr	0.7061	0.7062	0.7064	0.7056	0.7055	0.7055	0.7045	0.7070	n/a	n/a	0.7064	0.7048	0.7062	[a]0.7054	[a]0.7083	[a]0.7051	[a]0.7051
Estimated ^{87}Sr/^{86}Sr	0.7065	0.7064	0.7064	0.7062	0.7061	0.7061	0.7271	0.7055	n/a	n/a	0.7065	0.7040	0.7039	0.7039	0.7140	0.7041	0.7040
Geological mixing model + weathering flux (k)																	
Estimated ^{87}Sr/^{86}Sr	0.7061	0.7062	0.7061	0.7056	0.7055	0.7055	0.7271	0.7070	n/a	n/a	0.7064	0.7048	0.7062	0.7054	0.7083	0.7051	0.7051
Precambrian k	1	1	1	1	1	1	1	1	n/a	n/a	1	1	1	1	1	1	1
Paleogene/Neogene k	1.2	1.0	1.1	1.2	1.3	1.3	0.0	0.5	n/a	n/a	1.0	0.2	0.0	0.2	3.9	0.2	0.3
Quaternary sediments k	1.1	1.0	1.1	1.2	1.3	1.3	0.0	0.5	n/a	n/a	1.0	0.4	0.8	0.7	4.3	0.2	0.3
Quaternary volcanics k	1.1	1.0	1.1	1.2	1.3	1.3	0.0	0.4	n/a	n/a	1.0	0.2	0.0	0.7	3.9	0.2	0.3

[a] Data from van der Lubbe et al. (2017).

2.2. Climate

The Koppen climate classification for the southern extent of the LCB catchment is hot semi-arid (Precipitation < Evaporation). The central-northern LCB catchment, Lake Chamo and Lake Abaya are all tropical savannah with higher rainfall, but with severe dry seasons and frequent droughts. The LCB catchment has two rainy seasons: a longer season from March to May and a shorter season from October to November, with ~500 mm a^{-1} (Fig. 1b). The highlands northwest of LCB, including the Lake Abaya and Lake Chamo catchments, experience significantly higher (ca. >1000 mm a^{-1}; Fig. 1b) and unimodal rainfall spanning March to November (Segele and Lamb, 2005; Williams and Funk, 2011).

2.3. Hydrology

Lake Chew Bahir (498 m a.s.l.) is an ephemeral wetland at its northerly extent (Fig. 1c), which intermittently fills in a southerly direction during the wet seasons (Fig. 1d) with a maximum lake surface area of 2486 km^2 (Fischer et al., 2020). The LCB basin overflows southwards to Lake Turkana in northern Kenya when the overflow sill at 543 m a.s.l. is surpassed (overflow sill elevations, lake water surface areas and locations are given in Table 3). The volume of LCB in recorded history has fluctuated from complete desiccation to a 2000 km^2 lake in 1960 CE (Golubtsov and Habteselassie, 2010), with a reported depth of 8 m in the late 19th century (Grove et al., 1975). It is perennially fed by the Weyto and Segen Rivers (Fig. 2), which drain the north-western and north-eastern sides of the catchment, respectively. The Weyto River is the main surface inflow with an average flow rate of 72 m^3/s (2.27 km^3/a), approximately thrice that of the Segen (Supplementary Table 1) (JICA, 2012). The tectonic basin is bound by the Teltele-Konso Plateau and the Hammar Range to the east and west, respectively. Lake Chamo (1109 m a.s.l.) and Lake Abaya (1176 m a.s.l.) lie to the northeast of LCB (Fig. 1b), whereby Lake Abaya is occasionally connected to Lake Chamo via an overflow sill at 1194 m a.s.l. during high rainfall periods; however, this occurs infrequently under the modern climatic regime where lake levels only fluctuate by 0−1 m (Belete et al., 2015). The smaller Lake Chamo is connected to LCB catchment via an overflow sill at 1123 m a.s.l. via the Segen River when precipitation exceeds the long-term average (Belete et al., 2015).

Groundwater flow in the LCB basin generally follows the surface topography along a north-south gradient towards Lake Turkana (JICA, 2012). Recharge typically occurs on the elevated rift margins which receive more rainfall (Bretzler et al., 2011). The three main aquifer types in the basin relate to the three geological units: 1) granitic-gneissic basement rocks, 2) volcanic rocks and 3) unconsolidated Quaternary sediments. Crystalline basement rock aquifers, such as those in the Hammar Range, receive localised recharge associated with fracture and intergranular permeability and have low storage potential (Kebede et al., 2013). The volcanic aquifers are extensive and contain fracture permeability leading to localised

recharge with low storage potential and hydraulic conductivity. The unconsolidated sedimentary aquifers are located on the low elevation rift floor and are tectonically defined by the marginal/alluvial graben structures (Kebede et al., 2010a, b).

Previous hydrogeological investigations have mainly focused on the central MER, with data availability in the southern MER limited to commercial reports (e.g., JICA, 2012; Halcrow et al., 2008). Due to the low porosity and storage potential of LCB basin aquifers, most of the groundwater potential is localised in shallow wadi bed sediments that overlay the basement rocks. Recharge typically occurs through wadi sediments which is enhanced during flooding events, commonly allowing localised recharge 'pulses' to occur. Groundwater flow typically occurs in the direction of the rift flanks towards the rift floor via stream baseflow (Kebede et al., 2010b) and spring flow is less than 1−5 l/s (JICA, 2012). There is a general increase in the groundwater salinity and chemistry from Ca−Mg HCO$_3$ in the highlands to Na−HCO$_3$−SO$_4$−Cl type in the rift floor, possibly due solute remobilisation from thin evaporite lenses within the lacustrine sediments (Kebede et al., 2010a, b). Groundwater flow between Ethiopia and Kenya is considered to be negligible (JICA, 2012; Kebede et al., 2010a).

3. Methods

3.1. Field procedures

In November 2018, 20 water samples were collected during a field campaign in the LCB, and Lake Chamo and Lake Abaya catchments (Fig. 2). Due to LCB's remote location and difficulty of access, to the best of the authors' knowledge there are hardly any published hydrochemistry, Sr and O isotope data for the LCB catchment to date. Here, we provide the first high-resolution catchment wide study of LCB. The eastern dry catchments and large parts of the south-eastern margins of the LCB basin were inaccessible due to security concerns, but we note that these areas warrant further investigation.

Seven groundwater samples were collected from frequently pumped (all wells were being actively used prior to sampling), driven-point wells (India Mark II wells that are common in rural communities in eastern Africa) at <50 m depth. Water parameters were measured using a HI98194 (Hanna Instruments) multi-meter instrument, including pH, electrical conductivity (EC), total dissolved solids (TDS), temperature and oxidation-reduction potential (ORP). Prior to sampling, the wells were purged until these water parameters stabilised. Five lake samples were collected from LCB (n = 2), Lake Chamo (n = 2) and Lake Abaya (n = 1) as well as seven samples from the Weyto and Segen Rivers and their tributaries and one cold spring (Fig. 2). Total alkalinity concentrations were measured using the endpoint titration method and a Hach digital titrator within 24 h of sampling. Samples for anions and stable water isotopes (δ^{18}O and δ^2H) were immediately filtered through 0.45 μm nylon filters and collected in 60 ml High Density Poly-Ethylene (HDPE) bottles and 5.9 ml exetainer® glass vials (Labco),

Table 3
General characteristics of Lake Chew Bahir (LCB), Lake Chamo (LC) and Lake Abaya (LA). Surface area data from Fischer et al. (2020).

	LCB	LC	LA
Latitude (°N)	4.857−4.766	5.966−5.709	6.589−5.774
Longitude(°E)	36.911−36.888	37.552−37.627	37.616−38.051
Elevation (m a.s.l.)	498	1109	1176
Modern lake surface area (km^2)	~43	310	1081
Maximum lake surface area (km^2)	2486	394	1557
Modern maximum water depth (m)	1−2	13	13
Overflow elevation (m a.s.l.)	543	1123	1194
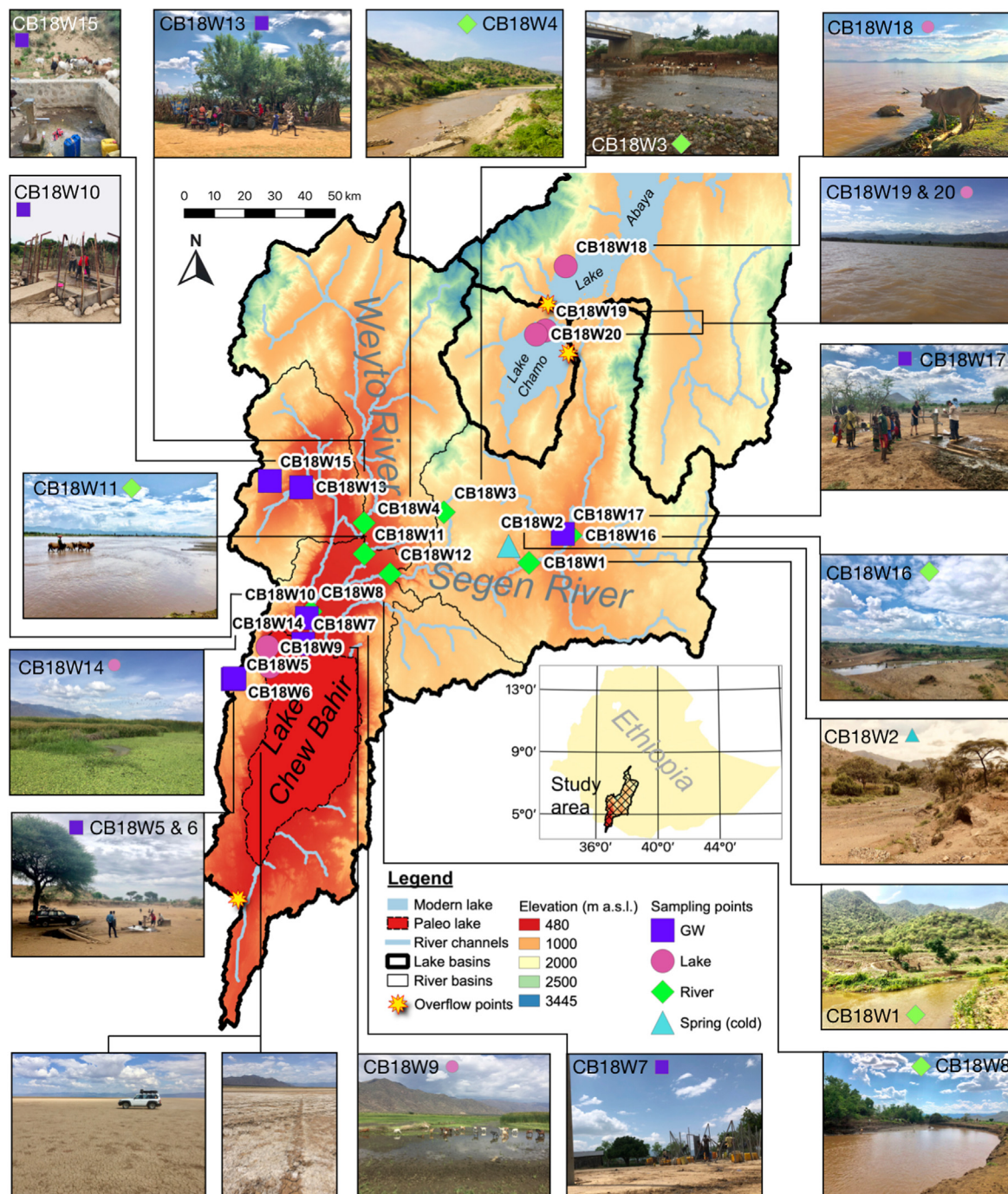
Fig. 2. Digital Elevation Model (DEM) of study site indicating the three major lakes investigated: Lake Abaya, Lake Chamo and Lake Chew Bahir. Sampling locations for groundwater (purple squares), lakes (magenta circles), rivers (green diamonds and springs (blue triangles) are indicated on the map. The paleo extent of Lake Chew Bahir is indicated by a black dashed line. Overflow points are shown as yellow stars at the catchment boundaries (Fischer et al., 2020). (For interpretation of the references to colour in this figure legend, the reader is referred to the Web version of this article.)

respectively, with no further treatment. Cation, $^{87}Sr/^{86}Sr$ and trace element samples were collected in 60 ml acid-cleaned HDPE bottles, and immediately acidified with ~1 ml of Suprapur® (Merck) 65% HNO_3.

3.2. Chemical analysis

Cation and anion concentrations were analysed using ion chromatography compact IC Flex and Compact IC Plus from Metrohm at the University of Tübingen, Germany. The limits of detection were as follows: Na (0.1 ppm), K, Ca, Mg, Cl, PO_4 (0.05 ppm), F (0.005 ppm), SO_4 (0.5 ppm). Water $\delta^{18}O$, δ^2H and $^{87}Sr/^{86}Sr$ were analysed at the Max Planck Institute for Chemistry in Mainz, Germany. $\delta^{18}O$ and δ^2H were measured using a Picarro cavity ring down laser spectrometer and are reported as a per mil (‰) deviation from the international standard VSMOW. The overall precision on analyses were ±0.1‰ $\delta^{18}O$ and ±1.1‰ δ^2H (2σ, n = 15) and calibrated using the VSMOW international standard and two

in-house standards with isotopic compositions of 0.2 and 7.0‰ for δ^{18}O and 1.2 and 45.8‰ for δ^2H, referenced to the international VSMOW-SLAP scale. Strontium concentrations were measured using a Thermo Scientific Element XR high-resolution ICP-MS. To correct for drift during measurements, In was used as an internal standard. Lake water standard TMDA-51.3 was measured repeatedly to ensure measurement accuracy and precision (less than ±10%). For ^{87}Sr/^{86}Sr analyses, Sr was separated from samples using DGA resin (Eichrom), using a prep*FAST*-MC™ system (Elemental Scientific) based on the method from Romaniello et al. (2015). Approximately 100 ng of purified Sr was then loaded onto tungsten filaments with Ta-fluoride activator and ^{87}Sr/^{86}Sr was measured using a ThermoFisher Triton™ Thermal Ionisation Mass Spectrometer. Replicate measurements of international standard NIST SRM-987 run with these samples yielded an average ^{87}Sr/^{86}Sr value of 0.71026 ± 0.00001 (2σ, n = 8). The Sr concentrations of the total procedural blanks were below the limit of detection (<0.3 ppb).

3.3. Coupled δ^{18}O and ^{87}Sr/^{86}Sr mass balance modelling

3.3.1. δ^{18}O model

A δ^{18}O$_L$-enabled mass balance lake model (Gibson et al., 2016) was used to quantify modern lake balance sensitivity and paleo-changes in δ^{18}O lake composition based on well-established previous models (Craig and Gordon, 1965; Gat, 1996; Gibson and Edwards, 2002; Gonfiantini, 1986; Horita et al., 2008; Jones et al., 2016). The change in lake water volume (km^3 a^{-1}) is given as:

$$\frac{dV}{dt} = P + Q_i - E - Q_o \qquad (1)$$

where V is the volume (km^3) at time t (a), P is precipitation volume (km^3 a^{-1}) on the maximum lake surface area per unit time (2486 km^2; Fischer et al., 2020), E is evaporation (km^3 a^{-1}) from the lake surface per unit time, Q_i and Q_o are the total inflows and outflows (km^3 a^{-1}), respectively (Supplementary Table 1), including the sum of all surface and groundwater flows.

The change in δ^{18}O$_L$ (‰) and water volume at time t was calculated by assuming that the lake is well-mixed, given as:

$$\frac{d}{dt}(V\delta_L) = P\delta_P + Q_i\delta_i - E\delta_E - Q_o\delta_L \qquad (2)$$

where δ_P, δ_i, δ_E, and δ_L are the δ^{18}O of precipitation, inflows, evaporation and LCB, respectively. Modern LCB is a shallow (<2 m depth) lake system, with a relatively homogenous hydrochemistry based on our water sampling (see Section 4). The term $Q_i\delta_i$ is defined as:

$$Q_i\delta_i = R_i\delta_{ri} + G_i\delta_{gi} + L_i\delta_{li} \qquad (3)$$

where G_i is the groundwater inflow, R_i is the riverine inflow, L_i is the overflow from Lake Chamo and their isotopic composition are δ_{gi}, δ_{ri} and δ_{li}, respectively. G_i is difficult to estimate due to highly variable flow rates (Mechal et al., 2017) and fluctuating water tables which vary significantly over short distances (Ayenew et al., 2008; Furi et al., 2012; Kebede et al., 2007; Tenalem et al., 2009). Here, a mass balance approach was used to determine groundwater inflow into LCB based on the measured ^{87}Sr/^{86}Sr ratios and concentrations. Given the modern Sr concentrations and ^{87}Sr/^{86}Sr$_L$ of a 0.15 km^3 LCB and using the annual inflow volumes of the Segen and Weyto Rivers and measured Sr concentrations and ^{87}Sr/^{86}Sr$_R$ (Supplementary Table 1), a mass balance approach was used to estimate the missing groundwater flow parameter to give an absolute groundwater inflow (G_i) of ~0.25 km^3 a^{-1}.

The term L_i in Equation. 3 represents the lake overflow from Lake Chamo with isotopic composition of δ_{li}. Lake Chamo overflow into LCB is initiated if P exceeds 2% of modern P, based on previous DEM and overflow lake balance modelling output (Fischer et al., 2020). Lake Chamo overflows at a rate of 10% of the volume of the Segen River at each time step, as the natural overflow of Lake Chamo is via the Segen River.

The term $R_i\delta_{ri}$ in Equation (3) represents the riverine input and is given as:

$$R_i\delta_{ri} = S_i\delta_{si} + W_i\delta_{wi} \qquad (4)$$

where S_i is the inflow from the Segen River, with a mean isotopic composition δ_{si} and W_i is the inflow from the Weyto River with a mean isotopic composition of δ_{wi}. To parameterise flow, the average annual estimates from gauge flow data from the Weyto River (27 years of data, station ID: 083002; JICA, 2012) and Segen River (3 years of data, station ID: 083001; JICA, 2012) were used, which yielded annual inflows of 2.27 and 0.71 km^3 a^{-1}, respectively.

The term $Q_o\delta_L$ in Equation (2) is defined as:

$$Q_o\delta_L = G_o\delta_L + L_o\delta_L \qquad (5)$$

where G_o is the groundwater outflow, calculated as the residual of Equation (1) assuming steady state conditions ($Q_i + P = Q_o + E$), for an estimated modern LCB volume of 0.15 km^3, yielding an annual outflow of 2.84 km^3 a^{-1}. L_o is the surface overflow from LCB to Lake Turkana, calculated as the surplus volume greater than 83.17 km^3 — the maximum extent of LCB (Fischer et al., 2020). The groundwater outflow isotopic composition is equal to the value of LCB water at the previous time step.

The open-water evaporation term, E, was calculated by Fischer et al. (2020) to be 1908 mm using the Penmann-Monteith equation relative to the evaporating surface area of LCB. The surface area was calculated indirectly from DEM model output from Fischer et al. (2020) using an empirical relationship between volume and surface area calculated specifically for LCB and given in Supplementary Figure 1. Based on modern lake surface area of ~0.15 km^3, this gave an initial surface area of ~207 km^2 with a resulting value for E of 0.39 km^3 a^{-1}.

The δ_P of P represents the calculated mean annual isotopic composition of rainfall, calculated for the LCB area using the Online Isotopes in Precipitation Calculator (https://wateriso.utah.edu/waterisotopes/pages/data_access/form.html; see Section 4.1.1). The δ^{18}O of the other inflows were determined from the end-members of samples from the 2018 field campaign, which were taken in between the dry and the rainy seasons (Supplementary Table 1). The most downstream samples (closest to LCB) before the confluence point of the two rivers were used to prescribe δ_{si} and δ_{wi}. Average groundwater δ^{18}O from the seven sampled sites was used for the groundwater end-member (δ_{gi}). The value for δ_{li} (overflow into LCB) is the average of measured Lake Chamo water.

As δ_E is difficult to measure and is typically calculated (Skrzypek et al., 2015) using the Craig and Gordon (1965) evaporation model, given as:

$$\delta_E = \frac{\alpha^+\delta_L - h\delta_A - \varepsilon}{1 - h + 0.001\varepsilon_k} \quad (‰) \qquad (6)$$

where a^+ is the equilibrium isotopic fractionation factor that is dependent on the measured temperature at the evaporating lake surface and is derived from experimental values (Horita and Wesolowski, 1994), given as:

$$\alpha^+\left(^{18}O\right) = \exp\left(-\frac{7.685}{10^3} + \frac{6.7123}{273.15 + T} - \frac{1666.4}{(273.15 + T)^2} + \frac{350410}{(273.15 + T)^3}\right) \tag{7}$$

where T is the temperature of the lake surface (30.5 °C). Sensitivity analyses considering the effect of a ± 10 °C change on the resultant $\delta^{18}O_L$ are shown in Section 5.3. The term h is the relative humidity corrected for the saturation vapour pressure (Supplementary Table 1), εk is the kinetic fractionation factor defined as 14.2(1- h) (Gonfiantini, 1986) and δA is the isotopic value of the air vapour over the lake assuming atmospheric moisture is at equilibrium with P given by:

$$\delta_A = (\delta_P - \varepsilon^+)\big/\left(1 + 10^{-3} \cdot \varepsilon^+\right) \quad (\text{‰}) \tag{8}$$

where $\varepsilon^+ = 1000(1-\alpha^+)$ (Gibson et al., 2016).

To solve for δ_L, Equation (6) is substituted into Equation (2) (i.e. Equation (4) in Gibson et al., 2016). Under constant hydrological steady state conditions (dV/dt = 0), Equation (2) can be simplified and integrated with respect to time, assuming constant values for $\delta_I, \delta_A, \varepsilon^+, \varepsilon^k, h, I, Q$ and E to yield Equation (9), an expression for δ_L at time t, on a yearly timestep. Here, the dimensionless term x is used to express the water lost to evaporation as a ratio of E/(P + Q_i), and m is used to describe the temporal enrichment slope (from evaporation).

$$\delta_L(t) = \delta_s - (\delta_s - \delta_o)\exp\left[-(1 + mx)\left(\frac{(P + Q_i t)}{V}\right)\right] \quad (\text{‰}) \tag{9}$$

where δ_o is the composition $\delta_L(t-1)$ of the previous time step. Here m and x are dimensionless and defined as:

$$m = \frac{\left(h - 10^{-3}\left(^\varepsilon k + \frac{\varepsilon^+}{\alpha^+}\right)\right)}{\left(1 - h + 10^{-3 *\varepsilon} k\right)} \quad (\text{dimensionless}) \tag{10}$$

and:

$$x = (\delta_s - (\delta_i + \delta_P) / (m(\delta^* - \delta_s)) \quad (\text{dimensionless}) \tag{11}$$

where δ^* is the limiting isotopic composition that a desiccating lake would approach under non steady state conditions as it recedes (V approaches 0). This is given as:

$$\delta^* = \frac{\left(\frac{h\delta_A + \varepsilon_K + \varepsilon^+}{a^+}\right)}{\left(h - 10^{-3} \times \left(\frac{+\varepsilon_K + \varepsilon^+}{a^+}\right)\right)} \quad (\text{‰}) \tag{12}$$

where δ_s is the steady state isotopic composition of the lake given by Gonfiantini (1986) and Gat (1996) as t approaches ∞, where δ_0 is the initial isotopic composition of the lake at t_0 and δ_i is the total

isotopic composition of inflows.

$$\delta_s = (xm\delta^* + (\delta_i + \delta_P) / (1 + mx) \quad (\text{‰}) \tag{13}$$

3.3.2. Sr model

To estimate the sensitivity of LCB to temporal changes in Sr fluxes from sub-catchments and overflow from adjacent basins, we used a Sr model from Hart et al. (2004) combined with our O isotope model. The simple mass balance model is given by:

$$^{87}\text{Sr}/^{86}\text{Sr}_{lake} = f_{Sr\ Weyto}\left(^{87}\text{Sr}\big/^{86}\text{Sr}_{Sr\ Weyto}\right) + f_{Sr\ Segen}\left(^{87}\text{Sr}\big/^{86}\text{Sr}_{Sr\ Segen}\right) + f_{Sr\ groundwater}\left(^{87}\text{Sr}\big/^{86}\text{Sr}_{Sr\ groundwater}\right)$$
$$+ f_{Sr\ Lake\ Chamo}\left(^{87}\text{Sr}\big/^{86}\text{Sr}_{Sr\ Lake\ Chamo}\right) + f_{Sr\ P}\left(^{87}\text{Sr}\big/^{86}\text{Sr}_{Sr\ P}\right) \tag{14}$$

where f is the fraction of Sr from each major Sr flux (Supplementary Table 1). Average $^{87}\text{Sr}/^{86}\text{Sr}$ values from the water sampling campaign were used for the riverine, lake and groundwater end-members. Sample CB18W8 was excluded as it was a small tributary of the Weyto River, and we could not confirm its flow routing connectivity to the greater Weyto River. The Sr contribution from rainfall (f_{SrP}) to lake water is typically low and was not considered significant due to the inland location (~1000 km from Indian Ocean) of LCB.

3.3.3. Model parameters

Using the initial conditions given in Supplementary Table 1, the model was run with a 1000-year spin-up time to reach steady state conditions for an estimated modern LCB volume of 0.15 km^3, with average modern lake water values for $\delta^{18}O_L$ = +3.8‰ and $^{87}\text{Sr}/^{86}\text{Sr}_L$ = 0.7064 (see sections 4.1.3 and 4.3.2). This initialised the model until the system was equilibrated with respect to flow terms, under steady state conditions (Q_i + P = Q_o + E). The adjustment to the initial flow terms directly resulting from the spin up is shown in Supplementary Table 1.

To assess how $\delta^{18}O_L$ and $^{87}\text{Sr}/^{86}\text{Sr}_L$ respond to regional climate change and hydrological reorganisation, three scenarios were considered with varying degrees of catchment connectivity: 1) Closed terminal LCB, 2) Semi-open terminal LCB (parameter L_i; overflow from Lake Chamo activated), and 3) Open flow-through LCB (parameter L_o; LCB overflow to Lake Turkana activated; Table 4). In Scenario 3, full lake connectivity is assumed whereby Lake Abaya, Lake Chamo, LCB and Lake Turkana form a cascading lake system. Evidence for past overflow in the form of paleo-channels in the landscape is visible from satellite imagery. A step-wise increase in P of 25%, incrementally over a 1000-year period was considered in all scenarios to simulate conditions at the onset of the AHP, in line with modelled estimates from Fischer et al. (2020). A 25% increase in P is similar to previous estimates of increased rainfall during the AHP in other EARS lakes, such as

Table 4
Modelling lake scenarios for increased rainfall during the African Humid Period.

Scenario	Inflow from LC	Outflow to LT	ΔP (%)	ΔQ_{rivers} (%)
1: Closed terminal LCB	N	N	+25	+150
2: Open terminal LCB	Y	N	+25	+150
3: Open flow-through LCB	Y	Y	+25	+300

paleo-Lake Suguta in Kenya (Borchardt and Trauth, 2012; Garcin et al., 2009; Junginger et al., 2014; Junginger and Trauth, 2013), and estimates across south-eastern equatorial Africa (20%) (Otto-Bliesner et al., 2014). In Scenarios 1 and 2, LCB reached 25% of its maximum volume (~20 km^3) as the inflows of the Segen River (S_i) and the Weyto River (W_i) increased by 150% relative to modern day. In Scenario 3, where LCB overflows into Lake Turkana, S_i and W_i were increased by 300% relative to modern day (Table 4).

Our model was run with an annual resolution for a period of 1000 years, followed by 1000 years of steady-state conditions. This timescale was chosen to reflect the abrupt onset of the changes to hydroclimate observed in the AHP (Beck et al., 2019; Junginger and Trauth, 2013; Tierney and deMenocal, 2013; Trauth et al., 2018). A detailed description of prescribed inflow and outflow fluxes are provided in Section 3.3.1 and initial conditions are given in Supplementary Table 1.

4. Results

4.1. Stable isotopes $\delta^{18}O$ and δ^2H

4.1.1. Rainfall

The rainfall stable isotope ($\delta^{18}O_P$ and δ^2H_P) data from all Ethiopian stations in the Global Network of Isotopes in Precipitation (GNIP; https://www.iaea.org/services/networks/gnip) were compiled. Addis Ababa is the only continuously-monitored GNIP station in Ethiopia (1961−2016 CE) at ~2400 m a.s.l., with high weighted mean $\delta^{18}O_P$ and δ^2H_P values of −1.3 ± 0.8‰ and +3.3 ± 5.7‰, respectively (Fig. 3a). There are no rainfall isotope data for the lower elevation LCB area (~500 m a.s.l), therefore, theoretical values for $\delta^{18}O_P$ (+1.6‰) and δ^2H_P (+24.0‰) were sourced from https://wateriso.utah.edu/waterisotopes/pages/data_access/form.html (Fig. 3a), and calculated over the lower elevation LCB site, which falls on the Local Meteoric and Global Meteoric Water Lines (Fig. 3a). The calculated mean rainfall value is offset in $\delta^{18}O$ from Addis Ababa rainfall (~2300 m asl) by ca. +2.8‰. This is consistent with a decrease in $\delta^{18}O_P$ with increasing elevation at a rate of ~ -0.1-0.2‰/100 m, which, given the elevation difference between the sites (~1800 m), results in a +1.8 to +3.6‰ offset. River $\delta^{18}O_R$ (section 4.1.2) were slightly lower than the calculated mean $\delta^{18}O_P$ for LCB as most river headwaters are found on the higher elevation rift flanks, therefore, it would be more appropriate to compare these to Addis Ababa weighted mean rainfall.

4.1.2. Surface and sub-surface waters

The Weyto and Segen Rivers had mean $\delta^{18}O_R$ values of 0.2‰ and −0.7‰ and δ^2H_R values of 4.6‰ and 8.1‰, respectively. The $\delta^{18}O_R$ values were offset from weighted mean rainfall by +0.5 to +1.5‰ and $\delta^{18}O_R$ values increased downstream (Fig. 3b). These stable isotope values are similar to previously published data for MER rivers (Ayenew et al., 2008; Bretzler et al., 2011; Cockerton et al., 2013; Demlie et al., 2007a; Levin et al., 2009) and fall on a Local Evaporation Line with a slope of 4.50 and an intercept of 7.51 (Fig. 3b). Generally, MER river water $\delta^{18}O_R$ largely falls on the Local Evaporation Line and are offset from weighted mean rainfall by +1.0 to +2.0‰ (Fig. 3c) with a low d-excess, consistent with our

results. This is likely due to an enrichment in ^{18}O caused by evaporation, which is typical of arid areas (Levin et al., 2009). In contrast, average groundwater $\delta^{18}O$ ($\delta^{18}O_G$) from the LCB catchment was lower (−2.0‰, ±0.9‰) than weighed mean rainfall. The upper Hammar Range group on the rift margins had the lowest $\delta^{18}O_G$ values (−2.5‰), whereas groundwaters sampled from the rift floor group (−1.4‰) and upper mixed group were higher (−1.2‰) (Fig. 3d), and closer to weighted mean rainfall. This is consistent with previously measurements of MER groundwaters, which generally exhibited lower mean $\delta^{18}O_G$ values on the rift margins (−2.5‰) and higher values in the low elevation rift area (−1.2‰; Mechal et al., 2016, Fig. 3d). The groundwater isotope composition across Ethiopia is typically biased towards the wet season precipitation values, where high-intensity storms are an important recharge source (Bedaso and Wu, 2021).

4.1.3. Lakes

The average $\delta^{18}O_L$ values of LCB, Lake Chamo and Lake Abaya were +3.8‰, +5.4‰ and +5.6‰, respectively (Fig. 3e). The higher $\delta^{18}O_L$ of lakes Chamo and Abaya suggest higher evaporative conditions in these large, permanent lakes compared to LCB which is ephemeral. MER $\delta^{18}O_L$ is typically offset compared to weighted mean rainfall (Fig. 3c) by approximately +10‰, due to evaporative isotopic enrichment of lake waters. The evaporative enrichment of lakes Abaya, Chamo and LCB appear slightly lower than the MER average with offsets between ~+3.0 and +6.0‰.

4.2. Major anions and cations

The hydrochemical characteristics of surface and groundwaters in the LCB basin are summarised here and all data are provided in Supplementary Table 2 and Fig. 4. The major inflows to LCB, the Segen and Weyto Rivers, are characterised by waters with a narrow pH range (7.98−8.74), low EC (<498 μS/cm), low TDS (<249 mg/l) and low total alkalinity (<178 mg/l). River waters have no dominant cation, and anions are dominated by HCO_3^-. Low TDS, NO_3 (<1 mg/l) and PO_4 (<0.1 mg/l) (Supplementary Table 2), coupled with a lack of large-scale agriculture or industry suggest minimal anthropogenic input. LCB had higher concentrations of dissolved solids compared to riverine inputs (EC:750−780 μS/cm and TDS: 375−390 ppm; Supplementary Table 2), but exhibited lower EC and TDS than Lake Abaya and Lake Chamo (1044−1611 μS/cm and 522−806 ppm, respectively; Supplementary Table 2). The pH (7.99−7.49) and total alkalinity (306−339 mg/l) were also lower in LCB compared to the other lakes. LCB waters had no dominant cation, but HCO_3^- was the dominant anion, similar to riverine waters (Supplementary Table 2). Lake Abaya and Chamo displayed more characteristic 'soda lake' hydrochemistry as cations and anions were dominated by Na/K and HCO_3^-, respectively (Fig. 4).

Groundwaters typically had lower pH values (<7.62, Supplementary Table 2) compared to surface waters, but higher EC (1090−4194 μS/cm) and TDS values (523−2097 ppm) up to an order of magnitude greater than surface waters. Group 1 groundwaters from the Upper Hammar Range rift margins of the LCB basin (CB18W5, CB18W6, CB18W13 and CB18W15; Fig. 2) cluster together in terms of hydrochemistry, but do not have a dominant
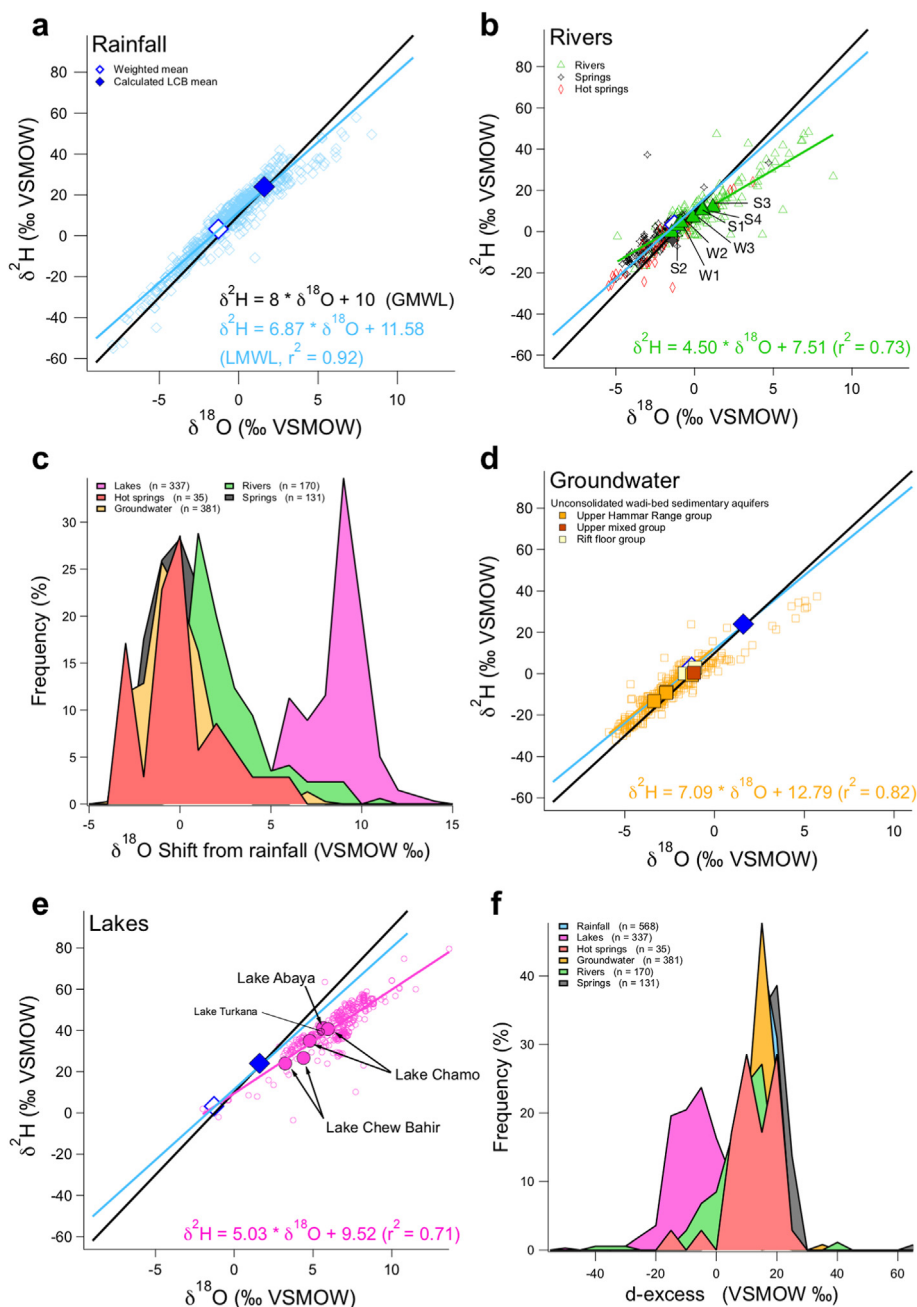
Fig. 3. Compilation of water stable isotope data for Ethiopia (Ayenew et al., 2008; Bretzler et al., 2011; Cockerton et al., 2013; Darling et al., 1996; Demlie et al., 2007a; Demlie et al., 2007b; Fontes et al., 1970; Furi et al., 2012; Gizaw, 2002; Gonfiantini et al., 1973; IAEA, 2019; Kebede, 2004; Kebede et al., 2005; Kebede et al., 2009; Kebede et al., 2010b; Kebede, 2001; Levin et al., 2009; McKenzie et al., 2001; Mechal et al., 2017; Odada, 2001; Schoell et al., 1976; Tekleab et al., 2014; Yitbarek et al., 2012) and the data collected in this study. Panel a: Scatterplot of δ^2H and $\delta^{18}O$ of rainfall from various sites in Ethiopia including Addis Ababa (n = 362), Addis Ababa West (n = 2), Adu Bariye (n = 5), Alemeya (n = 13), Asela (n = 7), Awassa (n = 19), Butajira (n = 2), Combolcha (n = 7), Dessie (n = 8), Diredawa (n = 12), Hagere Selam (n = 17), Harar (n = 6), Hidolola (n = 4), Kobo (n = 7), Kofele (n = 15), Mega (n = 4), Moyale (n = 4), Neghelle (n = 3), Silte (n = 2), Soddo (n = 16), Woldiya (n = 7), Weledi (n = 8), Yavello (n = 3) and Ziway (n = 3) as well as the Global Meteoric Water Line (GMWL) and the calculated Local Meteoric Water Line (LMWL). Calculated mean rainfall value for Lake Chew Bahir was derived from https://wateriso.utah.edu/waterisotopes/pages/data_access/form.html. Panel b: Scatterplot of δ^2H and $\delta^{18}O$ of rivers (open green triangles), hot springs (open red diamonds) and springs (open grey square diamonds) and samples from this study in the Chew Bahir catchment (filled triangles). Panel c: Plot of frequency (%) and $\delta^{18}O$ shift from weighted mean rainfall from the Addis Ababa station. Panel d: Scatterplot of δ^2H and $\delta^{18}O$ of groundwater from Ethiopia (open squares) and groundwater wells from the Chew Bahir catchment (filled squares). Panel e: Scatterplot of δ^2H and $\delta^{18}O$ of lakes in the MER, Ethiopia (open circles) and samples from this study (filled circles). Panel f: Plot of frequency (%) and d-excess using the equation d-excess = $\delta^2H - 8*\delta^{18}O$. (For interpretation of the references to colour in this figure legend, the reader is referred to the Web version of this article.)

cation or anion (Fig. 4). Group 2 (Upper mixed) (CB18W17) and Group 3 (rift floor samples) (CB18W7 and CB18W10) groundwaters could be grouped together, as cations were dominated in Na/K, similar to Lake Abaya and Lake Chamo. Anions were dominated by SO_4^{2-} and Cl^- (Fig. 4).

4.3. Sr isotope geochemistry

4.3.1. Riverine and subsurface waters

Riverine Sr concentrations (<349 ppb) were lower than those of groundwaters (400−1285 ppb; Table S2, Fig. 5). Riverine $^{87}Sr/^{86}Sr_R$
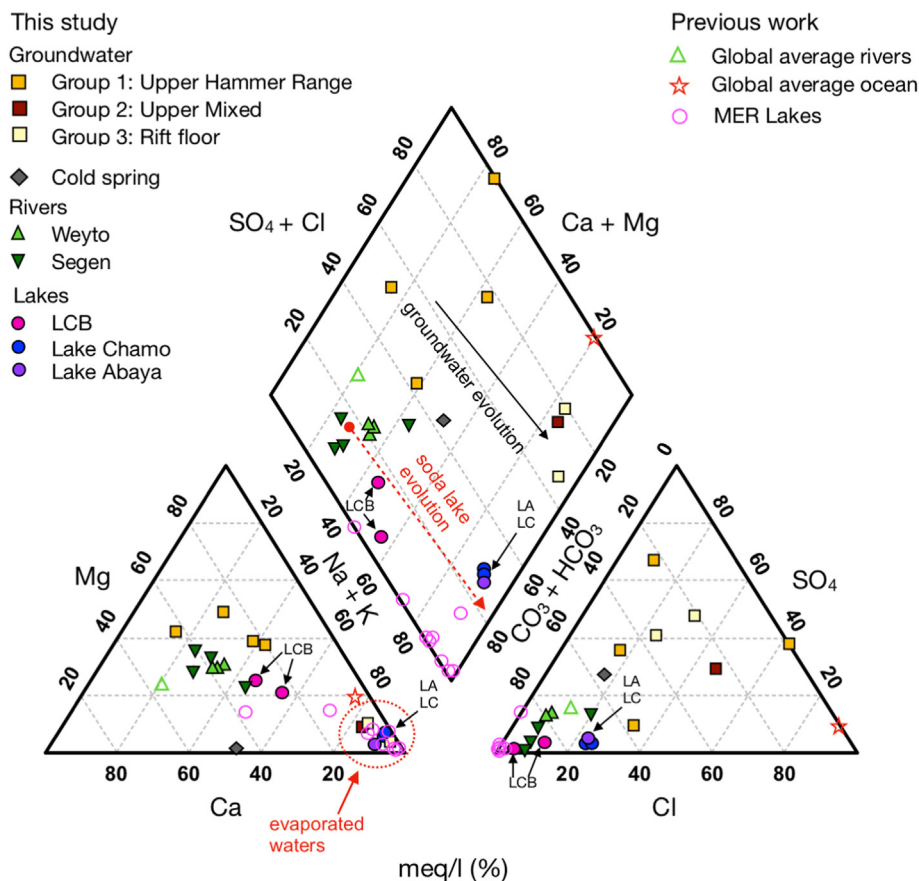
Fig. 4. Groundwater and surface water hydrochemistry of the Chew Bahir catchment as well as Lake Abaya (LA) and Lake Chamo (LC) expressed in meq/L (%). Global average rivers (Lowenstein and Risacher, 2009), global average ocean (Lowenstein and Risacher, 2009) and MER Lake hydro-chemistry (Kebede et al., 1994) are also indicated. When Fl or CO_3 data were unavailable it was assumed their input was negligible as Cl and HCO_3 were the dominant anions.

were generally low (relative to the modern seawater value of ~0.7091; Spooner, 1976) and characteristic of waters draining young and non-radiogenic volcanic rocks (Fig. 5). The range of $^{87}Sr/^{86}Sr_R$ in the Segen River was lower (0.7045−0.7070) than the Weyto (0.7061−0.7082). This trend is also reflected in the most evolved downstream waters of the main river channel just before the Segen and Weyto Rivers confluence, where the Weyto River $^{87}Sr/^{86}Sr_R$ was more radiogenic (0.7061) than the Segen River (0.7055). This is despite the Segen River catchment having a greater proportion of Precambrian basement rocks with more radiogenic $^{87}Sr/^{86}Sr$ (Table 2).

Groundwaters had the most radiogenic $^{87}Sr/^{86}Sr_G$ signatures in this study, but were spatially variable. Group 1 exhibited the highest $^{87}Sr/^{86}Sr_G$ with a range of 0.7080−0.7104 (Table S2, Fig. 5). In contrast, Group 2 had a lower $^{87}Sr/^{86}Sr_G$ range (0.7042−0.7045), including a cold spring sample (0.7045). The low elevation rift floor groundwaters of Group 3 had the lowest Sr concentrations, whereas their $^{87}Sr/^{86}Sr_G$ values (0.7064) were in between the ranges of Group 1 and Group 2, and CB18W7 was similar to Weyto River waters.

4.3.2. Lakes

Lakes Abaya and Chamo (Fig. 5) had low Sr concentrations (<140 ppb), similar to riverine waters in the LCB catchment, compared to LCB (~390 ppb). The average $^{87}Sr/^{86}Sr_L$ of lakes Chew Bahir, Chamo and Abaya were 0.7064, 0.7047 and 0.7062, respectively (Fig. 5). LCB had the most radiogenic Sr lake waters, which were very similar to Group 3 groundwaters.

5. Discussion

5.1. LCB catchment dynamics

The dominant control on riverine trace element hydrochemistry is water-rock interactions from silicate weathering (Fig. 6). Low Cl/Sr ratios relative to the marine value show enrichment in Sr with respect to Cl (Fig. 7c). Further, the Na/Cl molar ratio is greater than unity for all riverine samples, suggesting an Na excess relative to Cl (Fig. 7b). Waters with Na/Cl molar ratios above unity may reflect enhanced silicate weathering due to the dissolution of feldspar minerals by carbonic acid releasing HCO_3^- (Rajmohan and Elango, 2004). This may explain why the anions of all riverine and lake waters were dominated by HCO_3^- (Fig. 4).

Lake Abaya and Lake Chamo were dominated by Na/K cations, similar to Group 2 and 3 groundwaters (Fig. 4). This is typical of terminal soda lakes which accumulate high salt concentrations that are released via chemical weathering in the surrounding catchments and transferred as inflow via streams to form evaporating lake brines (Hardie et al., 1978). Typically, Ca and Mg reach saturation first, resulting in the precipitation of alkaline earth carbonates (Deocampo and Jones, 2014), whereas Na and K remain in solution longer, subsequently increasing the pH (e.g., 9.10−9.13; Table S2) and alkalinity of the lake water. In contrast to LA and LC, LCB is fresher and indicative of shorter water residence times, which do not allow high salt concentrations to accumulate. Lakes Chamo, Abaya and LCB fit with the hydrochemical range of previously reported MER lakes (Fig. 4), are less fresh than Lakes Ziway,
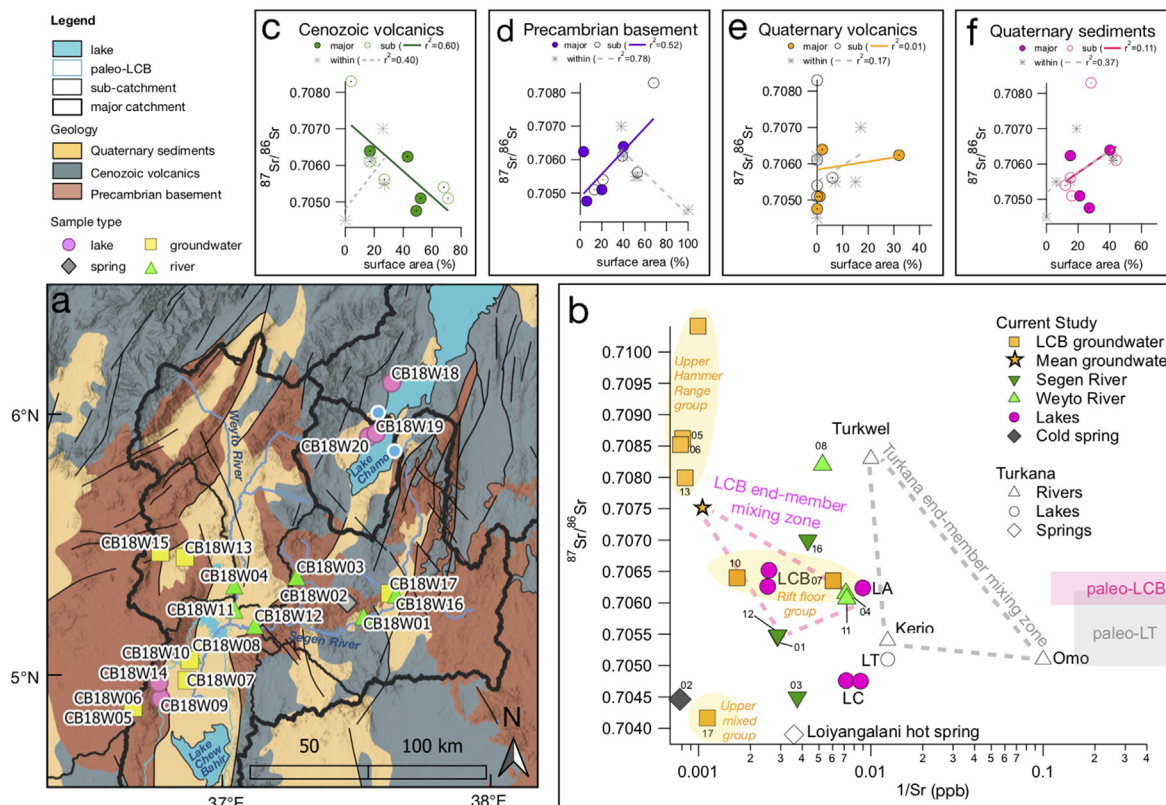
Fig. 5. Panel a: Lithological map of the LCB basin and sampling locations. Panel b: Cross plot of $^{87}Sr/^{86}Sr$ and 1/Sr (ppb) showing the end-member mixing zone for LCB (this study) and Lake Turkana (van der Lubbe et al., 2017). Panels c–f: Cross plots of the $^{87}Sr/^{86}Sr$ of LCB catchment surface waters (from Table 2) and the percentage of lithological surface cover. Yellow star in Panel b indicates the mean composition of all sampled groundwaters, the groundwater end-member used in the lake balance model. (For interpretation of the references to colour in this figure legend, the reader is referred to the Web version of this article.)

and Awassa, but not as evolved as Lake Shala or Lake Turkana, where dissolved solids may experience longer residence times.

Groundwaters were hydro-chemically distinct from surface waters with spatial trends within the catchment. Groundwater typically flows from the upper rift to the rift floor (JICA, 2012), where LCB acts as a semi-aquitard with limited flow from LCB towards Lake Turkana (Kebede et al., 2010a). Although groundwater has higher concentrations of dissolved solids relative to surface waters, this is not likely to be caused by evaporative concentration as groundwater stable water isotope ratios lie on the Global Meteoric Water Line, rather than an evaporation line (Fig. 3d). Groundwater $\delta^{18}O_G$ generally increases with decreasing elevation, which may reflect an altitudinal effect on $\delta^{18}O_P$; this is generally $0.5‰$ km^{-1} for Ethiopian surface waters (Levin et al., 2009) and $-0.9‰$ km^{-1} for groundwaters (Haji et al., 2021). Group 1 groundwaters on the western elevated rift margins were dominated by water rock interactions, and moved towards more hydrochemically evolved waters in the rift floor (Group 3) (Fig. 6). Multiple processes occur during water-rock interactions such as dissolution, precipitation, hydrolysis, ion exchange and oxidation-reduction reactions, which may alter the geochemical signature of groundwaters (Haji et al., 2021; Kebede et al., 2005). Group 1 groundwaters from the Upper Hammer Range were dominated by Ca/Mg cations and Group 2 and 3 groundwaters were dominated by Na/K (Fig. 4), suggesting longer residence times, with enhanced water-rock interactions and reverse weathering processes (authigenic clay mineral formation removing dissolved cations and alkalinity) typical of MER rift floor groundwaters (Kebede et al., 2005; Ayenew et al., 2008). Dissolution of evaporites or soil salts such as gypsum or trona in alluvial aquifers could increase both SO_4

and Na relative to surface waters, whilst ion exchange processes or Ca carbonate mineral precipitation may remove Ca and Mg from solution, progressively reducing dissolved Ca and Mg in solution along groundwater flow paths (Bennett et al., 2021).

5.2. Hydrological and lithological controls on $^{87}Sr/^{86}Sr$

The extreme differences in the $^{87}Sr/^{86}Sr$ of the two dominant lithologies in the EARS (Precambrian basement vs Cenozoic volcanic rocks; Table 1) renders $^{87}Sr/^{86}Sr_{R,L,G}$ a useful hydrological tracer in LCB. Further, it permits paleo-$^{87}Sr/^{86}Sr_C$ from fossil carbonates to be used to reveal changes in paleohydrology (Joordens et al., 2011; van der Lubbe et al., 2017). To determine whether LCB falls within the end-member $^{87}Sr/^{86}Sr$ inflow values, a three-component $^{87}Sr/^{86}Sr$ mixing model including average groundwater and riverine inputs from the Weyto and Segen Rivers as end-members are used (Fig. 5). LCB falls within the groundwater and riverine end-member mixing zone which suggests that these flows can account for LCB $^{87}Sr/^{86}Sr_L$ values. This mixing model also appears applicable to paleo LCB as it covers the total range of measured $^{87}Sr/^{86}Sr_C$ from LCB sedimentary cores over the AHP (Junginger, unpublished data; van der Lubbe et al., 2017), supporting the use of our model to probe variations in $^{87}Sr/^{86}Sr_L$ resulting from Late Quaternary climate change. A similar mixing zone was created using a three-component mixing model for Lake Turkana based on previously published surface water $^{87}Sr/^{86}Sr_C$ data (van der Lubbe et al., 2017). Here, Lake Turkana falls slightly outside the theoretical mixing zone, which suggests a missing 'low' $^{87}Sr/^{86}Sr_{R,G}$ source. The mixing model for Turkana is based on limited point-source information, which may be biased towards the sampling season, and not
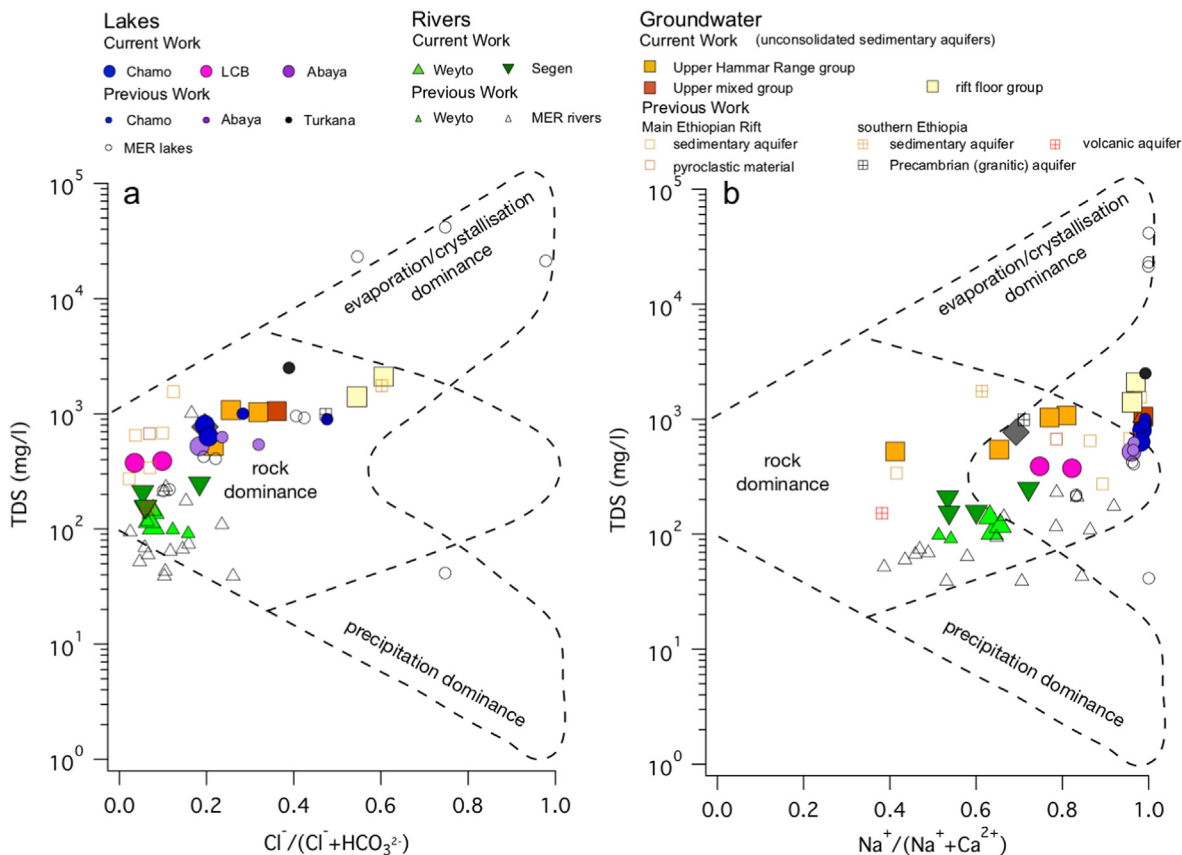
Fig. 6. Gibbs plot of hydrological data from this study and regional data for MER lakes (JICA, 2012) and southern Ethiopian groundwaters (Woldemariyam and Ayenew, 2016). Panel a; TDS versus Cl(Cl + HCO₃) and Panel b; TE + DS Na/(Na + Ca), which show the dominance of waters by precipitation, lithology or evaporation process.
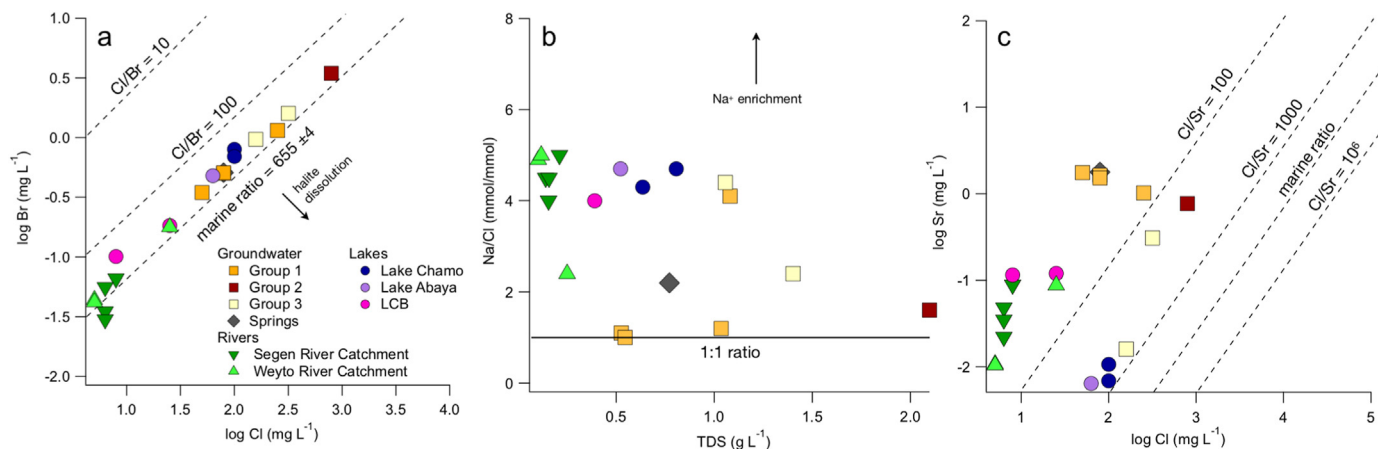
Fig. 7. Panel a: Cross plot of log Br and log Cl for surface and groundwaters, marine ratio (655 ± 4) (Alcalá and Custodio, 2008) is shown. Panel b: Cross plot of the Na/Cl molar ratio and TDS. Panel c: Cross plot of log Sr and log Cl.

representative of annual average inflows. Further, the Omo catchment, where >85% of Lake Turkana's inflows originate, has been influenced by a recent increase in anthropogenic activity over past decades. As Turkana is a larger lake system with longer response times, changes in Omo River $^{87}Sr/^{86}Sr_R$ from anthropogenic activity may not yet be apparent in Lake Turkana. Whilst anthropogenic influences are difficult to rule out, the modern lake $^{87}Sr/^{86}Sr_L$ ratio of 0.7051 is similar to the most recently reported paleo-Turkana $^{87}Sr/^{86}Sr_C$ at 500 years BP (0.7050) and 2000 years BP (0.7051)

(van der Lubbe et al., 2017). Additionally, variability in hydrothermal input (e.g., Loiyangalani hot spring in the south-eastern Turkana catchment) may also act as an additional minor $^{87}Sr/^{86}Sr$ inflow end-member for this lake system. Although beyond the scope of this study, further investigation is warranted to improve the constraints on $^{87}Sr/^{86}Sr$ in paleo-Lake Turkana.

Segen and Weyto $^{87}Sr/^{86}Sr_R$ values ranged from 0.7045 to 0.7070 and 0.7061 to 0.7082, respectively. Surprisingly, the Segen River waters overall were less radiogenic than the Weyto River, even

though this catchment contains a larger proportion of Precambrian basement rocks (53 and 39%, respectively; Table 2), which have more radiogenic mean $^{87}Sr/^{86}Sr$ due to their older age and Rb/Sr ratios (Table 1). There was also disparity in surface lithology and lake water $^{87}Sr/^{86}Sr$ values in the Chamo and Abaya catchments, which both have a small percentage surface cover comprised of older radiogenic bedrock (6 and 3%, respectively) and are dominated by Cenozoic volcanic and sedimentary deposits, but had significantly different $^{87}Sr/^{86}Sr_L$. Lake Chamo had a less radiogenic $^{87}Sr/^{86}Sr_L$ signature (0.7048) compared to that of Lake Abaya (0.7062), which was closer to the values of LCB (0.7064). This suggests that surface water $^{87}Sr/^{86}Sr_R$ in our study catchments is not solely controlled by lithology.

Broadly, chemical weathering rates are largely controlled by the temperature and pressure at which the constituent minerals formed (Goldich, 1938), the specific surface area of mineral surfaces (West et al., 2005), climate (Meybeck, 1987; White and Brantley, 2003), and vegetation (Moulton et al., 2000). Although not discussed here in detail, tectonic activity is coupled to weathering rates by controlling the supply of fresh mineral surfaces and influencing global climate (Raymo et al., 1988). Different weathering rates occur due to mineral surface areas and rock permeability and, thus, reactivity with aqueous solutions may account for the unequal contribution of bedrock lithologies to the dissolved Sr flux (Gibbs et al., 1999). To investigate the relationship between upstream lithology and surface water $^{87}Sr/^{86}Sr$, the lithology for the individual sample locations and catchment areas was calculated (apart from CB18W8 where a connection to the major river channel could not be established; Table 2). Surface lithology was determined for major catchments (Chew Bahir, Abaya, Chamo and Turkana), sub-catchments (Weyto, Segen, Turkwel, Keiro and Omo) and within catchment samples, defined as the surface cover of the area upstream of the riverine sample point (Table 2). The predicted $^{87}Sr/^{86}Sr$ of catchment surface waters was corrected for the differences in weathering rates normalised to granite following W_{norm} values given in Bataille and Bowen (2012; see Table 2). There was a moderate correlation between measured $^{87}Sr/^{86}Sr$ and the proportions of Precambrian granitic/gneisses and Neogene/Paleogene volcanics in the catchments ($r^2 = 0.53$ and 0.67, respectively; Fig. 6). Quaternary sediments showed a negligable relationship to $^{87}Sr/^{86}Sr$ values of catchment waters, which may reflect the fact that they represent an integrated mix of the catchment lithology, evaporites and potentially aeolian input.

The $^{87}Sr/^{86}Sr$ values estimated from catchment lithologies were similar (± 0.004) to measured surface water values for the Weyto and LCB catchments (Table 2). The estimated $^{87}Sr/^{86}Sr$ of the Segen River catchment waters were typically higher than measured values, with larger discrepancies for the smaller tributaries. For example, although sample CB18W3 had 100% upstream surface cover comprising of Precambrian granitic/gneissic rocks, the $^{87}Sr/^{86}Sr_R$ of the river water was unradiogenic (0.7045), suggesting a disconnect between the surface lithology and surface water $^{87}Sr/^{86}Sr$ in this tributary. In all other catchments except the Turkwel, the estimated $^{87}Sr/^{86}Sr$ was lower than the measured values.

To account for the different weathering flux of lithological units, we introduced a relative weathering flux term (k). The use of a k value reduces these parameters into a single term whereby similar k values across catchments would suggest a single dominant control on weathering rates. The k value was solved by inverse modelling for each catchment utilising the measured $^{87}Sr/^{86}Sr$ values of catchments using the following equation:

$$R_{waterbody} = \frac{R_p\left(f_p \times Sr_p \times k_p\right)}{\left(f_p \times Sr_p \times k_p\right) + \left(f_q \times Sr_q \times k_q\right) + (f_n \times Sr_n \times k_n)} +$$
$$\frac{R_n(f_n \times Sr_n \times k_n)}{\left(f_p \times Sr_p \times k_p\right) + \left(f_q \times Sr_q \times k_q\right) + (f_n \times Sr_n \times k_n)} +$$
$$\frac{R_q\left(f_q \times Sr_q \times k_q\right)}{\left(f_p \times Sr_p \times k_p\right) + \left(f_q \times Sr_q \times k_q\right) + (f_n \times Sr_n \times k_n)}$$

$$(15)$$

where $R_{waterbody}$ is the Sr measured isotopic ratio of a given waterbody (e.g., LCB), R_x is the average Sr isotopic ratio of a given lithological unit (denoted as *p*: Precambrian metamorphic basement, *q*: Quaternary sediments and alluvium and *n*: Neogene/Paleogene volcanics; Table 1), f_x is the fraction of the catchment area covered by a given lithology, *Sr* is the Sr concentration of a given lithology, and *k* is the weathering flux of a given lithology. The *k* values are normalised relative to the granitic/gneissic Precambrian units ($k_p = 1$) (Table 2) and reflect the differences of Sr weathering fluxes between catchments.

There are clear differences in *k* values between catchments. The LCB catchment *k* values for each lithology are approximately one, suggesting congruent weathering at the catchment scale. However, the LCB sub-catchments, and the Turkwel, Omo, Abaya, Chamo, Turkana and Keiro catchments exhibited *k* values from 0 to 4.3 (Table 2). One explanation could be the large range in Sr concentrations, $^{87}Sr/^{86}Sr$ ratios and age variability of the southern Ethiopian Precambrian basement rock itself creating a large range in $^{87}Sr/^{86}Sr$ flux variability (Table 1). Alternatively, there could be a contribution of Sr from the dissolution of aeolian-derived material (long-range transported dust or volcanic ash) that does not represent the local surface lithology. Importantly, this does not affect the interpretation of our modelling results as we use catchment-averaged $^{87}Sr/^{86}Sr$ ratios, but may be a critical consideration for future studies focusing on sub-catchment scales.

Another important consideration at LCB to explain $^{87}Sr/^{86}Sr_R$ is the influence of groundwater. The unexpectedly high $^{87}Sr/^{86}Sr_R$ for the Weyto River samples relative to their surface geology may be explained in terms of groundwater input (baseflow) from a more radiogenic source. The role of groundwater in the maintenance of baseflow is important in rivers and wetlands (Baillie et al., 2007), particularly in semi-arid regions as one of the most important low-flow hydrological parameters (Mwakalila et al., 2002). The groundwaters sampled in the Weyto River basin were classified as Group 1 (Fig. 2, Table 2), and have the most radiogenic $^{87}Sr/^{86}Sr_G$ (0.7080−0.7104) of all waters measured in this study (Table S2, Fig. 5). These groundwaters drain unconsolidated alluvial sediment aquifers overlying Precambrian granitic and gneissic rocks (Fig. 6), the weathering of which was the likely dominant local source of the sediments in the dry wadi bed aquifers in this part of the catchment. The groundwaters in Group 2, however, had low $^{87}Sr/^{86}Sr_G$, suggesting a feature of the eastern rift flank may be less radiogenic $^{87}Sr/^{86}Sr_G$ (Fig. 5). Although better spatial coverage of groundwater is required to draw any firm conclusions, a less radiogenic groundwater baseflow component in the Segen River catchment would provide an explanation for the lower $^{87}Sr/^{86}Sr_R$ measured for the Segen River relative to the catchment lithology. This would also be consistent with congruent weathering at the catchment scale.

The importance of groundwater inflow for LCB is demonstrated by the average $^{87}Sr/^{86}Sr_R$ end-member input for LCB (combined Weyto and Segen) being less radiogenic than LCB lake water, thus, requiring a more radiogenic $^{87}Sr/^{86}Sr$ end-member to achieve mass

balance. As average groundwaters had more radiogenic $^{87}Sr/^{86}Sr_G$, they likely represent an important end-member in the Sr mass balance of LCB. Further, the Group 3 groundwaters in the rift floor north of LCB, although further along the groundwater flow path and likely more evolved, are most similar in concentration and $^{87}Sr/^{86}Sr$ to riverine and LCB waters (Fig. 5). We attribute this to the rift floor being a zone of surface-water-groundwater interaction where mixing of riverine and shallow groundwater occurs. Additionally, for a mass balance model of terminal LCB, a large proportion of surface inflows must be lost to groundwater outflow (Supplementary Table 1), and this likely occurs in the deltaic wetland region in the northern part of LCB.

5.3. Hydro-balance modelling of $^{87}Sr/^{86}Sr$ and $\delta^{18}O$

Sedimentary records from LCB provide evidence of wetter conditions during the AHP due to the distinct mineral assemblages in sediment layers which correspond to wet phases (Foerster et al., 2018; Foerster et al., 2012; Foerster et al., 2015; Viehberg et al., 2018). In the following sections, we explore the role of hydrological re-organisation on $^{87}Sr/^{86}Sr_L$ and $\delta^{18}O_L$, modelled over

Quaternary timescales and the potential of using combined paleo $^{87}Sr/^{86}Sr_C$ and $\delta^{18}O_C$ as a proxy of catchment size and interconnectivity. Lake hydro-balance modelling (Fig. 8) allowed us to explore changes in the isotope composition of LCB over three scenarios at the onset of the AHP, assuming a 25% precipitation increase (Table 4). In the model simulations, we prescribe modern values of $\delta^{18}O$ for all inflow parameters. However, during the AHP, global isotope-enabled rainfall models suggest Ethiopian $\delta^{18}O_P$ was ~ −1‰ lower (LeGrande and Schmidt, 2009). We apply this offset to δ_{ri} and δ_P and reran the model simulations (Fig. 8b; grey dashed line) to show the impact of an isotope change in paleo inflows on $\delta^{18}O_L$.

The percentage of dissolved Sr delivered to LCB from each end-member (Weyto River, groundwater etc.), including the percentage of buffering from stored Sr in LCB, is shown in Fig. 8c at the start and end of the modelling period. In all scenarios, the initial $\delta^{18}O_L$ and $^{87}Sr/^{86}Sr_L$ of LCB was +3.8‰ and 0.7064, respectively, to reflect modern values (Supplementary Table 2). Theoretical water residence times based on the Sr concentrations of the maximum volume of a closed LCB (Fig. 9a) and a flow-through LCB (Fig. 9b) were also calculated following Yuretich and Cerling (1983):
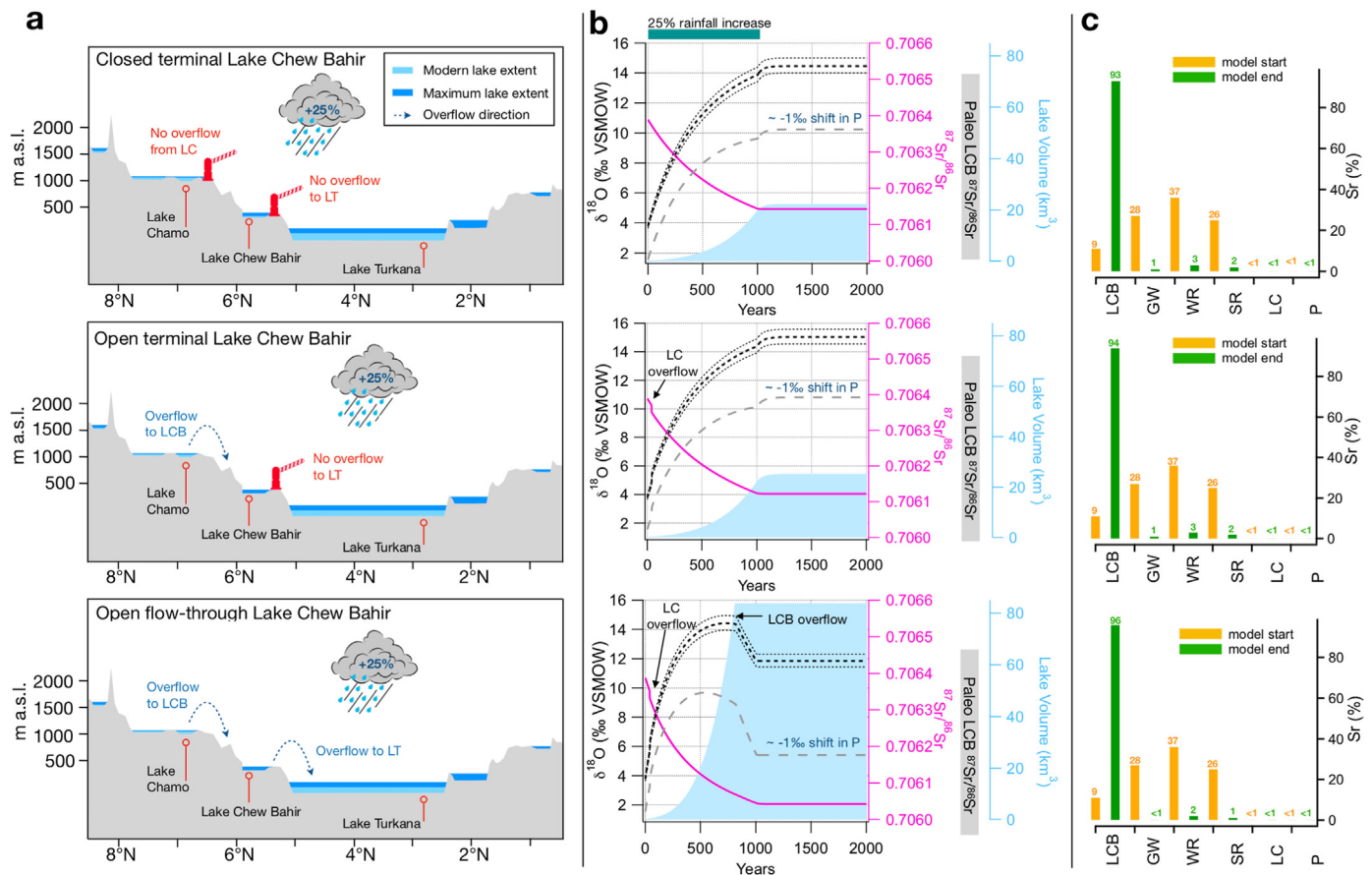
Fig. 8. Output from the combined Sr and O model over three different scenarios: Closed terminal LCB, Open terminal LCB and Open flow-through LCB under the conditions described in Table 4. Panel a shows a cartoon of each of the three scenarios. Panel b shows the isotopic (O and Sr) and corresponding LCB lake volume over the three scenarios. The paleo-LCB $^{87}Sr/^{86}Sr$ range of microfossils from van der Lubbe et al. (2017) and Junginger et al. unpublished data are indicated. The points when overflow switches on in the model from Lake Chamo and LCB are also indicated. The grey dashed lines show the modelling output if a concomitant change in δ_P and δ_{ri} occurred with the P increase. The sensitivity to change in temperature of ±10 °C are also shown as error bars next to the $\delta^{18}O_L$ modelled output. Panel c shows the percentage contributions from each reservoir (LCB: Lake Chew Bahir; GW: groundwater, WR: Weyto River, SR: Segen River, LC: Lake Chamo and P: Precipitation) of dissolved Sr into LCB at the start and end of the modelling period. At the start of the modelling period most of the dissolved Sr is derived from the Weyto (37%) and Segen Rivers (26%), whereas at the end of the modelling period, after a large lake has formed most of the dissolved Sr comes at a single annual time step comes from the LCB itself (the dissolved Sr already present in the lake from the previous time step).
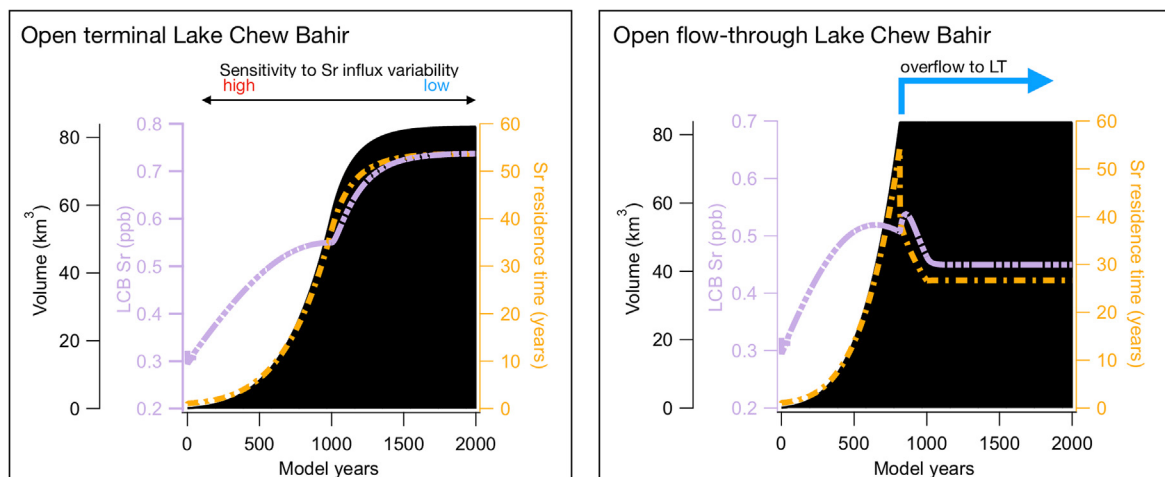
Fig. 9. Sr water residence times for LCB for Open terminal LCB and Open flow-through LCB modelling scenarios.

$$\tau_i = \frac{V_{lake} \times Mi}{Mi\left(V_{GW} + V_{overflow}\right)} \tag{16}$$

where τ is the annual residence time of the solute i, Mi is the amount of solute i in the water body, V_{lake} is the lake volume and the annual flux of the solute leaving the water body via groundwater outflow (V_{GW}) and surface overflow to Turkana ($V_{overflow}$) assuming ideal conditions with a well-mixed, unstratified lake. Overflow to Lake Turkana is initiated once the overflow threshold is surpassed, using the output from the lake balance modelling. Under modern closed-lake conditions, Sr residence times are ~1 year and are more sensitive to changes in Sr influxes.

5.3.1. Scenario 1: closed terminal Lake Chew Bahir

Under closed-lake conditions, modelled $^{87}Sr/^{86}Sr_L$ decreased from 0.7064 to ~0.7062 (Fig. 8a), and $\delta^{18}O_L$ increased to ~14‰ by model year 2000. This suggests a large range (~10‰) in $\delta^{18}O$ can be acheieved due to intra-catchment dynamics alone, i.e., no inter-catchment connectivity. The increase in $\delta^{18}O_L$ reflects the enhanced influence of evaporation in an expanding semi-arid lake that increases approximately 8-fold in surface area over the modelling period. Further, the modelled $\delta^{18}O_L$ is within the range of reported in modern day MER lakes (Fig. 3e). The decrease in $^{87}Sr/^{86}Sr_L$ is directly related to increased surface inflow with less radiogenic $^{87}Sr/^{86}Sr_R$, and occurs directly in phase with linear increases in inflows.

5.3.2. Scenario 2: open terminal Lake Chew Bahir

Another scenario during the AHP is hydrological reorganisation including additional inflow from Lake Chamo via the Segen River, which infrequently occurs under modern conditions when precipitation exceeds the long-term average. Interestingly, although the inflow from Lake Chamo resulted in a larger lake than in Scenario 1 (Fig. 8b), $^{87}Sr/^{86}Sr_L$ showed an initial change at the activation of Lake Chamo overflow, but this overflow made little appreciable difference compared to Scenario 1 over the whole modelling period. At the end of the modelling period, $\delta^{18}O_L$ was ~+15‰ (~1‰ higher than Scenario 1). Thus, overflow from Lake Chamo into LCB is unlikely to drive major changes in lake water chemistry.

5.3.3. Scenario 3: open flow-through Lake Chew Bahir

Scenario 3 considers an inter-connected lake system where LCB overflows and creates a large N−S cascading lake system connecting Lake Abaya, Lake Chamo, LCB and finally Lake Turkana. The $\delta^{18}O_L$ change over the modelled period was significantly different in this scenario. Similar to other scenarios, $\delta^{18}O_L$ increased over the modelling period until the overflow point was surpassed and overflow was initiated to Lake Turkana. At this point, $\delta^{18}O_L$ rapidly decreases from ~+14.0‰ and stabilises at +12.0‰ when steady state conditions begin at model year 1000. Under humid conditions when LCB is a flow-through system, $\delta^{18}O_L$ is still likely to be high, but trending towards lower values than other scenarios by up to −2.0‰. This is consistent with $\delta^{18}O$ reconstructions of ostracods from outcrops at Lake Turkana, where a −1.5‰ decrease occurred in the fossil record during phases of overflow and connectivity to the White Nile (Beck et al., 2019). Our modelling suggests that the transition from terminal to flow-through lake conditions in lake systems like LCB may be even more pronounced.

Modelled $^{87}Sr/^{86}Sr_L$ in LCB also changed significantly in this scenario from 0.7064 to ~0.7060, which is greater in magnitude than the change in the terminal LCB scenarios (Fig. 8). This suggests that the greatest change in $^{87}Sr/^{86}Sr_L$ occurs via a transition from smaller terminal lake to a large flow-through lake. A decrease in the residence times of dissolved Sr (~55 years to 25 years) occurred after LCB switched to a flow-through system, increasing the lake's sensitivity to changes in surface water inflows (Fig. 9b).

5.4. Lake water $\delta^{18}O$ change at the AHP onset

Dynamic changes in $\delta^{18}O_L$ have been reported in the endogenic calcite record from LCB lake cores with a range of +0.5 to +9.0‰ (VPDB) over the AHP (Viehberg et al., 2018). Once converted to the VSMOW scale (Coplen et al., 1998), assuming temperature dependent fractionation between water and calcite (Kim et al., 2007) and the modern lake water temperature of ~30.5 °C, we estimate that lake water ranged from +4.0 to +12.6‰ (VSMOW) during the AHP period. This is comparable to the range of $\delta^{18}O_L$ in our modelled results simulating the onset of the AHP (+4.0 to +14.5‰; Fig. 8). Lake water $\delta^{18}O_L$ is sensitive to three main factors: 1) the $\delta^{18}O_P$ of the precipitation moisture source, 2) groundwater input, and 3) the degree of evaporative fractionation (Leng and Marshall, 2004; Leng et al., 1999a, b). At LCB, changes in the first factor, ($\delta^{18}O_P$) may occur due to changes in the strength of the East African Monsoon or West African Monsoon (Viehberg et al., 2018), bringing rainfall from the

Atlantic or Indian Ocean, respectively. Modelled rainfall isotope values from coupled atmospheric-ocean circulation models, suggest a potential ~-1‰ (eg. LeGrande and Schmidt, 2009) change in rainfall $\delta^{18}O$ during the Holocene. If we consider this in our modelling, a concomitant change in δ_P and consequently δ_{ri} has a large impact on $\delta^{18}O_L$, resulting in an offset at the end of the modelling period of ~-6‰ compared to simulations where δ_P was held constant (Fig. 8b). Lower δ_P acts to 'buffer' the overall increase in $\delta^{18}O_L$ driven by evaporation in our model simulations. In the same way, increases in groundwater inflow with lower $\delta^{18}O$ than rainfall, would also act to buffer increases due to evaporation resulting in lower $\delta^{18}O_L$. The third factor, evaporation, shows the greatest total impact on $\delta^{18}O_L$, resulting in an overall change of ~10‰. This can be seen in terminal LCB Scenarios 1 and 2 where δ_P and G_i are held constant and the change in $\delta^{18}O_L$ is driven by evaporative fractionation as LCB expands in surface area and water residence times increase (Fig. 9).

5.5. Lake water $^{87}Sr/^{86}Sr$ change at the AHP onset

Scenarios 1 and 2 cover approximately half the variability of $^{87}Sr/^{86}Sr_C$ derived from measurements of carbonate microfossil material at LCB over the AHP (0.7065−0.7060; van der Lubbe et al., 2017; Junginger et al., unpublished data). The third scenario, where LCB overflowed to Lake Turkana, showed the greatest range in $^{87}Sr/^{86}Sr_L$. Sustained connectivity to Lake Turkana creates an extra outflow of Sr from LCB, effectively flushing Sr until a new steady state is reached. Consequently, estimated Sr residence times for the open flow-through LCB scenario are ~25 years lower (Fig. 9b).

Our maximum lake water residence time of ~55 years suggests a dynamic lake system which could respond quickly to changes in Sr influxes. This contrasts the record from Lake Turkana, which shows smooth and gradual changes in $^{87}Sr/^{86}Sr_C$ over the AHP, most likely due to the larger buffering capacity of this lake (~200 times larger than LCB at present day). Dissolution of lake basin evaporites, formed from past water pulses and subsequent evaporation episodes, could also provide an additional source of Sr during lake-filling episodes, the influence of which is difficult to account for. This could lag the response time of lake water $^{87}Sr/^{86}Sr_L$ to hydrological reorganisation. For example, if we consider the most extreme example of the complete desiccation of the maximum volume of LCB where 100% of the Sr in the water is precipitated as evaporites on the lake basin floor, we can suggest a potential upper limit of this process. Based on modern lake concentrations of Sr (394 ppb) and a maximum surface volume of ~83 km^3 an additional 3.3×10^7 kg of Sr would be released into LCB during filling episodes. This would effectively act as an additional source of 'recycled' Sr with the $^{87}Sr/^{86}Sr_L$ of past lake water. If we assume this is released at a constant rate during lake filling, this could represent a maximum of 0.1−4% of the total Sr input on an annual time step. In reality, not all lake Sr would be converted to surface evaporites and a proportion would be removed as groundwater outflow and depending on the time interval separating lake draining and filling episodes, evaporites may also buried via sedimentation processes estimated at 0.1−1.3 mm a^{-1} (Foerster et al., 2012).

5.6. Sensitivity analysis on the surface-water-to-groundwater ratio

The larger range of $^{87}Sr/^{86}Sr_C$ (0.7065−0.7060) measured in microfossils from LCB (van der Lubbe et al., 2017) could not be simulated by our model (~0.7064−0.7060) considering only changes in catchment connectivity. This suggests an additional source of more radiogenic Sr outside of our prescribed model conditions. Groundwater has both much higher Sr concentrations compared to surface waters (Table S2) and is typically more
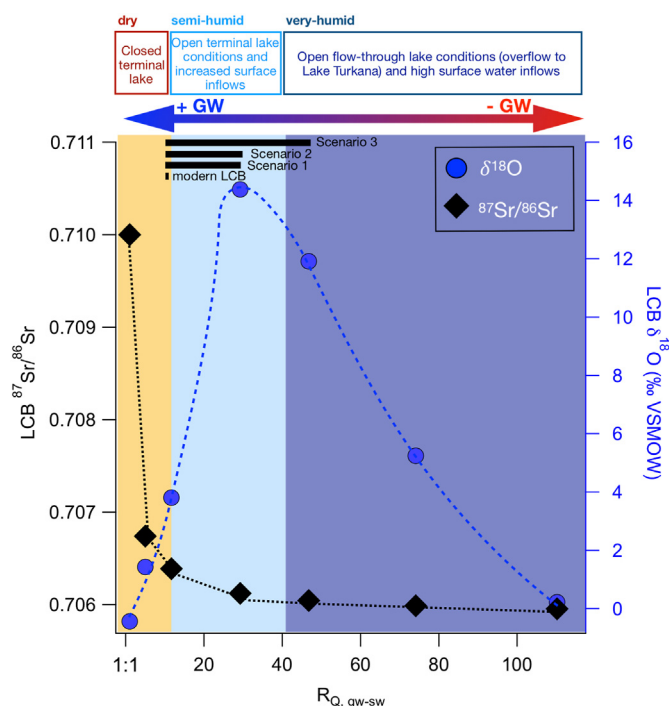

Fig. 10. Sensitivity cross-plot of LCB $^{87}Sr/^{86}Sr_L$ and $\delta^{18}O_L$ to changes in groundwater/surface water flow ($R_{Q, gw:sw}$) denoting the modern values and approximate shifts from closed to open conditions.

radiogenic $^{87}Sr/^{86}Sr_G$. Our hydro-balance shows that the modern ratio of surface water and groundwater inputs based on flow ($R_{Q,sw/gw}$) is 11:1, however, the Sr flux surface-water-to-groundwater ratio ($R_{Sr,sw/gw}$) is much lower (4:1) compared to the ratio of inflows, revealing that changes in groundwater inflow has a large impact on the overall Sr budget to LCB. In our model simulations groundwater inflows (G_i) were held constant. Fig. 10 shows the impact and sensitivity of LCB to changes in groundwater inflows by altering the $R_{Q,sw/gw}$ ratio, and the consequent impact on both $^{87}Sr/^{86}Sr_L$ and $\delta^{18}O_L$. This revealed that the most dynamic changes in $^{87}Sr/^{86}Sr_L$ occur under dry conditions as the $R_{Q,sw/gw}$ approaches 1. Conversely during very humid conditions, when a flow-through lake has been established, $^{87}Sr/^{86}Sr_L$ tends to be more stable due to the buffering capacity of a larger lake system. More radiogenic $^{87}Sr/^{86}Sr_L$ may be explained by an increase in groundwater flow into LCB due to either a rising water table or reduced surface water inflow. Lower $^{87}Sr/^{86}Sr_L$ during the AHP may be explained by reduced groundwater inflow or higher surface water inflow relative to today (higher $R_{Q,sw/gw}$), for example, in very humid conditions when there is overflow to Lake Turkana (Fig. 10). Large changes in precipitation will ultimately change the water table height; however, groundwater response times are typically slow, e.g., estimated at 100−1000 years in Olduvai gorge, Tanzania (Cuthbert et al., 2017), compared to runoff and are out of step with meteorological and surface hydrological change (Cuthbert et al., 2019). It may then be reasonable to assume that changes in groundwater inflow and outflow will be slow to respond at the onset of a humid period, and the isotopic response of LCB lake water will be dominated by the changes in surface water inflows. Over time groundwater will likely play a more important buffering role, especially in maintaining higher lake levels in a drying climate and allowing groundwater refugia to develop (Cuthbert et al., 2017). Therefore, groundwater inflow may buffer surface inflows to varying degrees, which should be reflected by changes in $^{87}Sr/^{86}Sr$. Whilst beyond the scope of this

study, an improved understanding of groundwater flow dynamics and age in southern Ethiopia would be invaluable for improving paleoclimatic reconstructions using $^{87}Sr/^{86}Sr$.

Changes in $R_{Q,sw/gw}$ also has implications for $\delta^{18}O_L$. At the start of Scenario 2 (dry conditions with a low $R_{Q,sw/gw}$), water residence times are shorter (Fig. 9), reducing the impact of evaporative ^{18}O enrichment and resulting in lower LCB $\delta^{18}O_L$ (Fig. 10). Conversely, under very humid conditions in Scenario 3, water residence times are reduced after flow-through conditions are established, which also results in lower $\delta^{18}O_L$ (Fig. 10). Higher $\delta^{18}O_L$ occurs as the $R_{Q,sw/gw}$ increases until the overflow point, after which connectivity to Lake Turkana reduces the lake water residence time (Figs. 8–10). In our modelling results, the lowest $\delta^{18}O_L$ values occurred under the two extreme lake scenarios: 1) under dry, closed terminal lake conditions with a low groundwater to surface water ratio and 2) under very humid, open flow-through lake conditions where LCB became part of a large cascading lake system (Fig. 10). Here, the additional use of $^{87}Sr/^{86}Sr$ in fossil carbonates can help distinguish whether conditions were dry (high $^{87}Sr/^{86}Sr$) or very humid (low $^{87}Sr/^{86}Sr$) and could serve as a framework for interpreting the lacustrine fossil $\delta^{18}O_C$ record. Based on our modelling, we suggest that flow-through conditions to Lake Turkana, simulated by increasing surface inflows by 300% and rainfall by 25%, result in a decrease in LCB $\delta^{18}O_L$ of $-2‰$, which decreases to $-10‰$ with concomitant change in rainfall precipitation of $-1‰$ relative to present day. Low $\delta^{18}O_C$ values between ~+0 and +3‰ (VPDB) were reported in the LCB paleo record from Viehberg et al. (2018) during the AHP, in conjunction with other proxy indicators (e.g., Ca/Ti) suggesting established lake conditions and not the dry/small lake end-member scenario. Our modelling suggests such low values necessitates a connection to Lake Turkana and higher inflows (beyond those of our modelled scenarios) or lower input rainfall isotopic composition. Dating of paleo-shorelines would also be beneficial in determining the timing of these phases. We suggest that $\delta^{18}O_C$ alone would be insufficient to differentiate lake conditions, such as an open versus closed lake, but in combination with $^{87}Sr/^{86}Sr_C$, the extent of lake expansion and trends (i.e. draining or filling) in hydroclimate may be better interpreted.

6. Conclusions

Our study provides the first known major hydrochemical investigation of the Lake Chew Bahir catchment in southern Ethiopia. The major, trace, and Sr and O isotopic composition of surface and groundwaters reported in this study are within the range of previously published data in the EARS, suggesting the LCB catchment is a good analogue for other semi-arid catchments in the region. Groundwater-surface water interactions at terminal, semi-arid LCB plays a significant role in water hydrochemistry. The Sr mass balance of LCB cannot be achieved by only including surface water inflows, or explain the modern lake water $^{87}Sr/^{86}Sr_L$ ratios. This demonstrates the important role of groundwater in dryland lake basins and supports the hypothesis that perennial springs likely play a central buffering role in sustaining water supplies in areas which typically experience climatically induced large-scale surface water fluctuations (Cuthbert et al., 2019).

Based on model simulations, LCB has short (1–55 years) Sr residence times, and $\delta^{18}O$ is sensitive to the evaporative conditions and lake water residence times. Higher $\delta^{18}O$ is likely indicative of a larger closed-lake system. Lake $\delta^{18}O_L$ values greater than +12.0‰ suggest a closed lake system, whereas a decreasing trend in $\delta^{18}O_L$ indicates a flow-through lake and subsequent connectivity to Lake Turkana. Coupled lower $^{87}Sr/^{86}Sr$ and higher $\delta^{18}O$ would suggest large-scale hydrological reorganisation, able to support a flow-through lake system where the Sr budget was dominated by

surface inflows. Isotopic data from microfossils could provide key insights on paleo-hydrological connectivity between LCB and Lake Turkana and allow time periods of cascading lake systems to be identified. Conversely, periods dominated and buffered by groundwater inflows indicated by lower $\delta^{18}O_L$ and higher $^{87}Sr/^{86}Sr_L$ may also be readily identified. This likely played an integral role in the availability of freshwater resources for our human ancestors in the region during documented climatic instability over the late Quaternary (Viehberg et al., 2018; Foerster et al., 2018). The combined use of $^{87}Sr/^{86}Sr_C$ and $\delta^{18}O_C$ can provide important insights to change in hydroclimate in southern Ethiopia, and other similar arid and semi-arid lowland sites.

Author contributions

Declaration of competing interest

The authors declare that they have no known competing financial interests or personal relationships that could have appeared to influence the work reported in this paper.

Acknowledgements

Appendix A. Supplementary data

Supplementary data to this article can be found online at https://doi.org/10.1016/j.quascirev.2022.107387.

References

Alcalá, F.J., Custodio, E., 2008. Using the Cl/Br ratio as a tracer to identify the origin of salinity in aquifers in Spain and Portugal. J. Hydrol. 359, 189–207.

Asrat, A., Barbey, P., Gleizes, G., 2001. The precambrian geology of Ethiopia: a review. Afr. Geosci. Rev. 8, 271–288.

Asrat, A., Barbey, P., 2003. Petrology, geochronology and Sr-Nd isotopic geochemistry of the Konso pluton, South-western Ethiopia: implications for transition from convergence to extension in the Mozambique Belt. Int. J. Earth Sci. 92, 873–890.

Ayenew, T., Kebede, S., Alemyahu, T., 2008. Environmental isotopes and hydrochemical study applied to surface water and groundwater interaction in the Awash River basin. Hydrol. Process. 22, 1548–1563.

Baddouh, M.b., Meyers, S.R., Carroll, A.R., Beard, B.L., Johnson, C.M., 2016. Lacustrine 87Sr/86Sr as a tracer to reconstruct Milankovitch forcing of the Eocene hydrologic cycle. Earth Planet Sci. Lett. 448, 62–68.

Baillie, M.N., Hogan, J.F., Ekwurzel, B., Wahi, A.K., Eastoe, C.J., 2007. Quantifying water sources to a semiarid riparian ecosystem, San Pedro River, Arizona. J. Geophys. Res.: Biogeosciences 112.

Bataille, C.P., Bowen, G.J., 2012. Mapping 87Sr/86Sr variations in bedrock and water for large scale provenance studies. Chem. Geol. 304–305, 39–52.

Beck, C.C., Feibel, C.S., Wright, J.D., Mortlock, R.A., 2019. Onset of the african humid period by 13.9 kyr BP at kabua gorge, Turkana basin, Kenya. Holocene 29, 1011–1019.

Bedaso, Z., Wu, S.-Y., 2021. Linking precipitation and groundwater isotopes in Ethiopia - implications from local meteoric water lines and isoscapes. J. Hydrol. 596, 126074.

Belete, A., Beccaluva, L., Bianchini, G., Colombani, N., Fazzini, M., Marchina, C., Natali, C., Rango, T., 2015. Water–rock interaction and lake hydrochemistry in the main Ethiopian rift. In: Billi, P. (Ed.), Landscapes and Landforms of Ethiopia. Springer Netherlands, Dordrecht, pp. 307–321.

Bennett, G., Van Reybrouck, J., Shemsanga, C., Kisaka, M., Tomašek, I., Fontijn, K., Kervyn, M., Walraevens, K., 2021. Hydrochemical characterisation of high-fluoride groundwater and development of a conceptual groundwater flow model using a combined hydrogeological and hydrochemical approach on an active volcano: mount meru, northern Tanzania. Water 13, 2159.

Bloszies, C., Forman, S.L., Wright, D.K., 2015. Water level history for lake Turkana, Kenya in the past 15,000years and a variable transition from the african humid period to holocene aridity. Global Planet. Change 132, 64–76.

Bonini, M., Corti, G., Innocenti, F., Manetti, P., Mazzarini, F., Abebe, T., Pecskay, Z., 2005. Evolution of the Main Ethiopian Rift in the frame of Afar and Kenya rifts propagation. Tectonics 24.

Borchardt, S., Trauth, M.H., 2012. Remotely-sensed evapotranspiration estimates for an improved hydrological modeling of the early Holocene mega-lake Suguta, northern Kenya Rift. Palaeogeogr. Palaeoclimatol. Palaeoecol. 361–362, 14–20.

Bretzler, A., Osenbrück, K., Gloaguen, R., Ruprecht, J.S., Kebede, S., Stadler, S., 2011. Groundwater origin and flow dynamics in active rift systems – a multi-isotope approach in the Main Ethiopian Rift. J. Hydrol. 402, 274–289.

Chamberlain, C.P., Wan, X., Graham, S.A., Carroll, A.R., Doebbert, A.C., Sageman, B.B., Blisniuk, P., Kent-Corson, M.L., Wang, Z., Chengshan, W., 2013. Stable isotopic evidence for climate and basin evolution of the Late Cretaceous Songliao basin, China. Palaeogeogr. Palaeoclimatol. Palaeoecol. 385, 106–124.

Clement, J., Caroff, M., Hemond, C., Tiercelin, J., Bollinger, C., Guillou, H., Cotten, J., 2003. Pleistocene magmatism in a lithospheric transition area: petrogenesis of alkaline and peralkaline lavas from the Baringo-Bogoria Basin. Can. J. Earth Sci. 40 (9), 1239–1257.

Cockerton, H.E., Street-Perrott, F.A., Leng, M.J., Barker, P.A., Horstwood, M.S.A., Pashley, V., 2013. Stable-isotope (H, O, and Si) evidence for seasonal variations in hydrology and Si cycling from modern waters in the Nile Basin: implications for interpreting the Quaternary record. Quat. Sci. Rev. 66, 4–21.

Coplen, T.B., 1996. New guidelines for reporting stable hydrogen, carbon, and oxygen isotope-ratio data. Geochem. Cosmochim. Acta 60, 3359–3360.

Cohen, A., Talbot, M.R., Awramik, S.M., Dettman, D.L., Abell, P., 1997. Lake Level and Paleoenvironmental History of Lake Tanganyika, Africa, as Inferred from Late Holocene and Modern Stromatolites.

Craig, H., Gordon, L.I., 1965. Deuterium and oxygen-18 variations in the ocean and the marine atmosper. In: Proceedings of a Conference on Stable Isotopes in Oceanographic Studies and Paleotemperatures. Spoleto, Italy, pp. 9–130.

Cuthbert, M.O., Gleeson, T., Moosdorf, N., Befus, K.M., Schneider, A., Hartmann, J., Lehner, B., 2019. Global patterns and dynamics of climate–groundwater interactions. Nat. Clim. Change 9, 137–141.

Cuthbert, M.O., Gleeson, T., Reynolds, S.C., Bennett, M.R., Newton, A.C., McCormack, C.J., Ashley, G.M., 2017. Modelling the role of groundwater hydro-refugia in East African hominin evolution and dispersal. Nat. Commun. 8, 15696.

Darling, W.G., Gizaw, B., Arusei, M.K., 1996. Lake-groundwater relationships and fluid-rock interaction in the East African Rift Valley: isotopic evidence. J. Afr. Earth Sci. 22, 423–431.

Davidson, A., 1983. The Omo river project: reconnaissance geology and geochemistry of parts of Illubabor, Kefa, Gamu Gofa and Sidamo, Ethiopia. Ethiop. Inst. Geol. Surv. Bull. 2, 89.

Demlie, M., Ayenew, T., Wohnlich, S., 2007a. Comprehensive hydrological and hydrogeological study of topographically closed lakes in highland Ethiopia: the case of Hayq and Ardibo. J. Hydrol. 339, 145–158.

Demlie, M., Wohnlich, S., Gizaw, B., Stichler, W., 2007b. Groundwater recharge in the Akaki catchment, central Ethiopia: evidence from environmental isotopes (δ18O, δ2H and 3H) and chloride mass balance. Hydrol. Process. 21, 807–818.

Deocampo, D.M., Jones, B.F., 2014. 7.13 - geochemistry of saline lakes. In: Holland, H.D., Turekian, K.K. (Eds.), Treatise on Geochemistry, second ed. Elsevier, Oxford, pp. 437–469.

Dettman, D.L., Palacios-Fest, M.R., Nkotagu, H.H., Cohen, A.S., 2005. Paleolimnological investigations of anthropogenic environmental change in Lake Tanganyika: VII. Carbonate isotope geochemistry as a record of riverine runoff. J. Paleolimnol. 34, 93–105.

Doebbert, A.C., Johnson, C.M., Carroll, A.R., Beard, B.L., Pietras, J.T., Rhodes Carson, M., Norsted, B., Throckmorton, L.A., 2014. Controls on Sr isotopic evolution in lacustrine systems: eocene green river formation, Wyoming. Chem. Geol. 380, 172–189.

Fischer, M.L., Markowska, M., Bachofer, F., Foerster, V.E., Asrat, A., Zielhofer, C., Trauth, M.H., Junginger, A., 2020. Determining the pace and magnitude of lake level changes in southern Ethiopia over the last 20,000 Years using lake balance modeling and SEBAL. Front. Earth Sci. 8.

Foerster, V., Deocampo, D.M., Asrat, A., Günter, C., Junginger, A., Krämer, K.H., Stroncik, N.A., Trauth, M.H., 2018. Towards an understanding of climate proxy formation in the Chew Bahir basin, southern Ethiopian Rift. Palaeogeogr. Palaeoclimatol. Palaeoecol. 501, 111–123.

Foerster, V., Junginger, A., Langkamp, O., Gebru, T., Asrat, A., Umer, M., Lamb, H.F., Wennrich, V., Rethemeyer, J., Nowaczyk, N., Trauth, M.H., Schaebitz, F., 2012. Climatic change recorded in the sediments of the Chew Bahir basin, southern Ethiopia, during the last 45,000 years. Quat. Int. 274, 25–37.

Foerster, V., Vogelsang, R., Junginger, A., Asrat, A., Lamb, H.F., Schaebitz, F., Trauth, M.H., 2015. Environmental change and human occupation of southern Ethiopia and northern Kenya during the last 20,000 years. Quat. Sci. Rev. 129, 333–340.

Fontes, J.-C., Maglione, G., Roche, M.-A., 1970. Eléments d'hydrologie isotopique dans le bassin du lac Tchad. International atomic energy, Vienna, pp. 209–219.

Forman, S.L., Wright, D.K., Bloszies, C., 2014. Variations in water level for lake Turkana in the past 8500 years near Mt. Porr, Kenya and the transition from the african humid period to holocene aridity. Quat. Sci. Rev. 97, 84–101.

Furi, W., Razack, M., Abiye, T.A., Kebede, S., Legesse, D., 2012. Hydrochemical characterization of complex volcanic aquifers in a continental rifted zone: the Middle Awash basin, Ethiopia. Hydrogeol. J. 20, 385–400.

Furman, T., Kalet, K.M., Bryce, J.G., Hanan, B.B., 2006. Tertiary mafic lavas of Turkana, Kenya: constraints on East African plume structure and the occurrence of high-μ volcanism in Africa. J. Petrol. 47, 1221–1244.

Garcin, Y., Junginger, A., Melnick, D., Olago, D.O., Strecker, M.R., Trauth, M.H., 2009. Late pleistocene–holocene rise and collapse of lake Suguta, northern Kenya rift. Quat. Sci. Rev. 28, 911–925.

Gat, J.R., 1996. Oxygen anf hydrogen isotopes in the hydrologic cycle. Annu. Rev. Earth Planet Sci. 24, 225–262.

George, R., Rogers, N., 2002. Plume dynamics beneath the African plate inferred from the geochemistry of the Tertiary basalts of southern Ethiopia. Contrib. Mineral. Petrol. 144, 286–304.

Gibbs, M.T., Bluth, G.J.S., Fawcett, P.J., Kump, L.R., 1999. Global chemical erosion over the last 250 my; variations due to changes in paleogeography, paleoclimate, and paleogeology. Am. J. Sci. 299, 611–651.

Gibson, J.J., Birks, S.J., Yi, Y., 2016. Stable isotope mass balance of lakes: a contemporary perspective. Quat. Sci. Rev. 131, 316–328.

Gibson, J.J., Edwards, T.W.D., 2002. Regional water balance trends and evaporation-transpiration partitioning from a stable isotope survey of lakes in northern Canada. Global Biogeochem. Cycles 16, 10-11-10-14.

Gizaw, B., 2002. Hydrochemical and Environmental Investigation of the Addis Ababa Region, Ethiopia. Unpublished PhD Thesis. Ludwig Macmillan, University of Munich, Munich.

Goldich, S.S., 1938. A study in rock-weathering. J. Geol. 46, 17–58.

Golubtsov, A.S., Habteselassie, R., 2010. Fish faunas of the Chamo-Abaya and Chew Bahir basins in southern portion of the Ethiopian Rift Valley: origin and prospects for survival. Aquat. Ecosys. Health Manag. 13, 47–55.

Gonfiantini, R., 1986. Chapter 3 – environmental isotopes in lake studies A2 - fritz, P. In: Fontes, J.C. (Ed.), The Terrestrial Environment, B. Elsevier, Amsterdam, pp. 113–168.

Gonfiantini, R., Borsi, S., Ferrara, G., Panichi, C., 1973. Isotopic composition of waters from the Danakil depression (Ethiopia). Earth Planet Sci. Lett. 18, 13–21.

Grove, A., Street, A., Goudie, A., 1975. Former lake levels and climatic change in the rift valley of southern Ethiopia. Geogr. J. 141, 177–194.

Haji, M., Qin, D., Guo, Y., Li, L., Wang, D., Karuppannan, S., Shube, H., 2021. Origin and geochemical evolution of groundwater in the Abaya Chamo basin of the Main Ethiopian Rift: application of multi-tracer approaches. Hydrogeol. J.

Halcrow, 2008. Rift valley lakes basin integrated resources development master plan study project, draft phase 2 report Part II prefeasibility studies, Halcrow group limited, and generation integrated rural development (GIRD) consultants unpublished report. Addis Ababa.

Hardie, L.A., Smoot, J.P., Eugster, H.P., 1978. Saline lakes and their deposits:a sedimentological approach. In: Matter, A., Tucker, M.E. (Eds.), Modern and Ancient Lake Sediments. Blackwell Scientific Publications, Oxford, pp. 7–42.

Hart, W.S., Quade, J., Madsen, D.B., Kaufman, D.S., Oviatt, C.G., 2004. The 87Sr/86Sr ratios of lacustrine carbonates and lake-level history of the Bonneville paleo-lake system. Geol. Soc. Am. Bull. 116, 1107–1119.

Horita, J., Rozanski, K., Cohen, S., 2008. Isotope effects in the evaporation of water: a status report of the Craig–Gordon model. Isot. Environ. Health Stud. 44, 23–49.

Horita, J., Wesolowski, D.J., 1994. Liquid-vapor fractionation of oxygen and hydrogen isotopes of water from the freezing to the critical temperature. Geochem. Cosmochim. Acta 58, 3425–3437.

IAEA, 2019. Global network of isotopes in rivers. The GNIR database. http://www-naweb.iaea.org/napc/ih/IHS_resources_isohis.html. (Accessed 7 February 2020).

Janzen, A., Bataille, C., Copeland, S.R., Quinn, R.L., Ambrose, S.H., Reed, D., Hamilton, M., Grimes, V., Richards, M.P., le Roux, P., Roberts, P., 2020. Spatial variation in bioavailable strontium isotope ratios (87Sr/86Sr) in Kenya and northern Tanzania: implications for ecology, paleoanthropology, and archaeology. Palaeogeogr. Palaeoclimatol. Palaeoecol. 560, 109957.

JICA, 2012. The Study on Groundwater Resources Assessment in the Rift Valley Lakes Basin in Ethiopia Final Report (Main Report). JICA, Kokusai Kogyo Co., Ltd., MoWE, Ethiopia.

Johnson, T.C., Malala, J.O., 2009. Lake Turkana and its link to the nile. In:

Dumont, H.J. (Ed.), The Nile: Origin, Environments, Limnology and Human Use. Springer Netherlands, Dordrecht, pp. 287–304.

Jones, M.D., Cuthbert, M.O., Leng, M.J., McGowan, S., Mariethoz, G., Arrowsmith, C., Sloane, H.J., Humphrey, K.K., Cross, I., 2016. Comparisons of observed and modelled lake δ18O variability. Quat. Sci. Rev. 131, 329–340.

Joordens, J.C.A., Vonhof, H.B., Feibel, C.S., Lourens, L.J., Dupont-Nivet, G., van der Lubbe, J.H.J.L., Sier, M.J., Davies, G.R., Kroon, D., 2011. An astronomically-tuned climate framework for hominins in the Turkana Basin. Earth Planet Sci. Lett. 307, 1–8.

Junginger, A., Roller, S., Olaka, L.A., Trauth, M.H., 2014. The effects of solar irradiation changes on the migration of the Congo Air Boundary and water levels of paleo-Lake Suguta, Northern Kenya Rift, during the African Humid Period (15–5ka BP). Palaeogeogr. Palaeoclimatol. Palaeoecol. 396, 1–16.

Junginger, A., Trauth, M.H., 2013. Hydrological constraints of paleo-lake Suguta in the northern Kenya rift during the african humid period (15–5kaBP). Global Planet. Change 111, 174–188.

Kebede, E., Mariam, Z.G., Ahlgren, I., 1994. The Ethiopian Rift Valley lakes: chemical characteristics of a salinity-alkalinity series. Hydrobiologia 288, 1–12.

Kebede, S., 2004. Environmental Isotopes and Geochemistry in Investigating Groundwater and Lake Hydrology: Cases from the Blue Nile Basin & the Ethiopian Rift (Ethiopia) Hydrogeology. Université d'Avignon et des Pays de Vaucluse d'Avignon, p. 162.

Kebede, S., 2013. Groundwater Potential, Recharge, Water Balance: Vital Numbers, Groundwater in Ethiopia: Features, Numbers and Opportunities. Springer Berlin Heidelberg, Berlin, Heidelberg, pp. 221–236.

Kebede, S., Ketema, A., Tesema, Z., 2010a. Features of groundwaters in basins shared between Ethiopia and Kenya and the implications for international legislation on transboundary aquifers. Hydrogeol. J. 18, 1685–1697.

Kebede, S., Travi, Y., Alemayehu, T., Ayenew, T., 2005. Groundwater recharge, circulation and geochemical evolution in the source region of the Blue Nile River, Ethiopia. Appl. Geochem. 20, 1658–1676.

Kebede, S., Travi, Y., Asrat, A., Alemayehu, T., Ayenew, T., Tessema, Z., 2007. Groundwater origin and flow along selected transects in Ethiopian rift volcanic aquifers. Hydrogeol. J. 16, 55.

Kebede, S., Travi, Y., Rozanski, K., 2009. The δ18O and δ2H enrichment of Ethiopian lakes. J. Hydrol. 365, 173–182.

Kebede, S., Travi, Y., Stadler, S., 2010b. Groundwaters of the Central Ethiopian Rift: diagnostic trends in trace elements, δ18O and major elements. Environ. Earth Sci. 61, 1641–1655.

Kebede, S.A., Tenalem, Umer, Mohammed, 2001. Application of isotope and water balance approaches for the study of the hydrogeological regime of the Bishoftu crater lakes, Ethiopia. Ethiopian Journal of Science 24, 151–166.

Kebede, T., Koeberl, C., 2003. Petrogenesis of A-type granitoids from the Wallagga area, western Ethiopia: constraints from mineralogy, bulk-rock chemistry, Nd and Sr isotopic compositions. Precambrian Res. 121, 1–24.

Kebede, T., Koeberl, C., Koller, F., 1999. Geology, geochemistry and petrogenesis of intrusive rocks of the Wallagga area, western Ethiopia. J. Afr. Earth Sci. 29, 715–734.

Kim, S.-T., Mucci, A., Taylor, B.E., 2007. Phosphoric acid fractionation factors for calcite and aragonite between 25 and 75 °C: Revisited. Chem. Geol. 246, 135–146.

LeGrande, A.N., Schmidt, G.A., 2009. Sources of Holocene variability of oxygen isotopes in paleoclimate archives. Clim. Past 5, 441–455.

Leng, M.J., Lamb, A.L., Lamb, H.F., Telford, R.J., 1999a. Palaeoclimatic implications of isotopic data from modern and early Holocene shells of the freshwater snail Melanoides tuberculata, from lakes in the Ethiopian Rift Valley. J. Paleolimnol. 21, 97–106.

Leng, M.J., Roberts, N., Reed, J.M., Sloane, H.J., 1999b. Late Quaternary palaeohydrology of the Konya Basin, Turkey, based on isotope studies of modern hydrology and lacustrine carbonates. J. Paleolimnol. 22 (2), 187–204.

Leng, M.J., Marshall, J.D., 2004. Palaeoclimate interpretation of stable isotope data from lake sediment archives. Quat. Sci. Rev. 23, 811–831.

Levin, N.E., Zipser, E.J., Cerling, T.E., 2009. Isotopic composition of waters from Ethiopia and Kenya: insights into moisture sources for eastern Africa. J. Geophys. Res. Atmos. 114.

Lowenstein, T.K., Risacher, F., 2009. Closed basin brine evolution and the influence of Ca–Cl inflow waters: death valley and bristol dry lake California, qaidam basin, China, and salar de Atacama, Chile. Aquat. Geochem. 15, 71–94.

McKenzie, J.M., Siegel, D.I., Patterson, W., McKenzie, D.J., 2001. A geochemical survey of spring water from the main Ethiopian rift valley, southern Ethiopia: implications for well-head protection. Hydrogeol. J. 9, 265–272.

Mechal, A., Birk, S., Dietzel, M., Leis, A., Winkler, G., Mogessie, A., Kebede, S., 2017. Groundwater flow dynamics in the complex aquifer system of Gidabo River Basin (Ethiopian Rift): a multi-proxy approach. Hydrogeol. J. 25, 519–538.

Meshesha, D., Shinjo, R., Matsumura, R., Chekol, T., 2011. Metasomatized lithospheric mantle beneath Turkana depression in southern Ethiopia (the East African Rift): geochemical and Sr–Nd–Pb isotopic characteristics. Contrib. Mineral. Petrol. 162, 889–907.

Meybeck, M., 1987. Global chemical weathering of surficial rocks estimated from river dissolved loads. Am. J. Sci. 287, 401–428.

Moulton, K.L., West, J., Berner, R.A., 2000. Solute flux and mineral mass balance approaches to the quantification of plant effects on silicate weathering. Am. J. Sci. 300, 539–570.

Mwakalila, S., Feyen, J., Wyseure, G., 2002. The influence of physical catchment properties on baseflow in semi-arid environments. J. Arid Environ. 52, 245–258.

Odada, E.O., 2001. Stable Isotopic Composition of East African Lake Waters. International Atomic Energy Agency (IAEA), pp. 43–48.

Otto-Bliesner, B.L., Russell, J.M., Clark, P.U., Liu, Z., Overpeck, J.T., Konecky, B., deMenocal, P., Nicholson, S.E., He, F., Lu, Z., 2014. Coherent changes of southeastern equatorial and northern African rainfall during the last deglaciation. Science 346, 1223–1227.

Rajmohan, N., Elango, L., 2004. Identification and evolution of hydrogeochemical processes in the groundwater environment in an area of the Palar and Cheyyar River Basins, Southern India. Environ. Geol. 46, 47–61.

Raymo, M.E., Ruddiman, W.F., Froelich, P.N., 1988. Influence of late Cenozoic mountain building on ocean geochemical cycles. Geology 16, 649–653.

Romaniello, S.J., Field, M.P., Smith, H.B., Gordon, G.W., Kim, M.H., Anbar, A.D., 2015. Fully automated chromatographic purification of Sr and Ca for isotopic analysis. J. Anal. Atomic Spectrom. 30, 1906–1912.

Schagerl, M., Renaut, R.W., 2016. Dipping into the soda lakes of East Africa. In: Schagerl, M. (Ed.), Soda Lakes of East Africa. Springer, Cham, Switzerland.

Schoell, M., Faber, E., Langguth, H., Pouchan, P., 1976. Survey on the isotopic composition of waters from NE Africa. Geologisches Jahrbuch. Reihe D, Mineralogie, Petrographie, Geochemie, Lagerstaettenkunde 197–213.

Segele, Z.T., Lamb, P.J., 2005. Characterization and variability of Kiremt rainy season over Ethiopia. Meteorol. Atmos. Phys. 89, 153–180.

Shinjo, R., Chekol, T., Meshesha, D., Itaya, T., Tatsumi, Y., 2011. Geochemistry and geochronology of the mafic lavas from the southeastern Ethiopian rift (the East African Rift System): assessment of models on magma sources, plume–lithosphere interaction and plume evolution. Contrib. Mineral. Petrol. 162, 209–230.

Skrzypek, G., Mydłowski, A., Dogramaci, S., Hedley, P., Gibson, J.J., Grierson, P.F., 2015. Estimation of evaporative loss based on the stable isotope composition of water using Hydrocalculator. J. Hydrol. 523, 781–789.

Spooner, E.T.C., 1976. The strontium isotopic composition of seawater, and seawater-oceanic crust interaction. Earth Planet Sci. Lett. 31 (1), 167–174.

Stewart, K., Rogers, N., 1996. Mantle plume and lithosphere contributions to basalts from southern Ethiopia. Earth Planet Sci. Lett. 139, 195–211.

Street-Perrott, F.A., Harrison, S.P., 1985. Lake level and climate Reconstructions. In: Hecht, A.D. (Ed.), Paleoclimate Analysis and Modeling. John Wiley and Sons, New York, pp. 291–340.

Talbot, M.R., Williams, M.A.J., Adamson, D.A., 2000. Strontium isotope evidence for late Pleistocene reestablishment of an integrated Nile drainage network. Geology 28, 343–346.

Teklay, M., Kröner, A., Mezger, K., Oberhänsli, R., 1998. Geochemistry, Pb-Pb single zircon ages and Nd-Sr isotope composition of Precambrian rocks from southern and eastern Ethiopia: implications for crustal evolution in East Africa. J. Afr. Earth Sci. 26, 207–227.

Tekleab, S., Wenninger, J., Uhlenbrook, S., 2014. Characterisation of stable isotopes to identify residence times and runoff components in two meso-scale catchments in the Abay/Upper Blue Nile basin, Ethiopia. Hydrol. Earth Syst. Sci. 18, 2415–2431.

Tenalem, A., Shimeles, F., Wisotzky, F., Demlie, M., Wohnlich, S., 2009. Hierarchical cluster analysis of hydrochemical data as a tool for assessing the evolution and dynamics of groundwater across the Ethiopia rift. Int. J. Phys. Sci. 4, 76–90.

Thieblemont, D., 2016. An Updated Geological Map of Africa at 1/10 000 000 Scale. 35th International Geological Congress : IGC 2016, Cape Town, South Africa.

Tierney, J.E., deMenocal, P.B., 2013. Abrupt shifts in horn of Africa hydroclimate since the last glacial maximum. Science 342, 843–846.

Trauth, M.H., Foerster, V., Junginger, A., Asrat, A., Lamb, H.F., Schaebitz, F., 2018. Abrupt or gradual? Change point analysis of the late Pleistocene–Holocene climate record from Chew Bahir, southern Ethiopia. Quaternary Research 90, 321–330.

Trauth, M.H., Maslin, M.A., Deino, A.L., Junginger, A., Lesoloyia, M., Odada, E.O., Olago, D.O., Olaka, L.A., Strecker, M.R., Tiedemann, R., 2010. Human evolution in a variable environment: the amplifier lakes of Eastern Africa. Quat. Sci. Rev. 29, 2981–2988.

van der Lubbe, H.J.L., Krause-Nehring, J., Junginger, A., Garcin, Y., Joordens, J.C.A., Davies, G.R., Beck, C., Feibel, C.S., Johnson, T.C., Vonhof, H.B., 2017. Gradual or abrupt? Changes in water source of lake Turkana (Kenya) during the african humid period inferred from Sr isotope ratios. Quat. Sci. Rev. 174, 1–12.

Viehberg, F.A., Just, J., Dean, J.R., Wagner, B., Franz, S.O., Klasen, N., Kleinen, T., Ludwig, P., Asrat, A., Lamb, H.F., Leng, M.J., Rethemeyer, J., Milodowski, A.E., Claussen, M., Schäbitz, F., 2018. Environmental change during MIS4 and MIS 3 opened corridors in the Horn of Africa for Homo sapiens expansion. Quat. Sci. Rev. 202, 139–153.

Vonhof, H.B., Joordens, J.C.A., Noback, M.L., van der Lubbe, J.H.J.L., Feibel, C.S., Kroon, D., 2013. Environmental and climatic control on seasonal stable isotope variation of freshwater molluscan bivalves in the Turkana Basin (Kenya).

Palaeogeogr. Palaeoclimatol. Palaeoecol. 383−384, 16−26.

West, A.J., Galy, A., Bickle, M., 2005. Tectonic and climatic controls on silicate weathering. Earth Planet Sci. Lett. 235, 211−228.

White, A.F., Brantley, S.L., 2003. The effect of time on the weathering of silicate minerals: why do weathering rates differ in the laboratory and field? Chem. Geol. 202, 479−506.

Williams, A.P., Funk, C., 2011. A westward extension of the warm pool leads to a westward extension of the Walker circulation, drying eastern Africa. Clim. Dynam. 37, 2417−2435.

Woldemariyam, F., Ayenew, T., 2016. Identification of hydrogeochemical processes in groundwater of Dawa River basin, southern Ethiopia. Environ. Monit. Assess. 188:8, 481.

Yitbarek, A., Razack, M., Ayenew, T., Zemedagegnehu, E., Azagegn, T., 2012. Hydrogeological and hydrochemical framework of Upper Awash River basin, Ethiopia: with special emphasis on inter-basins groundwater transfer between Blue Nile and Awash Rivers. J. Afr. Earth Sci. 65, 46−60.

Yuretich, R.F., Cerling, T.E., 1983. Hydrogeochemistry of Lake Turkana, Kenya: mass balance and mineral reactions in an alkaline lake. Geochem. Cosmochim. Acta 47, 1099−1109.

Appendix P5 – Buffering new risks? Environmental, social and economic changes in the Turkana Basin during and after the African Humid Period
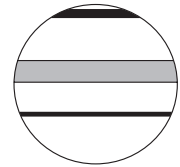
Buffering new risks? Environmental, social and economic changes in the Turkana Basin during and after the African Humid Period

Elisabeth Hildebrand,[1] Katherine M Grillo,[2] Kendra L Chritz,[3] Markus L Fischer,[4] Steven T Goldstein,[5] Anneke Janzen,[6] Annett Junginger,[4] Rahab N Kinyanjui,[7] Emmanuel Ndiema,[7] Elizabeth Sawchuk,[8] Amanuel Beyin[9] and Susan K Pfeiffer[10]

Abstract

This paper evaluates risk-oriented frameworks for explaining environmental, social, and economic changes faced by fishing and herding communities in the Turkana Basin during and after the African Humid Period (AHP, 15–5 ka). The orbitally-forced AHP created moist conditions, high lake levels, and unusual hydrological connections across much of northern and eastern Africa. As arid conditions set in and rainfall decreased between 5.3 and 3.9 ka in eastern Africa, Lake Turkana (NW Kenya) shrank dramatically. Shoreline retreat coincided with an expansion of open plains, creating new ecological conditions and potential opportunities for early herders in the basin. In this changing landscape, economies shifted from food procurement (fishing/hunting aquatic resources) to food production (herding), likely through both in-migration by pastoralists and adoption of herding by local fishers. Early pastoralists also built at least seven megalithic pillar sites that served as communal cemeteries during this time. Recent research has shown that local environmental dynamics – both during and after the AHP – were complex, demanding a more careful interrogation of the notion that post-AHP life entailed new and/or heightened risks. Risk-buffering strategies might include mobility, diversification, physical storage, and exchange. Archaeologists working around Lake Turkana have proposed that economic shifts from fishing to pastoralism entailed increased mobility as a risk-buffering strategy to deal with aridity and resource unpredictability, and that pillar sites – as fixed landmarks in an unstable landscape – provided settings for congregation and exchange amongst increasingly mobile herding communities. However, recent research has shown that local environmental dynamics in the Lake Turkana basin – both during and after the AHP – were more complex than previously thought, necessitating re-evaluation of the notion that post-AHP life entailed new and/or heightened risks. Here, we explore risk buffering strategies (e.g. mobility, diversification, physical storage and/or exchange) as only one category of potential explanation for the new social practices observed in the region at this time. Gauging their applicability requires us to (a) assess the spatial mobility of communities and individuals interred at pillar sites; (b) evaluate whether and how mobility strategies may have changed as pastoralism supplanted fishing; and (c) examine alternative explanations for social and economic changes.

Keywords

Africa, fisher-hunter-gatherer, Holocene, mobility, pastoralism, risk

Received 14 October 2021; revised manuscript accepted 30 July 2022

Introduction

In many parts of the world, scholars have viewed risk reduction as a potential motive for early food production, especially in temporally variable or unpredictable environments (Cohen, 2009; D'Alpoim Guedes, 2011; Peacock, 1998; Stein, 1989; Wetterstrom, 1993). This idea has been influential in Africa, particularly in areas where herding developed before farming (see reviews by Garcea, 2020; Gifford-Gonzalez, 2005; Lander and Russell, 2018; Lesur et al., 2014; Marshall et al., 2011). In an initial continent-wide synthesis, Marshall and Hildebrand (2002) used ethnoarchaeological examples to argue that the origins and spread of pastoralism came about through the desire to manage unpredictable resource access and achieve social and economic goals. Examining the "moving frontier" of pastoral spread through northern and eastern Africa, Sawchuk et al. (2018) suggested that commemorative practices among some early pastoral groups strengthened social networks in ways that would mediate challenges, uncertainties (and potential risks) of either bringing herds and people to a new area, or

[1]Stony Brook University, Stony Brook, NY, USA
[2]University of Florida, Gainesville, FL, USA
[3]University of British Columbia, Vancouver, BC, Canada
[4]University of Tubingen, Tubingen, Baden-Württemberg, Germany
[5]Max Planck Institute for the Science of Human History, Jena, Thüringen, Germany
[6]University of Tennessee-Knoxville, Knoxville, TN, USA
[7]National Museums of Kenya, Nairobi, Kenya
[8]University of Alberta, Edmonton, AB, Canada
[9]University of Louisville, Louisville, KY, USA
[10]University of Toronto, ON, Canada

*Steven T Goldstein is now affiliated to University of Pittsburgh, Pittsburgh, PA, USA and Elizabeth Sawchuk is now affiliated to Cleveland Museum of Natural History, Cleveland, OH, USA

Corresponding author:
Elisabeth Hildebrand, Social & Behavioral Sciences (SBS), Stony Brook University, Room 501-South, Stony Brook 11794-4364, USA.
Email: elisabeth.hildebrand@stonybrook.edu
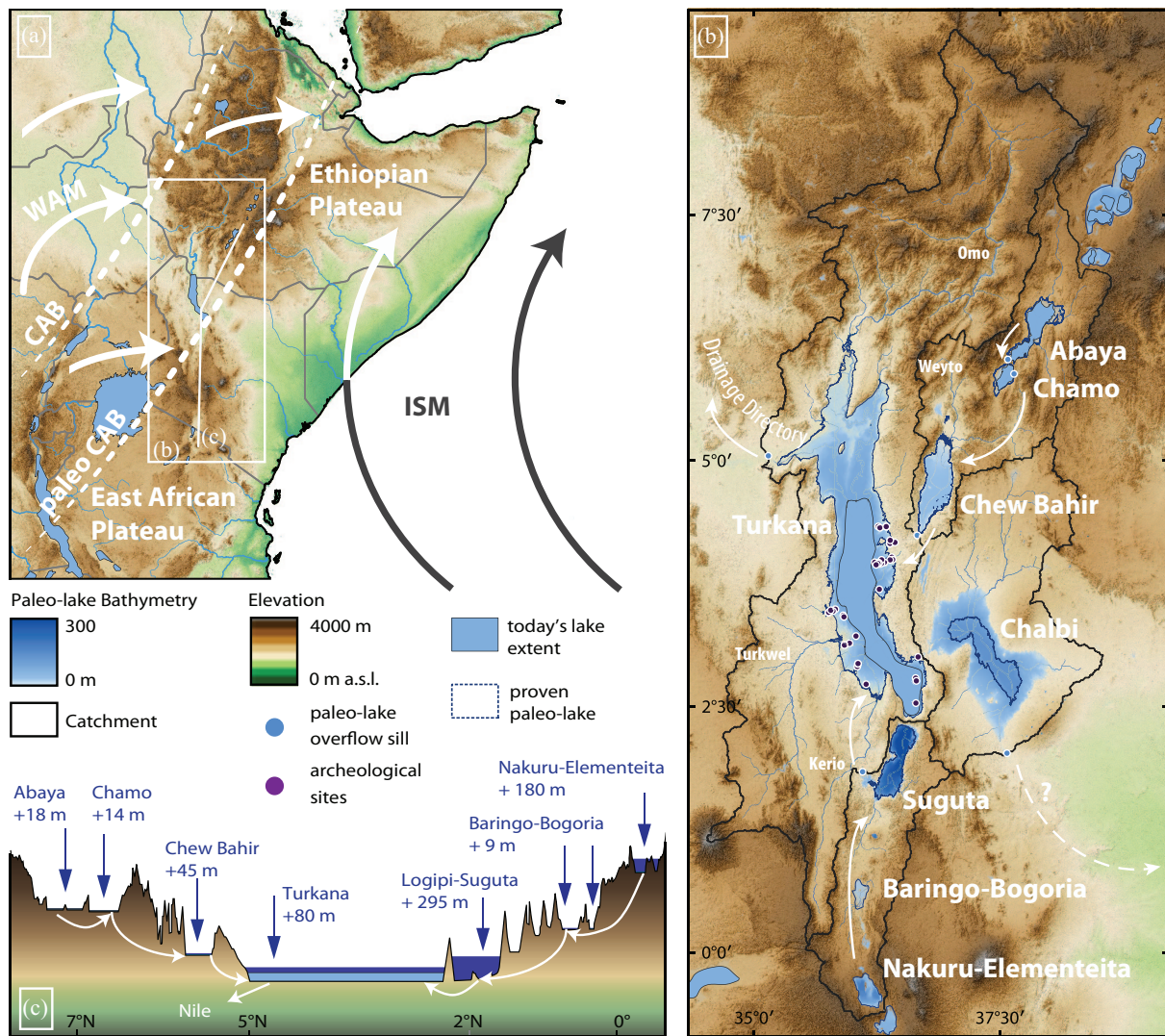
Figure 1. Topography, major wind trajectories, and outlines of modern-day lakes and paleo-lakes of eastern Africa. Dashed lines of paleo-lakes show proven maximum paleo-lake shores (Fischer et al., 2020; Junginger et al., 2014; and references therein), whereas "?" are paleo-lake outlines calculated using the QGIS 3.20 fill sink elevation: (a) topography of Eastern Africa with location of modern-day Congo Air Boundary (CAB) and presumed paleo-CAB. Trajectories of the West African Monsoon (WAM) and Indian Summer Monsoon (ISM) are shown as arrows, (b) topography of Lake Turkana's extended catchment during the AHP highstand, and (c) cross-section through the East African Rift System with all lakes that have overspilled to Lake Turkana during phases of maximum humidity during the AHP. Maps are based on OpenStreetMaps and SRTM.

incorporating animal husbandry into fishing-hunting-gathering economies. Marshall et al. (2011), noting different responses to different kinds of risk among contemporary pastoralists, modeled distinct environmental and social processes shaping the early stages of animal husbandry in northern versus southern Kenya. All of these works rest on an implicit assumption that humans perceive risk (defined here as unpredictable hazards and/or resource scarcities) in similar, generalizable ways. However, ethnographic records (reviewed in the next section) attest to a wide variety of views on what constitutes risk, what nature or severity of threat it poses, and what behaviors or strategies are appropriate to either mitigate or counter it, depending on local environments, economic orientations, and cultural beliefs. Because local environmental conditions and historical contingencies surely shaped early pastoralists' experiences and decisions, motives for socio-economic changes must be evaluated locally. Here, we use the Turkana Basin in eastern Africa (Figure 1) as a case study for reevaluating relationships between risk management and the spread of pastoralism in Africa, broadly.

For decades, risk has figured in discussions of early pastoralism in eastern Africa, with increasing recognition of the region's

unique environmental and social history (Chritz et al., 2019; Gifford-Gonzalez, 1998, 2000). First, eastern African rainfall patterns and vegetation would have been distinct from those in the potential source areas where pastoralism was practiced previously (Sudan, Ethiopia). Second, the earliest herding in NW Kenya coincided with the end of the African Humid Period (AHP, ca. 15–5 ka; all ages in this paper are in ka cal BP), with recession of Lake Turkana and neighboring lakes, alongside new vegetation and faunal composition 5–4 ka (Barker et al., 2004; Bloszies et al., 2015; Costa et al., 2014; Foerster et al., 2012; Garcin et al., 2012; Junginger and Trauth, 2013). However, this correlation does not prove that increasing aridity caused the spread of pastoralism; even if some kind of causality is established, its mechanisms are complex (pull vs push) and need not invoke risk as a motive. Third, the processes by which pastoralism spread are not yet clear: immigrant pastoralists presumably brought livestock, and at this time the Turkana Basin sees dramatic new patterns of ceramic and lithic production, burial traditions, and construction of monumental architecture (Goldstein, 2019; Grillo et al., 2022; Hildebrand et al., 2018; Keding, 2017). However, biodistance

analyses based on dental morphology are inconsistent with a major population replacement of forager communities by incoming herders (Sawchuk, 2017), so early pastoralism around Lake Turkana likely entailed both migration of people and diffusion of livestock and knowledge.

Deeper theoretical engagement, and new paleoenvironmental and archaeological data call for a critical evaluation of the idea that risk (or the desire to manage it) was a likely factor shaping profound economic and social changes around Lake Turkana c. 5–4 ka. A risk-centered interpretation of these changes runs as follows: if one supposes that AHP fishing-hunting-gathering (FHG) groups had a fairly secure existence living with low mobility near productive, predictable fishing grounds, then aridification and lake recession could have made FHG economies more unpredictable (and risky). In this situation, pastoralism would have entailed or allowed a more mobile existence, helping groups accommodate fluctuations in rainfall, depleted fishing, and geographic unpredictability of pasture and terrestrial plant and animal resources. Activities related to the construction and use of pillar sites could have drawn dispersed populations together often enough to exchange information and strategize actions that would reduce economic risks overall. This interpretive framework implies that mobility, herding, and pillar sites all constitute adaptations to heightened risks of the newly arid post-AHP world and dovetails neatly with Halstead and O'Shea's (1989) suggestion that mobility is a prime way to counter risk. However, many elements within it rely on unproven assumptions and shaky causal relations.

Other motivating factors may have been in play. For example, over time newly exposed plains by the retreating lakeshore could have offered prime pasture for incoming pastoralists, or herders could have been attracted by the opportunity to broaden their economy by incorporating fishing, or populations of fishers and herders may have realized that economic symbiosis might be beneficial to both. Some of these potential explanations also involve environmental changes and economic decisions, but the risk calculations involve different factors.

Over the past five decades, archaeology has undergone successive waves of enthusiasm for interpreting the impacts of climate change on human societies, the impacts of humans on the environments around them, and (most recently) the development of two-way human-environment relations (reviewed in Contreras, 2017). Contreras points out that all such studies have faced the same fundamental difficulties: paleoenvironmental and archaeological data may be collected at different spatial and temporal scales, chronological precision may be insufficient to establish true correlation, and causal mechanisms may not be clear. This is true in our own study area and period. In terms of scale, we are only beginning to understand the local environmental effects of NW Kenya's dramatic humid-to-arid transition in climate, and the economic ramifications for FHG communities. In terms of chronological precision, the dates of pastoral beginnings are still too vague to determine their exact relation to falling lake levels and vegetation changes. In terms of mechanisms, several aspects are uncertain beyond the population relations described above: pastoralism was spreading from areas that underwent post-AHP aridification slightly earlier, so that any in-migrating pastoralist groups may have had prior experiences with these phenomena. In addition, our understanding of how communities would perceive risk, and act upon those perceptions, remains elusive.

To revisit/revise explanations of early food production in NW Kenya, and build upon Marshall et al. (2011)'s perspectives on pastoral risk with Contreras's (2017) caveats in mind, we offer new comparative perspectives on risks that people living around Lake Turkana may have faced during and after the AHP. First, we turn to ethnographic and historic records to better understand how people in FHG and pastoralist groups may respond to environmental and economic risks. Second, we present new paleoclimate and paleoenvironmental data to evaluate risks that FHG groups might have faced during the AHP around Lake Turkana and neighboring basins of Chew Bahir and Suguta. We offer a brief synthesis of AHP archaeological sites to help discern how FHG groups positioned themselves on the landscape, and we assess the utility of existing data on early pastoralists. Finally, we consider the challenges of scale, precision, and mechanism as they apply to our current knowledge.

Understanding risk in fishing-hunting-gathering and pastoral economies

Foreshadowed by individual studies (e.g. Wiessner, 1982), Halstead and O'Shea (1989) launched a conversation about risk and uncertainty that has contributed valuable insights over the past three decades. This work directed archaeologists to examine not just average conditions and normative behaviors, but spatial and temporal variations in resource availability that could stimulate novel strategies. Their definitions of risk-buffering mechanisms – mobility, diversification, physical storage, and exchange (Halstead and O'Shea, 1989) – catalyzed new efforts to identify and explain these behaviors in the archaeological record. Since then, discussions of risk have continued in both archaeology and human ecology (e.g. Bliege Bird et al., 2002; Cashdan, 1990; Halstead and Jones, 1989; Miller et al., 2011; Strawhacker et al., 2020; Winterhalder, 2007; Zavodny et al., 2017).

Most archaeological discussions of risk and uncertainty have concerned either farmers or hunter-gatherer groups focusing on terrestrial resources, rather than pastoralist or FHG societies. These perspectives emphasize storage, sharing, and intensification of use or processing, rather than mobility (but see Marshall et al., 2011; Moore, 2011) as potential risk buffering mechanisms. Northwest Kenya offers the opportunity to make an explicit comparison of risk across the transition – from FHG to pastoralism – between two economic systems that have seen less attention, and unpack the variables necessary to evaluate mobility as a potential buffering mechanism in each economy. Ethnographic and ethnoarchaeological data demonstrate how FGH and pastoralist groups might experience, conceptualize, and respond to risk in different ways than farmers and terrestrial hunter-gatherers. By presenting these perspectives, and engaging with nuanced definitions of mobility in recent studies of contemporary pastoralists, we are not claiming specific, direct historical analogies between any ethnographic sources and archaeological subjects (*sensu* Wylie, 1985). Rather, we seek to situate the discussion of risk in the eastern African Holocene within a frame that explicitly acknowledges factors relevant to fishing and pastoral economies.

Considering risk in FHG economies

Archaeologists have long recognized that economies with a special focus on aquatic resources-be they FHG groups during the AHP, Mesolithic fisher – foragers of northern Europe, or various "shell mound" groups in the Americas – are distinct from those based primarily on terrestrial resources (e.g. Boethius et al., 2020; Fischer et al., 2007; Gaspar et al., 2011; Maritan et al., 2018; Marquardt and Watson, 2005; McQuade and O'Donnell, 2007; Richards and Schulting, 2006; Robson and Ritchie, 2019; Sutton, 1977). It follows that such groups may experience and perceive risk in ways that are linked to distinctive aspects of their environments' physiography and seasonality, and their technological repertoires and systems of social organization. Around Lake Turkana, the ethnographic record furnishes important analogs when considering fishing practices by FHG societies during the African Humid Period and earlier periods (Gifford-Gonzalez et al., 1999; Smith, 2018).

Relatively little information is available about historic mobility and settlement patterns by contemporary FHG peoples or peoples whose pastoralist economies include fishing components. Derbyshire (2019) describes numerous and longstanding Turkana fishing communities on the western lakeshore and their preference (*contra* development schemes) for impermanent and moveable settlements/structures. Along the northeast lakeshore, prior to the mid-1970s, men from specialist groups within Dassanach agropastoralist societies moved within an ~80 km stretch to fish and hunt while family members stayed in Ethiopian farming settlements. Stewart and Gifford-Gonzalez (1994) note their creation of both long- and short-term base camps, fish processing camps, and fish waste discard sites. El-molo FHG communities today live in two permanent villages on the southeastern shores of Lake Turkana, but previously lived in smaller and more widespread settlements on the northern, eastern, and southern edges of Lake Turkana and on its islands (Dyson and Fuchs, 1937; Kiura, 2005a, 2005b; Sobania, 1988; Vagnby and Jacobs, 1974).

Stewart (1989: 70–77) and Smith (2018) emphasize the significance of certain habitats at specific times of year: deep-water river mouths early in the rainy season, receding waters as the wet season ends, shallow basins where fish may be easy targets (e.g. Ferguson's Gulf in Turkana today) and deltas with slow, narrow channels (e.g. the Kerio Delta in Turkana today). Smith's interviews reveal Turkana fishermen's rich knowledge of different implements and multiple potential fishing sites that could be used in different seasons or depending on particular weather developments. Gifford-Gonzalez et al. (1999) note variable yields from day to day and depending on habitat and target species. Scherer (1978: 65–77) describes working groups of different sizes and gender compositions among El-molo, conducting spear-fishing (individual men), net fishing (large group of women, arranging their individual nets in a series and helped by small children), and spear or harpoon hunting of crocodiles and hippos (groups of 2–4 men). Other methods employed by contemporary fishing communities around Lake Turkana include the construction of weirs and the use of both thrust/drag and stationary baskets (Scherer, 1978: 66–70).

Although contemporary methods in fishing and aquatic hunting likely differ from AHP practices in many ways, they impart several important lessons. First, some forms of mobility are likely to have been central to the AHP FHG economic strategy, even within routine seasonal and interannual patterns of rainfall and water body flow. Second, AHP fishing groups likely had a repertoire of technologies that could be deployed in diverse locations along lakeshores, rivers, and deltas, potentially insulating groups from risks that would accrue if they focused on a single method, place, or habitat. Third, the specifics of contemporary fishing practices reveal ways in which unusually rapid changes in lake level – or even more subtle changes in seasonality of rainfall and water movement through rivers into lakes – could have made fishing systems less predictable, introducing new risks and opportunities as bays dried or filled, river deltas moved, and flooding or spawning times shifted.

A fourth insight arises from Derbyshire's (2019) observation that – *contra* ethnographic accounts emphasizing the pastoral elements of their economy – Turkana people living in shoreline communities have been involved in fishing for more than a century. Oral histories and linguistics place the origins of the Turkana ethnic group in eastern Uganda and South Sudan, far from the lake; oral accounts describe not a simple history of migration but a complex tapestry of movements, fusion with/separation from other groups, and economic adjustments to changing social, political, and environmental circumstances (Lamphear, 1988). Despite their notional roots elsewhere and the high value placed on animal husbandry, a substantial subset of the emerging Turkana ethnic group has gravitated to the shore and become expert in fishing technologies suitable for Rift lake environments. Similarly, pastoralist Dassanach groups on the eastern side of the lake have long included fishing communities (Gifford-Gonzalez et al., 1999; Sobania, 1988). Histories for other pastoralist groups such as Samburu echo some of these notes, recounting periods when herders suffered crises and livestock losses, moved to the lake, and merged (at least temporarily) with local fishing groups such as El-molo (Sobania, 1988). Together, these histories provide valuable alternatives to the idea that people turned to herding as a way to mitigate risks in fishing at the end of the AHP; it is equally plausible that herders, encountering many obstacles in a new and rapidly changing environment, found their way to the lakeshore with some livestock and joined forces with local fishers to invent a new livelihood, retaining some cultural features from both groups. Derbyshire (2021: 5; see also Derbyshire et al., 2021) and Lane (2013) both note that archaeological and historical records attest to considerable fluidity in social identities and economic foci since the advent of pastoralism in eastern Africa 5000 years ago.

Risk perception and strategic action in pastoral economic contexts

Risks faced by pastoral communities have been studied in a wide array of environments and from a variety of disciplinary standpoints within and outside of anthropology. Reviewing this work, Bollig and Göbel (1997) describe the singular constraints and opportunities of animal husbandry. They identify risks related to droughts (of variable duration), diseases (of variable contagion and morbidity), demographic growth pressures/demands, and degree of involvement in capitalist economic systems. They also emphasize the need to distinguish between different scales of risk (i.e. individual/family vs larger groups). Compared to other subsistence economies, pastoral advantages include mobility, both in terms of the ability to easily move to prime areas or away from difficulties (*contra* farmers), and the possession of resources that can move themselves (*contra* hunter-gatherers); the variety of pastoral products (meat, dairy, leather, dung, and possibly horn/antler); and rapid growth and reproduction of livestock under optimal conditions. Disadvantages include potential catastrophic losses during epidemics and droughts, and biological constraints on reproduction (animal and human) that delay recovery from these crises. These insights, and other observations by McCabe (1997), White (1997), Van Dijk (1997), and Mace and Sear (1997) in Africa and others on other continents, reveal fundamental differences in how pastoralists experience risk in comparison to people following other economic strategies.

Longstanding models of pastoralist behavior emphasized equilibrium dynamics, in which herders presumably maintain stable numbers of livestock below "carrying capacities" for rangeland ecosystems (see Galaty and Johnson, 1990). Scholars now favor disequilibrium (nonequilibrium) frameworks for understanding the ecology of pastoralism in arid and semi-arid environments, acknowledging relatively predictable, unavoidable droughts that periodically decimate livestock holdings (Behnke and Scoones, 1993; Ellis and Swift, 1988; see also McCabe, 2021). Herders plan for these droughts and manage livestock accordingly, typically by emphasizing responsive, flexible patterns of mobility and building livestock redundancy into the system. A synthesis by Roe et al. (1998) reconsiders "risk" as understood by pastoralists managing herds as part of disequilibrial systems, and notes that rather than trying to avoid hazards altogether they instead aim to avoid systemic failures by proactively planning and improving response, as Turkana pastoralists do routinely today (see McCabe, 2004). The long-term resilience of pastoralist systems, as discussed by Wright (2019), depends entirely on their adaptive capacity for withstanding these risks.

Using contemporary ethnographic and ecological research to build models for the behavior of early pastoralists across eastern Africa is notably fraught, because today, livestock holdings include camels, and herders are well-integrated into market systems. Also, it is well documented that the predictability of key resources in Kenya can change even within a few decades due to social or environmental factors. Boles et al. (2019) and McCabe (1997) describe several cases in which predictable environments have suddenly transformed, for example, due to causes such as government-imposed circumscription of movements and prohibitions on controlled pasture burning. Although environmental conditions are far drier today than they were 5000 years ago, it remains unclear how predictable or unpredictable resources would have been in the past. This returns us to Contreras's (2017) concerns about temporal precision – *How (un)predictable were the environments in Turkana during the exact time that herding began?* – and about mechanisms of change – *Were the main agents of early animal husbandry around Lake Turkana incoming pastoralists, local FHG groups, or a combination of the two? And what were their primary motives?* Although answers to these questions are not yet firmly in hand, recent paleoenvironmental research has helped delineate the nature of unpredictability during and just after the AHP, putting us in a better position to interrogate and build upon existing archaeological data.

Evaluating relations between mobility, risk, and reliability

Mobility has long been conceptualized in binary terms (i.e. "sedentary" vs "mobile") or as a spectrum (from "sedentary" to "highly mobile"). Today, multi-scalar reckonings of mobility within and beyond Africa acknowledge the universality of movement – of people(s), their ideas, and their material cultures. Scholars emphasize its centrality to individuals' daily lives and to social groups' uses of landscapes (Antonites and Ashley, 2016; Honeychurch, 2015; Kahn, 2013; Salazar and Smart, 2011; Ventresca Miller and Makarewicz, 2017; Whallon, 2006). Ethnographic and historical records for pastoral societies throughout eastern Africa (e.g. Dyson-Hudson and Dyson-Hudson, 1980; Pas Schrijver, 2019; Western and Dunne, 1979), including extensive ethnographic work among contemporary pastoralists living in the Turkana Basin (e.g. Little and Leslie, 1999; McCabe, 2004; McCabe et al., 1999; Sobania, 2011), attest to mobility's centrality to pastoralist lifeways, as structured by settlement needs, grazing requirements for livestock, and other factors.

These studies demonstrate diverse mobility systems among eastern African pastoralists, including seasonal, but flexible, strategies in which houses and households or partial households move periodically (or as needed) to accommodate arid, unpredictable, or changing environments (Behnke and Scoones, 1993; Homewood, 2008). Cattle, sheep, goats, and donkeys have various needs for pasture, water, and salt, and patterns of livestock mobility (i.e. grazing decisions) are structured by numerous factors including distribution of those resources across dry- and rainy-season landscapes, herd sizes, settlement densities, etc. (see Coppolillo, 2000). Residential mobility is particularly crucial during dry seasons and drought situations because relocating entire households or sending individuals who guard cattle to temporary camps near preferential niche pastures can reduce strain on both herders and livestock (Butt, 2010; Butt et al., 2009). Logistical movement of cattle is also a common response to heightened risks of raiding and/or conflict (Kaimba et al., 2011). It can accompany fluid aggregation and disaggregation of households as circumstances permit (Pike, 2004).

These perspectives reframe Halstead and O'Shea (1989)'s view of mobility as a possible response to risk and/or uncertainty. In pastoral societies, mobility is much more than a response to

risk: it is a fundamental element of the food production system. A wide array of factors may shape decisions about moving people and herds. Scholars trying to discern motives for an economic shift to pastoralism therefore face equifinalities. For example, FHG groups adopting pastoralism could have been countering risk through diversification (broadening their subsistence base to include domestic animals), or through mobility (focusing on resources that can be moved across an unpredictable landscape) – either of which might require or prompt reconfigurations of other social practices as well. At the same time, any pastoralists migrating into northwest Kenya from nearby areas may have had to adjust their mobility strategies to meet new or rapidly changing environments around Lake Turkana. To understand these changes, and the AHP conditions that preceded them, we now turn to climate and environmental records.

Climate and ecology records during and after the AHP

The AHP saw abrupt, pronounced lake level rises in most of northern and eastern Africa following a 20%–45% increase in precipitation due to a northern hemisphere insolation maximum (Barker et al., 2004; DeMenocal et al., 2000; Fischer et al., 2020; Junginger and Trauth, 2013). However, recent studies of lake sediments and strandlines have shown that AHP climatic conditions varied diachronically and geographically (Grant et al., 2017; Shanahan et al., 2015). Quantities and seasonality of precipitation in different areas would have been governed by both insolation effects on monsoon strength, and lateral shifts in the Congo Air Boundary (Junginger and Trauth, 2013). Paleoenvironmental indicators, including isotopic records showing regional and local changes in vegetation, cast the major transition to dry conditions at ~5 ka in a new light, and force a reconsideration of how changes in precipitation and environments might have presented challenges and opportunities to FHG communities and early pastoralists at various times and places.

Lake sediments

Lake sediments provide valuable tools for reconstructing past lake levels, water chemistry, and hydrological connections. Strand lines (wave cut notches, beach berms or shell beds) indicate past lake level elevations. Microfossils (e.g. ostracods, diatoms) support evaluation of lake water chemistries. Fish bones and biogenic carbonates can be used to infer the evaporative status via $\delta^{18}O$, and $^{87}Sr/^{86}Sr$ analyses can indicate water provenance and past hydrological connections. Pollen, phytoliths and leaf waxes preserved in lake sediments give insights into local and regional vegetation. Together, these proxies provide a basis for developing Lake Balance Models (LBM) and scenarios for past climate change.

Geochronology of lake sediments poses several challenges. Erosion of exposed sediments can displace evidence, and shoreline elevation reconstructions can vary due to measurement devices and/or isostatic rebound (Garcin et al., 2009; Melnick et al., 2012). Diverse processes can produce "reservoir effects": carbonates in lake sediments may yield dates that are too old, either due to inputs from old carbonate rocks in the catchment or hydrothermal activity. A study at Lake Asal has dated living snails to 2.2–1.7 ka (Gasse and Fontes, 1989). Parallel dating studies have shown age differences of 500-1500 years (Lake Abiyata: organic versus inorganic matter, see Gibert et al., 1999), and 1700-2200 years (Suguta: charcoal vs gastropods; see Garcin et al., 2009; Junginger et al., 2014). Parallel radiocarbon measurements on different materials in Lake Turkana sediments showed that reservoir ages can vary over time, and different materials can bear different reservoir ages, for example, similar ages for

shorelines deposited and living gastropods (Beck et al., 2019; Garcin et al., 2012). Thus, records based solely on carbonate ages should be taken with caution, whereas radiocarbon ages from charcoal or terrestrial plants are more reliable.

Reservoir effects can hinder precise chronological comparisons between different lake records. However, scholars agree on the broad outlines of the AHP and are investigating its sub-regional expressions. Besides generally enhanced moisture availability, equatorial Eastern Africa likely received additional moisture through a third rainy season in August-September, when the Congo Air Boundary pushed farther eastward than it usually does today (Beck et al., 2019; Bloszies et al., 2015; Costa et al., 2014; Junginger and Trauth, 2013). Moisture from the Atlantic-derived West African monsoon was recycled through vegetation in the Congo Basin and reached the Suguta and southern Turkana catchment (Camberlin, 1997; Junginger and Trauth, 2013; Nicholson, 1996). Major drought events during the AHP correlate with cold spells in the Northern Hemisphere (e.g. the Younger Dryas, YD), and small-scale events likely relate to small-scale solar irradiation changes also observed in West African and Indian Monsoon domains (Gupta et al., 2003; Junginger et al., 2014; Neff et al., 2001; Stager et al., 2002; Weldeab et al., 2007). Below, we review the response time and magnitude of Paleolakes Suguta, Chew Bahir, and Turkana to small and larger drought events, which depend on lake depths, catchment size, and thus the amount of water needed to establish and/or maintain water levels through drought periods.

Paleolake Suguta. Paleolake Suguta (today saline Lake Logipi) has a catchment of 13,000 km[2] incorporating the East African Plateau region. During the AHP, water from Lakes Nakuru-Elementeita, Bogoria, and Baringo overflowed into the Suguta basin (Figure 1). The paleolake record is based on shoreline elevations measured with differential GPS, lake sediment investigations of gastropods, grain sizes, Total Organic Carbon (TOC) and C/N ratios, and LBM. The exact onset of the AHP is unclear but maximum shorelines ~13.9 ka indicate Suguta was then ~300 m deep and 2200 km[2] (Figure 2a). During the YD (12.8–11.6 ka) Suguta desiccated completely but high lake levels resumed ~11.6 ka. Amidst generally high lake levels during the AHP, sediments and strandlines record at least nine distinct regression episodes between 11 ka and 8.5 ka; Suguta dropped 90 and 150 m within <100 years. Its rapid, high-amplitude lake level fluctuations echo regional records: recessions correlate with short-term moisture reductions recorded in Kilimanjaro dust deposits, likely caused by brief changes in solar irradiation (Garcin et al., 2009; Junginger and Trauth, 2013; Junginger et al., 2014).

LBM suggests the Suguta catchment received 21%–26% more rainfall than today during the AHP. Suguta would have spilled over into the Kerio-Turkana catchment during highstand episodes. Suguta's middle Holocene recession and final desiccation began after 6.7 ka and took ~1700 years (Borchardt and Trauth, 2012; Junginger and Trauth, 2013).

Lake Chew Bahir. At the foothills of the Southern Ethiopian Plateau, the Chew Bahir (*Ch'ew Bahir* = Salt Sea in Amharic) basin today has a 20,650 km[2] catchment fed by the Weyto and Segan Rivers (Figure 1). During the AHP, Lakes Abaya and Chamo temporarily overflowed into this basin; by 240 years after AHP onset, Chew Bahir attained a >2500 km[2] surface area and 45 m depth, and overflowed into the Turkana Basin (Figure 2b). Chew Bahir lake level research combines concentration of Potassium (K) in the lake sediments and LBM. K changes in the sediments reflect authigenic clay alteration due to pH changes in lake waters and thus water levels (Foerster et al., 2018). LBM shows a dependency of input waters from Abaya/Chamo with 20 to 30% increased precipitation during highstand. Shallow lake

bathymetry makes Chew Bahir sensitive to even short-term moisture changes. It dried up quickly and often within a 50-year period at 13.2–11.7, 11–10.7, 9.8–9.0, 7.8–7.5, and 7.1–6.8 ka (Fischer et al., 2020). Beginning ~6 ka, Chew Bahir lake levels declined for 1000 years, including 14 short episodes where K records indicate complete desiccation (Fischer et al., 2020; Foerster et al., 2012, 2018; Trauth et al., 2018).

Lake Turkana. Lake Turkana's catchment (138,000 km[2]) includes both SW Ethiopia (Omo River) and western Kenya (Turkwel and Kerio Rivers). Today the Omo delivers the vast majority of incoming water, but during the AHP the Kerio and Turkwel made substantial contributions, and Suguta and Chew Bahir spillovers gave variable inputs. Lake Turkana rose >80 m above its present level and increased in surface area from 6500 km[2] toward >22,500 km[2], before overflowing into the Nile Basin (Bloszies et al., 2015; Garcin et al., 2009; Junginger and Trauth, 2013; van der Lubbe et al., 2017; Figure 2c). LBM suggests these changes required a 20% increase in moisture (Hastenrath and Kutzbach, 1983).

Several lake level investigations have integrated observations from many locations and prior publications. Perhaps due to different proxies and reservoir effect handling, they differ in some details but agree on fundamentals. At AHP onset it is unclear whether Lake Turkana started to rise from a + 50 m or + 20 m paleo-lake level (Figure 2c). Between at least four distinct spillover episodes, Turkana dropped by 20–80 m (Beck et al., 2019; Bloszies et al., 2015; Garcin et al., 2012).

Recession may have occurred in multiple stages, with scholars suggesting slightly different timing: Whereas Bloszies et al. (2015) suggest highstands persisted to 5.1 ka, followed by a rapid recession, Garcin et al. (2012) describe an initial drop to 15 m below spillover level 6.4–5.2 ka, followed by a dramatic drop of 50 m between 5.2 and 5.0 ka. The loss of spillover from Suguta and Chew Bahir likely contributed to Turkana's regression (Junginger and Trauth, 2013). Despite this, and noticeable shifts in Lake Turkana's outline as the AHP ended, strontium isotope ratios suggest water provenance changed only gradually (van der Lubbe et al., 2017). Shoreline elevations 4.5–1.5 ka are not well known, but thought to be lower than most prior recession episodes.

Botanical records

In addition to lake level records, isotopic records from sedimentary leaf waxes can reveal geographic and temporal variation beyond simple aridification as the AHP ended. Deuterium isotope values (δD) of leaf waxes can be used to reconstruct isotopic values of past precipitation. Similarly, stable carbon isotopes (δ^{13}C) of leaf waxes can show the relative contribution of C_3 (woody plants, shrubs and forbs) and C_4 (tropical lowland grasses) vegetation. Depending on sampling locations, records may reflect conditions aggregated across major parts of Lake Turkana's catchment (basinal scale), or more localized (sub-basinal) areas. Like the lake records described above, they reveal geographic and temporal variation beyond simple aridification as the AHP ended.

Leaf wax δD values correlate to precipitation values, but plant form imparts an isotopic fractionation which must be corrected for (Garcin et al., 2012; Sachse et al., 2006, 2012). Using leaf wax δD values in *n*-alkanoic acids in southern basin piston core sediment sequences (Morrissey, 2014), we can explore variations in paleo-precipitation: from ~12 ka to 6 ka, $δD_{precip}$ fluctuates between −20‰ and 20‰ (Figure 2d). Though values remain low relative to the rest of the sequence, significant and consistent δD enrichment indicates aridity from ~6 kya to the present (Figure 2d), following orbitally-mediated hydrological changes.
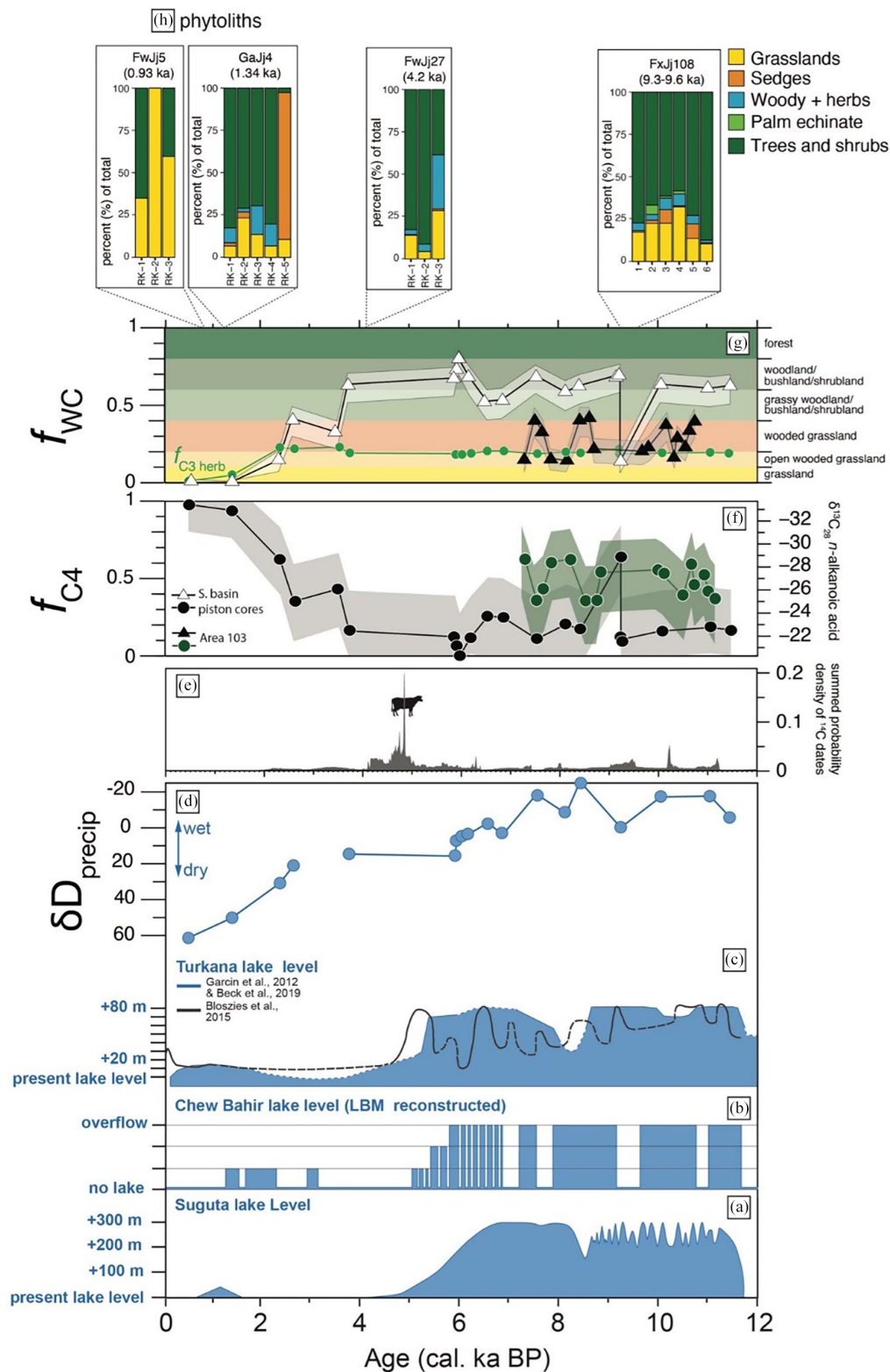
Figure 2. Paleoclimatic and paleoenvironmental records. (a–c) Lake level reconstructions for Suguta (a) (Junginger et al., 2014), Chew Bahir (b) (Fischer et al., 2020), Lake Turkana (c). (d) Leaf wax δD$_{precip}$ values calculated from leaf wax δD values from southern Turkana Basin piston core data. Precipitation δD was calculated by first estimating the apparent fractionation (ε$_{app}$) of deuterium by plant form using enrichment values and methods in Sachse et al. (2012). (e) Summed probability density (SPD) plot of dates from Holocene-aged Turkana archaeological sites (SI Table 2); cow denotes appearance of livestock in the archaeological record. SPD was created from probability densities of calibrated radiocarbon dates in R using the package "rcarbon" (Crema and Bevan, 2021). (f) Changing fractions of C$_4$ plants (f_{C4}) calculated from δ^{13}C$_{wax}$ values using a simple two-endmember linear mixing model with δ^{13}C$_{wax}$ values from modern African C$_3$ and C$_4$ plants (Garcin et al., 2014). Shading represents error in estimated f_{C4} due to natural variation in δ^{13}C$_{wax}$ values of endmembers. Leaf waxes were extracted from southern Turkana piston cores (black, Morrissey, 2014) and northern Turkana lacustrine sediments (green, Chritz et al., 2019). (g) Changing fractions of woody cover (f_{wc}) in leaf wax records from southern (white) and northern (black) Turkana Basin (SI Table 1). Estimated f_{wc} calculated from δ^{13}C$_{wax}$ values of modern African vegetation (Garcin et al., 2014). Due to a lack of *n*-alkanoic acid δ^{13}C values from modern vegetation, the closest *n*-alkane analog (C$_{29}$) was used. We then followed the methods of Magill et al. (2013) to estimate ε$_{C29-SOM}$ and calculate approximate δ^{13}C$_{29}$ values from δ^{13}C$_{SOM}$ to generate a sedimentary C$_{29}$ woody cover model using data from Cerling et al. (2011). The resulting equation relating sedimentary δ^{13}C$_{29}$ values to fraction woody cover is f_{wc} = (sin(-1.743693 - 0.085482 δ^{13}C$_{29}$))^2. (h). Representation of various plant types in phytolith assemblages from the east side of Lake Turkana (local & basinal inputs).

Leaf wax δ^{13}C records from northern (Area 103 sediments, 16 samples), and southern ends of Lake Turkana (piston cores, 21 samples) indicate variable responses to climatic changes (Figure 2f, SI Table 1; Chritz et al., 2019; Morrissey, 2014). Using a linear two-end member mixing model and C$_3$/C$_4$ endmember values from an Africa-wide dataset (Garcin et al., 2014), fraction C$_4$ (f_{C4}) contributions to sedimentary leaf waxes were calculated. In the north, where sediments were deposited quickly by the Omo River, C$_4$ plants' representation within the biomass fluctuated between 30% and 60% without any clear direction of change between 10.5 and 6 ka. Leaf wax records are unavailable for more recent periods, but pollen records from Core 8P in the north end of Lake Turkana show grass input fluctuating generally between 40% and 60% from 2.5 ka to recent times (Mohammed et al., 1996). In the south, deposition was slower and likely reflected conditions in the Turkwel and Kerio catchments; here, f_{C4} represented ≤20% of the contributing biomass 12–4 ka, and then increased to 100% from 4 ka to present (Figure 2f). Comparing northern and southern cores, it is clear that the two sub-areas of Lake Turkana's catchment experienced very distinct sequences of ecological change.

Woody cover is another dimension of the past environments people encountered that we can extract from δ^{13}C$_{wax}$ records. Fraction woody cover (f_{wc}) estimates were calculated using an arcsine squared model (Cerling et al., 2011), employing the Garcin et al. (2014) modern Africa wax dataset, and aligning these values to modern African woody cover models for soil organic matter (Cerling et al., 2011; Magill et al., 2013; Figure 2g). Though this woody cover model cannot distinguish between trees and shrubs (Cerling et al., 2011), f_{wc} estimates for Turkana allow us to use UNESCO biome classifications (White, 1983) to describe past environments. In Area 103, reconstructed f_{wc} indicates a wooded grassland to open wooded grassland environment for the northern Turkana catchment. Piston core data indicate that the southern Turkana catchment had a more wooded/bushy environment until 4 ka; following the appearance of herders (Figure 2e), the environment progressively opened and became a grassland by around 1.5 ka (Figure 2g).

Phytolith samples from archaeological sites can provide further insight in heterogeneous patterns of vegetation in the basin. East of Lake Turkana, phytoliths show vegetation structure changed through time: on the Karari Ridge, FxJj108 was wooded bushland with palm trees 9.6–9.3 ka. Near Ileret, vegetation at FwJj27 and FwJj5 shifted from more wooded to open wooded grasslands from 4.2 to 0.93 ka. At Koobi Fora, phytolith data from Dongondien (GaJi4) indicate grassy woodlands with significant presence of wetlands/swampy habitats (Kinyanjui, 2018) (Figure 2h).

Herbivore isotope records

Isotopic records from herbivore tooth enamel (SI Figure 1) have generated more local pictures of vegetative changes in NW Kenya, and support comparisons between lake-margin versus inland areas (see discussion in Chritz et al., 2019). Broadly, the representation of grazers in APP taxa (Artiodactyla, Perissodactyla, Proboscidea; following Cerling et al., 2015) from archaeological sites decreases over time. The representation of grazers at archaeological sites is >60% during the AHP (SI Figure 1). A suite of samples from the four AHP sites in and west of Lothagam give a granular depiction of local vegetation change: the Napudet Basin alternated between a shallow bay (highstands) and pasture for C$_4$ grazers (recessions) (Chritz et al., 2019). Post-AHP, tooth enamel isotopic records (c. 5–4 ka) are only available from adjacent archaeological sites Dongodien and GaJi2 on Koobi Fora Ridge, which would have formed a peninsula on Turkana's eastern shore as the lake was shrinking. These samples, from the earliest livestock in eastern Africa, show a shift to diets richer in C$_3$ resources (Chritz et al., 2019). Taken altogether these data, along with leaf wax based paleoenvironmental reconstructions (Figure 2f and g), show that even during the AHP when environments were predominantly woody/bushy/shrubby, landscapes held enough C$_4$ grasses to support large-bodied grazers. A significant expansion in C$_4$ grasses didn't occur until after herders had arrived in the basin.

Together, the records of lake levels, leaf waxes, phytoliths, and herbivore tooth isotopes all indicate considerable dynamism in climate and environment across the AHP and immediately thereafter. Recurring lake level fluctuations for Turkana, Suguta, and Chew Bahir would have made fishing less predictable at various points, necessitating flexible strategies in terms of both technology and mobility. Leaf wax isotopic records indicate vegetation fluctuations in the north end of the Turkana Basin, which would have affected terrestrial resources for HGF groups during the AHP. The transition to post-AHP conditions may have had multiple steps, with lake regressions occurring earlier and more dramatically than vegetation change. Here, however, we run into issues of scale: current leaf wax data indicate vegetation changes on sub-basinal scales, and lake level data reflect regional climate events that produced locally important changes in shorelines. Applying paleoenvironmental knowledge to the archaeological record also encounters issues of chronological precision and causality, as the next section will demonstrate.

The archaeological record

Archaeological expressions of human settlement episodes in the Turkana Basin 15–4 ka encompass a range of site types, from small scatters to localities with multiple phases of occupation and mortuary activities by FHG groups, and from ephemeral signs of pastoral occupation to communal cemeteries built for multi-generational use. Understanding of how these sites were situated on local landscapes is an essential foundation for discussing economic and social changes that may (or may not) be linked to risk/response.

Fisher-hunter-gatherers around Lake Turkana during the African Humid Period

Research beginning in the 1960s revealed numerous FHG sites around Lake Turkana (Table 1, Figure 3). AHP fishing sites produced barbed bone points and lithic assemblages rich in small or backed pieces; some, such as Lowasera and Lothagam-Lokam (hereafter referred to as Lokam), also had larger stone tools made from non-obsidian volcanics. A subset of sites had pottery (FxJj12N, GaJj12, GaJi3), some with decorations reminiscent of AHP sites near Khartoum (FxJj12N). This, along with barbed bone points, led scholars to include Turkana in syntheses postulating or critiquing the idea of broad cultural links across northern/eastern Africa (Holl, 2005; Keding, 2017; Sutton, 1977; see also Yellen, 1998). Dates for early-researched sites and localities (where available) are regarded as imprecise due to possible contamination (apatite) or reservoir effect (fish bone, shell) (see Collett and Robertshaw, 1983). Furthermore, many are from undated erosional contexts. Recent research has expanded the range of known sites and behaviors (Kokito, Dilit, Nataruk; see Beyin, 2021; Beyin et al., 2017; Mirazón Lahr et al., 2016a), and furnished more reliable dates for previously researched sites (Lothagam Lokam). Reliable dates, calibrations, and probability distributions appear in Table 2 and Figure 4; a comprehensive list of all dates appears in SI Table 2.

Turkana AHP sites are situated along elevated lakeshores (Wright et al., 2015), and often have barbed bone points indicative of aquatic pursuits. While many areas around Lake Turkana have not been systematically surveyed, both Barthelme (1981) and Beyin (Beyin, 2011; Beyin et al., 2017) covered substantial areas in diverse physiographic settings. Thus, careful comparison of AHP site contexts and use histories (Table 1) yields valuable perspectives. Most known AHP sites were located at the edge of protected bays or lagoons, near the mouths of local watercourses, and along peninsulas. Certain locations around the lake offered

Table 1. AHP fishing sites around Lake Turkana (clockwise from north end). Elevations (m above sea level) are in **bold** if a site has been georeferenced, and in *italic* if a site is not georeferenced but located precisely enough with respect to known landforms so that elevation data are likely to be within the range indicated. A * indicates that current site information is not precise enough to estimate elevation.

| Sites, elevations	Situation within local landscape during periods of occupation or use.	References
FxJj12: **435 m** FxJj12N: **448 m**	Paleobeaches 2 km east of the Kokoi Horst. During AHP, Kokoi landmass would have been an island or peninsula sheltering the channel or bays east of it from heavy wind and waves.	Barthelme (1985: 98–127)
GaJj1: **431 m** GaJj2: **431 m** GaJj12: **425 m**	Highstand beach on upper Koobi Fora Ridge, which would have protruded into Lake Turkana as a peninsula. Each of the three sites appears to cover a broad area and have multiple occupation horizons.	Barthelme (1985: 26–68; 86–97)
GaJi11: **433 m**	On SE slope of Koobi Fora ridge; would have overlooked enlarged Alia Bay during AHP. Barthelme suggests it represents an occupation/use of a near-shore *Etheria* reef/sandbar as a fishing station in a manner paralleling recent fishing practices of El Molo.	Barthelme (1985: 69–85)
GaJi3: **423 m**	Lower down in western Koobi Fora Ridge. Low density of artifacts interpreted as short occupational duration.	Barthelme (1985: 128–134)
Lowasera: **439 m**	East side of small paleo-inlet on NE corner of Alia Bay during AHP. Small water-course (usually dry today, likely active during AHP) enters the area from the NE.	Phillipson (1977)
Nataruk: **449 m**	Gently sloping lagoon. *In situ* human remains suggest local violent deaths occurred 10.5–9.5 ka. Nataruk's elevation suggests deposition during a modest regression phase.	Mirazón Lahr et al. (2016a, 2016b), Stojanowski et al. (2016)
Lothagam-Lokam: **455 m**	Locality >1 km² between two north-south volcanic ridges that together constituted a peninsula jutting into the AHP mega-lake. Beach deposits are in elevated areas at or near spillover elevations, with numerous concentrations of habitation and mortuary remains from c. 10 to 6 ka The shallow Napudet Bay lay <1 km to the west, over the lesser volcanic ridge.	Robbins (1967, 1972, 1974, 1980), Goldstein (2019) S/E
Zu-13 *	Site just SW of the main outcrop of the Napudet Hills, overlooking the Napudet Basin, which was a shallow bay during the AHP.	Robbins (1972) S
Bb-9, Zu-10, Zu-6, Zu-7, Sand Spit: *Napudet Basin elevations are 420–450 m asl.*	Sites at various elevations within the Napudet Basin/Bay, which was inundated and dried several times during the AHP. All sites would have been submerged during maximum transgression phases. Zu-6 has pottery with dotted wavy line motif; Bb9, Zu-6, and Zu-10 have human remains; at Zu-10 an arrow point was embedded in a human torso.	Robbins (1972, 1980), Phenice et al. (1980) S
Kokito 1: **447 m** Kokito 2: **437 m** Dilit: **450 m**	Inlet where lake waters intrude into gaps/valleys in the Losedok ridge system, near where a local stream/river would have entered the lake. Kokito 1 and 2 show occupations of near-highstand beaches during the early AHP by aceramic FHG groups with backed geometric tools and barbed bone points; occupations were ~13.5 ka and at times during the intervals 13.3–12.6 ka and 11.2–10.2 ka. Dilit (7.5 ka) had fauna, lithics, an ostrich eggshell (OES) bead, and non-diagnostic pottery.	Beyin et al. (2017), Prendergast and Beyin (2018), Beyin (2011, 2021) S/E

various combinations of terrestrial animal, plant, and aquatic resources at different times of year and under different climate conditions. Diversity in FHG site types appear to reflect the complexity of settlement systems that were developed to make use of these landscapes. Several sites/localities show evidence for multiple phases of occupation separated by centuries or millennia, indicating renewed use when lake levels and other conditions once again made an area particularly advantageous. As shorelines shifted during the AHP's transgressions and regressions, FHG groups necessarily relocated: some sites are located along highstand beaches, while others are at lower elevations. The notion of the AHP as a time of stasis and low risk can be rejected by a record of human responses to shifting shorelines. Fishing areas must have changed in depth or seasonality, grown, shifted, or disappeared, such that human groups would have had to make regular adjustments in settlement locations, mobility strategies, and fishing methods and tools.

Suggestions that FHG groups in riverine settings in the Sahara and Sudan "continually occupied the same sites for long periods of time throughout the year" (Garcea, 2006: 214) invite considerations of mobility among fishing groups around Lake Turkana. Stewart (1989: 76) contrasts riverine versus lakeshore

fishing: whereas rivers "provide directional movement and it is only a matter of devising appropriate implements to trap what flows past," shoreline fishing requires intimate knowledge of fish ecology and behavior, targeting waters that are shallow or receding. Around Lake Turkana, Stewart (1989: 160–168) distinguishes between the "selective fishing" (using spears or harpoons to hunt a few species of aquatic prey) demonstrated in assemblages from FHG sites near highstand elevation, and more diverse, less selective assemblages from GaJi3 and later occupational phases at Lokam and Lowasera, indicative of using weirs or ring nets. Given significant routine seasonal and year-to-year fluctuations in lake level (observed today, and likely in the past) all of the fishing methods described above – selective or not – would have required groups to shift their fishing areas, and possibly even site locations, multiple times per year. FHG groups living around Lake Turkana may have moved more often than the riverine peoples of the Sahara and Sudanese Nile.

Middle Holocene aridity and the advent of herding

Herding first appears in the Lake Turkana Basin in the mid-Holocene arid phase just after the AHP, ~5–4 ka. Distinct from
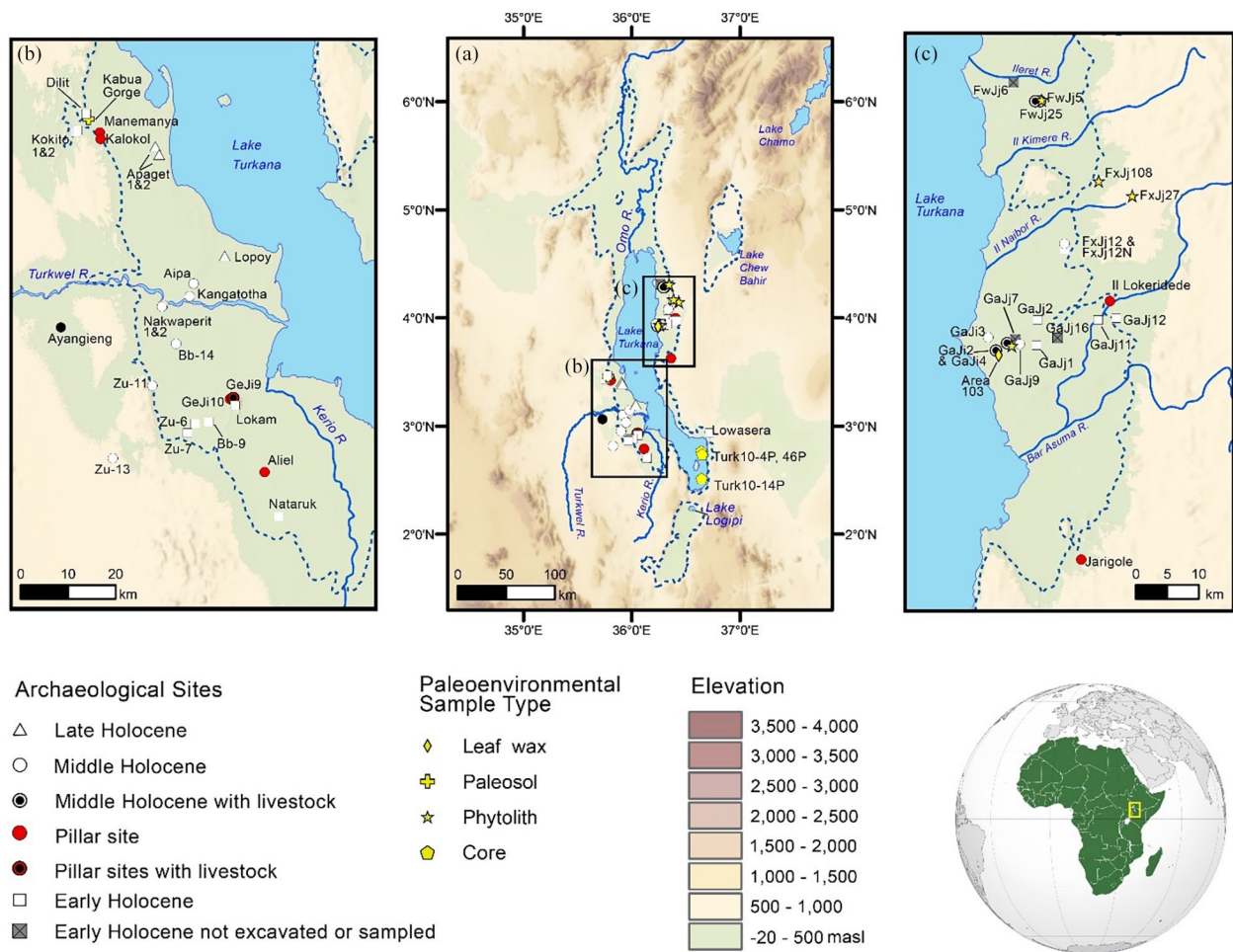
Figure 3. (a) Archaeological sites and paleoenvironmental sampling areas of the study area with respect to paleo-lakes as well as modern lakes and major rivers. (b) Detail of Lake Turkana's western shore near the Kerio and Turkwel River inputs. Note that sites Zu-6, 7, 11, and 13, as well as Bb-9 and Bb-14 (Robbins, 1972) cannot be reliably mapped using currently available information. (c) Detail of Lake Turkana's eastern shore from the Ileret to Bar Asuma River inputs.

preceding AHP industries, lithic technology associated with herding economies entailed a greater emphasis on a more uniform strategy of obsidian blade and bladelet production (Goldstein, 2019). Obsidian use by early herders was fairly localized but North Island sources required watercraft (Ndiema et al., 2010, 2011). Sand-tempered ceramics from this period, often highly decorated, represent the earliest known examples of Nderit tradition pottery, which later spread south to central Kenya and Tanzania (Grillo et al., 2022; Wandibba, 1980).

Most archaeological data for this period is from megalithic "pillar site" cemeteries, and must be interpreted through a mortuary lens with the appropriate caveats. At least seven pillar sites with megalithic basalt columns, elevated platforms, stone circles and/or cairns were constructed near Lake Turkana's 5 ka paleo-shoreline (Figure 3; SI Table 3; see also Githinji (1994), Grillo and Hildebrand (2013), Hildebrand et al. (2011, 2018), Hildebrand and Grillo (2012, in press); Koch et al. (2002), Nelson (1995), Sawchuk et al. (2018, 2019a, 2019b, in press); Wilshaw et al., 2016). At the six pillar sites that have seen excavation, charcoal and ostrich eggshell yielded secure dates between 5.3 and 4.3 ka; mortuary components include primary and sometimes secondary burials. At least two sites have revealed deliberately constructed mortuary cavities containing high densities of burials. Buried individuals span all ages and both sexes, often with highly individualized ornaments including various types of stone and ostrich eggshell beads, perforated animal teeth and hippo tusks,

ivory bangles and rings, and remnants of headpieces decorated with rodent teeth. At the seventh site (Aliel, unexcavated), a surface ceramic sample yielded a slightly earlier date. Nderit pottery is present at some pillar sites but not all. We have previously noted the absence of evidence for social stratification, and have suggested that communal cemeteries may have helped to unite otherwise dispersed herding groups inhabiting an unpredictable, changing landscape (Hildebrand et al., 2018; Sawchuk et al., 2018). While this interpretation remains plausible, current evidence from pillar site architecture, artifacts, and interred individuals cannot be tied back to their community's perceptions of risk or mobility patterns in an explicit fashion.

Few pastoral habitation sites have been located or excavated (Table 3). This limits our knowledge of settlement patterns and day-to-day life. Chronological ambiguities compound the challenge: early research at habitation sites yielded unreliable dates on bone, shell, and burned earth, and charcoal dates for Dongodien and GaJi2 are secure but have wide calibrated age ranges (Table 2; Figure 4; SI Table 2). Even if more secure dates are obtained, locational relationships between sites and contemporary lakeshores may remain imprecise because Lake Turkana receded so rapidly. All of these factors make it difficult, based on current data, to understand pastoral approaches to landscape use and mobility, assess the relative importance of fishing versus aquatic resources to groups in the immediate aftermath of the AHP, and gauge the degree to which people perceived their environments as risky.

Table 2. Reliable radiocarbon dates for early and middle Holocene archaeological sites around Lake Turkana. To be considered reliable, samples must be from charcoal or ostrich eggshell, and from an excavated (not surface) context. Probability distribution curves for radiocarbon dates presented in Table 2. Radiocarbon dates were calibrated in R using package "rcarbon" (Crema and Bevan, 2021). We used a 50/50 IntCal20 (Reimer et al., 2020) and SHCal20 (Hogg et al., 2020) mixed calibration curve. Probability distributions for these dates appear in Figure 4.

| Name	SASES	Site type	Lab #	Context	Material	14C date	Intcal20 median	Calibrated upper age limit (BP)	Calibrated lower age limit (BP)	References
Il Lokeridede	Gaji23	Pillar site	TO-4911	E121N111, 95–100 cm below datum	Charcoal	4180 ± 60	4693	4841	4526	Koch et al. (2002), Koch (1994); Koch pers. comm
Jarigole	Gbjjl	Pillar site	AA85132	Upper cap fill	OES bead	4251 ± 39	4749	4865	4618	Hildebrand and Grillo (2012)
Jarigole	Gbjjl	Pillar site	AA85131	Intermediate cap fill	OES bead	4381 ± 39	4932	5206	4843	Hildebrand and Grillo (2012)
Jarigole	Gbjjl	Pillar site	AA85133	Intermediate cap fill	OES bead	4401 ± 39	4949	5263	4849	Hildebrand and Grillo (2012)
Jarigole	Gbjjl	Pillar site	AA85134	Lower cap fill	OES bead	5156 ± 60	5883	6163	5720	Hildebrand and Grillo (2012)
Aliel	None	Pillar site	Beta-447866	Dated sherd is from surface	Pottery bulk organics	4490 ± 30	5153	5290	4975	Hildebrand and Grillo (2012)
Lothagam West	Gejil0	Pillar site	ISGS-A1494	Center of platform near top of burial pit	Charcoal	4290 ± 20	4845	4869	4737	Hildebrand et al. (2011)
Lothagam North	Gejl9	Pillar site	ISGS-A2624	Far west platform (beyond edge of mortuary cavity); ashy area at base of platform	Charcoal	4280 ± 15	4842	4862	4738	Hildebrand et al. (2018)
Lothagam North	Gejl9	Pillar site	ISGS-A3792	Cap deposits above western edge of mortuary cavity	OES bead	3845 ± 20	4216	4396	4097	Hildebrand et al. (2018)
Lothagam North	Gejl9	Pillar site	ISGS-A3793	Amidst cluster of perforated hippo tusks capping Bundle Burial B26B/C/D, near base and western edge of mortuary cavity	Charcoal	4135 ± 20	4643	4814	4526	Hildebrand et al. (2018)
Lothagam North	Gejl9	Pillar site	ISGS-A1505	Central platform, cap deposits	OES bead	4165 ± 20	4692	4823	4575	Hildebrand and Grillo (2012)
Lothagam North	Gejl9	Pillar site	ISGS-A1492	Central platform, base of cap/top of mortuary cavity	OES bead	4265 ± 15	4836	4859	4658	Hildebrand et al. (2011)
Lothagam North	Gejl9	Pillar site	ISGS-A2625	Central platform, within mortuary cavity near Burial B2	Charcoal	4140 ± 20	4655	4815	4528	Hildebrand et al. (2018)
Lothagam North	Gejl9	Pillar site	ISGS-A1491	Eastern platform, top of pebble-rich layer between surface and stone pavement	OES bead	4385 ± 15	4922	5027	4859	Hildebrand et al. (2011)
Lothagam North	Gejl9	Pillar site	ISGS-A2649	Pit in stone circle	OES frag	4240 ± 20	4748	4851	4648	Hildebrand et al. (2018)
Kalokol	Gcjh3	Pillar site	ISGS-A1493	Central platform, fill below/adjacent to pillar area	OES frag	3890 ± 15	4310	4409	4161	Hildebrand et al. (2011)
Manemanya	Gcjh5	Pillar site	ISGS-A1504	Platform cap fill	OES bead	4255 ± 20	4829	4857	4653	Hildebrand and Grillo (2012)
Manemanya	Gcjh5	Pillar site	ISGS-A1490	Platform just above burial (B2)	OES bead	3805 ± 15	4168	4239	4090	Hildebrand et al. (2011)
Koobi Fora Ridge	Gaji2	Habitation	P-2609	Excavated	Charcoal	3970 ± 60	4397	4572	4158	Barthelme (1985:143)

(Continued)

Table 2. (Continued)

Name	SASES	Site type	Lab #	Context	Material	14C date	Intcal20 median	Calibrated upper age limit (BP)	Calibrated lower age limit (BP)	References
Koobi Fora Ridge	Gaji2	Habitation	SUA-634	Excavated	Charcoal	4160 ± 100	4661	4922	4305	Barthelme (1985:143)
Dongodien	Gaji4	Habitation	P-2610	Unit 5 C	Charcoal	3890 ± 60	4293	4507	4093	Barthelme (1985: 23)
Dongodien	Gaji4	Habitation	SUA-637	Unit 5 C	Charcoal	3945 ± 135	4326	4817	3986	Barthelme (1985: 181)
Dongodien	Gaji4	Habitation	Beta-252053	Horizon B	Charcoal	4180 ± 40	4701	4834	4533	Ashley et al. (2017)
Dongodien	Gaji4	Habitation	Beta-252054	Horizon B	Charcoal	4240 ± 40	4741	4860	4586	Ashley et al. (2017)
Dongodien	Gaji4	Habitation	Beta-252056	Horizon B	Charcoal	4180 ± 40	4701	4834	4533	Ashley et al. (2017)
Nakwaperit 1	None	Habitation	ISGS-A3795	N523E781 L2, hard intact sediment. Plotted.	Charcoal	4965 ± 25	5658	5731	5597	
Lothagam	Geji11	Habitation	UCLA-2124A	Upper excavation	Charcoal	6300 ± 800	7083	8765	5320	Robbins and Lynch (1978: 619–620)
Kokito 1	GcJh11	Habitation	ISGS-A3752	D/V 9 cm bs	Charcoal	14,745 ± 50	18,063	18,209	17,881	Beyin et al. (2017)
Kokito 1	GcJh11	Habitation	ISGS-A1715	A/V 16 cm bs	Charcoal	9060 ± 30	10,216	10,244	10,182	Beyin et al. (2017)
Kokito 1	GcJh11	Habitation	ISGS-A3721	D/IV 24 cm bs	Charcoal	9600 ± 25	10,928	11,104	10,750	Beyin et al. (2017)
Kokito 1	GcJh11	Habitation	ISGS-A1714	A/III 25 cm bs	Charcoal	9785 ± 35	11,204	11,248	11,116	Beyin et al. (2017)
Kokito 1	GcJh11	Habitation	ISGS-A3722	D/III 40 cm bs	Charcoal	11,530 ± 25	13,386	13,455	13,316	Beyin et al. (2017)
Kokito 2	GcJh12	Habitation	ISGS-A3723	B/II 30 cm bs	Charcoal	11,670 ± 25	13,512	13,590	13,456	Beyin et al. (2017)
Kokito 2	GcJh12	Habitation	ISGS-A3028	B/II 44 cm bs	Charcoal	11,670 ± 35	13,512	13,595	13,448	Beyin et al. (2017)
Kokito 2	GcJh12	Habitation	ISGS-A3720	Bn/II 34 cm bs	Charcoal	11,705 ± 25	13,549	13,597	13,482	Beyin et al. (2017)
Kokito 2	GcJh12	Habitation	ISGS-A3724	Bn/III 19 cm bs	Charcoal	11,735 ± 30	13,551	13,734	13,486	Beyin et al. (2017)

A comprehensive list of all radiocarbon dates (including dates on shell, bone, burned earth, and material from surface) appears in SI Table 2a. A list of all non-radiocarbon dates (via OSL or U-Series) appears in SI Table 2b.
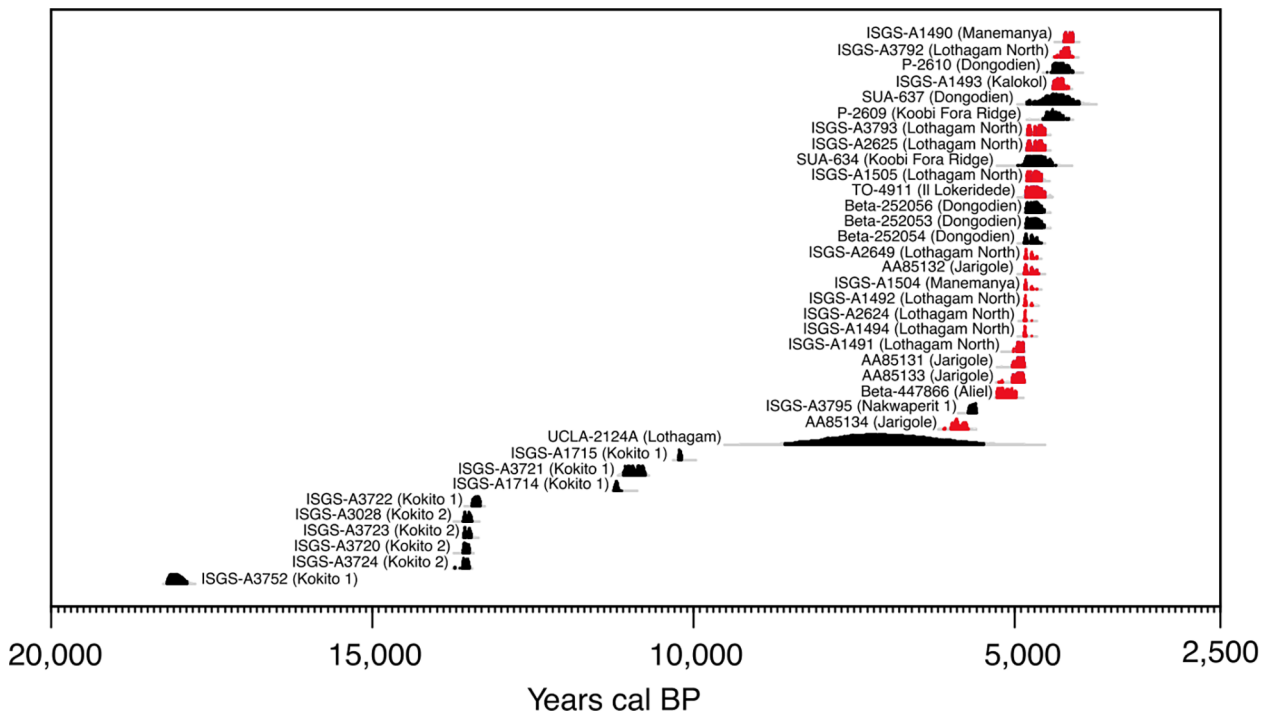
Figure 4. Probability distribution curves for radiocarbon dates presented in Table 2. Radiocarbon dates were calibrated in R using package "rcarbon" (Crema and Bevan, 2021). We used a 50/50 IntCal20 (Reimer et al., 2020) and SHCal20 (Hogg et al., 2020) mixed calibration curve. Pillar sites are red; all other sites are black.

"Before and after" versus processes of change

This brief archaeological review reveals the ways current data may or may not be substantial enough to evaluate potential differences in risk and/or mobility during AHP versus post-AHP times. An even more fundamental challenge to causal interpretations is that "before and after" contrasts do not necessarily illuminate the conditions and challenges people faced during the actual time of economic transition. Caprines are present by 4.5 ka in a burial context at Lothagam North (Hildebrand et al., 2018), and by 4 ka at Dongodien (Marshall et al., 1984), but it would be premature to rule out a slightly earlier presence of livestock. Most identifiable fauna from mortuary contexts at the pillar sites represent charismatic wild species like hippo, lion, and hyena that likely do not reflect typical subsistence activities. Archaeological coverage of the tail end of the AHP is thin: Nakwaperit 1, the sole archaeological occurrence securely dated to this time (5.7 ka on excavated OES), has Nderit pottery on the surface, raising the possibility of cultural shifts even before the lake's recession. Given that leaf wax data now suggest that vegetation changes may have unfolded for centuries after Turkana's dramatic recession, we must consider two chronologically distinct environmental processes that might – or might not – have posed new risks, and triggered changes in economy, technology, and mobility. Thus, current chronological imprecision hinders causal interpretation. Resolving these questions may hinge on new excavations in areas spanning the environmental transition to post-AHP conditions. For example Lokam's northern end may preserve early recessional shorelines, Also, along the Lower Turkwel, outcrops stretching several km east from Nakwaperit 1 may capture sites that followed retreating shorelines and deltas during the 5.3–3.9 ka recession.

Discussion: Ways forward

The Turkana Basin provides a signature example of how difficult it can be to articulate theory and data on questions of risk, even in research areas that have fairly well-developed archaeological data sets. This archaeological case also shows how critical it is to attack such issues from both ends – theory and data – and how both the (possible) risks and (possible) responses must be subject to independent interrogation via paleoenvironmental data.

Fisher-hunter-gatherer groups during the African Humid Period

Although leaf wax records confirm the operation of global insolation effects on precipitation within the Turkana catchment (Figure 2d), lake sediments demonstrate that Lakes Suguta, Chew Bahir, and Turkana varied in the timing and speed of AHP onset, the timing, severity, and duration of recessions during the AHP, and the speed of final recessions ~5 ka. The contrast between shallow Chew Bahir versus deep Suguta, and between abrupt versus gentle shorelines around Lake Turkana also may have been important in shaping local fishing practices and preferred technologies. Availability of good fishing grounds likely varied in time and space. Current data suggest that amidst environmental shifts, relatively mobile FHG groups selected specific kinds of settings for fishing and habitation. Many sites lie within peninsulas, inlets, areas near large bays, and points where internal drainages entered Lake Turkana. Although site size is difficult to assess, current data do not suggest large-scale settlements. Among other things, these data call for reflection on the proposed idea of sedentism/territoriality and interpersonal violence in the early Holocene (Mirazón Lahr et al., 2016a, but see Stojanowski et al., 2016). Mirazón Lahr et al. (2016a: 387) cite the presence of pottery in AHP contexts as possible evidence for food storage and therefore reduced mobility in a stable and resource-abundant landscape, but other scenarios are possible. A certain degree of mobility would have been necessary to meet seasonal, year-to-year, and longer-term shifts in lake levels and fishing areas, and would not necessarily preclude small-scale ceramic production for cooking/processing fish, shellfish, and/or other foods. We emphasize that FHG groups would have faced substantial risks and uncertainties throughout the AHP, long before the dramatic drop in lake level 5.3–3.9 ka.

Table 3. Middle Holocene habitation sites around Lake Turkana, clockwise from northeast end. S = Sites studied through survey only; S/E = Sites studied through survey and excavation. Elevations are in **bold** if a site has been georeferenced, and in *italic* if a site is not georeferenced but located precisely enough with respect to known landforms so that elevation data are likely to be within the range indicated. A * indicates that current site information is not precise enough to estimate elevation.

Site	Context during occupation	References
Ileret Stone Bowl site (FwJj5): **442 m**	0.5 km south of a westbound river channel. Main occupation layer deposited after major lake regression and incision of the laga. Location near freshwater spring, and possible use when shoreline was distant, suggest use during arid phases. Obsidian artifacts indicate travel/exchange as far as Suguta (south) and Ethiopian highlands (north).	Ashley et al. (2011), Barthelme (1985), see also Ndiema (2011), Ndiema et al. (2010, 2011), Nash et al. (2011) S/E
Dongodien (GaJi4): **414 m** Koobi Fora Ridge (GaJi2): **414 m**	Adjacent sites on south flanks of Koobi Fora Ridge about halfway between highstand and present shore. Artifacts accumulated just above beach sands at both sites, indicating people lived near the shore. At Dongodien, a slight transgression deposited shallow-water sediments over the occupation horizon, before a major recession. Both sites produced abundant caprines, some cattle, and wild terrestrial and aquatic fauna. Neither yielded barbed bone points, suggesting a shift away from fishing and aquatic hunting. Dongodien obsidian came from diverse sources.	Ashley et al. (2011, 2017), Barthelme (1985: 137–192), Marshall et al. (1984), Ndiema (2011), Ndiema et al. (2010, 2011) S/E
Zu-11: *442 ± 12*	West side of Napudet basin. Nderit and other ceramics, lava stone blades, and wild terrestrial fauna.	Robbins (1972) S
Bb14 *	Overlooks Lorungalup River. Nderit pottery.	Phenice et al. (1980) Robbins (1972) S
Nakwaperit 1: **442 m** Nakwaperit 2: **455 m**	Multiple sites along 1 km of outcrops of lacustrine and deltaic deposits on south bank of Turkwel River. Nakwaperit 1 has Nderit pottery on the surface, an eroding burial, and subsurface charcoal dated to 5.7 ka; Nakwaperit 2 has Nderit pottery on the surface, multiple burials, and an intact habitation layer as yet undated.	Hildebrand (2019) S/E
Kangatotha: **443 m**	Atop outcrops of lacustrine & deltaic deposits on north bank of Turkwel River east of Nakwaperit. Nderit pottery, small lithics.	Robbins (1972) S

Ethnographic observations of FHG groups hold lessons for archaeologists trying to document economic strategies during the AHP for their own sake, or to serve as a baseline for investigating "fishing to herding" transitions around Lake Turkana and elsewhere in Africa. Better knowledge of contemporary fishing practices can help us envision a variety of technologies that people might have deployed in the past, and examine site records (faunal, or lithic) that might reveal their use. Understanding the potential significance of different habitats for fishing and aquatic hunting can inspire us to develop more precise, locally situated models of lake level shifts' potential impacts on people's livelihoods, for example, how changes in lake levels might or might not spoil some productive environments and create new opportunities elsewhere. These could then be reformulated as hypotheses that might be testable in specific areas. For example, a null hypothesis might state that across the entire AHP, sites located at highstand beaches should have similar lithic assemblages to those located along recessional shorelines; refutation of this null hypothesis might support interpretations of shifts in technology in response to lake level changes.

The advent of pastoralism

Insights from pastoral ethnographic records and rangeland ecology – together with Contreras's (2017) caveats regarding our means of evaluating scale, precision, and mechanisms of environmental and social change – can help recalibrate archaeological theories about risks experienced by early herders. First, we can interrogate paleoenvironmental data to determine whether, when, where, and how unpredictability became acute, identifying possible times and places of special tension. Second, we can attempt to discern variation or continuity in material culture between tension points versus more stable times and places. Third, we must give particular attention to scale, seeking to maximize chronological precision in both types of records at possible tension points/places, while avoiding generalizations from one well-studied site or locality to too broad an area or time segment.

Lake level drops would have reshaped shorelines, emptied bays, and exposed new plains. While it is tempting to leap to a generalized inference that the landscape was "predictably unpredictable" during the centuries of recession, the local effects of these recessions would have varied depending on littoral slope: People living along steeper lake margins near Suguta, and where Lake Turkana hit adjacent volcanic ridges, would have seen less dramatic landscape changes than those living by Chew Bahir or in shallow areas where a small drop in lake level could cause a long-distance shoreline retreat.

Leaf wax $\delta^{13}C$ records demonstrate that Lake Turkana's southern catchments maintained predominantly C_3 vegetation at least 1000 years after lake levels began falling. A shift to C_4 plants began ~4 ka, such that significant vegetation change in Turkwel/Kerio catchments did not occur until pastoralism was already established around the lake. Parallel $\delta^{13}C$ data is not yet available for Turkana's northern catchment (Omo), so post-AHP changes in SW Ethiopian highland vegetation are not known. Capturing this information is essential in order to determine whether vegetation changes were unified, or offset, between northern and southern catchments. Conducting leaf wax $\delta^{13}C$ and phytolith studies on sediments from Suguta, Chew Bahir, and hyper-local catchments that collected in small areas but didn't connect to Lake Turkana (e.g. Ayaningeng Inland Delta ~50 km west of today's lakeshore) would allow us to assess unpredictability with more spatial precision. An expanded set of tooth enamel isotopic records could also strengthen our knowledge of local environmental change.

On the archaeological side, even as we pursue additional (and better-dated) assemblages, we can use new methods to query behaviors that may have been responses to risk, such as human movements, social networks, and exchange. "Material mobility," the movement of objects and animals, is a potential indicator of any or all of those. It is ripe for comparison within and between periods.

Research into obsidian sourcing (Nash et al., 2011; Ndiema et al., 2010, 2011) has already made substantial contributions to our understanding of early pastoral movements and/or exchange networks, but has not yet been applied comprehensively to AHP assemblages. Similar methods may help to identify clay sources, and track movement of pottery vessels after manufacture. A first goal would be to examine variation in source diversity *among* sites of a particular time period. One could then query distinctions *between* periods to see if, for example, pastoral sites demonstrated a greater diversity of sources than AHP sites. Even if we cannot definitively attribute an instance of heightened material mobility to exchange versus other social interaction versus movements of individuals or people, the increased circulation of objects (whatever the proximate cause) might be an indication of risk mitigation through more spatially extended, or frequently mobilized, social networks.

Mobility

Ethnographic and ethnoarchaeological records testify to mobility among contemporary people pursuing fishing economies, with movements of individuals or groups of fishers shaped by seasonal changes in habitat, targeted prey species, technologies, and momentary conditions. Lake level records of fluctuating shorelines of Chew Bahir, Suguta, and Lake Turkana during the AHP virtually guarantee that FHG groups around these lakes made major adjustments in their movements and technologies to cope with interannual and more long-term changes. Although certain sites/areas (e.g. Lokam) may have been within reach of a broad array of different types of fishing grounds and therefore less vulnerable to some of these changes, we should revise our view of AHP FHGs to recognize their possibly substantial degree of locational and technological flexibility.

For herders, human mobility must be acknowledged as a feature of their livelihood, and so not necessarily a response to risk *per se*. The great variety of movement types among contemporary pastoralists (of selected individuals or an entire group, across short or long distances, undertaken periodically or only *in extremis*) underlines the daunting nature of reconstructing pastoral mobilities in the past. This is particularly true for the earliest pastoralists around Lake Turkana, who were navigating new landscapes, knowledge systems, and/or organizations in a changing climate. To date, settlement data for early pastoralists around Turkana is woefully inadequate to the task of understanding settlement systems. However, human remains from AHP sites and pastoralist cemeteries support possible examination of human mobility via strontium (Sr) isotope analysis of tooth enamel. Construction of an Sr isoscape for the circum-Turkana region, plus bulk and serial sampling of teeth from humans recovered from archaeological sites, may reveal whether, and how, patterns of human movement differed between FHG and pastoral phases, and from site to site within each phase.

Conclusions

Increased risk, or an increasing desire to mitigate risk, has figured in many proposed explanations for early food production proposed in different parts of the world, particularly in contexts where environments were becoming more arid. The Turkana Basin of eastern Africa, where the transition from FHG to pastoral economies is associated with a major aridification event, might at first glance seem to be an obvious example of this phenomenon. However, attempts to evaluate causal relationships between paleoenvironmental events and human behavioral changes have been hampered by (among other issues) familiar problems of dissimilar paleoenvironmental and archaeological analytic scales, both spatial and chronological.

Decades of fieldwork near Lake Turkana have now generated extensive paleoenvironmental sequences and rich archaeological assemblages that do not yet support unequivocal answers, but rather reveal the complexity of the task before us. Contrary to previous suggestions that AHP conditions offered stable resources, we find that fishing communities likely faced substantial risks throughout the AHP. As the AHP ended, lake levels dropped rapidly but terrestrial vegetation may have changed more gradually than previously thought. The mechanisms through which herding took hold around Lake Turkana are still murky. There is an extensive middle ground between diffusionist interpretations (e.g. that fishers encountering catastrophic lake level changes adopted livestock obtained through exchange), and migrationist interpretations (e.g. that pastoralists moved into the area and took over, with little interest in lacustrine resources). For example, it may be that *both* fishers and herders were encountering new risks and new opportunities together and joined forces to invent a hybrid livelihood, retaining some economic and cultural features from both groups. Equally, incoming pastoralists may already have had their own traditions of fishing and aquatic resource use before they reached Turkana's shores. While these potential interpretations do not negate the general idea of risk as an influential mechanism, they demonstrate how difficult it is to pinpoint exactly how risks might have operated, and evaluate risk reduction against other possible motives for socioeconomic change. They also may serve as a caution in other parts of Africa where datasets are less secure. This work will contribute to productive comparisons of fishing-to-herding transitions between regions, between areas with different rainfall regimes, and between lacustrine versus riverine versus inland settings (e.g. Garcea, 2006; Khalidi et al., 2020).

Methodological advances offer encouraging opportunities for paleoenvironmental analysis that can help evaluate risk on more local geographic scales in Turkana and other research areas. They also provide more direct ways to assess mobility of people, livestock, and objects that might – or might not – indicate human strategies to mitigate risk. While these research tools will generate exciting new datasets, the paramount challenge is to situate interpretations within a framework that incorporates momentary, seasonal, and long-term dilemmas faced by communities of fishers and pastoralists. This requires explicit efforts to understand mobility systems, attitudes toward risk and risk mitigation, and other factors that structure decision-making by communities actively practicing these economic strategies. Archaeologists should continue to incorporate ethnographic information into their models, and to gain new perspectives via ethnoarchaeological research with fishing and pastoralist communities. Finally, as demonstrated elsewhere by Duwe and Preucel (2019), new collaborations with local research partners from these communities should yield insights that enhance interpretive frameworks.

ORCID iDs

Elisabeth Hildebrand https://orcid.org/0000-0002-4071-6068
Kendra L Chritz https://orcid.org/0000-0001-9665-0304
Elizabeth Sawchuk https://orcid.org/0000-0003-4398-2174
Susan K Pfeiffer https://orcid.org/0000-0003-0248-0530

Supplemental material

Supplemental material for this article is available online.

References

Antonites A and Ashley CZ (2016) The mobilities turn and archaeology: New perspectives on socio-political complexity in thirteenth-century northern South Africa. *Azania: Archaeological Research in Africa* 51: 469–488.

Ashley GM, Ndiema EK, Spencer JQG et al. (2011) Paleoenvironmental context of archaeological sites, implications for subsistence strategies under Holocene climate change, northern Kenya. *Geoarchaeology* 26(6): 809–837.

Ashley GM, Ndiema EK, Spencer JQG et al. (2017) Paleoenvironmental reconstruction of Dongodien, Lake Turkana, Kenya and OSL dating of site occupation during late Holocene climate change. *African Archaeological Review* 34: 345–362.

Barker PA, Talbot MR, Street-Perrott FA et al. (2004) Late Quaternary climatic variability in intertropical Africa. In: Battarbee RW, Gasse F and Stickley CE (eds) *Past Climate Variability Through Europe and Africa: Developments in Paleoenvironmental Research*, vol. 6. Dordrecht: Springer, pp.117–138.

Barthelme J (1981) Late Pleistocene-Holocene Prehistory Northeast of Lake Turkana, Kenya. Unpublished PhD thesis, University of California, Berkeley.

Barthelme J (1985) *Fisher-Hunters and Neolithic Pastoralists in East Turkana, Kenya*. Oxford: BAR International Series.

Beck CC, Feibel CS, Wright JD et al. (2019) Onset of the African Humid Period by 13.9 kyr BP at Kabua Gorge, Turkana Basin, Kenya. *The Holocene* 29: 1011–1019.

Behnke RH and Scoones I (1993) Rethinking range ecology: Implications for rangeland management in Africa. In: Behnke RH, Scoones I and Kerven C (eds) *Range Ecology at Disequilibrium: New Models of Natural Variability and Pastoral Adaptation in African Savannas*. London: Overseas Development Institute, pp.1–30.

Beyin A (2011) Recent archaeological survey and excavation around the greater Kalokol artea, west side of Lake Turkana: Preliminary findings. *Nyame Akuma* 75(1): 40–50.

Beyin A (2021) Human settlement successions and lithic technology in the Kalokol area (west Lake Turkana, Kenya) during the African Humid Period. *Azania: Archaeological Research in Africa* 56(4): 425–462.

Beyin A, Prendergast ME, Grillo KM et al. (2017) New radiocarbon dates for terminal Pleistocene and early Holocene settlements in West Turkana, northern Kenya. *Quaternary Science Reviews* 168: 208–215.

Bliege Bird R, Bird DW, Smith EA et al. (2002) Risk and reciprocity in Meriam food sharing. *Evolution and Human Behavior* 23: 297–321.

Bloszies C, Forman SL and Wright DK (2015) Water level history for Lake Turkana, Kenya in the past 15,000 years and a variable transition from the African Humid Period to Holocene aridity. *Global and Planetary Change* 132: 64–76.

Boethius A, Bergsvik KA and Nilsson B (2020) Knowledge from the ancient sea – a long-term perspective of human impact on aquatic life in Mesolithic Scandinavia. *The Holocene* 30(5): 632–645.

Boles OJC, Shoemaker A, Courtney Mustaphi CJ et al. (2019) Historical ecologies of pastoralist overgrazing in Kenya: Long-term perspectives on cause and effect. *Human Ecology* 47(3): 419–434.

Bollig M and Göbel B (1997) Risk, uncertainty, and pastoralism: An introduction. *Nomadic Peoples* 1(1): 5–21.

Borchardt S and Trauth MH (2012) Remotely-sensed evapotranspiration estimates for an improved hydrological modeling of the early Holocene mega-lake Suguta, northern Kenya Rift. *Palaeogeography, Palaeoclimatology, Palaeoecology* 361-362: 14–20.

Butt B (2010) Seasonal space-time dynamics of cattle behavior and mobility among Maasai pastoralists in semi-arid Kenya. *Journal of Arid Environments* 74: 403–413.

Butt B, Shortridge A and WinklerPrins AMG (2009) Pastoral herd management, drought coping strategies, and cattle mobility in southern Kenya. *Annals of the Association of American Geographers* 99: 309–334.

Camberlin P (1997) Rainfall anomalies in the source region of the Nile and their connection with the Indian summer monsoon. *Journal of Climate* 10: 1380–1392.

Cashdan E (ed.) (1990) *Risk and Uncertainty in Tribal and Peasant Economies*. Boulder, CO: Westview Press.

Cerling TE, Andanje SA, Blumenthal SA et al. (2015) Dietary changes of large herbivores in the Turkana Basin, Kenya from 4 to 1 Ma. *Proceedings of the National Academy of Sciences of the United States of America* 112(37): 11467–11472.

Cerling TE, Wynn JG, Andanje SA et al. (2011) Woody cover and hominin environments in the past 6 million years. *Nature* 476(7358): 51–56.

Chritz KL, Cerling TE, Freeman KH et al. (2019) Climate, ecology, and the spread of herding in eastern Africa. *Quaternary Science Reviews* 204: 119–132.

Cohen MN (2009) Introduction: Rethinking the Origins of Agriculture. *Current Anthropology* 50(5): 591–595.

Collett D and Robertshaw P (1983) Problems in the interpretation of radiocarbon dates: The Pastoral Neolithic of East Africa. *African Archaeological Review* 1: 57–74.

Contreras D (2017) Correlation is not enough: Building better arguments in the archaeology of human-environment interactions. In: Contreras D (ed.) *The Archaeology of Human-Environment Interactions: Strategies for Investigating Anthropogenic Landscapes, Dynamic Environments, and Climate Change in the Human Past*. London: Routledge, pp.3–22.

Coppolillo PB (2000) The landscape ecology of pastoral herding: Spatial analysis of land use and livestock production in East Africa. *Human Ecology* 28: 527–560.

Costa K, Russell J, Konecky B et al. (2014) Isotopic reconstruction of the African Humid Period and Congo Air Boundary migration at Lake Tana, Ethiopia. *Quaternary Science Reviews* 83: 58–67.

Crema ER and Bevan A (2021) Inference from large sets of radiocarbon dates: Software and methods. *Radiocarbon* 63(1): 23–39. DOI: 10.1017/RDC.2020.95

DeMenocal P, Ortiz J, Guilderson T et al. (2000) Abrupt onset and termination of the African Humid Period: Rapid climate responses to gradual insolation forcing. *Quaternary Science Reviews* 19: 347–361.

Derbyshire S (2021) *Remembering Turkana: Material Histories and Contemporary Livelihoods in North-Western Kenya*. New York, NY: Routledge.

Derbyshire SF (2019) Trade, development and destitution: A material culture history of fishing on the western shore of Lake Turkana, northern Kenya. *African Studies* 78: 324–346.

Derbyshire SF, Nami JE, Akall G et al. (2021) Divining the future: Making sense of ecological uncertainty in Turkana, northern Kenya. *Land* 10: 885.

Duwe S and Preucel RW (eds) (2019) *The Continuous Path: Pueblo Movement and the Archaeology of Becoming*. Tucson, AZ: University of Arizona Press.

Dyson-Hudson R and Dyson-Hudson N (1980) Nomadic pastoralism. *Annual Review of Anthropology* 9: 15–61.

Dyson WS and Fuchs VE (1937) The Elmolo. *The Journal of the Royal Anthropological Institute of Great Britain and Ireland* 67: 327–338.

D'Alpoim Guedes J (2011) Millets, rice, social complexity, and the spread of agriculture to the Chengdu Plain and southwest China. *Rice* 4: 104–113.

Ellis JE and Swift DM (1988) Stability of African pastoral ecosystems: Alternate paradigms and implications for development. *Rangeland Ecology and Management* 41(6): 450–459.

Fischer A, Olsen J, Richards M et al. (2007) Coast–inland mobility and diet in the Danish Mesolithic and Neolithic: Evidence from stable isotope values of humans and dogs. *Journal of Archaeological Science* 34: 2125–2150.

Fischer ML, Markowska M, Bachofer F et al. (2020) Determining the pace and magnitude of lake level changes in southern Ethiopia over the last 20,000 years using lake balance modeling and SEBAL. *Earth Science Frontiers* 8: 197. DOI: 10.3389/feart.2020.00197

Foerster V, Deocampo DM, Asrat A et al. (2018) Towards an understanding of climate proxy formation in the Chew Bahir basin, southern Ethiopian Rift. *Palaeogeography, Palaeoclimatology, Palaeoecology* 501: 111–123. DOI: 10.1016/j.palaeo.2018.04.009

Foerster V, Junginger A, Langkamp O et al. (2012) Climatic change recorded in the sediments of the Chew Bahir basin, southern Ethiopia, during the last 45,000 years. *Quaternary International* 274: 25–37.

Galaty J and Johnson D (eds) (1990) *The World of Pastoralism: Herding Systems in Comparative Perspective*. New York, NY: Guildford Press.

Garcea EAA (2006) Semi-permanent foragers in semi-arid environments of North Africa. *World Archaeology* 38(2): 197–219.

Garcea EAA (2020) *The Prehistory of the Sudan*. Cham, Switzerland: Springer.

Garcin Y, Junginger A, Melnick D et al. (2009) Late Pleistocene–Holocene rise and collapse of Lake Suguta, northern Kenya Rift. *Quaternary Science Reviews* 28: 911–925.

Garcin Y, Melnick D, Strecker MR et al. (2012) East African mid-Holocene wet–dry transition recorded in palaeo-shorelines of Lake Turkana, northern Kenya Rift. *Earth and Planetary Science Letters* 331-332: 322–334.

Garcin Y, Schefuß E, Schwab VF et al. (2014) Reconstructing C 3 and C 4 vegetation cover using n-alkane carbon isotope ratios in recent lake sediments from Cameroon, Western Central Africa. *Geochimica et Cosmochimica Acta* 142: 482–500.

Gaspar MD, Klokler DM and DeBlasis P (2011) Traditional fishing, mollusk gathering, and the shell mound builders of Santa Catarina, Brazil. *Journal of Ethnobiology* 31(2): 188–212.

Gasse F and Fontes JC (1989) Palaeoenvironments and palaeohydrology of a tropical closed lake (Lake Asal, Djibouti) since 10,000 yr B.P. *Palaeogeography, Palaeoclimatology, Palaeoecology* 69: 67–102.

Gibert E, Travi Y, Massault M et al. (1999) Comparing carbonate and organic AMS-^{14}C ages in Lake Abiyata sediments (Ethiopia): Hydrochemistry and paleoenvironmental implications. *Radiocarbon* 41(3): 271–286.

Gifford-Gonzalez D (1998) Early pastoralists in East Africa: Ecological and social dimensions. *Journal of Anthropological Archaeology* 17(2): 166–200.

Gifford-Gonzalez D (2000) Animal disease challenges to the emergence of pastoralism in sub-Saharan Africa. *African Archaeological Review* 17: 95–139.

Gifford-Gonzalez D (2005) Pastoralism and its consequences. In: Stahl AB (ed.) *African Archaeology: A Critical Introduction*. London: Blackwell, pp.187–224.

Gifford-Gonzalez D, Stewart KM and Rybczynski N (1999) Human activities and site formation at modern lake margin foraging camps in Kenya. *Journal of Anthropological Archaeology* 18(4): 397–440.

Githinji CK (1994) *Il Lokeridede: A Pastoral Neolithic mortuary site east of Lake Turkana, Kenya*. Unpublished MA thesis, University of Nairobi.

Goldstein ST (2019) Lithic technological strategies of the earliest herders at Lake Turkana, northern Kenya. *Antiquity* 93: 1495–1514.

Grant KM, Rohling EJ, Westerhold T et al. (2017) A 3 million year index for North African humidity/aridity and the implication of potential pan-African Humid Periods. *Quaternary Science Reviews* 171: 100–118.

Grillo KM and Hildebrand EA (2013) The context of early megalithic architecture in eastern Africa: The Turkana Basin *c*.5000-4000 BP. *Azania: Archaeological Research in Africa* 48: 193–217.

Grillo KM, McKeeby Z and Hildebrand EA (2022) "Nderit Ware" and the origins of pastoralist pottery in eastern Africa. *Quaternary International* 608-609: 226–242.

Gupta AK, Anderson DM and Overpeck JT (2003) Abrupt changes in the Asian southwest monsoon during the Holocene and their links to the North Atlantic Ocean. *Nature* 421: 354–357.

Halstead P and Jones G (1989) Agrarian ecology in the Greek Islands: Time stress, scale and risk. *The Journal of Hellenic Studies* 109: 41–55.

Halstead P and O'Shea J (eds) (1989) *Bad Year Economics: Cultural Responses to Risk and Uncertainty*. Cambridge: Cambridge University Press.

Halstead P and O'Shea J (1989) Introduction: Cultural responses to risk and uncertainty. In: Halstead P and O'Shea J (eds) *Bad Year Economics: Cultural Responses to Risk and Uncertainty*. Cambridge: Cambridge University Press, pp.1–7.

Hastenrath S and Kutzbach JE (1983) Paleoclimatic estimates from water and energy budgets of East African lakes. *Quaternary Research* 19: 141–153.

Hildebrand EA (2019) *Nakwaperit survey and excavations 2018: A short report for the National Museums of Kenya* (amended March 2019). Document on file, NMK-Nairobi.

Hildebrand EA and Grillo KM (2012) Early herders and monumental sites in eastern Africa: Dating and interpretation. *Antiquity* 86: 338–352.

Hildebrand EA, Grillo KM, Sawchuk EA et al. (2018) A monumental cemetery built by eastern Africa's first herders near Lake Turkana, Kenya. *Proceedings of the National Academy of Sciences of the United States of America* 115: 8942–8947.

Hildebrand EA, Shea JJ and Grillo KM (2011) Four middle Holocene pillar sites in West Turkana, Kenya. *Journal of Field Archaeology* 36: 181–200.

Hogg AG, Heaton TJ, Hua Q et al. (2020) SHCal20 Southern Hemisphere calibration, 0–55,000 years cal BP. *Radiocarbon* 62(4): 759–778.

Holl AFC (2005) Holocene 'aquatic' adaptations in north tropical Africa. In: Stahl AB (ed.) *African Archaeology: A Critical Introduction*. London: Blackwell, pp.174–186.

Homewood K (2008) *Ecology of African Pastoralist Societies*. Oxford: James Currey.

Honeychurch W (2015) *Inner Asia and the Spatial Politics of Empire: Archaeology, Mobility, and Culture Contact*. New York, NY: Springer.

Junginger A, Roller S, Olaka LA et al. (2014) The effects of solar irradiation changes on the migration of the Congo Air Boundary and water levels of paleo-Lake Suguta, northern Kenya

Rift, during the African Humid Period (15–5ka BP). *Palaeogeography, Palaeoclimatology, Palaeoecology* 396: 1–16.

Junginger A and Trauth MH (2013) Hydrological constraints of paleo-Lake Suguta in the Northern Kenya Rift during the African Humid Period (15–5ka BP). *Global and Planetary Change* 111: 174–188.

Kahn JG (2013) Anthropological archaeology in 2012: Mobility, economy, and transformation. *American Anthropologist* 115: 248–261.

Kaimba GK, Njehia BK and Guliye AY (2011) Effects of cattle rustling and household characteristics on migration decisions and herd size amongst pastoralists in Baringo District, Kenya. *Pastoralism: Research Policy and Practice* 1: 18. DOI: 10.1186/2041-7136-1-18

Keding B (2017) Middle Holocene fisher-hunter-gatherers of Lake Turkana in Kenya and their cultural connections with the north: The pottery. *Journal of African Archaeology* 15: 42–76.

Khalidi L, Mologni C, Ménard C et al. (2020) 9000 years of human lakeside adaptation in the Ethiopian Afar: Fisher-foragers and the first pastoralists in the Lake Abhe basin during the African Humid Period. *Quaternary Science Reviews* 243: 106459.

Kinyanjui R (2018) Phytolith analysed to compare changes in vegetation structure of Koobi Fora and Olorgesailie Basins through Mid-Pleistocene-Holocene periods. Unpublished PhD thesis, University of Witwatersrand, Johannesburg.

Kiura P (2005a) El-molo: The forgotten people of Lake Turkana. *Kenya Past & Present* 35: 11–16.

Kiura P (2005b) *An ethnoarchaeology and stable isotope study on the diets of three modern groups of people in northern Kenya.* Unpublished PhD thesis, Rutgers University.

Koch CP (1994) The Jarigole mortuary tradition: New light on Pastoral Neolithic burial practices. *Paper presented at the 16th Meeting of the South African Archaeological Association*, Pietermaritsburg, South Africa.

Koch CP, Pavlish LA, Farquhar RM et al. (2002) INAA of pottery from Il Lokeridede and Jarigole, Koobi Fora Region, Kenya. In: Jerem E and Biro KT (eds) *Archaeometry 98: Proceedings of the 31st Symposium Budapest*, April 26–May 3 1998, Volume II (BAR International Series 1043). Oxford: Archaeopress, pp. 587–92.

Lamphear J (1988) The people of the grey bull: The origin and expansion of the Turkana. *Journal of African History* 29(1): 27–39.

Lander F and Russell T (2018) The archaeological evidence for the appearance of pastoralism and farming in southern Africa. *PLoS One* 13(6): e0198941.

Lane PJ (2013) The archaeology of pastoralism and stock-keeping in East Africa. In: Mitchell P and Lane PJ (eds) *Oxford Handbook of African Archaeology*. Oxford: Oxford University Press, pp.585–601.

Lesur J, Hildebrand EA, Abawa G et al. (2014) The advent of herding in the horn of Africa: New data from Ethiopia, Djibouti and Somaliland. *Quaternary International* 343: 148–158.

Little MA and Leslie PW (eds) (1999) Turkana herders of the dry savanna: Ecology and biobehavioral response of nomads to an uncertain environment. *Research Monographs on Human Population Biology*, vol. 13. Oxford: Oxford University Press.

Mace R and Sear R (1997) Reproductive decisions by Gabbra pastoralists in the face of demographic risks. *Nomadic Peoples* 1(1): 151–163.

Magill CR, Ashley GM and Freeman KH (2013) Ecosystem variability and early human habitats in eastern Africa. *Proceedings of the National Academy of Sciences of the United States of America* 110(4): 1167–1174.

Maritan L, Iacumin P, Zerboni A et al. (2018) Fish and salt: The successful recipe of White Nile Mesolithic hunter-gatherer-fishers. *Journal of Archaeological Science* 92: 48–62.

Marquardt WH and Watson PW (2005) The Green River Shell Mound Archaic: Conclusions. In: Marquardt WH and Watson PJ (eds) *Archaeology of the Middle Green River Region, Kentucky. Institute of Archaeology and Paleoenvironmental Studies, Monograph 5*. Gainesville: University of Florida, pp.629–647.

Marshall F, Grillo K and Arco L (2011) Prehistoric pastoralists and social responses to climatic risk in East Africa. In: Miller NE, Moore KM and Ryan K (eds) *Sustainable Liveways: Cultural Persistence in an Ever-Changing Environment*. Philadelphia, PA: University of Pennsylvania Museum, pp.38–73.

Marshall F and Hildebrand E (2002) Cattle before crops: The beginnings of food production in Africa. *Journal of World Prehistory* 16: 99–143.

Marshall F, Stewart K and Barthelme J (1984) Early domestic stock at Dongodien in northern Kenya. *Azania* 19: 120–127.

McCabe JT (1997) Risk and uncertainty among the Maasai of the Ngorongoro Conservation Area. *Nomadic Peoples* 1(1): 54-65.

McCabe JT (2004) *Cattle Bring Us to Our Enemies: Turkana Ecology, Politics, and Raiding in a Disequilibrium System*. Ann Arbor, MI: University of Michigan Press.

McCabe JT (2021) Pastoralist ecologies. *Oxford Research Encyclopedias in Anthropology*. Epub ahead of print 22 January 2021. DOI: 10.1093/acrefore/9780190854584.013.305.

McCabe JT, Dyson-Hudson R and Wienpahl J (1999) Nomadic movements. In: Little MA and Leslie PW (eds) *Turkana Herders of the Dry Savannah: Ecology and Biobehavioural Response of Nomads to an Uncertain Environment*. Oxford: Oxford University Press, pp.109–121.

McQuade M and O'Donnell L (2007) Late Mesolithic fish traps from the Liffey estuary, Dublin, Ireland. *Antiquity* 81: 569–584.

Melnick D, Garcin Y, Quinteros J et al. (2012) Steady rifting in northern Kenya inferred from deformed Holocene lake shorelines of the Suguta and Turkana basins. *Earth and Planetary Science Letters* 331–332: 335–346.

Miller NE, Moore KM and Ryan K (eds) (2011) *Sustainable Liveways: Cultural Persistence in an Ever-Changing Environment*. Philadelphia, PA: University of Pennsylvania Museum.

Mirazón Lahr M, Rivera F, Power RK et al. (2016a) Inter-group violence among early Holocene hunter-gatherers of West Turkana, Kenya. *Nature* 529: 394–398.

Mirazón Lahr M, Rivera F, Power RK et al. (2016b) Mirazón Lahr et al. Reply. *Nature* 539: E10–E11.

Mohammed MU, Bonnefille R and Johnson TC (1996) Pollen and isotopic records in late Holocene sediments from Lake Turkana, Kenya. *Palaeogeography, Palaeoclimatology, Palaeoecology* 119(3-4): 371–383.

Moore K (2011) Grace under pressure: Responses to changing environments by herders and fishers in the Formative Lake Titicaca Basin, Bolivia. In: Miller NE and Ryan K (eds) *Sustainable Liveways: Cultural Persistence in an Ever-Changing Environment*. Philadelphia, PA: University of Pennsylvania Museum, pp.244–272.

Morrissey A (2014) Stratigraphic framework and Quaternary paleolimnology of the Lake Turkana Rift, Kenya. Unpublished PhD thesis, Syracuse University.

Nash BP, Merrick HV and Brown FH (2011) Obsidian types from Holocene sites around Lake Turkana, and other localities in northern Kenya. *Journal of Archaeological Science* 38: 1371–1376.

Ndiema EK (2011) Mobility and subsistence patterns among mid-Holocene pastoralists at Koobi Fora, northern Kenya: New archaeological sites and evidence from obsidian sourcing and geochemical characterization. Unpublished PhD thesis, Rutgers University.

Ndiema EK, Dillian CD and Braun DR (2010) Interaction and exchange across the transition to pastoralism, Lake Turkana,

Kenya. In: Dillian CD and White C (eds) *Trade and Exchange: Archaeological Studies From Prehistory and History*. New York, NY: Springer, pp.95–110.

Ndiema KE, Dillian CD, Braun DR et al. (2011) Transport and subsistence patterns at the transition to pastoralism, Koobi Fora, Kenya. *Archaeometry* 53: 1085–1098.

Neff U, Burns SJ, Mangini A et al. (2001) Strong coherence between solar variability and the monsoon in Oman between 9 and 6 kyr ago. *Nature* 411: 290–293.

Nelson CM (1995) The work of the Koobi Fora Field School at the Jarigole Pillar Site. *Kenya Past and Present* 27: 49–63.

Nicholson SE (1996) A review of climate dynamics and climate variability in eastern Africa. In: Johnson TC and Odada EO (eds) *Limnology, Climatology, and Paleoclimatology of the East African Lakes*. London: Routledge, pp.25–56.

Pas Schrijver A (2019) *Pastoralists, mobility and conservation: Shifting rules of access and control of grazing resources in Kenya's northern drylands*. Unpublished PhD thesis, Stockholm University.

Peacock S (1998) Putting down roots: The emergence of wild plant food production on the Canadian Plateau. Unpublished PhD thesis, University of Victoria.

Phenice TW, Robbins LH and Lynch BM (1980) Late Stone Age burials from sites located to the west of Lothagam. In: Angel JL, Phenice TW, Robbins LH et al. (eds) *Late Stone-Age Fishermen of Lothagam, Kenya*. East Lansing (MI): Michigan State University, pp.174–185.

Phillipson DW (1977) Lowasera. *Azania* 7 12: 1–32.

Pike IL (2004) The biosocial consequences of life on the run: A case study from Turkana District, Kenya. *Human Organization* 63: 221–235.

Prendergast ME and Beyin A (2018) Fishing in a fluctuating landscape: Terminal Pleistocene and early Holocene subsistence strategies in the Lake Turkana Basin, Kenya. *Quaternary International* 471: 203–218.

Reimer PJ, Austin W, Bard E et al. (2020) The IntCal20 northern hemisphere radiocarbon age calibration curve (0–55 cal kBP). *Radiocarbon* 62(4): 725–757.

Richards MP and Schulting RJ (2006) Touch not the fish: The Mesolithic-Neolithic change of diet and its significance. *Antiquity* 80(308): 444–456.

Robbins LH (1967) A recent archaeological discovery in the Turkana District of northern Kenya. *Azania* 2(1): 69–73.

Robbins LH (1972) Archeology in the Turkana District, Kenya. *Science* 176: 359–366.

Robbins LH (1974) *The Lothagam Site: A Late Stone Age Fishing Settlement in the Lake Rudolf Basin, Kenya* East Lansing, MI: Publications of the Museum, Michigan State University.

Robbins LH (1980) *Lopoy and Lothagam*. East Lansing, MI: Publications of the Museum, Michigan State University.

Robbins LH and Lynch BM (1978) New evidence on the use of microliths from the Lake Turkana Basin, East Africa. *Current Anthropology* 19(3): 619–620.

Robson HK and Ritchie K (2019) The early Mesolithic fisheries of southern Scandinavia. In: Groß D, Lübke H, Meadows J et al. (eds) Working at the Sharp End: *From Bone and Antler to Early Mesolithic Life in Northern Europe. Untersuchungen und Materialien Zzur Steinzeit in Schleswig-Holstein und im Ostseeraum 10*. Kiel/Hamburg: Wachholtz/Murmann Publishers, pp. 290–303.

Roe E, Huntsinger L and Labnow K (1998) High-reliability pastoralism versus risk-averse pastoralism. *Journal of Environment and Development* 7(4): 387–421.

Sachse D, Billault I, Bowen GJ et al. (2012) Molecular paleohydrology: Interpreting the hydrogen-isotopic composition of lipid biomarkers from photosynthesizing organisms. *Annual Review of Earth and Planetary Sciences* 40(1): 221–249.

Sachse D, Radke J and Gleixner G (2006) δD values of individual n-alkanes from terrestrial plants along a climatic gradient – Implications for the sedimentary biomarker record. *Organic Geochemistry* 37(4): 469–483.

Salazar NB and Smart A (2011) Anthropological takes on (im) mobility. *Identities* 18: i–ix.

Sawchuk EA (2017) Social change and human population movements: Dental morphology in Holocene eastern Africa. Unpublished PhD thesis, University of Toronto.

Sawchuk EA, Pfeiffer S, Klehm CE et al. (2019a) The bioarchaeology of mid-Holocene pastoralist cemeteries west of Lake Turkana, Kenya. *Archaeological and Anthropological Sciences* 11: 6221–6241.

Sawchuk EA, Grillo KM, Janzen A et al. (2019b) Rethinking pillar sites across Lake Turkana: New excavations at Jarigole (GbJj1). *Paper presented at the East African Association for Paleoanthropology and Paleontology Biennial Meeting*, Nairobi.

Sawchuk EA, Goldstein ST, Grillo KM et al. (2018) Cemeteries on a moving frontier: Mortuary practices and the spread of pastoralism from the Sahara into eastern Africa. *Journal of Anthropological Archaeology* 51: 187–205.

Sawchuk EA, Hildebrand EA, Hill AC et al. (in press) *The Jarigole Mortuary Tradition reconsidered*. Submitted to Antiquity.

Scherer JC (1978) *Fisherfolk of the desert: An ethnography of the Elmolo of Kenya*. Unpublished PhD thesis, University of Virginia.

Shanahan TM, McKay NP, Hughen KA et al. (2015) The time-transgressive termination of the African Humid Period. *Nature Geoscience* 8(2): 140–144.

Smith BD (2018) Hunting in yellow waters: An ethnoarchaeological perspective on selective fishing on Lake Turkana. *Quaternary International* 471: 241–251.

Sobania N (1988) Fishermen herders: Subsistence, survival and cultural change in northern Kenya. *Journal of African History* 29: 41–56.

Sobania N (2011) The formation of ethnic identity in South Omo: The Dassenech. *Journal of Eastern African Studies* 5: 195–210.

Stager JC, Mayewski PA and Meeker LD (2002) Cooling cycles, Heinrich event 1, and the desiccation of Lake Victoria. *Palaeogeography, Palaeoclimatology, Palaeoecology* 183: 169–178.

Stein G (1989) Strategies of risk reduction in herding and hunting systems of Neolithic southeast Anatolia. In: Crabtree P, Campana D and Ryan K (eds) *Early Animal Domestication and Its Cultural Context*. Masca Research Papers in Science and Archaeology, Special Supplement to Volume 6. Philadelphia, PA: MASCA, the University Museum of Archaeology and Anthropology, University of Pennsylvania, pp.87–97.

Stewart KM (1989) *Fishing Sites of North and East Africa in the Late Pleistocene and Holocene: Environmental Change and Human Adaptation*. BAR International Series 521.

Stewart KM and Gifford-Gonzalez D (1994) An ethnoarchaeological contribution to identifying hominid fish processing sites. *Journal of Archaeological Science* 21: 237–248.

Stojanowski CM, Seidel AC, Fulginiti LC et al. (2016) Contesting the massacre at Nataruk. *Nature* 539(7630): E8–E10.

Strawhacker C, Snitker G, Peeples MA et al. (2020) A landscape perspective on climate-driven risks to food security: Exploring the relationship between climate and social transformation in the prehispanic U.S. Southwest. *American Antiquity* 85(3): 427–451.

Sutton JEG (1977) The African Aqualithic. *Antiquity* 51: 25–34.

Trauth MH, Foerster V, Junginger A et al. (2018) Abrupt or gradual? Change point analysis of the late Pleistocene-Holocene climate record from Chew Bahir, southern Ethiopia. *Quaternary Research* 90: 321–330.

Vagnby B and Jacobs AH (1974) Kenya: Traditional housing of the Elmolo. *Ekistics* 38(227): 240–243.

van der Lubbe HJ, Krause-Nehring J, Junginger A et al. (2017) Gradual or abrupt? Changes in water source of Lake Turkana (Kenya) during the African Humid Period inferred from Sr isotope ratios. *Quaternary Science Reviews* 174: 1–12.

Van Dijk H (1997) Risk agro-pastoral decision making and natural resource management in Fulbe society, central Mali. *Nomadic Peoples* 1(1): 108–132.

Ventresca Miller AR and Makarewicz CA (eds) (2017) *Isotopic Investigations of Pastoralism in Prehistory*. New York, NY: Routledge.

Wandibba S (1980) The application of attribute analysis to the study of Later Stone Age/Neolithic pottery ceramics in Kenya (summary). In Leakey R and Ogot B (eds) *Proceedings of the 8th Panafrican Congress of Prehistory and Quaternary Studies, Nairobi, 5 to 10 September 1977*. Nairobi: International Louis Leakey Memorial Institute for African Prehistory, pp. 283–85.

Weldeab S, Lea DW, Schneider RR et al. (2007) Centennial scale climate instabilities in a wet early Holocene West African monsoon. *Geophysical Research Letters* 34: L24702.

Western D and Dunne T (1979) Environmental aspects of settlement site decisions among pastoral Maasai. *Human Ecology* 7: 75–98.

Wetterstrom W (1993) Foraging and farming in Egypt: The transition from hunting and gathering to horticulture in the Nile Valley. In: Shaw T, Sinclair P, Andah B and Okpoko A (eds) *The Archaeology of Africa: Food, Metals and Towns*. London: Routledge, pp.165–226.

Whallon R (2006) Social networks and information: Non-"utilitarian" mobility among hunter-gatherers. *Journal of Anthropological Archaeology* 25: 259–270.

White C (1997) The effect of poverty on risk reduction strategies of Fulani nomads in Niger. *Nomadic Peoples* 1(1): 90–117.

White F (1983) *The Vegetation of Africa*. Paris, France: UNESCO.

Wiessner P (1982) Risk, reciprocity and social influences on !Kung San economics. In: Leacock ER and Lee RB (eds) *Politics and History in Band Societies*. Cambridge: Cambridge University Press, pp.61–84.

Wilshaw A, Muwonge H, Rivera F et al. (2016) Aliel: A mid-holocene stone platform with cairn and single pillar in West Turkana, Kenya. *Nyame Akuma* 86: 51–59.

Winterhalder B (2007) Risk and decision-making. In: Dunbar RIM and Barrett L (eds) *Oxford Handbook of Evolutionary Psychology*. Oxford: Oxford University Press, pp.433–445.

Wright DK (2019) Long-term dynamics of pastoral ecology in northern Kenya: An old model for new resilience. *Journal of Anthropological Archaeology* 55: 101068.

Wright DK, Forman SL, Kiura P et al. (2015) Lakeside view: Sociocultural responses to changing water levels of Lake Turkana, Kenya. *African Archaeological Review* 32: 335–367.

Wylie A (1985) The reaction against analogy. *Advances in Archaeological Method and Theory* 8: 63–110.

Yellen J (1998) Barbed bone points: Tradition and continuity in Saharan and sub-Saharan Africa. *African Archaeological Review* 15: 173–198.

Zavodny E, Culleton BJ, McClure SB et al. (2017) Minimizing risk on the margins: Insights on Iron Age agriculture from stable isotope analyses in central Croatia. *Journal of Anthropological Archaeology* 48: 250–261.

Appendix P6 – Human-environmental interactions and seismic activity in a Late Bronze to Early Iron Age settlement center in the southeastern Caucasus

Check for updates

Human-environmental interactions and seismic activity in a Late Bronze to Early Iron Age settlement center in the southeastern Caucasus

Hans Von Suchodoletz[1]*, Giorgi Kirkitadze[2], Tiiu Koff[3],
Markus L. Fischer[1,4], Rosa M. Poch[5], Azra Khosravichenar[1],
Birgit Schneider[1], Bruno Glaser[6], Susanne Lindauer[7],
Silvan Hoth[8], Anna Skokan[9], Levan Navrozashvili[2],
Mikheil Lobjanidze[2], Mate Akhalaia[2], Levan Losaberidze[10] and
Mikheil Elashvili[2]

[1]University of Leipzig, Institute of Geography, Leipzig, Germany, [2]Ilia State University, School of Natural
Sciences and Engineering, Tbilisi, Georgia, [3]Tallinn University, Institute of Ecology, Tallinn, Estonia,
[4]University of Tübingen, Department of Geosciences, Tübingen, Germany, [5]Universitat de Lleida,
Departament de Medi Ambient i Ciències del Sòl, Lleida, Spain, [6]Martin-Luther University Halle-
Wittenberg, Institute of Agricultural and Nutritional Sciences, Soil Biogeochemistry, Halle/Saale,
Germany, [7]Curt-Engelhorn-Zentrum Archaeometrie gGmbH, Mannheim, Germany, [8]Equinor ASA,
Stavanger, Norway, [9]TU Dresden, Institute of Geography, Dresden, Germany, [10]Society of Young
Archeologists of Georgia, Tbilisi, Georgia

Long-term human-environmental interactions in naturally fragile drylands are a
focus of geomorphological and geoarchaeological research. Furthermore,
many dryland societies were also affected by seismic activity. The semi-arid
Shiraki Plain in the tectonically active southeastern Caucasus is currently
covered by steppe and largely devoid of settlements. However, numerous
Late Bronze to Early Iron Age city-type settlements suggest early state
formation between ca. 3.2-2.5 ka that abruptly ended after that time. A
paleolake was postulated for the lowest plain, and nearby pollen records
suggest forest clearcutting of the upper altitudes under a more humid
climate during the Late Bronze/Early Iron Ages. Furthermore, also an impact
of earthquakes on regional Early Iron Age settlements was suggested. However,
regional paleoenvironmental changes and paleoseismicity were not
systematically studied so far. We combined geomorphological,
sedimentological, chronological and paleoecological data with hydrological
modelling to reconstruct regional Holocene paleoenvironmental changes, to
identify natural and human causes and to study possible seismic events during
the Late Bronze/Early Iron Ages. Our results show a balanced to negative Early
to Mid-Holocene water balance probably caused by forested upper slopes.
Hence, no lake but a pellic Vertisol developed in the lowest plain. Following,
Late Bronze/Early Iron Age forest clear-cutting caused lake formation and the
deposition of lacustrine sediments derived from soil erosion. Subsequently,
regional aridification caused slow lake desiccation. Remains of freshwater fishes
indicate that the lake potentially offered valuable ecosystem services for

regional prehistoric societies even during the desiccation period. Finally, colluvial coverage of the lake sediments during the last centuries could have been linked with hydrological extremes during the Little Ice Age. Our study demonstrates that the Holocene hydrological balance of the Shiraki Plain was and is situated near a major hydrological threshold, making the landscape very sensitive to small-scale human or natural influences with severe consequences for local societies. Furthermore, seismites in the studied sediments do not indicate an influence of earthquakes on the main and late phases of Late Bronze/Early Iron Age settlement. Altogether, our study underlines the high value of multi-disciplinary approaches to investigate human-environmental interactions and paleoseismicity in drylands on millennial to centennial time scales.

1 Introduction

The dynamics of human-environmental interactions on centennial to millennial timescales that are characterized by thresholds are a focus of geomorphological and geoarchaeological research (Dotterweich, 2008; Harden et al., 2014; Barton et al., 2016; Menges et al., 2019; Dong et al., 2020; Liu et al., 2021). Especially naturally fragile drylands (Fletcher et al., 2013) are ideal to investigate such long-term interactions: On the one hand, human societies in drylands are highly affected by even small-scale environmental variations (Schmidt et al., 2011; Balbo et al., 2016), and on the other hand, drylands sensitively react towards small-scale human disturbances (Neff et al., 2008; Suchodoletz et al., 2010; O'Henry et al., 2017; Rosen et al., 2019). Furthermore, given that many drylands are located in tectonically active regions, next to environmental and societal factors also destructive seismic events impacted the local prehistoric societies (Nur and Cline, 2000; Force, 2017; Lazar et al., 2020).

Located between Mesopotamia and the Eurasian steppes, the southern Caucasus (Georgia, Armenia, Azerbaijan) occupies a distinctive place in Old World archaeology (Smith, 2005; Manning et al., 2018). Given its location in the active continental Arabia-Eurasia collisional zone this region is characterized by strong seismic activity (Ismail-Zadeh et al., 2020), forming a natural hazard also for former regional societies (Varazanashvili et al., 2011). Here and in the neighboring regions of eastern Turkey and northwestern Iran, the Late Bronze to Early Iron Ages between about 3.5 and 2.8 ka were characterized by large fortified permanent settlements and an increasing sociopolitical hierarchy and complexity, leading to the development of the region's first territorial polities with complex bureaucracies (Smith, 2005; Sagona, 2018; Erb-Satullo et al., 2019; Herrmann and Hammer, 2019). One important settlement center during that time was the Shiraki Plain in the semi-humid to semi-arid southeastern Caucasian lowlands that is largely devoid of settlements today (Figure 1). Here, several Late Bronze to Early Iron Age city-type fortified settlements of the so-called Lchashen-Tsitelgori tradition (Sagona, 2018) were found during the last years, suggesting early state formation since ca. 3.2 ka (Furtwängler et al., 1998; Maisuradze and Mindiashivili, 1999; Winter, 1999; Pitskhelauri et al., 2016; Bukhrashvili et al., 2019) (Figure 2). However, this phase of intensive settlement, maybe also extending over the Middle Iron Age (Manning et al., 2018), abruptly ended around 2.5 ka, and only minor human activity seemed to have continued afterwards (Arnhold et al., 2020). Based on destroyed wall structures and secondary buildings that were built on top of a former building layer in the intensively studied Didnauri settlement (Figure 2), it was suggested that the region was affected by strong seismic activity during the beginning of the Early Iron Ages (Pitskhelauri, 2018). The Shiraki Plain and its surroundings currently lack surficial water resources and mostly show a typical steppe vegetation dominated by grassland. However, a paleolake was suggested for the lowest part of the plain (Maruashvili, 1971), and pollen records from the nearby Udabno region (Figure 1) with similar climatic and environmental conditions and a similar Late Bronze/Early Iron Age settlement history (Kunze, 2017) suggest intensive forestation of the upper altitudes until the Late Bronze Age under a more humid climate compared with today (Kvavadze and Todria, 1992). Therefore, besides substantial variations of human activity this also suggests different environmental and hydrological conditions in this region during the past. However, unlike the well-studied humid western Caucasian lowlands and regions >1,000 m a.s.l. in the Lesser Caucasus mountain range (Connor and Sagona, 2007a; Connor et al., 2007b; Messager et al., 2013; Joannin et al., 2014; Connor et al., 2018), existing studies from the lower-altitude semi-humid to semi-arid south-eastern Caucasus region are limited to scattered pollen records with generally rather poor chronostratigraphic control (Gogichaishvili, 1984; Connor and Kvavadze, 2008), or to fluvial-geomorphological (Ollivier et al.,
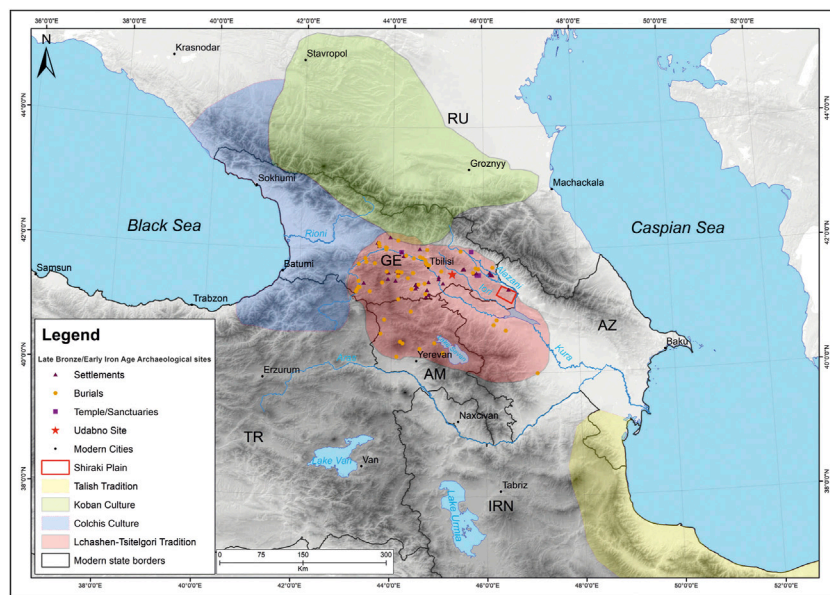
FIGURE 1
The Caucasus region with the distribution of Late Bronze/Early Iron Age cultures (Sagona, 2018). The Shiraki Plain is shown with a red rectangle, and the Udabno region with similar ecologic and climatic conditions as well as a similar prehistoric settlement history with a red star. The topography is based on an SRTM DTM (http://www2.jpl.nasa.gov/srtm) [GE = Georgia, RU = Russia, AZ = Azerbaijan, AM = Armenia, TR = Turkey, IRN = Iran].
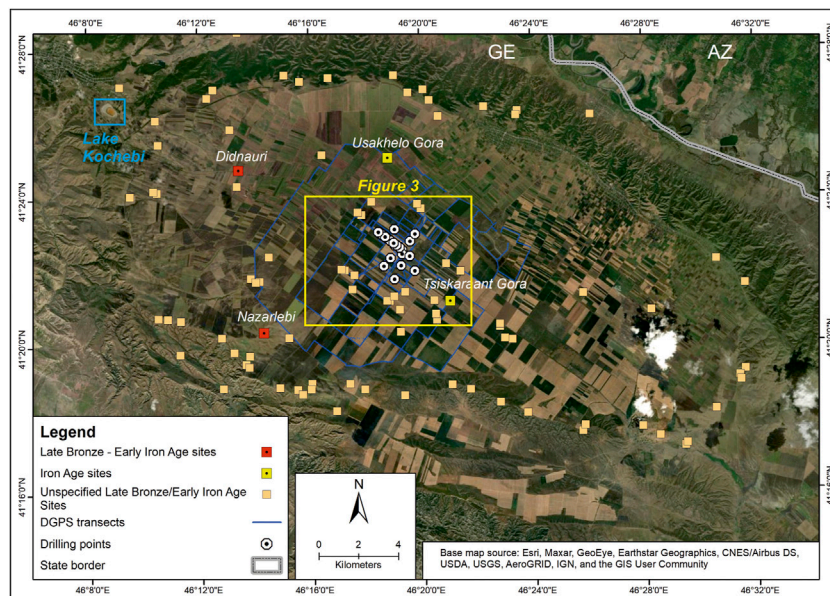
FIGURE 2
The Shiraki Plain with Late Bronze/Early Iron Age archaeological sites (Varazashvili and Pitskhelauri, 2011) and the core drillings and DGPS transects of this study. The area shown in Figure 3 is indicated with a yellow rectangle, and Lake Kochebi west of the plain with a blue rectangle [GE = Georgia, AZ = Azerbaijan].

2015, 2016; Suchodoletz et al., 2015, 2018), paleoecological (Bliedtner et al., 2018, 2020a; Suchodoletz et al., 2020) or paleoclimatic (Bliedtner et al., 2020b) investigations of fluvial sediments. However, due to their discontinuous character fluvial sediment archives generally show a relatively poor chronological resolution (Lewin and Macklin, 2003). Therefore, Holocene human-environmental interactions in the semi-humid to semi-arid south-eastern Caucasus region are currently not well understood. Furthermore, beyond the historical period the possible impact of seismic events on former regional societies has not been studied so far (Varazanashvili et al., 2011).

During this multi-disciplinary study that was carried out on the semi-arid Shiraki Plain we combined geomorphological, sedimentological, chronological and paleoecological data as well as hydrological modelling to: (i) Reconstruct regional paleoenvironmental changes during the Holocene, (ii) identify possible natural versus human causes, and (iii) study possible seismic events during the Late Bronze/Early Iron Ages. Our study will help to better understand human-environmental interactions in the fragile drylands of the southeastern Caucasus especially during the Late Bronze to Early Iron Age period when early state formation occurred in this region.

2 Study area

The endorheic Shiraki Plain is located in eastern Georgia between ca. 41°18′ and 41°27′N, and 46°11′ and 46°30′E (Figure 2) at altitudes between about 550 and 650 m a.s.l., covering a catchment area of about 300 km². To the west, south, and north the plain is surrounded by low mountain ridges with highest altitudes of up to 970 m a.s.l. The plain forms part of the Kura Fold-and-Thrust-Belt, consisting of a series of south-vergent faults and thrusts that are composed of deformed Plio-/Pleistocene flysch to molasse sediments. These are formed by conglomerates, sands, loams, clays and sandstones (Gamkrelidze, 2003; Forte et al., 2010).

The regional climate is continental semi-arid. Mean temperatures range between ca. -4°C in January and ca. 23°C in July, and mean annual precipitation is around 490 mm (Furtwängler et al., 1998). The surface of the Shiraki Plain is covered by Vertisols (Matchavariani, 2019). The current xerophytic vegetation is characterized by steppe species such as *Allium atroviolaceum*, *Muscari tenuiflorum* and *Puccinellia distans*, and large parts of the plain are used for intensive agriculture of wheat and sunflowers (Furtwängler et al., 1998).

Permanent surface water is currently largely missing in the plain and on the surrounding mountain ridges, but seasonal creeks descend from the slopes. Due to this lack of permanent surface water resources the area is largely devoid of settlements today, and only in the northern part some larger villages are located. In contrast, west of the Shiraki Plain a seasonal salt lake
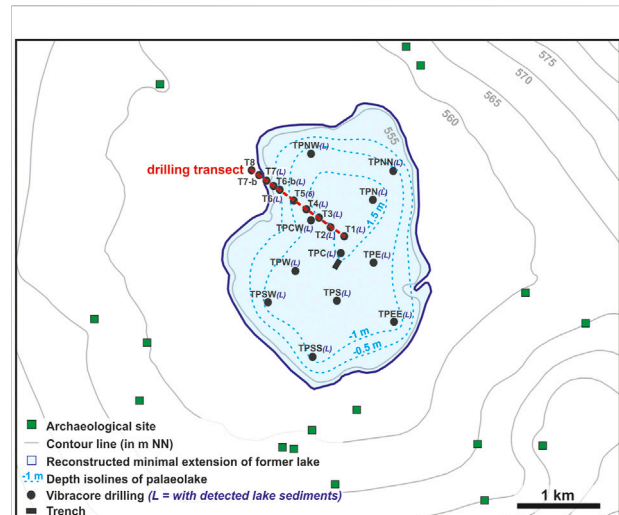
FIGURE 3
The lowest part of the Shiraki Plain with Late Bronze/Early Iron Age archaeological sites (Varazashvili and Pitskhelauri, 2011), core drillings, the studied trench and the maximal extension of the endorheic palaeolake based on the results of the occurrence of lake sediments that was extrapolated to the lowest part of the Shiraki Plain. However, given that lake sediments must have been deposited below a water column of unknown depth, the real maximal extension of the lake must have been somewhat larger than shown here.

(Lake Kochebi) is located at an altitude of ca. 780 m a.s.l. (Figure 2).

3 Methods

3.1 Field work

3.1.1 Stratigraphical mapping

To detect and map the extension of the formerly postulated paleolake (Maruashvili, 1971, 478f.), we applied vibracore drillings in the deepest parts of the plain using an Atlas Copco Cobra Pro hammer with a 60 mm diameter open corer: In a first step, 11 drillings were irregularly distributed over the topographically deepest part of the plain to verify and roughly outline the distribution of the possible paleolake sediments. In a second step, 10 further drillings were performed along a transect from the approximate center of the paleolake towards the northwest until the lacustrine sediments disappeared. Whereas the initial distance between the transect drillings in the approximate center of the paleolake was 200 m, to properly map the largest spatial extension of lacustrine sediments we reduced the drillings to distances of 100 m between drillings T6 and T8 at the northwestern transect margin (Figure 3). Supported by Ad-hoc (2005) and the Munsell soil color chart, the
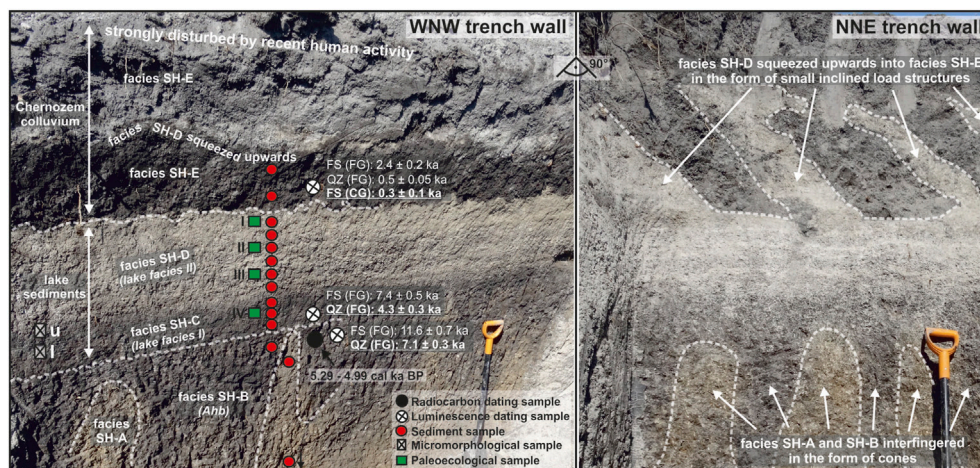
FIGURE 4
The stratigraphy of the trench with the locations of numerical dating, sediment, paleoecological and micromorphological samples. The luminescence results are given for feldspar (FS), quartz (QZ), fine grain (FG) and coarse grain (CG), and the preferred ages are underlined. Please note that the uppermost part of facies SH-E in the left-hand figure was not wetted, so that it appears lighter than the lower part of this material. The two trench walls are rectangular to each other. A version of this figure without any labellings and drawings can be found in Supplementary Figure S1.

sediments were mapped according to basic field properties (approximate grain size, wet sediment color, structure, stone content, sedimentary/pedogenic horizons, carbonate content, hydroxymorphic features, occurrence of gypsum crystals). The grain size distribution was classified according to Jahn et al. (2006). To obtain a detailed stratigraphy of the lacustrine and their over- and underlying sediments, in the approximate center of the paleolake an artificial ca. 3 m deep trench was dug into NNE - SSW direction using a shovel excavator (Figure 3). Similar to the drillings, basic field properties of the sediments were described according to Jahn et al. (2006) and Ad-hoc (2005).

3.1.2 Delineating the paleolake extension

First, we first built up a well-resolved digital terrain model (DTM) of the central Shiraki Plain by performing differential GPS (D-GPS) measurements with a resolution of some centimeters during September and November 2019 using a Stonex device operating with the Georgian CORS system (http://geocors.napr.gov.ge/SBC/spider-business-center). To cover a large area, these measurements were conducted along transects from a slowly moving vehicle. Later, these point measurements were interpolated in Arc Map GIS 10.4. 1 using the "Topo To Raster" tool, and a raster DTM was constructed that was integrated into the existing SRTM DTM. Subsequently, we properly mapped the highest altitude of lake sediments that were detected in the drilling transect, and then extrapolated this altitude to the complete central part of the Shiraki Plain using the newly creating well-resolved DTM.

3.2 Laboratory analyses

3.2.1 Sedimentological analyses

Fourteen sediment samples were taken from the main sedimentological units in the trench for sediment analyses (Figure 4). Prior to the analyses the samples were air-dried, and material >2 mm was removed by sieving.

Grain size was measured using 10 g of bulk sample material. After removing organic matter with 35% H_2O_2, the samples were dispersed in 10 ml 0.4 N sodium pyrophosphate solution ($Na_4P_2O_7$), and subsequently treated in an ultrasonic bath for ca. 45 min. The sand content (63–2000 μm) was determined by wet sieving, and the clay and silt content by measuring the material <63 μm with X-ray granulometry (XRG) using the SediGraph III 5120 (Micromeritics).

Calcium carbonate contents were determined according to Scheibler (Schlichting et al., 1995): Depending on the pre-tested approximate carbonate content, 1–10 g of material were filled into an Eijkelkamp Calcimeter apparatus, and 10% HCl was added continuously until the reaction ceased. Carbonate-bound C was calculated based on the CO_2 volume that was produced during the reaction.

Element distributions were measured on 32 mm-pellets that were produced by mixing and pressing 8 g of the ground material with 2 g CEREOX Licowax prior to measurement with a Spectro Xepos X-ray fluorescence spectrometer.

Measurements of mass-specific magnetic susceptibility (χ) were performed using a Bartington MS3 magnetic susceptibility meter equipped with a MS2B dual frequency sensor. After softly grounding and densely packing the

material into plastic boxes, volumetric magnetic susceptibility was measured with a frequency of 0.465 kHz (κ_{LF}). Normalizing κ_{LF} with the sample mass yielded mass-specific magnetic susceptibility χ.

Total carbon and nitrogen were determined using a Vario EL cube elemental analyser on material that was ground in a vibratory mill for ca. 10 min (required grain size <30 μm). *Total organic carbon (TOC)* was calculated by subtracting inorganic carbon (calculated from carbonate-bound C) from total carbon.

Black carbon (BC) content and its aromaticity were determined by measuring benzene polycarboxylic acids (BPCA) contents and patterns, respectively, according to Glaser et al. (1998) with the first step modified by Brodowski et al. (2005). This method comprises metal removal with 4 M trifluoroacetic acid (Brodowski et al., 2005), followed by nitric acid digestion (170°C, 8 h under pressure), cation exchange chromatography, derivatization (trimethylsilylation) and gas chromatography with flame ionization detection (Glaser et al., 1998). The sum of the individual BPCAs was converted to the black carbon content by multiplication with 2.27 (conversion factor for charcoal; Glaser et al., 1998). The challenge of the samples under study was their high gypsum content, which interfered with BPCA analysis probably due to complexation with dissolved Ca during the procedure. The best compromise to solve this problem was to use smaller amounts of material for the analysis (100 mg instead of 500 mg).

3.2.2 Numerical dating

Numerical dating was carried out in the CEZ radiocarbon laboratory Mannheim (Germany).

3.2.2.1 Radiocarbon dating

For radiocarbon dating we used one bulk sediment sample (location see Figure 4). The sample was prepared with the Acid-Base-Acid method (Steinhof et al., 2017), and the bulk organic matter after removing NaOH-soluble organic matter was dated. The age was calibrated using the software SwissCal applying the Intcal20 calibration curve (Reimer et al., 2020).

3.2.2.2 Luminescence dating

For luminescence dating three samples were taken (locations see Figure 4) during night, and directly packed into light-proof plastic bags. To sample only material that was not influenced by sunlight, we removed the outer 20 cm of the material right before sampling. Sample preparation under subdued red light included sieving recovering material between 90 and 200 μm and <90 μm, following treatment with 10 and 30% HCl to remove carbonate, and with 10 and 37% H_2O_2 for about 14 days to remove organic matter. Only for sample MAL-10551 (55 cm) the coarse grain fraction 90–200 μm could be obtained in a datable amount. However, given a still very low amount of material we did not apply any density separation or etching to this fraction, resulting

in a polymineral coarse grain fraction. Furthermore, for all samples the polymineral fine grain fraction 4–11 μm was separated from the sieve fraction <90 μm according to Stoke's Law in Atterberg settling tubes. The luminescence measurements were carried out on a Risø TL-DA-20 luminescence reader equipped with a $^{90}Sr/^{90}Y$ β-source (0.056 Gy/s for coarse grain, 0.074 Gy/s for fine grain). For the polymineral coarse (90–200 μm) and fine grain (4–11 μm) measurements applying the post-IR IR protocol of Buylaert et al. (2012) with a measurement temperature of 290 °C (pIRIR$_{290}$), we used a BG3/BG39 filter combination. We also aimed to compare feldspar and quartz fine grain measurement with respect to bleaching, since quartz bleaches faster than the feldspar pIRIR$_{290}$ signal (Kars et al., 2014). However, since also the fine grain fraction did not consist of enough material to etch away the feldspar, we measured the fine grain quartz signal by applying the single aliquot regeneration protocol of Murray and Wintle (2000) using an U340 filter that largely removes the feldspar emission. The a-values of polymineral and quartz fine grain were measured with an ^{241}Am α-source (0.115 Gy/s), and the a-value of 0.08 ± 0.03 for feldspar coarse grain was taken as a mean value from various literature about this kind of material (Wallinga et al., 2001; Rees-Jones and Tite, 2007; Kreutzer et al., 2018). Anomalous fading of the polymineral samples was tested by comparing the luminescence signals of not irradiated discs with those of irradiated discs directly after irradiation, and after seven and after 30 days following irradiation.

In parallel with the luminescence samples, ca. 500 g of material were taken from the same positions during daylight for dose rate determination. Given that samples MAL-10551 and MAL-10552 were located near stratigraphic borders, for both samples additional dose rate samples from facies SH-D were taken from nearby positions assumed to contribute ca. 30% of the gamma dose rate (see Table 1). After drying the samples at 105 °C for 24 h, dose rates were measured with low-level γ-spectrometry using a Canberra GCW4023 device. Given deep sediment desiccation for an unknown period after lake desiccation as could be recognized when opening the trench, a water content of 15 ± 10% was assumed to encompass the water contents of the complete burial periods. The cosmic dose rate was calculated according to Prescott and Hutton (1988), assuming a density of the overlying sediments of 1.6 g/cm³. The parameters used for age calculation and the luminescence ages are shown in Table 1.

3.2.3 Micromorphological analyses

One oriented block was taken for micromorphological analyses. After air-drying and impregnating with Oldopal P 80-21, the hardened block was cut and sliced into an upper (u) and a lower (l) 70 * 50 mm thin section (locations see Figure 4). Micromorphological description and analysis of the thin sections has been done under an Olympus BX51 petrographic microscope, following the guidelines of Stoops (2021).

TABLE 1 Measurement parameters and results of luminescence dating from the trench.

Sample number	Sample depth and facies	Th [ppm]	U [ppm]	K [%]	Assumed water content [%]	Kind of measurement	Dose rate [Gy/ka]	Cosmic dose rate [Gy/ka]	Equivalence dose [Gy]	a-value	Anomalous fading	Age [ka]
MAL-10551	55 cm (facies SH-E)	6.24 ± 1.17	2.0 ± 0.08	1.62 ± 0.05	15 ± 10	fine-grained feldspar	3.71 ± 0.32	0.22 ± 0.02	8.83 ± 0.56	0.18 ± 0.02	no	2.38 ± 0.21
						fine-grained quartz	2.77 ± 0.23	0.22 ± 0.02	1.34 ± 0.06	0.05 ± 0.02		0.48 ± 0.05
						coarse-grained feldspar	2.40 ± 0.61	0.22 ± 0.02	0.76 ± 0.19	0.08 ± 0.03**	no	0.32 ± 0.09
	70 cm (facies SH-D)*	3.26 ± 0.11	1.16 ± 0.05	0.83 ± 0.03								
MAL-10552	125 cm (facies SH-C)	7.34 ± 0.21	1.78 ± 0.07	1.86 ± 0.06	15 ± 10	fine-grained feldspar	3.26 ± 0.22	0.20 ± 0.02	23.83 ± 0.28	0.09 ± 0.02	yes	7.35 ± 0.49
						fine-grained quartz	3.04 ± 0.21	0.20 ± 0.02	12.85 ± 0.1	0.06 ± 0.02		4.25 ± 0.3
	110 cm (facies SH-D)*	4.10 ± 0.14	1.16 ± 0.05	1.01 ± 0.04								
MAL-10553	155 cm (facies SH-B)	6.48 ± 0.18	1.62 ± 0.06	1.80 ± 0.06	15 ± 10	fine-grained feldspar	3.03 ± 0.20	0.19 ± 0.02	35.06 ± 0.31	0.08 ± 0.02	yes	11.6 ± 0.7
						fine-grained quartz	2.83 ± 0.20	0.19 ± 0.02	20.12 ± 0.15	0.05 ± 0.02		7.1 ± 0.5s

*assumed to contribute ca. 30% of the gamma dose rate.

[a]Taken from literature (Wallinga et al., 2001; Rees-Jones and Tite, 2007; Kreutzer et al., 2018).

3.2.4 Paleoecological analyses

Four sediment samples of about 1 kg were taken for paleoecological analyses (locations see Figure 4), and sieved with distilled water with mesh widths of 0.71 and 0.21 mm, respectively. Subsequently, organic material such as charcoal, bones, teeth or seeds was analyzed using an Amscope binocular (magnification = 40).

3.3 Hydrological modelling

Based on a DTM (SRTM C-band; Farr et al., 2007) we delineated the catchment boundaries using ArcGIS 10.3, defining the lowest point of the basin manually. Subsequently, we processed the catchment DTM using the freq function of the R raster-package of Hijmans (2020) to calculate the geomorphologically possible maximal lake size and volume (All calculations are available at Gihub: https://github.com/MLFischer/Shiraki-Plain-Water-Balance, 03/22).

Then, we used three Holocene time periods to calculate the water balance of the catchment. Paleoenvironmental and paleoclimatic data were taken from a pollen reconstruction that covers the period around the Late Bronze/Early Iron Ages in the Udabno region ca. 80 km to the west with very similar ecological and climate conditions (Kvavadze and Todria, 1992): (a) The Early/Mid Holocene with a mainly forest-covered basin above and fertile meadow grassland below the timberline at ca. 700 m a.s.l. For this period a similar annual temperature as today and a maximal precipitation amount as for period (b) were assumed. (b) The Late Bronze/Early Iron Ages with a clear-cut basin covered by fertile meadow grassland, a lake with a size of at least 5 km^2 (taken from this study), a reconstructed higher annual temperature of ca. 1.5 °C and higher precipitation of ca. 200–300 mm/a compared with today, and (c) a modern-day climate scenario with a drier grassland-covered basin and no lake. For the modern period, for comparison we also calculated the water balance for the altitude of current salt Lake Kochebi (located ca. 230 m higher than the lowest part of the Shiraki Plain) (location see Figure 2).

Based on major (paleo-)environmental properties as summarized in Supplementary Table S1, for each time period and land cover we used an established parametrization approach (e.g. Brutsaert, 1982; Bougealt, 1991; Blodgett et al., 1997; Bergner et al., 2003) to calculate the actual evapotranspiration rate (ETa). Climate variables such as air temperature, relative humidity, surface conditions (surface drag coefficient, albedo, emissivity and soil moisture availability) were parametrized following Bougealt, 1991, and using the paleoenvironmental reconstructions of Kvavadze and Todria (1992). Cloud coverage was achieved using a global cloud coverage

dataset (Wilson and Jetz, 2016), and the cloud parameter was set according to Budyko (1974). Insolation was set according to Laskar et al. (2004). Modern-day climate variables were set using global gridded climate data (New et al., 2002). Temperature differences to the modern-day conditions were applied either using the paleoclimate reconstruction of Kvavadze and Todria (1992), or by using adiabatic average temperature gradients. Based on the precipitation and evapotranspiration rates we calculated the annual water flux volumes regarding the different land cover proportions within the basin.

4 Results

4.1 Field work

4.1.1 Stratigraphical mapping

To facilitate the stratigraphical description, we start here with the detailed description of the trench in the lowest part of the Shiraki Plain to establish the different facies, and then continue with the description of the drilling cores.
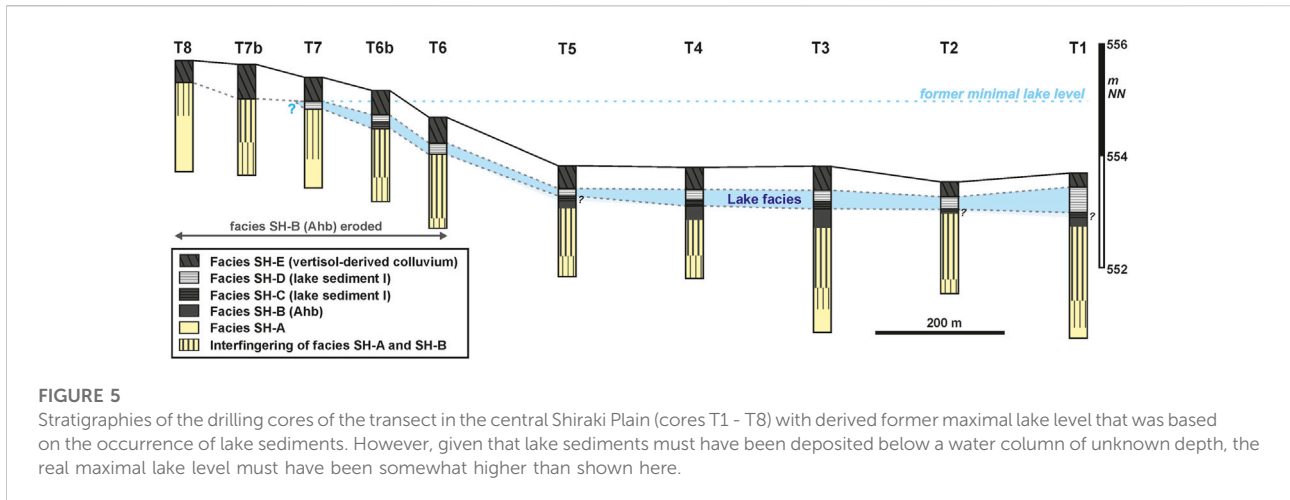
4.1.1.1 Trench

The facies described from bottom to top are shown in Figure 4:

- Facies SH-A (300 - 144 cm): The base of the trench is formed by brown (10YR4/3) carbonate-rich heavy clay with a polyedric structure. This material contains *in-situ* carbonate, gypsum, and iron oxide precipitations. Given the very fine grain sizes, we suggest that these deposits could represent limnic sediments of a paleolake. Between ca. 250 and 144 cm facies SH-A and SH-B are interfingered with each other, and the vertical cones in the interfingering zone showed widths of ca. 20 cm. We suggest that these deformation structures were linked with seismic shocks.

- Facies SH-B (144 - 135 cm): This facies consists of very dark gray (10YR3/1) heavy clay with a polyedric structure, and contains less gypsum precipitations and much less carbonate compared with facies SH-A. In some parts also reddish iron oxide stains were found. Given its high clay content and shiny slickensides on the aggregate surfaces, this material was interpreted as the Ahb horizon of a buried pellic Vertisol that had developed on the surface of facies SH-A and was overprinted by light-coloured gypsum precipitations. Given that it is not a surficial but buried soil, possibly formerly existing vertical cracks should not be recognizable any more.

- Facies SH-C (135 - 113 cm): Similar to facies SH-B this facies consists of black (7.5YR2.5/1) heavy clay with a fine polyedric structure. However, in difference to the former slight horizontal layering was recognizable. The matrix of this facies is mostly free of carbonate, and contains some mycelia-like gypsum precipitations and brownish iron oxide stains. This facies was interpreted as layered lacustrine sediments mostly consisting

FIGURE 5
Stratigraphies of the drilling cores of the transect in the central Shiraki Plain (cores T1 - T8) with derived former maximal lake level that was based on the occurrence of lake sediments. However, given that lake sediments must have been deposited below a water column of unknown depth, the real maximal lake level must have been somewhat higher than shown here.

of eroded Vertisol material from the surrounding slopes (lake facies I).

- Facies SH-D (113 - 70 cm): This facies consists of dark reddish gray (5YR4/2), (dark) grayish brown (10YR4/2) and brown (7.5YR5/2) up to 1 cm thick evaporative carbonate and gypsum layers alternating with clastic layers of heavy clay that are broken by desiccation cracks. Numerous *in-situ* gypsum precipitations cause a pseudosand structure of the greyish evaporative layers, whereof the proportion increases upwards. This facies was interpreted as lacustrine sediments of a successively drying lake (lake facies II).

- Facies SH-E (70 - 0 cm): This facies unconformably overlies facies SH-D, and consists of carbonate-rich black (7.5YR2.5/1) heavy clay with a polyedric structure and shiny slickensides on the aggregate surfaces. This material contains carbonate and gypsum precipitations. It was interpreted as a vertisol-derived colluvial layer. In the WNW trench wall, at ca. 40 cm depth a ca. 10 cm thick layer of material of facies SH-D was intercalated. However, in the neighbouring NNE trench wall it could be recognized that this material forms part of a series of small inclined load structures that were detached from the upper part of facies SH-D and squeezed into the material of facies SH-E. We suggest that these inclined load structures were linked with seismic shocks. The upper part of facies SH-E was strongly disturbed by recent human activity (recent Ap horizon).

4.1.1.2 Drillings

The lowest parts of all drillings were formed by facies SH-A. However, with increasing distance from the former lake center such as in drillings T7 and T8 (Figure 3), the grain size of this facies coarsened and changed from heavy clay to silty clay. The intermixture of facies SH-A and SH-B (Figure 4) was found in all cores (Figure 5). Unfortunately, given the similar sediment properties of facies SH-B and SH-C these could not well be differentiated from each other in the cores. However, black-

coloured material potentially originating from one of both facies was mostly found in the center of the plain, but not in cores TPCW, TPSS and T6 - T8. Overlying facies SH-D was detected in all cores but cores T7B and T8. Although facies SH-B was eroded in core T7B, some intermixing of this facies and facies SH-E was observed here. Facies SH-E was found in all cores. The core stratigraphies are listed in Supplementary Tables S2, 3, and the stratigraphy of the drilling transect is shown in Figure 5.

4.1.2 Delineating the maximal paleolake extension

To build up the well-resolved DTM of the central Shiraki Plain we measured 10,700 points with D-GPS. These points showed altitudes between 554 and 642 m a.s.l. The larger study area was covered with an irregular grid of measurement transects that followed existing earth roads, being denser in the central part of the plain where the study area is located (Figure 2). The maximal paleolake extension was derived by taking the altitude of core T7 that forms the northwesternmost drilling core of the transect towards the former northwestern lake margin where lake sediments (facies SH-D) were observed (555.34 m a.s.l.; Figure 5), and subsequently following this contour line in the newly created well-resolved DTM. This resulted in a maximal lake extent of ca. 6.2 km^2.

4.2 Laboratory analyses

4.2.1 Sedimentological analyses

The results of the sedimentological analyses are shown in Figure 6, and the data can be found in Supplementary Table S4.

The *grain size* is largely dominated by clay, with irregularly varying values between 73 and 98% found throughout the sequence. The sand fraction strongly fluctuates between 0.5 and 21% within the sequence, showing the lowest values
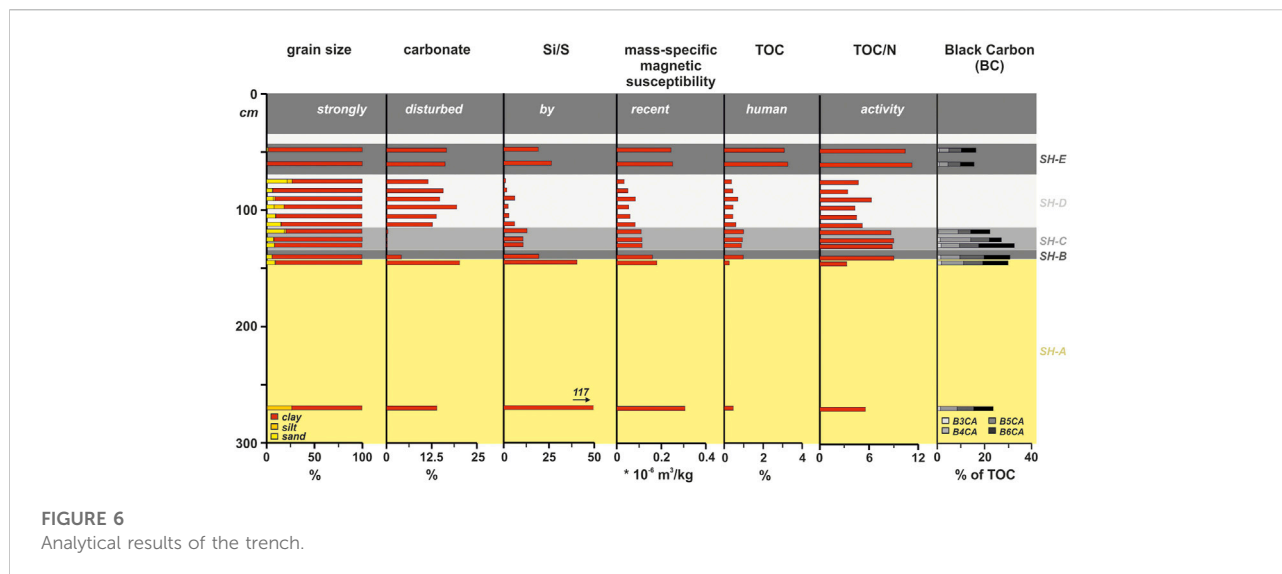
FIGURE 6
Analytical results of the trench.

TABLE 2 Results of radiocarbon dating from the trench.

Sample depth	Sample number	Material	$\delta^{13}C$ (‰)	C (%)	^{14}C age (year BP)	Calibrated ^{14}C age (cal. ka BC)
132 cm	MAMS-46350	sediment matrix	−24.5	1.0	4,481 ± 26	3.34 - 3.03

in facies SH-E. However, most of the sand was formed by *in-situ* precipitated gypsum crystals (pseudosand).

Calcium carbonate contents varied between 14 and 20% in facies SH-A. Facies SH-B showed a sharp drop to a value of 4%, and in facies SH-C carbonate contents dropped even more down to values between 0.4 and 0.2%. In facies SH-D carbonate values strongly increased to values between 20 and 11%, and similar values around 16% were also found in facies SH-E.

To analyze the inorganic *element distributions*, we first correlated the elements Si, Ti, Al, Fe, Rb, K, Zr, Ti, Mn, P, Ca, Mg and S in a correlation matrix. These elements are commonly included in element ratios that are used to trace grain sizes (Croudace et al., 2006), possible volcanic provenances (Zielhofer et al., 2017), paleo-redox conditions (Koinig et al., 2003) or human impact (Holliday and Gartner, 2007), or form the main components of silicates, gypsum and carbonates (Salminen, 2005). The results showed that the highest negative correlations exist between the siliciclastic elements Ti, Rb, Zr, Si and Al as well as Fe on the one hand, and Ca and S forming the main components of calcium carbonate and gypsum on the other hand (Supplementary Table S5). Therefore, we used the ratio Si/S to trace changes between siliciclastic layers and layers

characterized by a high content of (evaporative) gypsum. This ratio shows high values between 117 and 40 in facies SH-A, an intermediate value of 20 in facies SH-B, slightly lower values between 13 and 10 in facies SH-C, an upwards decreasing trend from 6 to 1 in facies SH-D, and intermediate values between 20 and 26 in facies SH-E.

Relatively high values of *mass-specific magnetic susceptibility* (χ) between 0.31 and 0.18 * 10^{-6} m^3/kg were measured in facies SH-A, and a slightly lower value of 0.16 * 10^{-6} m^3/kg in facies SH-B. Uniform intermediate values of 0.11* 10^{-6} m^3/kg were found in facies SH-C, and in facies SH-D low values with an upwards decreasing trend from 0.08 to 0.03 * 10^{-6} m^3/kg were observed. Facies SH-E showed higher values around 0.25 * 10^{-6} m^3/kg.

Facies SH-A showed relatively low values of *total organic carbon (TOC)* between 0.3 and 0.5%. In contrast, facies SH-B showed a higher value of 1.0% that only slightly dropped to 0.9% in facies SH-C. Facies SH-D showed lower values between 0.4 and 0.7% that strongly increased to values between 3.1 and 3.3% in facies SH-E. Low *TOC/N ratios* between 3 and 6 in facies SH-A increase to values around 9 in facies SH-B and SH-C, subsequently decreasing to values between 3 and 7 in facies SH-D. In facies SH-E this ratio increases again to values around 11.
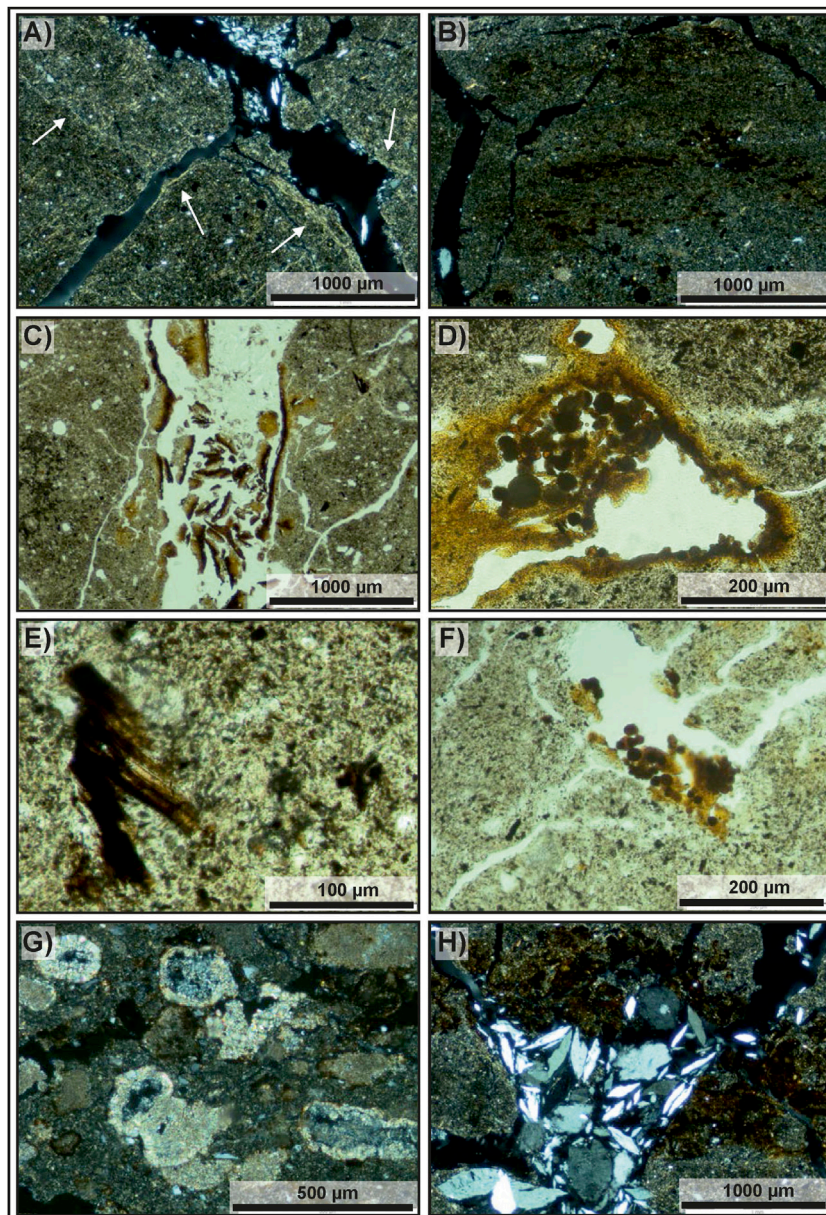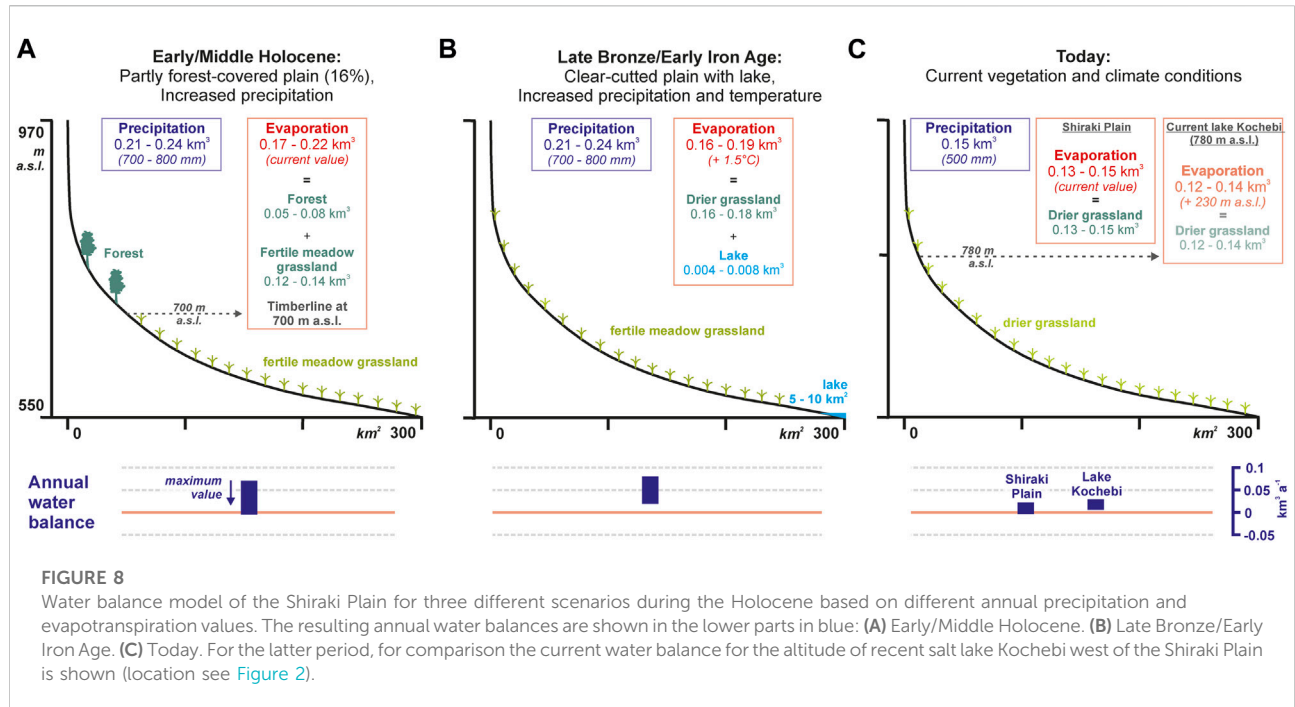
FIGURE 7
Lower sample (l): **(A)** Porostriation along fissures (arrows) resulting from stress (argilloturbation) due to swelling-shrinking. Some gypsum lenses occur at the top as loose discontinuous infillings. **(B)** Upper part of the reduced material, with layered sorting of particle sizes and subhorizontal organic intercalations. **(C)** Hypocoating of Fe-oxihydroxides along a pore (dark line) that has been broken by swelling-shrinking (argilloturbation) and is seen now as infilling of fragments together with gypsum lenses. **(D)** Hypocoatings of Fe-oxihydroxides around pores, and loose infilling of iron spheres, pseudomorphs after pyrite framboids. Some of the pseudomorphs show luster under incident light, which indicates that pyrite oxidation has not been complete. Upper sample (u): **(E)** Dark inclusions in the groundmass corresponding to particulate organic matter. **(F)** Loose discontinuous infilling of Fe nodules, pseudomorphs after pyrite framboids developed on organic materials. **(G)** Geodic nodules of sparite. **(H)** Loose continuous infilling of lenticular gypsum in a biopore (note the root section) together with an impregnative hypocoating of Fe-oxyhydroxides.

Black carbon (BC) contents ranged between 0.8 and 6.1 g kg^{-1} in all facies but SH-D, where no black carbon could be detected. Black carbon contribution to TOC ranged between 19 and 37% in all but facies SH-D. The patterns of the individual benzenepolycarboxylic acids showed an equal contribution of benzenetetracarboxylic acids (B4CA), benzenepentacarboxylic acid (B5CA) and benzenehexacarboxylic acid (B6CA), demonstrating a similar high degree of condensation (Supplementary Table S6).

FIGURE 8
Water balance model of the Shiraki Plain for three different scenarios during the Holocene based on different annual precipitation and evapotranspiration values. The resulting annual water balances are shown in the lower parts in blue: **(A)** Early/Middle Holocene. **(B)** Late Bronze/Early Iron Age. **(C)** Today. For the latter period, for comparison the current water balance for the altitude of recent salt lake Kochebi west of the Shiraki Plain is shown (location see Figure 2).

4.2.2 Numerical dating
4.2.2.1 Radiocarbon dating
The results of radiocarbon dating can be found in Table 2, and the age is shown in its stratigraphic position in Figure 4.

4.2.2.2 Luminescence dating
Luminescence dating yielded different ages for different grain sizes and minerals, ranging between 11.6 ± 0.7 ka and 0.32 ± 0.09 ka. However, the ages of the three samples are in the stratigraphic order. The results of luminescence dating can be found in Table 1, and the ages are shown in their stratigraphic positions in Figure 4.

4.2.3 Micromorphological analyses
Lower sample (l) and approximately the lower half of upper sample (u) were taken from facies SH-C, and showed a blocky structure that was highly separated by fissures. This structure was moderately bioturbated, and most pores were occupied by lenticular gypsum crystals of different sizes that showed frequent inclusions. The birefringence fabric of the micromass is porostriated, i.e. shows stress features along the fissures what reflects some swelling-shrinking processes linked to argilloturbation (Figure 7A). Due to abundant very small organic particles the micromass is speckled. Upwards, organic material increases as layered amorphous intercalations (Figure 7B). Pedofeatures not related to gypsum precipitation include redoximorphic phenomena such as nodules of Fe- and Mn- oxi-hydroxides as well as

clusters of small spheres of Fe-oxides after pyrite framboids (Figure 7C). The latter are often located next to organic residues, and some of those spheres still keep some unaltered pyrite inside (Figure 7D). The redoximorphic pattern can be classified as stage F or G of Vepraskas et al. (2018), meaning extreme, permanent reduction conditions.

The upper part of sample (u) was taken from facies SH-C. This sample is composed of a 0.5 cm thick layer of lenticular gypsum crystals that underlies clayey material with a lighter color compared with the clayey material of sample (l), but that also contains microparticles of organic matter (Figure 7E). Fe-oxide pseudomorphs after pyrite are equally present (Figure 7F), and the redoximorphic pattern corresponds to stage B of Vepraskas et al. (2018) indicating moderate reduction conditions. As the most striking pedofeatures of this sample we find micrite and geodic sparitic nodules of probably biogenic origin that could be derived from algae or other organisms living in shallow water conditions (Freytet and Verrecchia, 2002) (Figure 7G). In particular, infillings of calcitic excrements in channels are difficult to explain, unless they were made by fauna mixing materials with different calcite contents (Figure 7G).

Scans of the thin sections of both samples can be found in Supplementary Figure S2.

4.2.4 Paleoecological analyses
Different types of organic material were detected in the samples, i.e. charcoal, plant or wood tissues, plant roots,
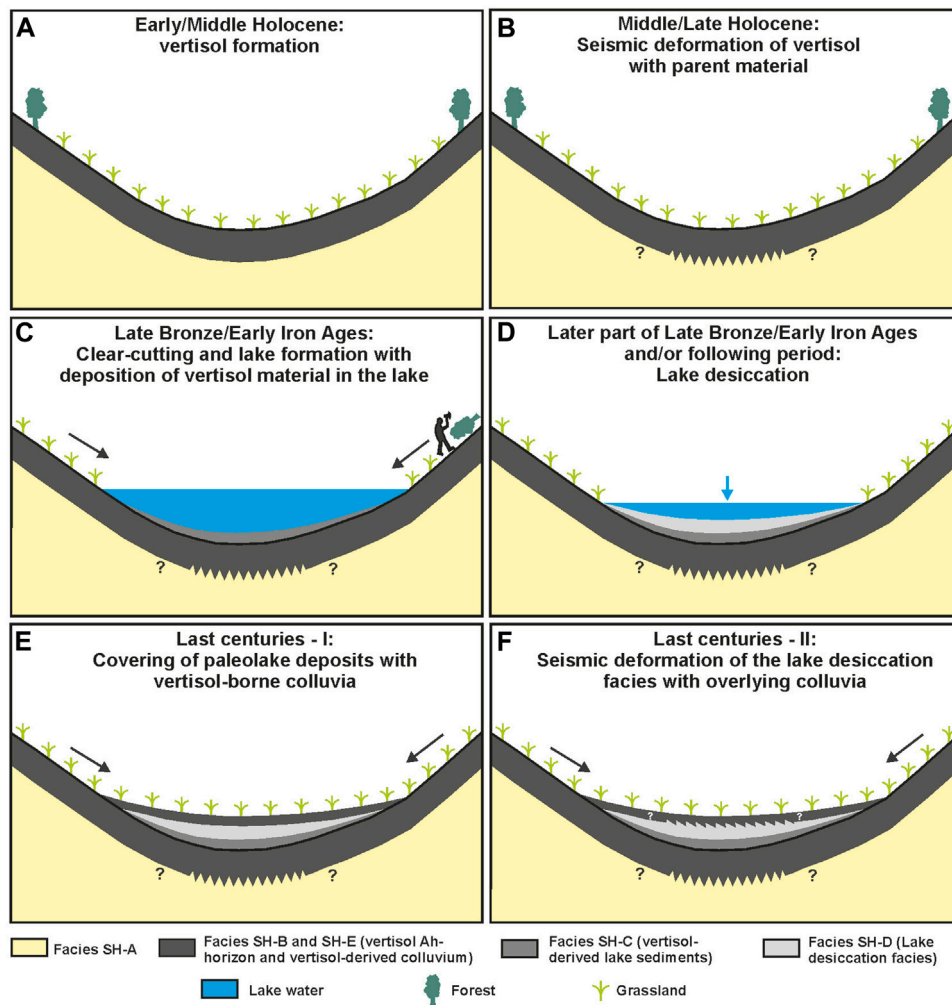
FIGURE 9
Landscape evolution of the Shiraki Plain: **(A)** Early/Middle Holocene. **(B)** Middle/Late Holocene. **(C)** Late Bronze/Early Iron Ages. **(D)** Later part of Late Bronze/Early Iron Ages and/or following period. **(E)** Last centuries−I. **(F)** Last centuries−II.

probably fish bones that could not be assigned to certain species, and in samples I and II fish teeth of the family *Cyprinidae* (sample locations see Figure 4).

The results are listed in Supplementary Table S7, and a photo of fish teeth and probably fish bones from sample II is shown in Supplementary Figure S3.

4.3 Hydrological modelling

The minimal Holocene lake size of ca. 6.2 km² that was calculated during this study should have hosted a water volume of ca. 0.006 km³. This water volume is much lower compared with the value of ca. 0.75 km³ for a lake with a size of about 70 km² that would have formed at the altitude of the theoretical

modern-day outflow of the plain at ca. 577.5 m a.s.l. However, according to our data that water level was never reached during the Holocene, i.e. the Shiraki Plain was always endorheic during that period.

For the Early/Mid Holocene we assumed a similar temperature as today and calculated an ETa of 481–565 mm a^{-1} on fertile meadow grassland and of up to 1,092–1,648 mm a^{-1} over forests, and for the Late Bronze/Early Iron Ages with a reconstructed higher temperature of ca. 1.5°C (Kvavadze and Todria, 1992) an ETa of 517–607 mm a^{-1} over fertile meadow grassland and of 822 mm a^{-1} over the paleolake. For the modern-day climate we calculated an ETa over drier grassland of 429–508 mm a^{-1}, and for the conditions at the ca. 230 m higher altitude of current salt lake Kochebi this results in a slightly lower current drier grassland ETa of 400–475 mm a^{-1}.

For the Early/Mid Holocene with an assumed maximal precipitation amount of 700–800 mm a^{-1} (0.21–0.24 km³ a^{-1}) and the timberline located at 700 m a.s.l we calculated an ETa volume over forests of 0.05–0.08 km³ a^{-1}, and for the fertile meadow grassland below the timberline an ETa volume of 0.12–0.14 km³ a^{-1}. This would result in a balanced water budget of -0.02–0.06 km³ a^{-1} (Figure 8A). For the Late Bronze/Early Iron Ages with a reconstructed precipitation amount of 700–800 mm a^{-1} (0.21–0.24 km³ a^{-1}; Kvavadze and Todria, 1992), for a lake size of 5–10 km² we calculated an ETa volume of 0.004–0.008 km³ a^{-1}, and a fertile meadow grassland ETa (covering the rest of the basin) of 0.16–0.18 km³ a^{-1}. This results in a positive water budget between 0.02 and 0.08 km³ a^{-1} (Figure 8B). For the modern-day time with a precipitation amount of about 500 mm a^{-1} (0.15 km³ a^{-1}) and a drier grassland evapotranspiration of 0.13–0.15 km³ a^{-1}, this results in an overall balanced water budget of -0.002–0.022 km³ a^{-1}, and for the climatic conditions at the ca. 230 m higher altitude of current salt lake Kochebi the model shows a slightly positive water budget of 0.007–0.029 km³ a^{-1} (Figure 8C).

5 Discussion

5.1 Holocene landscape evolution of the Shiraki Plain

Based on our stratigraphical, chronological, sedimentological, micromorphological and paleoecological data we reconstructed the Holocene landscape evolution of the Shiraki Plain:

i) During the Early/Mid-Holocene no lake existed in the central part of the Shiraki Plain (Figure 9A). Instead, the clay-rich material parent material (facies SH-A) was overprinted by Vertisol formation (facies SH-B) what is also confirmed by our analytical data: Depending on the local conditions Vertisols show strongly varying TOC contents that also encompass the measured value of ca. 1%, and similar TOC/N ratios around or slightly higher than 10 were also reported from other Vertisols (Virmani et al., 1982; de la Rosa et al., 2008). BC was hardly studied in Vertisols so far. However, according to Reisser et al. (2016), next to the contents of organic carbon and clay one factor that strongly determines the soil BC dynamics is the regional climate. Accordingly, our measured proportion of BC of TOC of about 30% and the equal proportions of the benzenepolycarboxylic acids B4CA, B5Ca and B6Ca (Figure 6) are typical for Chernozems (Rodionov et al., 2010) that are found in regions with climate conditions that are similar as those of the Shiraki Plain (Strouhalová et al., 2019). No numerical ages are available for the start of Vertisol formation. However, the bulk sediment radiocarbon

age of 5.3 - 5.0 cal ka BP from facies SH-B, averaging the age of organic matter in the soil matrix (Wang and Amundson, 1996), demonstrates that Vertisol formation must have lasted at least until that time. Looking at the luminescence ages, fine-grained feldspar pIRIR$_{290}$ dating gave a minimum age of 11.6 ± 0.7 ka (no fading correction applied), and fine-grained quartz an age of 7.1 ± 0.3 ka. Soil turbation processes cause the input of bleached mineral grains into the soil matrix also after sediment deposition (Bateman et al., 2003). Hence, in difference to the radiocarbon ages dating the soil organic matter, the luminescence ages should reflect argilloturbation linked with Vertisol formation. The large difference between both luminescence ages can possibly be explained with the much better bleachability of quartz compared with the pIRIR$_{290}$ feldspar luminescence signal (Kars et al., 2014). The cone-like intercalation of facies SH-A and SH-B indicates a strong seismic event when the Vertisol (SH-B) was already well developed, i.e. this event must have occurred during the Mid-to Late Holocene (Figure 9B).

ii) A permanent lake must subsequently have covered the pellic Vertisol in the central part of the Shiraki Plain. The first lake phase is reflected by horizontally layered facies SH-C (Figure 9C). Besides the layering, its (permanent) lacustrine character is demonstrated by micromorphology that showed pyrite formation and redoximorphic stages F or G (Figures 7C,D), indicating permanent reduction conditions (Vepraskas et al., 2018). These must have been caused by longer-lasting permanent covering of the sediments by lake water. The sedimentological properties of facies SH-C with a TOC content around 0.9%, the grayish to black color, TOC/N ratio around 9, equal proportions of the benzenepolycarboxylic acids B4CA, B5Ca and B6Ca and proportions of BC of TOC of ca. 33 to 22% are similar with those of the underlying Vertisol horizon (facies SH-B; Figure 6). This indicates the origin of facies SH-C from eroded Vertisols around the lake. Lower values of magnetic susceptibility compared with facies SH-B could possibly be explained with partial destruction of the magnetic signal under anoxic conditions (Hanesch and Scholger, 2005) (Figure 6). The origin of facies SH-C from eroded Vertisols is also supported by the observation that the Vertisol horizon (facies SH-B) was not detected between transect cores T6 and T8 located towards the former lake margin: The flat topography and rapid covering by lake water should have protected the Vertisol against soil erosion in the central plain, whereas it was eroded from the not water-covered and steeper parts of the plain beyond the paleolake shore (Figure 5). Fine-grained feldspar pIRIR$_{290}$ luminescence dating gave a minimum age of 7.4 ± 0.5 ka (not corrected for anomalous fading) for facies SH-C, and fine-grained quartz an age of 4.3 ± 0.3 ka. Given the better bleachability of quartz compared with the pIRIR$_{290}$ signal (Kars et al., 2014), the quartz age probably best approximates

the depositional age of the lake sediments. Archaeological finds show intensive settlement of the Shiraki region during the Late Bronze to Early Iron Ages since ca. 3.2 ka (Furtwängler et al., 1998, 1999; Maisuradze and Mindiashivili, 1999; Pitskhelauri et al., 2016; Bukhrashvili et al., 2019). Given that no large-scale human settlement is known from the Shiraki Plain prior to that time, the Vertisols must have been eroded by agricultural activity of that culture. Hence, on the one hand the chronological difference between the luminescence-dated start of Vertisol erosion reflected by the deposition of black-colored lacustrine facies SH-C, and the start of intensive human activity some centuries later, can possibly be explained by so far incomplete numerical dating of the archeological finds. Thus, further numerical dating of archaeological sites could result in older ages. On the other hand, this difference could also be explained by insufficient bleaching of the fine-grained vertisol-derived material during its colluvial transport from the slopes towards the central lake basin (Fuchs and Lang, 2008).

iii) After an unknown period of time the lake must have dried out. This process is indicated by facies SH-D formed by the alternation of clastic clayey with evaporitic carbonate and gypsum layers (Figure 9D). Accordingly, unlike lower lake facies SH-C with <1% carbonate facies SH-D contains ca. 10–20% carbonate. Likewise, increasing sand contents up to >21% can be attributed to gypsum crystals (pseudosand) that were not destroyed during preparation of the grain size samples (Figure 6). In facies SH-D the micromorphological analyses show only moderate reduction conditions as indicated by stage B of the redoximorphic pattern (Vepraskas et al., 2018). Furthermore, shallower lake conditions compared with facies SH-C are also indicated by micrite and geodic sparitic nodules of probably biogenic origin likely derived from algae or other organisms living in shallow water conditions (Freytet and Verrecchia, 2002), and regular desiccation of the lake bed is indicated by numerous desiccation cracks within the clayey layers. The upwards increasing proportion of evaporitic carbonate and gypsum compared with clastic clayey material probably reflects an intensified desiccation trend with time. This trend is also indicated by upwards decreasing Si/S ratios and decreasing values of mass-specific susceptibility, reflecting the relative increase of S-containing gypsum and parallel decrease of siliciclastic material towards the top, respectively (Figure 6). Fish teeth of the family *Cyprinidae* (including species such as carps and minnows) were found in upper facies SH-D. These species are not seasonal, and require fresh or at least brackish water conditions (Kottelat and Freyhof, 2007). Hence, also during the final period of lake desiccation the lake must have had longer stable phases with fresh or brackish water, allowing the establishment of stable fish populations that could potentially have been used by the local populations. This also demonstrates that the desiccation process must

have continued over a longer period. Going from the central plain towards its margin, facies SH-C was detected up to transect core T7 (Figure 5). Based on its altitude we derived a maximal lake extent of ca. 6.2 km^2 and maximal depth of >1.5 m (Figures 3, 5). However, given that deposition of facies SH-C must have been linked with a water column of unknown depth, these calculated maximal values should actually be minimum values. There are no numerical ages for the end of lake desiccation, however, the luminescence sample taken from overlying facies SH-E gave a fine-grained feldspar pIRIR$_{290}$ age of 2.4 ± 0.2 ka, a fine-grained quartz age of 0.5 ± 0.05 ka and a coarse-grained feldspar pIRIR$_{290}$ age of 0.3 ± 0.1 ka. Both feldspar pIRIR$_{290}$ ages did not show anomalous fading. The older fine-grained quartz age compared with the coarse-grained feldspar pIRIR$_{290}$ age probably indicates that slower bleaching of the latter signal compared with quartz (Kars et al., 2014) must have been counterbalanced by the better bleachability of coarse compared with fine grains (Olley et al., 1998). However, it is also possible that due to argilloturbation, causing the input of younger material, these youngest ages are to some degree underestimated (Bateman et al., 2003). Hence, the youngest coarse-grained feldspar pIRIR$_{290}$ age of 0.3 ± 0.1 ka should represent a *terminus ante quem* for lake desiccation. Accordingly, also historic maps from the 18th century AD (= ca. 0.3 ka) do not show a lake or swamp in the central Shiraki Plain (Vakhushti Bagrationi Institute of Geography Tbilisi, 1997).

iv) Finally, during the last centuries the dried paleolake was covered by a colluvium (facies SH-E) (Figure 9E), although on the current soil map this material is shown as part of the regional surficial Vertisols (Matchavariani 2019). Besides its black color also the TOC/N-ratio of ca. 10-11 is similar with the values for the buried Vertisol (facies SH-B), supporting an origin of this material from eroded surrounding Vertisols. Significantly higher TOC contents of >3% and higher values of the magnetic susceptibility compared with facies SH-B can possibly be explained with the longer time of Vertisol formation and current agriculture, causing continued input of organic material and magnetic enhancement (Jordanova and Jordanova, 1999). However, the lower proportion of BC of TOC of about 16% should indicate a dilution of BC by other kinds of organic material. Given the large absence of human settlements following the Late Bronze/Early Iron Ages (Arnhold et al., 2020), definite causes for the deposition of the colluvial layer cannot be given here. However, a strong phase of fluvial activity was detected in the regional rivers for a later phase of the Little Ice Age between 0.5 and 0.4 ka (Suchodoletz et al., 2018). This phase must have been linked with at least seasonal stronger discharge caused by more intensive precipitation compared with today. Although the total precipitation amount was obviously not enough to cause renewed longer-lasting lake

formation in the Shiraki Plain, we suggest that due to preceding anthropogenic deforestation extreme precipitation events during that time could have caused surface erosion and colluvial deposition in the semi-arid landscape of the central Shiraki Plain also without direct human influence. Following its deposition, colluvial facies SH-E was interfingered with underlying facies SH-D by a strong seismic event in the form of inclined load structures (Figure 9F).

5.2 Changes of the hydrological balance between natural and human controls

Hydrological modelling helped to retrace the observed changes of the regional hydrological balance of the Shiraki Plain, and to identify possible natural and human drivers:

(i) From the neighbouring Udabno region showing comparable ecological and climatic conditions, we know that prior to the Late Bronze/Early Iron Ages the slopes above 700 m a.s.l. have been intensively forested, and that species-rich meadows were found below 700 m a.s.l. (Kvavadze and Todria, 1992). The detailed regional climate evolution of that period is not known, so that we applied the maximal precipitation amount of 700–800 mm that was reconstructed for the Late Bronze/Early Iron Ages and the current annual temperature. Given that at least parts of that period in the southern Caucasus were warmer compared with today (Connor and Sagona, 2007a) and drier compared with the Late Bronze/Early Iron Age (Connor and Kvavadze, 2008; Bliedtner et al., 2020b), the calculated water balances for that time should represent maximum values. Using those parameters, we obtained a balanced instead of a positive water budget that would be required for lake formation. Hence, the observed existence of a terrestrial Vertisol and not a lake in the central Shiraki Plain for this time could be supported by hydrological modelling.

(ii) In the Udabno region the forests were largely clear-cut during the Late Bronze/Early Iron Ages, and annual temperatures were up to 1.5 °C and annual precipitation 200–300 mm higher compared with today (Kvavadze and Todria, 1992). Using those parameters also for the Shiraki Plain that was settled by the same cultures, we obtained a positive water budget that even remained positive when the reconstructed paleolake surface with a higher ETa was taken into account. Thus, observed lake formation, indicating a significant change of the regional water budget during that time, could be retraced by hydrological modelling. Since we did not change the annual precipitation amount compared with the period before, and even used a higher annual temperature leading to higher ETa values for hydrological modelling, the change towards a positive water budget must have been caused by the large-scale human-induced regional forest clearcutting that reduced regional

(iii) Using the current climate and the drier grassland vegetation of the Shiraki Plain for hydrological modelling, we again obtained a balanced water budget. This could explain the observed lake desiccation. Since grassland vegetation in the whole catchment has probably persisted since clear-cutting during the Late Bronze/Early Iron Ages, that change of the water budget must have been linked with the regional aridification trend that was observed since that time (Kvavadze and Todria, 1992; Bliedtner et al., 2020b). Interestingly, when using the present environmental conditions of the ca. 230 m higher altitude where the current salt lake Kochebi is located, we obtained a slightly positive water balance what could possibly explain the existence of that lake. Although next to climatic parameters lake formation is also influenced by hydrogeological factors (winter, 1999), however, two other similar salt lakes in the Gareja region are located at about 760 m a.s.l. (Jikurebi lake) and at about 820 m a.s.l. (Kopatadze lake), respectively. Hence, the existence of those lakes seems to confirm that the current water budget of the Shiraki Plain is very close to positive values, i.e. that also smaller-scale changes of the controlling factors could currently cause a shift towards a positive water budget allowing lake formation.

However, limitations of such kind of hydrological modelling remain, as unquantified processes may affect the water balance as well. These include e.g. cloud cover changes, whereof no paleo information is available. Further unquantified processes could be seasonality changes, rapid snow melt and/or intensified run-off within the basin. Additionally, specific values for a class-specific ETa may differ interannually, as the vegetation reacts in a dynamic way to the available moisture. Therefore, our ETa estimates represent the best-possible long-time averages using this method.

Altogether, our hydrological modelling suggests that the Holocene hydrological balance of the Shiraki Plain was and is situated near a major hydrological threshold (White, 2019). That means that also relatively small-scale human or natural changes of the regional water balance caused a change from balanced/negative to positive values or vice versa, with significant geoecological changes due to lake formation or desiccation in the central Shiraki Plain. These changes should also strongly have influenced the living conditions of former local societies by supply or removal of water and fish resources.

5.3 Paleoseismic activity

The Shiraki Plain forms part of the NW-SE trending Kura Fold-and-Thrust-Belt which accommodated ~25 km of shortening (Forte et al., 2010). While thrust front advance is generally towards the SW defining the southern margin of the Shiraki Plain, Forte et al. (2010) postulated the presence of a backthrust at its northern margin. According to these authors, the neotectonic expression of the latter structure in the field suggests its relatively young age. It follows that SW-directed thrust belt dynamics, including backthrusting towards the NE, controlled the formation of the endorheiic Shiraki Plain. Historic as well as recent seismic activity (Varazanashvili et al., 2011; Ismail-Zadeh et al., 2020; Kldiashvili, 2021) suggests that these processes are still ongoing. The latter authors documented three large earthquakes in the Alaverdi region located ca. 100 km to the northwest during the last 500 years. These occurred in 1530 (reconstructed magnitude 5.7), between 1667 and 1668, and in 1742 AD (reconstructed magnitude 7).

Seismites are deformational structures attributable to seismic shocks, and classification schemes including tentative links to earthquake magnitudes were proposed by Rodriguez-Pascua et al. (2000) and Moretti and Sabato (2007). During the last years such structures in lacustrine sediments received growing interest as archives for paleoseismic activity (Archer et al., 2019). However, many of such studies have focused on lakes in high-relief regions that are also susceptible to slope failures not related to earthquakes, rendering the seismicity interpretation more difficult. In contrast, the stratigraphic sequence of the Shiraki region records deposition in a relatively low relief region and should therefore provide an ideal archive for past seismicity. The geometries observed at the base of the trench walls (Figure 4) indicate an interfingering of facies SH-A and SH-B in the form of vertical cones, and are interpreted as load structures (Moretti and Sabato, 2007). Given that the internal layering is difficult to recognize, these structures may represent pillow structures according to Rodriguez-Pascua et al. (2000) which these authors tentatively linked with an up to magnitude 7 earthquake. As shown in Figure 4, these cones are unconformably overlain by lake facies SH-C and SH-D. Within the uppermost part of SH-D, a series of inclined load structures, verging towards WNW, are observed (Figure 4). A similar situation is also interpreted from cores TPNW and TPE, since material of facies SH-D was found within facies SH-E here (Supplementary Table S2; location of the cores see Figure 3). The absence of internal layering hinders a further definition of these soft-sediment deformation features. However, we note that the load structures between SH-A and SH-B are vertical, whereas a sense of shear with top to the WNW-direction must have been present during the formation of the inclined load structures in SH-D and SH-E (Supplementary Figure S1). The strike of these inclined load structures is at a right angle to the main tectonic transport direction of the Greater Caucasus with top to the SW-direction and available fault plane solutions (Forte et al., 2010; Ismail-Zadeh et al., 2020). According to the latter authors, all active faults in the Shiraki Plain trend NW-SE and no perpendicular accommodation structures have been mapped yet (Supplementary Figure S4).

The above observations indicate the presence of two distinct seismites. These are separated from each other by at least one angular unconformity that is represented by lake facies I (SH-C) and the lower part of lake facies II (SH-D), and thus record two individual earthquakes. Based on the available chronological data the first earthquake must have occurred when the Vertisol, represented by facies SH-B, was already well developed but vertisol-derived lake facies I (SH-C) was still not deposited. Hence, the first event must have occurred during the Middle to Late Holocene prior to the intensive phase of Late Bronze/Early Iron Age settlement with large-scale soil erosion. The second earthquake must have occurred when the colluvial layer (SH-E) already covered the paleolake sediments (facies SH-D), i.e. during the last centuries. However, given the available dating we cannot safely attribute the latter seismic event to a certain historic earthquake mentioned above (Varazanashvili et al., 2011; Kldiashvili, 2021). Altogether, based on our available data the two recorded strong seismic events should not have occurred during the main and late phases of the Late Bronze/Early Iron Age settlement period. Therefore our data do not support the hypothesis of Pitskhelauri (2018), who suggests strong seismic activity in the Shiraki Plain during the start of the Early Iron Age.

6 Conclusion

Using a multi-disciplinary approach, during our study in the semi-arid Shiraki Plain we reconstructed Holocene human-environmental interactions in an important Late Bronze/Early Iron Age settlement center in the southeastern Caucasus. Our data show a balanced to negative water balance during the Early and Middle Holocene, so that no lake could develop in the lowest part of the plain but a terrestrial vertisol had formed instead. It is very likely that similar with the neighbouring Udabno region forestation of the higher altitudes contributed to the balanced to negative water balance. Subsequently Late Bronze/Early Iron age human activity since at latest 3.2 ka obviously changed the regional water balance by forest clearcutting, leading to the formation of a lake with a size of several square kilometres in the lowest part of the plain. However, the lake level never reached the necessary altitude for an outflow so that the lake always remained endorheic. Strong human impact on the landscape during that intensive settlement period is also demonstrated by the deposition of vertisol-derived material on the lake bottom resulting from soil erosion processes. Subsequently the lake dried out during a longer period, probably caused by a regionally observed aridification trend. Given that freshwater fishes could thrive in the lake even during parts of the desiccation period, the lake potentially offered valuable ecosystem services for the regional prehistoric societies of that period. During the last centuries the lake sediments were covered by a vertisol-derived colluvium, and given the absence of large-scale human activity between the Early Iron Ages and the recent period its

deposition must have been linked with hydrological extremes during the Little Ice Age. Also seismites were detected in the studied sediments that were probably related with two individual earthquakes. Given that one event must have occurred prior to the intensive phase of Late Bronze/Early Iron Age settlement, and the second after large-scale colluvial deposition during the last centuries, strong earthquakes did obviously not affect the main and late phases of Late Bronze/Early Iron Age settlement in the Shiraki Plain.

Our study demonstrates that the Holocene hydrological balance of the Shiraki Plain was and is situated near a major hydrological threshold. Consequently, also relatively small-scale human or natural influences on this semi-arid landscape can cause significant geoecological changes that strongly affected the living conditions of local societies due to lake formation or desiccation in the central part of the plain. Hence, the results of our study underline the high fragility of drylands towards also small-scale external perturbations, and demonstrate the high value of multi-disciplinary approaches to investigate their long-term evolution on millennial and centennial time scales.

Data availability statement

The original contributions presented in the study are included in the article/Supplementary Material, and further inquiries can be directed to the corresponding author.

Author contributions

HvS—study design, stratigraphical field work and analysis, data compilation, writing; GK—D-GPS and GIS analyses and mapping, writing; TK—paleoecological analyses, writing; MLF—hydrological modelling, writing; RMP—micromorphological analyses, writing; AK—stratigraphical field work and analysis, writing; BS—laboratory analyses, writing; BG—laboratory analyses, writing; SL—numerical dating, writing; SH—evaluation of paleoseismicity, writing; AS—stratigraphical field work and laboratory analyses; LN—stratigraphical field work, writing; ML—stratigraphical field work, writing; MA—archeological field work and data compilation; LL—archeological field work

and data compilation, writing; ME—study design, data compilation, writing.

Conflict of interest

The authors declare that the research was conducted in the absence of any commercial or financial relationships that could be construed as a potential conflict of interest.

Publisher's note

All claims expressed in this article are solely those of the authors and do not necessarily represent those of their affiliated organizations, or those of the publisher, the editors and the reviewers. Any product that may be evaluated in this article, or claim that may be made by its manufacturer, is not guaranteed or endorsed by the publisher.

Supplementary material

The Supplementary Material for this article can be found online at: https://www.frontiersin.org/articles/10.3389/feart.2022.964188/full#supplementary-material

References

Ad-hoc, A. G. B. (2005). *Bodenkundliche Kartieranleitung*. Hannover: Federal Institute for Geosciences and Natural Resources in collaboration with the State Geological Services. 5th ed.

Archer, C., Noble, P., Rosen, M. R., Sagnotti, L., Florindo, F., Mensing, S., et al. (2019). Lakes as paleoseismic records in a seismically-active, low-relief area (Rieti Basin, central Italy). *Quat. Sci. Rev.* 211, 186–207. doi:10.1016/j.quascirev.2019.03.004

Arnhold, S., Bukhrashvili, P., Fassbinder, J., Tskvitinidze, Z., Abele, J., and Davitashvili, S. (2020). Untersuchungen in Samreklo 2019. *Mittl. Dtsch. Orient-Gesellschaft Berl.* 152, 111–123.

Balbo, A. L., Gómez-Baggethun, E., Salpeteur, M., Puy, A., Biagetti, S., and Scheffran, J. (2016). Resilience of small-scale societies: A view from drylands. *Ecol. Soc.* 21, 53. doi:10.5751/ES-08327-210253

Barton, M. C., Ullah, I. I. T., Bergin, S. M., Sarjoughian, H. S., Mayer, G. R., Bernabeu-Auban, J. E., et al. (2016). Experimental socioecology: Integrative science for Anthropocene landscape dynamics. *Anthropocene* 13, 34–45. doi:10.1016/j.ancene.2015.12.004

Bateman, M. D., Frederick, C., Jaiswal, M. J., and Singhvi, A. K. (2003). Investigations into the potential effects of pedoturbation on luminescence dating. *Quat. Sci. Rev.* 22, 1169–1176. doi:10.1016/s0277-3791(03)00019-2

Bergner, A. G., Trauth, M. H., and Bookhagen, B. (2003). Paleoprecipitation estimates for the Lake Naivasha basin (Kenya) during the last 175 ky using a lake-balance model. *Glob. Planet. Change* 36, 117–136. doi:10.1016/s0921-8181(02)00178-9

Bliedtner, M., Suchodoletz, H. v., Schäfer, I., Welte, C., Salazar, G., Szidat, S., et al. (2020a). Age and origin of leaf wax n-alkanes in fluvial sediment-paleosol sequences, and implications for paleoenvironmental reconstructions. *Hydrol. Earth Syst. Sc.* 24, 2105–2120. doi:10.5194/hess-24-2105-2020

Bliedtner, M., Zech, R., Kühn, P., Schneider, B., Zielhofer, C., and Suchodoletz, H. v. (2018). The potential of leaf wax biomarkers from fluvial soil-sediment sequences for paleovegetation reconstructions - upper Alazani River, central southern Greater Caucasus (Georgia). *Quat. Sci. Rev.* 196, 62–79. doi:10.1016/j.quascirev.2018.07.029

Bliedtner, M., Zech, R., Schäfer, I., and Suchodoletz, H. v. (2020b). A first Holocene leaf wax isotope-based paleoclimate record from the semi-humid to semi-arid south-eastern Caucasian lowlands. *J. Quat. Sci.* 35, 625–633. doi:10.1002/jqs.3210

Blodgett, T. A., Lenters, J. D., and Isacks, B. L. (1997). Constraints on the origin of paleolake expansions in the central Andes. *Earth Interact.* 1, 1–28. doi:10.1175/1087-3562(1997)001<0001:cotoop>2.0.co;2

Bougealt, P. (1991). "Parameterization of land surface processes in numerical weather prediction," in *Land surface evaporation: Measurement and parameterization*. Editors T. J. Schmugge and J. C. Andre (New York: Springer), 55–92.

Brodowski, S., Rodionov, A., Haumaier, L., Glaser, B., and Amelung, W. (2005). Revised black carbon assessment using benzene polycarboxylic acids. *Org. Geochem.* 36, 1299–1310. doi:10.1016/j.orggeochem.2005.03.011

Brutsaert, W. H. (1982). *Evaporation into the atmosphere: Theory, history, applications*. Dordrecht: D. Reidel Publishing.

Budyko, M. I. (1974). *Climate and life*. New York: International Geophysics Series 18, Academic Press.

Bukhrashvili, P., Blocher, F., Tskvitinidze, Z., and Davitashvili, S. (2019). Ausgrabungen in Nazarlebi, Kachetien (Georgien) 2017 und 2018. *Mittl. Dtsch. Orient-Gesellschaft Berl.* 151, 271–294.

Buylaert, J.-P., Jain, M., Murray, A. S., Thomsen, K. J., Thiel, C., and Sohbati, R. A. (2012). A robust feldspar luminescence dating method for Middle and Late Pleistocene sediments. *Boreas* 41, 435–451. doi:10.1111/j.1502-3885.2012.00248.x

Connor, S. E., Colombaroli, D., Confortini, F., Gobet, E., Ilyashuk, B. P., Ilyashuk, E. A., et al. (2018). Long-term population dynamics: Theory and reality in a peatland ecosystem. *J. Ecol.* 106, 333–346. doi:10.1111/1365-2745.12865

Connor, S. E., and Kvavadze, E. V. (2008). Modelling late Quaternary changes in plant distribution, vegetation and climate using pollen data from Georgia, Caucasus. *J. Biogeogr.* 36, 529–545. doi:10.1111/j.1365-2699.2008.02019.x

Connor, S. E., and Sagona, A., (2007a). "Environment and society in the late prehistory of southern Georgia, Caucasus," in *Les Cultures du Caucase (Vie-IIIe millénaires avant notre ère). Leurs relations avec le Proche-Orient*. Editors B. Lyonnet (Paris: CNRS. Éditions Recherche sur les Civilisations), 21–36.

Connor, S. E., Thomas, I., and Kvavadze, E. (2007b). A 5600-yr history of changing vegetation, sea levels and human impacts from the Black Sea coast of Georgia. *Holocene* 17, 25–36. doi:10.1177/0959683607073270

Croudace, I. W., Rindby, A., and Rothwell, G. (2006). "Itrax: Description and evaluation of a new multi-function X-ray core scanner," in *New techniques in sediment core analysis*. Editors R. G. Rothwell (London: Geological Society London, Special Publications) 267, 51–63.

de la Rosa, J. M., Knicker, H., López-Capel, E., Manning, D. A. C., González-Perez, J. A., and González-Vila, F. J. (2008). Direct detection of Black Carbon in soils by Py-GC/MS, carbon-13 NMR spectroscopy and thermogravimetric techniques. *Soil Sci. Soc. Am. J.* 72, 258–267. doi:10.2136/sssaj2007.0031

Dong, G., Li, R., Lu, M., Zhang, G., and James, N. (2020). Evolution of human-environmental interactions in China from the late Paleolithic to the Bronze Age. *Prog. Phys. Geogr. Earth Environ.* 44, 233–250. doi:10.1177/0309133319876802

Dotterweich, M. (2008). The history of soil erosion and fluvial deposits in small catchments of central Europe: Deciphering the long-term interaction between humans and the environment - a review. *Geomorphology* 101, 192–208. doi:10.1016/j.geomorph.2008.05.023

Erb-Satullo, N. L., Jachvliani, D., Kalayci, T., Puturidze, M., and Simon, K. (2019). Investigating the spatial organisation of Bronze and iron age fortress complexes in the south Caucasus. *Antiquity* 93, 412–431. doi:10.15184/aqy.2018.191

Farr, T. G., Rosen, P. A., Caro, E., Crippen, R., Duren, R., Hensley, S., et al. (2007). The shuttle radar topography mission. *Rev. Geophys.* 45, RG2004–33. doi:10.1029/2005rg000183

Fletcher, W., Faust, D., and Zielhofer, C. (2013). Fragile landscape systems. *Catena* 103, 1–2. doi:10.1016/j.catena.2012.02.006

Force, E. R. (2017). Seismic environments of prehistoric settlements in northern Mesopotamia: A review of current knowledge. *Bull. Am. Sch. Orient. Res.* 378, 55–69. doi:10.5615/bullamerschoorie.378.0055

Forte, A., Cowgill, E., Bernardin, T., Kreylos, O., and Hamann, B. (2010). Late Cenozoic deformation of the Kura Fold-thrust belt, southern Greater Caucasus. *Geol. Soc. Am. Bull.* 122, 465–486. doi:10.1130/b26464.1

Freytet, P., and Verrecchia, E. P. (2002). Lacustrine and palustrine carbonate petrography: An overview. *J. Paleolimnol.* 27, 221–237. doi:10.1023/a:1014263722766

Fuchs, M., and Lang, A. (2008). Luminescence dating of hillslope deposits - a review. *Geomorphology* 109, 17–26. doi:10.1016/j.geomorph.2008.08.025

Furtwängler, A. E., Knauß, F., and Motzenbäcker, I. (1998). Archäologische Expedition in Kachetien 1997. Ausgrabungen in Shiraki. *Eurasia Antiq.* 4, 309–364.

Furtwängler, A. E., Knauß, F., and Motzenbäcker, I. (1999). Archäologische Expedition in Kachetien 1998. Ausgrabungen in Shiraki. *Eurasia Antiq.* 4, 233–270.

Gamkrelidze, I. P. (2003). *Geological map of Georgia 1:500,000*. Tbilisi: Georgian State Department of Geology and National Oil Company "SAQNAFTOBI".

Glaser, B., Haumaier, L., Guggenberger, G., and Zech, W. (1998). Black carbon in soils: The use of benzenecarboxylic acids as specific markers. *Org. Geochem.* 29, 811–819. doi:10.1016/s0146-6380(98)00194-6

Gogichaishvili, L. K. (1984). "Vegetational and climatic history of the Western part of the Kura river basin," in *Palaeoclimates, palaeoenvironments and human communities in the eastern Mediterranean region in later prehistory*. Editors e. d. Bintliff and W. van Zeist (Oxford: BAR International Series), 133, 325–341.

Hanesch, M., and Scholger, R. (2005). The influence of soil type on the magnetic susceptibility measured throughout soil profiles. *Geophys. J. Int.* 161, 50–56. doi:10.1111/j.1365-246x.2005.02577.x

Harden, C. P., Chin, A., English, M. R., Fu, R., Galvin, K. A., Gerlak, A. K., et al. (2014). Understanding human-landscape interactions in the "Anthropocene". *Environ. Manage.* 53, 4–13. doi:10.1007/s00267-013-0082-0

Herrmann, J. T., and Hammer, E. L. (2019). Archaeo-geophysical survey of Bronze and Iron Age fortress landscapes of the south Caucasus. *J. Archaeol. Sci. Rep.* 24, 663–676. doi:10.1016/j.jasrep.2019.02.019

Hijmans, R. J. (2020). Raster: Geographic data analysis and modeling. Available at: https://CRAN.R-project.org/package=raster (Accessed October 11, 2021).

Holliday, V. T., and Gartner, W. G. (2007). Methods of soil P analysis in archaeology. *J. Archaeol. Sci.* 34, 301–333. doi:10.1016/j.jas.2006.05.004

Ismail-Zadeh, A., Adamia, S., Chabukiani, A., Chelidze, T., Cloethingh, S., Floyd, M., et al. (2020). Geodynamics, seismicity, and seismic hazards of the Caucasus. *Earth. Sci. Rev.* 207, 103222. doi:10.1016/j.earscirev.2020.103222

Jahn, R., Blume, H. P., Asio, V. B., Spaargaren, O., and Schad, P. (2006). *Guidelines for soil description*. Rome: FAO. fourth edition.

Joannin, S., Ali, A. A., Ollivier, V., Roiron, P., Peyron, O., Chevaux, S., et al. (2014). Vegetation, fire and climate history of the Lesser Caucasus: A new Holocene record from Zarishat fen (Armenia). *J. Quat. Sci.* 29, 70–82. doi:10.1002/jqs.2679

Jordanova, D., and Jordanova, N. (1999). Magnetic characteristics of different soil types from Bulgaria. *Studia Geophys. Geod.* 43, 303–318. doi:10.1023/a:1023398728538

Kars, R. H., Reimann, T., Ankjaergaard, C., and Wallinga, J. (2014). Bleaching of the post-IR IRSL signal: New insights for feldspar luminescence dating. *Boreas* 43, 780–791. doi:10.1111/bor.12082

Kldiashvili, D. (2021). "Earthquakes in ancient Georgia IV-XVIII centuries," *Manuscript of SRNSFG grant FR 217804* (Tbilisi: Korneli Kekelidze Georgian National Centre of Manuscripts).

Koinig, K. A., Shotyk, W., Lotter, A. F., Ohlendorf, C., and Sturm, M. (2003). 9000 years of geochemical evolution of lithogenic major and trace elements in the sediment of an alpine lake - the role of climate, vegetation, and landuse history. *J. Paleolimnol.* 30, 307–320. doi:10.1023/a:1026080712312

Kottelat, M., and Freyhof, J. (2007). *Handbook of European freshwater fishes*. Berlin: Publications Kottelat, Cornol and Freyhof.

Kreutzer, S., Martin, L., Dubernet, S., and Mercier, N. (2018). The IR-RF alpha-Efficiency of K-feldspar. *Radiat. Meas.* 120, 148–156. doi:10.1016/j.radmeas.2018.04.019

Kunze, R. (2017). Living and working in Late Bronze/Early Iron Age Georgia: The settlements of Udabno in Kakheti (eastern Georgia) and a contribution to metallurgy based on a field survey in the upper Alazani River basin. *Stud. Cauc. Archaeol.* 3, 54–83.

Kvavadze, E. V., and Todria, V. T. (1992). *Ecologic conditions for the humans of the Bronze and early Iron Age in Udabno Gareji (eastern Georgia) according to paleoclimate data*. Tbilisi: Metsniereba. *(in Russian)*.

Laskar, J., Robutel, P., Joutel, F., Gastineau, M., Correia, A. C. M., and Levrard, B. (2004). A long-term numerical solution for the insolation quantities of the Earth. *Astron. Astrophys.* 428, 261–285. doi:10.1051/0004-6361:20041335

Lazar, M., Cline, E. H., Nickelsberg, R., Shahack-Gross, R., and Yasur-Landau, A. (2020). Earthquake damage as a catalyst to abandonment of a middle Bronze age settlement: Tel Kabri, Israel. *PLoS ONE* 15 (9), e0239079. doi:10.1371/journal.pone.0239079

Lewin, J., and Macklin, M. G. (2003). Preservation potential for Late Quaternary river alluvium. *J. Quat. Sci.* 18, 107–120. doi:10.1002/jqs.738

Liu, X., Lu, R., Jia, F., Li, X., Li, X., Li, M., et al. (2021). The strategy and environmental significance of Neolithic subsistence in the Mu Us Desert, China. *Quat. Int.* 574, 68–77. doi:10.1016/j.quaint.2020.12.006

Maisuradze, B., and Mindiashvili, G. (1999). Aeroarchaeology of Shiraki. *Dziebani* 4, 29–36. *(in Georgian)*.

Manning, S. W., Smith, A. T., Khatchadourian, L., Badalyan, R., Lindsay, I., Green, A., et al. (2018). A new chronological model for the Bronze and Iron Age south Caucasus: Radiocarbon results from project ArAGATS, Armenia. *Antiquity* 92, 1530–1551. doi:10.15184/aqy.2018.171

Maruashvili, L. I. (1971). "Geomorphology of Georgia," in *The relief of the Georgian SSR in the aspects of layers, origin, dynamics and history* (Tbilisi: Edition Metsnerieba). *(in Russian)*.

Matchavariani, L., (2019). *The soils of Georgia*. Cham: Springer Nature.

Menges, J., Hovius, N., Andermann, C., Dietze, M., Sowboda, C., Cook, C. L., et al. (2019). Late Holocene landscape collapse of a trans-Himalayan dryland: Human impact and aridification. *Geophys. Res. Lett.* 46, 13814–13824. doi:10.1029/2019gl084192

Messager, E., Belmecheri, S., Grafenstein, U. von, Nomade, S., Ollivier, V., Voinchet, P., et al. (2013). Late Quaternary record of the vegetation and catchment-related changes from lake Paravani (Javakheti, south Caucasus). *Quat. Sci. Rev.* 77, 125–140. doi:10.1016/j.quascirev.2013.07.011

Moretti, M., and Sabato, L. (2007). Recognition of trigger mechanisms for soft-sediment deformation in the Pleistocene lacustrine deposits of the Sant'Arcangelo Basin (Southern Italy): Seismic shock vs. overloading. *Sediment. Geol.* 196, 31–45. doi:10.1016/j.sedgeo.2006.05.012

Murray, A. S., and Wintle, A. G. (2000). Luminescence dating of quartz using an improved single-aliquot regenerative-dose protocol. *Radiat. Meas.* 32, 57–73. doi:10.1016/s1350-4487(99)00253-x

Neff, J. C., Ballantyne, A. P., Farmer, G. L., Mahowald, N. M., Conroy, J. L., Landry, C. C., et al. (2008). Increasing eolian dust deposition in the western United States linked to human activity. *Nat. Geosci.* 1, 189–195. doi:10.1038/ngeo133

New, M., Lister, D., Hulme, M., and Makin, I. (2002). A high-resolution data set of surface climate over global land areas. *Clim. Res.* 21, 1–25. doi:10.3354/cr021001

Nur, A., and Cline, E. H. (2000). Poseidon's horses: Plate tectonics and earthquake storms in the late Bronze Age Aegean and eastern Mediterranean. *J. Archaeol. Sci.* 27, 43–63. doi:10.1006/jasc.1999.0431

O'Henry, D. O., Cordova, C. E., Portillo, M., Albert, R.-M., deWitt, R., and Emery-Barbier, A. (2017). Blame it on the goats? Desertification in the Near East during the Holocene. *Holocene* 27, 625–637. doi:10.1177/0959683616670470

Olley, J., Caitcheon, G., and Murray, A. (1998). The distribution of apparent dose as determined by optical stimulated luminescence in small aliquots of fluvial quartz: Implications for dating young sediments. *Quat. Sci. Rev.* 17, 1033–1040. doi:10.1016/s0277-3791(97)00090-5

Ollivier, V., Fontugne, M., Lyonnet, B., and Chataigner, C. (2016). Base level changes, river avulsions and Holocene human settlement dynamics in the Caspian Sea area (middle Kura valley, South Caucasus). *Quat. Int.* 395, 79–94. doi:10.1016/j.quaint.2015.03.017

Ollivier, V., Fontugne, M., and Lyonnet, B. (2015). Geomorphic response and ^{14}C chronology of base-level changes induced by Late Quaternary Caspian Sea mobility (middle Kura Valley, Azerbaijan). *Geomorphology* 230, 109–124. doi:10.1016/j.geomorph.2014.11.010

Pitskhelauri, K. (2018). "Brief report of archaeological works on Didnauri settlement and burial," in *Collection of brief reports from 2017 archaeological expeditions*. Editors N. Antidze (Tbilisi: National Agency of Cultural Heritage Protection of Georgia), 24–29.

Pitskhelauri, K., Elashvili, M., Kirkitadze, G., Navrozashvili, L., Adikashvili, L., Janelidze, Z., et al. (2016). Reconstruction of the paleoenvironment of the Shiraki plain - traces of early state formations in southern Caucasus. Preliminary results. *Proc. Georgian Natl. Acad. Sci.* 1, 86–100. *(in Georgian)*.

Prescott, J., and Hutton, J. (1988). Cosmic ray and gamma ray dosimetry for TL and ESR. *Int. J. Radiat. Appl. Instrum. Part D. Nucl. Tracks Radiat. Meas.* 14, 223–227. doi:10.1016/1359-0189(88)90069-6

Rees-Jones, J., and Tite, M. S. (2007). Optical dating results for British archaeological sediments. *Archaeometry* 39, 177–187. doi:10.1111/j.1475-4754.1997.tb00797.x

Reimer, P. J., Austin, W. E. N., Bard, E., Bayliss, A., Blackwell, P. G., Bronk Ramsey, C., et al. (2020). The IntCal20 northern hemisphere radiocarbon age calibration curve (0-55 cal kBP). *Radiocarbon* 62, 725–757. doi:10.1017/rdc.2020.41

Reisser, M., Purves, R. S., Schmidt, M. W. I., and Abiven, S. (2016). Pyrogenic carbon in soils: A literature-based inventory and a global estimation of its content in soil organic carbon and stocks. *Front. Earth Sci.* 4, 1–14. doi:10.3389/feart.2016.00080

Rodionov, A., Amelung, W., Peinemann, N., Haumaier, L., Zhang, X., Kleber, M., et al. (2010). Black carbon in grassland ecosystems of the world. *Glob. Biogeochem. Cycles* 24, GB3013. doi:10.1029/2009GB003669

Rodríguez-Pascua, M. A., Calvo, J. P., de Vicente, G., and Gómez-Gras, D. (2000). Soft-sediment deformation structures interpreted as seismites in lacustrine sediments of the Prebetic Zone, SE Spain, and their potential use as indicators of earthquake magnitudes during the Late Miocene. *Sediment. Geol.* 135, 117–135. doi:10.1016/s0037-0738(00)00067-1

Rosen, A. M., Hart, T. C., Farquhar, J., Schneider, J. S., and Yadmaa, T. (2019). Holocene vegetation cycles, land-use, and human adaptations to desertification in the Gobi Desert of Mongolia. *Veg. Hist. Archaeobot.* 28, 295–309. doi:10.1007/s00334-018-0710-y

Sagona, A. (2018). *The archaeology of the Caucasus*. Cambridge: Cambridge University Press.

Salminen, R., (2005). *Geochemical Atlas of Europe. Part 1: Background information, methodology and maps*. Espoo: Geological Survey of Finland.

Schlichting, E., Blume, H. P., and Stahr, K. (1995). *Bodenkundliches praktikum*. Berlin: Blackwell Wissenschaftsverlag.

Schmidt, A., Quigley, M., Fattahi, M., Azizi, G., Maghsoudi, M., and Fazeli, H. (2011). Holocene settlement shifts and palaeoenvironments on the Central Iranian Plateau: Investigating linked systems. *Holocene* 21, 583–595. doi:10.1177/0959683610385961

Smith, A. T. (2005). Prometheus unbound: Southern Caucasia in prehistory. *J. World Prehist.* 19, 229–279. doi:10.1007/s10963-006-9005-9

Steinhof, A., Altenburg, M., and Machts, H. (2017). Sample preparation at the Jena 14C laboratory. *Radiocarbon* 59, 815–830. doi:10.1017/rdc.2017.50

Stoops, G. (2021). *Guidelines for analysis and description of soil and regolith thin sections*. Hoboken, NJ: John Wiley & Sons. 2nd ed.

Strouhalová, B., Ertlen, D., Šefrna, L., Novák, T. J., Virágh, K., and Schwartz, D. (2019). Assessing the vegetation history of European chernozems through qualitative near infrared spectroscopy. *Quaternaire* 30, 227–241. doi:10.4000/quaternaire.12101

Suchodoletz, H. v., Gärtner, A., Zielhofer, C., and Faust, D. (2018). Eemian and post-Eemian fluvial dynamics in the Lesser Caucasus. *Quat. Sci. Rev.* 191, 189–203. doi:10.1016/j.quascirev.2018.05.012

Suchodoletz, H. v., Menz, M., Kühn, P., Sukhishvili, L., and Faust, D. (2015). Fluvial sediments of the Algeti River in southeastern Georgia - an archive of Late Quaternary landscape activity and stability in the Transcaucasian region. *Catena* 130, 95–107. doi:10.1016/j.catena.2014.06.019

Suchodoletz, H. v., Richter, C., Walther, F., Bliedtner, M., Eloshvili, M., Losaberidze, L., et al. (2020). Land snail assemblages in Holocene floodplain research - an example from the southern Caucasus. *E G - Quat. Sci. J.* 69, 247–260. doi:10.5194/egqsj-69-247-2020

Suchodoletz, H. von, Oberhänsli, H., Faust, D., Fuchs, M., Blanchet, C., Goldhammer, T., et al. (2010). The evolution of Saharan dust input on Lanzarote (Canary Islands)—influenced by human activity in the northwest Sahara during the early Holocene? *Holocene* 20, 169–179. doi:10.1177/0959683609350385

Vakhushti Bagrationi Institute of Geography Tbilisi (1997). *Atlas of Georgia by Vakhushti Bagrationi*. Tbilisi: Tbilisi State University.

Varazanashvili, O., Tsereteli, N., and Tsereteli, E. (2011). *Historical earthquakes in Georgia (up to 1900): Source analysis and catalogue compilation*. Tbilisi: Institute of Geophysics I. Javakhishvili Tbilisi State University.

Varazashvili, V., and Pitskhelauri, K. (2011). *Results of archaeological research of Ilia State University at the Iori Upland*. Khornabuji: Ilia State University Publishing, 42–105. (in Georgian).

Vepraskas, M. J., Lindbo, D. L., and Stolt, M. H. (2018). "Redoximorphic features," in *Interpretation of micromorphological features of soils and regoliths*Editors e. d. G. Stoops, V. Marcelino, and F. Mees (Amsterdam: Elsevier), 425–445.

Virmani, S. M., Sahrawat, K. L., and Burford, J. R. (1982). *Physical and chemical properties of vertisols and their management*. New Delhi, India: Twelfth International Congress of Soil Science. 8-16 February 1982.

Wallinga, J., Murray, A. S., Duller, G. A. T., and Törnqvist, T. E. (2001). Testing optically stimulated luminescence dating of sand-sized quartz and feldspar from fluvial deposits. *Earth Planet. Sci. Lett.* 193, 617–630. doi:10.1016/s0012-821x(01)00526-x

Wang, Y., Amundson, R., and Trumbore, S. (1996). Radiocarbon dating of soil organic matter. *Quat. Res.* 45, 282–288. doi:10.1006/qres.1996.0029

White, H. E. (2019). Theses and dissertations (comprehensive). 2176. Available at: https://scholars.wlu.ca/etd/2176 (Accessed March 21, 2022).

Wilson, A. M., and Jetz, W. (2016). Remotely sensed high-resolution global cloud dynamics for predicting ecosystem and biodiversity distributions. *PLoS Biol.* 14 (3), e1002415. doi:10.1371/journal.pbio.1002415

Winter, T. C. (1999). Relation of streams, lakes, and wetlands to groundwater flow systems. *Hydrogeol. J.* 7, 28–45. doi:10.1007/s100400050178

Zielhofer, C., Suchodoletz, H. v., Fletcher, W. J., Schneider, B., Dietze, E., Schlegel, M., et al. (2017). Millennial-scale fluctuations in Saharan dust supply across the decline of the African humid period. *Quat. Sci. Rev.* 171, 119–135. doi:10.1016/j.quascirev.2017.07.010